Universidad Autónoma de Madrid

Departamento de Física Teórica

Memoria de Tesis Doctoral

Raiders of the Lost ALP

por

Jesús Bonilla García

presentada ante el Departamento de Física Teórica
de la Universidad Autónoma de Madrid
para la obtención del Título de Doctor en Ciencias

Tesis Doctoral dirigida por

Prof. Mª Belén Gavela Legazpi

Catedrática del Departamento de Física Teórica
de la Universidad Autónoma de Madrid

20 de octubre de 2023, Madrid

Agradecimientos

Hacer un doctorado es un camino largo y desafiante, que requiere una gran implicación, dedicación y perseverancia. Sin embargo, paradójicamente, siento que este tiempo ha transcurrido en un abrir y cerrar de ojos. Mirando hacia atrás, es verdaderamente impresionante reproducir cada pequeño paso que me ha llevado hasta este momento de mi vida. Es por eso que quiero aprovechar estas páginas para dar las gracias a todas las personas que me han brindado su apoyo y ánimos en estos años, pues su ayuda ha sido fundamental para llegar a ser quien soy ahora.

En primer lugar, quiero dar las gracias a Belén, quien ha sido mi directora y guía durante mi doctorado e incluso desde algunos años antes. Ella me ha enseñado a desenvolverme y comprender un mundo lleno de operadores, diagramas y Lagrangianos, de congresos, cursos y seminarios, y a ser parte de él. Gracias, Belén, por tus consejos, tu dedicación y también por tu exigencia, que ha hecho que dé lo mejor de mí, aprenda todo lo que he aprendido en esta etapa y crezca como persona. También quiero agradecerte todo tu apoyo, especialmente a la hora de mirar hacia mi futuro, y pensar siempre en las motivaciones y aspiraciones de tus estudiantes.

Quiero agradecer también a todas las personas con las que he tenido la fortuna de colaborar a lo largo de mi carrera académica y, en especial, a todas las personas del IFT. Con todos vosotros, he compartido una pasión por el conocimiento y la exploración científica. Cada interacción y cada proyecto han sido una gran fuente de aprendizaje y enriquecimiento profesional. El ambiente de compañerismo en el IFT, tanto con los estudiantes de doctorado como con los investigadores senior, ha sido fundamental para nutrir mi crecimiento como investigador y persona. Por todo ello, quiero expresar mi más sincero agradecimiento a mis colegas y compañeros del IFT, cuya colaboración y amistad han dejado una huella permanente en mi trayectoria.

Merecen una mención especial mis dos "hermanos mayores de doctorado", Ilaria y Pablo, quienes me han aconsejado y ayudado en muchas ocasiones a lo largo de estos años de doctorado. Pablo, muchas gracias por tu apoyo y, sobre todo, por tu amistad y por haber sido tan buen guía tanto en San Diego como en Hamburgo. Gracias a ti, he conocido un montón de lugares increíbles. Queda pendiente volver a tomarnos una buena hamburguesa en The Bird o en el Rocky's (¡espero que no llegues muy tarde!). Y a ti, Ilaria, gracias por toda tu ayuda y por compartir conmigo todo lo que sabes. Siempre he podido contar contigo en esta etapa para cualquier duda que tenía, tanto a nivel académico como personal.

Por supuesto, no puedo olvidarme de darles las gracias a la Pocha Gang del IFT. Gracias a todos vosotros, a los nuevos miembros: Xavi, Dani, Fer, Paco y Emilia; y, por supuesto, a los miembros clásicos: Jose y Manu. Vuestra amistad ha sido imprescindible para mantener la cordura durante el doctorado, y gracias a vuestra sabiduría, he podido comprender verdaderamente las implicaciones del SM. Con vosotros, he compartido un montón de experiencias y siempre habéis estado ahí cuando lo he necesitado. Sois uno de los recuerdos más bonitos que me llevo de esta etapa.

Fuera del mundo académico, quiero mostrar mi sincero agradecimiento a los fisicolentos. A lo largo de todos estos años, su amistad ha sido un verdadero tesoro en mi vida. Aunque nuestras trayectorias profesionales difieren, siempre hemos compartido inquietudes y apasionantes discusiones sobre el futuro y mucho más. Gracias a Henar, Lema, Lel, Álvaro, Ana, César, Josekas, Juanma, Loeches, Marío, Tobias y, por supuesto, a Patry; vuestra amistad ha sido un regalo inestimable, y estoy eternamente agradecido por contar con personas tan especiales en mi vida.

Por último, mi más profundo agradecimiento a toda mi familia. Gracias a mis tíos, tías, primos y primas, que siempre han estado ahí desde que era pequeño. A Juan, Mari, Nina y María del Mar, con quienes me he sentido arropado y querido desde el primer minuto. A mi abuela, a quien quiero muchísimo, y a mi hermano, de quien estoy profundamente orgulloso. A mis padres, que siempre me han brindado un apoyo incondicional a lo largo de mi trayectoria académica, dándome toda la motivación y todas las oportunidades para seguir estudiando y creciendo como persona. Sin vosotros, no habría llegado hasta aquí. Y gracias con todo mi corazón a ti, Patry, que te has convertido en familia. Quiero expresar mi agradecimiento por todo tu apoyo y amor. Tu presencia en mi vida ha sido un regalo y tu cariño ha sido la mejor ayuda para cada desafío al que he enfrentado. Gracias por ser mi confidente y por ayudarme a sacar la mejor versión de mí mismo.

Gracias a todos vosotros por vuestra presencia y afecto. Siento una profunda gratitud por tener una familia tan maravillosa.

Publications

This doctoral thesis is based on the following scientific publications:

Refereed journal articles

[1] **One-loop corrections to ALP couplings**
J. Bonilla, I. Brivio, M. B. Gavela and V. Sanz
JHEP ***11*** *(2021) 168* and *arXiv:2107.11392 [hep-ph]*

[2] **Nonresonant searches for axion-like particles in vector boson scattering processes at the LHC**
J. Bonilla, I. Brivio, J. Machado-Rodríguez and J. F. de Trocóniz
JHEP ***06*** *(2022) 113* and *arXiv:2202.03450 [hep-ph]*

[3] **The cost of an ALP solution to the neutral B-anomalies**
J. Bonilla, A. de Giorgi, B. Gavela, L. Merlo and M. Ramos
JHEP ***02*** *(2023) 138* and *arXiv:2209.11247 [hep-ph]*

Preprints

[4] **Neutral B-anomalies from an on-shell scalar exchange**
J. Bonilla, A. de Giorgi and M. Ramos
arXiv:2211.05135 [hep-ph]

Proceedings

[5] **One-loop corrections to ALP effective couplings**
J. Bonilla, I. Brivio, M. B. Gavela and V. Sanz
PoS ***EPS-HEP2021*** *(2022) 497* and *arXiv:2111.14750 [hep-ph]*

[6] **Nonresonant Searches for Axion-Like Particles at the LHC: Implications for Vector Boson Scattering**
J. Bonilla, I. Brivio, J. Machado-Rodríguez and J. F. de Trocóniz
PoS ***EPS-HEP2021*** *(2022) 692*

[7] **ALP one-loop corrections and nonresonant searches**
J. Bonilla
56th Rencontres de Moriond on Electroweak Interactions and Unified Theories
arXiv:2205.09156 [hep-ph]

Abstract

While the Standard Model (SM) of Particle Physics describes with exceptional accuracy a vast amount of natural phenomena, it fails to explain certain experimental observations and theoretical challenges. Thus, extensions of the model are required to address these limitations. This thesis focuses on the exploration of Axion-Like Particles (ALPs) as a suitable extension of the SM. Given the ubiquity of ALPs in several beyond SM models, we employ a model-independent effective field theory framework to investigate the potential interactions between ALPs and the SM particles. Subsequently, the results presented in this thesis can be categorized into two main parts.

On one hand, as the experimental searches for ALPs have become increasingly diverse and precise, they call for the necessity to take into account radiative corrections to the ALP effective theory. In this thesis, the full set of one-loop corrections for the dimension-5 ALP Lagrangian is derived, manifesting their significant impact on experimental ALP searches. Notably, these corrections offer an approach to probe ALP couplings that may be challenging to test directly but induce a sizeable impact on other interactions that are highly constrained by experimental data.

On the other hand, this thesis investigates the phenomenological implications of ALPs in experimental high-energy searches. Specifically, we explore the contributions of ALPs to rare processes within collider searches. For instance, a novel search targeting vector-boson scattering processes is proposed, exploiting the derivative nature of ALPs to probe their electroweak couplings to massive gauge bosons. Moreover, we explore the impact of ALPs on flavor observables, with a particular emphasis on investigating flavor anomalies associated with the B-meson sector.

While the experimental detection of ALPs remains fruitless at present, the research conducted in this thesis has been productive in systematically exploring the ALP parameter space. Through rigorous analysis, new excluded regions within the parameter space have been identified, providing valuable constraints on potential ALP couplings. Furthermore, these studies have suggested novel promising avenues and valuable strategies to probe these elusive particles in upcoming experiments.

Resumen

Aunque el Modelo Estándar (ME) de Física de Partículas describe con una precisión excepcional una vasta cantidad de fenómenos naturales, no logra explicar ciertas observaciones experimentales y cuestiones teóricas. Por lo tanto, el modelo requiere de extensiones para abordar estas limitaciones. Esta tesis se centra en la exploración de partículas tipo axión (PTAs) como una posible extensión del ME. Dada la ubicuidad de las PTAs en varios modelos más allá del ME, empleamos el marco teórico de las teorías de campos efectivas, que son independientes de los modelos concretos, para investigar las posibles interacciones entre PTAs y las partículas del ME. Posteriormente, los resultados presentados en esta tesis se pueden categorizar en dos partes principales.

Por un lado, dado que las búsquedas experimentales de PTAs se han vuelto cada vez más diversas y precisas, es necesario tener en cuenta las correcciones radiativas a la teoría efectiva de las PTAs. En esta tesis, se deriva el conjunto completo de correcciones a un loop para el Lagrangiano de las PTAs de dimensión 5, manifestando su impacto significativo en las búsquedas experimentales de PTAs. Específicamente, estas correcciones ofrecen un nuevo enfoque para investigar acoplos de las PTAs que pueden ser difíciles de testar directamente, pero que inducen un impacto considerable en otras interacciones áltamente constreñidas por los datos experimentales.

Por otro lado, esta tesis investiga las implicaciones fenomenológicas de las PTAs en búsquedas experimentales de alta energía. Específicamente, exploramos las contribuciones de las PTAs a procesos raros en búsquedas de colisionadores. Por ejemplo, proponemos una nueva búsqueda centrada en los procesos de dispersión de bosones vectoriales, aprovechando la naturaleza derivativa de las PTAs para investigar sus acoplamientos electrodébiles con los bosones gauge masivos. Además, exploramos el impacto de las PTAs en observables del sabor, con un énfasis particular en investigar las anomalías de sabor asociadas al sector de los mesones B.

Aunque la detección experimental de PTAs sigue siendo infructuosa en la actualidad, la investigación realizada en esta tesis ha sido productiva en la exploración sistemática del espacio de parámetros de las PTAs. Mediante un análisis riguroso, se han identificado nuevas regiones excluidas dentro del espacio de parámetros, proporcionando valiosas restricciones sobre posibles acoplamientos de las PTAs. Además, estos estudios han sugerido nuevas y prometedoras vías y estrategias para investigar estas elusivas partículas en futuros experimentos.

Contents

Motivations and goals

The Standard Model (SM) of particle physics [8–13] provides a framework for understanding three out of the four fundamental forces of nature that govern the interactions among the fundamental building blocks of matter of the visible world: the strong interaction, the weak interaction and electromagnetism. The SM has been extensively tested in a wide variety of experiments and has accurately predicted many observations at collider energy scales and below with an extraordinary accuracy.

Notwithstanding the considerable achievements of the SM, there remain still empirical observations that cannot be satisfactorily explained by this theory (in addition to our lack of understanding of gravitation at the quantum level). Among these, the most notable are:

- **Dark matter**: Cosmological observations have indicated that only 5% of the energy density in our universe is composed of ordinary matter. About 26% should be made of cold dark matter, which only interacts weakly (if at all aside from gravity) with SM particles. Yet, the SM does not supply any suitable fundamental particle candidate for this new type of matter.

- **Dark energy**: About 69% of the energy density in our universe is in the form of "dark energy". This expression encodes a constant energy density for the vacuum, which is responsible of the accelerated expansion of the universe. However, attempts to intuitively understand this energy as a vacuum energy of the SM fields lead to a huge mismatch with respect to cosmological observations.

- **Neutrino masses**: As originally formulated, neutrinos are massless particles in the SM. However, the empirical observation of neutrino oscillations implies that at least two neutrino masses are different from zero. The actual mechanism that gives rise to these masses and explains their smallness, as well as the Dirac or Majorana nature of neutrinos, is still unknown.

- **Matter-antimatter asymmetry**: Astrophysical observations indicate that the universe is mostly made of matter. However, the SM predicts that matter and antimatter should be produced in almost equal amounts in early stages of the universe (assuming there is no asymmetry as an initial condition). Despite the fact that SM provides the "ingredients" to produce matter-antimatter asymmetry, these have been proven to be insufficient to explain the observed amount of asymmetry.

In addition to the aforementioned evidences for physics beyond the SM (BSM), some experimental observations have indicated deviations in other phenomena. These anomalies include, for example, measurements in the neutrino sector, as well as decay rates of heavy hadrons, such as B-mesons. However, the statistical significance of these anomalies is currently insufficient to classify them as evidence for new physics. On the other hand, they are identified as potential probes of unexplored hidden sectors of new BSM physics.

Furthermore, beyond the previously noted experimental questions, the structure of the SM itself presents certain concerns. These refer to fine-tuning issues, where certain parameters are required to have specific values without any theoretical justification. The most notable fine-tuning issues in the SM include the following:

- **The electroweak hierarchy problem**: Scalar particles, such as the Higgs boson, do not posses any symmetry that protects its mass against sensitivity to higher scales via radiative corrections, resulting in a quadratic dependence of the mass on that scale of hypothetical new physics. As a consequence, in the presence of physics with higher energy scales, the bare mass of the Higgs boson in the SM Lagrangian must be fine-tuned such that those corrections are partially cancelled, leading to the experimentally observed "light" mass of the Higgs boson.

- **The flavour puzzle**: The masses of the quarks and leptons arise from their Yukawa interactions with the Higgs boson. However, the scale of these masses is much smaller than the electroweak scale, for no good reason. Strictly speaking, this is not a naturalness issue: Yukawa couplings are protected by the chiral symmetry of the Lagrangian in the limit of small masses. Yet, the orders of magnitude differences in the fermion masses are puzzling. Furthermore, the remarked hierarchy among the three generations of fermions, plus the huge differences in the quark and lepton mixing matrices suggest that there is an underlying structure yet to be discovered.

- **The strong CP problem**: Quantum chromodynamics (QCD), the theory that describes strong interactions, a priori may contain a topological CP-odd term that is regulated by a parameter named $\overline{\theta}$, which characterizes the vacuum of the theory. This term should result in a non-zero contribution to the neutron electric dipole moment. However, current constraints on the latter require $\overline{\theta}$ to be fine-tuned to an extremely small value: $\overline{\theta} \lesssim 10^{-10}$, which results in a restoration of the CP symmetry in the QCD sector. This is surprising, as it is not required by gauge invariance and CP-symmetry is explicitly violated in other sectors of the SM.

In my research I have mainly focused on topics that are not directly connected to the latter, the strong CP problem of QCD, but are, however, inspired by and related to it. As mentioned above, the strong CP problem is a fine-tuning problem: mathematically there is no inconsistency with a value of $\overline{\theta}$ equal to 0. However, such a constrained value with no theoretical explanation calls for an underlying BSM mechanism. Several models have been proposed in the literature as a possible solution to the strong CP problem. One of the most appealing proposals are the so-called Peccei-Quinn (PQ) solutions. These try to extend the SM by implementing a new global symmetry classically conserved at the Lagrangian level, but explicitly broken at the quantum level by a chiral anomaly via QCD instanton effects. Thus, a rotation of such symmetry is used to render $\overline{\theta}$ unphysical. Typically, that symmetry is referred to as the PQ symmetry.

At low-energies, the PQ symmetry is spontaneously broken, originating a new light pseudoscalar in the spectrum, as mandated by the Goldstone theorem: the axion. Because of the explicit breaking of the PQ symmetry due to the chiral anomaly, the axion is not a true Goldstone boson (GB), but rather a pseudo-Goldstone boson (pGB). Because of this nature, axions typically exhibit derivative plus anomalous couplings with SM particles and have a small mass (induced precisely by the aforementioned chiral anomaly in QCD). Additionally, in a large fraction of the parameter space, the axion also turns out to constitute a perfect candidate for the explanation of dark matter. This attribute has turned the axion into one of the most appealing extensions of the SM.

Many different axion models have been proposed. The most popular ones are the so-called invisible axion models. In those, the axion energy scale is pushed up to large energies, which pushes down the axion mass and suppresses its couplings with SM particles, avoiding experimental constraints. On the other hand, in recent years extended models have allowed to implement solutions with heavier-than-standard and lighter-than-standard axions.

Nevertheless, the interest on pGBs extends far beyond true axion models. Theories of pGBs appear in many BSM proposals, typically unrelated to the strong CP problem, as SM singlets. Generally, these are referred to as axion-like particles (ALPs). Some paradigmatic examples include the Majoron, related to the spontaneous breaking of lepton number, as a dynamical explanation of the smallness of neutrino masses; or axiflavons, from dynamical flavour theories. Moreover, they are also predicted in theories with extra compact dimensions, for instance string theories, which predict a plethora of $U(1)$ symmetries and ALPs. In practice, the main difference between a true axion and an ALP is that the former attempts to solve the strong CP problem, which typically imposes strict relations between the axion mass and energy scale. Therefore, the exploration of the ALP parameter space does not suffer from the stringent constraints that usually apply to the canonical QCD axion.

Given the current absence of experimental axion and ALP signals, the ALP effective field theory (EFT) offers a model-independent approach to investigate their interactions with SM particles. This framework is characterized by a simple Lagrangian with few parameters, including the ALP mass and scale and some Wilson coefficients that encode the dependence on the specific ALP model. While many previous studies have focused on effective interactions with lighter particles like photons or electrons, the gauge invariant formulation of the effective ALP theory allows for interactions with heavier particles, such as electroweak (EW) bosons. These interactions exhibit a more intriguing phenomenology and can be explored across a broader range of energies in comparison with the usual axion low-energy searches. Those include, for example, collider ALP searches. These analyses hold a particular significance for specific models with pGBs that either do not couple to light particles or possess masses too heavy to be probed at low-energies.

The main goal of this thesis is to enable the discovery an axion or ALP signal at high energy searches or, if not detected, to derive the corresponding constraints on the ALP parameter space. This goal can be further subdivided into two additional objectives. On one hand, ALP searches have reached a level of precision and are so diverse that experimental sensitivity requires to compute the radiative corrections to effective ALP couplings. Thus, in this thesis I present the one-loop corrected ALP EFT, and explore its phenomenological consequences for experiments. On the other hand, I focus on ALP searches at collider experiments. For instance, novel searches on ALP interactions are explored. These includes a proposal for exploring scattering processes that are potentially mediated by off-shell ALPs,

testing their EW couplings. In addition, I study the impact of ALPs on several flavour anomalies, with special emphasis on the B-meson sector and its semileptonic decays.

This thesis is organized as follows: in Chapters 1 to 3 I present the state of art of the SM, axions and ALPs. Then, Chapters 4 to 6 include the original contribution of the thesis. The conclusions are summarized in Chapter 7.

Motivación y objetivos

El Modelo Estándar (ME) de la física de partículas [8–13] proporciona un marco teórico que permite explicar tres de las cuatro fuerzas fundamentales de la naturaleza que rigen las interacciones entre los bloques fundamentales de la materia del mundo visible: la interacción fuerte, la interacción débil y el electromagnetismo. El ME ha sido ampliamente testado en una vasta variedad de experimentos y ha predicho con extraordinaria precisión muchas observaciones en las escalas de energía típicas de los colisionadores de partículas y por debajo de estas.

A pesar de los considerables logros del ME, todavía existen observaciones empíricas que no pueden explicarse satisfactoriamente mediante esta teoría (además de nuestra falta de comprensión de la gravedad a nivel cuántico). Entre las más notables se encuentran:

- **Materia oscura**: Las observaciones cosmológicas han indicado que solo el 5 % de la densidad de energía en nuestro universo está compuesta de materia ordinaria. Alrededor del 26 % debería estar formado por materia oscura fría, que solo interactuaría débilmente (si es que lo hace más allá de la interacción gravitatoria) con las partículas del ME. Sin embargo, el ME no comprende ninguna partícula fundamental que sea un candidato adecuado para este nuevo tipo de materia.

- **Energía oscura**: Alrededor del 69 % de la densidad de energía en nuestro universo se encuentra en forma de “energía oscura". Esta expresión se refiere a una densidad de energía constante para el vacío, que es responsable de la expansión acelerada del universo. Sin embargo, los intentos de entender intuitivamente esta energía como una energía de vacío de los campos del ME conducen a una gran discrepancia con respecto a las observaciones cosmológicas.

- **Masas de los neutrinos**: Según se formularon originalmente, los neutrinos no tienen masa en el ME. Sin embargo, la observación empírica de las oscilaciones de neutrinos implica que al menos dos neutrinos tienen una masa distinta de cero. El mecanismo que daría lugar a estas masas y explicaría su ligereza, así como la naturaleza de Dirac o Majorana de los neutrinos, todavía se desconoce.

- **Asimetría materia-antimateria**: Las observaciones astrofísicas indican que el universo está compuesto principalmente de materia. Sin embargo, el ME predice que la materia y la antimateria deberían producirse en cantidades casi iguales en las etapas iniciales del universo (asumiendo que como condición inicial no hay asimatería). A pesar de que el

ME proporciona los “ingredientes"para producir la asimetría materia-antimateria, se ha demostrado que estos son insuficientes para explicar la cantidad de asimetría observada.

Además de las evidencias previamente mencionadas para la física más allá del ME, algunas observaciones experimentales han indicado desviaciones en otros fenómenos. Estas anomalías incluyen, por ejemplo, mediciones en el sector de los neutrinos, así como en los ratios de desintegración de hadrones pesados, como los mesones B. Sin embargo, la significancia estadística de estas anomalías es actualmente insuficiente para clasificarlas como evidencia de nueva física. Por otro lado, se identifican como posibles rastros de sectores inexplorados que podrían ocultar nueva física más allá del ME.

Aparte de las cuestiones experimentales mencionadas anteriormente, la estructura del ME en sí misma presenta ciertas preocupaciones. Estas se refieren a problemas de ajuste fino, donde se requiere que ciertos parámetros tengan valores específicos sin ninguna justificación teórica. Los problemas de ajuste fino más notables en el ME incluyen los siguientes:

- **El problema de la jerarquía electrodébil**: Las partículas escalares, como el bosón de Higgs, no poseen ninguna simetría que proteja su masa frente a la sensibilidad a escalas más altas a través de correcciones radiativas, lo que resulta en una dependencia cuadrática de la masa en la escala de nueva física. Como consecuencia, en presencia de física con escalas de energía más altas, la masa “desnuda” del bosón de Higgs en el Lagrangiano del ME debe ajustarse finamente para que esas correcciones se cancelen parcialmente, lo que conduce a la “ligera” masa que se observa experimentalmente para el bosón de Higgs.

- **El puzzle del sabor**: Las masas de los quarks y leptones surgen de sus interacciones de Yukawa con el bosón de Higgs. Sin embargo, la escala de estas masas es mucho menor que la escala electrodébil, sin razón aparente. Estrictamente hablando, esto no es un problema de naturalidad: los acoplos de Yukawa están protegidos por la simetría quiral del Lagrangiano en el límite de masas pequeñas. Sin embargo, las diferencias en órdenes de magnitud en las masas de fermiones son desconcertantes. Además, la destacada jerarquía entre las tres generaciones de fermiones, junto con las enormes diferencias en las matrices de mezcla de quarks y leptones, sugiere que existe una estructura subyacente aún por descubrir.

- **El problema CP fuerte**: La cromodinámica cuántica (CDC), la teoría que describe las interacciones fuertes, a priori puede contener un término topológico impar bajo CP que está regulado por un parámetro llamado $\overline{\theta}$, que caracteriza el vacío de la teoría. Este término debería dar lugar a una contribución no nula al momento dipolar eléctrico del neutrón. Sin embargo, las restricciones actuales sobre este último requieren que $\overline{\theta}$ esté ajustado finamente a un valor extremadamente pequeño: $\overline{\theta} \lesssim 10^{-10}$, lo que resulta en una restauración de la simetría CP en el sector de CDC. Esto es sorprendente, ya que la invariancia gauge no prohibe dicho término y la simetría CP está explícitamente rota en otros sectores del ME.

En mi investigación, me he centrado principalmente en temas que no están directamente relacionados con este último problema, el problema CP fuerte de CDC, pero que están, sin embargo, inspirados y relacionados con él. Como se mencionó anteriormente, el problema CP fuerte es un problema de ajuste fino: matemáticamente, el valor $\overline{\theta}$ igual a 0 no es inconsistente. Sin embargo, un valor tan restringido sin ninguna explicación teórica

apunta hacia un mecanismo subyacente de nueva física más allá del ME. Varios modelos se han propuesto en la literatura como posible solución al problema CP fuerte. Una de las propuestas más atractivas son las llamadas soluciones de Peccei-Quinn (PQ). Estas tratan de extender el ME implementando una nueva simetría global conservada a nivel del Lagrangiano, pero explícitamente rota a nivel cuántico por la anomalía quiral a través del efectos de los instantones de CDC. De esta manera, se puede realizar una rotación de dicha simetría para hacer que $\overline{\theta}$ se vuelta físicamente irrelevante. Típicamente, esta simetría se conoce como simetría de PQ.

At bajas energías, la simetría de PQ se rompe espontáneamente, originando un nuevo pseudoscalar ligero en el espectro, como se deriva del teorema de Goldstone: el axión. Debido a la ruptura explícita de la simetría de PQ debido a la anomalía quiral, el axión no es un verdadero bosón de Goldstone (BG), sino más bien un pseudo-bosón de Goldstone (pBG). Debido a esta naturaleza, los axiones típicamente exhiben acoplamientos derivativos y anómalos con las partículas del ME y tienen una masa muy ligera (inducida precisamente por la anteriormente mencionada anomalía quiral de CDC). Además, en una gran parte del espacio de parámetros, el axión también resulta ser un candidato perfecto para explicar la materia oscura. Esta característica ha convertido al axión en una de las extensiones más atractivas del ME.

Se han propuesto muchos modelos diferentes de axiones. Los más populares son los llamados modelos de axiones invisibles. En estos, la escala de energía del axión toma un valor muy elevado, lo que reduce su masa y suprime sus acoplos con las partículas del ME, evitando los límites experimentales. Por otro lado, en los últimos años, se han propuesto modelos extendidos que implementan soluciones con axiones más pesados o más ligeros que el axion estándar.

No obstante, el interés en los pBGs se extiende mucho más allá de los modelos de axiones. Teorías de pBGs aparecen en muchas propuestas de física más allá del ME, típicamente no relacionadas con el problema CP fuerte, como singletes del ME. Generalmente, estos se conocen como "partículas tipo axión" (PTAs). Algunos ejemplos paradigmáticos incluyen el Majorón, relacionado con la ruptura espontánea del número leptónico, como una explicación dinámica de la ligereza de las masas de neutrinos; o los axiflavones, en teorías dinámicas del sabor. Además, también se predicen en teorías con dimensiones extra compactificadas, por ejemplo, en teorías de cuerdas, que predicen una plétora de simetrías $U(1)$ y PTAs. En la práctica, la principal diferencia entre un verdadero axión y una PTA es que el primero intenta resolver el problema CP fuerte, lo que típicamente impone una relación estricta entre la masa y la escala de energía del axión. Por lo tanto, la exploración del espacio de parámetros de las PTAs no sufre las estrictas restricciones que normalmente se aplican al axión canónico de CDC.

Dada la actual ausencia de señales experimentales de axiones y PTAs, la teoría efectiva de PTAs nos permite investigar sus interacciones con partículas del ME de forma independiente de los modelos concretos de PTAs. Este marco teórico se caracteriza por un Lagrangiano simple con pocos parámetros, que incluyen la masa y la escala de la PTA, así como algunos coeficientes de Wilson que codifican la dependencia en los modelos específicos de PTAs. Si bien muchos estudios anteriores se han centrado en las interacciones efectivas con las partículas más ligeras, como fotones o electrones, la formulación invariante gauge de la teoría efectiva de las PTAs permite interacciones con partículas más pesadas, como los bosones electrodébiles (ED). Estas interacciones exhiben una fenomenología más interesante

y pueden ser exploradas en un rango de energías más amplio en comparación con las búsquedas usuales de axiones a bajas energías. Esto incluye, por ejemplo, búsquedas de PTAs en colisionadores. Estos análisis tienen una importancia particular para modelos específicos con pBGs que o bien no se acoplan a partículas ligeras o poseen masas demasiado pesadas como para ser producidos a bajas energías.

El objetivo principal de esta tesis es posibilitar el descubrimiento de una señal de axiones o PTAs en búsquedas de alta energía o, de no ser detectadas, derivar las correspondientes restricciones en el espacio de parámetros de las PTAs. Este objetivo se puede subdividir en dos objetivos adicionales. Por un lado, las búsquedas de PTAs han alcanzado un nivel de precisión y son tan diversas que la sensibilidad experimental requiere calcular las correcciones radiativas a los acoplos efectivos de las PTAs. Por lo tanto, en esta tesis presento la teoría efectiva de las PTAs corregida a nivel de un loop y exploro sus consecuencias fenomenológicas para los experimentos. Por otro lado, me enfoco en las búsquedas de PTAs en experimentos de colisionadores. Por ejemplo, se estudian posibles nuevas búsquedas de PTAs, incluida una propuesta para explorar procesos de dispersión potencialmente mediados por PTAs fuera de su capa de masas, testando sus acoplamientos ED. Además, estudio el impacto de las PTAs en varias anomalías de sabor, con especial énfasis en el sector de los mesones B y sus desintegraciones semileptónicas.

Esta tesis está organizada de la siguiente manera: en los Capítulos 1 al 3 presento el estado del arte del ME, los axiones y las PTAs. Luego, los Capítulos 4 al 6 incluyen la contribución original de la tesis. Las conclusiones se resumen en el Capítulo 7.

Part I

Foundations

Chapter 1

The Standard Model of Particle Physics

Multiple experimental tests of the SM have been carried out, yielding to a remarkable accuracy in predicting a wide variety of phenomena at energy scales below the TeV. The basic structure of the SM can be condensed in a very elegant way in the following Lagrangian

$$\mathscr{L}_{\rm SM} = \mathscr{L}_{\rm gauge} + \mathscr{L}_{\rm Dirac} + \mathscr{L}_{\rm Yukawa} + \mathscr{L}_{\Phi} + \mathscr{L}_{\theta}\,, \tag{1.0.1}$$

with

$$\begin{aligned}
\mathscr{L}_{\rm gauge} &= -\frac{1}{4}G^{\alpha}_{\mu\nu}G^{\mu\nu,\alpha} - \frac{1}{4}W^{i}_{\mu\nu}W^{\mu\nu,i} - \frac{1}{4}B_{\mu\nu}B^{\mu\nu}\,,\\
\mathscr{L}_{\rm Dirac} &= i\overline{Q}_L \not{D} Q_L + i\overline{U}_R \not{D} U_R + i\overline{D}_R \not{D} D_R + i\overline{L}_L \not{D} L_L + i\overline{E}_R \not{D} E_R\,,\\
\mathscr{L}_{\rm Yukawa} &= -\overline{Q}_L \mathbf{Y}_u \widetilde{\Phi} U_R - \overline{Q}_L \mathbf{Y}_d \Phi D_R - \overline{L}_L \mathbf{Y}_e \Phi E_R + \text{h.c.}\,,\\
\mathscr{L}_{\Phi} &= (D_\mu \Phi)^\dagger D^\mu \Phi - \mu^2 \Phi^\dagger \Phi - \lambda \left(\Phi^\dagger \Phi\right)^2\,,\\
\mathscr{L}_{\theta} &= \theta \frac{\alpha_S}{8\pi} G^{\alpha}_{\mu\nu} \widetilde{G}^{\mu\nu,\alpha}\,.
\end{aligned} \tag{1.0.2}$$

In the next sections I will provide an explanation for each of the fields and terms that constitute this Lagrangian, discussing their meaning and properties. Additionally, I will explore the fundamental aspects of the SM and I will present the most stringent experimental measurements of its constituent parameters.

1.1 SM symmetries & particle content

The SM is a Quantum Field Theory (QFT) that has been formulated based on the basic principles of special relativity, locality and causality. Those principles are enforced by imposing Lorentz symmetry [14]. As a consequence, particles are interpreted as excitations of fundamental fields that correspond to distinct representations of the Lorentz symmetry group: (*spin-0*) scalars, (*spin-1/2*) fermions and (*spin-1*) gauge bosons.

Another essential ingredient of the SM is gauge symmetries, which are local symmetries that govern the interactions among the SM fields. The gauge group of the SM plays a

crucial role in the theory, as it determines the properties and behavior of the fundamental particles and in particular of the force mediators. Its symmetry group is

$$G_{\text{SM}} = SU(3)_c \times SU(2)_L \times U(1)_Y \,, \tag{1.1.3}$$

where each separated symmetry group in G_{SM} corresponds to a distinct fundamental interaction. For instance, $SU(3)_c$ corresponds to quantum chromodynamics (QCD), which is the theory that describes the strong interactions among quarks and gluons. On the other hand, $SU(2)_L$ and $U(1)_Y$ depict electroweak (EW) interactions, namely weak isospin and weak hypercharge, respectively. After electroweak symmetry breaking (EWSB), which will be discussed in the next section, a combination of these last two groups results in $U(1)_{\text{em}}$, which describes quantum electrodynamics (QED), the QFT corresponding to electromagnetic interactions among charged particles and photons.

The gauge bosons are the mediators of the interactions in the SM. Each of them is associated to the generators of its corresponding gauge group. In consequence, the SM has in total 12 gauge bosons: 8 gluons, represented as G^α_μ (with $\alpha = 1, \ldots, 8$), and 4 EW gauge bosons: 3 bosons W^i_μ (with $i = 1, 2, 3$) for weak isospin and B_μ for weak hypercharge. In the SM Lagrangian, the kinetic terms that correspond to these gauge fields are represented in Eq. (1.0.2) as

$$\mathscr{L}_{\text{gauge}} = -\frac{1}{4} G^\alpha_{\mu\nu} G^{\mu\nu,\alpha} - \frac{1}{4} W^i_{\mu\nu} W^{\mu\nu,i} - \frac{1}{4} B_{\mu\nu} B^{\mu\nu} \,, \tag{1.1.4}$$

where $G^\alpha_{\mu\nu}$, $W^i_{\mu\nu}$ and $B_{\mu\nu}$ are respectively the field strength tensors of $SU(3)_c$, $SU(2)_L$ and $U(1)_Y$, which can be written as

$$\begin{aligned} G^\alpha_{\mu\nu} &= \partial_\mu G^\alpha_\nu - \partial_\nu G^\alpha_\mu + g_S \, f_{\alpha\beta\gamma} G^\beta_\mu G^\gamma_\nu \,, \\ W^i_{\mu\nu} &= \partial_\mu W^i_\nu - \partial_\nu W^i_\mu + g \, \epsilon_{ijk} W^j_\mu W^k_\nu \,, \\ B_{\mu\nu} &= \partial_\mu B_\nu - \partial_\nu B_\mu \,, \end{aligned} \tag{1.1.5}$$

with $f_{\alpha\beta\gamma}$ and ϵ_{ijk} being respectively the structure constants of the $SU(3)$ and $SU(2)$ non-abelian Lie groups, and g_S and g the strong and weak gauge group coupling constants. In addition we also define a g' coupling constant that is the corresponding to $U(1)_Y$.

The first two terms in Eq. (1.1.5) correspond to the kinetic energy of a massless gauge boson. The last term describes the gauge boson self-interactions, which are only present for non-abelian groups, i.e. $SU(3)_c$ and $SU(2)_L$.

Here it should be noted that experimental evidence shows that among the 12 physics gauge bosons that have been discovered, only 9 of them (8 gluons and 1 photon) are massless. The other 3 EW bosons (the two $W^\pm$ bosons and the Z boson) are indeed massive. A tree-level (Lagrangian level) mass for gauge bosons is however not possible, as it would imply a direct violation of gauge symmetry. In the SM, the mechanism that provides a mass for these bosons, namely the Higgs mechanism, is implemented via spontaneous symmetry breaking [12,13], by means of a complex scalar field. The gist of the mechanism is that, while the Lagrangian is exactly symmetric, the lowest-energy spectrum does not need to exhibit the symmetry: the symmetry is thus exact but "hidden". More details will be discussed in Sec. 1.2.

While the gauge group determines the number of gauge bosons and their properties, the representation of the matter fields under such group is arbitrary, taken from the empirical

	$SU(3)_c$	$SU(2)_L$	$U(1)_Y$
Q_L	**3**	**2**	1/6
U_R	**3**	**1**	2/3
D_R	**3**	**1**	-1/3
L_L	**1**	**2**	-1/2
E_R	**1**	**1**	-1
Φ	**1**	**2**	1/2

Table 1.1: Transformation properties of the SM fermions and Higgs field under the SM gauge group $G_{\rm SM} = SU(3)_c \times SU(2)_L \times U(1)_Y$.

observation of natural processes, with only a single restriction: gauge anomaly cancellation as a consequence of gauge symmetry preservation. Experimental evidence has led to the classification of observed fermions into three distinct "generations" (sometimes also referred as "families" or "flavours"). Particles in different families share the same gauge charges but exhibit different masses and mixings.

Each family of fermions contains a total of five fermion fields, which are usually distinguished according to their gauge charges. On the one hand, there are 3 quark fields, which are charged under both the strong and EW interactions. In addition, these fields can also be classified according to their representation under $SU(2)_L$. For instance, there are two right-handed (RH) $SU(2)_L$ singlet fields, U_R and D_R, and a left-handed (LH) doublet quark field Q_L. On the other hand, leptons are only charge under the EW gauge groups and do not experience the strong force. In the lepton sector there is only one RH $SU(2)_L$ singlet, E_R, and one LH doublet L_L.

It is customary to express these fields as a multiplet representation of the three different flavours, so that the Lagrangian for the three families can be written in a compact way. Making explicit the components we can write them as

$$\begin{aligned} &\bullet \text{ Leptons:} \quad L_L = \begin{pmatrix} \nu_L^e \\ e_L \end{pmatrix}, \begin{pmatrix} \nu_L^\mu \\ \mu_L \end{pmatrix}, \begin{pmatrix} \nu_L^\tau \\ \tau_L \end{pmatrix}, \qquad E_R = \{e_R,\, \mu_R,\, \tau_R\}\ , \\ &\bullet \text{ Quarks:} \quad Q_L = \begin{pmatrix} u_L \\ d_L \end{pmatrix}, \begin{pmatrix} c_L \\ s_L \end{pmatrix}, \begin{pmatrix} t_L \\ b_L \end{pmatrix}, \qquad \begin{aligned} U_R &= \{u_R,\, c_R,\, t_R\}\ , \\ D_R &= \{d_R,\, s_R,\, b_R\}\ . \end{aligned} \end{aligned} \tag{1.1.6}$$

Notice that the SM does not contain a field corresponding to right-handed neutrinos, as at the time of its construction they were not necessary in the absence of evidence for neutrino masses.

The transformation properties of the fermions fields under the SM gauge group $G_{\rm SM}$ is determined by how these particles interact: under $SU(3)_c$ quarks transform as the fundamental representation of the group (triplets) while leptons are in a singlet representation. Regarding the weak interactions, it has been observed that fermion fields of different chiralities, left-handed (LH) or right-handed (RH) chirality, undergo different transformations. For instance, as said before, under $SU(2)_L$ only LH fields transform (as doublets), while RH fields are singlets, showing explicitly the $V-A$ Lorentz structure of $SU(2)_L$. On the other hand, both LH and RH fields transform under $U(1)_Y$, but again different chiral multiplets in Eq. (1.1.6) possess different EW hypercharges. Further details on the SM fermion charges under $G_{\rm SM}$ are shown in Tab. 1.1.

The interaction terms of the SM fermions are located in the $\mathscr{L}_{\text{Dirac}}$ term of the SM Lagrangian in Eq. (1.0.2). The principle of gauge invariance imposes that, for $\mathscr{L}_{\text{SM}}$ to be invariant under a gauge transformation, the usual derivative ∂_μ in the fermion kinetic terms must be replaced by a "covariant derivative" D_μ which depends on the gauge fields. Then, $\mathscr{L}_{\text{Dirac}}$ takes the form

$$\mathscr{L}_{\text{Dirac}} = i\overline{Q}_L \not{D} Q_L + i\overline{U}_R \not{D} U_R + i\overline{D}_R \not{D} D_R + i\overline{L}_L \not{D} L_L + i\overline{E}_R \not{D} E_R \,, \tag{1.1.7}$$

where $\not{D} = D_\mu \gamma^\mu$, and γ^μ are the Dirac gamma matrices. Furthermore, the explicit dependence of D_μ on the gauge fields for each fermion can be written as:

$$\begin{aligned}
D_\mu Q_L &= \left(\partial_\mu + i\,\frac{g_s}{2}\lambda^\alpha G^\alpha_\mu + i\,\frac{g}{2}\sigma^i W^i_\mu + i\,\frac{g'}{6}B_\mu\right) Q_L \,, \\
D_\mu U_R &= \left(\partial_\mu + i\,\frac{g_s}{2}\lambda^\alpha G^\alpha_\mu + i\,\frac{2g'}{3}B_\mu\right) U_R \,, \\
D_\mu D_R &= \left(\partial_\mu + i\,\frac{g_s}{2}\lambda^\alpha G^\alpha_\mu - i\,\frac{g'}{3}B_\mu\right) D_R \,, \\
D_\mu L_L &= \left(\partial_\mu + i\,\frac{g}{2}\sigma^i W^i_\mu - i\,\frac{g'}{2}B_\mu\right) L_L \,, \\
D_\mu E_L &= \left(\partial_\mu - i\,g' B_\mu\right) E_R \,,
\end{aligned} \tag{1.1.8}$$

where λ^α and σ^i denote the Gell-Mann and Pauli matrices, respectively.

Finally, the SM also contains a complex scalar particle, the Higgs field, denoted as Φ. This scalar boson is a singlet under QCD gauge group, but, in contrast, it is charged under the EW gauge group (see Tab 1.1). Higgs interactions with other bosons are encoded in $\mathscr{L}_\Phi$ in Eq. (1.0.2):

$$\mathscr{L}_\Phi = (D_\mu \Phi)^\dagger D^\mu \Phi - V(\Phi) = (D_\mu \Phi)^\dagger D^\mu \Phi - \mu^2 \Phi^\dagger \Phi - \lambda \left(\Phi^\dagger \Phi\right)^2 \,, \tag{1.1.9}$$

where

$$D_\mu \Phi = \left(\partial_\mu + i\,\frac{g}{2}\sigma^i W^i_\mu + i\,\frac{g'}{2}B_\mu\right) \Phi \,, \tag{1.1.10}$$

and μ and λ are two constants that characterize the Higgs field self-interactions in the scalar potential $V(\Phi)$. Notice that, being a complex $SU(2)_L$ doublet, Φ comprises a total of four independent degrees of freedom (dofs).

Within the SM, the "purpose" of the Higgs field is to trigger EWSB. That is, the minimum value of Φ is not zero. The potential $V(\Phi)$ induces a "vacuum expectation value" (vev) for Φ which breaks the EW group $SU(2)_L \times U(1)_Y$ down to $U(1)_{\text{em}}$: the electromagnetic (EM) interactions (See Sec. 1.2).

1.2 Electroweak symmetry breaking

The EW interaction is satisfactorily described in the SM by the $SU(2)_L \times U(1)_Y$ gauge group. In this scenario, fermions are split in chiral multiplets in such a way that LH fields are $SU(2)_L$ doublets while RH fields are singlets. However, this picture is incomplete, as it

would imply that both EW gauge bosons and SM fermions are all massless particles, under the assumption that the SM Lagrangian must be invariant under a gauge transformation. However, experimental evidence shows that the EW gauge bosons (W and Z) and the physical fermions are massive. [1] The piece that is missing is precisely the Higgs field Φ. Within the EW sector, the purpose of the Higgs is to trigger EWSB: the Higgs field induces spontaneous breaking of the EW gauge symmetry down to EM. Therefore, even though the Lagrangian is exactly invariant under a gauge transformation, the spectrum of particles does not constitute a representation of the local EW gauge group, and then masses for gauge bosons and fermions can arise.

In order to understand the general lines of the Higgs mechanism, let us consider the most general renormalizable Lagrangian for the Higgs doublet, which was already defined on Eq. (1.1.9). The latter includes a potential for the Higgs of the form

$$V(\Phi) = \mu^2 \Phi^\dagger \Phi + \lambda \left(\Phi^\dagger \Phi \right)^2 . \tag{1.2.11}$$

If the quadratic term in the previous potential is negative[2], that is $\mu^2 < 0$, then the field configuration of Φ minimizes the potential is not invariant under the EW gauge group. In other words, the vev v of the Higgs field is different from zero and can be defined as

$$\langle \Phi^\dagger \Phi \rangle \equiv \frac{v^2}{2} = -\frac{\mu^2}{\lambda} . \tag{1.2.12}$$

According to the Goldstone theorem [15, 16], whenever a global symmetry is spontaneously broken in a quantum field theory, a spin-0 massless particle must appear in the low-energy spectrum for each broken symmetry generator. These particles are named *Goldstone bosons* (GB). Within EWSB, the Higgs vev spontaneously breaks a total of three generators encoded in the EW gauge group. However, such symmetries are not global, but local (gauge) symmetries. As a consequence, the Goldstone fields (corresponding to three out of the four dofs of Φ) are not realized as independent GB, but are "eaten" by the massless EW gauge bosons (each of them comprising two independent dofs). Therefore, after EWSB, the physical spectrum of particles contains three massive EW gauge bosons (each of them depicted by three dofs): the two W bosons and the Z boson. Thus, at low-energies EW gauge symmetry is still exact, but "hidden".

After EWSB, the remaining dof of the Higgs doublet Φ (out of the original four dofs) can be parametrized around the minimum energy configuration as

$$\Phi = \frac{1}{\sqrt{2}} \begin{matrix} 0 \\ v + h \end{matrix} , \tag{1.2.13}$$

where h is identified as the physical Higgs boson, which was discovered at LHC in 2012 [17, 18]. Thus, the kinetic term in $\mathscr{L}_\Phi$ is rewritten as

$$\left(D_\mu \Phi \right)^\dagger D^\mu \Phi = \frac{1}{2} \partial_\mu h \partial^\mu h + \frac{g^2 (v+h)^2}{4} W_\mu^+ W^{\mu,-} + \frac{(g^2 + g'^2)(v+h)^2}{8} Z_\mu Z^\mu . \tag{1.2.14}$$

[1] Physical neutrinos are a special case, as their masses, evidenced by neutrino oscillations measurements, might not only arise from the Higgs mechanism, but they could also present contributions from additional sources depending on their Dirac or Majorana nature.

[2] Notice that $\lambda > 0$ is always a requirement so that the Higgs potential is bounded by below.

The physical gauge bosons can be expressed in terms of W^i_μ and B_μ as

$$W^\pm_\mu = \frac{W^1_\mu \mp i W^2_\mu}{\sqrt{2}}\,, \tag{1.2.15}$$

$$A_\mu = \cos\theta_w B_\mu + \sin\theta_w W^3_\mu\,, \tag{1.2.16}$$

$$Z_\mu = -\sin\theta_w B_\mu + \cos\theta_w W^3_\mu\,, \tag{1.2.17}$$

where $W^\pm_\mu$ corresponds the physical W bosons, Z_μ is the weak Z boson and A_μ is the photon field, and θ_w is the so-called weak angle, which is a function of g and g', and at tree level it reads

$$\tan\theta_w = \frac{g'}{g}\,. \tag{1.2.18}$$

Its experimental value has been measured with exceptional precision. The most recent world average value can be found in Ref [19]: $s^2_w = 0.22339(10)$.

From Eq. (1.2.14) we can read the masses for Z and W bosons that arise from the Higgs mechanism:

$$M_W = \frac{vg}{2}\,, \qquad M_Z = \frac{v\sqrt{g^2+g'^2}}{2}\,, \tag{1.2.19}$$

whose world average measurements read [19]

$$M_W = 80.377 \pm 0.012 \text{ GeV}\,, \qquad M_Z = 91.1876 \pm 0.0021 \text{ GeV}\,, \tag{1.2.20}$$

while the photon field remains massless. This can be understood as the fact that the Higgs mechanism does not break completely the whole EW gauge group. Instead, the breaking pattern is $SU(2)_L \times U(1)_Y \to U(1)_{\text{em}}$. In other words, EM is the residual gauge symmetry that "survives" EWSB, as an explicit symmetry of the spectrum. As a result, there is no mass term for the photon. Additionally, the electromagnetic coupling constant can be computed in terms of g and g' at tree level as

$$e = g\sin\theta_w = g'\cos\theta_w\,. \tag{1.2.21}$$

1.3 Flavour structure in the fermion sector

As stated in the previous sectors, a priori there are no mass terms for the SM fermions in the Lagrangian due to gauge invariance. However, gauge symmetry allows for interaction terms between fermions and the Higgs doublet, which are encoded in $\mathscr{L}_{\text{Yukawa}}$ in Eq. (1.0.2) and read:

$$\mathscr{L}_{\text{Yukawa}} = -\overline{Q}_L \mathbf{Y}_u \widetilde{\Phi} U_R - \overline{Q}_L \mathbf{Y}_d \Phi D_R - \overline{L}_L \mathbf{Y}_e \Phi E_R + \text{h.c.}\,, \tag{1.3.22}$$

where $\mathbf{Y}_{u,d,e}$ are 3×3 matrices in flavour space and $\widetilde{\Phi} = i\sigma^2\Phi^*$.

From this equation, it can be verified that upon expanding the Higgs doublet around the minimum of its potential, additional mass terms for the fermions emerge in the Lagrangian. The Dirac mass matrices for the physical fermions are computed in terms of the Yukawa matrices and the Higgs vev as

$$\mathbf{M}_f \equiv \frac{\mathbf{Y}_f v}{\sqrt{2}}\,, \tag{1.3.23}$$

In other words, in the same way that the Higgs vev allows for EW gauge bosons to have mass without an explicit breaking of gauge invariance (only an spontaneous breaking), it is also responsible of the masses of the fermions. Moreover, it should be noted that, as a consequence of this mechanism, the interactions between the physical Higgs h and fermions are proportional to the fermions masses.

In all generality, $\mathbf{M}_f$ are non-diagonal complex matrices in flavour space. Nevertheless, they can be transform into a diagonal form via redefinitions of the fermion fields. For instance, a real and diagonal form can be found by implementing the following redefinitions

$$\begin{aligned} U_L &\to \mathbf{V}_u U_L\,, & D_L &\to \mathbf{V}_d D_L\,, & L_L &\to \mathbf{V}_e L_L\,, \\ U_R &\to \mathbf{U}_u U_R\,, & D_R &\to \mathbf{U}_d D_R\,, & E_R &\to \mathbf{U}_e E_R\,, \end{aligned} \tag{1.3.24}$$

in such a way that

$$\begin{aligned} \mathbf{V}_u^\dagger \mathbf{M}_u \mathbf{U}_u &= \mathbf{M}_u^{\text{diag}} = \text{diagonal}(m_u,\, m_c,\, m_t)\,, \\ \mathbf{V}_d^\dagger \mathbf{M}_d \mathbf{U}_d &= \mathbf{M}_d^{\text{diag}} = \text{diagonal}(m_d,\, m_s,\, m_b)\,, \\ \mathbf{V}_e^\dagger \mathbf{M}_e \mathbf{U}_e &= \mathbf{M}_e^{\text{diag}} = \text{diagonal}(m_e,\, m_\mu,\, m_\tau)\,, \end{aligned} \tag{1.3.25}$$

where m_f are the masses of the physical fermions, and the matrices $\mathbf{V}$ and $\mathbf{U}$ are unitary matrices: $\mathbf{V}_f^\dagger \mathbf{V}_f = \mathbb{1}$ and $\mathbf{U}_f^\dagger \mathbf{U}_f = \mathbb{1}$.

After the change of basis in Eq. (1.3.25), fermion mass matrices are now diagonal and represent the masses of the physical fermions of the SM. The most recent world average values of the charged lepton and quark mass measurements are provided by the Particle Data Group collaboration in their 2022 report [19], which provides the following results

$$\begin{aligned} m_u &= 2.16^{+0.49}_{-0.26}\ \text{MeV}\,, & m_d &= 4.67^{+0.48}_{-0.17}\ \text{MeV} & m_e &= 510.99895000(15)\ \text{keV}\,, \\ m_c &= 1.27 \pm 0.02\ \text{GeV}\,, & m_s &= 93.4^{+8.6}_{-3.4}\ \text{MeV}\,, & m_\mu &= 105.6583755(23)\ \text{MeV}\,, \\ m_t &= 172.69 \pm 0.30\ \text{GeV}\,, & m_b &= 4.18^{+0.03}_{-0.02}\ \text{GeV}\,, & m_\tau &= 1776.86 \pm 0.12\ \text{MeV}\,. \end{aligned} \tag{1.3.26}$$

The transformations in Eq. (1.3.24) are not a symmetry of other terms pf the SM Lagrangian. For instance, due to the unitarity of the $\mathbf{U}$ and $\mathbf{V}$ matrices the interaction terms between fermions and photons, gluons and Z bosons, which are coupled to neutral currents of fermions, remain invariant. However, the interaction between LH quarks and W bosons are modified. Thus, the flavour-changing charged current interactions of the SM quark sector read

$$\mathscr{L}_{\text{SM}} \supset -\frac{g}{\sqrt{2}}\ \overline{U}_L \gamma^\mu W_\mu^+ \mathbf{V}_{\text{CKM}} D_L + \text{h.c.} \quad , \tag{1.3.27}$$

where $\mathbf{V}_{\text{CKM}}$ is an unitary matrix given by $\mathbf{V}_{\text{CKM}} = \mathbf{V}_u \mathbf{V}_d^\dagger$, known as the Cabibbo-Kobayashi-Maskawa (CKM) matrix [20, 21] which encodes the resulting flavour-mixing in the quark sector [19]:

$$\mathbf{V}_{\text{CKM}} = \begin{pmatrix} V_{ud} & V_{us} & V_{ub} \\ V_{cd} & V_{cs} & V_{cb} \\ V_{td} & V_{ts} & V_{tb} \end{pmatrix} . \tag{1.3.28}$$

As an unitary 3×3 matrix, $\mathbf{V}_{\text{CKM}}$ comprises four independent dofs, which allow for several distinct parametrizations. A simple choice in terms of three mixing angles (θ_{12}, θ_{23}

and θ_{13}) and a CP-violating complex phase (δ) reads

$$\begin{aligned}\mathbf{V}_{\text{CKM}} &= \begin{pmatrix}1 & 0 & 0\\ 0 & c_{23} & s_{23}\\ 0 & -s_{23} & c_{23}\end{pmatrix}\begin{pmatrix}c_{13} & 0 & s_{13}e^{-i\delta}\\ 0 & 1 & 0\\ -s_{13}e^{i\delta} & 0 & c_{13}\end{pmatrix}\begin{pmatrix}c_{12} & s_{12} & 0\\ -s_{12} & c_{12} & 0\\ 0 & 0 & 1\end{pmatrix}\\ &= \begin{pmatrix}c_{12}c_{13} & s_{12}c_{13} & s_{13}e^{-i\delta}\\ -s_{12}c_{23} - c_{12}s_{23}s_{13}e^{i\delta} & c_{12}c_{23} - s_{12}s_{23}s_{13}e^{i\delta} & s_{23}c_{13}\\ s_{12}s_{23} - c_{12}c_{23}s_{13}e^{i\delta} & -c_{12}s_{23} - s_{12}c_{23}s_{13}e^{i\delta} & c_{23}c_{13}\end{pmatrix},\end{aligned} \tag{1.3.29}$$

where $c_{ij} = \cos\theta_{ij}$ and $s_{ij} = \sin\theta_{ij}$. The angles θ_{ij} can be chosen to lie in the first quadrant, and thus $c_{ij},\ s_{ij} \geq 0$.

As stated before, the quark mass matrices $\mathbf{M}_u$ and $\mathbf{M}_d$, being general 3×3 complex matrices, contain several CP-odd phases. Some of them are just unphysical phases which are be removed away via field redefinitions form Eq. (1.3.25), but others may survive as potential physical CP-odd measurable parameters. Within the EW sector of the SM, the CKM matrix is the only source of flavour mixing and CP-breaking. It is responsible of all flavour transitions that are measured in meson decays and scattering processes, an all CP-violating transitions observed up to now. However, some other phases from $\mathbf{M}_u$ and $\mathbf{M}_d$, which are independent of δ, may reappear within the QCD sector of the SM and mix with the θ-parameter from $\mathscr{L}_\theta$. This would result into another source of CP-violation within the SM. However, when measured, it seems to be absent from the QCD Lagrangian, originating the so-called Strong CP problem that is widely explained within this Thesis in Ch. 2.

The different elements of the CKM matrix have been measured by a variety of experiments. The last global fit obtained by Particle Data Group collaboration in 2022 [19] gives the following result for the absolute value of the CKM matrix elements:

$$|\mathbf{V}_{\text{CKM}}| = \begin{pmatrix}0.97435 \pm 0.00016 & 0.22500 \pm 0.00067 & 0.00369 \pm 0.00011\\ 0.22486 \pm 0.00067 & 0.97349 \pm 0.00016 & 0.04182^{+0.00085}_{-0.00074}\\ 0.00857^{+0.00020}_{-0.00018} & 0.04110^{+0.00083}_{-0.00072} & 0.999118^{+0.000031}_{-0.000036}\end{pmatrix}, \tag{1.3.30}$$

and the complex phase of the CKM matrix is also measured to be: $\delta = 1.144 \pm 0.02$. In addition, its unitarity has also been tested with excellent accuracy.

On the other hand, at this point it should be noticed that the SM predicts no flavour-mixing in the lepton sector. This can be derived from the fermion field redefinitions in Eq. (1.3.24): since Eq. (1.3.22) lacks a mass term for neutrinos, the LH lepton doublet L_L can be rotated as a whole and as a result $\mathscr{L}_{\text{Dirac}}$ remains invariant. In other words, any unitary rotation of the LH charged leptons E_L can be compensated by the same rotation for the LH neutrino fields ν_L in the interaction terms with W bosons. Therefore, flavour-mixing charged current interactions are not induced in the lepton sector within the SM.

Nevertheless, mixing in the leptonic sector has been measured in the last two decades in the phenomenon known as "neutrino oscillations", best explained in terms of neutrinos with different masses. The origin of neutrino masses is still uncertain. One simple option is to enlarge the SM fermion sector with a RH neutrino field, N_R, singlet of the whole SM gauge group, which allows for a Dirac mass for neutrinos, analogously to the other SM fermions. Given they gauge charges of the LH lepton doublet L_L, a more interesting scenario is possible though: neutrinos may be "Majorana" particles. In simple terms, a Majorana particle is a fermion which is its own antiparticle. Majorana fermions present additional mass terms

beyond the standard Dirac masses. For the LH neutrinos, such "Majorana masses" would arise from the effective 5-dimensional operator known as the Weinberg operator [22]

$$\mathscr{L}_{\text{effective}} \supset \frac{\overline{L_L^c}\,\widetilde{\Phi}^* \quad \widetilde{\Phi}^\dagger L_L}{\Lambda}\,, \tag{1.3.31}$$

where Λ is the energy scale of the BSM sector from which the operator would arise and $L_L^c = i\gamma_0\gamma_2 L_L^T$. After Φ takes a non-zero vev, the former describes a Majorana mass term for ν_L. In addition, it also provides an explanation for the smallness of neutrino masses with respect to other SM fermions: neutrino masses are predicted to be proportional to $\sim v^2/\Lambda$, where typically $\Lambda \gg v$ is assumed. Thus, the heavier the exotic sector is with respect to the SM, the lighter neutrinos are expected to be. That is the reason why this mechanism for the generation of neutrino masses is commonly known as the *seesaw* mechanism [23]. In contrast, in the Dirac case light neutrino masses are explained in terms of small Yukawa couplings. The true nature of neutrino masses is a question which is still unresolved and object of strong experimental searches.

Even though the origin of these masses is still uncertain, flavour-mixing has been measured within the neutrino sector in a similar way as it is present for the quark interaction with W bosons. In particular, for leptons the mixing matrix is known as the Pontecorvo-Maki-Nakagawa-Sakata (PMNS) matrix [24,25] $\mathbf{U}_{\text{PMNS}}$. It can be parametrized in a similar way than the CKM matrix in Eq. (1.3.29), by three mixing angles and a CP complex phase. In addition the PMNS matrix could also present two extra CP complex phases depending on whether neutrinos are Dirac or Majorana particles.

A recent global fit for the PMNS parameters by the NuFit collaboration can be found in Ref. [26]. For instance, the following 3σ regions for the absolute value of its matrix elements are measured

$$|\mathbf{U}_{\text{PMNS}}| = \begin{pmatrix} 0.801 \to 0.845 & 0.513 \to 0.579 & 0.143 \to 0.155 \\ 0.234 \to 0.500 & 0.471 \to 0.689 & 0.637 \to 0.776 \\ 0.271 \to 0.525 & 0.477 \to 0.694 & 0.613 \to 0.756 \end{pmatrix}, \tag{1.3.32}$$

and the PMNS CP phase is measured to be $\delta = 195^\circ{}^{+51^\circ}_{-25^\circ}$ and $\delta = 286^\circ{}^{+27^\circ}_{-32^\circ}$ for *normal* neutrino ordering (NO) and *inverted* ordering (IO) respectively. These two situations refer to the different arrangements of neutrinos masses that are allowed experimentally with the current data. The former corresponds to the case in which the mass eigenstates $\{\nu_1, \nu_2, \nu_3\}$ are arranged in ascending order in mass: $(m_1 < m_2 < m_3)$. These eigenstates are defined as those states primarily composed of the flavor eigenstates ν_e, ν_μ and ν_τ respectively. In contrast, inverted ordering describes the case in which ν_3 corresponds to the lightest state $(m_3 < m_1 < m_2)$. On the other hand, the possible Majorana CP-odd phases, if there are any, are far from being within the experimental reach.

Finally, it is noteworthy the substantial differences between the CKM and PMNS matrices. On one hand, the CKM matrix is almost equal to the identity matrix, which means that quark-favour mixing is strongly suppressed within the SM. On the other hand, the PMNS matrix significantly departs from the identity matrix, inducing a large effect in lepton flavour mixing observables such as neutrino oscillations experiments. These huge differences, in addition with the family structure of the SM, for which there is no underlying explanation, is part of the so-called *flavour puzzle* of the SM, which is still an open question.

Chapter 2

The Strong CP problem and axions

In the previous chapter I have discussed the fundamental components of the SM. These includes the gauge symmetry which originates the fundamental interactions, the fermion content and the Higgs mechanism that is responsible for all fundamental particle masses in the SM. Nevertheless, there is a last piece of the SM Lagrangian in Eq. (1.0.2) which I did not address: $\mathscr{L}_\theta$. In this chapter I will show how such term induces a fine-tunning problem in the QCD sector of the SM: the so-called "Strong CP problem". Solutions could lead to the presence of a new fundamental particle within the SM particle spectrum at low-energies, namely the "axion".

2.1 CP violation in QCD

Let us consider the QCD sector Lagrangian below EWSB, $\mathscr{L}_{\rm QCD}$, within the total SM Lagrangian in Eq. (1.0.2)

$$\mathscr{L}_{\rm QCD} = -\frac{1}{4}G^\alpha_{\mu\nu}G^{\mu\nu,\alpha} + \theta\frac{\alpha_S}{8\pi}G^\alpha_{\mu\nu}\widetilde{G}^{\mu\nu,\alpha} + \sum_{Q=U,D} i\overline{Q}\not{D}Q - \overline{Q}_L\mathbf{M}_Q Q_R + \text{h.c.}\,, \tag{2.1.1}$$

where $Q = Q_R + Q_L$ and $\mathbf{M}_u$ and $\mathbf{M}_d$ are the 3×3 complex quark mass matrices defined in Eq. (1.3.23). The second term in Eq. (2.1.1), which corresponds to $\mathscr{L}_\theta$ in Eq. (1.0.2), is the so-called θ-term, since it is parametrized by a dimensionless parameter θ. It can be shown that the interaction term $G^\alpha_{\mu\nu}\widetilde{G}^{\mu\nu,\alpha}$ is odd under a CP transformation. For instance, in the classical limit $G^\alpha_{\mu\nu}\widetilde{G}^{\mu\nu,\alpha}$ can be written in terms of the chromoelectric $\vec{E}$ and chromomagnetic fields $\vec{B}$ as $-4\vec{E}\cdot\vec{B}$, which is odd under P and a T transformations. Moreover, the CPT theorem [27] states that a combined simultaneous transformation of C, P and T must be a fundamental symmetry of nature under the only assumption of Lorentz invariance for any local QFT. Therefore, the quantity $G^\alpha_{\mu\nu}\widetilde{G}^{\mu\nu,\alpha}$ must also be CP-odd. In contrast, the gluon field kinetic term in Eq. (2.1.1) can be written in the classical limit as $\sim (E^2 - B^2)$ which is even under P and CP.

On the other hand, a priori one could think that the θ-term can be disregarded from the QCD Lagrangian since it can be proven to be a total derivative. For instance, let us

define a vector K^μ in terms of the gluon fields as

$$K^\mu \equiv 2\epsilon^{\mu\nu\rho\sigma} A^\alpha_\nu \left[\partial_\rho A^\alpha_\sigma - \frac{2g}{3} f_{\alpha\beta\gamma} A^\beta_\rho A^\gamma_\sigma \right] = \epsilon^{\mu\nu\rho\sigma} A^\alpha_\nu \left[G^\alpha_{\rho\sigma} + \frac{2g}{3} f_{\alpha\beta\gamma} A^\beta_\rho A^\gamma_\sigma \right] , \tag{2.1.2}$$

which satisfies

$$\partial_\mu K^\mu = \partial_\mu \left[\epsilon^{\mu\nu\rho\sigma} A^\alpha_\nu \left[G^\alpha_{\rho\sigma} + \frac{2g_S}{3} f_{\alpha\beta\gamma} A^\beta_\rho A^\gamma_\sigma \right] \right] = G^\alpha_{\mu\nu} \widetilde{G}^{\mu\nu,\alpha} . \tag{2.1.3}$$

The expression above would suggest that the θ-term does not contribute to the equations of motion (EOMs), but only to the action ($S = \int \mathrm{d}^4x \, \mathcal{L}$) as a boundary term. Therefore, it could be set to zero by setting the boundary condition for the gluon fields: $A^a_\mu \sim \mathcal{O}\left(1/r^{1+\epsilon}\right)$, with $\epsilon > 0$, in the limit $r \to \infty$.

However, the last statement is not true. For QCD (and, in general, for interactions described by non-abelian gauge groups) there are some gauge-field configurations that do not decay fast enough at large distances ($r \to \infty$), and they thus add a finite contribution to the action S. These configurations are called *instantons* [28–30]. Instantons are classical finite-action solutions of the EOM of the gluon-fields in *Euclidean space*. Euclidean spacetime is a reparametrization of Minkovski spacetime, where we define the *Euclidean time* as $\tau \equiv it$, so that the metric turns into an Euclidean metric $(+,+,+,+)$ in four dimensions. In this space, the Yang-Mills Lagrangian $\mathscr{L}_{\text{gauge}}$ in Eq. (1.0.2) is written as

$$S_E \supset -\frac{1}{2} \int \mathrm{d}^4x \, \mathrm{Tr}\left[G_{\mu\nu} G^{\mu\nu} \right] , \tag{2.1.4}$$

where S_E is the *Euclidean action* and $G_{\mu\nu} \equiv G^\alpha_{\mu\nu} \lambda^\alpha / 2$. In order for this term to have a finite action, we require that in the limit $r \to \infty$, $G_{\mu\nu} G^{\mu\nu}$ decrease at a higher rate than r^4 (where here $r \equiv (\tau^2 + \vec{x}^2)^{1/2}$):

$$G_{\mu\nu} G^{\mu\nu} \sim \mathcal{O}\left[\frac{1}{r^{4+\epsilon}} \right] , \qquad \Rightarrow \qquad G_{\mu\nu} \sim \mathcal{O}\left[\frac{1}{r^{2+\epsilon}} \right] . \tag{2.1.5}$$

Nevertheless, the previous condition does not directly imply that the gluon-fields $A_\mu \equiv A^\alpha_\mu \lambda^\alpha / 2$ themselves behave as $\mathcal{O}(1/r^{1+\epsilon})$ at large distances. In particular, at $r \to \infty$ the configuration of these fields can be any gauge transformation of the null field state $A_\mu = 0$. These configurations are called *pure gauge* configurations. For any field A_μ, the gauge-transformed field $A^{(\Omega)}_\mu$ is computed as

$$A^{(\Omega)}_\mu = \Omega A_\mu \Omega^{-1} + \frac{i}{g_S} \Omega \partial_\mu \Omega^{-1} , \tag{2.1.6}$$

where Ω is an element of the QCD gauge group: $SU(3)_c$. Thus, a pure gauge configuration of A_μ can be written at large distances as

$$A_\mu = \frac{i}{g_S} \Omega \partial_\mu \Omega^{-1} + \mathcal{O}\left[\frac{1}{r^{1+\epsilon}} \right] . \tag{2.1.7}$$

Notice that at large distances, $\Omega(x)$ is evaluated in the "surface" of a (infinite-radius) 3-sphere (S^3). Thus, $\Omega(x)$ are functions of only the 3 angles that define each point in S^3 in

the four-dimensional Euclidean space. Therefore, pure gauge configurations are determined by a map from S^3 to the elements of the gauge group: $\Omega(x) : S^3 \to SU(3)_c$.

It can be shown [28–30] that for $SU(3)_c$ (and in general for all $SU(N)$ Lie groups) all these maps can be characterized by an integer ν, that is commonly named *winding number* or *Pontryagin index*. In particular, every map is homotopic to one of the so-called *standard maps*:

$$\Omega^{(\nu)}(x) = \left(\frac{\tau + i\vec{\sigma}\cdot\vec{x}}{r}\right)^{\nu}, \tag{2.1.8}$$

where $\vec{\sigma}$ are the Pauli matrices. This statement means that any possible map from S^3 to $SU(3)_c$ can be continuously deformed into one of the maps described by Eq. (2.1.8), for some particular ν. However, maps with different winding numbers are not connected through a continuous deformation. In particular, if the vector field A_μ is a configuration with $\nu \neq 0$, it can never be continuously deformed to reach the configuration $A_\mu = 0$, that actually has winding number $\nu = 0$.

Moreover, given the above expressions for $\Omega^{(\nu)}(x)$ in Eq. (2.1.8), the pure gauge piece of A_μ in Eq. (2.1.7) behaves exactly as $\mathcal{O}(1/r)$ at high distances. Then, the θ-term, $\sim \theta G^\alpha_{\mu\nu}\tilde{G}^{\mu\nu,\alpha}$, does provide a finite contribution to the action. Using Eq. (2.1.3), it follows that

$$\begin{aligned} S_E \supset \int \mathrm{d}^4x\, G^\alpha_{\mu\nu}\tilde{G}^{\mu\nu,\alpha} &= \int \mathrm{d}^4x\, \partial_\mu K^\mu\,, \\ &= \lim_{r\to\infty} \int \mathrm{d}^3\sigma_\mu\, K^\mu\,, \\ &= \lim_{r\to\infty} \int \mathrm{d}^3\sigma_\mu\, \epsilon^{\mu\nu\rho\sigma} A^\alpha_\nu \left(G^\alpha_{\rho\sigma} + \frac{2g_S}{3} f_{\alpha\beta\gamma} A^\beta_\rho A^\gamma_\sigma\right), \end{aligned} \tag{2.1.9}$$

where we have applied the Gauss theorem, with $\mathrm{d}^3\sigma_\mu$ denoting the differential area element in the surface of the (infinite-radius) 3-sphere. As the field-strength tensor $G^\alpha_{\rho\sigma}$ behaves as $\mathcal{O}(1/r^{2+\epsilon})$ at high distances, the first term in the integral vanishes in the limit $r \to \infty$. Therefore, only the second term remains:

$$\begin{aligned} \int \mathrm{d}^4x\, G^a_{\mu\nu}\tilde{G}^{a\mu\nu} &= \frac{2g_S}{3} \lim_{r\to\infty} \int \mathrm{d}^3\sigma_\mu\, \epsilon^{\mu\nu\rho\sigma} A^\alpha_\nu A^\beta_\rho A^\gamma_\sigma f_{\alpha\beta\gamma}\,, \\ &= \frac{4g_S}{3} \lim_{r\to\infty} \int \mathrm{d}^3\sigma_\mu\, \epsilon^{\mu\nu\rho\sigma} \mathrm{Tr}\left[A_\nu A_\rho A_\sigma\right], \\ &= -\frac{4i}{3g_S^2} \lim_{r\to\infty} \int \mathrm{d}^3\sigma_\mu\, \epsilon^{\mu\nu\rho\sigma} \mathrm{Tr}\left[\Omega\partial_\nu\Omega^{-1}\Omega\partial_\rho\Omega^{-1}\Omega\partial_\sigma\Omega^{-1}\right]. \end{aligned} \tag{2.1.10}$$

Finally, given the expression of the maps $\Omega^{(\nu)}$ from Eq. 2.1.8, it follows that

$$\int \mathrm{d}^4x\, G^a_{\mu\nu}\tilde{G}^{a\mu\nu} = \frac{32\pi^2\nu}{g_S^2} = \frac{8\pi\nu}{\alpha_S}, \tag{2.1.11}$$

which is obviously non-zero for $\nu \neq 0$.

Summing up, even though the θ-term of the QCD Lagrangian is a total derivative, it gives a finite non-zero contribution to the action, that is proportional to the winding number. Therefore, it can have a physical impact: it is measurable experimentally. Also, since the θ-term is a source of CP-violation, a priori CP-violating processes are expected to be measured within the realm of strong interactions.

On the other hand, this is not the only source of CP-violation in the QCD Lagrangian in Eq. (2.1.1). As discussed in Sec. 1.3, the quark mass matrices $\mathbf{M}_u$ and $\mathbf{M}_d$ comprise several CP-odd phases, which may potentially source CP-violation within the QCD sector (beyond the complex phase δ of the CKM matrix in the EW sector). In order to illustrate this, let us assume $\mathbf{M}_u$ and $\mathbf{M}_d$ are written as diagonal matrices with complex eigenvalues denoted by $m_\psi e^{i\delta_\psi}$, where m_ψ is the physical mass of the quarks ψ and δ_ψ are generic phases (which are independent of the δ), for $\psi = \{u, d, c, s, t, b\}$. Therefore, the mass term in Eq. (2.1.1) can be rewritten as the sum of individual mass terms for each quark flavour as follows

$$\begin{aligned} -\sum_Q \overline{Q}_L \mathbf{M}_Q Q_R + \text{h.c.} &= -\sum_\psi \overline{\psi}_L m_\psi e^{i\delta_\psi}\psi_R + \overline{\psi}_R m_\psi e^{-i\delta_\psi}\psi_L \quad , \\ &= -\sum_\psi m_\psi \cos\delta_\psi \overline{\psi}\psi + i m_\psi \sin\delta_\psi \overline{\psi}\gamma^5\psi \quad . \end{aligned} \tag{2.1.12}$$

Moreover, if we work under the assumption that the complex phases are small ($\delta_\psi \ll 1$), we can further approximate the previous expression as

$$-\sum_Q \overline{Q}_L \mathbf{M}_Q Q_R + \text{h.c.} \approx -\sum_\psi m_\psi \overline{\psi}\psi + i m_\psi \delta_\psi \overline{\psi}\gamma^5\psi \quad . \tag{2.1.13}$$

The first term in the previous equation is just the ordinary mass term for the quarks, which is CP-even: $\sim \overline{\psi}\psi = \overline{\psi}_L\psi_R + \overline{\psi}_R\psi_L$. The second term ($\sim \overline{\psi}\gamma^5\psi = \overline{\psi}_L\psi_R - \overline{\psi}_R\psi_L$) is instead odd under a CP transformation, though. Thus, a priori it comprises another source of CP-violation within QCD. Moreover, the latter is also proportional to the complex phases δ_ψ. This means that if the mass matrix of the quarks were real, as the usual consideration, the mass term must preserve CP symmetry. Later, it will be shown that an axial $U(1)$ transformation ($U(1)_A$) of the ψ quark fields can be used to rotate away all these CP phases in Eq. (2.1.13) from the mass matrices. However, by doing so the δ_ψ phases are instead reabsorbed into the θ-parameter. Thus, all the QCD sources of CP-violation become concentrated in a new parameter, $\overline{\theta}$, which we will define in the next section.

2.2 The missing meson problem

In this section we will expound the relevance of QCD instantons in hadronic physics, and their relation with the θ-parameter, by explaining their implications in the solution of the so-called "missing meson problem" [31] also referred as "the $U(1)_A$ problem". The latter is related to the understanding of the mass of the η' meson, which, from symmetry arguments, was expected to be as light as pions or kaons. However, when measured, it was turned to be as heavy as the proton.

In order to illustrate this problem let us consider the fermionic Lagrangian for the three lightest quark flavours of the SM: u, d and s:

$$\mathscr{L} = \sum_{q=u,d,s} \bar{q}\ \left(i\not{D} - m_q\right)\ q\,. \tag{2.2.14}$$

Since the confinement scale of QCD, Λ_{QCD}, is of the order of ~ 300 MeV, it is indeed a good approximation to neglect the quark masses in the Lagrangian above in comparison with the physical scale of the theory: $m_q \ll \Lambda_{\text{QCD}}$. Thus, if we further disregard other interactions than QCD (i.e. electroweak interactions), the Lagrangian presents an approximate (classical)

symmetry under the flavour group $U(3)_L \times U(3)_R$, under which the light quarks transform as

$$\begin{pmatrix} u_L \\ d_L \\ s_L \end{pmatrix} \to \mathbf{U}_L \begin{pmatrix} u_L \\ d_L \\ s_L \end{pmatrix} , \qquad \begin{pmatrix} u_R \\ d_R \\ s_R \end{pmatrix} \to \mathbf{U}_R \begin{pmatrix} u_R \\ d_R \\ s_R \end{pmatrix} , \tag{2.2.15}$$

with $\mathbf{U}_L$ and $\mathbf{U}_R$ an element of the symmetry groups $U(3)_L$ and $U(3)_R$ respectively.

The symmetry group $U(3)_L \times U(3)_R$, that transforms separately fermions with different chiralities, can be here reparametrized in terms of vector and axial transformations as $U(3)_L \times U(3)_R = SU(3)_V \times SU(3)_A \times U(1)_V \times U(1)_A$, where vector refers to a transformation of LH and RH quarks with the same angle ($V = R + L$), and axial refers to a transformation with opposite angle ($A = R - L$). The currents associated to these transformations are given by the following expressions

$$j_V^\mu = \overline{q}\gamma^\mu q\,, \qquad j_{V,\,a}^\mu = \overline{q}\gamma^\mu \quad \frac{\lambda^a}{2} \quad q\,, \tag{2.2.16}$$

for the $U(1)_V$ and $SU(3)_V$ vectorial transformations respectively, and

$$j_A^\mu = \overline{q}\gamma^\mu\gamma^5 q\,, \qquad j_{A,\,a}^\mu = \overline{q}\gamma^\mu\gamma^5 \quad \frac{\lambda^a}{2} \quad q\,, \tag{2.2.17}$$

for the $U(1)_A$ and $SU(3)_A$ axial transformations. Notice that here the Gell-Mann matrices λ^a (with $a = 1, \ldots, 8$) are matrices in flavour space defined by the $\{u, d, s\}$ flavours and not in colour space. Also, q here represents the 3-component flavour vector $q = (u, d, s)^T$.

Among the symmetry groups above, the axial transformations $U(1)_A$ and $SU(3)_A$ are explicitly broken in the Lagrangian by the mass term of the quarks, that we have neglected in the previous paragraphs. On the other hand, the $SU(3)_V$ vectorial transformation is only broken by the mass differences between quarks, [1] and finally, $U(1)_V$ is conserved at Lagrangian level even if all quark masses are kept.

Notwithstanding, not all the symmetries depicted above are manifestly realized in nature in the low-energy hadron spectrum. For instance, only the vectorial groups are manifestly realized. Indeed, after QCD confinement, the axial symmetries $U(1)_A \times SU(3)_A$ are spontaneously broken by the non-zero value of the quark condensate $\langle\overline{q}q\rangle \neq 0$. According to the Goldstone theorem [15,16], in the QCD confinement scenario, one would naively expect to find 9 massless GBs in the hadron spectrum: 8 corresponding to the spontaneously broken $SU(3)_A$ symmetry, plus 1 corresponding to $U(1)_A$. Nevertheless, as the spontaneously broken symmetries are not exact but approximate (due to quark masses), these particles are not massless but gain a small mass, and are referred to as *pseudo-Goldstone bosons* (pGB).

However, only 8 light pGBs are found in the QCD hadron spectrum. Those are [19]: three pions, π^0 ($m_{\pi^0} \approx 135$ MeV) and $\pi^\pm$ ($m_{\pi^\pm} \approx 139$ MeV); four kaons, K^0, $\overline{K}^0$ ($m_{K^0} \approx m_{\overline{K}^0} \approx 498$ MeV) and $K^\pm$ ($m_{K^\pm} \approx 494$ MeV); and the η meson ($m_\eta \approx 548$ MeV), which

[1] In the full SM, a flavour $SU(3)_V$ vectorial transformation is not only broken by the quark mass differences, but also by the different EW hypercharges.

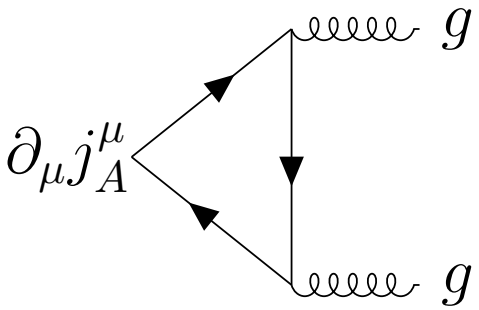

Figure 2.1: One-loop triangle diagram corresponding to the chiral anomaly of the axial current $j^\mu_A = \overline{\psi}\gamma^\mu\gamma^5\psi$ at quantum level, where the fermions ψ run in the loop.

correspond to the $SU(3)_A$ generators. Notice that those pGB mesons containing a s quark in their composition tend to be more massive. The reason is that the strange quark mass (m_s), which is the symmetry breaking parameter for $SU(3)_A$, is larger than m_u and m_d. However, the ninth meson, the η' meson, corresponding to $U(1)_A$ is much heavier than the others, as heavy as a proton, ($m_{\eta'} \approx 958$ MeV) and thus cannot be classified as a pGB. The lack of an explanation for the large value of $m_{\eta'}$ in comparison with the other light mesons is the so-called "missing meson problem" or "$U(1)_A$ problem" [31].

A dynamical explanation to the $U(1)_A$ problem was found by 'tHooft [29, 32, 33], who pointed out that the $U(1)_A$ is explicitly broken due to the Adler-Bell-Jackiw (ABJ) anomaly [34, 35] (sometimes also referred as the "axial" or "chiral" anomaly) due to QCD. Ergo, the natural scale of this symmetry breaking is the QCD scale. It follows that, even in the massless quark scenario, $U(1)_A$ is never a good symmetry of the QCD Lagrangian, and thus the η' meson gets additional contributions to its mass, resulting in a final value as large as the proton mass.

To gain an understanding of the ABJ anomaly's implications with respect to the $U(1)_A$ transformation of the SM quarks, let us first examine a concrete scenario involving the axial rotation of a quark ψ, with mass m_ψ, by an angle β, which transforms the quark field as

$$U(1)_A : \psi \to e^{-i\beta\gamma^5}\psi = \begin{cases} e^{-i\beta}\psi_R\,, \\ e^{+i\beta}\psi_L\,, \end{cases} \tag{2.2.18}$$

and whose associated axial current reads $j^\mu_A = \overline{\psi}\gamma^\mu\gamma^5\psi$. Since $U(1)_A$ is explicitly broken by the mass terms, the divergence of the current is different from zero by a term proportional to m_ψ already at the classical level. Nevertheless, due to the chiral anomaly extra (anomalous) terms appear in the expression for the divergence of j^μ_A, so that the full divergence reads

$$\partial_\mu j^\mu_A = -i2m_\psi\overline{\psi}\gamma^5\psi + \frac{\alpha_S}{4\pi}G^\alpha_{\mu\nu}\widetilde{G}^{\alpha,\mu\nu}\,, \tag{2.2.19}$$

where the second one corresponds to the ABJ anomaly and can be obtained by computing the triangle Feynman diagram in Fig. 2.1 or via the path integral Fujikawa method [36]. Thus, it is clear that even if the case where quark ψ were exactly massless, $U(1)_A$ would be *classically* conserved (that is, no term in the Lagrangian breaks the symmetry), but still explicitly broken *at quantum level* due to the chiral anomaly. In consequence, given the expression in Eq. (2.2.19), if an infinitesimal axial rotation $U(1)_A$ of angle β is performed

the resulting variation in the Lagrangian reads

$$\psi \xrightarrow{U(1)_A} e^{-i\beta\gamma^5}\psi\,, \qquad \rightarrow \qquad \delta\mathscr{L} = \beta\partial_\mu j^\mu_A = -i2m_\psi\beta\overline{\psi}\gamma^5\psi + \beta\frac{\alpha_S}{4\pi}G^\alpha_{\mu\nu}\widetilde{G}^{\alpha,\mu\nu}\,, \tag{2.2.20}$$

where, as we discussed in the previous section, the second term must be kept even though it is indeed a total derivative, as instanton field configurations lead to a non-zero contribution to the action.

Returning to Eqs. (2.1.1) and (2.1.13), if an axial rotation $U(1)_A$ is performed on each of the Standard Model quark fields ψ by angles $\beta = \delta_\psi/2$, then the QCD Lagrangian undergoes a transformation resulting in a new form that reads

$$\mathscr{L}_{\rm QCD} = -\frac{1}{4}G^\alpha_{\mu\nu}G^{\mu\nu,\alpha} + \left(\theta + \sum_\psi \delta_\psi\right)\frac{\alpha_S}{8\pi}G^\alpha_{\mu\nu}\widetilde{G}^{\mu\nu,\alpha} + \sum_\psi \overline{\psi}\;\; i\not{D} - m_\psi \;\; \psi\,. \tag{2.2.21}$$

Here we define the $\overline{\theta}$-parameter as

$$\overline{\theta} \equiv \theta + \arg\det(\mathbf{M}_Q)\,, \tag{2.2.22}$$

where in our case $\arg\det(\mathbf{M}_Q) = \sum_\psi \delta_\psi$.

To summarize, $\overline{\theta}$, the combination of the θ-parameter and the complex phases of the quark mass matrix in Eq. (2.2.22), is the only parameter source of CP-violation within the QCD sector once we consider all possible quark-field redefinitions. Thus, the latter is the only combination that has physical sense and can be measured experimentally. Within the QCD Lagrangian, $\overline{\theta}$ can be written as a global coefficient of the $G\widetilde{G}$ CP-odd term, in the basis with real quark masses, or it can be rotated to the quark mass matrix via axial transformation of the quark fields.

It is now obvious from Eq. (2.2.19) that, if at least one quark were massless, a chiral rotation of its field would be conserved at the classical level, but still broken at the quantum level by the anomaly. Therefore, by performing a chiral rotation of that massless quark field of angle $\beta = -\overline{\theta}/2$, the $\overline{\theta}$ parameter would be rotated away from the Lagrangian and, in consequence, it would not have physical implications at experiments. In other words, that would be a sufficient condition to turn $\overline{\theta}$ unphysical and erase all source of CP-violation within QCD.

2.3 Neutron electric dipole moment

The $\overline{\theta}$-parameter has a substantial impact on numerous observables in the domains of nuclear and hadronic physics. Specifically, a non-zero value of the $\overline{\theta}$-parameter induces contributions to the values of hadron masses and couplings, and may even modify the rate of synthesis of various heavy elements in the early universe [37]. Among different experimental approaches, the most sensitive probe of the $\overline{\theta}$ parameter is the measurement of the neutron electric dipole moment (nEDM). This quantity is strongly suppressed in the Standard Model, making it one of the best avenues for seeking new BSM physics. At the effective QED + QCD Lagrangian level, [2] the EDM interaction between neutrons and the electromagnetic

[2] When the whole gauge group of the SM is considered, the lowest dimensional effective operator that generates an EDM for the fermions arises instead at dimension-6: $i\Psi_L\sigma_{\mu\nu}\Psi_R\Phi F^{\mu\nu}/\Lambda^2 + \text{h.c.}$.

field can be written as

$$\mathscr{L}_{\text{nEDM}} = -\frac{i}{2} d_n \overline{n} \sigma_{\mu\nu} \gamma^5 n F^{\mu\nu} \supset -i d_n \overline{n} \quad \vec{\sigma} \cdot \vec{E} \quad n \,, \tag{2.3.23}$$

where n is the neutron field spinor, d_n denotes the nEDM and $\vec{E}$ is the electric field. The vertex above is a mass-dimension five coupling between the neutron and the photon field, and in consequence, it can not be present in the SM Lagrangian or in any renormalizable Lagrangian. It is induced at loop-level as an effective interaction though.

In contrast with magnetic dipole moments, EDMs change their direction under P and T transformations, and thus under CP. This is obvious from the $\vec{\sigma} \cdot \vec{E}$ dependence shown above. Therefore, in order to produce an effective EDM interaction it is required from the beginning the presence of one or several P and CP-odd couplings in the Lagrangian. As stated in the previous sections, this is exactly the case of the QCD $\overline{\theta}$-term. However, the SM comprises other sources of CP-violation within the EW interactions (see Sec. 1.3). Therefore, it is convenient to ask ourselves what would be the SM prediction for the nEDM, generated by the weak interactions, in the extreme case in which no source of CP-violation is present within QCD; $\overline{\theta} = 0$.

Setting aside the complex phase of the PMNS matrix for neutrino mixing, the other SM source of violation of CP is the complex phase of the CKM matrix defined in Eq. (1.3.29): δ. However, SM CP violating processes require the simultaneous presence of quarks from the three generations and non-vanishing flavour-mixing. Therefore, a non-zero value for the nEDM cannot be generated by one-loop processes. A simple way to illustrate this statement is that in any one-loop diagram originating an EDM for the quarks, for each CKM matrix element $(\mathbf{V}_{\text{CKM}})_{ij}$ in a W-boson vertex there is a second vertex with the conjugate element $(\mathbf{V}_{\text{CKM}})^*_{ij}$. Then, the complex phase δ cancels and the total amplitude must preserve CP. See illustration in Fig. 2.2. This means that the amplitude of this diagram must be proportional to the following factor

$$\mathcal{M}_{\text{one-loop}} \propto (\mathbf{V}_{\text{CKM}})_{uq} (\mathbf{V}_{\text{CKM}})^*_{uq} = |(\mathbf{V}_{\text{CKM}})_{uq}|^2 \,, \tag{2.3.24}$$

where q is the flavour of the internal down-like quark in Fig. 2.2, and thus the amplitude will always correspond to a CP-conserving process (e.g. magnetic moment for chirality flipping transitions). Thus, the one-loop diagram in Fig. 2.2 will never originate an EDM for the quarks. The next step in the perturbative expansion is to look for EDM contributions at two-loop order. An example of these diagrams is shown in Fig. 2.3.

The amplitude of the two-loop diagram in Fig. 2.3 must be proportional to the following product of CKM matrix elements

$$\mathcal{M}_{\text{two-loop}} \propto (\mathbf{V}_{\text{CKM}})_{uq} (\mathbf{V}_{\text{CKM}})^*_{q'q} (\mathbf{V}_{\text{CKM}})_{q'q''} (\mathbf{V}_{\text{CKM}})^*_{uq''} \,, \tag{2.3.25}$$

where q, q' and q'' are the internal quark flavours running in the loop. This combination is a priori complex, so we would expect a non-zero contribution to the quark EDM (and then, to the nEDM) from the sum of these two-diagrams. However, it was shown in Ref. [38] that the imaginary part of the sum of all two-loop contributions vanishes once we sum over all internal quarks flavours. As a consequence, in the SM the leading order contribution to the quark EDM is given at least at three-loop loop order in perturbation theory. An example of a three-loop diagram contributing to the quark EDM is shown in Fig. 2.4.

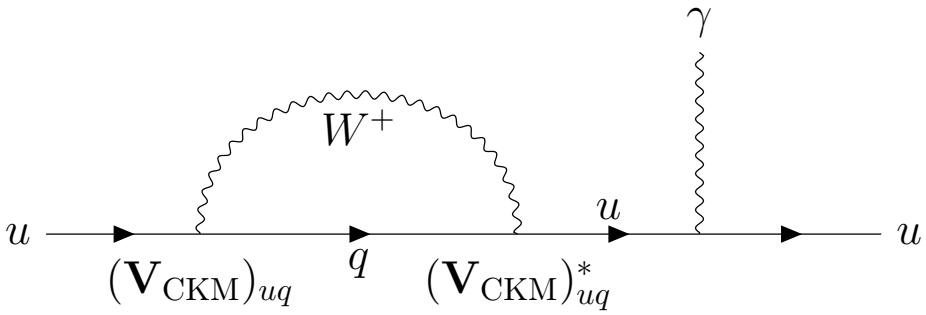

Figure 2.2: Example of hypothetical one-loop diagram for the SM EW contribution to the up-quark EDM. The photon external leg could be attached to any charged-particle leg.

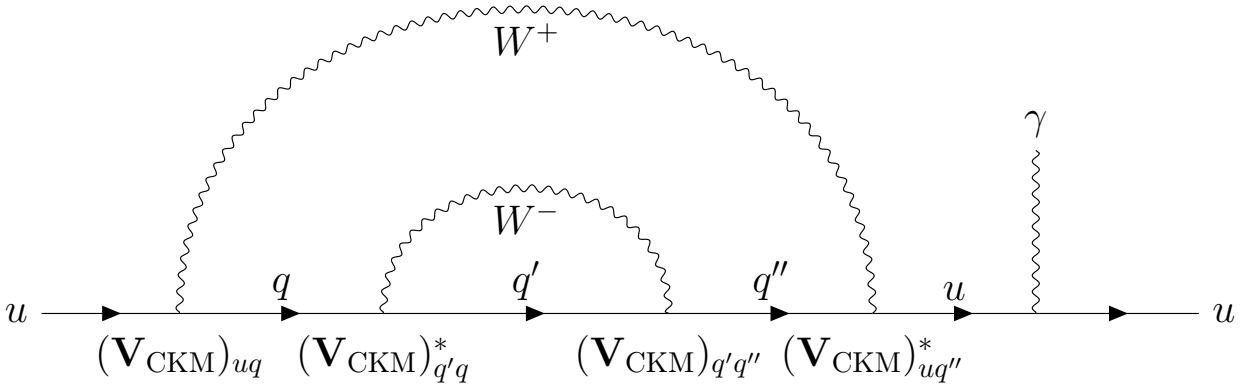

Figure 2.3: Example of hypothetical two-loop diagram for the SM EW contribution to the up-quark EDM. The photon external leg could be attached to any charged-particle leg.

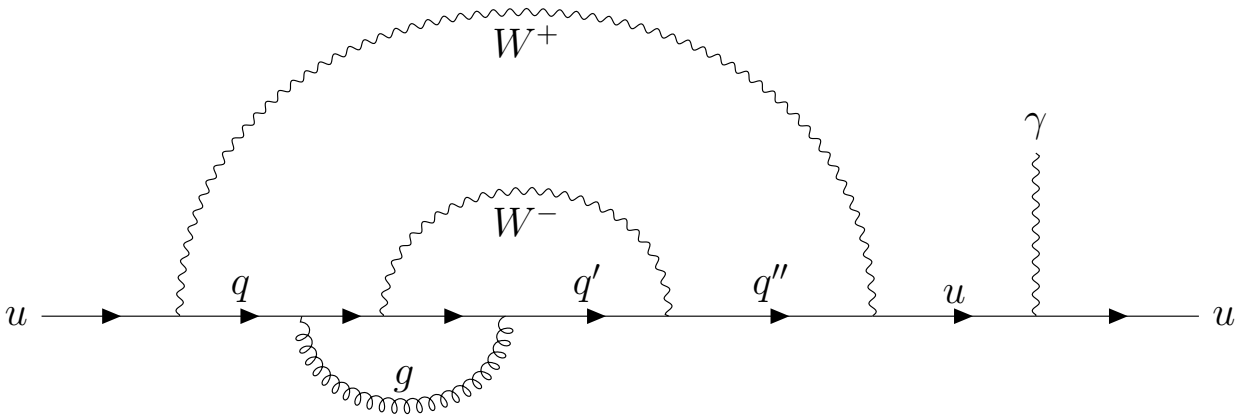

Figure 2.4: Example of a three-loop diagram for the SM EW contribution to the up-quark EDM. The photon external leg could be attached to any charged-particle leg.

Finally, when we consider the neutron as a whole particle beyond its individual valence quarks, other diagrams at the same order in perturbation theory are possible involving simultaneous interactions between valence quarks [39, 40]. An example of these diagrams is drawn in Fig. 2.5. These lead to the leading order contribution from the EW sector of the SM. Overall, considering the experimental value of the complex phase of the CKM matrix, the SM induced nEDM is expected to be of the following order of magnitude [41, 42]

$$d_n^{\mathrm{EW}} \sim 10^{-31} \ \mathrm{e}\cdot\mathrm{cm}\,. \tag{2.3.26}$$

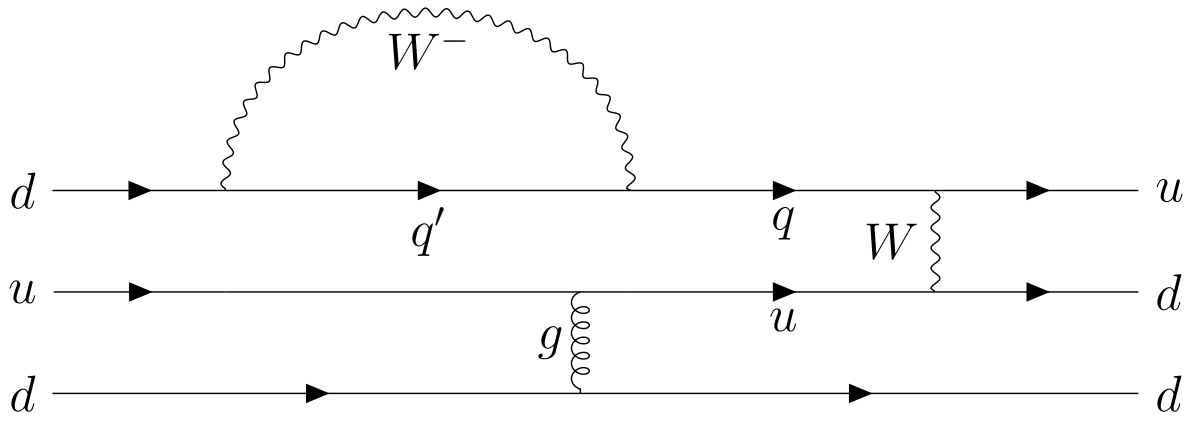

Figure 2.5: Example of a leading order diagram contributing to the nEDM from EW interactions in the SM. The photon external leg could be attached to any charged-particle leg.

Once we have estimated the numerical value of the EW contribution to the nEDM in Eq. (2.3.26), now we must compare this result to the contribution from the $\overline{\theta}$-term. A common approach is to perform a series of $U(1)_A$ rotations in order to trade the θ-term by a CP-violating operator $i\overline{\theta} m_\psi \overline{\psi}\gamma^5\psi \subset \delta\mathscr{L}_{\text{CP}}$ in the mass terms of the quarks. It can be shown that such operators induce an asymmetry in the charge distribution inside the neutron which results in a non-zero nEDM which depends on the value of the $\overline{\theta}$-parameter. Numerous estimations of this contribution can be found [43–49], yielding the following range

$$d_n^{\overline{\theta}} \sim (0.8 - 2) \times 10^{-15}\, \overline{\theta}\ \ \text{e} \cdot \text{cm}\,. \tag{2.3.27}$$

This is the point at which the Strong CP problem arises: when measured at experiments, no nEDM signal has been found. It seems that experimentally the $\overline{\theta}$ contribution is completely absent. According to Particle Data Group (2022) [50], the world average upper bound on the nEDM for the time being reads

$$d_n^{\text{exp}} < 1.8 \times 10^{-26}\ \ \text{e} \cdot \text{cm}\,, \tag{2.3.28}$$

at 90% C.L. Then, given Eq. (2.3.27), the latter translates into the following experimental constraint for the $\overline{\theta}$-parameter

$$\overline{\theta} \lesssim 10^{-11}\,. \tag{2.3.29}$$

Note that $\overline{\theta}$ was defined in Eq. (2.2.22) as the sum of two quantities (the original QCD θ-parameter and the complex phases of the quark mass matrices), which a priori are completely unrelated. Moreover, both quantities are angles, which means they are expected to take arbitrary values between 0 and 2π. These facts make the upper bound in Eq. (2.3.29) completely puzzling: even though $\overline{\theta}$, as an angle, may take any value between 0 and 2π, the experimental value turns out to be extremely suppressed with no underlying theoretical explanation within the SM framework.

This is what is called a *fine-tuning* problem: an experimental value of $\overline{\theta} \lesssim 10^{-11}$ is a priori mathematically possible and consistent with the theory. However, from the theoretical perspective, we would expect $\overline{\theta} \sim \mathcal{O}(1)$. Thus, such bound on $\overline{\theta}$ suggests for an explanation from BSM physics. This is what is called the *Strong CP problem* of QCD.

Future prospects on the nEDM are expected to reach an experimental sensitivity of 10^{-29} e·cm [51]. Also, proton EDM in coming into play with the same expected sensitivity, using storage rings [52]. Therefore, in the next years we would be able to probe experimentally the EW contribution in Eq. (2.3.26) for the nEDM.

2.4 Solutions to the Strong CP problem

Numerous attempts have been made in the literature to extend the SM in order to provide a theoretical basis for the unexpectedly suppressed value of $\overline{\theta}$. Broadly speaking, these efforts can be classified into three distinct solution types, which will be elaborated in next sections.

2.4.1 Massless quark solution

In Sec. 2.2 we explored the consequences of the ABJ anomaly with respect to performing chiral $U(1)_A$ of the SM quark fields. Additionally, we discussed that if one of the quarks of the SM were massless $\overline{\theta}$ would be rendered unphysical. For example, if the up quark, which is the lightest quark in the SM, were massless, an axial $U(1)_A$ rotation of the u field would be a classical symmetry of the QCD Lagrangian, but it would be explicitly broken at quantum level due to the ABJ anomaly. Thus, the divergence of the current associated to this symmetry would read

$$U(1)_A : u \to e^{-i\beta\gamma^5} u\,, \qquad \xrightarrow{m_u=0} \qquad \partial_\mu j^\mu_A = \frac{\alpha_S}{4\pi} G^\alpha_{\mu\nu} \widetilde{G}^{\alpha,\mu\nu}\,. \tag{2.4.30}$$

Therefore, a rotation of this kind with an angle $\beta = -\overline{\theta}/2$ would rotate away $\overline{\theta}$-term from the QCD Lagrangian and the Strong CP problem would be solved. However, the hypothesis that any of the quarks of the SM is massless have been ruled out by many results from lattice QCD simulations and chiral perturbation theory [53–58].

Yet another option is to consider new exotic massless quarks, charged under $SU(3)_c$. However, if those exist, a mechanism must be provided in order to "hide" them experimentally. The idea explored by some works in the literature is to "enlarge" the strong sector of the SM by extra gauge groups, under which the exotic quarks are also charged. Thus, assuming that the new confining scale is much larger than that of QCD, the exotic "hadrons" of the new group would be much heavier than the usual QCD hadrons, and then not accessible experimentally (excluding some possible new pGBs).

2.4.2 Nelson-Barr Mechanism

The Nelson-Barr mechanism [59–61] is a solution to the strong CP problem in which CP is assumed to be an exact symmetry of nature and only spontaneously broken. If CP is a fundamental symmetry, the $\overline{\theta}$-term would be absent from the QCD Lagrangian, as it would break CP explicitly. On the other hand, CP violation in the EW sector have been confirmed with great precision in the complex phase δ of the CKM matrix. This seems a priori incompatible with the assumption that CP is a fundamental symmetry. The solution within these models is simple: new scalar singlets are added, which develop a non-zero complex vevs, breaking spontaneously CP. Furthermore, the exotic sector is arranged in a way that the complex vevs only induces CP-violation within the EW sector, in the CKM matrix, but not in QCD, so $\overline{\theta}$ remains exactly zero at tree-level.

In order to do so, new vector-like quarks are introduced, which interact with the SM quarks through new scalars. Those scalars develop complex vevs, breaking spontaneously CP. However, charges and symmetries are imposed in such a way that, after EWSB, the total mass matrices of the quarks (SM + exotics) reads [62]

$$\widetilde{\mathbf{M}}_Q = \begin{matrix} \mu & B \\ 0 & \mathbf{M}_Q \end{matrix} \quad , \tag{2.4.31}$$

where $\mathbf{M}_Q$ (with $Q = u, d$) the usual 3×3 matrix of the SM quarks, μ is the $n \times n$ mass matrix of the new n exotics quarks and B is a $n \times 3$ interaction matrix between the SM and exotic sector. Notice that the 0 in one of the off-diagonal elements is enforced by the symmetries and/or charges of the models. Also, since CP is assumed, μ and $\mathbf{M}_Q$ are here real matrices, while B is complex since it is generated by the complex vevs of the extra scalar fields.

Notice that the structure of $\widetilde{\mathbf{M}}_Q$ always guarantees that $\arg\det \widetilde{\mathbf{M}}_Q = 0$. Since $\theta = 0$ at the Lagrangian level due to the CP-conservation, then also $\overline{\theta} = 0$ (at tree level) even though B is complex. On the other hand, the CKM phase in the SM is generated by integrating out the heavy exotic quarks.

However, it is important to note a potential limitation of Nelson-Barr-like models, that are based on the absence of a $\overline{\theta}$-term at tree level. $\overline{\theta}$ is not a technically natural parameter in the 'tHooft sense [63]. Since $\overline{\theta}$ is not protected by any symmetry, it may get contributions from the CP-violating CKM phase δ. These contributions may require sophisticated matter content in order to keep the induced value of $\overline{\theta}$ under control. The point is that, even if $\overline{\theta}$ is set to 0 at UV energies, the renormalization group equations may induce a non-zero sizable value at low-energies. For the SM matter content, the estimate of such loop contributions was already computed by Ellis and Gaillard in Ref. [64]. Here they found that the first infinite contribution to $\overline{\theta}$ from the CKM complex phase must arise at 7-loop in the perturbation theory. Therefore, even if $\overline{\theta}$ is set to 0 at the Planck scale, its running is so suppressed that at low-energies we would measure $\overline{\theta} \sim 10^{-16}$, that is negligible in comparison with nEDM upper bounds on $\overline{\theta}$.

2.4.3 Peccei-Quinn Mechanism

The basic ingredient behind the mechanism proposed by Roberto Peccei and Helen Quinn [65, 66] is to require that the Lagrangian has a classical symmetry analogous to the $U(1)_A$ discussed for massless quarks, but with all SM quarks massive. However, such symmetry is not present in the SM Lagrangian at low energies.

The idea is simple: Roberto Peccei and Helen Quinn's proposal is to enlarge the SM matter sector with an additional Higgs doublet, in such a way that Yukawa sector of the SM Lagrangian presents a new $U(1)_{\rm PQ}$ (Peccei-Quinn) global symmetry under which SM fermions transform axially. Thus, $U(1)_{\rm PQ}$ would be classically exact but explicitly broken at quantum level due to the ABJ anomaly, which allows us to rotate away $\overline{\theta}$. Phenomenologically, in order to "hide" the new symmetry at low energies (since it has not been observed experimentally), $U(1)_{\rm PQ}$ undergoes spontaneous symmetry breaking, originating a new light pGB in the low-energy spectrum, namely the *axion*.

Unfortunately, the original PQ model has been ruled out for the time being. However, a plethora of different axion models have been studied in the past decades. The basic axion

is called "canonical" QCD or *invisible* axion [65–73]. In such models the axion energy scale is much larger than the EW scale, suppressing interactions with SM particles and eluding experimental bounds. In addition to the former, recently several axion models have been proposed in which the axion is made heavier [74–90] or lighter [91–94] than the QCD axion. For example, in some of those the axion gets extra contributions to its mass by enlarging the gauge sector of the SM.

As of today, the axion solution remains a viable option, and an extensive experimental program is underway to search for these elusive particles. In the next section we explore the most relevant axion models proposed in the literature, as well as we review its basic properties.

2.5 Axion models

In this section, we provide a review of the paradigmatic axion models. The first axion model, the PQWW model, is discussed in detail. Subsequently, "invisible" axion models are reviewed. For instance, we explore the two most relevant invisible axion models, the KSVZ and DFSZ models, and the Kim-Choi composite axion. Finally, we comment on recent attempts to construct heavy axion models in which the axion mass is higher than that of the invisible axion.

2.5.1 Peccei-Quinn-Weinberg-Wilczek axion

In Sec. 1.2 we reviewed the Higgs mechanism, responsible for the SM quark masses via Yukawa couplings with the Higgs doublet. Later, in Sec. 2.2, it was stated that such couplings break explicitly at the classical level an axial transformation of the quark fields. Thus, $\overline{\theta}$ is a physical parameter that cannot be rotated away from the QCD Lagrangian, originating the Strong CP problem. However, given Eq. (1.3.22) it is worth to attempt to implement a symmetry $U(1)_{\rm PQ}$ on the SM Lagrangian by considering that the Higgs doublet Φ could also be rotated in order to render the quark mass terms invariant.

For instance, let us take the first term in the equation above try to implement an axial $U(1)$ symmetry for the up-like quarks: $U_R \to e^{-i\beta}U_R$ and $Q_L \to e^{+i\beta}Q_L$. The, the Φ Higgs doublet must transform under this $U(1)$ symmetry as $\widetilde{\Phi} \to e^{+i2\beta}\widetilde{\Phi}$: So that, the up-like quarks mass term by itself would be $U(1)$ invariant. However, in the down-like quarks mass term the Higgs doublet Φ necessarily transforms with the opposite phase: $\Phi \to e^{-i2\beta}\Phi$. Therefore, in order to make the latter invariant D_R must transform as: $D_R \to e^{+i3\beta}D_R$. Unfortunately, even though the $U(1)$ symmetry we just defined is a good symmetry of the Lagrangian at classical level, given the charge assignment of the quarks, the QCD chiral anomaly induced by the up-like and down-like quarks cancels. In other words, this $U(1)$ does not present a chiral anomaly for QCD and there is no way to implement a Peccei-Quinn symmetry in the SM Yukawa Lagrangian. [3]

[3] Indeed, any $U(1)$ symmetry of the SM Yukawa Lagrangian at classical level is just a combination of baryon number $U(1)_B$, lepton number $U(1)_L$ and hypercharge $U(1)_Y$ (or the corresponding rotations for the different fermion families). All of them are QCD anomaly-free, so no $U(1)_{\rm PQ}$ is present in the SM.

In 1977, Roberto Peccei and Helen Quinn overcame this situation in their proposal in Refs. [65, 66] by extending the Yukawa sector of the SM by one extra Higgs doublet: Φ_1 and Φ_2. In this picture, it is possible to rotate independently Φ_1 and Φ_2. Thus, we can identify a $U(1)_{\rm PQ}$ transformation, that is a classical symmetry of the Lagrangian, but is broken at quantum level by the ABJ anomaly in the QCD sector. Thus, rendering $\overline{\theta}$ unphysical and solving the Strong CP problem. Later, it was Weinberg and Wilczek [67, 68] who noticed the PQ model included the presence of an "axion", a light pGB a low-energies due to the spontaneous breaking of $U(1)_{\rm PQ}$: the Peccei-Quinn-Weinberg-Wilczek (PQWW) axion.

In the PQ model, the charges of the two Higgs doublet under the SM gauge group are the same as the original Higgs doublet: $\Phi_1(\mathbf{1},\mathbf{2},1/2)$ and $\Phi_2(\mathbf{1},\mathbf{2},1/2)$ under $SU(3)_c \times SU(2)_L \times U(1)_Y$. The Higgs sector of the Lagrangian is now extended as follows

$$\mathscr{L}_{\Phi_1,\Phi_2} = \sum_i \left(D_\mu \Phi_i\right)^\dagger D^\mu \Phi_i - V(\Phi_1,\Phi_2)\,, \tag{2.5.32}$$

where $V(\Phi_1,\Phi_2)$ is the scalar potential, which triggers EWSB by making Φ_1 and Φ_2 take non-zero vevs: v_1 and v_2. The original EW scale v is related to v_1 and v_2 as $v = \sqrt{v_1^2+v_2^2}$. Moreover, the four independent degrees of freedom of each doublet can be parametrized as follows in terms of these vevs as

$$\Phi_1 = \frac{1}{\sqrt{2}} \exp\left(i\eta_1/v_1\right) \begin{pmatrix} \phi_1^+ \\ v_1 + \phi_1^0 \end{pmatrix}, \qquad \Phi_2 = \frac{1}{\sqrt{2}} \exp\left(i\eta_2/v_2\right) \begin{pmatrix} \phi_2^+ \\ v_2 + \phi_2^0 \end{pmatrix}. \tag{2.5.33}$$

Regarding the Yukawa Lagrangian, for the quarks fields it can be written as

$$\mathscr{L}_{\rm Yukawa} \supset -\overline{Q_L}\mathbf{Y}_u \widetilde{\Phi}_2 U_R - \overline{Q_L}\mathbf{Y}_d \Phi_1 D_R + \text{h.c.}\,, \tag{2.5.34}$$

while for the lepton sector there is a choice whether to couple them to Φ_1 or Φ_2. Let us denote the two different possibilities by PQ-I and PQ-II respectively:

$$\text{PQ-I: } \mathscr{L}_{\rm Yukawa} \supset -\overline{L_L}\mathbf{Y}_e \Phi_1 E_R + \text{h.c.}\,, \qquad \text{PQ-II: } \mathscr{L}_{\rm Yukawa} \supset -\overline{L_L}\mathbf{Y}_e \Phi_2 E_R + \text{h.c.}\,. \tag{2.5.35}$$

Given the two Higgs doublets on this model, there are several global $U(1)$ transformations that are symmetries of the Lagrangian. For instance, among these symmetries we find baryon number ($U(1)_B$), lepton number ($U(1)_L$) and a global version of hypercharge ($U(1)_Y$), which are also present in the SM, but also the Peccei-Quinn symmetry $U(1)_{\rm PQ}$ can be identified.

In general, a generic transformation of $U(1)_{\rm PQ}$ by an angle β would correspond to the following field redefinitions

$$U(1)_{\rm PQ} = \begin{cases} U_R \to e^{-i\chi_u\beta} U_R\,, \\ D_R \to e^{-i\chi_d\beta} D_R\,, \\ E_R \to e^{-i\chi_e\beta} E_R\,, \\ Q_L \to e^{-i\chi_Q\beta} Q_L\,, \\ L_L \to e^{-i\chi_L\beta} L_L\,, \\ \Phi_1 \to e^{-i(\chi_Q-\chi_d)\beta} \Phi_1\,, \\ \Phi_2 \to e^{-i(\chi_u-\chi_Q)\beta} \Phi_2\,, \end{cases} \tag{2.5.36}$$

where χ_u, χ_d, χ_e, χ_Q and χ_L are the PQ charges under $U(1)_{\rm PQ}$ of U_R, D_R, E_R, Q_L and L_L, respectively. For the PQ-I model $\chi_e = \chi_L - \chi_Q + \chi_d$, while for PQ-II $\chi_e = \chi_L + \chi_Q - \chi_u$.

Notice here that $U(1)_{\rm PQ}$ is not uniquely defined, since there are four independent parameters $\{\chi_u, \chi_d, \chi_Q, \chi_L\}$ which up to this point are free. A common choice here is to fix the PQ charges of LH fermions to 0: $\chi_Q = \chi_L = 0$. This can be done by combining $U(1)_{\rm PQ}$ with $U(1)_B$ and $U(1)_L$, which are vectorial rotation of the fermions fields. The axion physical couplings to fermions only depend on the axial combination of PQ charges $(\chi_{\psi_R} - \chi_{\psi_L})$, where ψ_R and ψ_L denote the RH and LH chiralities of the fermion ψ respectively. Thus, this choice leaves such couplings unaffected. [4] Thus, after this choice, the PQ symmetry only depend on two free parameters: the PQ charges of RH quarks $\{\chi_u, \chi_d\}$.

Yet another condition on the PQ charges $\{\chi_u, \chi_d\}$ can be inferred by imposing that $U(1)_{\rm PQ}$ is orthogonal to $U(1)_Y$. Let us consider the axial dofs of the two Higgs doublets: η_1 and η_2. Under $U(1)_{\rm PQ}$ and $U(1)_Y$, those fields transform in a shift-symmetric way as

$$U(1)_{\rm PQ} = \begin{cases} \eta_1 \to \eta_1 + \beta v_1 \chi_d \,, \\ \eta_2 \to \eta_2 - \beta v_2 \chi_u \,, \end{cases} \qquad U(1)_Y = \begin{cases} \eta_1 \to \eta_1 - \frac{\beta}{2} v_1 \,, \\ \eta_2 \to \eta_2 - \frac{\beta}{2} v_2 \,. \end{cases} \tag{2.5.37}$$

After EWSB, η_1 and η_2 encode the physical field of the axion plus the would-be GB of $U(1)_Y$ (that is "eaten" by the Z boson in order to become massive), here denoted by G. The explicit expression of a and G in terms of η_1 and η_2 can be found by imposing the following shift-symmetric transformation rules

$$U(1)_{\rm PQ} = \begin{cases} a \to a - \beta f_{\rm PQ} \,, \\ G \to G \,, \end{cases} \qquad U(1)_Y = \begin{cases} a \to a \,, \\ G \to G - \frac{\beta}{2} v \,, \end{cases} \tag{2.5.38}$$

where $f_{\rm PQ}$ is the so-called "Peccei-Quinn energy scale" which is yet to be identified. After comparing Eqs. (2.5.37) and (2.5.38) it follows that

$$a = \frac{v_1 \eta_2 - v_2 \eta_1}{v} \,, \qquad G = \frac{v_1 \eta_1 + v_2 \eta_2}{v} \,, \tag{2.5.39}$$

and

$$\frac{\chi_u}{\chi_d} = \frac{v_1^2}{v_2^2} \,, \qquad U(1)_{\rm PQ} : a \to a - \beta \frac{v_1 v_2}{v} (\chi_u + \chi_d) \,. \tag{2.5.40}$$

Thus, $f_{\rm PQ}$ is identified in terms of v_1, v_2 and the PQ charges as

$$f_{\rm PQ} = \frac{v_1 v_2}{v} (\chi_u + \chi_d) \,. \tag{2.5.41}$$

Notice χ_u and χ_d are now related so that there is only one free parameter in the PQ charge assignment, which corresponds to a global normalization of the PQ charges. A common choice is to fix them to the following values

$$\chi_u = x \,, \qquad \chi_d = \frac{1}{x} \,, \tag{2.5.42}$$

[4] Physical couplings couplings of the PQWW axion to gluons and photons are also unaffected, as the anomalous coefficients of QCD and QED (as vectorial gauge interactions) only depend on the axial combination of PQ charges. On the other hand, the axion anomalous interaction to Z and W bosons may be modified.

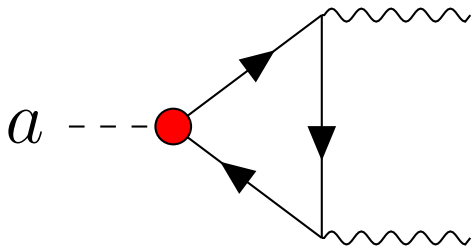

Figure 2.6: One-loop triangle diagram corresponding to the $aX\widetilde{X}$ anomalous interactions fo the axion with gauge bosons. The wavy legs denotes any pair of gauge bosons to which the axion couples to.

with $x = v_1/v_2$. Then, the PQ scale is computed as

$$f_{\rm PQ} = \frac{v_1 v_2}{v} \quad x + \frac{1}{x} \quad = v\,, \tag{2.5.43}$$

which corresponds exactly with the EW scale for such PQ charge assignment. It can be proved that for different PQ charges the same order of magnitude for $f_{\rm PQ}$ is maintained.

The PQWW axion couplings

Physical couplings between the PQWW axion and SM fermions can be easily deduced from Eqs. (2.5.34) and (2.5.35). Under EWSB, the Yukawa interactions of the PQ Lagrangian result in the following terms

$$\begin{aligned} \mathscr{L}_{\rm PQ} \supset & - \sum_{\psi} m_\psi \overline{\psi}_L e^{-ia(\chi_{\psi_R} - \chi_{\psi_L})/f_{\rm PQ}} \psi_R + \text{h.c.}\,, \\ = & - \sum_{\psi} m_\psi \overline{\psi}\psi + \frac{\partial_\mu a}{2f_{\rm PQ}} \sum_{\psi} (\chi_{\psi_R} - \chi_{\psi_L}) \overline{\psi}\gamma^\mu\gamma^5\psi + \mathcal{O}(\alpha)\frac{a}{f_{\rm PQ}} X\widetilde{X}\,, \end{aligned} \tag{2.5.44}$$

where the sum runs over $\psi = \{u, c, t, d, s, c, e, \mu, \tau\}$. The second line in the equation above is obtained by expanding the exponential up to order $\mathcal{O}(1/f_{\rm PQ})$ and then applying the EOMs of the SM fermions fields. [5] Notice that, as was anticipated before, the physical couplings of the axion with the SM fermions only depend on the axial combination of PQ charges. Additionally, such couplings depend on the derivative of a, i.e. are shift-symmetric under $U(1)_{\rm PQ}$.

The last term in Eq. (2.5.44) corresponds to the anomalous couplings of the axion to SM gauge bosons. Those are generated by the axial rotation of the fermions, that is implicitly performed when the fermion EOMs are applied. Alternatively, anomalous couplings can be understood as arising from the triangle diagram in Fig. 2.6, where the way legs in the final

[5] An alternative way to rewrite the axion interaction in their derivative shape is to perform an axion-dependent field redefinition of the SM fermions to the axion fields is removed from the Yukawa piece of the Lagrangian. Thus, the axion interaction terms are obtained from the fermions kinetic terms, yielding to the same relation as in Eq. (2.5.44).

state denote any pair of gauge bosons to which the axion couples to. At low-energy, this diagram induces interactions to and gluons and photons, which are given by the following terms in the Lagrangian

$$\mathscr{L}_{\rm PQ} \supset N\frac{\alpha_S}{8\pi}\frac{a}{f_{\rm PQ}}G^{\alpha}_{\mu\nu}\widetilde{G}^{\alpha,\mu\nu} + E\frac{\alpha_{\rm em}}{8\pi}\frac{a}{f_{\rm PQ}}F_{\mu\nu}\widetilde{F}^{\mu\nu}\,, \tag{2.5.45}$$

where N and E are respectively the QCD and QED anomalous coefficients of the fermions running in the loop. In terms of the PQ charges, those are computed as

$$N = 2\sum_{\psi}(\chi_{\psi_R}-\chi_{\psi_L})T(R_\psi)\,, \qquad E = 2\sum_{\psi}(\chi_{\psi_R}-\chi_{\psi_L})q_\psi^2\,, \tag{2.5.46}$$

where q_ψ is the EM charge of ψ, R_ψ is the representation under QCD gauge group and $T(R_\psi)$ is the Dynkin index of such representation, defined as $\mathrm{Tr}(T^aT^b) = T(R_\psi)\delta^{ab}$, begin T^a the generators of $SU(3)_c$ for the representation R_ψ. In particular, for the choice of PQ charges that we presented in the previous section, we find

$$N = N_f\left(x+\frac{1}{x}\right)\,, \qquad E = N_f\left(x+\frac{1}{x}\right)\times\begin{cases}8/3 \text{ for PQ-I}\,,\\ 2/3 \text{ for PQ-II}\,,\end{cases} \tag{2.5.47}$$

with $N_f = 3$ is the number of fermions families.

At this point it is customary to defined the "axion energy scale", f_a, as the original PQ scale over N

$$f_a \equiv \frac{f_{\rm PQ}}{N}\,, \tag{2.5.48}$$

which is the physical variable measured in any axion $G\widetilde{G}$ test. In addition, it suppresses all the axion couplings to SM particles. Thus, the coupling to $G\widetilde{G}$ is normalized to f_a and do not depends explicitly on the PQ charges:

$$\mathscr{L}_{\rm PQ} \supset \frac{\alpha_S}{8\pi}\frac{a}{f_a}G^{\alpha}_{\mu\nu}\widetilde{G}^{\alpha,\mu\nu} + \frac{E}{N}\frac{\alpha_{\rm em}}{8\pi}\frac{a}{f_a}F_{\mu\nu}\widetilde{F}^{\mu\nu}\,, \tag{2.5.49}$$

while the axion-photon coupling now depends on the quotient E/N. From Eq. (2.5.47), this ratio equals 8/3 for the PQ-I model, and 2/3 for PQ-II.

The QCD axion mass

The exact dependence of the axion mass on the axion scale f_a is one of the most robust predictions of the axion models, and is a direct consequence of the $a\,G\widetilde{G}$ coupling depicted in Eq. (2.5.49): after QCD confinement, the instanton field configurations generate a potential for the axion as a consequence of the non-perturbative QCD dynamics. All axion models possessing this common origin for their masses are collectively referred to as "QCD axions", including the original PQWW axion.

The QCD axion, alike to the η' meson, couples to $G\widetilde{G}$. However, typically it is expected to be much lighter than $m_{\eta'} \sim \Lambda_{\rm QCD}$, which seems contradictory. In other words, should not the axion get a mass of the order of $m_{\eta'} \sim \Lambda_{\rm QCD}$ given that it couples to $G\widetilde{G}$ as well? The answer is precisely that there is only one source of breaking due to the QCD instanton fields, the $G\widetilde{G}$ anomalous term, while there are two different pseudoscalars with anomalous couplings to QCD. As a consequence, below the QCD confinement scale there

is a mixing between both pseudoscalars and one combination will acquire a mass $\sim \Lambda_{\rm QCD}$, while the other would remain much lighter [95–98]. The first eigenstate is the one that is identified experimentally as the physical η' meson. On the other hand, the latter is identified as the physical QCD axion. In order to compute the explicit expressions of the pseudoscalar masses it is pertinent to construct the combined mass matrix in chiral perturbation theory (χPT), which describes the QCD mesons as the dynamical degrees of freedom bellow QCD confinement.

Following Refs. [95–98], let us consider an extension of the chiral theory that includes the QCD pseudoscalar mesons plus the axion as dynamical degrees of freedom. For the moment, let us denote here the original neutral pion, η and η' mesons and the axion as: $\{\pi_3, \eta_8, \eta_0, a_0\}$ and disregard the mixing corrections from heavier pseudoscalars (i.e. η_c). Thus, under QCD confinement, the mass terms induces a mixing among these pseudoscalars which results, after diagonalizing the mass matrix, into the physical mesons and the physical QCD axion, that we denote as: $\{\pi^0, \eta, \eta', a\}$. At leading order in the chiral expansion, the chiral Lagrangian includes the following terms

$$\begin{aligned}\mathscr{L}^{\chi\rm PT} \supset 2v_\chi^3 \Bigg[& m_u \cos\left(\frac{\pi_3}{f_\pi} + \frac{\eta_8}{\sqrt{3}f_\pi} + \frac{\sqrt{2}\eta_0}{\sqrt{3}f_\eta}\right) + m_d \cos\left(\frac{\pi_3}{f_\pi} - \frac{\eta_8}{\sqrt{3}f_\pi} - \frac{\sqrt{2}\eta_0}{\sqrt{3}f_\eta}\right) \\ & + m_s \cos\left(-\frac{2\eta_8}{\sqrt{3}f_\pi} + \frac{\sqrt{2}\eta_0}{\sqrt{3}f_\eta}\right) \Bigg] + K \cos\left(\frac{\sqrt{6}\eta_0}{f_\eta} + \frac{a_0}{f_a}\right) ,\end{aligned} \tag{2.5.50}$$

where v_χ is the QCD quark chiral condensate ($\langle \overline{q}q \rangle = v_\chi^3$), f_π and f_η are respectively the pion and η decay constants and K denotes the QCD anomaly contribution to the η_0 and a_0 fields from the instanton configurations.

By expanding the Lagrangian in Eq (2.5.50) we find the following mass matrix for the set $\{\pi_3, \eta_8, \eta_0, a_0\}$:

$$\mathbf{M^2} = \begin{pmatrix} \frac{2v_\chi^3}{f_\pi^2}(m_u + m_d) & \frac{2v_\chi^3}{\sqrt{3}f_\pi^2}(m_u - m_d) & \frac{4v_\chi^3}{\sqrt{6}f_\pi f_\eta}(m_u - m_d) & 0 \\ \frac{2v_\chi^3}{\sqrt{3}f_\pi^2}(m_u - m_d) & \frac{2v_\chi^3}{3f_\pi^2}(m_u + m_d + 4m_s) & \frac{4v_\chi^3}{3\sqrt{2}f_\pi f_\eta}(m_u + m_d - 2m_s) & 0 \\ \frac{4v_\chi^3}{\sqrt{6}f_\pi f_\eta}(m_u - m_d) & \frac{4v_\chi^3}{3\sqrt{2}f_\pi f_\eta}(m_u + m_d - 2m_s) & \frac{6K}{f_\eta^2} + \frac{4v_\chi^3}{3f_\eta^2}(m_u + m_d + m_s) & \frac{\sqrt{6}K}{f_\eta f_a} \\ 0 & 0 & \frac{\sqrt{6}K}{f_\eta f_a} & \frac{K}{f_a^2} \end{pmatrix} . \tag{2.5.51}$$

After diagonalizing the matrix above, the following expression for the mass of the physical QCD axion a is found:

$$m_a^2 = \frac{1}{f_a^2} \frac{K}{1 + \frac{K}{2v_\chi^3} \mathrm{Tr}\mathbf{M}_Q^{-1}} , \tag{2.5.52}$$

with $\mathbf{M}_Q = \mathrm{diag}(m_u, m_d, m_s)$.

Additionally, if we work under the assumption that f_a is much larger that any other scale ($f_a \gg f_\pi, f_\eta, K, v_\chi$) and disregard the mass of the lightest quarks with respect to $\mathcal{O}(\Lambda_{\rm QCD})$ scales ($m_u, m_d \ll v_\chi, K^{1/4}$), we can find an expression for v_χ^3 and K in terms of the pion mass and energy scale, and the quark masses that reads [95]

$$K \approx \frac{8}{9} v_\chi^3 m_s , \qquad v_\chi^3 \approx \frac{m_\pi^2 f_\pi^2}{2(m_u + m_d)} . \tag{2.5.53}$$

So that, the expression for m_a can be related to m_π and f_π as

$$m_a^2 f_a^2 \approx m_\pi^2 f_\pi^2 \frac{m_u m_d}{(m_u + m_d)^2} \,. \tag{2.5.54}$$

When the expression above is extended to include corrections from the mass of the strange quark, it becomes

$$m_a^2 \approx \frac{m_\pi^2 f_\pi^2}{f_a^2} \frac{4 m_u m_d m_s}{(m_u + m_d)(4 m_u m_s + 4 m_d m_s + 13 m_u m_d)} \,. \tag{2.5.55}$$

The Eq. (2.5.54) is one of the most robust predictions for the QCD axion. In particular, it tells us that for the PQWW axion, whose scale $f_a \approx v = 246$ GeV, m_a is expected to be of order $\mathcal{O}(100)$ keV, which is incompatible with the particle spectrum observed at experiments [69]. Therefore, excluding the first Peccei and Quinn's proposal. On the other hand, if f_a would be of the order of $10^9 - 10^{12}$ GeV, the m_a would be much lighter, $10^{-5} - 10^{-2}$ eV, and its couplings to SM particles would be so suppressed that it would elude experimental bounds. This is the case of the so-called *invisible* axion models, which are discussed in the next section.

After diagonalizing the $\mathbf{M^2}$ mass matrix, we find that the physical QCD axion field corresponds to the state

$$a \approx a_0 + \theta_{a\pi} \pi_3 + \theta_{a\eta} \eta_8 + \theta_{a\eta 0} \eta_0 \,, \tag{2.5.56}$$

where the mixing angles, working under the assumptions depicted above, reads

$$\theta_{a\pi} \approx -\frac{f_\pi}{2 f_a} \frac{m_d - m_u}{m_u + m_d} \,, \qquad \theta_{a\eta} \approx -\frac{f_\pi}{2\sqrt{3} f_a} \,, \qquad \theta_{a\eta'} \approx -\frac{-f_\eta}{\sqrt{6} f_a} \,, \tag{2.5.57}$$

plus some corrections $\mathcal{O}(m_{u,d}/m_s)$.

The QCD axion-photon coupling

The mixing between the QCD axion and pseudoscalar mesons does not only fixes the axion mass but also has a large impact on the axion phenomenology. As an example, this mixing induces an effective interaction between the QCD axion and photons which combines with the original $F\widetilde{F}$ coupling in Eq. (2.5.49). A customary parametrization of the axion-photon interaction is given by the following operator

$$\mathscr{L}_{a\gamma\gamma} = -\frac{1}{4} g_{a\gamma\gamma} a F_{\mu\nu} \widetilde{F}^{\mu\nu} \,, \tag{2.5.58}$$

where $g_{a\gamma\gamma}$ is an effective coupling constant $\mathcal{O}(1/f_a)$. For the QCD axion, such coupling constant is not only given by the anomalous EM coefficient of the $U(1)_{\rm PQ}$ symmetry depicted in Eq. (2.5.47), but it also gets contribution from the other pseudoscalar mesons. For instance, $g_{a\gamma\gamma}$ could be computed as

$$g_{a\gamma\gamma} = g^0_{a\gamma\gamma} + \theta_{a\pi} g_{\pi\gamma\gamma} + \theta_{a\eta} g_{\eta\gamma\gamma} + \theta_{a\eta'} g_{\eta'\gamma\gamma} \,, \tag{2.5.59}$$

where the first term correspond to the original coupling in Eq. (2.5.49), while the other are due to the mixing. Given the expression of the mixing angles in Eq. (2.5.57), the physical $g_{a\gamma\gamma}$ reads

$$g_{a\gamma\gamma} = -\frac{\alpha_{\rm em}}{2\pi f_a} \left(\frac{E}{N} - \frac{2}{3} \frac{m_u + 4 m_d}{m_u + m_d} \right) \,, \tag{2.5.60}$$

at leading order of the chiral expansion, where the first term corresponds to the original axion coupling, while the latter is originated from the mixing. When taking into account the NLO corrections from the χPT, a more accurate expression is found [99]

$$g_{a\gamma\gamma} = -\frac{\alpha_{\rm em}}{2\pi f_a}\left(\frac{E}{N} - 1.92(4)\right) \quad . \tag{2.5.61}$$

Summing up, the physical couplings to photon of the PQWW axion (and, in general, of any QCD axion), as that in Eq. (2.5.61), comprises two different contributions: first, the model-dependent contribution, that is originally present in the Lagrangian, and second, the contribution from the axion-meson mixing. The latter is model independent: it is exactly the same for all QCD models and, as the expression for $m_a^2 f_a^2$ in Eq. (2.5.54), it is a robust prediction that only relies under the assumption that the PQ symmetry is only broken by the QCD instantons.

As a final remark, mixing-induced couplings, such as that in Eq. (2.5.61), are not a particularity of the axion-photon interaction. Other model-independent components of couplings can be computed for the effective axion interaction with leptons, nucleons or EW bosons [100, 101].

2.5.2 Invisible axion models

Since the PQ original model can not be an accurate description of nature as a solution to the Strong CP problem, a natural question is whether the exotic matter sector can allow for much larger effective scales f_a.

We will review next the so-called *invisible axion models*. Those introduce new particles that raise the axion energy scale f_a to values much higher than the EW scale: $f_a \gg v$. The point is that all axion couplings to SM fields are proportional to $1/f_a$, and thus for very large f_a values the experimental constraints on axion couplings can be eluded. Additionally, due to the relation between the mass of the axion m_a and the scale in Eq. (2.5.54), these invisible axions are expected to be much lighter than the original PQWW axion. Typically, for such models an scale $f_a \sim \mathcal{O}(10^9) - \mathcal{O}(10^{12})$ GeV is phenomenologically viable, which implies an axion mass of $m_a \sim \mathcal{O}(10^{-5}) - \mathcal{O}(10^{-2})$ eV.

In this section we present the two most relevant invisible axion models: the DFSZ axion and the KSVZ axion. Both models raise the scale via the addition of an extra scalar singlet under the SM gauge group, but carrying PQ charges, whose vev $\sim f_a \gg v$. Additionally we also discuss the Kim-Choi axion, that is a composite axion model that increases the value of f_a via a new confining gauge group at high energies.

DFSZ axion

The Dine-Fischler-Srednicki-Zhitnitsky (DFSZ) axion model [71, 72], can be understood as an extension of the original PQ solution, enlarging only the matter sector of the SM with extra scalar particles. This model enlarges the SM Higgs sector by introducing a second Higgs doublet Φ_2. On the other hand, it also requires a new complex scalar S that would be a singlet of the SM gauge group $SU(3) \times SU(2) \times U(1)$, and serves to raise the overall axion scale. This field S would be charged under $U(1)_{PQ}$, as well as the SM quarks and the two Higgs doublets.

The Yukawa Lagrangian in this model is identical to the one of the PQ model, depicted in Eq. (2.5.34): the SM fermion masses are generated by the non-zero vevs of the two Higgs doublets Φ_1 and Φ_2. However, the scalar potential, $V(\Phi_1, \Phi_2, S)$, now also depends on the new scalar singlet S. In particular, the following interaction terms is introduced in the Lagrangian

$$V(\Phi_1, \Phi_2, S) \supset \lambda \Phi_1 \widetilde{\Phi}_2 S^2 + \text{h.c.}\,, \tag{2.5.62}$$

where λ is a dimensionless parameter. Given the PQ charge assignment in Eq. (2.5.36), such term imposes that S transforms as

$$U(1)_{\text{PQ}} : S \to e^{-i(\chi_u + \chi_d)/2} S\,, \tag{2.5.63}$$

where we have also imposed $\chi_Q = 0$ as in the previous section. Moreover, the scalar potential forces S to take a non-zero vev which is assumed to be much larger than the EW scale

$$\langle S \rangle = \frac{v_S}{\sqrt{2}} \gg v = \sqrt{v_1^2 + v_2^2}\,. \tag{2.5.64}$$

Then, we can parameterize S as follows

$$S = \frac{1}{\sqrt{2}}(v_S + \rho) e^{i\eta_S / v_S}\,, \tag{2.5.65}$$

where ρ corresponds to the massive radial excitations of S while η_S is the field that characterizes the axial component.

The DFSZ axion, a, appears in this model as a linear combination of the previous PQWW axion from Eq. (2.5.39) and η_S. In order to find the exact expression for the true axion, we impose that a is only shifted under $U(1)_{\text{PQ}}$, while it remains invariant under the orthogonal transformations. Thus, we find the following expression

$$a = \frac{1}{\sqrt{\left(\frac{v_S}{2}\right)^2 + \left(\frac{v_1 v_2}{v}\right)^2}} \left(\frac{v_S}{2}\eta_S - \frac{v_1 v_2^2}{v^2}\eta_1 + \frac{v_1^2 v_2}{v^2}\eta_2 \right) \approx \eta_S\,, \tag{2.5.66}$$

plus some correction terms $\mathcal{O}(v/v_S)$. Also, by imposing that under $U(1)_{\text{PQ}}$ a transforms as Eq. (2.5.38), it follows

$$f_{\text{PQ}} = \sqrt{\left(\frac{v_S}{2}\right)^2 + \left(\frac{v_1 v_2}{v}\right)^2}\,(\chi_u + \chi_d) \approx \frac{v_S}{2}\,(\chi_u + \chi_d) \gg v\,. \tag{2.5.67}$$

Summing up, due to the large hierarchy among the vevs of the scalars ($v_s \gg v_1, v_2$), the energy scale of the PQ sector is of the same order as the vev of the singlet S, $f_{\text{PQ}} \sim v_S$, and the DFSZ axion is mostly given by its axial component: $a \approx \eta_S$.

Finally, since the PQ charges of the SM fermions are exactly the same as in the original PQ model, the DFSZ axion couplings would correspond to those of the original PQWW. The only subtlety is that such couplings are now suppressed by the new large PQ scale. Thus, in the DFSZ model the axion couplings are suppressed by a factor $\sim v/v_S$ with respect to those of the PQWW axion. Since v_S is not determined by any experimental search and is a free parameter of the DFSZ model, those interactions can be arbitrarily suppressed, eluding all experimental bounds on axion searches. In addition, since the PQ symmetry is only broken by the QCD instantons, all the properties derived in previous section (for QCD axions) also apply here. In particular, QCD keeps being the only source of axion mass m_a, and the relation between m_a and f_a in Eq. (2.5.54) holds. Then the mass of the DFSZ axion is expected to be much lighter than that of the PQWW axion, by a factor $\sim v/v_S$.

KSVZ axion

The Kim-Shifman-Vainshtein-Zakharov (KSVZ) axion model [69, 70] is slightly different in comparison with the previous axion models. It still maintains the SM gauge sector, while it enlarges the SM matter content, but by exotic QCD colored fermions in this case. All the SM fermions and Higgs sector here are singlets of $U(1)_{\rm PQ}$, while the PQ symmetry is solely implemented via an exotic vector-like quark Q, charged (at least) under $SU(3)_c$, and a new singlet complex scalar S. The total Lagrangian of the KSVZ model reads

$$\mathscr{L} = \mathscr{L}_{\rm SM} + \mathscr{L}_{\rm KSVZ}\,, \tag{2.5.68}$$

where

$$\mathscr{L}_{\rm KSVZ} = i\overline{Q}\not{D}Q - \; y_Q S\overline{Q}_R Q_L + \text{h.c.} \; + \frac{1}{2}\partial_\mu S^*\partial^\mu S - \mu^2|S|^2 - \lambda|S|^4 - \lambda' \;\; \Phi^\dagger\Phi \;\; |S|^2\,, \tag{2.5.69}$$

where $\not{D}$ is the QCD covariant derivative, y_Q is the Yukawa coupling constant of Q and μ, λ and λ' are the parameters that characterize the scalar potential. This Lagrangian comprises two $U(1)$ symmetries. One of them is just a vectorial rotation of the Q quark, which is exact. On the other hand, the second one is an axial symmetry under which both Q and S must transform. The latter can be identified as the PQ symmetry, under which the fields are rotated as

$$U(1)_{\rm PQ} : Q_R \to e^{-i\beta/2}Q_R\,, \qquad Q_L \to e^{+i\beta/2}Q_L\,, \qquad S \to e^{-i\beta}S\,, \tag{2.5.70}$$

where, without loss of generality, we have chosen the following assignment of PQ charges: $\chi_{Q_R} = -\chi_{Q_L} = 1/2$, while the SM fermions are not charged under $U(1)_{\rm PQ}$. This symmetry is QCD anomalous due to the $SU(3)_c$ charge of Q, so that the Strong CP problem is solved.

At low energies, the scalar potential induces a non-zero vev for the S singlet, which breaks spontaneously the PQ symmetry. It can be directly identified as the energy scale associated to the PQ sector: $f_{\rm PQ}$. Thus, S can be parameterized as follows

$$S = \frac{1}{\sqrt{2}}(f_{\rm PQ} + \rho)e^{ia/f_{\rm PQ}}\,, \tag{2.5.71}$$

where ρ corresponds to the radial excitations of S, while the axial field can be directly identified as the KSVZ axion. Notice that given this expression and the PQ charges in Eq. (2.5.70), the shift transformation of a defined in Eq. (2.5.38) is trivially satisfied. Again, the KSVZ axion is a QCD axion. Thus, the relations for m_a in Eq. (2.5.54) and and the photon coupling in Eq. (2.5.61) also hold.

Additionally, ρ gains a mass of order $f_{\rm PQ}$, that is assumed to be much larger than the EW scale ($f_{\rm PQ} \gg v$). Thus, no low-energy impact is expected from ρ. The mass of Q is generated from the Yukawa interaction with S. After S takes a vev, we find $m_Q = y_Q f_{\rm PQ}/\sqrt{2} \gg v$. Therefore, both particles get decoupled, leaving the KSVZ axion as the only dynamical dof at low energies.

Regarding the a couplings to SM particles, in the KSVZ model a priori there are no tree-level interactions with SM fermions, since those are not charged under $U(1)_{\rm PQ}$. The axion anomalous couplings to gluons and photon are now determined by the PQ charges of Q. From Eq. (2.5.47), it follows

$$N_{\rm KSVZ} = 1\,, \qquad E_{\rm KSVZ} = 6\,q_Q^2\,. \tag{2.5.72}$$

Therefore, we identify the axion scale as $f_a = f_{\rm PQ}$. On the other hand, the model dependent piece of the axion-photon coupling in Eq. (2.5.61) depends on the EM charge of Q: q_Q.

It is worth to highlight that some extensions of the KSVZ model can be easily found by adding more exotic vector-like quarks Q_i, which may transform non-trivially under the EW gauge group of the SM. By doing so, the anomalous $N_{\rm KSVZ}$ and $E_{\rm KSVZ}$ gets contributions from all exotic vector-like quarks. Indeed, this would solve one of the issues of the original KSVZ model: heavy cosmological stable relics [102]. In simple words, it was discussed that the KSVZ Lagrangian encodes two $U(1)$ symmetries: the PQ symmetry and a vectorial transformation of Q, which is analogous to baryon number but for the exotic sector. The latter ensures the cosmological stability of Q, giving rise to fractionally charged baryons after QCD confinement. Such hadrons are strongly constrained [103, 104] experimentally. A viable solution is to provide the exotic quarks with EW charges. Thus, gauge invariance allows for renormalizable mixing terms between the exotic and the SM quarks, breaking the exotic and SM baryon number down to a single $U(1)_B$ under which all quarks (exotic plus SM) are charged. Therefore, fractionally charged baryons are rendered unstable.

Kim-Choi composite axion

The Kim-Choi (KC) axion model [73] constitutes a PQ solution to the Strong CP problem in which the axion is not a fundamental field of the new physics sector, but a composite particle instead. It inherits the basic ideas of the massless quark solution: new exotic massless quarks are introduced, so $\overline{\theta}$ becomes unphysical and can be safely removed away. However, it requires to enlarge the gauge sector of the SM. Indeed, in order to "hide" such exotic quarks at low-energies, a new non-abelian gauge group $SU(N)_a$ is assumed, usually referred as "axicolor" interaction, under which the new quarks are charged. $SU(N)_a$ is assumed to undergo confinement at an energy scale $\Lambda_a \gg \Lambda_{\rm QCD}$. Therefore, new exotic hadrons (*axihadrons*) acquire a large mass $\sim \Lambda_a$ and decouple from low-energy physics. Notwithstanding, the confinement of the axicolor group leads to the spontaneous breaking of global axial flavour symmetries in the exotic quark sector. Thus, light pseudoscalar mesons may appear in the spectrum as pGB of such symmetries, in a similar way as we discuss the case of the pions in Sec. 2.2. That is precisely the case of the Kim-Choi axion, which is now a bound state of the exotic massless quarks.

Even though one single massless quark is necessary in order to remove the $\overline{\theta}$-term from the Lagrangian, in their original proposal Kim and Choi postulated two exotic massless vector-like quarks, namely Q and ψ. The former is charged under both confining groups, QCD and axicolor, while the latter only has axicolor charge. The reason behind this idea is that the new confining axicolor group $SU(N)_a$ may present also an axicolor θ_a-term which also induces CP violation. While an axial rotation of Q rotates away the $\overline{\theta}$-term from the QCD Lagrangian, an independent rotation of ψ is used to also render θ_a unphysical.

Therefore the Lagrangian for the KC model is simply written as

$$\mathscr{L} = \mathscr{L}_{\rm SM} + \mathscr{L}_{\rm KC}\,, \qquad \mathscr{L}_{\rm KC} = i\overline{Q}\not{D}Q + i\overline{\psi}\not{D}\psi\,, \tag{2.5.73}$$

where $\not{D}$ now includes both the QCD and axicolor couplings. The QCD and axicolor charges of Q and ψ can be inferred from Tab. 2.1.

Let us know consider the confining process of the axicolor group. Assuming $SU(N)_a$ undergoes confinement at an arbitrarily high energy scale Λ_a, with $\Lambda_a \gg \Lambda_{\rm QCD}$, it is a good

	$SU(3)_c$	$SU(N)_a$
Q	**3**	**N**
ψ	**1**	**N**

Table 2.1: QCD and axicolor charges of the quark sector of the Kim-Choi axion model. The fields Q and ψ represent massless vector-like fermions. **N** denotes the fundamental representation $SU(N)_a$.

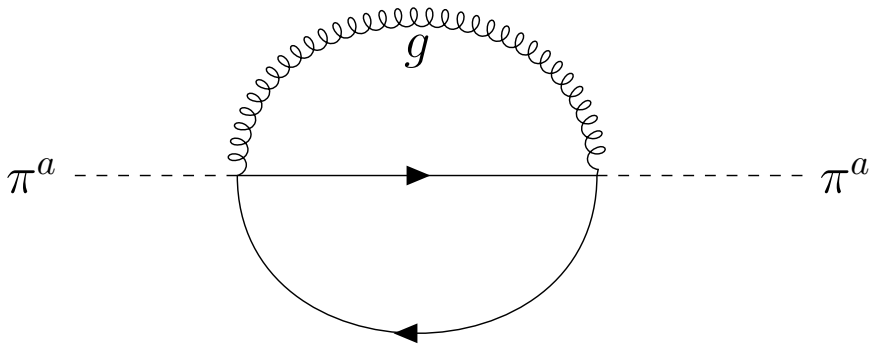

Figure 2.7: Gluon exchange loop diagram that originates the axipion mass from QCD in the Kim-Choi axion model. The internal fermionic lines corresponds to the quark components on the axipion π^a.

approximation to work in the limit of vanishing QCD coupling: $\alpha_S \to 0$. [6] In such limit, the different color charges of Q can be understood as different flavours. Thus, the Lagrangian in Eq. (2.5.73) comprises an approximate $U(4)_L \times U(4)_R = SU(4)_A \times SU(4)_V \times U(1)_A \times U(1)_V$ flavour symmetry, that is broken at low energies by QCD.

Analogously to the discussion in Sec. 2.2, after axicolor confinement the chiral condensate of the exotic quarks, given by

$$\left\langle \overline{Q}Q \right\rangle = \left\langle \overline{\psi}\psi \right\rangle \sim \Lambda_a^3 \,, \tag{2.5.74}$$

breaks spontaneously the axial symmetries: $SU(4)_A \times U(1)_A$, giving rise to potential light degrees of freedoms at low energies in the form of pseudo-Goldstone bosons. Let us call them *axipions* as an analogy of QCD confinement. Since $U(1)_A$ is anomalous under the axicolor group, its corresponding pGB, a singlet under all SM gauge groups, gains a mass of order $\sim \Lambda_a$. This is the equivalent of the η' meson in $SU(N)_a$. On the other hand, $SU(4)_A$ generates $4^2 - 1 = 15$ axipions, which are expected to have masses $\ll \Lambda_a$.

As stated before, $SU(4)_A$ is explicitly broken by QCD, so they become pseudo-GB instead of true GB. Notice that axipions are, all but one, colored particles. Therefore, they can acquire mass from gluon exchange diagrams, that are shown in Fig. 2.7. This is the analogous of the mechanism that originates different masses to the neutral pion π^0 and the charged pions $\pi^\pm$ through a photon exchange: $m^2_{\pi^\pm} - m^2_{\pi^0} \approx (35.6)^2$ MeV^2 [19]. A naive

[6] Due to the QCD β-function, α_S turns to be extremely suppressed at high energies. Thus, it is a good approximation to considering the decoupling of QCD interactions at UV energy scales.

estimation of the mass of the axipions can be found by scaling up the EM contribution to the mass of $\pi^{\pm}$. Then, the colored axipion masses are of order $M_{\pi^a} \sim \alpha_S \Lambda_a^2$. A more intricate computation of these masses leads to following expression [73]

$$M_{\pi^a} \approx \left(\frac{C_2(R_a)\alpha_S}{\alpha_{\rm em}}\right)^{1/2} \frac{F_a}{f_\pi}(35.6 \text{ MeV}) \,, \tag{2.5.75}$$

where $C_2(R_a)$ is the quadratic Casimir operator of the representation R_a under QCD of the axipion π^a, and $F_a = \Lambda_a/4\pi$ is the axipion decay constant, the equivalent to the PQ scale for the previous models. Assuming $F_a \sim 10^{10}$ GeV, the different axipion masses are estimated to be of order $\mathcal{O}(10^9) - \mathcal{O}(10^{10})$ GeV, depending on the different QCD representations. Thus, the axipions are not accessible at collider energies, eluding experimental searches on exotic colored scalars.

Notwithstanding, among the 15 axipions, there is only one corresponding to a singlet representation of QCD, which does not get its mass from the diagram in Fig. 2.7. It corresponds to the color-singlet current

$$j^\mu = \overline{Q}\gamma^\mu\gamma^5 Q - 3\overline{\psi}\gamma^\mu\gamma^5\psi \,, \tag{2.5.76}$$

which is classically conserved, but it anomalous under QCD. Its divergence is given by the expression

$$\partial_\mu j^\mu = N\frac{\alpha_S}{4\pi} G^\alpha_{\mu\nu}\widetilde{G}^{\alpha,\mu\nu} \tag{2.5.77}$$

where N here denotes the degree of the $SU(N)_a$ axicolor group. Instead, this pGB obtains its mass via the color anomaly and the QCD instanton effects. Therefore, it can be identified as a QCD axion: the KC axion.

Given the axion effective interactions induced by the quark current above,

$$\mathscr{L} \supset N\frac{\alpha_S}{4\pi F_a} a\, G^\alpha_{\mu\nu}\widetilde{G}^{\alpha,\mu\nu} \,, \tag{2.5.78}$$

the KC axion is identified as a (composite) invisible axion model, where the axion energy scale is computed as

$$f_a = \frac{F_a}{N} \,. \tag{2.5.79}$$

2.5.3 Heavy axion models

In the sections above, we have discussed the predominant models of axions in the literature: the invisible axion models. These models predict that axion are very light pGBs that couple extremely weakly to SM particles. Indeed, the relation between the axion mass m_a and scale f_a in Eq. (2.5.54) is one of the most robust predictions of the QCD axion, for which QCD instantons are the only source of breaking of the Peccei-Quinn symmetry.

Nevertheless, recently new different kinds of models have been proposed, in which new sources of PQ breaking are being to be considered. The essential ingredient is to extend the strong interacting sector of the SM, so that the axion potential receives supplementary contributions which make larger the right-hand side of Eq. (2.5.54). Thus, the extra contribution turn the axion into a much heavier particle in comparison with invisible axion models. These new models are commonly called *heavy axion models* [74–90].

Typically, such models enlarge the strong interactions sector by adding new confining groups, which confine at a scale $\Lambda'_{\rm QCD} \gg \Lambda_{\rm QCD}$. Therefore, the axion mass gets contributions, for instance, from two confining sources

$$m_a^2 f_a^2 \approx m_\pi^2 f_\pi^2 \frac{m_u m_d}{(m_u + m_d)^2} + \Lambda'^4_{\rm QCD}\,, \tag{2.5.80}$$

as an example.

On the other hand, heavy axion models have to deal with additional problems. For instance, in order to cancel all sources of CP breaking in the enlarged strong interacting sector, they have to impose some condition so that the extra θ'-terms become unphysical as well as $\overline{\theta}$. As an example, some authors have considered imposing extra discrete symmetries, in such a way that both θ-parameters are forced to be equal and can be rotated away simultaneously by the same PQ transformation [75, 77, 82, 83]. Other authors have proposed that QCD is actually contained into a larger group, that is spontaneously broken into $SU(3)_c$. In these models only the original $\overline{\theta}$-parameter is to be removed, but the "constrained" instantons from the broken group present an extra source of PQ-violation, raising the axion mass [84, 85].

Summing up, heavy axion models constitute a proof of concept that the PQ mechanism does not necessarily imply the existence of a light axion at low-energies. As a consequence, a larger region of the parameter-space, that typically was considered to belong to axion-like particles, may also provide a solution a solution to the Strong CP and be populated by true axions.

2.6 Experimental constraints on axions

The search for axions has predominantly focused on the exploration of invisible axion models, which are characterized by the robust relationship between m_a and f_a as described in Eq. (2.5.54), as discussed in the previous sections. Additionally, another robust prediction of such models is that all axion couplings to SM particles, including photons, nucleons, and electrons, are inversely proportional to f_a times some model-dependent coefficients of order unity.

The constraints on invisible axion models are typically derived from a wide range of astrophysical, cosmological, and laboratory-based observations, incorporating axion couplings to several particles. While it is challenging to establish an absolute lower bound for the axion scale f_a (an upper bound on the axion mass m_a) due to the model dependence of some of these searches, an approximate estimate can be extracted from data on the supernova SN1987a [92] of order

$$f_a \gtrsim 10^9 \text{ GeV}\,, \qquad m_a \lesssim 10^{-2} \text{ eV}\,. \tag{2.6.81}$$

In addition, we briefly mentioned in the introductory section of this chapter that axions were subsequently identified as excellent candidates for Dark Matter [100, 105–108]. In the early stages of the universe, axions can be generated through non-thermal processes, contributing significantly to the energy density of the universe. The most popular mechanism responsible for this phenomenon, known as the *misalignment mechanism*, arises from the invisible axion potential induced by QCD instantons. The underlying principle is simple: during the early universe, the axion can be understood as a classical oscillating field around

the minima of its potential. The energy density associated with these oscillations behaves as Cold Dark Matter with respect to the expansion rate of the universe. Therefore, to prevent the axion energy-density from exceeding the DM critical density, an upper bound on the axion scale f_a (a lower bound on the axion mass m_a) is required [100, 105–108]

$$f_a \lesssim 10^{12}\ \text{GeV}\,, \qquad m_a \gtrsim 10^{-6}\ \text{eV}\,. \tag{2.6.82}$$

However, the constraints above present a large variability with the universe history. In other words, those may change whether the PQ phase transition occurs before of after inflation. For instance, if the PQ symmetry undergoes spontaneous breaking right after inflation, DM axions could also be produced as the decay of topological defects, i.e. domain walls and strings, whose exact contribution is still uncertain.

Regarding experimental bounds on specific, model-dependent, axion effective couplings to SM particles, those will be discussed in Sec. 3.2 in association with experimental bounds on axion-like particles (pGBs with some shared properties with axions). See the plots in Figs. 3.1 and 3.2.

Chapter 3

Axion-like particles

In the previous sections we have reviewed in detail the Strong CP problem and the PQ mechanism as one of its most appealing solutions. Such solutions predicts predicts the presence of light pGBs at low-energies: axions. However, the motivation to consider pGBs as potential BSM particles extends beyond their role in addressing the strong CP problem and axion models. In general, pGBs can arise from diverse theoretical frameworks, which can be classified based on the global symmetry from which they originate. Several paradigmatic examples in physics are as follows: i) theories involving extra dimensions exhibit pGBs as a consequence of the behavior of the Wilson line encircling a compact dimension, which mimics a 4-dimensional axion; ii) dynamical explanations for the smallness of neutrino masses incorporate the Majoron, a pGB arising from a hidden $U(1)_L$ lepton symmetry [109] (the Majoron and the axion could even be identified [110, 111]); iii) string theory models, characterized by their rich structure, often possess a plethora of hidden $U(1)$ symmetries and axions [112]; iv) the Higgs boson itself which can have a pGB nature as in Composite-Higgs models [113] ; v) dynamical flavor theories encompass the concept of "axiflavons" as pGBs [114–116], among other relevant studies.

Due to their shared properties with axions as pGBs, these particles are commonly referred to as axion-like particles (ALPs). It is important to note, however, that ALPs feature an extended parameter space and do not address the Strong CP problem, which is the primary objective of the QCD axion. As a consequence, they do not gain its mass from QCD instantons effects, and therefore the relation in Eq. (2.5.54) does not apply. In other words, their mass m_a and the ALP energy scale of the exotic sector from which they are originated, f_a, are independent parameters.

In this Chapter we will explore the basic features of ALPs, as well as their experimental status. In Sec. 3.1 we present the effective field theory (EFT) describing the interactions between axion and ALPs and SM particles, while in Sec. 3.2 we review the experimental bounds on such couplings and other ALP theory parameters.

3.1 ALP linear effective Lagrangian

3.1.1 ALP EFT above EWSB

The formulation of the ALP effective Lagrangian dates back to the late 1980s, where significant contributions were made in the original works in Refs. [95, 96]. More recently, there have been a growing interest [1, 117–119] in such effective theory, associated with an intense effort to investigate in detail the ALP parameter space [2, 117, 120–133].

There is a certain arbitrariness in the definition of what an ALP is. The most common approach is based on the case of the QCD axion: they are defined as pGBs of classical symmetries of the Lagrangian, that are spontaneously realized, but explicitly broken at quantum level by chiral anomalies. Thus, in the ALP EFT, a is assumed to be a pseudoscalar boson, singlet of the SM gauge group, and described by a Lagrangian invariant under the shift symmetry $a \to a + constant$ (remnant of the global symmetry from which is originated), plus anomalous couplings which may break the shift invariance, together with a small mass term $m_a \ll f_a$. [1] At next-to-leading order (NLO) of the linear expansion on the ALP scale, that is up to $\mathcal{O}(1/f_a)$ suppression, this corresponds to operators with mass-dimension up to five. The complete Lagrangian can be written as

$$\mathscr{L} = \mathscr{L}_{\rm SM} + \mathscr{L}_a \,, \tag{3.1.1}$$

where the ALP sector is encoded in

$$\mathscr{L}_a = \frac{1}{2}\partial_\mu a \partial^\mu a - \frac{m_a^2}{2}a^2 + \mathscr{L}_a^{X\widetilde{X}} + \mathscr{L}_a^{\Psi} \,. \tag{3.1.2}$$

The $\mathscr{L}_a^{X\widetilde{X}}$ piece of the ALP Lagrangian comprises ALP anomalous interactions with SM gauge bosons,

$$\mathscr{L}_a^{X\widetilde{X}} = -c_{\widetilde{G}}\frac{a}{f_a}G^\alpha_{\mu\nu}\widetilde{G}^{\mu\nu,\alpha} - c_{\widetilde{W}}\frac{a}{f_a}W^i_{\mu\nu}\widetilde{W}^{\mu\nu,i} - c_{\widetilde{B}}\frac{a}{f_a}B_{\mu\nu}\widetilde{B}^{\mu\nu} \,, \tag{3.1.3}$$

where $c_{\widetilde{G}}$, $c_{\widetilde{W}}$ and $c_{\widetilde{B}}$ are (real) anomalous Wilson coefficients, [2]. On the other hand, $\mathscr{L}_a^{\Psi}$ describes the interaction with SM fermions,

$$\mathscr{L}_a^{\Psi} = \frac{\partial_\mu a}{f_a}\ \overline{Q}_L\gamma^\mu\hat{\mathbf{c}}_Q Q_L + \overline{U}_R\gamma^\mu\hat{\mathbf{c}}_u U_R + \overline{D}_R\gamma^\mu\hat{\mathbf{c}}_d D_R + \overline{L}_L\gamma^\mu\hat{\mathbf{c}}_L L_L + \overline{E}_R\gamma^\mu\hat{\mathbf{c}}_e E_R \quad , \tag{3.1.4}$$

where $\hat{\mathbf{c}}_\Psi$ are 3×3 hermitian matrices in flavour space that contains the Wilson coefficients for the ALP-fermion interactions. Notice that, being a a pseudoscalar, the bosonic Lagrangian $\mathscr{L}_a^{X\widetilde{X}}$ in Eq. (3.1.3) preserves CP, while in the fermion sector in Eq. (3.1.4), the complex

[1] In fact, as discussed in Sec. 2.5.1, in true axion models that mass is a byproduct of the anomalous couplings of ALP to the strong gauge sector of the theory [67, 68, 74–93]). Such couplings source a potential for the axion, and thus a mass. The ALP mass is usually represented by a more general explicit mass term in the Lagrangian. Therefore, breaking the typical relation between m_a and f_a for true axions from Eq. (2.5.54).

[2] The coefficients of gauge anomalous terms are often defined with a suppression factor with respect to the notation used here: $c_{\widetilde{X}} \to \alpha_X/(4\pi)c_{\widetilde{X}}$.

phases of $\hat{\mathbf{c}}_\Psi$ are a source of CP-breaking. Thus, if we further required CP-conservation, the condition $\hat{\mathbf{c}}_\Psi = \hat{\mathbf{c}}_\Psi^T$ would be imposed, so all the ALP couplings become real.

Before moving any further, let us recall for a moment how the Yukawa matrices are given a diagonal shape in the SM from Sec. 1.3. By applying the field redefinitions in Eq. (1.3.24), the SM fermion fields are rotated by unitary matrices in such a way that the mass matrices become diagonal. The other terms from the SM Lagrangian are left invariant, except for the quark interaction with W boson, for which the CKM mixing matrix introduced as the product of the rotation matrix of the LH quark fields: $\mathbf{V}_{\rm CKM} = \mathbf{V}_u \mathbf{V}_d^\dagger$, as explained earlier. Moving back to the ALP EFT, it is worth to highlight that the fermion operators in Eq. (3.1.4) are not invariant under such field rotations by unitary matrices. Indeed, after applying the transformation in Eq. (1.3.24), the $\mathscr{L}_a^\Psi$ can be written as

$$\begin{aligned}\mathscr{L}_a^\Psi = \frac{\partial_\mu a}{f_a} \quad & \overline{U}_L \gamma^\mu \mathbf{c}_U U_L + \overline{D}_L \gamma^\mu \mathbf{c}_D D_L + \overline{U}_R \gamma^\mu \mathbf{c}_u U_R + \overline{D}_R \gamma^\mu \mathbf{c}_d D_R \\ & + \overline{L}_L \gamma^\mu \mathbf{c}_L L_L + \overline{E}_R \gamma^\mu \mathbf{c}_e E_R \quad ,\end{aligned} \tag{3.1.5}$$

where the $\mathbf{c}_\Psi$ are defined as follows

$$\begin{aligned}\mathbf{c}_u = \mathbf{U}_u^\dagger \hat{\mathbf{c}}_u \mathbf{U}_u \,, \qquad & \mathbf{c}_d = \mathbf{U}_d^\dagger \hat{\mathbf{c}}_d \mathbf{U}_d \,, \qquad \mathbf{c}_Q = \mathbf{V}_u^\dagger \hat{\mathbf{c}}_Q \mathbf{V}_u \,, \\ & \mathbf{c}_e = \mathbf{U}_e^\dagger \hat{\mathbf{c}}_e \mathbf{U}_e \,, \qquad \mathbf{c}_L = \mathbf{V}_e^\dagger \hat{\mathbf{c}}_L \mathbf{V}_e \,.\end{aligned} \tag{3.1.6}$$

Notice that, due to these field redefinition, the ALP now couple with different strength to LH up-like and down-like quarks. Actually, both matrices are related via the CKM mixing matrix as [3]

$$\mathbf{c}_U \equiv \mathbf{c}_Q \,, \qquad \mathbf{c}_D \equiv \mathbf{V}_{\rm CKM}^\dagger \mathbf{c}_Q \mathbf{V}_{\rm CKM} \,. \tag{3.1.7}$$

It is noteworthy that, in order to avoid redundancies in the ALP basis presented in Eq. (3.1.2), up to four Wilson coefficient are not independent, as they can be removed by applying the conservation of baryon and lepton number. Classically, with neutrino masses disregarded, lepton number L_k ($k = e, \mu, \tau$) is separately conserved for each fermion generation, while for quarks, due to CKM mixing, only the total baryon number B is. In consequence, $N_f = 3$ couplings become redundant due to lepton number, in contrast to just one for baryon number. Indeed, the ALP coupling to the baryonic and leptonic currents reads

$$\frac{\partial_\mu a}{f_a} J_B^\mu = \frac{\partial_\mu a}{f_a} \quad \frac{\overline{U}\gamma^\mu U + \overline{D}\gamma^\mu D}{3} \quad = -\frac{N_f}{32\pi^2}\frac{a}{f_a} \quad g^2 W_{\mu\nu}^i \widetilde{W}^{\mu\nu,i} - g'^2 B_{\mu\nu}\widetilde{B}^{\mu\nu} \quad , \tag{3.1.8}$$

$$\frac{\partial_\mu a}{f_a} J_{L_k}^\mu = \frac{\partial_\mu a}{f_a} \quad \overline{E}^k \gamma^\mu E^k \quad = -\frac{1}{32\pi^2}\frac{a}{f_a} \quad g^2 W_{\mu\nu}^i \widetilde{W}^{\mu\nu,i} - g'^2 B_{\mu\nu}\widetilde{B}^{\mu\nu} \quad , \tag{3.1.9}$$

where in the last equation there is no sum over the k flavour index, and the right-hand side of these equations stems from the chiral anomalies of baryon and lepton number currents.

[3] Identifying the $\mathbf{c}_Q$ matrix as the physical couplings to LH up-like quarks or down-like quarks is a choice. Some works in the literature [3] has made the opposite identification ($\mathbf{c}_D \equiv \mathbf{c}_Q$), so that the CKM matrix appears instead in the coupling to LH up-like quarks.

Given the four identities in Eqs. (3.1.8)–(3.1.9), it is easy to see that among the set of couplings $\{c_{\widetilde{W}}, c_{\widetilde{B}}, (\mathbf{c}_\Psi)_{ii}\}$ (namely, among the two anomalous ALP couplings to EW bosons and the flavour-diagonal couplings to fermions) we can remove from the ALP EFT Lagrangian: i) four diagonal entries of fermion couplings; or ii) three diagonal entries of the fermions couplings plus one anomalous coupling to EW gauge bosons. Notice that, however, it is not possible to trade simultaneously both $c_{\widetilde{W}}$ and $c_{\widetilde{B}}$ by derivative fermionic operators. The reason is that the four expressions in Eqs. (3.1.8)–(3.1.9) only relates derivative operators to exactly the same combination of anomalous couplings in the right-hand side: $(g^2 W\widetilde{W} - g'^2 B\widetilde{B})$. Thus, once one of the two EW anomalous couplings is removed, then the other is fixed and only fermionic degrees of freedom can be reabsorbed.

3.1.2 Additional ALP operators and operator basis reduction

Purely bosonic basis

In some contexts, it may be pertinent to focus exclusively on the bosonic Lagrangian. The most general and complete *purely bosonic* effective ALP Lagrangian describing ALP couplings at NLO is extraordinarily simple, as it contains just four linearly independent effective operators [95, 96, 117, 134]. Those correspond to the three anomalous couplings to SM gauge bosons from Eq. (3.1.3) in $\mathscr{L}_a^{X\widetilde{X}}$ plus an extra mass-dimension 5 derivative operator that involves the Higgs doublet Φ,

$$\mathscr{L}_a^{\text{boson}} = -c_{\widetilde{G}}\frac{a}{f_a}G^\alpha_{\mu\nu}\widetilde{G}^{\mu\nu,\alpha} - c_{\widetilde{W}}\frac{a}{f_a}W^i_{\mu\nu}\widetilde{W}^{\mu\nu,i} - c_{\widetilde{B}}\frac{a}{f_a}B_{\mu\nu}\widetilde{B}^{\mu\nu} + c_{a\Phi}\frac{\partial_\mu a}{f_a}\;\Phi^\dagger i\overleftrightarrow{D_\mu}\Phi \quad , \tag{3.1.10}$$

where $c_{a\Phi}$ is a real constant and $\Phi^\dagger i\overleftrightarrow{D}_\mu\Phi = i\Phi^\dagger(D_\mu\Phi) - i(D_\mu\Phi^\dagger)\Phi$. The latter is usually disregarded from the whole ALP Lagrangian, as it can be rewritten as a linear combination of fermionic operators. Therefore, it will be redundant to add it to the complete set in Eq. (3.1.2).

The main impact of such operator is to induce a kinetic mixing between a and the would-be GB eaten by the Z boson after EWSB. It is customary to undo this mixing by performing an ALP-dependent Higgs field redefinition of the form $\Phi \to \Phi\, e^{ic_{a\Phi}a/f_a}$ [1,96,117, 135], which is equivalent to the application of the Higgs EOM. This delivers the following expression in terms of fermionic chirality-flipping operators up to order $\mathcal{O}(1/f_a)$

$$c_{a\Phi}\frac{\partial_\mu a}{f_a}\;\Phi^\dagger i\overleftrightarrow{D_\mu}\Phi \;= ic_{a\Phi}\frac{a}{f_a}\;\overline{Q}_L\mathbf{Y}_u\widetilde{\Phi}U_R - \overline{Q}_L\mathbf{Y}_d\Phi D_R - \overline{L}_L\mathbf{Y}_e\Phi E_R \;+\text{h.c.}\,. \tag{3.1.11}$$

In general, the expression above for $c_{a\Phi}\frac{\partial_\mu a}{f_a}\;\Phi^\dagger i\overleftrightarrow{D_\mu}\Phi$ can be rewritten in terms of derivative fermionic operators from Eq. (3.1.4) using the fermionic EOMs. It is important to note that there is not a unique way of performing this rewriting, and different choices can lead to equivalent expressions. The most general expression in terms of derivative, chirality-conserving operators reads

$$\begin{aligned} c_{a\Phi}\frac{\partial_\mu a}{f_a}\;\Phi^\dagger i\overleftrightarrow{D_\mu}\Phi \;= \frac{\partial_\mu a}{f_a}\;&\beta_Q\overline{Q}_L\gamma^\mu Q_L + \beta_u\overline{U}_R\gamma^\mu U_R + \beta_d\overline{D}_R\gamma^\mu D_R \\ &+\beta_L\overline{L}_L\gamma^\mu L_L + \beta_e\overline{E}_R\gamma^\mu E_R \quad , \end{aligned} \tag{3.1.12}$$

where the parameters $\{\beta_Q, \beta_u, \beta_d, \beta_L, \beta_e\}$ must satisfy

$$\beta_u - \beta_Q = -c_{a\Phi}\,, \qquad \beta_d - \beta_Q = c_{a\Phi}\,, \qquad \beta_e - \beta_L = c_{a\Phi}\,, \qquad 3\beta_Q + \beta_L = 0\,. \tag{3.1.13}$$

The first three conditions are imposed so that the derivative operators match the chirality-flipping operators from Eq. (3.1.11). However, the last condition is imposed so that the fermionic current which replaces the ALP-Φ operator is anomaly free, as expected for a bosonic operator. [4] A common option is to replace $\frac{\partial_\mu a}{f_a}\ \Phi^\dagger i\overleftrightarrow{D_\mu}\Phi$ by only RH currents [1,119], so

$$c_{a\Phi}\frac{\partial_\mu a}{f_a}\ \Phi^\dagger i\overleftrightarrow{D_\mu}\Phi\ = c_{a\Phi}\frac{\partial_\mu a}{f_a}\ \overline{D}_R\gamma^\mu D_R + \overline{E}_R\gamma^\mu E_R - \overline{U}_R\gamma^\mu U_R\ \ . \tag{3.1.14}$$

while other options include replacing it by a current proportional to hypercharge [96, 136], which is anomaly free.

It worth mentioning that some works include an additional purely bosonic 5-dimensional effective operator which is CP-odd. It reads: $\partial^2 a\,\Phi^\dagger\Phi$. However, when applying the EOMs of the ALP, it can be traded by $m_a^2 a\,\Phi^\dagger\Phi$, which is suppressed by the mass of the ALP. Thus, it customary to neglect such operator.

Chirality-flipping fermionic operators

Chirality-flip fermion currents are sometimes used to describe the ALP Lagrangian, together with the three anomalous gauge couplings from Eq. (3.1.3). That is, some or all of the chirality-conserving fermionic structures in $\mathscr{L}_a^\Psi$ from Eq. (3.1.4) are traded by chirality-flip ones, i.e

$$\mathscr{L}_a^\Psi \supset i\frac{a}{f_a}\ \overline{Q}_L\widetilde{\mathbf{Y}}_u\tilde{\Phi}U_R + \overline{Q}_L\widetilde{\mathbf{Y}}_d\Phi D_R + \overline{L}_L\widetilde{\mathbf{Y}}_e\Phi E_R\ + \text{h.c.}\,, \tag{3.1.15}$$

where $\widetilde{\mathbf{Y}}_u$, $\widetilde{\mathbf{Y}}_d$ and $\widetilde{\mathbf{Y}}_e$ are, a priori, completely general complex 3×3 matrices in flavour space containing the Wilson coefficient in the chirality-flipping basis. Although this is possible if done with care via fermionic EOMs, it could be misleading. The point is that, in all generality, the operators in Eq. (3.1.15) do not belong to the ALP Lagrangian in the sense that they are not invariant per se under the required shift symmetry $a \to a+constant$ (which in the ALP paradigm is assumed to be broken only by gauge anomalous currents).

Only in some particular cases the chirality-flip couplings are tradable for generic derivative (chirality-preserving) fermionic operators (plus redefinitions of the $\{c_{\widetilde{G}}, c_{\widetilde{W}}, c_{\widetilde{B}}\}$ anomalous coefficients). It should be noted here that the number of degrees of freedom of a hermitian coefficient matrix (as for chirality-preserving operators) differs in general from that of a general complex matrix (as for chirality-flip ones). In the general case, any complete and non-redundant basis made out of purely shift-invariant fermionic operators spans $5N_f^2-(N_f+1) = 41$ degrees of freedom [5], which differs from the $6N_f^2 = 54$ independent

[4] It is noteworthy that the last condition is a priori not strictly necessary in order to match the $a-\Phi$ operator into the ALP basis. However, if it is not imposed this operator cannot be completely replaced by only derivative fermionic operators, but also anomalous ALP couplings to gauge bosons are needed. The reason is that, if the chosen fermionic current is anomalous, the latter would generate anomalous couplings at one-loop level by a triangle diagram. Therefore, extra anomalous operators at tree-level are needed in order to cancel such contribution, so that the $a-\Phi$ operator remains anomaly-free as expected for a bosonic operator.

[5] This counting corresponds to the degrees of freedom of the five hermitian matrices $\mathbf{c}_\Psi$, minus those $1+N_f$ redundant degrees of freedom that are removed via baryon and lepton number rotations.

parameters of the chirality-flip set in Eq. (3.1.15). The precise combinations of chirality-flip structures which are equivalent to shift-invariant ALP couplings (plus anomalous gauge couplings) are identified in the next section. See also Ref. [118].

Basis reduction via equations of motion

One method for determining the relationship among redundant operators within a given set is to apply the EOMs of the involved fields and analyzing their transformations. In this case, we aim to establish the explicit relation between the operators in the ALP basis (chirality-conserving and anomalous operators), as defined in Eqs.(3.1.3)–(3.1.4), and the chirality-flipping operators introduced in the previous section, as defined in Eq.(3.1.15).

In the SM, the EOMs for the chiral fermions read

$$i\not{D}Q_L = \Phi \mathbf{Y}_d D_R + \widetilde{\Phi}\mathbf{Y}_u U_R\,, \qquad i\not{D}U_R = \widetilde{\Phi}^\dagger \mathbf{Y}_u^\dagger Q_L\,, \qquad i\not{D}D_R = \Phi^\dagger \mathbf{Y}_d^\dagger Q_L\,, \tag{3.1.16}$$

$$i\not{D}L_L = \Phi \mathbf{Y}_e E_R\,, \qquad i\not{D}E_R = \Phi^\dagger \mathbf{Y}_e^\dagger L_L\,, \tag{3.1.17}$$

where flavor index contractions are implicit. For the conjugate fields they imply

$$-i\overline{Q}_L \overleftarrow{\not{D}} = \overline{D}_R \mathbf{Y}_d^\dagger \Phi^\dagger + \overline{U}_R \mathbf{Y}_u^\dagger \tilde{\Phi}^\dagger\,, \quad -i\overline{U}_R \overleftarrow{\not{D}} = \overline{Q}_L \mathbf{Y}_u \tilde{\Phi}\,, \quad -i\overline{D}_R \overleftarrow{\not{D}} = \overline{Q}_L \mathbf{Y}_d \Phi\,, \tag{3.1.18}$$

$$-i\overline{L}_L \overleftarrow{\not{D}} = \overline{E}_R \mathbf{Y}_e^\dagger \Phi^\dagger\,, \qquad -i\overline{E}_R \overleftarrow{\not{D}} = \overline{L}_L \mathbf{Y}_e \Phi\,. \tag{3.1.19}$$

The use of fermion EOM is tantamount to chiral rotations of fermion fields, at the classical level. When considering loop effects, they must be supplemented by the contributions of the SM anomalous global currents, i.e.

$$\partial_\mu \ \overline{Q}_L^k \gamma^\mu Q_L^k \ \supset \frac{g'^2}{96\pi^2} B_{\mu\nu}\widetilde{B}^{\mu\nu} + \frac{3g^2}{32\pi^2} W^i_{\mu\nu}\widetilde{W}^{\mu\nu,i} + \frac{g_s^2}{16\pi^2} G^\alpha_{\mu\nu}\widetilde{G}^{\mu\nu,\alpha}\,, \tag{3.1.20}$$

$$\partial_\mu \ \overline{U}_R^k \gamma^\mu U_R^k \ \supset -\frac{g'^2}{12\pi^2} B_{\mu\nu}\widetilde{B}^{\mu\nu} - \frac{g_s^2}{32\pi^2} G^\alpha_{\mu\nu}\widetilde{G}^{\mu\nu,\alpha}\,, \tag{3.1.21}$$

$$\partial_\mu \ \overline{D}_R^k \gamma^\mu D_R^k \ \supset -\frac{g'^2}{48\pi^2} B_{\mu\nu}\widetilde{B}^{\mu\nu} - \frac{g_s^2}{32\pi^2} G^\alpha_{\mu\nu}\widetilde{G}^{\mu\nu,\alpha}\,, \tag{3.1.22}$$

$$\partial_\mu \ \overline{L}_L^k \gamma^\mu L_L^k \ \supset \frac{g'^2}{32\pi^2} B_{\mu\nu}\widetilde{B}^{\mu\nu} + \frac{g^2}{32\pi^2} W^\alpha_{\mu\nu}\tilde{W}^{\alpha\mu\nu}\,, \tag{3.1.23}$$

$$\partial_\mu \ \overline{E}_R^k \gamma^\mu E_R^k \ \supset -\frac{g'^2}{16\pi^2} B_{\mu\nu}\widetilde{B}^{\mu\nu}\,, \tag{3.1.24}$$

where we are not summing over the index k.

Finally, applying Eqs. (3.1.16)–(3.1.24), we can express the chirality-preserving operators in terms of chirality-flipping operators and anomalous operators. This rewriting can be expressed as follows

$$\begin{aligned} \frac{\partial_\mu a}{f_a} \ \overline{Q}_L \gamma^\mu \mathbf{c}_Q Q_L \ &= \ i\frac{a}{f_a} \ \overline{Q}_L \mathbf{c}_Q \mathbf{Y}_u \widetilde{\Phi} U_R + \overline{Q}_L \mathbf{c}_Q \mathbf{Y}_d \Phi D_R \ + \text{h.c.} \\ &\quad - \frac{1}{32\pi^2}\frac{a}{f_a} \ \frac{g'^2}{3} B_{\mu\nu}\widetilde{B}^{\mu\nu} + 3g^2 W^i_{\mu\nu}\widetilde{W}^{\mu\nu,i} + 2g_S^2 G^\alpha_{\mu\nu}\widetilde{G}^{\mu\nu,\alpha} \ \ \text{Tr}(\mathbf{c}_Q)\,, \end{aligned} \tag{3.1.25}$$

$$\frac{\partial_\mu a}{f_a}\ \overline{U}_R\gamma^\mu \mathbf{c}_u U_R \ = \ -i\frac{a}{f_a}\overline{Q}_L \mathbf{Y}_u \mathbf{c}_u \widetilde{\Phi} U_R + \text{h.c.} \\ + \frac{1}{32\pi^2}\frac{a}{f_a}\ \frac{8g'^2}{3}B_{\mu\nu}\widetilde{B}^{\mu\nu} + g_S^2 G^\alpha_{\mu\nu}\widetilde{G}^{\mu\nu,\alpha}\ \ \text{Tr}(\mathbf{c}_u)\,, \tag{3.1.26}$$

$$\frac{\partial_\mu a}{f_a}\ \overline{D}_R\gamma^\mu \mathbf{c}_d D_R \ = \ -i\frac{a}{f_a}\overline{Q}_L \mathbf{Y}_d \mathbf{c}_d \Phi D_R + \text{h.c.} \\ + \frac{1}{32\pi^2}\frac{a}{f_a}\ \frac{2g'^2}{3}B_{\mu\nu}\widetilde{B}^{\mu\nu} + g_S^2 G^\alpha_{\mu\nu}\widetilde{G}^{\mu\nu,\alpha}\ \ \text{Tr}(\mathbf{c}_d)\,, \tag{3.1.27}$$

$$\frac{\partial_\mu a}{f_a}\ \overline{L}_L\gamma^\mu \mathbf{c}_L L_L \ = \ i\frac{a}{f_a}\overline{L}_L \mathbf{c}_L \mathbf{Y}_e \Phi E_R + \text{h.c.} \\ - \frac{1}{32\pi^2}\frac{a}{f_a}\ g'^2 B_{\mu\nu}\widetilde{B}^{\mu\nu} + g^2 W^i_{\mu\nu}\widetilde{W}^{\mu\nu,i}\ \ \text{Tr}(\mathbf{c}_L)\,, \tag{3.1.28}$$

$$\frac{\partial_\mu a}{f_a}\ \overline{E}_R\gamma^\mu \mathbf{c}_e E_R \ = \ -i\frac{a}{f_a}\overline{L}_L \mathbf{Y}_e \mathbf{c}_e \Phi E_R + \text{h.c.} \ + \frac{g'^2}{16\pi^2}\frac{a}{f_a}B_{\mu\nu}\widetilde{B}^{\mu\nu}\text{Tr}(\mathbf{c}_e)\,. \tag{3.1.29}$$

Therefore, by combining the previous expressions, we can establish that the chirality-flipping operators from Eq. (3.1.15) can be rewritten in terms of chirality-preserving operators and anomalous operators only if their coupling matrices $\widetilde{\mathbf{Y}}_\psi$ satisfy the following condition

$$\widetilde{\mathbf{Y}}_\psi = \ \mathbf{c}_\psi^L \mathbf{Y}_\psi - \mathbf{Y}_\psi \mathbf{c}_\psi^R \ \ , \tag{3.1.30}$$

where $\mathbf{c}_\psi^R$ and $\mathbf{c}_\psi^L$ are the hermitian coupling matrices to RH and LH fermions in the chirality-preserving basis, and $\mathbf{Y}_\psi$ is the Yukawa matrix.

Basis reduction via field redefinitions

An alternative approach to establish relationships among redundant operators is through field redefinitions. It is expected that physical observables remain invariant under field redefinitions. Consequently, any variations observed in the effective Lagrangian resulting from a field redefinition can be interpreted as an equivalence between different operators. This property of EFTs is commonly known as the *equivalence theorem* [137, 138]. In this case, we will consider the ALP-dependent field redefinitions of the Higgs and fermion fields, which are necessary to establish connections and simplify the operator basis. These field redefinitions can be expressed as

$$\Phi \to \exp\ \ ix_\Phi \frac{a}{f_a}\ \ \Phi\,, \qquad \Psi \to \exp\ \ i\mathbf{x}_\Psi \frac{a}{f_a}\ \ \Psi \tag{3.1.31}$$

where $\Psi = \{Q_L, U_R, D_R, L_L, E_R\}$, $\mathbf{x}_\Psi$ are hermitian matrices in flavour space and x_Φ is a real constant. [6] Discussing the basis reduction in terms of field redefinitions rather than via

[6] A priori there is nothing preventing us from considering $\mathbf{x}_\Psi$ as arbitrary complex matrices and x_Φ as a complex number. However, due to the hermicity of the Lagrangian, it is only the hermitian component of the matrices $\mathbf{x}_\Psi$ and the real part of x_Φ that contributes to a variation in it.

the direct use of EOMs renders their impact on the anomalous operators more transparent: because the fermion rotations are chiral, contributions to the latter are generated through the axial anomaly.

The general procedure for reducing the operator basis is as follows. The rotations in Eq. (3.1.31) are first applied to the SM Lagrangian in Eq. (1.0.2). Then, an expansion up to order $\mathcal{O}(1/f_a)$ is performed next. The net shift resulting from the most general rotation reads [1, 117]

$$\begin{aligned}
\Delta\mathscr{L} = & -x_\Phi \frac{\partial_\mu a}{f_a} \Phi^\dagger i\overleftrightarrow{D_\mu}\Phi - \frac{\partial_\mu a}{f_a}{}_\Psi \overline{\Psi}\gamma^\mu \mathbf{x}_\Psi \Psi \\
& + i\frac{a}{f_a}\overline{Q}_L \left(\mathbf{x}_Q \mathbf{Y}_u - \mathbf{Y}_u \mathbf{x}_u + x_\Phi \mathbf{Y}_u\right) \widetilde{\Phi} U_R \\
& + i\frac{a}{f_a}\overline{Q}_L \left(\mathbf{x}_Q \mathbf{Y}_d - \mathbf{Y}_d \mathbf{x}_d - x_\Phi \mathbf{Y}_d\right) \Phi D_R \\
& + i\frac{a}{f_a}\overline{L}_L \left(\mathbf{x}_L \mathbf{Y}_e - \mathbf{Y}_e \mathbf{x}_e - x_\Phi \mathbf{Y}_e\right) \Phi E_R + \text{h.c.} \\
& - \frac{g'^2}{32\pi^2}\frac{a}{f_a} B_{\mu\nu}\widetilde{B}^{\mu\nu}\,\text{Tr}\left(\frac{1}{3}\mathbf{x}_Q - \frac{8}{3}\mathbf{x}_u - \frac{2}{3}\mathbf{x}_d + \mathbf{x}_L - 2\mathbf{x}_e\right) \\
& - \frac{g^2}{32\pi^2}\frac{a}{f_a} W^i_{\mu\nu}\widetilde{W}^{\mu\nu,i}\,\text{Tr}\left(3\mathbf{x}_Q + \mathbf{x}_L\right) \\
& - \frac{g_S^2}{32\pi^2}\frac{a}{f_a} G^\alpha_{\mu\nu}\widetilde{G}^{\mu\nu,\alpha}\,\text{Tr}\left(2\mathbf{x}_Q - \mathbf{x}_u - \mathbf{x}_d\right) .
\end{aligned} \tag{3.1.32}$$

At this point, one is free for instance to choose x_Φ and $\mathbf{x}_\Psi$ so that the terms in $\Delta\mathscr{L}$ cancel off against redundant operators in $\mathscr{L}_a$. Or to choose values for a combination of indices so as to remove one or all of the anomalous coefficients $c_{\widetilde{X}}$, for example. It is not hard to verify that each field transformation is equivalent, up to shifts to the anomalous bosonic operators, to the application of the EOM of the corresponding field in Eqs. (3.1.16)–(3.1.19), as shown in the previous section.

For instance, the relation in Eq. (3.1.14) can be easily proven by choosing $x_\Phi = c_{a\Phi}$ and $\mathbf{x}_u = -\mathbf{x}_d = -\mathbf{x}_e = c_{a\Phi}\mathbb{1}$, while $\mathbf{x}_Q = \mathbf{x}_L = 0$. Alternatively. the identities in Eqs. (3.1.25)–(3.1.29) can be demonstrated via fermionic field redefinitions under the choice $\mathbf{x}_\Psi = \mathbf{c}_\Psi$.

Summing up, field redefinitions offer an alternative approach for reducing the operator basis. By performing appropriate field transformations, one can establish equivalence relations among different ALP effective operators that are identical to the relations derived from EOMs up to order $\mathcal{O}(1/f_a)$.

Nevertheless, it should be noted that EOMs do not generally lead to equivalence theorems beyond first order in the perturbative expansion [137–139]. While EOMs establish equivalence relations at order $\mathcal{O}(1/f_a)$, they fail to provide the correct equivalence relations among effective operators at higher orders. In contrast, field redefinitions offer an approach that remains valid at all orders in the $1/f_a$ expansion. By considering the fermionic field redefinitions presented in Eq. (3.1.31), we can establish relations that holds to all orders in

$1/f_a$. As an example, for the U_R we find

$$\frac{\partial_\mu a}{f_a}\ \overline{U}_R\gamma^\mu \mathbf{c}_u U_R\ = \overline{Q}_L\ \ 1-e^{i\mathbf{c}_u a/f_a}\ \ \mathbf{Y}_u\widetilde{\Phi}U_R+\text{h.c.}+\mathcal{O}(\alpha)aX\widetilde{X}\,, \tag{3.1.33}$$

where the last term stands for the anomalous interaction terms from Eq. (3.1.25), which are exact at all orders. The exponential of the matrix $\mathbf{c}_Q$ must be understood here as the Taylor expansion of the exponential function. Thus, if we wish to make a computation at higher order than $\mathcal{O}(1/f_a)$, the expression above is the equivalence relation we must use to trade the chirality-preserving operator by chirality-flipping ones, instead than the one obtained via EOMs. [7]

3.1.3 ALP EFT below EWSB

The ALP EFT presented above in terms of gauge invariant operators leads to multiple experimental signals. The ultimate goal is to detect or constraint from data the set of fundamental independent variables $\{c_{\widetilde{G}}, c_{\widetilde{W}}, c_{\widetilde{B}}, \mathbf{c}_\Psi\}$ which are to be treated as free Lagrangian parameters.

After EWSB, the three anomalous gauge couplings from Eq. (3.1.3) induce five distinct phenomenological interactions with the physical gauge bosons: gluons, photons, W and Z bosons. Customarily, these couplings are codified as

$$\begin{aligned}\mathscr{L}_a \supset &-\frac{1}{4}g_{agg}aG^\alpha_{\mu\nu}\widetilde{G}^{\mu\nu,\alpha}-\frac{1}{4}g_{a\gamma\gamma}aF_{\mu\nu}\widetilde{F}^{\mu\nu}\\ &-\frac{1}{4}g_{a\gamma Z}aF_{\mu\nu}\widetilde{Z}^{\mu\nu}-\frac{1}{4}g_{aZZ}aZ_{\mu\nu}\widetilde{Z}^{\mu\nu}-\frac{1}{2}g_{aWW}aW^+_{\mu\nu}\widetilde{W}^{\mu\nu,-}\,,\end{aligned} \tag{3.1.34}$$

where $Z_{\mu\nu}$ and $W^\pm_{\mu\nu}$ are respectively the fields strength of Z and $W^\pm$ bosons, and

$$\begin{aligned} g_{agg}&=\frac{4}{f_a}c_{\widetilde{G}}\,, & g_{a\gamma\gamma}&=\frac{4}{f_a}\ \ c_w^2c_{\widetilde{B}}+s_w^2c_{\widetilde{W}}\ \ ,\\ g_{aWW}&=\frac{4}{f_a}c_{\widetilde{W}}\,, & g_{aZZ}&=\frac{4}{f_a}\ \ s_w^2c_{\widetilde{B}}+c_w^2c_{\widetilde{W}}\ \ , \qquad g_{a\gamma Z}=\frac{8}{f_a}c_ws_w\ \ c_{\widetilde{W}}-c_{\widetilde{B}}\ \ , \end{aligned} \tag{3.1.35}$$

where $c_w(s_w)$ is the cosine (sine) of the weak mixing angle.

It is noteworthy that in the two independent EW ALP couplings spawn four different interactions with the physical EW bosons after EWSB,

$$\{c_{\widetilde{W}}, c_{\widetilde{B}}\}\to\{g_{a\gamma\gamma}, g_{a\gamma Z}, g_{aZZ}, g_{aWW}\}\,, \tag{3.1.36}$$

which allows to overconstrain the electroweak gauge sector of the parameter space. In other words, the four phenomenological EW couplings are correlated, and, from the experimental

[7] At higher orders in the $1/f_a$ expansion, the chirality-preserving operator, which is of $\mathcal{O}(1/f_a)$, is effectively replaced by a tower of higher-order chirality-flipping operators that appear at all orders in $1/f_a$ and involve several ALPs fields in each effective vertex. However, despite the differences in the operator basis, both the chirality-preserving and chirality-flipping operator bases lead to the same physical observables. This equivalence between the two bases is consistent with the expected outcome based on the equivalence theorem.

point of view, this can be used to set constraints on one coupling based on the constraints on other couplings, barring fine-tuned cancellations.

Regarding the fermion sector, in order to discuss the phenomenological ALP couplings to the physical fermions it is more convenient to rewrite the fermion couplings using the chirality-flipping couplings depicted in Eq. (3.1.15), where the $\widetilde{\mathbf{Y}}_\Psi$ matrices are computed in terms of the chirality-preserving couplings $\mathbf{c}_\Psi$ as in Eq. (3.1.30). Therefore, after EWSB, the couplings are expressed in the fermion mass basis and the interaction terms read

$$\mathscr{L}_a \supset -i\frac{a}{f_a} \sum_{\Psi} \sum_{k,l} (m_{\Psi^k} - m_{\Psi^l}) \left[\mathbf{K}^S_\Psi\right]_{kl} \Psi^k \Psi^l + (m_{\Psi^k} + m_{\Psi^l}) \left[\mathbf{K}^P_\Psi\right]_{kl} \Psi^k \gamma^5 \Psi^l \quad , \tag{3.1.37}$$

where $\Psi = \{U, D, E\}$, k and l are flavour indices, m_{Ψ^k} denotes the mass of the flavour component Ψ^k and the matrices $\mathbf{K}^S$ and $\mathbf{K}^P$ are defined as

$$\mathbf{K}^{S,P}_\Psi \equiv \frac{1}{2} \left[\mathbf{c}^R_\Psi \pm \mathbf{c}^L_\Psi\right] \quad , \tag{3.1.38}$$

with the sum (difference) of the operator coefficients $\mathbf{c}^{R,L}_\Psi$ corresponding to the scalar (pseudoscalar) components of $\mathbf{K}^{S,P}_\Psi$.

It should be noted also that Eq. (3.1.37) shows then that only pseudoscalar couplings contribute at tree-level of the EFT to flavour-diagonal interactions, while both scalar and pseudoscalar contributions are present for the off-diagonal ones. Moreover, all tree-level ALP-fermion interactions are proportional to the masses of the fermions involved, which is not obvious in the chirality-preserving basis. Therefore, the naive expectation is that phenomenological couplings with light fermions are subdominant with respect to couplings with heavier fermions.

3.2 Experimental constraints on ALPs

Experimental searches for ALPs are closely linked to searches for axions. The main reason is that axion searches encompass regions of parameter space that are not exclusive to invisible axions, in particular where the relation between f_a and m_a from Eq. (2.5.54) does not hold, and then have the potential to discover ALPs as well. Therefore, the constraints presented below in this section can be interpreted in terms of both invisible axions and ALPs. [8]

We present experimental bounds on different axion and ALPs couplings to SM particles from the ALP Linear EFT. These includes the predominant bound on photons and gluons, as well as bounds on fermions or massive gauge bosons. The bounds are presented in Figs. 3.1, 3.2, where we show the excluded regions on the $\{m_a, g_{aVV}\}$ or $\{m_a, \mathbf{c}_\Psi\}$ parameter plane, where g_{aVV} denotes a generic anomalous coupling between a and gauge bosons, by several experimental searches.

[8] In addition, heavy axion models address the strong CP problem but predicts a value of the axion the mass shifted by large confining scales (see Sec. 2.5). Then, those are expected to be found on regions of the parameter space typically associated to ALPs.

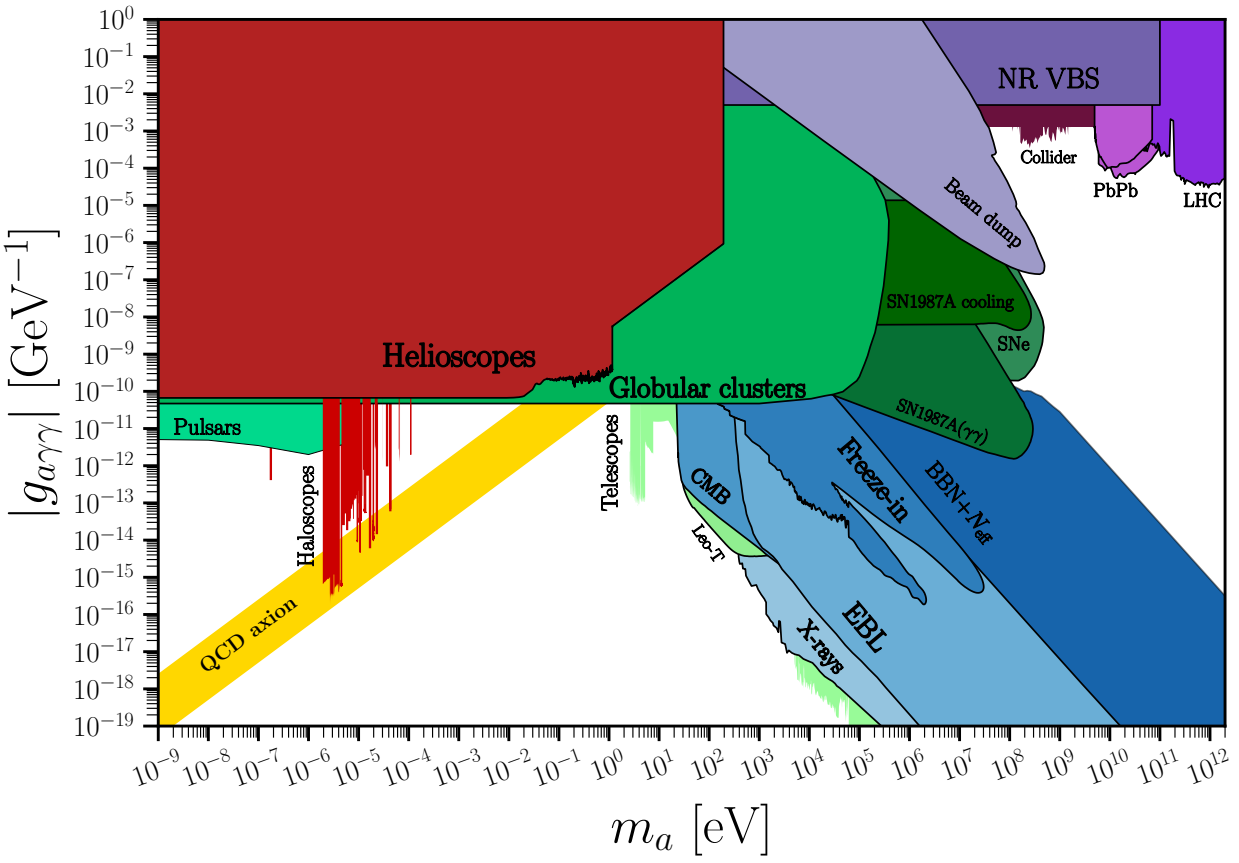

Figure 3.1: Constraints on the axion coupling to photons $g_{a\gamma\gamma}$ as a function of the axion mass m_a. Figure adapted from [140].

3.2.1 ALP coupling to photons

The interaction between ALPs and photons is encoded in the $aF\widetilde{F}$ term in $\mathscr{L}_a^{X\widetilde{X}}$ from Eq. (3.1.34). For the QCD axion, the $g_{a\gamma\gamma}$ coupling constant comprises two independent contributions: a first term that depends on the axion model and a second model-independent term from the mixing with light mesons from Eq. (2.5.61). On the other hand, for ALPs it is a free parameter of the Effective Lagrangian. Experimental bounds on $g_{a\gamma\gamma}$ are represented in Fig. 3.1 for a wide range of ALP masses and couplings.

First of all, in yellow we present the "QCD axion" band, that encompass the prediction for the QCD axion for several invisible axion models.

Among the searches represented here, many of them are based on the *Primakoff conversion* effect [141, 142]: in the presence of an external magnetic field $\vec{B}$, the axion coupling to photons in Eq. (3.1.34) may generate an axion-photon conversion process. For instance, that is the case of bounds represented in red, which comprise experiments aiming to measure a direct ALP signal. Those include helioscopes searching for solar axions, such as CAST [143, 144] and haloscopes aiming to detect DM axions/ALPs via resonant cavities: here we include ADMX [145–148], ADMX SLIC [149], CAPP [150–155], RBF [156], HAYSTAC [157–159], QUAX [160–162] and ORGAN [163, 164].

On the other hand, bounds stemming from astrophysics are represented in green color. Those include searches for ALPs produced in strong magnetic fields at pulsars [165],

bounds based on stellar evolution at globular clusters [166, 167], bounds form supernovae (SNe) [168], the limit form the gas temperature of Leo-T galaxy [169] and the effect of ALPs on SN1987A. The latter includes the cooling effect [168] or ALPs decaying into photons, contributing to the supernova explosion energy [170]. In addition we find telescopes searches, that aim to measure DM ALPs decaying into pairs of photons, such as MUSE [171], VIMOS [172], HTS [173, 174], XMM-Newton [175], NuSTAR [176–178] and INTEGRAL [179].

In blue color we show bounds arising from cosmological observables. Typically, these assume that ALPs are the main constituent of DM and has a role on the cosmological evolution of the universe. Among these, we find searches for distortions on the CMB [180, 181], searches on X-ray backgrounds [182], ALP contributions to the extragalactic background light (EBL) spectrum [182], limits from Plack [183] based on Big Bang Nucleosynthesis (BBN) and ΔN_{eff}, and the irreducible freeze-in ALP abundance [184].

Finally, in purple we represent bounds stemming from collider and high-energy experiments. Here we find results from beam dump experiments [185–189], limits from light-by-light scattering in Pb-Pb nuclei collisions at CMS [190] and ATLAS [191] and bounds from pp collisions at LHC [192], among others [122, 192–195]. Additionally, we also show our plot derived from nonresonant Vector-Boson scattering (NR VBS) in Ref. [2]. In this work we use CMS data on the production of pairs of massive vector bosons in VBS processes to establish a new experimental bound on ALPs. Working under the assumption that off-shell ALPs can mediate such processes, new bound can be extracted, that have the property of being independent on the ALP mass and decat width. On Chapter 5 we discuss in detail these experimental limits and Ref [2].

3.2.2 ALP coupling to gluons

The coupling between axions/ALPs and gluons is determined by the $aG\widetilde{G}$ term in the Lagrangian $\mathcal{L}_a^{X\widetilde{X}}$, described in Eq.(3.1.34). In the case of ALPs, the coupling constant g_{agg} is a free parameter of the Lagrangian, allowing for the possibility that ALPs may not couple to gluons at all. However, for true axions, the coupling to gluons is mandatory in order to solve the Strong CP problem.

Certain QCD axion models have been developed in which the ratio of the QED and QCD anomalous coefficients, denoted as E/N, approximately equals 1.92. This feature allows for partial cancellation between the model-dependent and model-independent contributions to the photon coupling in Eq. (2.5.61). Such axion models are often referred to as *photophobic* axion models, since the interaction to photons is strongly suppressed. In the context of these models, the bounds on the photon coupling presented in Fig. 3.1 may be eluded, allowing for true axions in a range of masses that a priori seems to be excluded. Considering this perspective, it becomes necessary to investigate the bounds in the parameter space for the gluon interactions.

One of the best experimental observables to test this coupling is the branching ratio for the rare kaon decay process $K^+ \to \pi^+ + \text{invisible}$. In the SM the main contribution to such branching factor is due to neutrinos (which are not detected in the decay process): $K^+ \to \pi^+ \overline{\nu}\nu$. However, if a is assumed to be light and stable at collider distances, the process $K^+ \to \pi^+ a$, where a goes undetected, can contribute to measurement of the previous kaon branching fraction. Recent measurements [196] of the latter leads to the following limit on

g_{agg} [133]:

$$|g_{agg}| \lesssim 3 \times 10^{-6}\ \text{GeV}^{-1} \qquad \text{for } m_a \lesssim 100\ \text{MeV}\,. \tag{3.2.39}$$

In addition, the ALP-gluon coupling can be tested as well in collider experiments. For instance, mono-jet and di-jet searches at the LHC have established robust limits on g_{agg} for high values of m_a [121, 197–199]. In those processes, an ALP is produced in association with one or two gluons and/or quarks, which later are measured as jets, while a escapes detection. By combining the results for those searches, the limits on g_{agg} that we obtained read

$$|g_{agg}| \lesssim \begin{cases} 3 \times 10^{-5}\ \text{GeV}^{-1} & \text{for } m_a \lesssim 1\ \text{GeV}\,, \\ 7 \times 10^{-5}\ \text{GeV}^{-1} & \text{for } 1\ \text{GeV} \lesssim m_a \lesssim 1\ \text{TeV}\,. \end{cases} \tag{3.2.40}$$

3.2.3 ALP coupling to electrons

ALP couplings to fermions can also be tested. In particular, couplings to electrons are of special interested, due to their impact on experimental and astrophysical observables. From Eq. (3.1.37) we deduced that flavour-diagonal couplings to fermions only depend on the axial combination of ALP-fermionic couplings. Therefore, we can defined the ALP coupling to physical electrons as follows

$$\mathscr{L}_a \supset \frac{c_{ee}}{f_a}\partial_\mu a \;\; \bar{e}\gamma^\mu\gamma^5 e \;\; = -2im_e\frac{c_{ee}}{f_a}a \;\; \bar{e}\gamma^5 e \;\; + \mathcal{O}(\alpha_{\text{em}})\,, \tag{3.2.41}$$

with

$$c_{ee} \equiv (\mathbf{c}_e - \mathbf{c}_L)_{ee}\ . \tag{3.2.42}$$

In Fig. 3.2 we represent experimental bounds on the quotient c_{ee}/f_a for a wide range of values of the ALP mass and coupling to electrons.

First, analogously to Fig. 3.1, we have represented the predictions for the QCD axion couplings as a band in yellow for different invisible axion models.

In red, we show direct detection experiments aiming to detect DM ALPs/axions. Those include searches at GERDA [201], XENON1T [202–204] and XENONnT [205].

Bounds in green are those arising from astrophysics observables. Among these we find measurement of the brightness of Red Giant stars, which set bounds on c_{ee}/f_a from energy loss arguments [206] and bounds from SN1987A. The latter are originally those bounds on the ALP-photon interactions that we presented in Fig. 3.1. However, they can be recasted into new limits on the ALP-electron couplings by taking into account the loop-impact of the latter on the photon interaction [200]. The same argument can be used to obtained bounds from cosmological observations, represented here in blue color, such as the irreducible freeze-in ALP abundance [184] or effects on BBN [200, 207].

Finally, bounds stemming from electron beam dump experiments are shown in purple. The latter are taken from Ref. [208] and encompass ALP searches at NA64 [209–211], SLAC-E137 [212], SLAC-E141 [186], Fermilab-E774 [213] and Orsay [214].

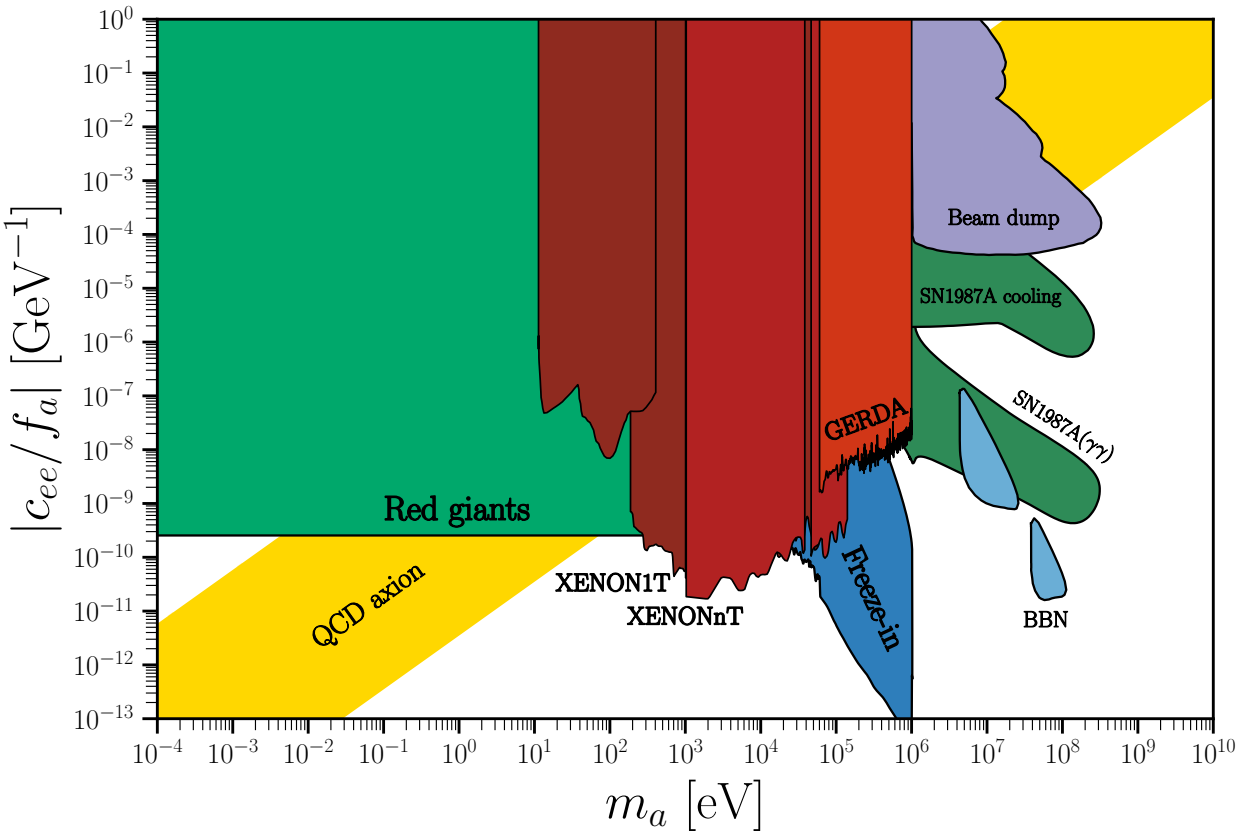

Figure 3.2: Constraints on the axion coupling to electrons as a function of the axion mass m_a. Figure adapted from [140, 200].

3.2.4 ALP coupling to massive vector bosons

The principle of gauge invariance imposes that if an ALP exhibits couplings to photons, it must also possess interactions with other heavy EW bosons. [9] While the ALP-photons couplings are subject to significant constraints from low-energy experiments, such as helioscopes and haloscopes, as well as astrophysical observations, the couplings to heavy EW bosons can be explored more effectively in high-energy collider experiments, where the bounds arising from photon couplings are less stringent. Consequently, collider experiments play a critical role in examining the anomalous interactions of ALPs with EW bosons, complementing the constraints derived from low-energy ALP searches.

Chapter 5, which contains our work from Ref. [2], provides an extensive analysis of the constraints imposed on the ALP couplings to EW heavy bosons: $\{g_{a\gamma Z}, g_{aZZ}, g_{aWW}\}$. Here we investigate the ALP interactions by focusing on nonresonant VBS searches performed at the CMS experiment at the LHC. The chapter comprises a detailed comparison with the prior constraints on ALP EW couplings found in existing literature. Consequently, the present section just provides a concise overview of the experimental limits outlined in

[9] Among the set of the four phenomenological electroweak couplings $\{g_{a\gamma\gamma}, g_{a\gamma Z}, g_{aZZ}, g_{aWW}\}$, only one of them, at maximum, can be fixed to 0 given their expressions in terms of $c_{\widetilde{B}}$ and $c_{\widetilde{W}}$ from Eq. (3.1.35).

Ch. 5.

ALP-γZ interaction

The ALP-γZ interaction arises from the $aF\widetilde{Z}$ term in the $\mathscr{L}_a^{X\widetilde{X}}$ Lagrangian from Eq. (3.1.34). The most stringent constraints on this coupling originate from precise measurements of Z-boson observables obtained at LEP. Specifically, ALPs with masses lighter than the Z-boson mass are expected to contribute to the decay process $Z \to \gamma + a$.

For instance, if ALPs are assumed to be stable at collider distances, stringent bounds on $g_{a\gamma Z}$ are established from the non-observation of exotic $Z \to \gamma +$ invisible decays at LEP [101, 125]:

$$|g_{a\gamma Z}| \lesssim 6 \times 10^{-5}\ \text{GeV}^{-1} \qquad \text{for } m_a \lesssim 400\ \text{MeV}\,. \tag{3.2.43}$$

If the assumption of a stable ALP is relaxed, the latter constraint can be replaced by the more conservative bound due to the measurement of the total Z-decay width at LEP, that extends up to $m_a \lesssim M_Z$ [117, 125]:

$$|g_{a\gamma Z}| \lesssim 2 \times 10^{-3}\ \text{GeV}^{-1} \qquad \text{for } m_a \lesssim M_Z\,. \tag{3.2.44}$$

For higher values of m_a the bounds are dominated by LHC measurements. In particular our work in Ref. [2] imposes

$$|g_{a\gamma Z}| \lesssim 5 \times 10^{-3}\ \text{GeV}^{-1} \qquad \text{for } m_a \lesssim 100\ \text{GeV}\,, \tag{3.2.45}$$

from the non-observation of exotic events in nonresonant VBS processes at CMS.

Finally, for masses above 100 GeV the dominant bounds stem from resonant triboson searches [125]:

$$|g_{a\gamma Z}| \lesssim 5 \times 10^{-2}\ \text{GeV}^{-1} \qquad \text{for } 100\ \text{GeV} \lesssim m_a \lesssim 500\ \text{GeV}\,. \tag{3.2.46}$$

ALP-ZZ interaction

The ALP interaction with Z-bosons arises from the term $aZ\widetilde{Z}$ from Eq. (3.1.34). Unlike the case of $g_{a\gamma Z}$, it cannot be inferred from Z-boson decay processes, which make it much harder to test experimentally. Best constraints on g_{aZZ} stem from LHC measurements. In particular, LHC searches for exotic mono-Z processes give rise to the following limit

$$|g_{aZZ}| \lesssim 8 \times 10^{-4}\ \text{GeV}^{-1} \qquad \text{for } m_a \lesssim 400\ \text{MeV}\,. \tag{3.2.47}$$

At higher masses, we derive in our work in Ref. [2] the following bound from nonresonant VBS processes at CMS:

$$|g_{aZZ}| \lesssim 3 \times 10^{-3}\ \text{GeV}^{-1} \qquad \text{for } m_a \lesssim 100\ \text{GeV}\,. \tag{3.2.48}$$

ALP-WW interaction

ALP couplings to W-bosons stem from the $aW\widetilde{W}$ term from Eq. (3.1.34). At one-loop order, g_{aWW} contributes to rare meson decay process (e.g. $K^+ \to \pi^+ a$) if a is assumed

to be light. Analogously to the case of the ALP-gluon coupling, recent measurements [196] of the Kaon branching fraction for the charged kaon decay process into pions and neutrinos ($K^+ \to \pi^+ \overline{\nu}\nu$) set the following bound on g_{aWW} [133]:

$$|g_{agg}| \lesssim 3 \times 10^{-6}\ \text{GeV}^{-1} \qquad \text{for } m_a \lesssim 400\ \text{MeV}\,. \tag{3.2.49}$$

Again, for larger values of the ALP mass, we derive in our work in Ref. [2] the a bound from nonresonant VBS processes at CMS that reads

$$|g_{aWW}| \lesssim 3 \times 10^{-3}\ \text{GeV}^{-1} \qquad \text{for } m_a \lesssim 100\ \text{GeV}\,. \tag{3.2.50}$$

Finally, above 100 GeV, the best constraint is derived from triboson searches at the CMS experiment [215]:

$$|g_{aWW}| \lesssim 2 \times 10^{-2}\ \text{GeV}^{-1} \qquad \text{for } 200\ \text{GeV} \lesssim m_a \lesssim 600\ \text{GeV}\,. \tag{3.2.51}$$

3.2.5 ALP coupling to nucleons

At low energies, below QCD confinement, the couplings between ALPs and fermions lead to an effective interaction with nucleons. This interaction can be described by a Lagrangian that incorporates nucleons as the dynamic degrees of freedom. Analogously to the fermionic ALP Lagrangian presented in Eq. (3.1.4), we can express this interaction using an effective operator

$$\mathscr{L}_a \supset \frac{C_{aN}}{2f_a}\partial_\mu a \;\; \overline{\Psi}_N \gamma^\mu \gamma^5 \Psi_N \quad , \tag{3.2.52}$$

where C_{aN} denotes the ALP-nucleon coupling constant and $N = \{p, n\}$ denotes the nucleon (proton or neutron) represented by the spinor field Ψ_N. This effective Lagrangian captures the net interaction between ALPs and nucleons at low energies, considering the fermionic nature of nucleons and the derivative nature of ALPs.

The effective interaction described above is subject to strong constraints from astrophysical observations, particularly related to the cooling of celestial objects due to ALP emission. The most stringent bound on these couplings arises from measurements of the luminosities of nearby isolated neutron stars, as reported in Ref. [216]. These measurements have led to the derivation of the following upper limits on the ALP-nucleon interactions:

$$|C_{ap}/f_a| \lesssim 1.6 \times 10^{-9}\ \text{GeV}^{-1}\,, \qquad |C_{an}/f_a| \lesssim 1.4 \times 10^{-9}\ \text{GeV}^{-1}\,, \tag{3.2.53}$$

for ALP masses $m_a \lesssim 16$ meV.

Part II

Raiders of the Lost ALP

Chapter 4

One-loop corrections to ALP couplings

This chapter contains the publication in Ref. [1]. The main goal of this work is to compute and quantify the complete set of one-loop corrections to interactions between ALPs and SM particles, which is needed from the experimental point of view to explore the ALP parameter space optimally. Indeed, the present experimental accuracy calls for taking into account radiative corrections in some channels. For simplicity, CP-symmetry is assumed in the ALP sector. Neutrino masses are disregarded, and no RH neutrino field is considered. In addition, CKM mixing is also neglected.

In Sec. 2, the mass dimension $d = 5$ ALP linear effective Lagrangian is presented, clarifying the relations among alternative (complete and non-redundant) operator bases. The precise combinations of ALP anomalous couplings to gauge bosons involved in trading different bases are identified. This includes the relations stemming from the anomalous global baryon and lepton number currents. Additionally, in Sec. 3 we discuss *non-renormalization theorems*, which ensure that in some particular choices of the ALP operator basis, anomalous couplings are not renormalized at any loop order in perturbation theory, and only get finite corrections.

The complete one-loop corrections are presented in Sec. 4, including all divergent and finite terms, to all possible CP-even couplings of an ALP to SM gauge fields and fermions, but restricted to flavour diagonal external channels. The computation is performed for a generic off-shell ALP and on-shell SM particles, in the covariant R_ξ gauge. As a byproduct, the UV divergent terms of the computations allow to obtain the ALP renormalization group equations straightforwardly. In addition, different kinematic limits for the ALP mass vs. fermion and gauge boson masses are presented, which may be relevant for several experimental searches.

In Sec. 5 the impact of one-loop corrections on gauge-invariance relations is discussed. EW gauge invariance imposes fixed relations among ALP effective couplings to photons, Z bosons and W bosons at tree-level. One-loop corrections demonstrate that these tree-level relations are modified at the loop order. The results are interpreted here in terms of higher dimensional operators that, when the Higgs doublet Φ is considered, render gauge invariance explicit again.

Finally, a phenomenological study is contained in Sec. 6. As an illustrative example, we explore how experimental ALP searches can take advantage of one-loop corrections in order to establish new upper limits on the parameter space. The ALP-top couplings are analyzed in two regimes: heavy and light ALPs. We study how the ALP-top coupling interaction $(c_{tt}/f_a)\partial_\mu a(\bar{t}\gamma^\mu\gamma^5 t)$ can be constrained by LHC measurements of top-pair final state processes for heavy ALPs. These channels are enhanced by gluon fusion at one-loop via a top loop, with a sizeable cross-section even when the tree-level coupling ALP-gluon would be zero. Derived bounds can be found in Fig. 10. Additionally, ALP-top effective interaction is also constrained for light ALPs by computing its loop impact on ALP-electron interactions. Constraints from astrophysical observations and DM direct detection searches on the ALP-electron coupling are thus recasted on the effective ALP-top interaction, leading to new upper limits for previously unexplored areas of the parameter space. These limits are shown in Fig. 11.

Published for SISSA by Springer

Received: August 23, 2021
Accepted: November 14, 2021
Published: November 22, 2021

One-loop corrections to ALP couplings

J. Bonilla,[a] **I. Brivio,**[b] **M.B. Gavela**[a] **and V. Sanz**[c,d]

[a] *Departamento de Física Teórica, Universidad Autónoma de Madrid, and Instituto de Física Teórica IFT-UAM/CSIC, Cantoblanco, E-28049, Madrid, Spain*

[b] *Institut für Theoretische Physik, Universität Heidelberg, Philosophenweg 16, D-69120 Heidelberg, Germany*

[c] *Instituto de Física Corpuscular (IFIC), Universidad de Valencia-CSIC, E-46980 Valencia, Spain*

[d] *Department of Physics and Astronomy, University of Sussex, Brighton BN1 9QH, U.K.*

E-mail: jesus.bonilla@uam.es, brivio@thphys.uni-heidelberg.de, belen.gavela@uam.es, veronica.sanz@uv.es

Abstract: The plethora of increasingly precise experiments which hunt for axion-like particles (ALPs), as well as their widely different energy reach, call for the theoretical understanding of ALP couplings at loop-level. We derive the one-loop contributions to ALP-SM effective couplings, including finite corrections. The complete leading-order — dimension five — effective linear Lagrangian is considered. The ALP is left off-shell, which is of particular impact on LHC and accelerator searches of ALP couplings to $\gamma\gamma$, ZZ, $Z\gamma$, WW, gluons and fermions. All results are obtained in the covariant R_ξ gauge. A few phenomenological consequences are also explored as illustration, with flavour diagonal channels in the case of fermions: in particular, we explore constraints on the coupling of the ALP to top quarks, that can be extracted from LHC data, from astrophysical sources and from Dark Matter direct detection experiments such as PandaX, LUX and XENON1T. Furthermore, we clarify the relation between alternative ALP bases, the role of gauge anomalous couplings and their interface with chirality-conserving and chirality-flip fermion interactions, and we briefly discuss renormalization group aspects.

Keywords: Beyond Standard Model, Effective Field Theories, Renormalization Group

ArXiv ePrint: 2107.11392

https://doi.org/10.1007/JHEP11(2021)168

JHEP11(2021)168

Contents

JHEP11(2021)168

1 Introduction

The field of axions and axion-like particles (ALPs) is undergoing a phase of spectacular development, both theoretical and experimental. This should come as no surprise. No firm signal of new physics has shown up yet at colliders or elsewhere, which transforms the fine-tuning issues of the Standard Model of particle physics (SM) in most pressing ones, and also impacts on the dark matter (DM) quest. The silence of data is calling for a rerouting guided by fundamental issues such as the strong CP problem, as well as for an open-minded approach to hunt for the generic tell-tale of global hidden symmetries: derivative couplings, as in the case of axions and ALPs.

Indeed, axions appear in dynamical solutions to the strong CP problem as the pseudo Goldstone-bosons (pGB) of a global chiral U(1) symmetry [1–4]. Theories of pGBs extend well beyond those true axions, though. They appear in a plethora of beyond the SM (BSM) constructions, typically as SM scalar singlets, and often receive the generic name of ALPs (in particular when gauge anomalous couplings are present in addition to pure derivative ones). Paradigmatic examples of pGBs physics include: i) theories with extra dimensions, because the Wilson line around a compact dimension behaves as a 4-dimensional axion; ii) dynamical explanations to the smallness of neutrino masses, with the Majoron [5] as a pGB of a hidden U(1) lepton symmetry (the Majoron and the axion could even be identified [6, 7]); iv) string theory models, which tend to have a plethora of hidden U(1)'s and axions [8]; iv) dynamical flavour theories ("axiflavons" [9–11]), to cite just a few examples. As a wonderful byproduct, axions and a variety of ALPs are often excellent candidates to account for DM.

The landscape of experimental searches for axions and/or ALPs is undergoing a flourishing period, covering orders of magnitude in energy scale and using very different techniques. In particular, the couplings of ALPs to heavy SM bosons are under increasing experimental scrutiny [12–20]. Indeed, because of electroweak gauge invariance they are generically expected at the same level as the photonic interactions. Through the ensemble of ALP bosonic couplings, ALP scales ranging from hundreds of GeV to several TeV are within

JHEP11(2021)168

the reach of the LHC and of future collider experiments, favored by the prospects of increasing energy and precision. In addition, the impact of ALP electroweak couplings on flavour rare decays is already setting impressive constraints on the ALP parameter space [21, 22] (for ALP masses below 5 GeV), offering a complementary window of high-precision.

A model-independent approach to the search for a true axion or an ALP — both denoted here as a — is that of effective Lagrangians, with the tower of effective operators weighted down by its BSM scale f_a. The parameter space is then simply defined by the mass vs. scale $\{m_a, f_a\}$ plane, with $m_a \ll f_a$ and the model-dependence encoded in the arbitrary operator coefficients. The couplings are mainly derivative — proportional to the ALP momentum — as befits pGBs, plus anomalous couplings to gauge field strengths. The practical difference between a canonical QCD axion [3, 4] which solves the strong CP problem and generic ALPs is that for the latter f_a and m_a are treated as independent parameters. The exploration of the ALP parameter space is thus free from the stringent phenomenological constraints which hold for the canonical QCD axion.[1] For the purpose of this work, the difference between a true axion and an ALP is of no consequence and the name ALP will be used indistinctly.

We explore at one-loop order all possible CP-even operators coupling one pseudoscalar ALP to SM fields: to the gluon, the photon, $W^{\pm}$, Z, the Higgs particle and to fermions, at next-to leading order (NLO) of the linear effective field theory (EFT) formulation, i.e. mass dimension five operators. The approach is in the same spirit as the usual SMEFT theory, but including the ALP a as an additional low-energy active field. The necessity to address these interactions at loop-level stems, on one side, from the high precision experimentally achieved in certain channels, and on the other from the very different energy scales explored by different experiments. Motivated by the latter, updated studies of the renormalization group evolution of the ALP effective Lagrangian have already appeared very recently [43, 44].

We provide here the complete one-loop corrections, i.e. divergent and finite contributions, for an off-shell ALP and on-shell SM fields. Previously, those corrections had been worked out only for the contributions to the axion-photon-photon coupling $g_{a\gamma\gamma}$ and to the axion leptonic coupling (in certain limits), for an on-shell ALP [14]. Recently, fermionic contributions to $g_{a\gamma Z}$ have also appeared [44] for an on-shell ALP. The physical impact of our results will be presented as contributions to the set of measurable CP-even interactions $\{g_{a\gamma\gamma}, g_{aWW}, g_{aZZ}, g_{a\gamma Z}, g_{agg}, c_{\rm f}\}$, where the first five denote ALP anomalous couplings to gauge bosons and f denotes a generic fermion, with the SM fields on-shell. All our computations are performed in the covariant R_ξ gauge. The only restriction on fermions is that flavour diagonal channels are computed, disregarding generation mixing. Neutrino masses are disregarded as well.

Furthermore, the constraints that gauge invariance imposes on the complete set of ALP couplings will be discussed, showing how the one-loop corrections modify the tree-level

[1] The anomalous coupling to gluons is necessarily present for axions that solve the strong CP problem. For true axions, the precise relation between m_a and f_a depends on the characteristics of the strong interacting sector of the theory: QCD in the case of the canonical axion, and an enlarged confining sector for true axions which are either heavier [23–39] or lighter [40–42] than the canonical QCD axion.

JHEP11(2021)168

gauge invariance relations which relate physical channels. The results impact in particular the variety of LHC and collider ALP searches.

We will also clarify the one-loop impact of ALP-fermion couplings on gauge anomalous ALP interactions. This will allow to elucidate ongoing discussions in the literature on the relation between different types of complete and non-redundant bases of operators. Some aspects of the RG running above the electroweak scale will be briefly discussed as well.

The structure of the paper can be easily inferred from the Table of Contents.

2 Effective Lagrangian

The formulation of the CP-even ALP effective Lagrangian at next-to-leading order (NLO) of the linear expansion, i.e. up to $\mathcal{O}(1/f_a)$ couplings of mass dimension five, is discussed next assuming the field a to be a pseudoscalar. A complete basis of independent ALP operators — bosonic plus fermionic — is considered, and its relation to other complete bases and to the purely bosonic one is also clarified.

In addition to ALP kinetic energy and mass terms, any ALP EFT is defined by an ensemble of effective operators which are invariant under the shift symmetry $a \to a + c$ where c is a constant (i.e. purely derivative ALP couplings, as it would befit Goldstone bosons) plus ALP-gauge couplings resulting from the axial anomaly of the form $aX_{\mu\nu}\tilde{X}^{\mu\nu}$, where $X_{\mu\nu}$ denotes a generic SM gauge field strength and $\tilde{X}^{\mu\nu}$ its dual $\tilde{X}^{\mu\nu} \equiv \frac{1}{2}\epsilon^{\mu\nu\rho\sigma}X_{\rho\sigma}$ with $\varepsilon^{0123} = 1$.[2]

2.1 Complete and non-redundant bases

A complete and non-redundant ALP effective Lagrangian is given at $\mathcal{O}(1/f_a)$ by

$$\mathscr{L}_{\rm ALP} = \mathscr{L}_{\rm SM} + \mathscr{L}_a^{\rm total}\,, \tag{2.1}$$

where $\mathscr{L}_{\rm SM}$ denotes the SM Lagrangian,

$$\begin{aligned}\mathscr{L}_{\rm SM} = &-\frac{1}{4}W^{\alpha}_{\mu\nu}W^{\alpha\mu\nu} - \frac{1}{4}B_{\mu\nu}B^{\mu\nu} - \frac{1}{4}G^{a}_{\mu\nu}G^{a\mu\nu} + D_\mu\Phi^\dagger D^\mu\Phi + \sum_{\rm f}\bar{\rm f}\, i\not{D}\,{\rm f}\\ &- \Big[\bar{Q}_L Y_d \Phi d_R + \bar{Q}_L Y_u \tilde{\Phi} u_R + \bar{L}_L Y_e \Phi e_R + \text{h.c.}\Big] - V(\Phi^\dagger\Phi)\,.\end{aligned} \tag{2.2}$$

Here, the index f runs over the chiral fermion fields ${\rm f} = \{Q_L, u_R, d_R, L_L, e_R\}$ which are vectors in three-dimensional flavour space, $Y_{\rm f}$ denote $n_g \times n_g$ Yukawa matrices in flavour space, where n_g denotes the number of fermion generations, Φ is the Higgs doublet with $\tilde{\Phi} = i\sigma^2\Phi^*$, and $V(\Phi^\dagger\Phi)$ is the Higgs potential. In this equation, $G_{\mu\nu}$, $W_{\mu\nu}$ and $B_{\mu\nu}$ denote respectively the $\mathrm{SU}(3)_c$, $\mathrm{SU}(2)_L$ and $\mathrm{U}(1)_Y$ gauge field strengths. Neutrino masses are disregarded here and all through this work; no right-handed neutrino fields will be considered.

[2] We do not consider other shift-invariant ALP couplings to gauge fields which have been recently argued to be independent in some BSM theories [45].

JHEP11(2021)168

All possible shift-invariant fermionic coupling of mass dimension five are contained in the set

$$\mathbf{O}_u \equiv \frac{\partial_\mu a}{f_a}\,(\bar{u}_R\gamma^\mu u_R)\,, \qquad \mathbf{O}_d \equiv \frac{\partial_\mu a}{f_a}\left(\bar{d}_R\gamma^\mu d_R\right), \qquad \mathbf{O}_Q \equiv \frac{\partial_\mu a}{f_a}\left(\bar{Q}_L\gamma^\mu Q_L\right), \tag{2.3}$$

$$\mathbf{O}_L \equiv \frac{\partial_\mu a}{f_a}\left(\bar{Q}_L\gamma^\mu Q_L\right), \qquad \mathbf{O}_e \equiv \frac{\partial_\mu a}{f_a}\,(\bar{e}_R\gamma^\mu e_R) \tag{2.4}$$

in a compact notation in which each of these terms is a $n_g \times n_g$ matrix in flavour space, with flavour indices $\{i, j\}$ left implicit, e.g. $\mathbf{O}_u \equiv \{\mathbf{O}_u^{ij} = \partial_\mu a/f_a\,(\bar{u}_R^i\gamma_\mu u_R^j)\}$. The question is how many of those fermionic couplings can be included in a complete and non-redundant basis of ALP operators.

The most general CP-conserving ALP effective Lagrangian $\mathscr{L}_a^{\rm total}$, including *bosonic and fermionic* ALP couplings [46, 47], admits many possible choices of basis. A *complete and non-redundant basis* — to be used in this paper — is that defined by the Lagrangian

$$\mathscr{L}_a^{\rm total} = \frac{1}{2}\partial_\mu a\partial^\mu a + \frac{m_a^2}{2}a^2 + c_{\tilde{W}}\mathbf{O}_{\tilde{W}} + c_{\tilde{B}}\mathbf{O}_{\tilde{B}} + c_{\tilde{G}}\mathbf{O}_{\tilde{G}} + \sum_{\mathrm{f}=u,d,e}\mathbf{c}_{\mathrm{f}}\mathbf{O}_{\mathrm{f}} + \sum_{\mathrm{f}=Q,L}\mathbf{c}_{\mathrm{f}}\boldsymbol{\emptyset}_{\mathrm{f}}, \tag{2.5}$$

where the effective operators are as given in table 1, and the coefficients $\mathbf{c}_{\mathrm{f}}$ are $n_g \times n_g$ hermitian tensors; in addition, because of the assumption of CP conservation, they will obey $\mathbf{c}_{\mathrm{f}} = \mathbf{c}_{\mathrm{f}}^T$. The convention to be used for the $\mathbf{c}\,\mathbf{O}$ products is the popular one in which their implicit flavour indices $\{i, j\}$ are *not* contracted as a matrix product, but as follows:

$$\mathbf{c}\,\mathbf{O} \equiv \sum_{i,j}(\mathbf{c})_{ij}\,\mathbf{O}^{ij}\,. \tag{2.6}$$

Note that the fermionic basis is chosen here to include all possible right-handed currents, while — in order to avoid redundancies — one of the quark operators made out of left-handed currents has been excluded (see $\boldsymbol{\emptyset}_Q$) together with all diagonal elements of the leptonic operators made out of left-handed currents ($\boldsymbol{\emptyset}_L$), as indicated in short-hand notation, i.e.

$$\boldsymbol{\emptyset}_Q \equiv \left\{\mathbf{O}_Q^{ij} = \frac{\partial_\mu a}{f_a}\,(\bar{Q}_L^i\gamma_\mu Q_L^j) \quad \text{where} \quad i, j \neq 1, 1\right\} \tag{2.7}$$

$$\boldsymbol{\emptyset}_L \equiv \left\{\mathbf{O}_L^{ij} = \frac{\partial_\mu a}{f_a}\,(\bar{L}_L^i\gamma_\mu L_L^j) \quad \text{where} \quad i \neq j\right\}. \tag{2.8}$$

The exclusion of the $(\boldsymbol{\emptyset}_Q)_{11}$ element can be replaced by that of any other of the diagonal elements of $\boldsymbol{\emptyset}_Q$.

It follows that the most general CP-conserving ALP Lagrangian is described by a total of

$$3(\text{bosonic}) + [n_g(5n_g+3)/2 - 1](\text{fermionic}) = 2 + n_g(5n_g+3)/2 \tag{2.9}$$

independent couplings, i.e. 6 couplings in the case of just one generation, and 29 couplings for $n_g = 3$.

The key point to identify redundancies, and the origin of the different number of degrees of freedom for quarks and leptons, is related to baryon and lepton number conservation.

JHEP11(2021)168

$\mathbf{O}_{\tilde{W}} = -\frac{a}{f_a} W^{\alpha}_{\mu\nu} \tilde{W}^{\alpha\mu\nu}$	$\mathbf{O}_{\tilde{B}} = -\frac{a}{f_a} B_{\mu\nu} \tilde{B}^{\mu\nu}$	$\mathbf{O}_{\tilde{G}} = -\frac{a}{f_a} G^{a}_{\mu\nu} \tilde{G}^{a\mu\nu}$
$\mathbf{O}_u = \frac{\partial_\mu a}{f_a} (\bar{u}_R \gamma^\mu u_R)$	$\mathbf{O}_d = \frac{\partial_\mu a}{f_a} \left(\bar{d}_R \gamma^\mu d_R\right)$	$\mathbf{O}_e = \frac{\partial_\mu a}{f_a} (\bar{e}_R \gamma^\mu e_R)$
$\boldsymbol{\phi}_Q = \frac{\partial_\mu a}{f_a} \left(\bar{Q}_L \gamma^\mu Q_L\right)_{i,j\neq 1,1}$	$\boldsymbol{\phi}_L = \frac{\partial_\mu a}{f_a} \left(\bar{L}_L \gamma^\mu L_L\right)_{i\neq j}$	

Table 1. A complete and non-redundant basis of bosonic+fermionic operators, in the presence of quark mixing. Each fermionic structure is a $n_g \times n_g$ matrix in flavour space, with flavour indices $\{i, j\}$ left implicit except in the operators on the last row (which become redundant — for $n_g = 1$). For the anomalous terms, a "hatted" renaming will be used when convenient, $\hat{\mathbf{O}}_{\tilde{X}} \equiv \alpha_X/4\pi\, \mathbf{O}_{\tilde{X}}$, see text.

Classically, with neutrino masses disregarded (only the SM left-handed neutrino fields are considered), lepton number L_i is separately conserved for each generation i (i.e. L_e, L_μ and L_τ for $n_g = 3$), while for quarks with all generations mixed only the total baryon number B is. In consequence, n_g leptonic diagonal couplings become redundant, in contrast to just one for quarks. Indeed, the ALP coupling to the baryonic and leptonic currents reads (see appendix B.2)

$$\frac{\partial_\mu a}{f_a} J^\mu_B = \mathrm{Tr}\left[\frac{\mathbf{O}_Q + \mathbf{O}_u + \mathbf{O}_d}{3}\right] = \frac{n_g}{32\pi^2}\left(g^2 \mathbf{O}_{\tilde{W}} - g'^2 \mathbf{O}_{\tilde{B}}\right), \tag{2.10}$$

$$\frac{\partial_\mu a}{f_a} J^\mu_{L_i} = [\mathbf{O}_L + \mathbf{O}_e]^{ii} = \frac{1}{32\pi^2}\left(g^2 \mathbf{O}_{\tilde{W}} - g'^2 \mathbf{O}_{\tilde{B}}\right), \tag{2.11}$$

where in the last equation there is no sum over the i index, and the right-hand side of these equations stems from the fermion rotations involved. These relations provide one constraint on diagonal quark operators and n_g constraints on diagonal leptonic operators, which reduce in consequence the number of independent degrees of freedom.

Eqs. (2.10) and (2.11) also illustrate that the ALP coupling to the $B + L$ current J^μ_{B+L} is anomalous, where L denotes total lepton number $L = \sum_i L_i$, which is precisely why that coupling can be traded by purely derivative operators.[3] The $B - L$ current J^μ_{B-L} is instead exactly conserved,

$$\frac{\partial_\mu a}{f_a} J^\mu_{B+L} = \mathrm{Tr}\left[\frac{\mathbf{O}_Q + \mathbf{O}_u + \mathbf{O}_d}{3} + \mathbf{O}_L + \mathbf{O}_e\right] = \frac{n_g}{16\pi^2}\left(g^2 \mathbf{O}_{\tilde{W}} - g'^2 \mathbf{O}_{\tilde{B}}\right), \tag{2.12}$$

$$\frac{\partial_\mu a}{f_a} J^\mu_{B-L} = \mathrm{Tr}\left[\frac{\mathbf{O}_Q + \mathbf{O}_u + \mathbf{O}_d}{3} - \mathbf{O}_L - \mathbf{O}_e\right] = 0\,. \tag{2.13}$$

The role of the left-handed and right-handed ALP operators in table 1. can be exchanged. For completeness, we discuss in the next subsection other fair choices of shift-invariant fermionic operators — e.g. containing all possible left-handed currents.

[3] This is analogous to how the Peccei-Quinn current, precisely because it is anomalous, allows to rotate away the $\bar{\theta}$ terms which combine fermion mass and anomalous gauge terms.

JHEP11(2021)168

A frequent redefinition. Often in the literature [14, 15, 44, 48–50] the normalization used for the ALP coupling to gauge anomalous currents differs slightly from that in table 1. We will denote with a hat ("hat basis") that variant:

$$\hat{\mathbf{O}}_{\tilde{B}} \equiv \frac{\alpha_1}{4\pi}\mathbf{O}_{\tilde{B}}\,, \qquad \hat{\mathbf{O}}_{\tilde{W}} \equiv \frac{\alpha_2}{4\pi}\mathbf{O}_{\tilde{W}}\,, \qquad \hat{\mathbf{O}}_{\tilde{G}} \equiv \frac{\alpha_s}{4\pi}\mathbf{O}_{\tilde{G}}\,, \tag{2.14}$$

where $\alpha_1 = g'^2/4\pi$, $\alpha_2 = g^2/4\pi$ and $\alpha_s = g_s^2/4\pi$ denote respectively the $\mathrm{SU}(3)_c$, $\mathrm{SU}(2)_L$ and $\mathrm{U}(1)$ fine structure constants. The corresponding Wilson coefficients of the ALP anomalous gauge couplings are simply related by

$$c_{\tilde{B}} = \hat{c}_{\tilde{B}}\,\frac{\alpha_1}{4\pi}\,, \qquad c_{\tilde{W}} = \hat{c}_{\tilde{W}}\,\frac{\alpha_2}{4\pi}\,, \qquad c_{\tilde{G}} = \hat{c}_{\tilde{G}}\,\frac{\alpha_s}{4\pi}\,. \tag{2.15}$$

2.2 Alternative complete basis

Many choices of complete basis other than that in eq. (2.5) and table 1 are possible, as far as the total number of independent couplings is consistently maintained. Several examples have been proposed in the literature.

Chirality-conserving fermionic alternatives. A valid option is to include in the basis *all* possible operators made out of left-handed fields, including all diagonal couplings, i.e. all $n_g \times (n_g+1)/2$ operators $\mathbf{O}_Q$ and all $n_g \times (n_g+1)/2$ operators $\mathbf{O}_L$, see eqs. (2.3) and (2.4). With respect to the choice in table 1, and still maintaining in the basis the three anomalous couplings, this would require — to avoid redundancies — to drop all flavour diagonal leptonic operators in $\mathbf{O}_{\mathrm{e}}$ (i.e. replace $\mathbf{O}_e \to \not{\mathbf{O}}_e \equiv \partial_\mu a/f_a\ (\bar{e}_R\gamma^\mu e_R)_{i\neq j}$, plus one of the flavour-diagonal ones in $\mathbf{O}_{\mathrm{f}=u}$ or $\mathbf{O}_{\mathrm{f}=d}$. Several other intermediate exchange patterns are legitimate as far as the number of degrees of freedom is consistently maintained.

It is also valid to omit from the basis some of the anomalous bosonic operators, substituting them for flavour-diagonal fermionic couplings. Indeed, eqs. (2.10) and (2.11) show that a complete and non-redundant basis would result for instance from substituting $\not{\mathbf{O}}_Q$ in table 1 by the whole set $\mathbf{O}_Q$ together with the omission of either $\mathbf{O}_{\tilde{W}}$ or $\mathbf{O}_{\tilde{B}}$, or other similar tradings involving the lepton sector.

The case $n_g = 1$. In the simplified case of one generation, the operators $\not{\mathbf{O}}_{\{Q,L\}}$ in the basis in table 1 are absent and pure right-handed operators suffice in addition to the three anomalous ones. That is, for just one generation the set of operators $\{\mathbf{O}_{\tilde{W}}, \mathbf{O}_{\tilde{B}}, \mathbf{O}_{\tilde{G}}, \mathbf{O}_u, \mathbf{O}_d\,\mathbf{O}_e\}$ in table 1 suffices to form a complete basis of linearly independent operators, unlike for $n_g > 1$. Indeed, in the one-generation case the following relations hold

$$\mathbf{O}_Q = -\left[\mathbf{O}_u + \mathbf{O}_d\right] + \frac{3}{32\pi^2}\left(g^2\mathbf{O}_{\tilde{W}} - g'^2\mathbf{O}_{\tilde{B}}\right)\,, \tag{2.16}$$

$$\mathbf{O}_L = -\mathbf{O}_e + \frac{1}{32\pi^2}\left(g^2\mathbf{O}_{\tilde{W}} - g'^2\mathbf{O}_{\tilde{B}}\right)\,, \tag{2.17}$$

which demonstrate that it would be redundant to consider any element of $\mathbf{O}_Q$ and $\mathbf{O}_L$ in addition to all possible operators made out of right-handed currents plus the three anomalous couplings.

JHEP11(2021)168

No flavour mixing, CKM $= \mathbb{1}$. When $n_g > 1$ but CKM flavour mixing is disregarded, the quark sector mirrors what is described above for the lepton sector. There will be then n_g quark baryon charges independently conserved, each of them obeying separately an equation alike to eq. (2.11), instead of only the combined one eq. (2.10). In consequence, n_g constraints follow on the diagonal elements of the quark sector, and all diagonal elements of $\mathbf{O}_Q$ become redundant (assuming that the complete set of right-handed quark currents is retained in the basis together with the anomalous operators). In other words, when CKM mixing is disregarded, a complete and non-redundant basis is given by that in table 1 albeit with the redefinition

$$\not{\mathbf{O}}_Q \equiv \left\{ \mathbf{O}_Q^{ij} = \frac{\partial_\mu a}{f_a} \left(\bar{Q}_L^i \gamma_\mu Q_L^j\right) \quad \text{where } i \neq j \right\} \tag{2.18}$$

We will use this simplified framework in the one-loop computations in section 4.

On the use of chirality-flip fermionic operators. Chirality-flip fermion currents are sometimes used to describe the ALP Lagrangian, together with the three anomalous gauge couplings. That is, some or all of the chirality-conserving fermionic structures in table 1 are traded by chirality-flip ones, i.e.

$$\mathbf{O}_{u\Phi} \equiv i\,\frac{a}{f_a}\bar{Q}_L\,\widetilde{\Phi}\,u_R\,, \quad \mathbf{O}_{d\Phi} \equiv i\,\frac{a}{f_a}\bar{Q}_L\,\Phi\,d_R\,, \quad \mathbf{O}_{e\Phi} \equiv i\,\frac{a}{f_a}\bar{L}_L\,\Phi\,e_R\,. \tag{2.19}$$

Although this is possible if done with care, it could be misleading. The point is that, in all generality, the operators in eq. (2.19) do not belong to the ALP Lagrangian in the sense that they are not invariant *per se* under the required shift symmetry $a \to a + c$ (which in the ALP paradigm is assumed to be broken only by gauge anomalous currents).

Only in some particular cases the chirality-flip couplings are tradable for generic chirality-preserving ones (plus redefinitions of the $c_{\tilde{X}}$ anomalous coefficients). For instance, this is the case for just one fermion generation or when the EFT respects Minimal Flavour Violation (MFV).[4] Otherwise, it suffices to note here that the number of degrees of freedom of a hermitian coefficient matrix (as for chirality-preserving operators) differs in general from that of a general $n_g \times n_g$ matrix (as for chirality-flip ones). In the CP-even case, any complete and non-redundant basis made out of purely shift-invariant fermionic operators spans $n_g(5n_g+3)/2 - 1$ degrees of freedom — see eq. (2.9), which differs from the $3n_g^2$ independent parameters of the chirality-flip set $\{\mathbf{O}_{u\Phi}, \mathbf{O}_{d\Phi}, \mathbf{O}_{e\Phi}\}$ in eq. (2.19). The precise combinations of chirality-flip structures which are equivalent to shift-invariant ALP couplings (plus anomalous gauge couplings) are identified in appendix B.2, see also ref. [43].

Trading anomalous operators by fermionic ones. Anomalous gauge couplings are intrinsically non shift-invariant. Chirality-flip structures will thus necessarily appear if anomalous operators were to be traded by purely fermionic ones. It is shown in appendix B.3 how each of the operators $\mathbf{O}_{\tilde{B}}$, $\mathbf{O}_{\tilde{W}}$ and $\mathbf{O}_{\tilde{G}}$ can be traded by a combination of purely fermionic structures which necessarily includes chirality-flip terms.

[4] This requires the coefficients of the chirality-flip operators to be proportional to the corresponding Yukawa matrices.

JHEP11(2021)168

Let us consider here as illustration the situation when only one anomalous gauge coupling is removed from the complete Lagrangian. Eq. (2.12) showed that $\mathbf{O}_{\tilde{W}}$ can be removed without introducing any chirality-flip operator if $\mathbf{O}_{\tilde{B}}$ is maintained, and viceversa, as a consequence of $B+L$ being an anomalous global symmetry of the SM. For instance, in our basis in table 1 it would suffice to replace either $\mathbf{O}_{\tilde{W}}$ or $\mathbf{O}_{\tilde{B}}$ by a trace of chirality-conserving fermionic structures defined in eqs. (2.3) and (2.4). In contrast, the combination of $\mathbf{O}_{\tilde{B}}$ and $\mathbf{O}_{\tilde{W}}$ with opposite sign to that in eq. (2.12) does not correspond to an anomalous current, and thus requires chirality-flip structures when traded by fermionic currents, namely

$$\begin{aligned}\frac{n_g}{16\pi^2}\left(g'^2\mathbf{O}_{\tilde{B}}+g^2\mathbf{O}_{\tilde{W}}\right) &= 2\,\mathrm{Tr}\,\mathbf{O}_L - 2(Y_e\mathbf{O}_{e\Phi}+\mathrm{h.c.})\\ &= \frac{2}{3}\,\mathrm{Tr}\left(\mathbf{O}_Q-2\mathbf{O}_u+4\mathbf{O}_d\right)+2\left(Y_d\mathbf{O}_{d\Phi}-Y_u\mathbf{O}_{u\Phi}+\mathrm{h.c.}\right)\,. \end{aligned} \tag{2.20}$$

Analogously, and as expected from the non-perturbative nature of $a\,G_{\mu\nu}\tilde{G^{\mu\nu}}$ and the fact that this term may induce a potential for the ALP field,[5] it is not possible to remove $\mathbf{O}_{\tilde{G}}$ altogether in favour of another anomalous coupling plus purely chirality-conserving (and thus shift-invariant) terms. For instance, some alternative equivalences of interest are

$$\mathbf{O}_{\tilde{G}} = -\frac{32\pi^2}{n_g g_s^2}\left[\mathrm{Tr}\,\mathbf{O}_d+(Y_d\mathbf{O}_{d\Phi}+\mathrm{h.c.})\right]-\frac{2}{3}\frac{g'^2}{g_s^2}\mathbf{O}_{\tilde{B}}\,, \tag{2.21}$$

$$\mathbf{O}_{\tilde{G}} = -\frac{32\pi^2}{n_g g_s^2}\left[\mathrm{Tr}\,\mathbf{O}_u+(Y_u\mathbf{O}_{u\Phi}+\mathrm{h.c.})\right]-\frac{8}{3}\frac{g'^2}{g_s^2}\mathbf{O}_{\tilde{B}}\,, \tag{2.22}$$

$$\mathbf{O}_{\tilde{G}} = \frac{32\pi^2}{3n_g g_s^2}\left[\mathrm{Tr}\left(\mathbf{O}_u-4\mathbf{O}_d\right)+(Y_u\mathbf{O}_{u\Phi}-4Y_d\mathbf{O}_{d\Phi}+\mathrm{h.c.})\right]\,. \tag{2.23}$$

An interesting question in the chirality-flip vs. chirality conserving arena is that of the one-loop ($\mathcal{O}(\alpha_X)$) impact of fermionic operators on anomalous ALP-couplings. The results allow to understand which combinations of chirality-flip operators discussed are exactly equivalent to purely derivative fermionic ones. That this happens at all could seem paradoxical from the quantum loop perspective, as chirality-flip operators will exclusively induce at one-loop corrections proportional to fermion masses squared, while derivative chirality-conserving operators contribute in addition a finite and mass independent term, which is the contribution from the chiral anomaly of the fermionic currents. Nevertheless, the relations above among both type of fermionic structures — see also appendix B.2 — are precisely such that the matching holds at any order. An illustrative example of the one-loop matching of chirality flip and chirality conserving contributions can be found at the end of section B.1.

2.3 Purely bosonic basis

The addition of an ALP to the SM interactions is an enlargement of the scalar sector of the low-energy theory. In some contexts, it may be pertinent to focus exclusively on the bosonic Lagrangian.

[5] In fact, it is well-known that $\mathbf{O}_{\tilde{G}}$ generates a scalar potential for the QCD axion [3, 4].

JHEP11(2021)168

$\mathbf{O}_{\tilde{W}} = -\frac{a}{f_a} W^{\alpha}_{\mu\nu} \tilde{W}^{\alpha\mu\nu}$	$\mathbf{O}_{\tilde{B}} = -\frac{a}{f_a} B_{\mu\nu} \tilde{B}^{\mu\nu}$	$\mathbf{O}_{\tilde{G}} = -\frac{a}{f_a} G^{a}_{\mu\nu} \tilde{G}^{a\mu\nu}$
$\mathbf{O}_{a\Phi} = \frac{\partial^\mu a}{f_a} \left(\Phi^\dagger i \overleftrightarrow{D_\mu} \Phi\right)$		

Table 2. Purely bosonic operator basis.

The most general and complete *purely bosonic* effective ALP Lagrangian describing CP-even couplings at NLO is extraordinarily simple. It contains just four linearly independent effective operators [17, 46, 47, 51]:

$$\mathscr{L}_a^{\text{bosonic}} = c_{\tilde{W}} \mathbf{O}_{\tilde{W}} + c_{\tilde{B}} \mathbf{O}_{\tilde{B}} + c_{\tilde{G}} \mathbf{O}_{\tilde{G}} + c_{a\Phi} \mathbf{O}_{a\Phi} \,, \tag{2.24}$$

where $c_{a\Phi}$ is a real constant and

$$\mathbf{O}_{a\Phi} \equiv \frac{\partial^\mu a}{f_a} \left(\Phi^\dagger i \overleftrightarrow{D_\mu} \Phi\right) \,, \tag{2.25}$$

being $\Phi^\dagger i \overleftrightarrow{D}_\mu \Phi = i\Phi^\dagger (D_\mu \Phi) - i (D_\mu \Phi^\dagger)\Phi$. The purely bosonic basis is summarized in table 2. The operator $\mathbf{O}_{a\Phi}$ is equivalent to a precise linear combination of the fermionic operators in table 1:

$$\mathbf{O}_{a\Phi} = \text{Tr}\left(\mathbf{O}_e + \mathbf{O}_d - \mathbf{O}_u\right) \,, \tag{2.26}$$

and it would have thus been redundant to add it to the set in table 1. The direct impact of $\mathbf{O}_{a\Phi}$ is to induce a kinetic mixing between a and the would-be Goldstone boson eaten by the Z boson. This mixing is cumbersome to work with, and it can be removed via a Higgs field redefinition of the form $\Phi \to \Phi\, e^{i c_{a\Phi} a/f_a}$ [17, 46, 52], which is equivalent to the application of the Higgs EOM. This delivers chirality-flip operators that can next be turned via the fermionic EOM into the chirality-conserving combination in eq. (2.26). Note that no trace of anomalous gauge couplings remains in the final expression eq. (2.26) in spite of the fermion rotations involved, as expected for a purely bosonic ALP interaction. A comprehensive discussion of how the anomalous terms that *a priori* could be induced by fermion rotations cancel each other for this operator can be found in appendix B.1.

Finally, note that $\mathbf{O}_{a\Phi}$ could be kept as one of the operators of a complete and non-redundant basis at the expense of some other coupling. Eq. (2.26) shows that it could be included at the price of omitting any of the diagonal operators of the right-handed set $\{\mathbf{O}_e, \mathbf{O}_d, \mathbf{O}_u\}$. Another possibility — among many — is for $\mathbf{O}_{a\Phi}$ to replace certain flavour-diagonal fermionic couplings of the left-handed set $\{\mathbf{O}_Q, \mathbf{O}_L\}$, as indicated by the identity (see appendix B.1)

$$\mathbf{O}_{a\Phi} = -\,\text{Tr}\left(\mathbf{O}_L + \mathbf{O}_Q + 2\mathbf{O}_u\right) + \frac{1}{8\pi^2}\left(g^2 \mathbf{O}_{\tilde{W}} - g'^2 \mathbf{O}_{\tilde{B}}\right) n_g \,. \tag{2.27}$$

This equation also suggests yet another alternative: to include $\mathbf{O}_{a\Phi}$ in the complete and non-redundant basis at the expense of omitting either $\mathbf{O}_{\tilde{W}}$ or $\mathbf{O}_{\tilde{B}}$. The exact expression of the degrees of freedom which may be replaced by $\mathbf{O}_{a\Phi}$ is to be analyzed for each possible basis.

JHEP11(2021)168

2.4 Phenomenological parameters

The ALP EFT presented above in terms of $\mathrm{SU}(3)_c \times \mathrm{SU}(2)_L \times \mathrm{U}(1)_Y$ gauge invariant operators leads to multiple experimental signals. The ultimate goal is to detect or constraint from data the set of fundamental independent variables

$$\{c_{\tilde{W}}\,, c_{\tilde{B}}\,, c_{\tilde{G}}\,, \mathbf{c}_{\mathrm{f}}\}\,, \tag{2.28}$$

which are to be treated as free Lagrangian parameters.

The three anomalous gauge couplings, $\mathbf{O}_{\tilde{G}}$, $\mathbf{O}_{\tilde{W}}$ and $\mathbf{O}_{\tilde{B}}$, induce five distinct physical interactions with gluons, photons, W and Z bosons, which are customarily codified as

$$\mathscr{L}_a \supset -\frac{1}{4} g_{agg}\, a\, G_{\mu\nu}\widetilde{G}^{\mu\nu} - \frac{1}{4} g_{a\gamma\gamma} a F_{\mu\nu}\tilde{F}^{\mu\nu} - \frac{1}{4} g_{a\gamma Z} a F_{\mu\nu}\tilde{Z}^{\mu\nu} - \frac{1}{4} g_{aZZ} a Z_{\mu\nu}\tilde{Z}^{\mu\nu} - \frac{1}{2} g_{aWW} a W^{+}_{\mu\nu}\tilde{W}^{-\mu\nu}\,, \tag{2.29}$$

where

$$g_{agg} \equiv \frac{4}{f_a}\, c_{\tilde{G}}\,, \qquad g_{a\gamma\gamma} \equiv \frac{4}{f_a}\left(s_w^2\, c_{\tilde{W}} + c_w^2\, c_{\tilde{B}}\right), \tag{2.30}$$

$$g_{aWW} \equiv \frac{4}{f_a}\, c_{\tilde{W}}\,, \qquad g_{aZZ} \equiv \frac{4}{f_a}\left(c_w^2\, c_{\tilde{W}} + s_w^2\, c_{\tilde{B}}\right), \tag{2.31}$$

$$g_{a\gamma Z} \equiv \frac{8}{f_a}\, s_w c_w (c_{\tilde{W}} - c_{\tilde{B}})\,, \tag{2.32}$$

where s_w and c_w denote respectively the sine and cosine of the Weinberg mixing angle, given at tree-level by

$$c_w \equiv \frac{M_W}{M_Z}\,. \tag{2.33}$$

It follows that the two independent electroweak anomalous couplings may source four independent measurable quantities,

$$\{c_{\tilde{W}}, c_{\tilde{B}}\} \longrightarrow \{g_{a\gamma\gamma}, g_{aWW}, g_{aZZ}, g_{a\gamma Z}\}\,, \tag{2.34}$$

a fact that allows to overconstrain the electroweak gauge sector of the parameter space. In other words, electroweak gauge invariance imposes at tree-level the constraints

$$\begin{aligned} g_{aWW} &= g_{a\gamma\gamma} + \frac{c_w}{2s_w} g_{a\gamma Z}\,, \\ g_{aZZ} &= g_{a\gamma\gamma} + \frac{c_w^2 - s_w^2}{2c_w s_w} g_{a\gamma Z}\,. \end{aligned} \tag{2.35}$$

From the experimental point of view these two expressions are quite useful, since they can be used to set constraints on one coupling based on the constraints on other couplings, barring fine-tuned cancellations. For example, $g_{a\gamma\gamma}$ is strongly constrained from multiple experiments, while g_{aZZ} is harder to measure directly. Nevertheless, applying eq. (2.35) one can translate the constraints on $g_{a\gamma\gamma}$ into constraints on g_{aZZ} that are stronger than those extracted from direct searches of the latter. This approach has already led to cross-relations among different measurements, resulting in a noticeable reduction of parameter space allowed by present data [14, 53]. It is thus relevant from the phenomenological point of

JHEP11(2021)168

view to determine how the relations in eq. (2.35) are modified when one-loop corrections are taken into account. We will address this task in section 5.

It is also convenient for later use to consider the following combination of the couplings in eq. (2.31) and (2.32), which corresponds to the $aB_{\mu\nu}\tilde{B}_{\mu\nu}$ coupling:

$$g_{aBB} \equiv \frac{4}{f_a}\, c_{\tilde{B}} = g_{aWW} - \frac{1}{2 s_w c_w} g_{a\gamma Z}\,. \tag{2.36}$$

Furthermore, in the cases in which the hatted basis of gauge invariant operators in eq. (2.15) is preferred as description, the corresponding phenomenological parameters $\hat{g}_{iXX}$ follow trivially form the substitution $\{c_i \longrightarrow \hat{c}_i\,, g_{iXX} \longrightarrow \hat{g}_{iXX}\}$ in eqs. (2.30)–(2.32), i.e.

$$\hat{g}_{aGG} \equiv \frac{4}{f_a}\,\hat{c}_{\tilde{G}}\,, \qquad \hat{g}_{aWW} \equiv \frac{4}{f_a}\,\hat{c}_{\tilde{W}}\,, \qquad \hat{g}_{aBB} \equiv \frac{4}{f_a}\,\hat{c}_{\tilde{B}}\,, \tag{2.37}$$

with the relation between c_i and $\hat{c}_i$ as discussed in eq. (2.15).

In all cases, the data on fermion EFT couplings can be directly expressed in terms of the EFT Lagrangian parameter matrix $\mathbf{c}_{\rm f}$ corresponding to the complete basis in table 1. For practical purposes, a simplified notation can be useful when considering flavour-diagonal transitions. The latter are proportional only to the axial part of the fermionic derivative couplings, i.e. the coupling has Lorentz structure R−L. For instance, a general — basis independent — definition of phenomenological flavour-diagonal couplings can be written as

$$c_u \equiv (\mathbf{c}_u - \mathbf{c}_Q)^{11}\,, \qquad c_c \equiv (\mathbf{c}_u - \mathbf{c}_Q)^{22}\,, \qquad c_t \equiv (\mathbf{c}_u - \mathbf{c}_Q)^{33}\,, \tag{2.38}$$

$$c_d \equiv (\mathbf{c}_d - U^\dagger \mathbf{c}_Q U)^{11}\,, \qquad c_s \equiv (\mathbf{c}_d - U^\dagger \mathbf{c}_Q U)^{22}\,, \qquad c_b \equiv (\mathbf{c}_d - U^\dagger \mathbf{c}_Q U)^{33}\,, \tag{2.39}$$

$$c_e \equiv (\mathbf{c}_e - \mathbf{c}_L)^{11}\,, \qquad c_\mu \equiv (\mathbf{c}_e - \mathbf{c}_L)^{22}\,, \qquad c_\tau \equiv (\mathbf{c}_e - \mathbf{c}_L)^{33}\,, \tag{2.40}$$

where $U = U_{\rm CKM}$ is the CKM mixing matrix. This notation simplifies further in the particular complete basis in table 1 in which *de facto* $(\mathbf{c}_Q)^{11} = 0$ and $(\mathbf{c}_L)^{i=j} = 0$, e.g.

$$c_u = (\mathbf{c}_u)^{11}\,, \quad c_e = (\mathbf{c}_e)^{11}\,, \quad c_\mu = (\mathbf{c}_e)^{22}\,, \quad c_\tau = (\mathbf{c}_e)^{33}\,. \tag{2.41}$$

3 Non-renormalization theorems

The renormalization group (RG) properties of the ALP effective coupling have received considerable attention lately.

Above the electroweak scale. CP-odd anomalous gauge couplings within the SM, i.e. Lagrangian terms of the generic form $\alpha_X X_{\mu\nu}\tilde{X}^{\mu\nu}$ where $X_{\mu\nu}$ denotes a generic gauge field strength and α_X its fine structure coupling, are not multiplicatively renormalized at any order in perturbation theory. The reason is their topological character, which ensures anomaly matching conditions [54]. Indeed the combinations $\alpha_1/2\pi B\tilde{B}$, $\alpha_2/2\pi\, W\tilde{W}$ and $\alpha_s/2\pi\, G\tilde{G}$ appear in the Lagrangian multiplied by "θ" angles which are periodic variables with periodicity 2π, and cannot thus be multiplicatively renormalized [55, 56]. This can be inferred from the fact that a chiral rotation induces a contribution to the divergence of the axial current J_μ precisely of the form

$$\partial_\mu J_\mu \supset \frac{\alpha_X}{2\pi} X_{\mu\nu}\tilde{X}^{\mu\nu}\,. \tag{3.1}$$

JHEP11(2021)168

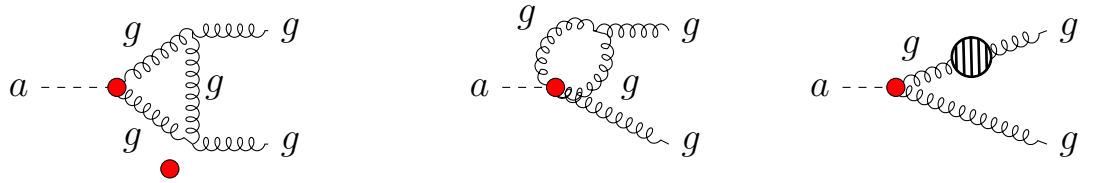

Figure 1. One-loop diagrams which renormalize the effective $a\,G\tilde{G}$ interaction. The blob in the last diagram stands for one-loop gluon and quark contributions (a similar contribution holds for the other external gauge leg).

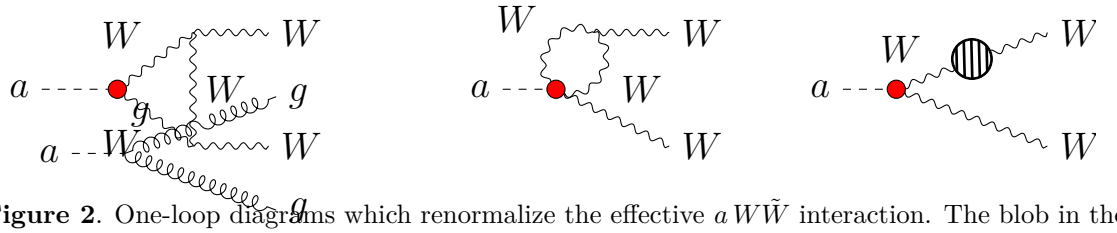

Figure 2. One-loop diagrams which renormalize the effective $a\,W\tilde{W}$ interaction. The blob in the last diagram stands for one-loop W and $\mathrm{SU}(2)_L$ charged fermion contributions (a similar contribution holds for the other external gauge leg).

Now, when considering ALP-SM anomalous couplings, the ratio a/f_a plays the role of an effective angle. The non-renormalization theorems thus apply as well to ALP couplings of the form $c_X/(2\pi f)\,a\,X_{\mu\nu}\tilde{X}^{\mu\nu}$, where $2\pi f$ is the periodicity of a [57]. In consequence, no UV divergent terms can result from corrections to the combinations $\alpha_1/2\pi\,\mathbf{O}_{\tilde{W}}$, $\alpha_2/2\pi\,\mathbf{O}_{\tilde{B}}$ and $\alpha_s/2\pi\,\mathbf{O}_{\tilde{G}}$. In other words, in the *hat basis* of effective ALP operators — see eqs. (2.14) and (2.15) — the β functions for the electroweak anomalous couplings must vanish,

$$\beta_{\hat{c}_{\tilde{B}}} = \frac{\mathrm{d}}{\mathrm{d}\log\mu}\hat{c}_{\tilde{B}} = 0\,, \qquad \beta_{\hat{c}_{\tilde{W}}} = \frac{\mathrm{d}}{\mathrm{d}\log\mu}\hat{c}_{\tilde{W}} = 0\,, \qquad \beta_{\hat{c}_{\tilde{G}}} = \frac{\mathrm{d}}{\mathrm{d}\log\mu}\hat{c}_{\tilde{G}} = 0\,. \tag{3.2}$$

It is easy to check these results at one-loop, from the contributions of the Feynman diagrams in figures 1, 2 and 3. Correspondingly, the RG evolution of the $\{c_{\tilde{G}}, c_{\tilde{W}}, c_{\tilde{B}}\}$ coefficients for the basis in table 1 reflects that of the α_i couplings, see eq. (2.15),

$$\beta_{c_{\tilde{B}}} = \frac{\mathrm{d}}{\mathrm{d}\log\mu}c_{\tilde{B}} = \beta_{\alpha_1} = \left(\frac{1}{12} + \frac{10}{9}n_g\right)\frac{\alpha_1}{\pi}\,c_{\tilde{B}} = \frac{41}{12}\frac{\alpha_1}{\pi}\,c_{\tilde{B}}\,, \tag{3.3}$$

$$\beta_{c_{\tilde{W}}} = \frac{\mathrm{d}}{\mathrm{d}\log\mu}c_{\tilde{W}} = \beta_{\alpha_2} = -\left(\frac{43}{12} - \frac{2}{3}n_g\right)\frac{\alpha_2}{\pi}\,c_{\tilde{W}} = -\frac{19}{12}\frac{\alpha_2}{\pi}\,c_{\tilde{W}}\,, \tag{3.4}$$

$$\beta_{c_{\tilde{G}}} = \frac{\mathrm{d}}{\mathrm{d}\log\mu}c_{\tilde{G}} = \beta_{\alpha_s} = -\left(\frac{11}{2} - \frac{2}{3}n_g\right)\frac{\alpha_s}{\pi}\,c_{\tilde{G}} = -\frac{7}{2}\frac{\alpha_s}{\pi}\,c_{\tilde{G}}\,, \tag{3.5}$$

where n_g is the number of generations of fermions, and $n_g = 3$ has been taken on the last equalities of these equations. This results had been previously derived in ref. [43].

The beta functions for the ALP-fermion couplings have been previously obtained as well, using a variety of fermionic bases, and we refer the reader to the corresponding literature [43, 44, 49]. The beta function for the bosonic operator $\mathbf{O}_{a\Phi}$ can be found In ref. [49], in a redundant basis which contemplates all possible operators.

JHEP11(2021)168

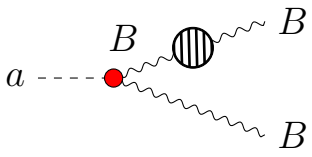

Figure 3. One-loop diagrams which renormalize the effective $a\,B\tilde{B}$ interaction. The blob in the last diagram stands for one-loop fermion contributions (a similar contribution holds for the other external gauge leg).

4 Complete one-loop contributions to ALP couplings

We present here the one-loop contributions to the phenomenological ALP couplings, including all finite corrections. The ALP field will be left off-shell (which is of practical interest for collider and other searches away from the ALP resonance, besides adapting trivially to ALP on-shell searches), while the external SM fields will be considered on-shell. For channels with external fermions, we only provide corrections to the flavour diagonal ones. Furthermore, CKM mixing is disregarded in the loop corrections to all couplings, which means the framework depicted in section 2.2 for CKM$=\mathbb{1}$. That is, the complete and non-redundant basis corresponds to that in table 1 with the proviso in eq. (2.18).

The operator basis used is that defined in eq. (2.5) and table 1. We will trade the set of two linearly independent electroweak anomalous couplings $\{c_{\tilde{W}}, c_{\tilde{B}}\}$ for the set of four phenomenological couplings $\{g_{a\gamma\gamma}, g_{aWW}, g_{aZZ}, g_{a\gamma Z}\}$ in eqs. (2.29)–(2.32), which are in consequence linked by gauge invariance (as shown at tree-level in eq. (2.35)). The latter means that the final one-loop results for a given effective electroweak coupling g^{eff}_{aXX} can be expressed in terms of just two tree-level phenomenological couplings of choice, e.g. in terms of the set $\{g_{aXX}, g_{aWW}\}$. These can be easily transcribed back in terms of the set $\{c_{\tilde{W}}, c_{\tilde{B}}\}$ if wished, using eqs. (2.30)–(2.32) and (2.36).

All computations have been carried out in the covariant R_ξ-gauge, with the help of `Mathematica` packages `FeynCalc` and `Package-X` [58, 59]. The individual one-loop diagrams are in general ξ-dependent. The same applies to each of the one-loop corrected amplitudes in the ensemble $\{g^{\text{eff}}_{a\gamma\gamma}, g^{\text{eff}}_{aWW}, g^{\text{eff}}_{aZZ}, g^{\text{eff}}_{a\gamma Z}\}$ resulting from directly inserting all possible tree-level phenomenological couplings $\{g_{a\gamma\gamma}, g_{aWW}, g_{aZZ}, g_{a\gamma Z}\}$. Their ξ-independence (with external SM fields on-shell) becomes explicit only when the gauge invariance relations in eq. (2.35) are applied to the electroweak radiative results, so as to reduce the parameter space. Details of ξ-dependent intermediate steps are provided in NotebookArchive.

Renormalization and measurable parameters. We will use as renormalization framework of the electroweak sector the scheme in which its four linearly independent parameters (other than fermion Yukawa couplings), i.e. the SU(2)$_L$ and U(1)$_Y$ coupling constants (g and g' respectively), the Higgs vev v and Higgs self-coupling denoted here $\tilde{\lambda}$, are to be traded by precisely measured input parameters as follows

$$\{g, g', v, \tilde{\lambda}\} \longrightarrow \{\alpha_{em}, M_Z, M_W, M_H\}|_{exp} \tag{4.1}$$

JHEP11(2021)168

where the experimental value of α_{em} is extracted from Thompson scattering (e.g. $Q^2 = 0$) and the values of M_W, M_Z and M_H are determined from their resonant peaks.[6] The ALP effective operators do not contribute to these observables at one-loop and $\mathcal{O}(1/f_a)$. In consequence, the relation between the Lagrangian parameters and those four observables is not modified with respect to the SM case. In other words, at tree-level it holds that

$$\begin{aligned} \alpha_{em} &= \frac{e^2}{4\pi} = \frac{g^2 g'^2}{4\pi(g^2+g'^2)} = \frac{\alpha_1\alpha_2}{\alpha_1+\alpha_2}\,, & M_W &= \frac{1}{2}\,gv\,, \\ M_Z &= \frac{1}{2}\sqrt{g^2+g'^2}v\,, & M_H^2 &= \tilde{\lambda}v^2\,, \end{aligned} \tag{4.2}$$

a set of relations that can be easily inverted. All other SM observable quantities to be predicted can be expressed in terms of those four input observables plus fermion masses. While the fermion masses of leptons have a direct physical meaning which allows simple renormalization procedures, in QCD due to confinement such a natural scale does not exist. Alike considerations apply to the QCD coupling strength α_s. The renormalization scale and scheme must be chosen with other criteria, based on simplicity and convergence. There are many alternative ways proposed to deal with the infrarred behaviour of the QCD coupling constant, that is, on how to extract from observables the strength of α_s at a variety of scales, see for instance ref. [60] and section 4.2.

One-loop corrections. Let us briefly rename with a bar the one-loop renormalized parameters whose values are to be identified with the experimentally inputs mentioned above, i.e. $\{\overline{\alpha}_{em}, \overline{M}_Z, \overline{M}_W, \overline{M}_H\}$. Their relation with the (unbarred) tree-level quantities can be written as

$$\begin{aligned} \overline{\alpha}_{em} &= \alpha_{em} + \delta\alpha_{em}\,, & \overline{M}_Z^2 &= M_Z^2 + \delta M_Z^2\,, \\ \overline{M}_W^2 &= M_W^2 + \delta M_W^2\,, & \overline{M}_H^2 &= M_H^2 + \delta M_H^2\,. \end{aligned} \tag{4.3}$$

While the symbol δ is used here for the corrections involved in the definition of the input parameters, we will use the symbol Δ for the physical predictions, that is, for the measurable deviations with respect to the SM, that follow for any other observable. Of particular practical interest is the Weinberg angle, defined at tree-level in eq. (2.33). Let us define a ratio $\bar{c}_w$ as

$$\bar{c}_w \equiv \frac{\overline{M}_W}{\overline{M}_Z} = c_w\left(1 + \frac{\Delta c_w}{c_w}\right)\,, \tag{4.4}$$

where

$$\frac{\Delta c_w}{c_w} = -\frac{1}{2}\left(\frac{\delta M_Z^2}{M_Z^2} - \frac{\delta M_W^2}{M_W^2}\right)\,, \tag{4.5}$$

and $\delta M^2_{V=Z,W}$ are computed in terms of the Z and W transverse self-energies as $\delta M_V^2 = \Sigma_V(q^2 = M_V^2)$, see whose exact expressions can be found in appendix D. The tree-level

[6] $\alpha_{em} = 1/137.035999139(31)$ at $Q^2 = 0$, $M_Z = 91.1876(21)\,\text{GeV}$, $M_W = 80.379(12)$ and $M_H = 125.25(17)\,\text{GeV}$.

JHEP11(2021)168

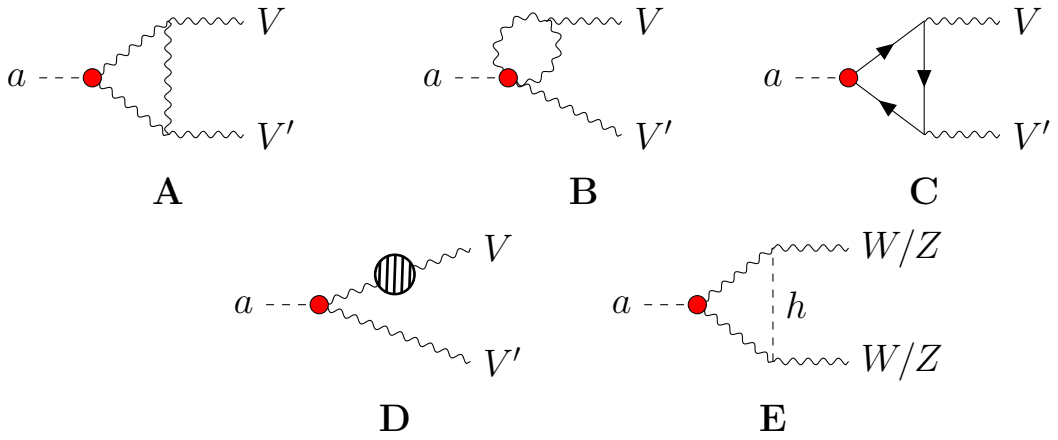

Figure 4. One-loop diagrams contributing to g_{agg}, $g_{a\gamma\gamma}$, $g_{a\gamma Z}$, g_{aZZ} and g_{aWW} at one-loop (the corresponding diagrams with Goldstone bosons and the diagrams exchanging the gauge boson legs are left implicit), where V and V' are either a gluon, a photon, a Z boson or a W boson. The last diagram only corrects insertions of the g_{aZZ} and g_{aWW} couplings.

variables $\{g_{a\gamma\gamma}, g_{a\gamma Z}, g_{aZZ}\}$ can now be written as a combination of the set $\{c_{\tilde{B}}, c_{\tilde{W}}\}$ and physical boson masses,

$$g_{a\gamma\gamma} = \frac{4}{f_a}(c_w^2 c_{\tilde{B}} + s_w^2 c_{\tilde{W}}) = \frac{4}{f_a}(\bar{c}_w^2 c_{\tilde{B}} + \bar{s}_w^2 c_{\tilde{W}}) + \frac{8}{f_a}\bar{c}_w^2(c_{\tilde{W}} - c_{\tilde{B}})\frac{\Delta c_w}{c_w}\,, \tag{4.6}$$

$$g_{a\gamma Z} = \frac{8}{f_a} c_w s_w (c_{\tilde{W}} - c_{\tilde{B}}) = \frac{8}{f_a}\bar{c}_w \bar{s}_w (c_{\tilde{W}} - c_{\tilde{B}})\left(1 + \frac{\bar{c}_w^2 - \bar{s}_w^2}{\bar{s}_w^2}\frac{\Delta c_w}{c_w}\right), \tag{4.7}$$

$$g_{aZZ} = \frac{4}{f_a}(s_w^2 c_{\tilde{B}} + c_w^2 c_{\tilde{W}}) = \frac{4}{f_a}(\bar{s}_w^2 c_{\tilde{B}} + \bar{c}_w^2 c_{\tilde{W}}) - \frac{8}{f_a}\bar{c}_w^2(c_{\tilde{W}} - c_{\tilde{B}})\frac{\Delta c_w}{c_w}\,. \tag{4.8}$$

We will denote below by $\{g_{agg}^{\rm eff}, g_{a\gamma\gamma}^{\rm eff}, g_{a\gamma Z}^{\rm eff}, g_{aZZ}^{\rm eff}, g_{aWW}^{\rm eff}, c_{\rm f}^{\rm eff}\}$ the physical amplitudes computed at one loop, which are to be compared with data. They will be expressed in terms of the tree-level variables $\{g_{agg}, g_{a\gamma\gamma}, g_{a\gamma Z}, g_{aZZ}, g_{aWW}, c_{\rm f}\}$ and SM quantities. The Δc_w corrections shown above are to be taken into account whenever a fit to the fundamental electroweak ALP variables $\{c_{\tilde{B}}, c_{\tilde{W}}\}$ is attempted from data, i.e. the equalities to the right in eqs. (4.6)–(4.8) must be used in the transcription. Aside from taking into account this proviso, the bars will be omitted from now on in all expressions.

4.1 ALP anomalous coupling to photons

The Feynman diagrams which induce one loop corrections to the effective anomalous ALP coupling to photons, $g_{a\gamma\gamma}$, are depicted in figure 4 **A**, **B**, **C** and **D**, with $V = V' = \gamma$ (which implies that W is the gauge boson running in the closed gauge loops, while the virtual gauge boson coupled to a in diagram **D** is either a photon or a Z boson). Among the four effective electroweak couplings, insertions of the set $\{g_{a\gamma\gamma}, g_{aWW}, g_{a\gamma Z}\}$ contribute to the one-loop corrected effective coupling $g_{a\gamma\gamma}^{\rm eff}$. Using the gauge-invariance relations eq. (2.35), we choose to express the final result in terms of just two of them, e.g. the set $\{g_{a\gamma\gamma}, g_{aWW}\}$,

JHEP11(2021)168

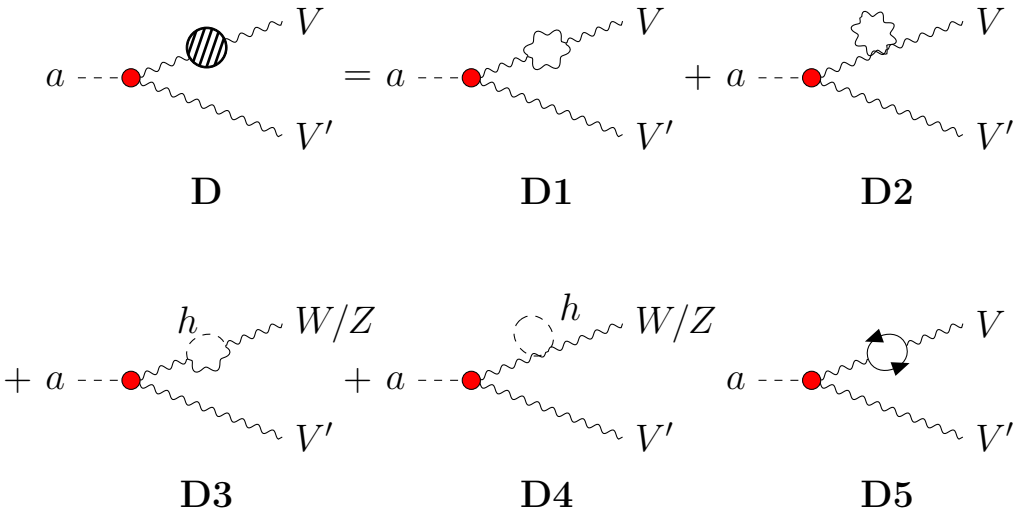

Figure 5. One-loop diagrams contributing to the correction to the external gauge boson legs. Diagrams with Goldstone bosons and Higgs tadpole diagrams are included. Notice that diagrams **D3** and **D4** are only present for a Z or W boson external legs.

plus fermionic couplings:

$$g^{\text{eff}}_{a\gamma\gamma} = g_{a\gamma\gamma}\left\{1+\frac{\alpha_{em}}{6\pi}A^{Z/\gamma\to\gamma}\right\}+\frac{2\alpha_{em}}{\pi}g_{aWW}B_2\left(\frac{4M_W^2}{p^2}\right)-\frac{\alpha_{em}}{\pi f_a}\sum_{\text{f}}c_{\text{f}}\,Q_{\text{f}}^2N_CB_1\left(\frac{4m_{\text{f}}^2}{p^2}\right), \tag{4.9}$$

where here and all through the rest of the paper (unless stated otherwise) the sum over fermions denotes all possible individual fermion flavours, $\text{f} = u, c, t, d, s, b, e, \mu, \tau$, and p denotes the 4-momentum of the ALP, N_C is the number of colours for a given fermion f (i.e. 3 for quarks and 1 for leptons), Q_{f} is its electric charge. The functions B_1 and B_2 have already been defined in ref. [14] as:

$$B_1(\tau)=1-\tau f^2(\tau)\,,\quad B_2(\tau)=1-(\tau-1)f^2(\tau)\,,\quad \text{with } f(\tau)=\begin{cases}\arcsin\frac{1}{\sqrt{\tau}} & \text{for } \tau\geq 1\\ \frac{\pi}{2}+\frac{i}{2}\ln\frac{1+\sqrt{1-\tau}}{1-\sqrt{1-\tau}} & \text{for } \tau<1\end{cases}. \tag{4.10}$$

The function $A^{Z/\gamma\to\gamma}$ encodes pure leg radiative corrections stemming from diagramas **D1**, **D2** and **D5** in figure 5 (with the virtual gauge boson attached to a being either a photon or a Z boson, while the W boson runs in the closed gauge loops),

$$A^{Z/\gamma\to\gamma}=1-2\sum_{\text{f}}Q_{\text{f}}^2N_C\log\left(\frac{\Lambda^2}{m_{\text{f}}^2}\right)+\frac{21}{2}\log\left(\frac{\Lambda^2}{M_W^2}\right). \tag{4.11}$$

This computation has been carried out in dimensional regularization, trading next the $1/\epsilon$ UV-divergent terms for an energy cutoff Λ via the $\overline{\text{MS}}$ prescription $1/\epsilon-\gamma_E+\log\left(4\pi\mu^2\right)\to\log\Lambda^2$. This leg correction correspond to the SM one-loop redefinition of α_{em}. Indeed, were the hatted basis of gauge operators to be used — in which α_1 and α_2 enter explicitly in the

JHEP11(2021)168

operators definition (see eqs. (2.15) and (2.37)), the one-loop corrections would read

$$\hat{g}^{\text{eff}}_{a\gamma\gamma} = \hat{g}_{a\gamma\gamma} + \frac{2\alpha_{em}}{\pi s_w^2}\hat{g}_{aWW} B_2\left(\frac{4M_W^2}{p^2}\right) - \frac{4}{f_a}\sum_{\text{f}} c_{\text{f}}\, Q_{\text{f}}^2 N_C B_1\left(\frac{4m_{\text{f}}^2}{p^2}\right), \tag{4.12}$$

a result which in the on-shell ALP limit reduces straightforwardly to that in ref. [14].

Eq. (4.9) could be rewritten if wished in terms of $\{c_{\tilde{B}}, c_{\tilde{W}}\}$ (and c_{f}) applying eq. (2.31) for g_{aWW} and the last equality in eq. (4.6) for $g_{a\gamma\gamma}$ (and analogously for eq. (4.12)).

For an on-shell ALP ($p^2 = m_a^2$) the one-loop corrected decay width is simply given by

$$\Gamma(a \to \gamma\gamma) = \frac{m_a^3 |g^{\text{eff}}_{a\gamma\gamma}|^2}{64\pi}, \tag{4.13}$$

or the equivalent expression in the hat basis with the replacement $g^{\text{eff}}_{a\gamma\gamma} \to \alpha_{em}/4\pi\, \hat{g}^{\text{eff}}_{a\gamma\gamma}$. We show next some limits of the exact results above for the functions B_1 and B_2, for an off-shell ALP, which are of interest in particular experimental contexts.

4.1.1 $g^{\text{eff}}_{a\gamma\gamma}$ for high, intermediate and low ALP p^2

- For $p^2 \to \infty$ ($p^2 \gg (m_{\text{f}}^2, M_Z^2, M_W^2)$), only the anomaly contribution remains from fermion coupling insertions. These contributions and those from g_{aWW} insertions reduce to, respectively,

$$B_1 = 1\,, \qquad B_2 = -\frac{1}{4}\left(\log\left(\frac{M_W^2}{p^2}\right) + i\pi\right)^2. \tag{4.14}$$

- For intermediate values of p^2 ($m_{\text{f}}^2 \ll p^2 \ll (M_Z^2, M_W^2) \ll m_t^2$), i.e. smaller than the top and all gauge bosons masses but larger than all other fermion masses, it results

$$B_1 = \begin{cases} 1\,, & \text{for light fermion insertions: } m_{\text{f}}^2 \ll p^2 \ll M_Z^2\,, \\ 0\,, & \text{for top quark insertion: } p^2 \ll M_Z^2 \ll m_t^2\,, \end{cases} \qquad B_2 = 0\,. \tag{4.15}$$

- For $p^2 \to 0$, i.e. smaller than all fermion masses, both functions vanish $B_1 = B_2 = 0$.

4.2 ALP anomalous coupling to gluons

The Feynman diagrams which induce one loop corrections to the effective anomalous coupling of an ALP to two gluons, g_{agg}, are depicted by diagrams **A**, **B**, **C** and **D** of figure 4 with $V = V' = g$ (which implies that all virtual gauge bosons are also gluons). Only the ALP-quark couplings c_{f}, and g_{agg} itself, can contribute at one-loop to the g^{eff}_{gaa} amplitude,

$$g^{\text{eff}}_{agg} = g_{agg}\left\{1 + \frac{\alpha_s}{12\pi}\, G^{gg}\right\} - \frac{\alpha_s}{2\pi f_a}\sum_{\substack{\text{f}=u,c,t,\\ d,s,b}} c_{\text{f}}\, B_1\left(\frac{4m_{\text{f}}^2}{p^2}\right), \tag{4.16}$$

where B_1 was defined in eq. (4.10), and the function G^{gg} encodes the corrections stemming from the vertex diagram **A** in figure 4 plus those from external leg corrections in diagrams **D1**, **D2** and **D5** of figure 5.

JHEP11(2021)168

We have performed the computation of g_{agg}^{eff} in the R_ξ gauge and using dimensional regularization. The latter respects gauge invariance and regulates both ultraviolet (UV) and infrared (IR) divergences when present, portraying both as poles in $1/\epsilon$ and thus mixing them. It is possible to separate UV and IR divergences, though, via the implementation as a previous step of any IR regularization procedure [61] — e.g. setting the external gluons off-shell or using an effective gluon "mass"[7] — so as to identify first the UV divergences, and then using this information on the complete pure dimensional regularization result. We obtain,

$$G^{gg} = -2 \sum_{\substack{\text{f}=u,c,t,\\ d,s,b}} \left(\frac{1}{\epsilon_{\text{UV}}} - \gamma_E + \log\left(\frac{4\pi\mu_{\text{UV}}^2}{m_{\text{f}}^2} \right) \right) + 33 \left(\frac{1}{\epsilon_{\text{UV}}} - \gamma_E + \log\left(\frac{4\pi\mu_{\text{UV}}^2}{p^2} \right) \right) - 9 \left(\frac{1}{\epsilon_{\text{IR}}} - \gamma_E + \log\left(-\frac{4\pi\mu_{\text{IR}}^2}{p^2} \right) \right)^2 - 33 \left(\frac{1}{\epsilon_{\text{IR}}} - \gamma_E + \log\left(\frac{4\pi\mu_{\text{IR}}^2}{p^2} \right) \right) + 36 + \frac{3\pi^2}{2} , \tag{4.17}$$

where ϵ_{UV} (ϵ_{IR}) and μ_{UV}^2 (μ_{IR}^2) account respectively for the UV (IR) divergence and renormalization scale. This result can be rewritten in terms of UV and IR cutoffs via the $\overline{\text{MS}}$ prescription

$$\frac{1}{\epsilon_{\text{UV}}} - \gamma_E + \log\left(4\pi\mu_{\text{UV}}^2\right) \to \log\Lambda^2 , \tag{4.18}$$

$$\frac{1}{\epsilon_{\text{IR}}} - \gamma_E + \log\left(4\pi\mu_{\text{IR}}^2\right) \to \log\lambda^2 , \tag{4.19}$$

where Λ and λ denote respectively the UV and IR energy cut-offs, leading to

$$G^{gg} = 33\log\left(\frac{\Lambda^2}{p^2}\right) - 2\sum_{\substack{\text{f}=u,c,t,\\ d,s,b}} \log\left(\frac{\Lambda^2}{m_{\text{f}}^2}\right) - 33\log\left(\frac{\lambda^2}{p^2}\right) - 9\left(\log\left(\frac{\lambda^2}{p^2}\right) + i\pi\right)^2 + 36 + \frac{3\pi^2}{2} . \tag{4.20}$$

When computing the probability for a given physical processes, the unphysical dependence on IR divergences will cancel with that stemming from soft and/or collinear gluon bremsstrahlung. In turn, the UV-divergent terms in this equation lead to the beta function for $c_{\tilde{G}}$ in eq. (3.5).

4.3 ALP anomalous coupling to Z plus photon

The effective $g_{a\gamma Z}$ coupling receives one-loop corrections from the fermion-ALP couplings c_{f} and from the complete set of electroweak couplings $\{g_{a\gamma\gamma}, g_{aWW}, g_{aZZ}, g_{a\gamma Z}\}$. The relevant

[7] It is meant here to simply replace the gluon propagator by a massive one. This is not a gauge invariant procedure and it thus leaves finite terms which are ξ-dependent and in consequence physically meaningless, but it allows to identify properly the UV divergences (and with this information restart the whole procedure using only dimensional regularization). It is of course possible to give a mass to the gluon in a gauge invariant way by "Higgsing" QCD: this would add the contribution of the would-be gluonic Goldstone bosons, and we checked that all the ξ-dependence would cancel then. Nevertheless, this Higgsed theory does not recuperate QCD in the massless gluon limit: for instance, the beta function is modified by the contribution of the extra scalar degrees of freedom present.

JHEP11(2021)168

Feynman diagrams are those in figures 4 and 5 (except diagram **E**), with the external vector bosons being either photon or Z, and with $V \neq V'$. In consequence, the gauge boson running in closed gauge loops can only be the W boson, while the virtual boson attached to a in diagrams **D1**, **D2** and **D5** is either Z or γ, and $V' = \gamma$ in diagrams **D3** and **D4**.

The results are shown to become ξ-independent — as they must — only when the gauge-electroweak parameter space is reduced to three couplings, using eq. (2.35). Applying the latter again, the electroweak set can be further reduced to two anomalous electroweak operators, that we choose to be the set $\{g_{a\gamma Z}, g_{aWW}\}$. The total result can be summarized as

$$g^{\text{eff}}_{a\gamma Z} = g_{a\gamma Z}\left\{1+\frac{\alpha_{em}}{12\pi}\left(A^{Z/\gamma\to\gamma}+\frac{1}{c_w^2 s_w^2}A^{Z/\gamma\to Z}\right)\right\}+\frac{\alpha_{em}}{\pi}\frac{c_w}{s_w}g_{aWW}\,A^{WW}+\frac{\alpha_{em}}{\pi c_w s_w}\sum_{\text{f}}\frac{c_{\text{f}}}{f_a}A^{\text{f}}, \tag{4.21}$$

where the exact expressions for all the functions in this equation can be found in appendix C.1, for an off-shell ALP and on-shell external SM particles. They are defined as follows:

- $A^{Z/\gamma\to\gamma}$ gathers the external leg corrections with a photon as final particle, (figure 5 **D1-D5** with $V = \gamma$ and $V' = Z$). Its expression was given in eq. (4.11).
- $A^{Z/\gamma\to Z}$ encodes the external leg corrections with Z as final particle (figure 5 **D1-D5** with $V = Z$ and $V' = \gamma$). It can be expanded as

$$A^{Z/\gamma\to Z} = A^{Z/\gamma\to Z}_{\text{ferm}} + A^{Z\to Z}_{\text{Higgs}} + A^{Z/\gamma\to Z}_{\text{gauge}}\,, \tag{4.22}$$

  where
  - $A^{Z/\gamma\to Z}_{\text{ferm}}$ accounts for the SM fermion loop corrections, figure 5 **D5**, see eq. (C.1).
  - $A^{Z\to Z}_{\text{Higgs}}$ encodes Higgs corrections to external legs in figure 5 **D3** and **D4**, see eq. (C.2).
  - $A^{Z/\gamma\to Z}_{\text{gauge}}$ gathers the gauge boson corrections to external legs in figure 5 **D1** and **D2** (with W bosons running in the loop), plus the $g_{a\gamma Z}$ component of the corrections stemming from $g_{a\gamma\gamma}$ and g_{aZZ} insertions in figure 5 **D1-D5**, projected on the parameter space $\{g_{a\gamma Z}, g_{aWW}\}$, see eq. (C.3).
- A^{WW} contains the contributions from direct vertex insertions of g_{aWW} in diagrams **A** and **B** of figure 4, plus the g_{aWW} component of the corrections stemming from $g_{a\gamma\gamma}$ and g_{aZZ} insertions in figure 5 **D1-D5** projected on the parameter space $\{g_{a\gamma Z}, g_{aWW}\}$, see eq. (C.4).
- A^{f} encodes the fermion triangle correction from diagram **C** in figure 4, see eq. (C.5).

Eq. (4.21) can be rewritten in terms of $\{c_{\tilde{B}}, c_{\tilde{W}}\}$ (and c_{f}) applying eq. (2.31) for g_{aWW} and the last equality in eq. (4.7) for $g_{a\gamma Z}$.

An example of physical process to which the exact results can be directly applied in case $m_a < M_Z$ is given by the decay width of a Z boson to photon plus ALP,

$$\Gamma(Z\to a\gamma) = \frac{M_Z^3|g^{\text{eff}}_{a\gamma Z}|^2}{384\pi}\left(1-\frac{m_a^2}{M_Z^2}\right)^3\,, \tag{4.23}$$

JHEP11(2021)168

while for $m_a > M_Z$, the ALP decay width into Z plus photon reads

$$\Gamma(a \to \gamma Z) = \frac{m_a^3 |g^{\rm eff}_{a\gamma Z}|^2}{128\pi} \left(1 - \frac{M_Z^2}{m_a^2}\right)^3 . \tag{4.24}$$

We illustrate next the results obtained above for a generic off-shell ALP in some particular limits of practical interest.

4.3.1 $g^{\rm eff}_{aZ\gamma}$ for high ALP p^2

For $p^2 \to \infty$, ($p^2 \gg (m_{\rm f}^2, M_Z^2, M_W^2)$), the anomaly contribution yields:

$$A^{\rm f} = 2 N_C Q_{\rm f}^2 s_w^2 \,, \tag{4.25}$$

while the correction proportional to g_{aWW} is given by

$$A^{WW} = \frac{42M_W^2 + M_Z^2}{12M_W^2} \log\left(\frac{\Lambda^2}{M_W^2}\right) - \sum_{\rm f} \frac{N_C Q_{\rm f}(T_{3,{\rm f}} - 2Q_{\rm f} s_w^2)}{3c_w^2} \log\left(\frac{\Lambda^2}{m_{\rm f}^2}\right) - \left(\log\left(\frac{M_W^2}{p^2}\right) + i\pi\right)^2 , \tag{4.26}$$

where the terms proportional to $\log\Lambda$ are kept, because consistency of the EFT expansion requires $p^2 < \Lambda^2$.

4.3.2 $g^{\rm eff}_{aZ\gamma}$ for intermediate and low ALP p^2

Both for $m_{\rm f}^2 \ll p^2 \ll (M_Z^2, M_W^2) \ll m_t^2$, where f refers to all fermion mass but the top one, and for $p^2 \to 0$ ($p^2 \ll (m_{\rm f}^2, M_Z^2)$), i.e. smaller than all fermion masses (which can apply for instance to Z decay to ALP + photon), the contribution of fermionic ALP couplings to $g^{\rm eff}_{aZ\gamma}$ is well approached by

$$A^{\rm f} = \begin{cases} 2N_C Q_{\rm f}^2 s_w^2 \,, & \text{for light fermions: } m_{\rm f}^2 \ll M_Z^2 \,, \\ \frac{3Q_t}{2} \,, & \text{for the top quark: } m_t^2 \gg M_Z^2 \,, \end{cases} \tag{4.27}$$

while the correction proportional to g_{aWW} reads

$$A^{WW} = \frac{42M_W^2 + M_Z^2}{12M_W^2} \log\left(\frac{\Lambda^2}{M_W^2}\right) - \sum_{\rm f} \frac{N_C Q_{\rm f}(T_{3,{\rm f}} - 2Q_{\rm f} s_w^2)}{3c_w^2} \log\left(\frac{\Lambda^2}{m_{\rm f}^2}\right) + \dots \,, \tag{4.28}$$

where dots stand for constant terms.

4.4 ALP anomalous coupling to ZZ

The effective g_{aZZ} coupling receives corrections induced by three of the four electroweak gauge couplings: the set $\{g_{aWW}, g_{aZZ}, g_{a\gamma Z}\}$, plus $\mathbf{c}_{\rm f}$ fermion corrections. All Feynman diagrams in figures 4 and 5 contribute with $V = V' = Z$. Using eq. (2.35), the contributions resulting from electroweak gauge insertions can be projected on a two-dimensional space of

JHEP11(2021)168

couplings, which we choose to be here $\{g_{aZZ}, g_{aWW}\}$. The total effective coupling g_{aZZ} can then be expressed as

$$g_{aZZ}^{\text{eff}} = g_{aZZ}\left\{1 + \frac{\alpha_{em}}{6\pi c_w^2 s_w^2}\left(A^{Z/\gamma\to Z} + B^{\text{Higgs}}\right)\right\} + \frac{\alpha_{em}}{\pi}\frac{c_w^2}{s_w^2} g_{aWW} B^{WW} + \frac{\alpha_{em}}{\pi c_w^2 s_w^2}\sum_{\text{f}} \frac{c_{\text{f}}}{f_a} B^{\text{f}}\,, \tag{4.29}$$

where the complete expressions for the functions in this expression can be found in appendix C.2. They correspond to:

- $A^{Z/\gamma\to Z}$ encodes corrections to the external legs (diagrams **D1-D5** in figure 5), see eq. (C.1) for the exact result.
- B^{Higgs} stems from the vertex insertion of g_{aZZ} with a Higgs particle exchanged between the two Z bosons (diagram **E** in figure 4), see eq. (C.10).
- B^{WW} collects the contributions proportional to g_{aWW} resulting from direct vertex insertions of g_{aWW} in figure 4 **A** and **B**, plus the g_{aWW} component of the contributions seeded by the insertion of $g_{a\gamma Z}$ in the external legs and then projected onto the parameter space $\{g_{aZZ}, g_{aWW}\}$, see eq. (C.11).
- Finally, the function B^{f} encodes the contributions from vertex insertions of the fermionic couplings c_{f} (figure 4 **C**), see eq. (C.12).

Eq. (4.29) can be rewritten in terms of $\{c_{\tilde{B}}, c_{\tilde{W}}\}$ (and c_{f}) applying eq. (2.31) for g_{aWW} and the last equality in eq. (4.8) for g_{aZZ}.

The results in this subsection can be applied to a variety of transitions in which the ALP may be on-shell or off-shell. For instance, for $m_a > 2M_Z$ the one-loop corrected ALP decay width into two Z bosons is simply given by

$$\Gamma(a \to ZZ) = \frac{m_a^3 |g_{aZZ}^{\text{eff}}|^2}{64\pi}\left(1 - \frac{4M_Z^2}{m_a^2}\right)^{3/2}. \tag{4.30}$$

We present next for illustration the limit of the complete results in appendix C.2 in the particular case of high ALP four-momentum squared, which can be of interest for instance for non-resonant collider ALP searches.[8]

4.4.1 g_{aZZ}^{eff} for high ALP p^2

For $p^2 \to \infty$ ($p^2 \gg (m_{\text{f}}^2, M_Z^2, M_W^2)$), only the anomaly contribution remains from the insertion of ALP-fermions couplings,

$$B^{\text{f}} = -N_C Q_{\text{f}}^2 s_w^4\,, \tag{4.31}$$

while the contribution proportional to g_{aWW} simplifies to

$$B^{WW} = \frac{42M_W^2 + M_Z^2}{12M_W^2}\log\left(\frac{\Lambda^2}{M_W^2}\right) - \sum_{\text{f}} \frac{N_C Q_{\text{f}}(T_{3,\text{f}} - 2Q_{\text{f}} s_w^2)}{3c_w^2}\log\left(\frac{\Lambda^2}{m_{\text{f}}^2}\right) - \frac{1}{2}\left(\log\left(\frac{M_W^2}{p^2}\right) + i\pi\right)^2, \tag{4.32}$$

[8] For intermediate ALP momentum ($m_{\text{f}}^2 \ll p^2 \ll (M_Z^2, M_W^2) \ll m_t^2$) and low four-momentum ($p^2 \ll (m_{\text{f}}^2, M_Z^2)$) the transition is not kinematically possible with the gauge bosons on-shell.

JHEP11(2021)168

and that proportional to g_{aZZ} corrected by Higgs boson exchange between external legs vanishes, $B^{\text{Higgs}} = 0$.

4.5 ALP anomalous coupling to W^+W^-

All four couplings in the ensemble $\{g_{a\gamma\gamma}, g_{aWW}, g_{aZZ}, g_{a\gamma Z}\}$ induce one-loop corrections to the effective g^{eff}_{aWW} coupling. All Feynman diagrams in figures 4 and 5 contribute. The complete results can be found in appendix C.3. Using eq. (2.35), the total result can be expressed for instance as a function of $\{g_{aWW}, g_{a\gamma\gamma}\}$ plus fermionic couplings,

$$g^{\text{eff}}_{aWW} = g_{aWW}\left\{1 + \frac{\alpha_{em}}{24\pi s_w^2}\left(A^{W\to W} + C^{WW} + C^{\text{Higgs}}\right)\right\} + \frac{\alpha_{em}}{2\pi} g_{a\gamma\gamma}\, C^{\gamma\gamma} + \frac{\alpha_{em}}{\pi s_w^2}\sum_{\text{f}} \frac{c_{\text{f}}}{f_a} C^{\text{f}}\,, \tag{4.33}$$

where:

- $A^{W\to W}$ contains two sources of one-loop external-leg SM corrections to the insertion of g_{aWW} itself: fermionic and Higgs corrections,

$$A^{W\to W} = A^{W\to W}_{\text{ferm}} + A^{W\to W}_{\text{Higgs}}\,, \tag{4.34}$$

  with only fermion doublets contributing to $A^{W\to W}_{\text{ferm}}$, see diagram **D5** in figure 5 and eq. (C.17), and the Higgs-dependent term $A^{W\to W}_{\text{Higgs}}$ stemming from diagrams **D3** and **D4** in figure 5, see eq. (C.18).

- C^{WW} accounts for corrections proportional to g_{aWW}, and gathers one-loop SM corrections on the external legs (figure 5 **D1** and **D2**) together with vertex ones (figure 4 **A** and **B**) (see eq. (C.19) for the complete expression):

  - The leg corrections and those from the vertex diagram **B** are directly seeded by the insertion of g_{aWW}.
  - The contributions originated from diagram **A** correspond to the combination of direct vertex insertions of g_{aWW}, plus the g_{aWW} component of the contributions seeded by $\{g_{aZZ}, g_{a\gamma Z}\}$ insertions projected onto the $\{g_{a\gamma\gamma}, g_{aWW}\}$ parameter space.

- C^{Higgs} is a pure vertex correction resulting from the direct insertion of g_{aWW} with the Higgs boson exchanged between the two W legs (diagram **E** in figure 4), see eq. (C.20).

- The vertex function $C^{\gamma\gamma}$ corresponds to figure 4 **A**, combining the results from the direct insertion of $g_{a\gamma\gamma}$ *and* the $g_{a\gamma\gamma}$ component of the contributions seeded by $\{g_{a\gamma Z}, g_{aZZ}\}$ insertions projected onto the $\{g_{\gamma\gamma}, g_{aWW}\}$ parameter space, see eq. (C.21).

- Finally, the vertex function C^{f} accounts for the fermionic triangle contributions (figure 4 **C**), induced by fermionic couplings c_{f} insertions, see eq. (C.22).

JHEP11(2021)168

Eq. (4.33) can be rewritten in terms of $\{c_{\tilde{B}}, c_{\tilde{W}}\}$ (and $c_{\rm f}$) applying eq. (2.31) for g_{aWW} and the last equality in eq. (4.6) for $g_{a\gamma\gamma}$.

We present next for illustration the high ALP four-momentum squared limit of the functions in eq. (4.33).

4.5.1 $g^{\rm eff}_{aWW}$ for high ALP p^2

In the limit $p^2 \to \infty$ ($p^2 \gg (m_{\rm f}^2, M_Z^2, M_W^2)$), the fermionic contribution to the anomaly vanishes. The same holds in this limit for the correction proportional to $g_{a\gamma\gamma}$ as well as that stemming from Higgs boson-exchange between the external W bosons,

$$C^{\rm f} = C^{\gamma\gamma} = C^{\rm Higgs} = 0\,. \tag{4.35}$$

The only non-vanishing contributions in this limit are those proportional to g_{aWW} itself and stemming from $A^{W\to W}$ and C^{WW}. The function $A^{W\to W}$ is independent of p^2: in consequence, it is not further simplifed from the relatively cumbersome complete expressions in eqs. (C.17) and eq. (C.18), see eq. (4.34). The function C^{WW} simplifies to

$$C^{WW} = 43\log\left(\frac{\Lambda^2}{M_W^2}\right) - 12\left(\log\left(\frac{M_W^2}{p^2}\right) + i\pi\right)^2 - 12 s_w^2 \log\left(\frac{\lambda^2}{M_W^2}\right)\left(1 + i\pi + \log\left(\frac{M_W^2}{p^2}\right)\right)\ldots\,, \tag{4.36}$$

where Λ is the UV cutoff (this logarithmic dependence cannot be disregarded in front of that in p^2 for EFT consistency), and λ denotes the IR cutoff. The computation has been carried out entirely in dimensional regularization, with the $1/\epsilon$ terms traded next for energy cutoffs via a protocol alike to that used for $g^{\rm eff}_{agg}$ — eq. (4.17) — and the prescription in eq. (4.18). The $\log\Lambda$ dependence contained in C^{WW} combined with that in the leg correction $A^{W\to W}$ determines the beta function for $c_{\tilde{W}}$ in eq. (3.4).

The two first terms in eq. (4.36) are the leading contributions for large enough p^2. The third term exhibits a logarithimic dependence on the IR cutoff which is instead physically irrelevant and can be disregarded, as it will exactly cancel for any physical observable against the contributions from soft and/or collinear photon brehmsstrahlung. The latter may also contribute additional finite terms to be combined with the finite and p^2 independent terms in C^{WW} (see the exact expression in eq. (C.19) in appendix C.3), encoded here by dots.

For intermediate ($m_{\rm f}^2 \ll p^2 \ll (M_Z^2, M_W^2) \ll m_t^2$) and low ($p^2 \ll (m_{\rm f}^2, M_Z^2)$) ALP four-momentum, the ALP-WW transition is again not kinematically possible for gauge bosons on-shell.

4.6 ALP fermionic couplings

The one-loop corrections to the effective ALP-fermion-fermion couplings are depicted in figures 6 and 7, where the internal wavy lines denote either the gluon in the case of the gluon-ALP coupling g_{agg} (only possible for quark final states) or electroweak gauge bosons. Contrary to the case for all previous effective couplings described, the individual contributions seeded by each of the electroweak couplings in the set $\{g_{a\gamma\gamma}, g_{aWW}, g_{aZZ}, g_{a\gamma Z}\}$ are separately gauge invariant. In other words, the ξ-independence of the results holds

JHEP11(2021)168

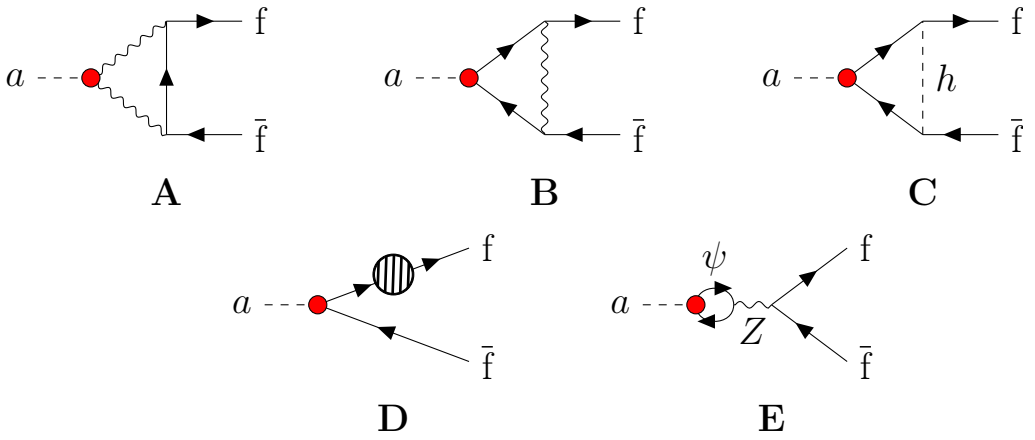

Figure 6. One-loop diagrams contributing to $c_{\rm f}$ at one-loop (plus the corresponding diagrams with Goldstone bosons). The wavy lines denote gauge bosons: gluons, photons, W and Z bosons.

already at the level of each one of those contributions, that is, prior to their projection onto a reduced parameter space of electroweak gauge couplings. For this reason, we will present those contributions individually. If wished, the reader can trivially project those results in the two-coupling $\{c_{\tilde{W}}, c_{\tilde{B}}\}$ parameter space, or on any other parameter space (e.g. $\{g_{a\gamma\gamma}, g_{aWW}\}$), using the gauge-invariance relations in eq. (2.35).

The results can be summarized as

$$\begin{aligned}\frac{c_{\rm f}^{\rm eff}}{f_a} = \frac{c_{\rm f}}{f_a}\left\{1+\frac{\alpha_{em}}{2\pi}D^{c_{\rm f}}+\frac{\alpha_s}{3\pi}D_g^{c_{\rm f}}\right\}+\frac{\alpha_{em}}{2\pi f_a}\left\{c_{\rm f'}D^{c_{\rm f'}}+\sum_\psi c_\psi D_{\rm mix}^{c_\psi}\right\}\\ +\frac{\alpha_{em}}{2\pi}\left\{g_{a\gamma\gamma}D^{\gamma\gamma}+g_{a\gamma Z}D^{\gamma Z}+g_{aZZ}D^{ZZ}+g_{aWW}D^{WW}\right\}+\frac{\alpha_s}{3\pi}\left\{g_{agg}D^{gg}\right\},\end{aligned} \tag{4.37}$$

where the sum over fermions runs over all possible flavours, $\psi = u, c, t, d, s, b, e, \mu, \tau$, and the terms in the second line account — respectively — for vertex insertions of the phenomenological ALP electroweak couplings $\{g_{a\gamma\gamma}, g_{a\gamma Z}, g_{aZZ}, g_{aWW}\}$ plus the anomalous gluon coupling g_{agg}: they all stem from diagram **A** in figure 6, and each term is separately gauge invariant. The complete expressions for the functions $D^{\gamma\gamma}$, $D^{\gamma Z}$, D^{ZZ} and D^{WW} can be found in eqs. (C.23)–(C.27) of appendix C.4. The first line in eq. (4.37) encodes instead insertions of:

- The fermionic coupling $c_{\rm f}$ itself accompanied by one-loop exchange of a gluon, encoded in $D_g^{c_{\rm f}}$, or by the one-loop exchange of either a photon, a Z, a W or a Higgs boson, i.e.

$$D^{c_{\rm f}} = D_\gamma^{c_{\rm f}} + D_Z^{c_{\rm f}} + D_W^{c_{\rm f}} + D_h^{c_{\rm f}}\,, \tag{4.38}$$

  where $D_W^{c_{\rm f}}$ is a pure leg correction from W exchange (figure 7 **D1**), and it is ξ-independent by itself, see eq. (C.31). In contrast, in to order get results in an explicitly gauge invariant formulation, the one-loop corrections due to photon or Z exchange — encoded respectively in $D_\gamma^{c_{\rm f}}$ and $D_Z^{c_{\rm f}}$ — require the combination of the vertex diagram **B** in figure 6 and the leg correction in figure 7 **D1**, see eqs. (C.29) and (C.30).

JHEP11(2021)168

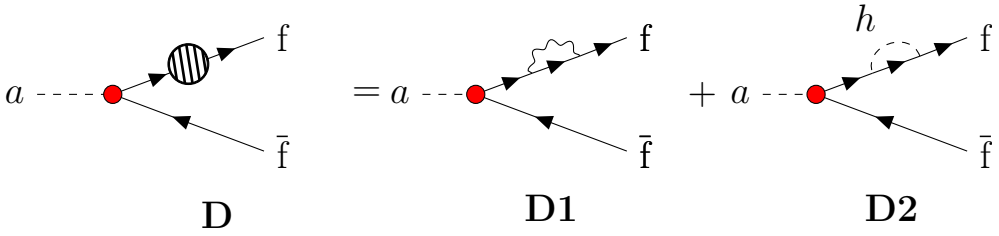

Figure 7. One-loop diagrams contributing to the correction to the external fermion legs. Diagrams with Goldstone bosons are included.

Similarly, manifest gauge invariance of the Higgs-exchange corrections — encoded in $a D_{ht}^{c_f}$ — results after combining the vertex correction in figure 6 **C** and the leg corrections in figure 7 **D2**, see eq. (C.33).

- The contribution from $c_{f'}$, where f' denotes the $SU(2)_L$ flavour partner of fermion f, encoded in the function $D^{c_{f'}}$ given in eq. (C.32). It corresponds to the vertex correction due to W exchange in figure 6 **B**, which is gauge invariant by itself.

- All possible fermionic contributions to the mixed a-Z correction in figure 6 **E**, which are encoded through the functions $D_{\rm mix}^{c_\psi}$, which are also separately gauge-invariant, see the complete result in eq. (C.34).

The results can be applied to a variety of physical transitions with an ALP on- or off-shell. For instance, for ALP decay into a fermionic $\bar{\rm f}{\rm f}$ channel when $m_a > 2\,m_{\rm f}$, the one-loop corrected width is simply obtained from

$$\Gamma(a \to {\rm f}\bar{\rm f}) = \frac{N_C m_a m_{\rm f}^2 |c_{\rm f}^{\rm eff}|^2}{8\pi f_a^2}\sqrt{1-\frac{4m_{\rm f}^2}{m_a^2}}\,. \tag{4.39}$$

For simplicity and for illustration purposes, we present next in this subsection some useful limits of the exact functions in appendix C.4, for a generic off-shell ALP.

4.7 $c_{\rm f}^{\rm eff}$ for high ALP p^2

For non-resonant searches at the LHC and other colliders, and/or for very heavy ALPs, the limit $m_{\rm f}^2 \ll (M_Z^2, M_W^2, M_H^2) \ll m_t^2 \ll p^2$ is of physical interest, where $m_{\rm f}$ refers to all fermion masses but the top one. In this subsection we set $m_{\rm f} = 0$ except in divergent terms.

4.7.1 Limit of light external fermions for ${\rm f} = u, d, s, b, e, \mu$

Let us first consider the contribution of gauge-anomalous couplings to $c_{\rm f}^{\rm eff}$. For instance, D^{gg} encodes the g_{agg} contribution with gluons running in the internal loop of diagram **A** in figure 6, which in this limit reduces to

$$D^{gg} = \left\{3\log\left(\frac{\Lambda^2}{m_{\rm f}^2}\right) - 4 - \frac{2\pi^2}{3} - \frac{1}{2}\left(\log\left(\frac{m_{\rm f}^2}{p^2}\right) + i\pi\right)^2\right\}. \tag{4.40}$$

JHEP11(2021)168

Analogously, $D^{\gamma\gamma}$ accounts for the $g_{a\gamma\gamma}$ insertion with two photons running in the internal loop of diagram **A** in figure 6, with an expression very close to that of D^{gg} which in this limit reduces to

$$D^{\gamma\gamma} = \frac{Q_{\rm f}^2}{2} D^{gg}\,, \tag{4.41}$$

while the $D^{\gamma Z}$ term stems from that same diagram with one photon and one Z boson in the internal loop,

$$D^{\gamma Z} = \frac{Q_{\rm f}\left(T_{3,\rm f} - 2Q_{\rm f} s_w^2\right)}{16 c_w s_w}\left\{12\log\left(\frac{\Lambda^2}{M_Z^2}\right) - 19 - \frac{2\pi^2}{3} - 2\left(\log\left(\frac{M_Z^2}{p^2}\right) + i\pi\right)^2 \right.$$
$$\left. - \log\left(\frac{m_{\rm f}^2}{M_Z^2}\right)\left[6 + 4i\pi + 4\log\left(\frac{M_Z^2}{p^2}\right)\right]\right\}. \tag{4.42}$$

Similarly, the same diagram in figure 6 **A** although with two internal Z bosons results in

$$D^{ZZ} = \frac{1}{8 c_w^2 s_w^2}\left\{\left(T_{3,\rm f}^2 - 2T_{3,\rm f} Q_{\rm f} s_w^2 + 2Q_t s_w^4\right)\left(6\log\left(\frac{\Lambda^2}{M_Z^2}\right) - 11\right)\right.$$
$$\left. + 4T_{3,\rm f}^2\left(1 + \log\left(\frac{M_Z^2}{p^2}\right) + i\pi\right) + 4Q_{\rm f}^2 s_w^2 (T_{3,\rm f} - Q_{\rm f} s_w^2)\left(\log\left(\frac{M_Z^2}{p^2}\right) + i\pi\right)^2\right\}, \tag{4.43}$$

while D^{WW} corresponds to that same diagram, albeit with internal W bosons,

$$D^{WW} = \begin{cases} \frac{1}{16 s_w^2}\left\{6\log\left(\frac{\Lambda^2}{p^2}\right) - 2\log\left(\frac{M_W^2}{p^2}\right) - 7 + 4i\pi\right\}, & \text{for leptons and quarks} \\ & \text{except top and bottom}\,, \\ \frac{1}{16 s_w^2}\left\{6\log\left(\frac{\Lambda^2}{p^2}\right) - 2\log\left(\frac{m_t^2}{p^2}\right) - 9 + 4i\pi\right\}, & \text{for the bottom quark}\,. \end{cases} \tag{4.44}$$

For the contributions resulting from the insertions of ALP fermionic couplings, the one-loop gluon corrections (vertex plus legs), and the analogous one-loop photon corrections lead in this limit to, respectively,

$$D_g^{c_{\rm f}} = -2\left\{1 - \frac{\pi^2}{6} + \log\left(\frac{\lambda^2}{m_{\rm f}^2}\right)\left(1 + i\pi + \log\left(\frac{m_{\rm f}^2}{p^2}\right)\right) + \frac{1}{2}\left(\log\left(\frac{m_{\rm f}^2}{p^2}\right) + i\pi\right)^2\right\}, \tag{4.45}$$

$$D_\gamma^{c_{\rm f}} = \frac{Q_{\rm f}^2}{2} D_g^{c_{\rm f}}\,, \tag{4.46}$$

where λ is an infrared cutoff which encodes the IR-divergent contributions to the $1/\epsilon$ dimensional regularization terms via the prescription in eq. (4.18), following the same protocol used for the gluonic IR divergences in eq. (4.17). and the photonic ones in eq. (4.36). Those unphysical IR logarithmic dependences will again exactly cancel in physical transitions against those from the phase space integral terms stemming from tree-level soft and/or collinear gluon and photon bremsstrahlung.

JHEP11(2021)168

In turn, Z exchange (vertex plus legs) is free from IR divergences and leads to

$$D_Z^{c_\mathrm{f}} = -\frac{Q_\mathrm{f} s_w^2 (T_{3,\mathrm{f}} - Q_\mathrm{f} s_w^2)}{2 c_w^2 s_w^2} \left\{ \frac{2\pi^2}{3} + \left(\log\left(\frac{M_Z^2}{p^2}\right) + i\pi \right)^2 \right\}. \tag{4.47}$$

The $c_\mathrm{f}^\mathrm{eff}$ component resulting from one-loop W-exchange corrections to ALP fermion-coupling insertions unfolds as explained as two ξ-independent contributions: i) the leg correction from the insertion of c_f in figure 7 **D1**, encoded in $D_W^{c_\mathrm{f}}$, which in this particular limit vanishes, and ii) the vertex correction induced by the insertion of the SU(2) flavour-partner coupling $c_{\mathrm{f}'}$ in figure 6 **B**, encoded in $D^{c_{\mathrm{f}'}}$:

$$D^{c_{\mathrm{f}'}} = \begin{cases} 0\,, & \text{for leptons and quarks} \\ & \text{except top and bottom}\,, \\ -\frac{m_t^2}{8 M_W^2 s_w^2} \left\{ \log\left(\frac{\Lambda^2}{p^2}\right) + \log\left(\frac{M_W^2}{p^2}\right) + \frac{7}{2} + 2i\pi \right\}, & \text{for the bottom quark}\,. \end{cases} \tag{4.48}$$

The one-loop Higgs corrections to c_f insertions also vanish in this limit, $D_h^{c_\mathrm{f}} = 0$. Finally, the mixed one-loop contribution to $c_\mathrm{f}^\mathrm{eff}$ from diagram **E** in figure 6 receives contributions from all possible ALP fermionic couplings — quarks and leptons, and it is also ξ-independent by itself. Its expression is particularly simple even in the exact case (see eq. (C.34) in appendix C), while in the present limit all contributions vanish but for that with the top quark running in the loop,

$$D_\mathrm{mix}^{c_t} = -\frac{3 T_{3,\mathrm{f}}\, m_t^2}{2 s_w^2 M_W^2} \left\{ \log\left(\frac{\Lambda^2}{p^2}\right) + 2 + i\pi \right\}, \tag{4.49}$$

where $T_{3,\mathrm{f}}$ denotes the third component of weak isospin for the external flavour f. The logarithimic dependence was already obtained in ref. [62]. This result shows that, in the limit under study, the top-coupling contribution can be the dominant one on the quest for signals of ALP couplings to light fermions, because the contributions are proportional to the mass of the fermion running in the loop and independent of the external flavour. In fact, this conclusion extends as well to the exact result in eq. (C.34). This may be very relevant for instance on the searches for ALP couplings to electrons in XENON and other experiments, see section 6.

4.7.2 Limit of light internal fermions for external f = t

The analogous high ALP p^2 results when the external fermion is the top, i.e. the contributions to c_t^eff neglecting light fermion masses, are reported next.

Let us consider first the impact of the insertions of ALP gauge anomalous couplings. In the case of the ALP-photon and ALP-gluon couplings, g_{agg} and $g_{a\gamma\gamma}$, the corresponding functions D^{gg} and $D^{\gamma\gamma}$ are exactly as those in eqs. (4.40) and (4.41) albeit with the

JHEP11(2021)168

replacement $m_{\rm f} \to m_t$. For the other anomalous couplings, the results simplify to

$$D^{\gamma Z} = \frac{Q_t\,(T_{3,t} - 2Q_t s_w^2)}{4 c_w s_w}\left\{3\log\left(\frac{\Lambda^2}{m_t^2}\right) - 4\right\}, \tag{4.50}$$

$$\begin{aligned} D^{ZZ} = \frac{1}{4c_w^2 s_w^2}\Bigg\{&(T_{3,t}^2 - 2T_{3,t}Q_t s_w^2 + 2Q_t s_w^4)\left(3\log\left(\frac{\Lambda^2}{m_t^2}\right) - 4\right) \\ &+ 2Q_t^2 s_w^2 (T_{3,t} - Q_t s_w^2)\left[\frac{2\pi^2}{3} + \frac{1}{2}\left(\log\left(\frac{m_t^2}{p^2}\right) + i\pi\right)^2\right] + 2T_{3,t}^2\left(\log\left(\frac{m_t^2}{p^2}\right) + i\pi\right)\Bigg\}, \end{aligned} \tag{4.51}$$

$$D^{WW} = \frac{1}{8 s_w^2}\left\{3\log\left(\frac{\Lambda^2}{p^2}\right) - \log\left(\frac{m_t^2}{p^2}\right) - 3 + 3i\pi\right\}. \tag{4.52}$$

In turn, the one-loop gluon and photon contributions to $c_t^{\rm eff}$ stemming from ALP-fermion couplings, i.e. $D_g^{c_{\rm f}}$ and $D_\gamma^{c_{\rm f}}$, are respectively identical to those found above for the light external fermion limit in eqs. (4.45) and (4.46). The rest of the one-loop boson corrections to insertions of ALP-fermion couplings reads in this limit:

$$\begin{aligned} D_Z^{c_t} = \frac{1}{2c_w^2 s_w^2}\Bigg\{&-\frac{m_t^2 T_{3,t}^2}{M_Z^2}\left(\log\left(\frac{\Lambda^2}{p^2}\right) + 2 + i\pi\right) - (T_{3,t}^2 + 4T_{3,t}Q_t s_w^2 - 4Q_t^2 s_w^4)\log\left(\frac{m_t^2}{M_Z^2}\right) \\ &- Q_t s_w^2 (T_{3,t} - Q_t s_w^2)\left[\frac{\pi^2}{3} + 2\log\left(\frac{m_t^2}{M_Z^2}\right)\left(\log\left(\frac{m_t^2}{p^2}\right) + i\pi\right) - \left(\log\left(\frac{m_t^2}{p^2}\right) + i\pi\right)^2\right]\Bigg\}, \end{aligned} \tag{4.53}$$

$$D_W^{c_t} = -\frac{m_t^2}{8 M_W^2 s_w^2}\left\{\log\left(\frac{\Lambda^2}{m_t^2}\right) + 1 + i\pi\right\}, \tag{4.54}$$

$$D_h^{c_t} = -\frac{m_t^2}{8\pi s_w^2 M_W^2}\left\{\log\left(\frac{\Lambda^2}{M_H^2}\right) + \log\left(\frac{p^2}{M_H^2}\right) - 2 - i\pi\right\}, \tag{4.55}$$

$$D_{\rm mix}^{c_\psi} = -\frac{3m_t^2}{4 s_w^2 M_W^2}\left\{\log\left(\frac{\Lambda^2}{m_t^2}\right) + 2 + i\pi\right\}, \tag{4.56}$$

while $D_W^{c_{\rm f'}} = 0$ with f' $= b$ in this particular case.

4.8 $c_{\rm f}^{\rm eff}$ for intermediate ALP p^2 and light fermions

We explicit now the limits for an ALP with a low p^2, smaller or equal than all SM boson gauge boson masses but larger than the mass squared of all light fermions $m_{\rm f}^2 \ll p^2 \ll M_Z^2, M_W^2, M_H^2$ with ${\rm f} = u, d, c, s, b, e, \mu, \tau$. This limit is of interest for instance when considering decays of a light ALP to leptons or light fermions, such as those searched for in rare decays.

The contribution stemming from the insertions of g_{agg} and $g_{a\gamma\gamma}$, i.e. the functions D^{gg} and $D^{\gamma\gamma}$, are again exactly as those in eqs. (4.40) and (4.41). For the other anomalous

JHEP11(2021)168

couplings, the results simplify in this limit to

$$D^{\gamma Z} = \frac{Q_{\rm f}\left(T_{3,\rm f} - 2Q_{\rm f}s_w^2\right)}{8c_w s_w}\left\{6\log\left(\frac{\Lambda^2}{M_Z^2}\right) - 13\right\}, \tag{4.57}$$

$$D^{ZZ} = \frac{\left(T_{3,\rm f}^2 - T_{3,\rm f}2Q_{\rm f}s_w^2 + 2Q_{\rm f}s_w^4\right)}{8c_w^2 s_w^2}\left\{6\log\left(\frac{\Lambda^2}{M_Z^2}\right) - 19\right\}, \tag{4.58}$$

$$D^{WW} = \frac{1}{16 s_w^2}\left\{6\log\left(\frac{\Lambda^2}{M_Z^2}\right) - 19\right\}. \tag{4.59}$$

The results for $D^{\gamma\gamma}$ and eqs. (4.57)–(4.59) have been addressed previously in ref. [14] for an on-shell ALP ($p^2 = m_a^2$); our results are in agreement with those, except for a minor factor in $D^{\gamma\gamma}$, eq. (4.41).

We consider next the impact of inserting ALP fermionic couplings. Their contributions vanish in this particular limit for the following functions:

$$D_Z^{c_{\rm f}} = D_W^{c_{\rm f}} = D_W^{c'_{\rm f}} = D_h^{c_{\rm f}} = 0\,, \tag{4.60}$$

while the gluon and photon corrections $D_g^{c_{\rm f}}$ and $D_\gamma^{c_{\rm f}}$ coincide with those in eqs. (4.45) and (4.46). Finally, the a-Z mixing corrections read in this limit [62]

$$D_{\rm mix}^{c_t} = -\frac{3T_{3,\rm f}\, m_t^2}{2s_w^2 M_W^2}\left\{\log\left(\frac{\Lambda^2}{m_t^2}\right)\right\}. \tag{4.61}$$

5 Gauge invariance at one-loop level

This section analyzes the modifications to the tree-level gauge invariance relations in eq. (2.35) and (2.36), which result from rewriting the only two independent parameters of the electroweak sector g_{aWW} and g_{aBB} (i.e. $c_{\tilde{W}}$ and $c_{\tilde{B}}$, see eqs. (2.31) and (2.36)) in terms of the measured phenomenological couplings, e.g.

$$\begin{aligned} g_{aWW} &= g_{a\gamma\gamma} + \frac{c_w}{2s_w} g_{a\gamma Z}\,, \\ g_{aBB} &= c_w^2 g_{a\gamma\gamma} + s_w^2 g_{aZZ} - c_w s_w g_{a\gamma Z}\,. \end{aligned} \tag{5.1}$$

Radiative corrections which include mass effects (spontaneously) break the explicit gauge invariance of the original Lagrangian in eq. (2.5) and table 1. In other words, corrections proportional to the Higgs vev v are to be expected, which can be summarized as contributions to both the original $\mathrm{SU}(2)_L \times \mathrm{U}(1)_Y$-invariant operators and to additional effective couplings which are not invariant under the electroweak (and custodial) symmetry. The results can then be encoded as the strength of the following set of four effective couplings

$$\left\{a\, B^{\mu\nu}\tilde{B}_{\mu\nu},\, a\, W^{\mu\nu}\tilde{W}_{\mu\nu},\, a\, B^{\mu\nu}\tilde{W}^3_{\mu\nu},\, a\, W_3^{\mu\nu}\tilde{W}_{3\,\mu\nu}\right\}, \tag{5.2}$$

where the last two are new and do not respect electroweak and custodial symmetries, while the first two were already present in the original gauge-invariant Lagrangian eq. (2.5). The

JHEP11(2021)168

radiative corrections to the $aW^1_{\mu\nu}\tilde{W}^{1\mu\nu}$ coupling must equal exactly those for the $aW^2_{\mu\nu}\tilde{W}^{2\mu\nu}$ coefficient because of electric charge conservation: $g^{\rm eff}_{aWW}$ will encode them as well as the identical ones for the $aW^3_{\mu\nu}\tilde{W}^{3\mu\nu}$ interaction, while the "excess" will be accounted for in the coefficient for a $a\,W_3^{\mu\nu}\tilde{W}_3$ interaction denoted Δ_{WW}. In turn, Δ_{BW} will encode corrections of the form $a\,B^{\mu\nu}\tilde{W}^3_{\mu\nu}$, i.e.

$$\delta\mathcal{L}_a^{\rm total} \supset \frac{1}{4}\Delta_{BW}aB_{\mu\nu}\tilde{W}^{3\mu\nu} + \frac{1}{4}\Delta_{WW}aW^3_{\mu\nu}\tilde{W}^{3\mu\nu}\,. \tag{5.3}$$

The two new effective couplings can be expressed as the following combinations of radiatively-corrected phenomenological parameters:

$$\begin{aligned}\Delta_{WW} &= \bar{s}_w^2\, g^{\rm eff}_{a\gamma\gamma} + \bar{c}_w^2\, g^{\rm eff}_{aZZ} + \bar{c}_w\bar{s}_w\, g^{\rm eff}_{a\gamma Z} - g^{\rm eff}_{aWW}\,,\\ \Delta_{BW} &= 2\bar{c}_w\bar{s}_w(g^{\rm eff}_{a\gamma\gamma} - g^{\rm eff}_{aZZ}) + (\bar{c}_w^2 - \bar{s}_w^2)g^{\rm eff}_{a\gamma Z}\,.\end{aligned} \tag{5.4}$$

It is straightforward to compute the exact values of Δ_{WW} and Δ_{BW} from the results for the effective couplings in section 4 and appendix C and the expression for $\bar{c}_w$ in eq. (4.4). The tree-level closed gauge-invariance relations in eq. (2.35) will be modified in consequence.

Gauge invariant ancestors of radiatively corrected couplings. As stated above, the operators $aB_{\mu\nu}\tilde{W}^{3\mu\nu}$ and $aW^3_{\mu\nu}\tilde{W}^{3\mu\nu}$ are neither custodial nor $\mathrm{SU}(2)_L$ invariant. Nevertheless, there must be a fully gauge-invariant formulation of any possible correction to the effective Lagrangian and its corrections, because electroweak gauge symmetry is unbroken in nature. Indeed, in generic EFTs, one-loop corrections are expected to give contributions to higher order terms in the EFT expansion. Both in the SMEFT and in the linear ALP EFT, these contributions are always finite, i.e. all UV-divergences are reabsorbed order-by-order in the EFT expansion. Well-known examples in the SM are the magnetic and electric dipole moments in the SM, whose gauge invariant version corresponds to operators with mass dimension six and above.

Higher order radiative corrections, and in particular mass dependent ones (which are equivalent to multiple Higgs insertions that then take a vev) can imply that a full tower of operators may be needed to formulate those corrections in a gauge invariant way. The putative $\mathrm{SU}(2)_L \times \mathrm{U}(1)_Y$-invariant ancestors of the four gauge anomalous couplings in the Lagrangian $\mathcal{L}_a^{\rm total} + \delta\mathcal{L}_a^{\rm total}$, i.e. eqs. (2.5) and eq. (5.3), can be formulated alike to those in ref. [63] for CP-conserving Higgs couplings. For our ALP set, we expect v-dependent radiative corrections encoded in the gauge invariant operators

$$(5+2n): \quad a\,(\Phi^\dagger\Phi)^n\, B^{\mu\nu}\tilde{B}_{\mu\nu}\,, \tag{5.5}$$

$$(5+2n): \quad a\,(\Phi^\dagger\Phi)^n\, W^{\mu\nu}\tilde{W}_{\mu\nu}\,, \tag{5.6}$$

$$(7+2n): \quad a\,(\Phi^\dagger\Phi)^n\,(\Phi^\dagger\vec{\sigma}\Phi)\,\vec{W}^{\mu\nu}\tilde{B}_{\mu\nu} \longrightarrow a\,B^{\mu\nu}\tilde{W}^3_{\mu\nu}\,, \tag{5.7}$$

$$(9+2n): \quad a\,(\Phi^\dagger\Phi)^n\,(\Phi^\dagger\vec{\sigma^a}\Phi)\,(\Phi^\dagger\vec{\sigma^b}\Phi)\,\vec{W}^{\mu\nu}_a\tilde{W}_{b\,\mu\nu} \longrightarrow a\,W_3^{\mu\nu}\tilde{W}^3_{\mu\nu}\,, \tag{5.8}$$

where n is integer, $n \geq 0$. In the last two lines it is indicated that those two towers of operators lead — after spontaneously symmetry breaking — to the custodial and $\mathrm{SU}(2)_L$ non-invariant couplings $a\,B^{\mu\nu}\tilde{W}^3_{\mu\nu}$ and $a\,W_3^{\mu\nu}\tilde{W}^3_{\mu\nu}$ postulated earlier: note that their mass

JHEP11(2021)168

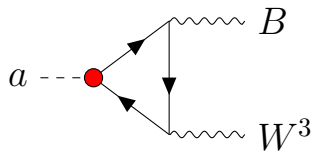

Figure 8. Illustration of fermionic one-loop contributions which induce an effective coupling $a\, B^{\mu\nu}\tilde{W}^3_{\mu\nu}$.

dimension is at least seven and nine, respectively, and that they vanish for $v = 0$. In contrast, the couplings in the first two lines can receive mass-independent one-loop corrections even for $n = 0$, as computed in the previous section. An important consequence of this is that loops induced by dimension-5 ALP operators can give UV-divergent contributions to the structures in (5.5) and (5.6) for $n = 0$, while contributions to all other structures must be finite. We find that this is indeed the case for Δ_{WW} and Δ_{BW}.

A pertinent question is the scale that would weight down those higher-dimension operators. Only one inverse power of f_a is possible, because ALP insertions must enter as powers of a/f_a, and only one ALP insertion is considered here. The remaining scale dependence must then correspond to either another BSM scale (not considered here) or simply to SM mass parameters when only SM radiative corrections are present as in the present work, i.e. to powers of the electroweak scale. These SM corrections should generate coefficient contributions proportional in addition to the SM sources of custodial breaking.

5.1 Gauge invariance relations among effective electroweak couplings at one-loop

It is easy to verify that $\Delta_{WW} = \Delta_{BW} = 0$ in the massless limit, i.e. for $v = 0$,[9] and the one-loop corrections to the anomalous gauge couplings satisfy the tree-level gauge invariance relations eq. (2.35). Instead, when mass corrections are taken into account, non-zero values for Δ_{WW} and Δ_{BW} do emerge. As an example, our results show that the contributions stemming from ALP-fermion coupling insertions — see figure 8 — are finite and take the general form

$$\Delta_{BW} = Y_L\,(F_L(m_1) - F_L(m_2)) + Y_{R1}\,F_R(m_1) - Y_{R2}\,F_R(m_2)\,, \tag{5.9}$$

where $m_{i=1,2}$ denote fermion masses of $\mathrm{SU}(2)_L$ fermion partners and the functions $F_R(m)$ and $F_L(m)$ cancel in the massless fermion limit, $F_{L,R}(0) = 0$. In other words, a non-vanishing Δ_{BW} coupling requires as expected that the sources of custodial breaking be at play: different fermion hypercharges and non-degenerate fermion partners running in the loop.

More in general, it follows from the analysis above that the tree-level gauge invariance relations in eq. (2.35) are to be substituted by the one-loop corrected ones, which we choose

[9] Moreover, the radiative correction to g_{aBB} is proportional as expected to $\sum_\psi y_\psi^2$, where y_ψ denote the fermion hypercharges.

JHEP11(2021)168

to parametrize as:

$$
\begin{aligned}
g^{\text{eff}}_{aWW} &= g^{\text{eff}}_{a\gamma\gamma} + \frac{\bar{c}_w}{2\bar{s}_w} g^{\text{eff}}_{a\gamma Z} - \frac{\bar{c}_w}{2\bar{s}_w}\Delta_{BW} - \Delta_{WW}\,, \\
g^{\text{eff}}_{aZZ} &= g^{\text{eff}}_{a\gamma\gamma} + \frac{\bar{c}_w^2 - \bar{s}_w^2}{2\bar{c}_w\bar{s}_w} g^{\text{eff}}_{a\gamma Z} - \frac{1}{2\bar{c}_w\bar{s}_w}\Delta_{BW}\,,
\end{aligned}
\tag{5.10}
$$

where $\bar{c}_w$ was defined in eq. (4.4). These one-loop corrections gauge invariance relations may impact on the limits inferred for a given coupling from the experimental bounds on another couplings known at present with higher precision (e.g. the bounds on the ALP-ZZ anomalous coupling obtained from the experimental limits on the ALP-$\gamma\gamma$ coupling in certain mass regimes [14, 53, 64]).

Limit $m_f^2, M_Z^2, M_W^2, M_H^2 \ll p^2 \leq m_t^2$. Because Δ_{WW} and Δ_{BW} vanish for $v = 0$, they vanish in the limit $p^2 \to \infty$. The contribution of the top quark may thus dominate for large p^2 close to m_t^2. That is, the contribution of the top-ALP coupling $\mathbf{c}_t$ may dominate in the limit in which all SM particle masses but the top one are neglected with respect to the ALP p^2:

$$
\Delta_{BW} \sim -c_t \frac{\alpha_{em}}{\pi c_w s_w}\frac{m_t^2}{p^2}\left\{6 + 6i\sqrt{1-\frac{4m_t^2}{p^2}}\, f\left(\frac{4m_t^2}{p^2}\right) - 4f\left(\frac{4m_t^2}{p^2}\right)^2\right\}, \tag{5.11}
$$

$$
\Delta_{WW} \sim c_t \frac{3\alpha_{em}}{2\pi s_w^2}\frac{m_t^2}{p^2}\left\{1 + m_t^2 \mathcal{C}\left(0, 0, p^2, m_t, 0, m_t\right)\right\}, \tag{5.12}
$$

where the function $f(\tau)$ was defined in eq. (4.10) and $\mathcal{C}$ is defined in eqs. (C.13)–(C.16) of appendix C.2. Notice that these expressions vanish in the limit $p^2 \to \infty$, as they must.

6 Some phenomenological consequences of loop-induced ALP couplings

High-precision measurements may be increasingly able to probe loop corrections to tree-level effective couplings. Currently, sensitivity to loop-induced couplings is particularly interesting when a tree-level coupling is suppressed and the loop contributions dominate.

In this section we are going to explore two examples of such situations: high-energy gluon-initiated production of an electroweak ALP, and very precise low-energy searches for ALPs which rely on couplings to electron-positron. In both cases, we focus on the loop effects of the ALP coupling to top quarks.

6.1 LHC probes for heavy ALPs

In the Lagrangian eq. (2.5), we provided the ALP with couplings to the whole SM: the electroweak bosons, gluons and fermions. This is a rather general coupling structure, yet ALPs may have restrictions on how they communicate at tree-level to the SM. For example, ALPs could originate from a UV sector participating in the mechanism of electroweak symmetry breaking, coupled to the $\mathrm{SU}(2)_L \times \mathrm{U}(1)_Y$ sector and not to the $\mathrm{SU}(3)_c$ one, e.g. in Composite Higgs models where an additional heavy CP-odd state arises as a partner to

JHEP11(2021)168

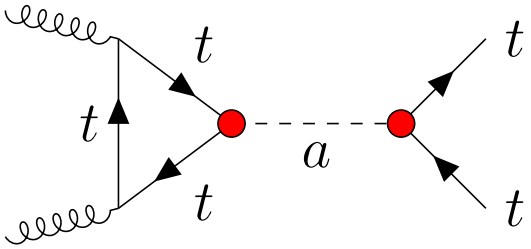

Figure 9. One-loop contribution to ALP production via gluon-fusion, and its decay to a pair of tops.

the Composite Higgs [65, 66]. This is just an example of theories with vanishing or very suppressed tree-level effective ALP-gluon coupling (g_{agg} in eq. (2.30)): an electroweak ALP.

These models of electroweak ALPs would be hard to probe at the LHC, as protons are mainly made of light quarks and gluons. Then, the leading contribution to gluon-fusion cross-section could correspond to integrating out tops. For definiteness, let us consider exclusively the ALP-top diagonal coupling c_t defined in eq. (2.38),

$$\mathscr{L} \supset c_t \frac{\partial_\mu a}{2f_a} \left(\bar{t}\gamma^\mu\gamma_5 t\right) . \tag{6.1}$$

The ALP production would then be mediated by a top running in the gluon loop and could be constrained, for instance, in $gg \to a \to t\bar{t}$ processes, as illustrated in figure 9. In this process, the ALP could be either resonant or non-resonant [19], depending on its mass.[10]

For definiteness, here we consider ALPs with $m_a > 2m_t$, such that the top-antitop pair can be resonant. This allows us to derive constraints from existing searches for resonances in $t\bar{t}$ final states, that are at a very mature stage in the LHC collaborations. This is true in particular at high-mass, where the fully hadronic topology can be accessed using jet substructure techniques. As an illustration of how LHC probes could be used to search for heavy ALPs, we re-interpret the recent ATLAS analysis [67] to set bounds on c_t/f_a.

We simulate separately the pure $gg \to a \to t\bar{t}$ signal and the component stemming from the interference of this process with SM $gg \to t\bar{t}$ production. Expressing g_{agg}^{eff} as a function of c_t as in eq. (4.16), the former scales with $(c_t/f_a)^4$ and the latter with $(c_t/f_a)^2$. The simulation is performed generating 10^5 events in each channel with `MadGraph5_aMC@NLO` [68], using an in-house UFO implementation of the Lagrangian in eq. (2.5). Variations of g_{agg}^{eff} with p^2 are neglected, as they only induce a few % correction to the numerical value of the gluon coupling. The imaginary part stemming from expanding the B_1 loop function is also subdominant and can be safely neglected in the simulation.

We perform a very simple analysis at parton level, without decaying the top quarks and without performing full parton shower and detector simulations. To partially compensate for this, a gaussian smearing with a 6% width is applied to the simulated top-antitop invariant mass ($m_{t\bar{t}}$) distribution, and the latter is multiplied by a $m_{t\bar{t}}$-dependent suppression factor

[10] A competing channel, that takes place at tree level, is $pp \to t\bar{t}a$ with $a \to t\bar{t}$. However, the phase-space suppression for this channel is stronger than the loop suppression in $gg \to t\bar{t}$. For example, for $m_a = 1\,\text{TeV}$, $\sigma(gg \to a)/\sigma(pp \to t\bar{t}a) \simeq 2 \times 10^4$.

JHEP11(2021)168

estimated from figure 2 in ref. [67], that accounts for the tagging efficiencies.[11] The acceptance correction is implemented by applying, at the generator level, the cuts reported in ref. [67] on the top quarks pseudo-rapidities $\eta_{t,\bar{t}}$ and transverse momenta $p_T(t,\bar{t})$, and on their rapidity and azimuthal-angle separations, $\Delta y_{t\bar{t}}$ and $\Delta\phi_{t\bar{t}}$ respectively.

The distribution obtained (summing signal and interference components) is compared to the difference between measured and predicted number of events in the $m_{t\bar{t}}$ spectra reported in ref. [67], that is available on HEPdata. We implement a basic test statistics constructing a χ^2 as

$$\chi^2(c_t/f_a) = \sum_k \frac{1}{\sigma_k^2}\left[\frac{c_t^4}{f_a^4}\,a_k + \frac{c_t^2}{f_a^2}\,i_k + b_k - d_k\right], \tag{6.2}$$

where the index k runs over the bins of the $m_{t\bar{t}}$ distributions for the 1- and 2-b-tagged signal regions, a_k (i_k) is the number of events estimated for the pure ALP signal (ALP-SM interference) in the k-th bin with $c_t/f_a = 1\,\text{TeV}^{-1}$. In this equation, b_k (d_k) is the number of expected background events (observed events) reported by the ATLAS Collaboration. Finally, the uncertainty σ_k is estimated by summing in quadrature the total systematic uncertainty reported by ATLAS, the statistical error $\sqrt{d_k}$ on the measured data points and the statistical uncertainty associated to our Monte Carlo simulation. As a conservative choice, bins with 0 observed events are removed from the analysis, as in this case a χ^2 statistics cannot be applied. We repeat this analysis for various values of m_a in the range from 1.6 to 4.6 TeV and extract, for each value, a 95%CL upper limit on c_t/f_a.

The results of this naive re-interpretation are shown in figure 10. The limits on f_a obtained lie at the boundaries of a good effective description of the ALP Lagrangian as, for $|c_t| = 1$, the bound on f_a is mostly below m_a. On the other hand, in a strongly interacting regime where $|c_t| \simeq 4\pi$ (as could be the case of a Composite Higgs model), the limits on f_a improve by an order of magnitude and result well above m_a. A dedicated analysis, potentially extended to the leptonic and semi-leptonic channels, could improve these bounds significantly.

6.2 Limits on the couplings to top quarks for light ALPs

Another interesting use of loop-induced ALP couplings appears when a tree-level coupling is very well measured and can provide a good constraint on loop-induced couplings, assuming no substantial cancellations happen between tree and loop-induced couplings. Among these, the loop-induced ALP-electron diagonal coupling c_e (defined in eq. (2.40)),

$$\mathscr{L} \supset c_e\,\frac{\partial_\mu a}{2f_a}\,(\bar{e}\gamma^\mu\gamma_5 e)\,, \tag{6.3}$$

is particularly interesting as electrons are found in stable matter. Astrophysical objects like red giants or precise non-collider experiments such as Dark Matter Direct Detection

[11] We assume that the efficiency for the ALP detection does not differ significantly from that for a Z'. A more detailed analysis would require simulating both particles and comparing how the fat-jet tagging efficiency varies depending on the coupling properties of the resonance. This dependence has been often found to be subdominant in previous studies, see e.g. refs. [69, 70].

JHEP11(2021)168

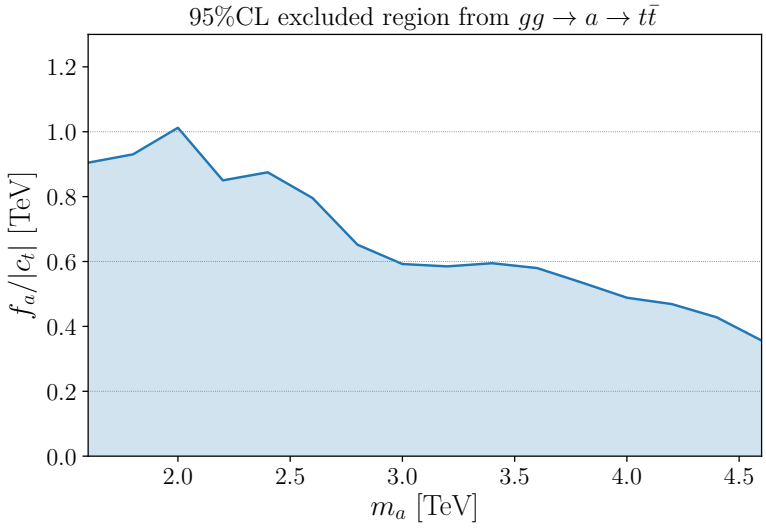

Figure 10. Limits on $f_a/|c_t|$, as a function of the ALP mass, extracted from the all-hadronic $t\bar{t}$ resonance search by ATLAS of ref. [67].

experiments provide an excellent handle on that coupling. Here we consider the current limits on the axion-electron coupling collected in ref. [71], that include results from Red Giants [72], Solar neutrinos [73] and LUX [74], which are derived for solar axions and extend to very low ALP masses, as well as from Edelweiss [75], PandaX [76], SuperCDMS [77] and XENON-1T [78–80], that cover the region $100\,\text{eV} \lesssim m_a \lesssim 100\,\text{keV}$ assuming the ALP to be the main DM constituent.[12] The most stringent bounds are those from red giants and from DM direct detection at XENON-1T, and give $|c_e^{\text{eff}}|\,(m_e/f_a) \lesssim 10^{-13}$.

These limits can be translated into limits on the diagonal ALP-top coupling, using the one-loop contributions computed in section 4.6, corresponding to diagram **E** in figure 6, see also refs. [62, 81]. Note that in DM direct detection experiments the typical energy range is the keV, hence our expressions must be taken in the limit of low-momentum exchange in the detector between the ALP and the electron, i.e. below the electron mass. In this case one finds the log-enhanced expression found in eq. (4.61), namely:

$$c_e^{\text{eff}} \simeq 2.48\, c_t\, \alpha_{em}\, \log\left(\frac{\Lambda^2}{m_t^2}\right) . \tag{6.4}$$

For consistency, the cutoff of the loop integrals Λ should be of the same order as f_a. As the Λ dependence is logarithmic we will use $\Lambda = 10^6$ TeV in this equation, to extract the bounds on f_a/c_t shown in figure 11,[13] from which it follows

$$f_a/|c_t| > 2.2 \times 10^6\,\text{TeV} \tag{6.5}$$

[12] Note that — strictly speaking — the bounds extracted from DM searches only apply in scenarios where the ALP is stable and can be produced with the correct relic abundance. Verifying the latter condition for the particular ALP scenario considered here is beyond the scope of this work.

[13] The value 10^6 TeV was chosen a posteriori, so as to match the limits on f_a.

JHEP11(2021)168

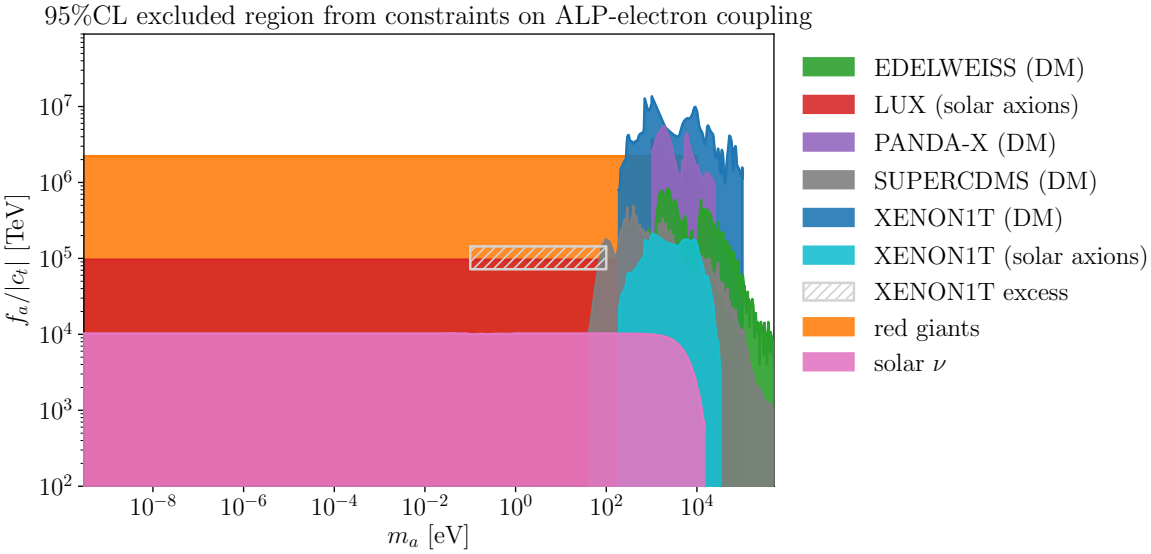

Figure 11. Limits on $f_a/|c_t|$ as a function of the ALP mass, extracted rescaling existing constraints on the ALP-electron coupling, taken from ref. [71]. The grey hatched box marks the region roughly compatible with the excess observed by XENON1T [79].

in the entire range considered. If the ALP is assumed to be DM, XENON1T bounds apply, leading to the stronger constraint

$$f_a/|c_t| > 1.4 \times 10^7 \text{ TeV} \,. \tag{6.6}$$

XENON1T recently observed an excess in their data, which could have been explained by solar axions coupled to electrons and/or photons in the mass range $m_a \sim 0.1 - 100\,\text{eV}$ for the QCD axion [79, 82]. Thus, instead of a limit, in this case XENON1T would identify a finite preferred region in the plane $(g_{a\gamma\gamma}, c_e/f_a)$. Unfortunately, this interpretation of a QCD axion is in conflict with the data from red giants. Nevertheless and for the sake of the exercise, one can consider what would be the preferred value for f_a/c_t if that XENON1T excess was taken at face value. Using then eq. (6.4), and the one-loop corrections to $g_{a\gamma\gamma}$ computed in section 4.1 which correspond to diagram **C** in figure 4, it follows that the induced value of $g_{a\gamma\gamma}$ is strongly suppressed for the ALP mass range considered here ($p^2 = m_a^2 \ll m_t^2$): $g_{a\gamma\gamma}^{\text{eff}} \lesssim 10^{-8} \alpha_{em} c_t/f_a \ll c_e^{\text{eff}}/f_a$. In this limit, the results from XENON1T could be interpreted as a preferred range for c_e^{eff} independent of $g_{a\gamma\gamma}$. This broadly includes values $2 \times 10^{-12} \lesssim |c_e^{\text{eff}}|(m_e/f_a) \lesssim 4 \times 10^{-12}$. The projection of this interval in terms of f_a/c_t is shown as a grey-hatched region in figure 11.

Finally, note that the type of analysis carried out in this subsection can be also applied to the flavour-diagonal ALP-bottom coupling c_b (defined in eq. (2.39)). Numerically, limits on f_a/c_b can be approximately estimated rescaling by m_b^2/m_t^2 [81] those on f_a/c_t in eqs. (6.5) and (6.6) above, leading respectively to $f_a/|c_b| > 1.0 \times 10^3$ TeV and $f_a/|c_b| > 6.5 \times 10^3$ TeV, for $\Lambda = 10^3$ TeV.

JHEP11(2021)168

7 Conclusions

The search for axions and ALPs is intensifying in both the energy and the precision frontiers. The vastly different energy regions explored range from those typical of astrophysics and low-energy laboratory experiments to collider energies. At the same time, increasingly precise probes are targeted e.g. photon and/or invisible channels in rare hadron decays and other low-energy channels. The point is well past in which the estimation of one-loop effects in the couplings of ALPs to SM particles is needed to explore optimally BSM physics through the detection of pseudo-Goldstone bosons signals. From the theoretical point of view, effective Lagrangian formulations allow to pursue this quest in a very model-independent way.

In this work, we have first clarified the relations among alternative — complete and non-redundant — CP-even bases for the $d = 5$ ALP linear effective Lagrangian. In doing so, we derived the exact relations between bases which differ in their choices of fermionic operators constructed with left-handed and right-handed currents and/or chirality-flip couplings. We identified the precise combinations of gauge anomalous couplings involved in trading different bases. This includes the relations stemming from the anomalous global $B + L$ current and the conserved $B - L$ one. Although we then chose to work on a complete and non-redundant basis containing gauge anomalous operators plus all possible right-handed fermionic currents and certain couplings made out of left-handed currents, the relations obtained will allow easy translation of the results to other bases.

Furthermore, illustrative practical checks of bases equivalences were as well performed. For instance, the purely bosonic operator $\mathbf{O}_{a\Phi}$ can be written either as a combination of right-handed fermion currents or as a combination of left-handed fermion currents, right-handed ones and gauge anomalous couplings: it is explicitly shown how all anomalous corrections vanish at one-loop level, as they should.

In a second step, we have computed the complete one-loop corrections — thus including all divergent and finite terms — to all possible CP-even couplings of an ALP to SM fields, for a generic off-shell ALP and on-shell SM particles. Our results are formulated in the form of the effective one-loop interactions $\{g^{\text{eff}}_{agg}, g^{\text{eff}}_{a\gamma\gamma}, g^{\text{eff}}_{aWW}, g^{\text{eff}}_{aZZ}, g^{\text{eff}}_{a\gamma Z}, c^{\text{eff}}_{\text{f}}\}$, where the latter is computed for all SM fermions — light and heavy — but restricted to flavour diagonal external channels. Moreover three-generation CKM mixing is disregarded in the loop corrections. Neutrino masses are disregarded as well. Our computations thus carry to novel territory previous studies restricted to on-shell ALPs and to certain channels and limits. All our computations have been performed in the covariant R_ξ gauge, and the intermediate ξ-dependent steps made publicly available at NotebookArchive, together with the exact final gauge-invariant results. The latter are shown as well in appendix C, while in the main text limits relevant for high, intermediate and low energy experiments are extracted. Particular attention has been dedicated to the isolation of infrared divergences when present. As a byproduct, the UV divergent terms of our computations also allowed to do a straightforward check of recent RG results in the literature in different bases.

An illustration of the reach of our results is the impact that any putative ALP coupling induces at one-loop on any other ALP interaction. For instance, we explored how, for heavy ALPs, the ALP-top coupling can be constrained by LHC measurements of top-pair final

JHEP11(2021)168

states, processes which are induced at one-loop by this coupling. These channels, pumped up by gluon fusion via a top loop, open up the possibility of studying many ALP final states with a sizeable cross-section, even when the tree-level coupling ALP-gluon would be zero. We also explored constraints on ALP-top interactions for light ALPs. In this case, the strictest limits are those derived from bounds on the ALP-electron coupling, extracted from astrophysical constraints and from DM Direct Detection searches [62].

An interesting point also clarified in this work is the one-loop modification of the electroweak tree-level gauge invariance relations. These are relevant as far as custodial symmetry breaking, i.e. mass and hypercharge differences, are relevant. We have determined these corrections, which will impact future one-loop extractions at LHC and other experiments of the sensitivity to a given ALP coupling from more precise data on another ALP coupling (e.g. g_{aWW} from data on $g^{\text{eff}}_{a\gamma\gamma}$ or $g^{\text{eff}}_{a\gamma Z}$, and similar analyses).

A plethora of experimental channels should be explored using the results of this paper. Future directions include the one-loop complete results with all external particles off-shell and also flavour non-diagonal channels. A related interesting task is the computation of box and other diagrams for certain physical processes, which is mandatory to cancel all infrared divergences in processes involving g_{agg}, g_{aWW} and $c^{\text{eff}}_{\text{f}}$. Finally, the analysis of the ALP bases should be extended to include CP violation in the ALP couplings. These and other exciting developments lie ahead in the BSM path to uncover novel pseudo-Goldstone boson physics.

Acknowledgments

We thank Gonzalo Alonso, Josemi No, Jorge Fernandez de Troconiz, Arturo de Giorgi, Luca Merlo and Pablo Quilez for illuminating discussions. The work of J.B. was e supported by the Spanish MICIU through the National Program FPU (grant number FPU18/03047). J.B. and M.B.G. acknowledge partial financial support by the Spanish MINECO through the Centro de excelencia Severo Ochoa Program under grant SEV-2016-0597, by the Spanish "Agencia Estatal de Investigacíon"(AEI) and the EU "Fondo Europeo de Desarrollo Regional" (FEDER) through the project PID2019-108892RB-I00/AEI/10.13039/501100011033. All authors acknowledge the European Union's Horizon 2020 research and innovation programme under the Marie Skłodowska-Curie grant agreement No. 860881-HIDDeN. VS acknowledges support from the UK STFC via Grant ST/L000504/1.

A Standard Model equations of motion

In this appendix we report the SM EOM for the fermion and Higgs fields, that are relevant for the discussion in section 2 and appendix B. For chiral fermions, the EOM read

$$i\not{D} Q_L = \Phi Y_d d_R + \tilde{\Phi} Y_u u_R\,, \qquad i\not{D} u_R = \tilde{\Phi}^\dagger Y_u^\dagger Q_L\,, \qquad i\not{D} d_R = \Phi^\dagger Y_d^\dagger Q_L\,, \tag{A.1}$$

$$i\not{D} L_L = \Phi Y_e e_R\,, \qquad i\not{D} e_R = \Phi^\dagger Y_e^\dagger L_L\,, \tag{A.2}$$

JHEP11(2021)168

where flavor index contractions are implicit. For the conjugate fields they imply

$$-i\bar{Q}_L \overleftarrow{\not{D}} = \bar{d}_R Y_d^\dagger \Phi^\dagger + \bar{u}_R Y_u^\dagger \tilde{\Phi}^\dagger\,, \qquad -i\bar{u}_R \overleftarrow{\not{D}} = \bar{Q}_L Y_u \tilde{\Phi}\,, \qquad -i\bar{d}_R \overleftarrow{\not{D}} = \bar{Q}_L Y_d \Phi\,, \tag{A.3}$$

$$-i\bar{L}_L \overleftarrow{\not{D}} = \bar{e}_R Y_e^\dagger \Phi^\dagger\,, \qquad -i\bar{e}_R \overleftarrow{\not{D}} = \bar{L}_L Y_e \Phi\,. \tag{A.4}$$

The EOM for the Higgs field reads

$$\Box\Phi_i = -\left[\bar{d}_R Y_d^\dagger (Q_L)_i + (\bar{Q}_L i\sigma^2)_i Y_u u_R + \bar{e}_R Y_e^\dagger (L_L)_i\right] + \frac{m_h^2}{2}\Phi_i - 2\lambda(\Phi^\dagger\Phi)\Phi_i\,, \tag{A.5}$$

$$\Box\Phi_i^\dagger = -\left[(\bar{Q}_L)_i Y_d d_R + \bar{u}_R Y_u^\dagger (i\sigma^2 Q_L)_i + (\bar{L}_L)_i Y_e e_R\right] + \frac{m_h^2}{2}\Phi_i^\dagger - 2\lambda(\Phi^\dagger\Phi)\Phi_i^\dagger\,, \tag{A.6}$$

where i is a free $\mathrm{SU}(2)_L$ index and we have taken $V(\Phi^\dagger\Phi) = -(m_H^2/2)\Phi^\dagger\Phi + \lambda(\Phi^\dagger\Phi)^2$, where m_H and λ denote respectively the Higgs mass and self-coupling.

The use of fermion EOM is tantamount to chiral rotations of fermion fields, at the classical level. When considering loop effects as in this work, they must be supplemented by the contributions of the SM anomalous global currents, i.e.

$$\partial_\mu(\bar{Q}_L^i \gamma^\mu Q_L^i) \supset \frac{g'^2}{96\pi^2} B_{\mu\nu}\tilde{B}^{\mu\nu} + \frac{3g^2}{32\pi^2} W^\alpha_{\mu\nu}\tilde{W}^{\alpha\mu\nu} + \frac{g_s^2}{16\pi^2} G^a_{\mu\nu}\tilde{G}^{a\mu\nu}\,, \tag{A.7}$$

$$\partial_\mu(\bar{u}_R^i \gamma^\mu u_R^i) \supset -\frac{g'^2}{12\pi^2} B_{\mu\nu}\tilde{B}^{\mu\nu} - \frac{g_s^2}{32\pi^2} G^a_{\mu\nu}\tilde{G}^{a\mu\nu}\,, \tag{A.8}$$

$$\partial_\mu(\bar{d}_R^i \gamma^\mu d_R^i) \supset -\frac{g'^2}{48\pi^2} B_{\mu\nu}\tilde{B}^{\mu\nu} - \frac{g_s^2}{32\pi^2} G^a_{\mu\nu}\tilde{G}^{a\mu\nu}\,, \tag{A.9}$$

$$\partial_\mu(\bar{L}_L^i \gamma^\mu L_L^i) \supset \frac{g'^2}{32\pi^2} B_{\mu\nu}\tilde{B}^{\mu\nu} + \frac{g^2}{32\pi^2} W^\alpha_{\mu\nu}\tilde{W}^{\alpha\mu\nu}\,, \tag{A.10}$$

$$\partial_\mu(\bar{e}_R^i \gamma^\mu e_R^i) \supset -\frac{g'^2}{16\pi^2} B_{\mu\nu}\tilde{B}^{\mu\nu}\,, \tag{A.11}$$

where we are not summing over the index i.

B Field redefinitions and operator basis reduction

In this appendix we consider the ALP-dependent field redefinitions that are required in order to relate and reduce the operator basis:

$$\Phi \mapsto \exp\left[i x_\Phi \frac{a}{f_a}\right]\Phi\,, \qquad\qquad \mathrm{f} \mapsto \exp\left[i \mathbf{x}_\mathrm{f} \frac{a}{f_a}\right]\mathrm{f}\,, \tag{B.1}$$

where in flavour space $\mathrm{f} = \{Q_L, u_R, d_R, L_L, e_R\}$ are vectors and $\mathbf{x}_\mathrm{f} = \mathbf{x}_\mathrm{f}^{ij}$ are tensors. For notation simplicity, the subindices $\{L, R\}$ will be omitted, i.e. $\mathrm{f} = \{Q_L, u_R, d_R, L_L, e_R\} \equiv \{Q, u, d, L, e\}$. We take all rotation parameters x_Φ and $\mathbf{x}_\mathrm{f}$ to be real, consistent with the assumption of CP conservation of the ALP couplings (the only CP-violation present is that of the SM contained in CKM, i.e. in the Yukawa matrices). Moreover, due to the hermicity of the Lagrangian it is only the symmetric component of the matrices $\mathbf{x}_\mathrm{f}$ that contributes to a variation in it. Then, from now on we assume $\mathbf{x}_\mathrm{f}$ to be symmetric, i.e. $\mathbf{x}_\mathrm{f}^{ij} = \mathbf{x}_\mathrm{f}^{ji}$, so $(\mathbf{x}_\mathrm{f} + \mathbf{x}_\mathrm{f}^T)/2 = \mathbf{x}_\mathrm{f}$. Discussing the basis reduction in terms of field redefinitions rather than

JHEP11(2021)168

via the direct use of EOMs makes their impact on the $\mathbf{O}_{\tilde{X}}$ operators more transparent: because the fermion rotations are chiral, contributions to the latter are generated through the axial anomaly.

The general procedure for reducing the operator basis is as follows. The rotations in (B.1) are first applied to $\mathscr{L}_{\rm SM}$ (eq. (2.2)), and an expansion at $O(1/f_a)$ is performed next. The net shift resulting from the most general rotation reads [17]

$$\begin{aligned}\Delta\mathscr{L}_{\rm SM} = &-x_\Phi\,\mathbf{O}_{a\Phi} - \sum_{\mathrm{f}=Q,u,d,L,e} \mathbf{x}_\mathrm{f}\mathbf{O}_\mathrm{f} + \Big[\left(\mathbf{x}_L Y_e - Y_e\mathbf{x}_e - x_\Phi Y_e\right)\mathbf{O}_{e\Phi}\\ &+ \left(\mathbf{x}_Q Y_d - Y_d\mathbf{x}_d - x_\Phi Y_d\right)\mathbf{O}_{d\Phi} + \left(\mathbf{x}_Q Y_u - Y_u\mathbf{x}_u + x_\Phi Y_u\right)\mathbf{O}_{u\Phi} + \mathrm{h.c.}\Big]\\ &+ \frac{g'^2}{32\pi^2}\mathbf{O}_{\tilde{B}}\,\mathrm{Tr}\left[\frac{1}{3}\mathbf{x}_Q - \frac{8}{3}\mathbf{x}_u - \frac{2}{3}\mathbf{x}_d + \mathbf{x}_L - 2\mathbf{x}_e\right] + \frac{g^2}{32\pi^2}\mathbf{O}_{\tilde{W}}\,\mathrm{Tr}\left[3\mathbf{x}_Q + \mathbf{x}_L\right]\\ &+ \frac{g_s^2}{32\pi^2}\mathbf{O}_{\tilde{G}}\,\mathrm{Tr}\left[2\mathbf{x}_Q - \mathbf{x}_u - \mathbf{x}_d\right]\,,\end{aligned} \tag{B.2}$$

where the anomalous operators $\mathbf{O}_{\tilde{X}}$ are defined in table 1, $\mathbf{O}_\mathrm{f}$ are the chirality-conserving fermionic operators defined in eqs. (2.3) (2.4), $\mathbf{O}_{\mathrm{f}\Phi}$ are the chirality-flip ones defined in eq. (2.19), and finally $\mathbf{O}_{a\Phi}$ is defined in table 2. The trace in the last two lines of eq. (B.2) is over flavor indices, while in the first two lines the implicit contraction of flavour index of the effective coefficients and operators respects the convention in eq. (2.6), e.g.

$$\left(\mathbf{x}_L Y_e - Y_e\mathbf{x}_e - x_\Phi Y_e\right)\mathbf{O}_{e\Phi} = \sum_{i,j}\left(\mathbf{x}_L Y_e - Y_e\mathbf{x}_e - x_\Phi Y_e\right)_{ij}\mathbf{O}_{e\Phi}^{ij}\,,\quad \text{etc.}\,,$$

while the expressions inside parenthesis are matrix products, i.e. $(\mathbf{x}_L Y_e)_{ij} = \sum_k (\mathbf{x}_L)_{ik}(Y_e)_{kj}$.

At this point, one is free for instance to choose x_Φ and $\mathbf{x}_\mathrm{f}$ so that the terms in $\Delta\mathscr{L}_{\rm SM}$ cancel off against redundant operators in $\mathscr{L}_a^{\rm total}$. Or to choose values for combination of indices so as to remove one or all of the anomalous coefficients $c_{\tilde{X}}$. It is not hard to verify that each field transformation is equivalent — up to shifts to the anomalous bosonic operators — to the application of the EOM of the corresponding field, provided in appendix A. In what follows, some specific applications of eq. (B.2) are developed.

B.1 Relation between $\mathbf{O}_{a\Phi}$ and fermionic operators

Eq. (B.2) indicates that in order to remove $\mathbf{O}_{a\Phi}$ one needs to fix $x_\Phi = c_{a\Phi}$. This Φ rotation comes at the price of introducing a set of chirality-flip operators [17, 46, 52], i.e.

$$\mathbf{O}_{a\Phi} = Y_u\mathbf{O}_{u\Phi} - Y_d\mathbf{O}_{d\Phi} - Y_e\mathbf{O}_{e\Phi} + \mathrm{h.c.}\,. \tag{B.3}$$

As $\mathbf{O}_{a\Phi}$ is a purely bosonic operator, the flavor structure of the fermionic operators in this equation necessarily reflects the SM flavour structure. In other words, it follows the MFV ansatz [83–85], where a $\mathrm{U}(3)^5$ global flavor symmetry is present in the Lagrangian but for the Yukawa couplings, which are treated as spurions.

The combination of chirality-flip operators obtained can be traded next for chirality-preserving ones (plus in some cases shifts in the $\mathbf{O}_{\tilde{X}}$ operator coefficients) by fixing the quantities $\mathbf{x}_\mathrm{f}$ such that the coefficients of $\mathbf{O}_{e\Phi}, \mathbf{O}_{u\Phi}, \mathbf{O}_{d\Phi}$ in eq. (B.2) cancel. This is

JHEP11(2021)168

equivalent to applying the transformations of the fermion fields in eqs. (B.5)–(B.9) below. For instance, it is possible to map $\mathbf{O}_{a\Phi}$ onto just 3 operators out of the whole set $\{\mathbf{O}_u, \mathbf{O}_d, \mathbf{O}_e, \mathbf{O}_Q, \mathbf{O}_L\}$, plus $\mathbf{O}_{\tilde{X}}$ operators. For example, the mapping onto the set $\{\mathbf{O}_u, \mathbf{O}_d, \mathbf{O}_e\}$ is achived choosing $\mathbf{x}_e^{ij} = \mathbf{x}_d^{ij} = -\mathbf{x}_u^{ij} = \delta^{ij}\, c_{a\Phi}$, and leads to eq. (2.26), that is a combination of only right-handed fermionic currents. As it can be easily checked from eq. (B.2), the contributions to gauge anomalous operators $\mathbf{O}_{\tilde{X}}$ cancel exactly in this case, which does not necessarily generalize to other choices.

For instance, one could alternatively map onto the set $\{\mathbf{O}_Q, \mathbf{O}_u, \mathbf{O}_L\}$ by choosing $\mathbf{x}_L^{ij} = \mathbf{x}_Q^{ij} = \mathbf{x}_u^{ij}/2 = \delta^{ij}\, c_{a\Phi}$, which leads to

$$\mathbf{O}_{a\Phi} = -\,\mathrm{Tr}\,(\mathbf{O}_L + \mathbf{O}_Q + 2\mathbf{O}_u) + \frac{1}{8\pi^2}\left(g^2\mathbf{O}_{\tilde{W}} - g'^2\mathbf{O}_{\tilde{B}}\right) n_g\,. \tag{B.4}$$

This result does not mean that $\mathbf{O}_{a\Phi}$ is anomalous! In fact, we have explicitly checked that when the product $c_{a\Phi}\mathbf{O}_{a\Phi}$ is considered at $\mathcal{O}(\alpha)$, the contribution from the $\mathbf{O}_{\tilde{X}}$ terms on the last bracket are compensated exactly by the anomalous contributions stemming from the insertion in figure 4 diagram **C** of the operators in the first bracket ($\mathbf{O}_u$, $\mathbf{O}_Q$ and $\mathbf{O}_L$), and only $\mathcal{O}(m_\mathrm{f}^2)$ finite terms of remain from the loop contribution. When instead the same computation is performed using the expression for $\mathbf{O}_{a\Phi}$ in eq. (2.26), i.e. as combination of the right-handed set $\{\mathbf{O}_u, \mathbf{O}_d, \mathbf{O}_e\}$, the anomalous contributions they induce cancel each other and only the same $\mathcal{O}(m_\mathrm{f}^2)$ terms are present, as they should.

B.2 Relations among fermionic operators

Collecting the terms proportional to $\mathbf{x}_\mathrm{f}$ in eq. (B.2) one can infer relations among the fermionic operators. Writing explicitly the flavor indices i, j, it follows that the relations between chirality preserving and chirality-flip operators (plus anomalous couplings) read fermion structures can be

$$\begin{aligned}\mathbf{O}_Q^{ij} = &\left[\mathbf{O}_{d\Phi}^{ik}\,(Y_d)_{jk} + \mathbf{O}_{u\Phi}^{ik}\,(Y_u)_{jk} + (\mathbf{O}_{d\Phi}^\dagger)^{kj}\,(Y_d^\dagger)_{ki} + (\mathbf{O}_{u\Phi}^\dagger)^{kj}\,(Y_u^\dagger)_{ki}\right] \\ &+ \left[\frac{g'^2}{96\pi^2}\mathbf{O}_{\tilde{B}} + \frac{3g^2}{32\pi^2}\mathbf{O}_{\tilde{W}} + \frac{g_s^2}{16\pi^2}\mathbf{O}_{\tilde{G}}\right]\delta^{ij}\,,\end{aligned} \tag{B.5}$$

$$\mathbf{O}_u^{ij} = \left[-\mathbf{O}_{u\Phi}^{kj}\,(Y_u)_{ki} - (\mathbf{O}_{u\Phi}^\dagger)^{ik}\,(Y_u^\dagger)_{jk}\right] - \left[\frac{g'^2}{12\pi^2}\mathbf{O}_{\tilde{B}} + \frac{g_s^2}{32\pi^2}\mathbf{O}_{\tilde{G}}\right]\delta^{ij}\,, \tag{B.6}$$

$$\mathbf{O}_d^{ij} = \left[-\mathbf{O}_{d\Phi}^{kj}\,(Y_d)_{ki} - (\mathbf{O}_{d\Phi}^\dagger)^{ik}\,(Y_d^\dagger)_{jk}\right] - \left[\frac{g'^2}{48\pi^2}\mathbf{O}_{\tilde{B}} + \frac{g_s^2}{32\pi^2}\mathbf{O}_{\tilde{G}}\right]\delta^{ij}\,, \tag{B.7}$$

$$\mathbf{O}_L^{ij} = \left[\mathbf{O}_{e\Phi}^{ik}\,(Y_e)_{jk} + (\mathbf{O}_{e\Phi}^\dagger)^{kj}\,(Y_e^\dagger)_{ki}\right] + \left[\frac{g'^2}{32\pi^2}\mathbf{O}_{\tilde{B}} + \frac{g^2}{32\pi^2}\mathbf{O}_{\tilde{W}}\right]\delta^{ij}\,, \tag{B.8}$$

$$\mathbf{O}_e^{ij} = \left[-\mathbf{O}_{e\Phi}^{kj}\,(Y_e)_{ki} - (\mathbf{O}_{e\Phi}^\dagger)^{ik}\,(Y_e^\dagger)_{jk}\right] - \frac{g'^2}{16\pi^2}\mathbf{O}_{\tilde{B}}\,\delta^{ij}\,, \tag{B.9}$$

where a sum over k is understood. Combining them, the relations between chirality-conserving operators and chirality-flip ones are determined.

The equations above showed how to express the chirality-conserving couplings as combinations of chirality-flip ones. What about the inverse relation? It is clear from the

JHEP11(2021)168

counting of degrees of freedom shown earlier that the latter cannot be achieved in all generality. Indeed, only very particular combinations — relatively weighed by Yukawa factors — of a given chirality-flip operator can be extracted from eqs. (B.5)–(B.9), and written in terms of chirality-conserving plus anomalous couplings: this reduces in practice their n_g^2 degrees of freedom per fermionic operator (which sums to a total of $3n_g^2$ fermionic parameters in the ALP Lagrangian) to an active number of $n_g(5n_g+3)/2-1$ fermionic parameters in total.

B.3 Purely fermionic bases: removing anomalous operators

Finally, one could ask whether the anomalous operators $\mathbf{O}_{\tilde{X}}$ could be removed altogether from the basis, trading them for fermionic structures. In order to do this, one needs to impose

$$\frac{g'^2}{32\pi^2}\,\mathrm{Tr}\left[\frac{1}{3}\mathbf{x}_Q-\frac{8}{3}\mathbf{x}_u-\frac{2}{3}\mathbf{x}_d+\mathbf{x}_L-2\mathbf{x}_e\right]=-c_{\tilde{B}}\,, \tag{B.10}$$

$$\frac{g^2}{32\pi^2}\,\mathrm{Tr}\left[3\mathbf{x}_Q+\mathbf{x}_L\right]=-c_{\tilde{W}}\,. \tag{B.11}$$

$$\frac{g_s^2}{32\pi^2}\,\mathrm{Tr}\left[2\mathbf{x}_Q-\mathbf{x}_u-\mathbf{x}_d\right]=-c_{\tilde{G}}\,. \tag{B.12}$$

It is not difficult to show explicitly that the anomalous bosonic operators cannot be completely replaced by purely chirality-conserving fermionic ones.[14] Indeed, it follows from eq. (B.2) that the conditions to remove all chirality-flip terms are

$$\begin{aligned}\mathbf{x}_Q Y_u-Y_u\mathbf{x}_u&=0\,,\\ \mathbf{x}_Q Y_d-Y_d\mathbf{x}_d&=0\,,\\ \mathbf{x}_L Y_e-Y_e\mathbf{x}_e&=0\,,\end{aligned} \tag{B.13}$$

and it is not possible to satisfy simultaneously these equations and the conditions in eqs. (B.10)–(B.12). Nevertheless, it is sufficient to relax two of the conditions in (B.13) in order for the system to be solvable. This implies that any solution of eqs. (B.5)–(B.9) always involve chirality-flip terms. One example is:

$$\mathbf{O}_{\tilde{B}}=-\frac{16\pi^2}{g'^2 n_g}\left[\mathrm{Tr}\,\mathbf{O}_e+(Y_e\mathbf{O}_{e\Phi}+\mathrm{h.c.})\right]\,, \tag{B.14}$$

$$\mathbf{O}_{\tilde{W}}=\frac{32\pi^2}{g^2 n_g}\left[\mathrm{Tr}\left(\mathbf{O}_L+\frac{1}{2}\mathbf{O}_e\right)-\left(\frac{Y_e}{2}\mathbf{O}_{e\Phi}+\mathrm{h.c.}\right)\right]\,, \tag{B.15}$$

$$\mathbf{O}_{\tilde{G}}=\frac{32\pi^2}{g_s^2 n_g}\left[\mathrm{Tr}\left(-\mathbf{O}_d+\frac{\mathbf{O}_e}{3}\right)-\left(Y_d\mathbf{O}_{d\Phi}-\frac{Y_e}{3}\mathbf{O}_{e\Phi}+\mathrm{h.c.}\right)\right]\,. \tag{B.16}$$

A final comment on the non-equivalence of anomalous couplings and shift-invariant fermionic ones is pertinent in the case of the gauge hypercharge, i.e. the operator $\mathbf{O}_{\tilde{B}}$. As it is well known, the pure gauge anomalous couplings can be written as total derivatives of non-gauge invariant quantities, $X_{\mu\nu}\tilde{X}^{\mu\nu}=\partial_\mu K_X^\mu$, a term that for pure U(1) gauge Lagrangians

[14] This is as expected on physical grounds, given the non-invariance of anomalous gauge couplings under the shift symmetry.

JHEP11(2021)168

does not contribute to the action because the gauge configurations die sufficiently fast at infinity, unlike for non-abelian groups. In this sense, it can appear at first sight surprising that the equations above show that the fermionic equivalent of $\mathbf{O}_{\tilde{B}}$ does include chirality-flip (and thus not-shift invariant) terms. Nevertheless, in the presence of fermions it is the combination of $\mathbf{O}_{\tilde{B}}$ and $\mathbf{O}_{\tilde{W}}$ in eq. (2.12) the one which is shift-invariant, because it corresponds to the non-conservation of the anomalous $B+L$ global U(1), while the combination of $\mathbf{O}_{\tilde{B}}$ and $\mathbf{O}_{\tilde{W}}$ with opposite sign is endowed with a non shift-invariant nature, see eq. (2.20).

C Complete — finite and divergent — corrections to effective couplings

We gather here the exact expressions for the one-loop corrections to the set of ALP-SM couplings $\{g_{a\gamma Z}, g_{aZZ}, g_{aWW}\}$ at $\mathcal{O}(1/f_a)$, for a generic off-shell ALP and on-shell external SM fields. These couplings were introduced and developed only in certain limits in section 4, while the complete expressions are presented below.

C.1 ALP-Z-photon anomalous coupling

The results for the one-loop corrected $g^{\text{eff}}_{a\gamma Z}$ have been introduced in section 4.3, where the results were also presented in certain limits. We collect in this appendix the exact expressions for the functions defined in that section (the complete expression for $A^{Z/\gamma\to\gamma}$ was already given in eq. (4.11)). All descriptions presented there for the origin of each term apply here as well. The intermediate ξ-dependent steps, together with the final ξ-independent expressions, can be found in NotebookArchive. The gauge invariant complete results are as follows:

$$\begin{aligned}
A^{Z/\gamma\to Z}_{\text{ferm}} = -2\sum_{\text{f}} N_C \Bigg\{ & \left(\frac{T^2_{3,\text{f}}}{2} - T_{3,\text{f}} Q_\text{f} s_w^2 + Q_\text{f}^2 s_w^4\right) \times \\
& \times \left(\log\left(\frac{\Lambda^2}{m_\text{f}^2}\right) + \frac{2}{3} + \frac{M_Z^2 - 2m_\text{f}^2}{M_Z^2 - 4m_\text{f}^2}\mathcal{DB}(M_Z^2, m_\text{f}, m_\text{f})\right) \\
& + \frac{m_\text{f}^2}{M_Z^2}\left(\frac{T^2_{3,\text{f}}}{2} + 2T_{3,\text{f}} Q_\text{f} s_w^2 - 2Q_\text{f}^2 s_w^4\right)\left(1 - \frac{2m_\text{f}^2}{M_Z^2 - 4m_\text{f}^2}\mathcal{DB}(M_Z^2, m_\text{f}, m_\text{f})\right) \\
& - c_w^2 Q_\text{f}(T_{3,\text{f}} - 2Q_\text{f} s_w^2)\left[\log\left(\frac{\Lambda^2}{m_\text{f}^2}\right)\right. \\
& \left. + \frac{12m_\text{f}^2 + 5M_Z^2}{3M_Z^2} + \frac{2m_\text{f}^2 + M_Z^2}{M_Z^2}\mathcal{DB}(M_Z^2, m_\text{f}, m_\text{f})\right]\Bigg\},
\end{aligned} \tag{C.1}$$

where $T_{3,\text{f}}$ denotes the weak isospin of fermion f.

The function $A^{Z\to Z}_{\text{Higgs}}$ for the Higgs corrections to external legs is given by

$$\begin{aligned}
A^{Z\to Z}_{\text{Higgs}} = \frac{1}{4}\Bigg\{ & \frac{M_Z^4 - 3M_Z^2 M_H^2 + M_H^4}{M_Z^4} + \frac{12M_Z^6 - 18M_Z^4 M_H^2 + 9M_Z^2 M_H^4 - 2M_H^6}{4M_Z^6}\log\left(\frac{M_H^2}{M_Z^2}\right) \\
& - \frac{36M_Z^6 - 32M_Z^4 M_H^2 + 13M_Z^2 M_H^4 - 2M_H^6}{2M_Z^4(M_H^2 - 4M_Z^2)}\mathcal{DB}(M_Z^2, M_Z, M_H)\Bigg\},
\end{aligned} \tag{C.2}$$

JHEP11(2021)168

while the gauge corrections to external legs proportional to $g_{a\gamma Z}$ are gathered in

$$\begin{aligned} A^{Z/\gamma\to Z}_{\text{gauge}} = -\frac{1}{2}\Bigg\{ & \frac{42M_W^4+M_Z^4}{2M_Z^4}\log\left(\frac{\Lambda^2}{M_W^2}\right)+\frac{M_W^4}{4M_Z^4}\log\left(\frac{M_W^2}{M_Z^2}\right) \\ & +\frac{180M_W^6+153M_W^4M_Z^2-12M_W^2M_Z^4-5M_Z^6}{3M_Z^6} \\ & +\frac{120M_W^6+108M_W^4M_Z^2+2M_W^2M_Z^4+M_Z^6}{4M_Z^6}\mathcal{DB}(M_Z^2,M_W,M_W)\Bigg\}\,. \end{aligned} \tag{C.3}$$

The function contributions A^{WW} which encodes the contributions proportional to g_{aWW} reads

$$\begin{aligned} A^{WW} \equiv \Bigg\{ & \frac{42M_W^2+M_Z^2}{12M_W^2}\log\left(\frac{\Lambda^2}{M_W^2}\right)+\frac{36M_W^4+93M_W^2M_Z^2+2M_Z^4}{9M_W^2M_Z^2} \\ & +\frac{24M_W^4+38M_W^2M_Z^2+M_Z^4}{12M_W^2M_Z^2}\mathcal{DB}(M_Z^2,M_W,M_W) \\ & -\frac{4(4M_W^2-p^2)}{p^2-M_Z^2}\left(f^2\left(\frac{4M_W^2}{p^2}\right)-f^2\left(\frac{4M_W^2}{M_Z^2}\right)\right) \\ & -\frac{1}{3c_w^2}\sum_{\text{f}}N_CQ_{\text{f}}(T_{3,\text{f}}-2Q_{\text{f}}s_w^2)\Bigg[\log\left(\frac{\Lambda^2}{m_{\text{f}}^2}\right) \\ & +\frac{12m_{\text{f}}^2+5M_Z^2}{3M_Z^2}+\frac{2m_{\text{f}}^2+M_Z^2}{M_Z^2}\mathcal{DB}(M_Z^2,m_{\text{f}},m_{\text{f}})\Bigg]\Bigg\}\,, \end{aligned} \tag{C.4}$$

while the complete result for the function A^{f} which encodes the fermion triangle correction is given by

$$A^{\text{f}} = Q_{\text{f}}N_C\left\{2Q_{\text{f}}s_w^2+\frac{4\left(T_{3,\text{f}}-2Q_{\text{f}}s_w^2\right)m_{\text{f}}^2}{p^2-M_Z^2}\left(f\left(\frac{4m_{\text{f}}^2}{p^2}\right)^2-f\left(\frac{4m_{\text{f}}^2}{M_Z^2}\right)^2\right)\right\}\,, \tag{C.5}$$

where the function $f(\tau)$ has been defined in eq. (4.10) and the function $\mathcal{DB}(p^2,m_1,m_2)$ corresponds to function `DiscB` in `Package-X` and is defined as

$$\mathcal{DB}(p^2,m_1,m_2) \equiv \frac{\sqrt{\rho(p^2,m_1^2,m_2^2)}}{p^2}\log\left(\frac{m_1^2+m_2^2-p^2+\sqrt{\rho(p^2,m_1^2,m_2^2)}}{2m_1m_2}\right)\,, \tag{C.6}$$

which is symmetric under $m_1\leftrightarrow m_2$ and can be simplified in some specific cases:

$$\mathcal{DB}(M^2,M,m) = \frac{m^2}{M^2}\sqrt{1-\frac{4M^2}{m^2}}\log\left(\frac{m^2+\sqrt{m^4-4M^2m^2}}{2Mm}\right)\,, \tag{C.7}$$

$$\mathcal{DB}(p^2,m,m) = 2i\sqrt{1-\frac{4m^2}{p^2}}f\left(\frac{4m^2}{p^2}\right)\,, \tag{C.8}$$

and the function ρ is the Källén function, that is defined as

$$\rho(a,b,c) \equiv a^4+b^4+c^4-2a^2b^2-2b^2c^2-2c^2a^2\,. \tag{C.9}$$

JHEP11(2021)168

C.2 ALP-ZZ anomalous coupling

The results for the one-loop corrected $g_{aZZ}^{\rm eff}$ have been introduced in section 4.4, where the results were also presented in certain limits. We collect in this appendix the exact expressions for the functions defined in that section. All descriptions presented there for the origin of each term apply here as well. The intermediate ξ-dependent steps, as well as the complete ξ-independent final expressions, can be found in NotebookArchive. The gauge invariant complete results, presented in the $\{g_{aZZ}, g_{aWW}\}$ subspace of anomalous electroweak couplings, are as follows:

The function $A^{Z/\gamma\to Z}$ which encodes corrections to the external legs were given in eq. (4.22) and (C.1)–(C.3). The function $B^{\rm Higgs}$ accounting for the vertex insertion of g_{aZZ} corrected at one-loop by Higgs exchange between the two Z bosons reads

$$\begin{aligned} B^{\rm Higgs} = 3\Bigg\{ & -\frac{2M_Z^2}{4M_Z^2-p^2}\mathcal{DB}(M_Z^2,M_Z,M_H)+\frac{2M_Z^2}{4M_Z^2-p^2}\mathcal{DB}(p^2,M_Z,M_Z) \\ & + M_Z^2\left(\frac{2M_H^2}{4M_Z^2-p^2}-1\right)\mathcal{C}(M_Z^2,M_Z^2,p^2,M_Z,M_H,M_Z)+\frac{M_H^2}{4M_Z^2-p^2}\log\left(\frac{M_H^2}{M_Z^2}\right)\Bigg\}. \end{aligned} \tag{C.10}$$

The contributions proportional to g_{aWW} encoded in B^{WW} are given by

$$\begin{aligned} B^{WW} = \Bigg(& \Bigg\{\frac{42M_W^2+M_Z^2}{12M_W^2}\log\left(\frac{\Lambda^2}{M_W^2}\right)+\frac{36M_W^4+75M_W^2M_Z^2+2M_Z^4}{9M_W^2M_Z^2} \\ & +\frac{24M_W^4+38M_W^2M_Z^2+M_Z^4}{12M_W^2M_Z^2}\mathcal{DB}(M_Z^2,M_W,M_W) \\ & -\frac{M_Z^4}{M_W^2(p^2-4M_Z^2)}\Big(\mathcal{DB}(p^2,M_W,M_W)-\mathcal{DB}(M_Z^2,M_W,M_W)\Big) \\ & +\left((4M_W^2-p^2)+\frac{M_Z^4(p^2-2M_Z^2)}{2M_W^2(p^2-4M_Z^2)}\right)\mathcal{C}(M_Z^2,M_Z^2,p^2,M_W,M_W,M_W)\Bigg\} \\ & -\frac{1}{3c_w^2}\sum_{\rm f}N_CQ_{\rm f}(T_{3,\rm f}-2Q_{\rm f}s_w^2)\Bigg\{\log\left(\frac{\Lambda^2}{m_{\rm f}^2}\right) \\ & +\frac{12m_{\rm f}^2+5M_Z^2}{3M_Z^2}+\frac{2m_{\rm f}^2+M_Z^2}{M_Z^2}\mathcal{DB}(M_Z^2,m_{\rm f},m_{\rm f})\Bigg\}\Bigg). \end{aligned} \tag{C.11}$$

Finally, the function $B^{\rm f}$ which encodes vertex insertions of fermionic couplings c_f reads

$$\begin{aligned} B^{\rm f} = -N_C\Bigg\{ & Q_{\rm f}^2s_w^4+T_{3,f}^2\frac{2m_{\rm f}^2}{(4M_Z^2-p^2)}\Big(\mathcal{DB}(p^2,m_{\rm f},m_{\rm f})-\mathcal{DB}(M_Z^2,m_{\rm f},m_{\rm f})\Big)+ \\ & +\frac{2m_{\rm f}^2}{(4M_Z^2-p^2)}\Big[M_Z^2(T_{3,\rm f}-2Q_{\rm f}s_w^2)^2+p^2Q_{\rm f}s_w^2(T_{3,\rm f}-Q_{\rm f}s_w^2)\Big]\,\mathcal{C}\left(M_Z^2,M_Z^2,p^2,m_{\rm f},m_{\rm f},m_{\rm f}\right)\Bigg\}, \end{aligned} \tag{C.12}$$

JHEP11(2021)168

where the function $\mathcal{C}(q_1^2, q_2^2, p^2, m_1, m_2, m_3)$ is the C_0 Passarino-Veltman function [86] and is defined by:

$$\mathcal{C}(q_1^2, q_2^2, p^2, m_1, m_2, m_3) \equiv$$
$$\int_0^1 \mathrm{d}x \int_0^x \mathrm{d}y \frac{1}{(x-y)yq_1^2 - (x-y)(x-1)q_2^2 - y(x-1)p^2 - ym_1^2 - (x-y)m_2^2 + (x-1)m_3^2}\,, \tag{C.13}$$

which can be reduced to a combination of $f(\tau)$ and $\mathcal{DB}$ functions (see eq. (4.10) and eqs. (C.6)–(C.8)) in the following cases:

$$\mathcal{C}(0,0,p^2,m,m,m) = -\frac{2}{p^2} f\left(\frac{4m^2}{p^2}\right)^2, \tag{C.14}$$

$$\mathcal{C}(0,M^2,p^2,m,m,m) = -\frac{2}{p^2-M^2}\left[f\left(\frac{4m^2}{p^2}\right)^2 - f\left(\frac{4m^2}{M^2}\right)^2\right], \tag{C.15}$$

$$\mathcal{C}(M^2,M^2,0,m,m,m) = \frac{1}{4m^2-M^2}\mathcal{DB}(M^2,m,m)\,. \tag{C.16}$$

C.3 ALP-WW anomalous coupling

The results for the one-loop corrected g_{aWW}^{eff} have been introduced in section 4.5, where the results were also presented in the high ALP p^2 limit. We collect in this appendix the exact expressions for the functions defined in that section. All descriptions presented there for the origin of each term apply here as well. The intermediate ξ-dependent steps, as well as the final ξ-independent results, can be found in NotebookArchive. The gauge invariant complete results, projected on the $\{g_{a\gamma\gamma}, g_{aWW}\}$ subspace of anomalous electroweak couplings are detailed next.

The function $A^{W\to W}$ results from the combination of fermionic and Higgs corrections, see eq. (4.34). Only fermion doublets can contribute to $A_{\text{ferm}}^{W\to W}$ (figure 5 **D5**):

$$\begin{aligned} A_{\text{ferm}}^{W\to W} = 2 \sum_{\substack{\mathrm{f}=u,c,t,\\ \nu_e,\nu_\mu,\nu_\tau}} N_C \Bigg\{ &-\log\left(\frac{\Lambda^2}{m_{\mathrm{f}}^2}\right) - \frac{3M_W^3(m_{\mathrm{f}}^2+m_{\mathrm{f}'}^2)+6(m_{\mathrm{f}}^2-m_{\mathrm{f}'}^2)^2+4M_W^4}{6M_W^2} \\ &+ \frac{(m_{\mathrm{f}}^2-m_{\mathrm{f}'}^2)^3 - M_W^6}{2M_W^6}\log\left(\frac{m_{\mathrm{f}}^2}{m_{\mathrm{f}'}^2}\right) + \mathcal{DB}(Mw^2, m_{\mathrm{f}}, m_{\mathrm{f}'})\times \\ &\times \frac{M_W^6(m_{\mathrm{f}}^2+m_{\mathrm{f}'}^2)+2M_W^4 m_{\mathrm{f}}^2 m_{\mathrm{f}'}^2 + M_W^2(m_{\mathrm{f}}^4-m_{\mathrm{f}'}^4)+(m_{\mathrm{f}}^2-m_{\mathrm{f}'}^2)^4+M_W^8}{M_W^4\,\rho(M_W^2,m_{\mathrm{f}}^2,m_{\mathrm{f}'}^2)} \Bigg\}, \end{aligned} \tag{C.17}$$

where Λ is an UV cutoff (see eq. (4.18)), m_{f} and $m_{\mathrm{f}'}$ denote the masses of the two fermion mass eigenstates.

The Higgs corrections to external legs gathered in $A_{\text{Higgs}}^{W\to W}$ (figure 5 **D3** and **D4**) read

$$\begin{aligned} A_{\text{Higgs}}^{W\to W} = &\frac{M_W^4 - 3M_W^2M_H^2 + M_H^4}{M_W^4} + \frac{12M_W^6 - 18M_W^4M_H^2 + 9M_W^2M_H^4 - 2M_H^6}{4M_W^6}\log\left(\frac{M_H^2}{M_W^2}\right) \\ &- \frac{36M_W^6 - 32M_W^4M_H^2 + 13M_W^2M_H^4 - 2M_H^6}{2M_W^4(M_H^2-4M_W^2)}\mathcal{DB}(M_W^2, M_W, M_H)\,. \end{aligned} \tag{C.18}$$

JHEP11(2021)168

The gauge corrections proportional to g_{aWW} encoded by C^{WW} are given by

$$
\begin{aligned}
C^{WW} = &\left\{ 43\log\left(\frac{\Lambda^2}{M_W^2}\right) + \frac{236M_W^4+33M_W^2M_Z^2+3M_Z^4}{3M_W^4} \right. \\
&+\left(\frac{36M_W^6-34M_W^4M_Z^2-M_W^2M_Z^4+8M_Z^6}{2M_W^4M_Z^2} - \frac{(24M_W^6-30M_W^4M_Z^2+24M_W^2M_Z^4-6M_Z^6)p^2}{2M_W^4M_Z^2(4M_W^2-p^2)}\right)\times \\
&\times \mathcal{DB}(M_W^2,M_W,M_Z) + \left(\frac{48M_W^8+108M_W^6M_Z^2-60M_W^4M_Z^4}{4M_W^6M_Z^2}\right. \\
&\left.+\frac{-17M_W^2M_Z^6+8M_Z^8}{4M_W^6M_Z^2} - \frac{(24M_W^6-54M_W^4M_Z^2+36M_W^2M_Z^4-6M_Z^6)p^2M_Z^2}{4M_W^6M_Z^2(4M_W^2-p^2)}\right)\log\left(\frac{M_W^2}{M_Z^2}\right) \\
&+12s_w^2(2M_W^2-p^2)\mathcal{C}(M_W^2,M_W^2,p^2,M_W,\lambda,M_W) - 12s_w^2\log\left(\frac{\lambda^2}{M_W^2}\right) \\
&\left.+6c_w^2\frac{16M_W^4+20M_W^2M_Z^2-6M_W^4-3p^2(4M_W^2+M_Z^2)+2p^4}{(4M_W^2-p^2)}\mathcal{C}(M_W^2,M_W^2,p^2,M_W,M_Z,M_W)\right\} \\
&+6(c_w^2-s_w^2)\left\{\frac{2M_Z^2}{c_w^2(4M_W^2-p^2)}\mathcal{DB}(p^2,M_Z,M_Z)\right. \\
&\left.+\left(2(4M_Z^2-p^2)-\frac{M_Z^2(2M_Z^2-p^2)}{c_w^2(4M_W^2-p^2)}\right)\mathcal{C}(M_W^2,M_W^2,p^2,M_Z,M_W,M_Z)\right\} \\
&+24s_w^2\left\{\frac{4M_Z^2}{M_W^2p^2(4M_W^2-p^2)}\mathcal{DB}(M_W^2,M_W,M_Z)\right. \\
&\left.+\frac{2M_Z^4}{p^2(4M_W^2-p^2)}\log\left(\frac{M_W^2}{M_Z^2}\right) - \frac{(p^2-M_Z^2)^2}{p^2}\mathcal{C}(M_W^2,M_W^2,p^2,0,M_W,M_Z)\right\},
\end{aligned}
\tag{C.19}
$$

where λ is again an IR cutoff, which encodes the IR contribution to the $1/\epsilon$ terms obtained in dimensional regularization via the prescription in eq. (4.18), with a protocol alike to that for gluon corrections in eq. (4.17).

The vertex function C^{Higgs} results from the direct vertex insertion of g_{aWW}, with the Higgs particle exchanged between the two W legs (diagram **E** in figure 4):

$$
\begin{aligned}
C^{\text{Higgs}} = 6\Bigg\{ &-\frac{2M_W^2}{4M_W^2-p^2}\mathcal{DB}(M_W^2,M_W,M_H) + \frac{2M_W^2}{4M_W^2-p^2}\mathcal{DB}(p^2,M_W,M_W) \\
&+M_W^2\left(\frac{2M_H^2}{4M_W^2-p^2}-1\right)\mathcal{C}(M_W^2,M_W^2,p^2,M_W,M_H,M_W) + \frac{M_H^2}{4M_W^2-p^2}\log\left(\frac{M_H^2}{M_W^2}\right)\Bigg\}.
\end{aligned}
\tag{C.20}
$$

The vertex function $C^{\gamma\gamma}$ is given by

$$
\begin{aligned}
C^{\gamma\gamma} = &-p^2\mathcal{C}(M_W^2,M_W^2,p^2,0,M_W,0) + \frac{M_Z^2}{c_w^2(4M_W^2-p^2)}\mathcal{DB}(p^2,M_Z,M_Z) \\
&+\left((4M_Z^2-p^2)-\frac{M_Z^2(2M_Z^2-p^2)}{2c_w^2(4M_W^2-p^2)}\right)\mathcal{C}(M_W^2,M_W^2,p^2,M_Z,M_W,M_Z) \\
&-\left(\frac{2M_Z^2}{p^2}+\frac{M_Z^2}{c_w^2(4M_W^2-p^2)}\right)\mathcal{DB}(M_W^2,M_W,M_Z) \\
&-\left(\frac{M_Z^2}{c_w^2p^2}-\frac{2M_W^2-M_Z^2}{2c_w^4(4M_W^2-p^2)}\right)\log\left(\frac{M_W^2}{M_Z^2}\right) + \frac{2(p^2-M_Z^2)^2}{p^2}\mathcal{C}(M_W^2,M_W^2,p^2,0,M_W,M_Z).
\end{aligned}
\tag{C.21}
$$

JHEP11(2021)168

Finally, the fermionic triangle contributions induced by $c_{\rm f}$ insertions (figure 4 **C**) lead to

$$C^{\rm f} = -N_C\Bigg\{\frac{m_{\rm f}^2}{4(4M_W^2-p^2)}\left(\frac{m_{\rm f}^2-m_{\rm f'}^2}{M_W^2}-1\right)\log\left(\frac{m_{\rm f}^2}{m_{\rm f'}^2}\right) + \frac{m_{\rm f}^2}{2(4M_W^2-p^2)}\left(\mathcal{DB}(p^2,m_{\rm f},m_{\rm f})-\mathcal{DB}(M_W^2,m_{\rm f},m_{\rm f'})\right) + \frac{m_{\rm f}^2(M_W^2-m_{\rm f}^2+m_{\rm f'}^2)}{2(4M_W^2-p^2)}\mathcal{C}\left(M_W^2,M_W^2,p^2,m_{\rm f},m_{\rm f'},m_{\rm f}\right)\Bigg\}. \tag{C.22}$$

C.4 ALP-fermion couplings

The results for the one-loop corrected $\boldsymbol{c}_{\rm f}^{\rm eff}$ have been introduced and presented in section 4.6 in certain limits of interest. We collect in this appendix the exact expressions for the functions defined in that section. All descriptions presented there for the origin of each term apply here as well. The intermediate ξ-dependent steps can be found in NotebookArchive. The gauge invariant complete results are as follows:

$$D^{gg} = \left\{3\log\left(\frac{\Lambda^2}{m_{\rm f}^2}\right)-4-p^2\mathcal{C}\left(m_{\rm f}^2,m_{\rm f}^2,p^2,0,m_{\rm f},0\right)\right\}. \tag{C.23}$$

$$D^{\gamma\gamma} = \frac{Q_{\rm f}^2}{2}D^{gg}, \tag{C.24}$$

where the function $\mathcal{C}$ was defined in eqs. (C.13)–(C.16), and

$$D^{\gamma Z} = \frac{Q_{\rm f}(T_{3,\rm f}-2Q_{\rm f}s_w^2)}{16c_w s_w}\Bigg\{12\log\left(\frac{\Lambda^2}{M_Z^2}\right)+2\frac{M_Z^2-8m_{\rm f}^2}{m_{\rm f}^2} +2\frac{2m_{\rm f}^2(M_Z^2+p^2)+M_Z^2p^2}{m_{\rm f}^2p^2}\mathcal{DB}(m_{\rm f}^2,m_{\rm f},M_Z) -\frac{12m_{\rm f}^4p^2-2m_{\rm f}^2M_Z^4-M_Z^4p^2}{m_{\rm f}^4p^2}\log\left(\frac{m_{\rm f}^2}{M_Z^2}\right)-4\frac{(M_Z^2-p^2)^2}{p^2}\mathcal{C}(m_{\rm f}^2,m_{\rm f}^2,p^2,0,m_{\rm f},M_Z)\Bigg\}. \tag{C.25}$$

$$D^{ZZ} = \frac{1}{8c_w^2s_w^2}\Bigg\{2\left(T_{3,\rm f}^2-2T_{3,\rm f}Q_{\rm f}s_w^2+2Q_{\rm f}^2s_w^4\right)\left(3\log\left(\frac{\Lambda^2}{M_Z^2}\right)+\frac{M_Z^2-4m_{\rm f}^2}{m_{\rm f}^2}\right) -\left(2(T_{3,\rm f}^2-6T_{3,\rm f}Q_{\rm f}s_w^2+6Q_{\rm f}^2s_w^4)+\frac{2M_Z^2T_{3,\rm f}^2}{m_{\rm f}^2}-\frac{M_Z^4}{m_{\rm f}^4}(T_{3,\rm f}^2-2T_{3,\rm f}Q_{\rm f}s_w^2+2Q_{\rm f}^2s_w^4)\right)\times \times\log\left(\frac{m_{\rm f}^2}{M_Z^2}\right)+4T_{3,\rm f}^2\mathcal{DB}(p^2,M_Z,M_Z) +\frac{2M_Z^2(T_{3,\rm f}^2-2T_{3,\rm f}Q_{\rm f}s_w^2+2Q_{\rm f}^2s_w^4)-8m_{\rm f}^2Q_{\rm f}s_w^2(T_{3,\rm f}-Q_{\rm f}s_w^2)}{m_{\rm f}^2}\mathcal{DB}(m_{\rm f}^2,m_{\rm f},M_Z) +4\left[M_Z^2(T_{3,\rm f}-2Q_{\rm f}s_w^2)^2+p^2Q_{\rm f}s_w^2(T_{3,\rm f}-Q_{\rm f}s_w^2)\right]\mathcal{C}(m_{\rm f}^2,m_{\rm f}^2,p^2,M_Z,m_{\rm f},M_Z)\Bigg\}, \tag{C.26}$$

JHEP11(2021)168

$$
\begin{aligned}
D^{WW} = \frac{1}{16 s_w^2}\Bigg\{ & 6\log\left(\frac{\Lambda^2}{M_W^2}\right) - \frac{2(3m_{\rm f}^2 + m_{\rm f'}^2 - M_W^2)}{m_{\rm f}^2} \\
& + 4\mathcal{DB}(p^2, M_W, M_W) - \frac{m_{\rm f}^4 + 2m_{\rm f}^2 m_{\rm f'}^2 - (m_{\rm f'}^2 - M_W^2)^2}{m_{\rm f}^4}\log\left(\frac{m_{\rm f'}^2}{M_W^2}\right) \\
& + \frac{2(m_{\rm f}^2 - m_{\rm f'}^2 + M_W^2)}{m_{\rm f}^2}\mathcal{DB}(m_{\rm f}^2, m_{\rm f'}, M_W) \\
& - 4\left(m_{\rm f}^2 - m_{\rm f'}^2 - M_W^2\right)\mathcal{C}(m_{\rm f}^2, m_{\rm f}^2, p^2, M_W, m_{\rm f'}, M_W)\Bigg\},
\end{aligned}
\tag{C.27}
$$

where the function $\mathcal{DB}$ was defined in eqs. (C.6)-(C.8).

The contributions to $\mathbf{c}_{\rm f}^{\rm eff}$ from insertions of ALP fermionic couplings are given by

$$
D_g^{c_{\rm f}} = -2\left\{1 + \log\left(\frac{\lambda^2}{m_{\rm f}^2}\right) + (p^2 - 2m_{\rm f}^2)\mathcal{C}\left(m_{\rm f}^2, m_{\rm f}^2, p^2, m_{\rm f}, \lambda, m_{\rm f}\right)\right\},
\tag{C.28}
$$

$$
D_\gamma^{c_{\rm f}} = \frac{Q_{\rm f}^2}{2} D_g^{c_{\rm f}},
\tag{C.29}
$$

$$
\begin{aligned}
D_Z^{c_{\rm f}} = \frac{1}{4c_w^2 s_w^2}\Bigg\{ & -\frac{2m_{\rm f}^2 T_{3,{\rm f}}^2}{M_Z^2}\log\left(\frac{\Lambda^2}{M_Z^2}\right) + 4(T_{3,{\rm f}}^2 + T_{3,{\rm f}} Q_{\rm f} s_w^2 - Q_{\rm f}^2 s_w^4) - \frac{4m_{\rm f}^2 T_{3,{\rm f}}^2}{M_Z^2} \\
& - \frac{4M_Z^2}{m_{\rm f}^2}(T_{3,{\rm f}}^2 - 2T_{3,{\rm f}} Q_{\rm f} s_w^2 + 2Q_{\rm f}^2 s_w^4) + \frac{1}{m_{\rm f}^4 M_Z^2}\Big[T_{3,{\rm f}}^2(2m_{\rm f}^6 - m_{\rm f}^4 M_Z^2 + 5m_{\rm f}^2 M_Z^4 - 2M_Z^6) \\
& - 4Q_{\rm f} s_w^2 (T_{3,{\rm f}} - Q_{\rm f} s_w^2) M_Z^2 (m_{\rm f}^4 + m_{\rm f}^2 M_Z^2 - M_Z^4)\Big]\log\left(\frac{m_{\rm f}^2}{M_Z^2}\right) \\
& + \frac{2}{m_{\rm f}^2(M_Z^2 - 4m_{\rm f}^2)}\Big[T_{3,{\rm f}}^2(-7m_{\rm f}^4 + 9m_{\rm f}^2 M_Z^2 - 2M_Z^4) \\
& - 4Q_{\rm f} s_w^2 (T_{3,{\rm f}} - Q_{\rm f} s_w^2)(m_{\rm f}^4 + 3m_{\rm f}^2 M_Z^2 - M_Z^4)\Big]\mathcal{DB}(m_{\rm f}^2, m_{\rm f}, M_Z) \\
& - \frac{2m_{\rm f}^2 T_{3,{\rm f}}^2}{M_Z^2}\mathcal{DB}(p^2, m_{\rm f}, m_{\rm f}) \\
& + 2\left[m_{\rm f}^2(T_{3,{\rm f}} - 2Q_{\rm f} s_w^2)^2 + 2p^2 Q_{\rm f} s_w^2 (T_{3,{\rm f}} - Q_{\rm f} s_w^2)\right]\mathcal{C}(m_{\rm f}^2, m_{\rm f}^2, p^2, m_{\rm f}, M_Z, m_{\rm f})\Bigg\}.
\end{aligned}
\tag{C.30}
$$

$$
\begin{aligned}
D_W^{c_{\rm f}} = -\frac{1}{16 s_w^2}\Bigg\{ & \frac{2m_{\rm f}^2}{M_W^2}\log\left(\frac{\Lambda^2}{M_W^2}\right) + \frac{2(m_{\rm f}^4 + 2m_{\rm f}^2 m_{\rm f'}^2 - 2m_{\rm f'}^4 - m_{\rm f}^2 M_W^2 - 2m_{\rm f'}^2 M_W^2 + 4M_W^4)}{m_{\rm f}^2 M_W^2} \\
& - \frac{m_{\rm f}^6 + 3m_{\rm f}^2(m_{\rm f}'^2 + M_W^2) - 2(m_{\rm f'}^6 - 3m_{\rm f'}^2 M_W^4 + 2M_W^6)}{m_{\rm f}^4 M_W^2}\log\left(\frac{m_{\rm f'}^2}{M_W^2}\right) \\
& + \frac{2}{m_{\rm f}^2 M_W^2 \rho(m_{\rm f}^2, m_{\rm f'}^2, M_W^2)}\Big[m_{\rm f}^8 - m_{\rm f}^6(m_{\rm f'}^2 + M_W^2) - m_{\rm f}^4(3m_{\rm f'}^4 + 2m_{\rm f'}^2 M_W^2 - 3M_W^4) \\
& + m_{\rm f}^2(5m_{\rm f'}^6 + m_{\rm f'}^4 M_W^2 + m_{\rm f'}^2 M_W^4 - 7M_W^6) - 2(m_{\rm f'}^2 - M_W^2)^3(m_{\rm f'}^2 + 2M_W^2)\Big]\mathcal{DB}(m_{\rm f}^2, m_{\rm f'}, M_W)\Bigg\},
\end{aligned}
\tag{C.31}
$$

JHEP11(2021)168

$$D^{c_{\mathrm{f}'}} = -\frac{m_{\mathrm{f}'}^2}{16 s_w^2}\left\{\frac{2}{M_W^2}\log\left(\frac{\Lambda^2}{M_W^2}\right) - \frac{3m_{\mathrm{f}}^4 - 2m_{\mathrm{f}}^2 m_{\mathrm{f}'}^2 + (m_{\mathrm{f}'}^2 - M_W^2)^2}{m_{\mathrm{f}}^4 M_W^2}\log\left(\frac{m_{\mathrm{f}'}^2}{M_W^2}\right)\right.$$
$$+\frac{2(2m_{\mathrm{f}}^2 + m_{\mathrm{f}'}^2 - M_W^2)}{m_{\mathrm{f}}^2 M_W^2} - \frac{2(m_{\mathrm{f}}^2 - m_{\mathrm{f}'}^2 + M_W^2)}{m_{\mathrm{f}}^2 M_W^2}\mathcal{DB}(m_{\mathrm{f}}^2, m_{\mathrm{f}'}, M_W) \tag{C.32}$$
$$\left.+\frac{2}{M_W^2}\mathcal{DB}(p^2, m_{\mathrm{f}}, m_{\mathrm{f}}) + 4\mathcal{C}(m_{\mathrm{f}}^2, m_{\mathrm{f}}^2, p^2, m_{\mathrm{f}'}, M_W, m_{\mathrm{f}'})\right\}.$$

$$D_h^{c_{\mathrm{f}}} = \frac{1}{16\pi s_w^2}\left\{-\frac{2m_{\mathrm{f}}^2}{M_W^2}\log\left(\frac{\Lambda^2}{M_H^2}\right) + \frac{2(2m_{\mathrm{f}}^2 - M_H^2)}{M_W^2}\right.$$
$$-\frac{2m_{\mathrm{f}}^4 - 3m_{\mathrm{f}}^2 M_H^2 + M_H^4}{m_{\mathrm{f}}^2 M_W^2}\log\left(\frac{m_{\mathrm{f}}^2}{M_H^2}\right) + \frac{2(m_{\mathrm{f}}^2 - M_H^2)}{M_W^2}\mathcal{DB}(m_{\mathrm{f}}^2, m_{\mathrm{f}}, M_H) \tag{C.33}$$
$$\left.+\frac{2m_{\mathrm{f}}^2}{M_W^2}\mathcal{DB}(p^2, m_{\mathrm{f}}, m_{\mathrm{f}}) + \frac{2m_{\mathrm{f}}^2(M_H^2 - 4m_{\mathrm{f}}^2)}{M_W^2}\mathcal{C}(m_{\mathrm{f}}^2, m_{\mathrm{f}}^2, p^2, m_{\mathrm{f}}, M_H, m_{\mathrm{f}})\right\}.$$

$$D_{\mathrm{mix}}^{c_\psi} = -\frac{T_{3,\mathrm{f}}}{s_w^2 M_W^2} N_C T_{3,\psi} m_\psi^2\left\{\log\left(\frac{\Lambda^2}{m_\psi^2}\right) + 2 + \mathcal{DB}(p^2, m_\psi, m_\psi)\right\}. \tag{C.34}$$

D One-loop corrections to the weak angle

In eq. (4.4) we defined a quantity $\bar{c}_w$ as the ratio of two input observables: the W and Z masses, whose renormalized formulation was expressed in terms of Δc_w, see eqs. (4.4), and (4.5). The exact Δc_w expression can be split in three parts,

$$\frac{\Delta c_w}{c_w} = \frac{\Delta c_w^{\mathrm{gauge}}}{c_w} + \frac{\Delta c_w^{\mathrm{Higgs}}}{c_w} + \frac{\Delta c_w^{\mathrm{ferm}}}{c_w}, \tag{D.1}$$

which correspond respectively to the gauge boson corrections to the self-energies, the Higgs corrections and the fermions corrections:

$$\frac{\Delta c_w^{\mathrm{gauge}}}{c_w} = \frac{\alpha_{em}}{\pi}\left\{\frac{42M_W^2 + M_Z^2}{48M_W^2}\log\left(\frac{\Lambda^2}{M_W^2}\right) + \frac{288M_W^6 + 696M_W^4 M_Z^2 - 74M_W^2 M_Z^4 - 3M_Z^6}{288M_W^4 M_Z^2}\right.$$
$$+\frac{80M_W^4 - 14M_W^2 M_Z^2 - M_Z^4}{192 s_w^2 c_w^2 M_W^4}\log\left(\frac{M_W^2}{M_Z^2}\right) + \frac{48M_W^6 + 68M_W^4 M_Z^2 - 16M_W^2 M_Z^4 - M_Z^6}{96 s_w^2 c_w^2 M_W^2 M_Z^6}\times$$
$$\left.\times\left[M_Z^2\mathcal{DB}(M_W^2, M_W, M_Z) - M_W^2\mathcal{DB}(M_Z^2, M_W, M_W)\right]\right\}, \tag{D.2}$$

$$\frac{\Delta c_w^{\mathrm{Higgs}}}{c_w} = \frac{\alpha_{em}}{\pi}\left\{\frac{M_H^4 - 24M_W^2 M_Z^2}{96M_W^4} + \frac{M_H^4[M_H^2(M_W^2 + M_Z^2) - 6M_W^2 M_Z^2]}{192M_W^6 M_Z^2}\log\left(\frac{M_W^2}{M_H^2}\right)\right.$$
$$-\frac{M_H^6 - 6M_H^4 M_Z^2 + 18M_H^2 M_Z^4 - 24M_Z^4}{192 s_w^2 M_W^2 M_Z^4}\log\left(\frac{M_W^2}{M_Z^2}\right)$$
$$+\frac{M_H^4 - 4M_H^2 M_Z^2 + 12M_Z^4}{96 s_w^2 M_W^2 M_Z^2}\mathcal{DB}(M_Z^2, M_Z, M_H) \tag{D.3}$$
$$\left.-\frac{M_H^4 - 4M_H^2 M_W^2 + 12M_W^4}{96 s_w^2 M_W^4}\mathcal{DB}(M_W^2, M_W, M_H)\right\},$$

JHEP11(2021)168

$$
\begin{aligned}
\frac{\Delta c_w^{\rm ferm}}{c_w} = \frac{\alpha_{em}}{\pi} \sum_{\substack{\mathrm{f}=u,c,t,\\ \nu_e,\nu_\mu,\nu_\tau}} \Bigg\{ & \frac{4(Q_{\mathrm{f}}^2+Q_{\mathrm{f}'}^2)s_w^2-1}{24c_w^2}\log\left(\frac{\Lambda^2}{m_{\mathrm{f}}^2}\right) \\
& + \frac{(m_{\mathrm{f}}^2-m_{\mathrm{f}'}^2)^2}{48s_w^2M_W^4} + \frac{24m_{\mathrm{f}}^2Q_{\mathrm{f}}(2Q_{\mathrm{f}}s_w^2-1)+24m_{\mathrm{f}'}^2Q_{\mathrm{f}'}(2Q_{\mathrm{f}'}s_w^2+1)+5M_Z^2(4s_w^2(Q_{\mathrm{f}}^2+Q_{\mathrm{f}'}^2)-1)}{72M_W^2} \\
& - \frac{(m_{\mathrm{f}}^2-m_{\mathrm{f}'}^2-M_W^2)^2(m_{\mathrm{f}}^2-m_{\mathrm{f}'}^2+2M_W^2)-2M_W^4M_Z^2(8Q_{\mathrm{f}'}^2s_w^4+4Q_{\mathrm{f}'}s_w^2+1)}{96s_w^2M_W^6}\log\left(\frac{m_{\mathrm{f}}^2}{m_{\mathrm{f}'}^2}\right) \\
& + \frac{(m_{\mathrm{f}}^2-m_{\mathrm{f}'}^2)^2+M_W^2(m_{\mathrm{f}}^2+m_{\mathrm{f}'}^2)-2M_W^4}{48s_w^2M_W^4}\mathcal{DB}(M_W^2,m_{\mathrm{f}},m_{\mathrm{f}'}) \\
& + \frac{(2m_{\mathrm{f}}^2+M_Z^2)(8Q_{\mathrm{f}}^2s_w^4-4Q_{\mathrm{f}}s_w^2+1)-3m_{\mathrm{f}}^2}{48s_w^2M_W^2}\mathcal{DB}(M_Z^2,m_{\mathrm{f}},m_{\mathrm{f}}) \\
& + \frac{(2m_{\mathrm{f}'}^2+M_Z^2)(8Q_{\mathrm{f}}^2s_w^4+4Q_{\mathrm{f}}s_w^2+1)-3m_{\mathrm{f}'}^2}{48s_w^2M_W^2}\mathcal{DB}(M_Z^2,m_{\mathrm{f}'},m_{\mathrm{f}'}) \Bigg\},
\end{aligned}
\tag{D.4}
$$

where the funcions $f(\tau)$ and $\mathcal{DB}(p^2,m_1,m_2)$ were defined in eq. (4.10) and eqs. (C.6)–(C.8).

These Δc_w corrections allow to express the tree-level phenomenological couplings $\{g_{a\gamma\gamma}, g_{a\gamma Z}, g_{aZZ}\}$ as a combination of the two fundamental Lagrangian parameters $\{c_{\tilde{B}}, c_{\tilde{W}}\}$ and observable quantities, see eqs. (4.6)–(4.8).

References

[1] R.D. Peccei and H.R. Quinn, *CP Conservation in the Presence of Instantons*, *Phys. Rev. Lett.* **38** (1977) 1440 [INSPIRE].

[2] R.D. Peccei and H.R. Quinn, *Constraints Imposed by CP Conservation in the Presence of Instantons*, *Phys. Rev. D* **16** (1977) 1791 [INSPIRE].

[3] S. Weinberg, *A New Light Boson?*, *Phys. Rev. Lett.* **40** (1978) 223 [INSPIRE].

[4] F. Wilczek, *Problem of Strong P and T Invariance in the Presence of Instantons*, *Phys. Rev. Lett.* **40** (1978) 279 [INSPIRE].

[5] G.B. Gelmini and M. Roncadelli, *Left-Handed Neutrino Mass Scale and Spontaneously Broken Lepton Number*, *Phys. Lett. B* **99** (1981) 411 [INSPIRE].

[6] P. Langacker, R.D. Peccei and T. Yanagida, *Invisible Axions and Light Neutrinos: Are They Connected?*, *Mod. Phys. Lett. A* **1** (1986) 541 [INSPIRE].

[7] G. Ballesteros, J. Redondo, A. Ringwald and C. Tamarit, *Standard Model-axion-seesaw-Higgs portal inflation. Five problems of particle physics and cosmology solved in one stroke*, *JCAP* **08** (2017) 001 [arXiv:1610.01639] [INSPIRE].

[8] M. Cicoli, *Axion-like Particles from String Compactifications*, in *9th Patras Workshop on Axions, WIMPs and WISPs*, pp. 235–242 (2013) [DOI] [arXiv:1309.6988] [INSPIRE].

[9] F. Wilczek, *Axions and Family Symmetry Breaking*, *Phys. Rev. Lett.* **49** (1982) 1549 [INSPIRE].

JHEP11(2021)168

[10] L. Calibbi, F. Goertz, D. Redigolo, R. Ziegler and J. Zupan, *Minimal axion model from flavor*, *Phys. Rev. D* **95** (2017) 095009 [arXiv:1612.08040] [INSPIRE].

[11] Y. Ema, K. Hamaguchi, T. Moroi and K. Nakayama, *Flaxion: a minimal extension to solve puzzles in the standard model*, *JHEP* **01** (2017) 096 [arXiv:1612.05492] [INSPIRE].

[12] J. Jaeckel and M. Spannowsky, *Probing MeV to* 90 *GeV axion-like particles with LEP and LHC*, *Phys. Lett. B* **753** (2016) 482 [arXiv:1509.00476] [INSPIRE].

[13] K. Mimasu and V. Sanz, *ALPs at Colliders*, *JHEP* **06** (2015) 173 [arXiv:1409.4792] [INSPIRE].

[14] M. Bauer, M. Neubert and A. Thamm, *Collider Probes of Axion-Like Particles*, *JHEP* **12** (2017) 044 [arXiv:1708.00443] [INSPIRE].

[15] M. Bauer, M. Heiles, M. Neubert and A. Thamm, *Axion-Like Particles at Future Colliders*, *Eur. Phys. J. C* **79** (2019) 74 [arXiv:1808.10323] [INSPIRE].

[16] C. Frugiuele, E. Fuchs, G. Perez and M. Schlaffer, *Relaxion and light (pseudo)scalars at the HL-LHC and lepton colliders*, *JHEP* **10** (2018) 151 [arXiv:1807.10842] [INSPIRE].

[17] I. Brivio, M.B. Gavela, L. Merlo, K. Mimasu, J.M. No, R. del Rey et al., *ALPs Effective Field Theory and Collider Signatures*, *Eur. Phys. J. C* **77** (2017) 572 [arXiv:1701.05379] [INSPIRE].

[18] N. Craig, A. Hook and S. Kasko, *The Photophobic ALP*, *JHEP* **09** (2018) 028 [arXiv:1805.06538] [INSPIRE].

[19] M.B. Gavela, J.M. No, V. Sanz and J.F. de Trocóniz, *Nonresonant Searches for Axionlike Particles at the LHC*, *Phys. Rev. Lett.* **124** (2020) 051802 [arXiv:1905.12953] [INSPIRE].

[20] J. Ebadi, S. Khatibi and M. Mohammadi Najafabadi, *New probes for axionlike particles at hadron colliders*, *Phys. Rev. D* **100** (2019) 015016 [arXiv:1901.03061] [INSPIRE].

[21] E. Izaguirre, T. Lin and B. Shuve, *Searching for Axionlike Particles in Flavor-Changing Neutral Current Processes*, *Phys. Rev. Lett.* **118** (2017) 111802 [arXiv:1611.09355] [INSPIRE].

[22] M. Freytsis, Z. Ligeti and J. Thaler, *Constraining the Axion Portal with* $B \to K l^+ l^-$, *Phys. Rev. D* **81** (2010) 034001 [arXiv:0911.5355] [INSPIRE].

[23] V.A. Rubakov, *Grand unification and heavy axion*, *JETP Lett.* **65** (1997) 621 [hep-ph/9703409] [INSPIRE].

[24] Z. Berezhiani, L. Gianfagna and M. Giannotti, *Strong CP problem and mirror world: The Weinberg-Wilczek axion revisited*, *Phys. Lett. B* **500** (2001) 286 [hep-ph/0009290] [INSPIRE].

[25] L. Gianfagna, M. Giannotti and F. Nesti, *Mirror world, supersymmetric axion and gamma ray bursts*, *JHEP* **10** (2004) 044 [hep-ph/0409185] [INSPIRE].

[26] S.D.H. Hsu and F. Sannino, *New solutions to the strong CP problem*, *Phys. Lett. B* **605** (2005) 369 [hep-ph/0408319] [INSPIRE].

[27] A. Hook, *Anomalous solutions to the strong CP problem*, *Phys. Rev. Lett.* **114** (2015) 141801 [arXiv:1411.3325] [INSPIRE].

[28] H. Fukuda, K. Harigaya, M. Ibe and T.T. Yanagida, *Model of visible QCD axion*, *Phys. Rev. D* **92** (2015) 015021 [arXiv:1504.06084] [INSPIRE].

[29] C.-W. Chiang, H. Fukuda, M. Ibe and T.T. Yanagida, 750 *GeV diphoton resonance in a visible heavy QCD axion model*, *Phys. Rev. D* **93** (2016) 095016 [arXiv:1602.07909] [INSPIRE].

[30] S. Dimopoulos, A. Hook, J. Huang and G. Marques-Tavares, *A collider observable QCD axion*, *JHEP* **11** (2016) 052 [arXiv:1606.03097] [INSPIRE].

JHEP11(2021)168

[31] T. Gherghetta, N. Nagata and M. Shifman, *A Visible QCD Axion from an Enlarged Color Group*, *Phys. Rev. D* **93** (2016) 115010 [arXiv:1604.01127] [INSPIRE].

[32] A. Kobakhidze, *Heavy axion in asymptotically safe QCD*, arXiv:1607.06552 [INSPIRE].

[33] P. Agrawal and K. Howe, *Factoring the Strong CP Problem*, *JHEP* **12** (2018) 029 [arXiv:1710.04213] [INSPIRE].

[34] P. Agrawal and K. Howe, *A Flavorful Factoring of the Strong CP Problem*, *JHEP* **12** (2018) 035 [arXiv:1712.05803] [INSPIRE].

[35] M.K. Gaillard, M.B. Gavela, R. Houtz, P. Quilez and R. Del Rey, *Color unified dynamical axion*, *Eur. Phys. J. C* **78** (2018) 972 [arXiv:1805.06465] [INSPIRE].

[36] M.A. Buen-Abad and J. Fan, *Dynamical axion misalignment with small instantons*, *JHEP* **12** (2019) 161 [arXiv:1911.05737] [INSPIRE].

[37] A. Hook, S. Kumar, Z. Liu and R. Sundrum, *High Quality QCD Axion and the LHC*, *Phys. Rev. Lett.* **124** (2020) 221801 [arXiv:1911.12364] [INSPIRE].

[38] C. Csáki, M. Ruhdorfer and Y. Shirman, *UV Sensitivity of the Axion Mass from Instantons in Partially Broken Gauge Groups*, *JHEP* **04** (2020) 031 [arXiv:1912.02197] [INSPIRE].

[39] T. Gherghetta and M.D. Nguyen, *A Composite Higgs with a Heavy Composite Axion*, *JHEP* **12** (2020) 094 [arXiv:2007.10875] [INSPIRE].

[40] A. Hook, *Solving the Hierarchy Problem Discretely*, *Phys. Rev. Lett.* **120** (2018) 261802 [arXiv:1802.10093] [INSPIRE].

[41] L. Di Luzio, B. Gavela, P. Quilez and A. Ringwald, *An even lighter QCD axion*, *JHEP* **05** (2021) 184 [arXiv:2102.00012] [INSPIRE].

[42] L. Di Luzio, B. Gavela, P. Quilez and A. Ringwald, *Dark matter from an even lighter QCD axion: trapped misalignment*, *JCAP* **10** (2021) 001 [arXiv:2102.01082] [INSPIRE].

[43] M. Chala, G. Guedes, M. Ramos and J. Santiago, *Running in the ALPs*, *Eur. Phys. J. C* **81** (2021) 181 [arXiv:2012.09017] [INSPIRE].

[44] M. Bauer, M. Neubert, S. Renner, M. Schnubel and A. Thamm, *The Low-Energy Effective Theory of Axions and ALPs*, *JHEP* **04** (2021) 063 [arXiv:2012.12272] [INSPIRE].

[45] Q. Bonnefoy, L. Di Luzio, C. Grojean, A. Paul and A.N. Rossia, *The anomalous case of axion EFTs and massive chiral gauge fields*, *JHEP* **07** (2021) 189 [arXiv:2011.10025] [INSPIRE].

[46] H. Georgi, D.B. Kaplan and L. Randall, *Manifesting the Invisible Axion at Low-energies*, *Phys. Lett. B* **169** (1986) 73 [INSPIRE].

[47] K. Choi, K. Kang and J.E. Kim, *Effects of η' in Low-energy Axion Physics*, *Phys. Lett. B* **181** (1986) 145 [INSPIRE].

[48] I.G. Irastorza and J. Redondo, *New experimental approaches in the search for axion-like particles*, *Prog. Part. Nucl. Phys.* **102** (2018) 89 [arXiv:1801.08127] [INSPIRE].

[49] J. Martin Camalich, M. Pospelov, P.N.H. Vuong, R. Ziegler and J. Zupan, *Quark Flavor Phenomenology of the QCD Axion*, *Phys. Rev. D* **102** (2020) 015023 [arXiv:2002.04623] [INSPIRE].

[50] A.M. Galda, M. Neubert and S. Renner, *ALP — SMEFT interference*, *JHEP* **06** (2021) 135 [arXiv:2105.01078] [INSPIRE].

[51] A. Salvio, A. Strumia and W. Xue, *Thermal axion production*, *JCAP* **01** (2014) 011 [arXiv:1310.6982] [INSPIRE].

JHEP11(2021)168

[52] M.B. Gavela, J. Gonzalez-Fraile, M.C. Gonzalez-Garcia, L. Merlo, S. Rigolin and J. Yepes, *CP violation with a dynamical Higgs*, *JHEP* **10** (2014) 044 [arXiv:1406.6367] [INSPIRE].

[53] G. Alonso-Álvarez, M.B. Gavela and P. Quilez, *Axion couplings to electroweak gauge bosons*, *Eur. Phys. J. C* **79** (2019) 223 [arXiv:1811.05466] [INSPIRE].

[54] G. 't Hooft, *Naturalness, chiral symmetry, and spontaneous chiral symmetry breaking*, *NATO Sci. Ser. B* **59** (1980) 135 [INSPIRE].

[55] D.B. Kaplan and A. Manohar, *Strange Matrix Elements in the Proton from Neutral Current Experiments*, *Nucl. Phys. B* **310** (1988) 527 [INSPIRE].

[56] C. Grojean, E.E. Jenkins, A.V. Manohar and M. Trott, *Renormalization Group Scaling of Higgs Operators and $h \to \gamma\gamma$*, *JHEP* **04** (2013) 016 [arXiv:1301.2588] [INSPIRE].

[57] P. Agrawal, A. Hook and J. Huang, *A CMB Millikan experiment with cosmic axiverse strings*, *JHEP* **07** (2020) 138 [arXiv:1912.02823] [INSPIRE].

[58] V. Shtabovenko, R. Mertig and F. Orellana, *FeynCalc 9.3: New features and improvements*, *Comput. Phys. Commun.* **256** (2020) 107478 [arXiv:2001.04407] [INSPIRE].

[59] H.H. Patel, *Package-X 2.0: A Mathematica package for the analytic calculation of one-loop integrals*, *Comput. Phys. Commun.* **218** (2017) 66 [arXiv:1612.00009] [INSPIRE].

[60] G.M. Prosperi, M. Raciti and C. Simolo, *On the running coupling constant in QCD*, *Prog. Part. Nucl. Phys.* **58** (2007) 387 [hep-ph/0607209] [INSPIRE].

[61] G. Heinrich, *Introduction to quantum chromodynamics and loop calculations*, August, 2018 [https://indico.in2p3.fr/event/16354/contributions/59530/].

[62] J.L. Feng, T. Moroi, H. Murayama and E. Schnapka, *Third generation familons, b factories, and neutrino cosmology*, *Phys. Rev. D* **57** (1998) 5875 [hep-ph/9709411] [INSPIRE].

[63] A. Helset, A. Martin and M. Trott, *The Geometric Standard Model Effective Field Theory*, *JHEP* **03** (2020) 163 [arXiv:2001.01453] [INSPIRE].

[64] M.B. Gavela, R. Houtz, P. Quilez, R. Del Rey and O. Sumensari, *Flavor constraints on electroweak ALP couplings*, *Eur. Phys. J. C* **79** (2019) 369 [arXiv:1901.02031] [INSPIRE].

[65] J.M. No, V. Sanz and J. Setford, *See-saw composite Higgs model at the LHC: Linking naturalness to the* 750 *GeV diphoton resonance*, *Phys. Rev. D* **93** (2016) 095010 [arXiv:1512.05700] [INSPIRE].

[66] D. Croon, V. Sanz and E.R.M. Tarrant, *Reheating with a composite Higgs boson*, *Phys. Rev. D* **94** (2016) 045010 [arXiv:1507.04653] [INSPIRE].

[67] ATLAS collaboration, *Search for $t\bar{t}$ resonances in fully hadronic final states in pp collisions at $\sqrt{s} = 13$ TeV with the ATLAS detector*, *JHEP* **10** (2020) 061 [arXiv:2005.05138] [INSPIRE].

[68] J. Alwall, M. Herquet, F. Maltoni, O. Mattelaer and T. Stelzer, *MadGraph 5: Going Beyond*, *JHEP* **06** (2011) 128 [arXiv:1106.0522] [INSPIRE].

[69] M. Gouzevitch, A. Oliveira, J. Rojo, R. Rosenfeld, G.P. Salam and V. Sanz, *Scale-invariant resonance tagging in multijet events and new physics in Higgs pair production*, *JHEP* **07** (2013) 148 [arXiv:1303.6636] [INSPIRE].

[70] G. Kasieczka et al., *The LHC Olympics 2020: A Community Challenge for Anomaly Detection in High Energy Physics*, arXiv:2101.08320 [INSPIRE].

[71] C. O'Hare, `cajohare/AxionLimits:AxionLimits` (version v1.0), July, 2020 [https://doi.org/10.5281/zenodo.3932430].

JHEP11(2021)168

[72] F. Capozzi and G. Raffelt, *Axion and neutrino bounds improved with new calibrations of the tip of the red-giant branch using geometric distance determinations*, *Phys. Rev. D* **102** (2020) 083007 [arXiv:2007.03694] [INSPIRE].

[73] P. Gondolo and G.G. Raffelt, *Solar neutrino limit on axions and keV-mass bosons*, *Phys. Rev. D* **79** (2009) 107301 [arXiv:0807.2926] [INSPIRE].

[74] LUX collaboration, *First Searches for Axions and Axionlike Particles with the LUX Experiment*, *Phys. Rev. Lett.* **118** (2017) 261301 [arXiv:1704.02297] [INSPIRE].

[75] EDELWEISS collaboration, *Searches for electron interactions induced by new physics in the EDELWEISS-III Germanium bolometers*, *Phys. Rev. D* **98** (2018) 082004 [arXiv:1808.02340] [INSPIRE].

[76] PandaX collaboration, *Limits on Axion Couplings from the First 80 Days of Data of the PandaX-II Experiment*, *Phys. Rev. Lett.* **119** (2017) 181806 [arXiv:1707.07921] [INSPIRE].

[77] SuperCDMS collaboration, *Constraints on dark photons and axionlike particles from the SuperCDMS Soudan experiment*, *Phys. Rev. D* **101** (2020) 052008 [*Erratum ibid.* **103** (2021) 039901] [arXiv:1911.11905] [INSPIRE].

[78] XENON collaboration, *Light Dark Matter Search with Ionization Signals in XENON1T*, *Phys. Rev. Lett.* **123** (2019) 251801 [arXiv:1907.11485] [INSPIRE].

[79] XENON collaboration, *Excess electronic recoil events in XENON1T*, *Phys. Rev. D* **102** (2020) 072004 [arXiv:2006.09721] [INSPIRE].

[80] K. Van Tilburg, *Stellar basins of gravitationally bound particles*, *Phys. Rev. D* **104** (2021) 023019 [arXiv:2006.12431] [INSPIRE].

[81] F. Arias-Aragón, F. D'Eramo, R.Z. Ferreira, L. Merlo and A. Notari, *Production of Thermal Axions across the ElectroWeak Phase Transition*, *JCAP* **03** (2021) 090 [arXiv:2012.04736] [INSPIRE].

[82] C. Gao, J. Liu, L.-T. Wang, X.-P. Wang, W. Xue and Y.-M. Zhong, *Reexamining the Solar Axion Explanation for the XENON1T Excess*, *Phys. Rev. Lett.* **125** (2020) 131806 [arXiv:2006.14598] [INSPIRE].

[83] R.S. Chivukula and H. Georgi, *Composite Technicolor Standard Model*, *Phys. Lett. B* **188** (1987) 99 [INSPIRE].

[84] L.J. Hall and L. Randall, *Weak scale effective supersymmetry*, *Phys. Rev. Lett.* **65** (1990) 2939 [INSPIRE].

[85] G. D'Ambrosio, G.F. Giudice, G. Isidori and A. Strumia, *Minimal flavor violation: An Effective field theory approach*, *Nucl. Phys. B* **645** (2002) 155 [hep-ph/0207036] [INSPIRE].

[86] G. Passarino and M.J.G. Veltman, *One Loop Corrections for e^+e^- Annihilation Into $\mu^+\mu^-$ in the Weinberg Model*, *Nucl. Phys. B* **160** (1979) 151 [INSPIRE].

JHEP11(2021)168

Chapter 5

Nonresonant Searches for Axion-Like Particles in Vector Boson Scattering Processes at the LHC

This chapter contains the publication in Ref. [2]. In this work a new experimental search for ALPs at collider experiments is proposed. Vector Boson Scattering (VBS) processes are targeted, aiming to detect a contribution from off-shell ALP-mediated channels. Such contribution occurs whenever the ALP is too light to be produced resonantly and takes advantage of the derivative nature of ALP couplings. In particular, this work considers the CMS searches for the EW production of ZZ, $Z\gamma$, $W^{\pm}\gamma$, $W^{\pm}Z$ and same-sign $W^{\pm}W^{\pm}$ pairs with large diboson invariant mass in association with two forward jets in VBS processes [217–220]. Nonresonant ALPs are expected to contribute to this processes leading to a distortion of the shape of the event distribution for large values of the invariant mass. Since no ALP signal is measured within the current data, bounds on the ALP parameter space are derived for masses $m_a \lesssim 100$ GeV. Projections of these limits are derived for Run 3 and HL-LHC.

The ALP Lagrangian is discussed in Sec. 2. ALP anomalous couplings to EW gauge bosons are considered. ALP interactions with fermions are shown to be negligible, as they lead to amplitudes proportional to fermion masses, that are unimportant in VBS processes. The interaction with gluons is disregarded but it is shown that, if considered, it would only contribute to a small enhancement of the ALP VBS cross sections, resulting in slightly better limits on the ALP couplings.

Sec. 3 analyzes the main characteristic properties of the ALP contribution to VBS processes. The functional dependence of the pure ALP processes and the ALP-SM interference on the anomalous coupling constants is discussed. Also, the most relevant region in order to distinguish between ALP and SM mediated VBS processes is identified, corresponding to the region of larger values for the diboson invariant mass. ALP-mediated channels tend to produce larger values of this parameter, due to the derivative enhancement of the cross sections. Moreover, the validity of the EFT expansion is discussed.

Details on the simulation of the ALP signal and interference, and the subsequent sta-

tistical analysis, are depicted in Sec. 4. The signal region defined for each channel is taken from the original CMS reference. The ALP signal is generated with the software MadGraph5_aMC@NLO 2.8.2 [221] employing the `ALP_linear` UFO model from [117, 222]. Parton showering, hadronization and decays are simulated with PYTHIA 8 [223]. Finally, the CMS detector simulation and reconstruction of the experimental objects is done with DELPHES 3 [224], including FastJet [225]. The expected ALP events at the CMS detector are obtained and characterized as a function of the EW ALP effective couplings. Finally, for the statistical analysis a log-likelihood is constructed based on a Poisson distribution. Systematic errors are described by nuisance parameters that are taken to be Gaussian-distributed, and we assign it a total size of 20% from adding different sources of uncertainty.

Finally Sec. 5 comprises the experimental limits on the EW ALP couplings derived in this work. These are presented in Tab. 5 in terms of the phenomenological couplings $\{g_{a\gamma\gamma}, g_{a\gamma Z}, g_{aZZ}, g_{aWW}\}$ and they are valid for ALP masses up to $m_a \lesssim 100$ GeV. Fig. 5 shows the allowed regions of the $\{c_{\widetilde{B}}/fa, c_{\widetilde{W}}/f_a\}$ plane for each individual channel and for the combined analysis. Additionally, projections for Run 3 LHC and HL-LHC are shown in Fig. 6. Finally, Sec. 6 shows the comparison between these bounds and other experimental limits on the four ALP phenomenological couplings to EW gauge bosons. Such comparison shows that our limits are competitive with respect to other experimental ALP searches, specially for the couplings to Z bosons and W bosons, g_{aZZ} and g_{aWW}, which are otherwise unconstrained for the region of large ALP masses. Our results have the advantage of being independent of any assumption on the existence of ALP-gluon and/or ALP-fermion couplings, unlike previous ordinary resonant searches, which typically rely on those interactions for the ALP production channel (i.e. gluon fusion) or impose restrictions on the ALP decay width.

The limits derived on the ALP couplings to ZZ, $Z\gamma$ and $W^{\pm}W^{\pm}$ pairs are very competitive for ALP masses up to 100 GeV. In addition, in ALP mass region from 1 to 100 GeV our results comprise the best limit on the ZZ and $W^{\pm}W^{\pm}$ couplings, which were previously unconstrained.

Published for SISSA by Springer

Received: February 28, 2022
Revised: May 3, 2022
Accepted: May 17, 2022
Published: June 20, 2022

Nonresonant searches for axion-like particles in vector boson scattering processes at the LHC

J. Bonilla,[a,b] **I. Brivio,**[c] **J. Machado-Rodríguez**[a,b] **and J.F. de Trocóniz**[a]

[a] *Departamento de Física Teórica, Universidad Autónoma de Madrid, Cantoblanco, E-28049, Madrid, Spain*
[b] *Instituto de Física Teórica IFT-UAM/CSIC, Cantoblanco, E-28049, Madrid, Spain*
[c] *Institut für Theoretische Physik, Universität Heidelberg, Philosophenweg 16, D-69120 Heidelberg, Germany*

E-mail: jesus.bonilla@uam.es, brivio@thphys.uni-heidelberg.de, jonathan.machado@uam.es, jorge.troconiz@uam.es

Abstract: We propose a new search for Axion-Like Particles (ALPs), targeting Vector Boson Scattering (VBS) processes at the LHC. We consider nonresonant ALP-mediated VBS, where the ALP participates as an off-shell mediator. This process occurs whenever the ALP is too light to be produced resonantly, and it takes advantage of the derivative nature of ALP interactions with the electroweak Standard Model bosons. We study the production of ZZ, $Z\gamma$, $W^{\pm}\gamma$, $W^{\pm}Z$ and $W^{\pm}W^{\pm}$ pairs with large diboson invariant masses in association with two jets. Working in a gauge-invariant framework, upper limits on ALP couplings to electroweak bosons are obtained from a reinterpretation of Run 2 public CMS VBS analyses. The constraints inferred on ALP couplings to ZZ, $Z\gamma$ and $W^{\pm}W^{\pm}$ pairs are very competitive for ALP masses up to 100 GeV. They have the advantage of being independent of the ALP coupling to gluons and of the ALP decay width. Simple projections for LHC Run 3 and HL-LHC are also calculated, demonstrating the power of future dedicated analyses at ATLAS and CMS.

Keywords: Axions and ALPs, Electroweak Precision Physics, Specific BSM Phenomenology

ArXiv ePrint: 2202.03450

https://doi.org/10.1007/JHEP06(2022)113

Contents

JHEP06(2022)113

1 Introduction

Axion-Like Particles (ALPs) constitute a particularly attractive class of hypothetical particles, that are predicted in a variety of Standard Model (SM) extensions, ranging from invisible axion models [1–8] to string theory [9]. They are defined as the pseudo-Goldstone bosons of a generic, spontaneously broken global symmetry, that is restored only at energy scales much higher compared to the electroweak (EW) one. Besides the Peccei-Quinn symmetry, typical examples are the lepton number [10–12] or flavor symmetries [13–15]. Being pseudo-Goldstone bosons, ALPs are pseudo-scalar particles, singlets under the SM gauge groups, and naturally much lighter than the beyond-SM (BSM) sector they originate from. As a consequence, they are most conveniently studied in an Effective Field Theory (EFT) framework, constructed as an expansion in inverse powers of the ALP characteristic scale f_a.

At the leading order, the ALP EFT only includes very few parameters (up to flavor indices). Nevertheless, the ranges allowed *a priori* for both the ALP mass m_a and scale f_a are extremely vast, spanning several orders of magnitude. As a result, the phenomenology of ALPs is one of the richest in particle and astroparticle physics. This peculiarity, together with their ubiquity in BSM models, has recently brought this class of particles into the spotlight, stimulating enormous theoretical and experimental advancements. A plethora of experiments searching for ALPs in different regimes and exploiting very diversified

techniques are either already taking data or scheduled to do so in the next decade, see e.g. [16, 17] for recent reports.

Most of these experiments are sensitive to ALPs coupling to photons, electrons or gluons. ALP interactions with the massive gauge bosons, on the other hand, are harder to access: at present, they can only be probed indirectly via loop corrections to low-energy processes [18–28] or directly at colliders. At the LHC, depending on the ALP mass and decay width, ALP-gauge interactions can be probed in V+ALP associated production processes, with $V = \gamma, Z, W^{\pm}$ and the ALP either escaping detection [29, 30] or decaying resonantly [31–33], in resonant ALP decays into diboson pairs [31], or in nonresonant processes where the ALP enters as an off-shell mediator. The latter were first studied in the context of inclusive diboson production at the LHC, where the ALP appears in s-channel, being produced via gluon fusion [34]. These channels are sensitive to the product of the ALP coupling to gluons with the relevant coupling to dibosons and probe previously unexplored areas of the ALP parameter space. Moreover, the nonresonant cross sections and kinematical distributions are found to be independent of the ALP mass from arbitrarily light masses up to masses of the order of 100 GeV [34]. The experimental strategy is to look for deviations with respect to SM expectations in the tails of the bosons transverse momenta or diboson mass distributions. ALP coupling limits derived from reinterpretations of CMS and ATLAS Run 2 measurements were presented in refs. [34, 35], while the CMS Collaboration has recently published a dedicated search for nonresonant ALP-mediated ZZ production in semileptonic final states at the LHC [36].

In this paper we study for the first time nonresonant ALP signals in EW Vector Boson Scattering (VBS) processes at the LHC (see [37] for a review). We focus on channels containing massive EW bosons: ALP EW VBS processes with the ALP going to a photon pair were studied in ref. [38] for the LHC, in ref. [39] for CLIC and in ref. [40] for the EIC. Figure 1 depicts the leading order Feynman diagrams for ALP-mediated EW production of $q_1 q_2 \to q_1' q_2' V_1 V_2$. The two jets in the final state, q_1' and q_2', are required to have a large invariant mass and to be well separated in rapidity. These processes are particularly convenient for a number of reasons: first, they allow us to access the couplings of the ALP to EW bosons independently of the coupling to gluons. At the same time, the richness of VBS in terms of different final states helps constraining the parameter space from multiple complementary directions.

Searching for signals beyond the SM in VBS final states is a major goal for the ATLAS and CMS experiments and both collaborations have recently reported Run 2 measurements of these processes [41–56]. These analyses allow us to perform a first comparison of the ALP VBS predictions to the data, a calibration of the available simulation tools and a calculation of educated predictions for higher LHC luminosities. Moreover, nonresonant searches are generally expected to become more and more competitive during the upcoming LHC runs. They will benefit, on the one hand, from the large increase in the accumulated statistics and, on the other, from the technological developments currently driven by studies of the Standard Model EFT (SMEFT) formalism, that are encouraging a global, comprehensive approach to new physics searches. Interestingly, while SMEFT analyses rely on the assumption of new particles being too heavy to be produced on-shell, nonresonant

JHEP06(2022)113

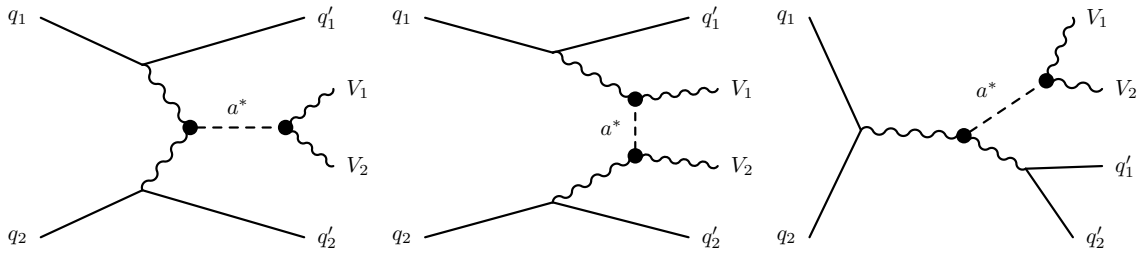

Figure 1. Feynman diagrams for ALP contributions to a generic process $q_1q_2 \to q_1'q_2'V_1V_2$. Fermion lines represent both quarks and antiquarks. In the last diagram, the final state quarks can be emitted from any of the outgoing bosons.

ALP searches target the opposite limit, i.e. where the ALP is *too light* to decay resonantly. In this way, they provide access to parameter space regions complementary to those probed in other LHC searches. In particular, compared to resonant or large-missing-momentum processes, they require only very minimal assumptions on the ALP decay width.

The manuscript is organized as follows: the theoretical framework adopted is defined in section 2. In section 3 we discuss the general characteristics of nonresonant ALP EW VBS production. The details of the ALP VBS simulation and analysis are explained in section 4. We first extract current constraints on ALP-gauge interactions from measurements of differential VBS observables published by the CMS Collaboration, and subsequently estimate projected limits for the LHC Run 3 and for the High Luminosity (HL-LHC) phase. The results are presented in section 5. In section 6 we compare them to other existing constraints. In section 7 we conclude.

2 The ALP effective Lagrangian

We define the ALP a as a pseudo-scalar state whose interactions are either manifestly invariant under shifts $a(x) \to a(x) + c$ (as befits its Goldstone origin) or generated via the chiral anomaly. Adopting an EFT approach, all ALP interactions are weighted down by inverse powers of the characteristic scale $f_a \gg m_a$, that is unknown and naturally close to the mass scale of the heavy sector the ALP originates from. We implicitly assume $f_a \gg v \simeq 246\,\text{GeV}$ and require all ALP interactions to be invariant under the full SM gauge group. We neglect CP violating terms and ALP-fermion interactions. The latter only give highly suppressed contributions at tree-level, as their physical impact is always proportional to the mass of the fermion itself and only light fermions appear in LO VBS diagrams.

The SM is then extended by the Lagrangian [57, 58]

$$\mathscr{L}_{\text{ALP}} = \frac{1}{4}\partial_\mu a \partial^\mu a - \frac{m_a^2}{2}a^2 - c_{\widetilde{B}}\frac{a}{f_a}B_{\mu\nu}\tilde{B}^{\mu\nu} - c_{\widetilde{W}}\frac{a}{f_a}W^i_{\mu\nu}\tilde{W}^{i\mu\nu} - c_{\widetilde{G}}\frac{a}{f_a}G^A_{\mu\nu}\tilde{G}^{A\mu\nu}\,, \qquad (2.1)$$

that contains a complete and non-redundant set of dimension-5 bosonic operators.[1] Here B_μ, W^i_μ, G^A_μ denote the bosons associated to the U(1), SU(2) and SU(3) gauge symmetries

[1] One more bosonic dimension 5 operator could be written down, namely $O_{a\Phi} = \partial^\mu a(\Phi^\dagger i\overleftrightarrow{D_\mu}\Phi)$, where Φ the Higgs doublet. However, this operator can be fully traded for ALP-fermion terms via the Higgs equations of motion [57]. Therefore, its impact on VBS processes is negligible.

JHEP06(2022)113

of the SM, respectively. The associated coupling constants will be denoted by g', g, g_s. Unless otherwise specified, we will use i, j, k and A, B, C to denote isospin and color indices. Covariant derivatives are defined with a minus sign convention, such that $W^i_{\mu\nu} = \partial_\mu W^i_\nu - \partial_\nu W^i_\mu + g\epsilon^{ijk} W^j_\mu W^k_\nu$ and analogously for gluons. Dual field strengths are defined as $\tilde{X}_{\mu\nu} = \frac{1}{2}\varepsilon_{\mu\nu\rho\sigma} X^{\rho\sigma}$.

In the analysis presented below, we only consider EW ALP contributions to the VBS processes, while we neglect those containing ALP-gluon interactions, which is tantamount to setting $c_{\widetilde{G}} = 0$. This is a very good approximation for the $W^\pm\gamma$, $W^\pm Z$ and same-sign $W^\pm W^\pm$ channels where the ALP QCD contribution is absent at tree level. For the ZZ and $Z\gamma$ channels, an ALP QCD contribution is present in principle. However, the ALP QCD component is reduced by requiring consistency with the limits obtained in [34–36], the rejection of the VBS selection cuts and the large diboson invariant masses involved. In particular, for values of the EW couplings $\gtrsim 1\,\text{TeV}^{-1}$, the theoretical prediction is dominated by the pure EW ALP signal, with a smaller contribution from the pure QCD ALP signal. Here, both the EW and QCD ALP signal components are positive and their interference is subdominant. This rules out the possibility of cancellations between the ALP EW and QCD components, and implies that the final bounds for $c_{\widetilde{W}}/f_a$ and $c_{\widetilde{B}}/f_a$ for $c_{\widetilde{G}} = 0$ are conservative.

It is then safe to restrict the parameter space to the four ALP couplings to the electroweak gauge bosons. In unitary gauge, they are usually parameterized as

$$\mathscr{L}_{\text{ALP,EW}} = -\frac{g_{a\gamma\gamma}}{4} a F^{\mu\nu}\tilde{F}_{\mu\nu} - \frac{g_{a\gamma Z}}{4} a Z^{\mu\nu}\tilde{F}_{\mu\nu} - \frac{g_{aZZ}}{4} a Z^{\mu\nu}\tilde{Z}_{\mu\nu} - \frac{g_{aWW}}{2} a W^{+\mu\nu}\tilde{W}^-_{\mu\nu}\,, \tag{2.2}$$

with $F_{\mu\nu}, Z_{\mu\nu}, W^\pm_{\mu\nu}$ are the field strengths of the photon, Z and $W^\pm$ bosons respectively,

$$g_{a\gamma\gamma} = \frac{4}{f_a}(s^2_\theta c_{\widetilde{W}} + c^2_\theta c_{\widetilde{B}})\,, \qquad g_{a\gamma Z} = \frac{4}{f_a} s_{2\theta}(c_{\widetilde{W}} - c_{\widetilde{B}})\,, \tag{2.3}$$

$$g_{aZZ} = \frac{4}{f_a}(c^2_\theta c_{\widetilde{W}} + s^2_\theta c_{\widetilde{B}})\,, \qquad g_{aWW} = \frac{4}{f_a} c_{\widetilde{W}}\,, \tag{2.4}$$

and s_θ, c_θ the sine and cosine of the weak mixing angle. For later convenience, we also define

$$g_{agg} = \frac{4}{f_a} c_{\widetilde{G}}\,. \tag{2.5}$$

3 General characteristics of ALP-mediated EW VBS production

We consider the production of ZZ, $Z\gamma$, $W^\pm\gamma$, $W^\pm Z$ and same-sign $W^\pm W^\pm$ pairs in association with two forward jets. These five VBS channels are those for which differential measurements of the diboson invariant mass (or transverse mass) have been reported by the CMS Collaboration, using data collected at the LHC Run 2. At parton level we treat them, for simplicity, as $2 \to 4$ scatterings, with either photons or weak bosons in the final state. As described in section 4, the weak bosons are decayed to leptons at a later stage.

ALPs give EW contributions to these processes via the diagram topologies shown in figure 1. All of them necessarily present two insertions of ALP operators, leading to

JHEP06(2022)113

Process	$c_{\widetilde{B}}^2$	$c_{\widetilde{W}}^2$	$c_{\widetilde{B}}c_{\widetilde{W}}$	$c_{\widetilde{B}}^4$	$c_{\widetilde{W}}^4$	$c_{\widetilde{B}}^2 c_{\widetilde{W}}^2$	$c_{\widetilde{B}}^3 c_{\widetilde{W}}$	$c_{\widetilde{B}} c_{\widetilde{W}}^3$
$pp \to jjZZ$	✓	✓	✓	✓	✓	✓	✓	✓
$pp \to jjZ\gamma$	✓	✓	✓	✓	✓	✓	✓	✓
$pp \to jjW^{\pm}\gamma$		✓	✓		✓	✓		✓
$pp \to jjW^{\pm}Z$		✓	✓		✓	✓		✓
$pp \to jjW^{\pm}W^{\pm}$		✓			✓			

Table 1. List of VBS processes considered in this work. For each, we indicate which terms in the polynomial dependence on $c_{\widetilde{W}}$, $c_{\widetilde{B}}$ (eq. (3.1)) are present in the parameterization of the ALP signal.

amplitudes that scale as f_a^{-2}, and cross sections of order f_a^{-4}. A generic VBS cross section, including both SM and EW ALP contributions, has the structure

$$\begin{aligned}
\sigma_{\text{ALP}} &= \sigma_{\text{SM}} + \frac{1}{f_a^2}\,\sigma_{\text{interf.}} + \frac{1}{f_a^4}\,\sigma_{\text{signal}}\,, \\
\sigma_{\text{interf.}} &= c_{\widetilde{B}}^2\,\sigma_{B2} + c_{\widetilde{W}}^2\,\sigma_{W2} + c_{\widetilde{B}}c_{\widetilde{W}}\,\sigma_{BW}\,, \\
\sigma_{\text{signal}} &= c_{\widetilde{B}}^4\,\sigma_{B4} + c_{\widetilde{W}}^4\,\sigma_{W4} + c_{\widetilde{B}}^2 c_{\widetilde{W}}^2\,\sigma_{B2W2} + c_{\widetilde{B}}^3 c_{\widetilde{W}}\,\sigma_{B3W} + c_{\widetilde{B}} c_{\widetilde{W}}^3\,\sigma_{BW3}\,,
\end{aligned} \tag{3.1}$$

where all the σ_i quantities can be evaluated numerically from the simulations. This structure holds after selection cuts. Not all processes receive contributions from all terms in this polynomial expansion: the dependence is summarized in table 1. The pattern observed can be easily explained: all processes with a W boson in final state require an insertion of $g_{aWW} \sim c_{\widetilde{W}}/f_a$. Pure $c_{\widetilde{B}}$ contributions are then absent, which means that these channels cannot constrain the ALP parameter space along the $c_{\widetilde{B}}$ axis. Same-sign $W^{\pm}W^{\pm}$ production represents an extreme case where $c_{\widetilde{B}}$ does not enter at all. Explicit expressions of $\sigma_{\text{interf.}}$, σ_{signal} are given in appendix A for the integrated cross-section of each channel, calculated after the selection cuts, see section 4.

Among the diagrams shown in figure 1, the first, where the ALP is exchanged in s-channel, only contributes to VBS with ZZ and $Z\gamma$ final states.[2] The second, with the ALP in t-channel, is relevant for all VBS processes, and it is the only one contributing to $W^{\pm}\gamma, W^{\pm}Z$ and $W^{\pm}W^{\pm}$. Finally, the third topology is triboson-like: although these diagrams were included for consistency in our calculation, we have verified that their contribution is efficiently suppressed with a cut on the dijet invariant mass $M_{q_1'q_2'} > 120\,\text{GeV}$.

We take the ALP to be too light for any of the V_1V_2 pairs to be produced resonantly. As a consequence, the ALP is always off-shell and its propagator acts as a suppression of the scattering amplitudes. However, this effect is overcompensated by the momentum enhancement induced by the ALP interaction vertices. The net result is that the ALP-mediated cross section falls more slowly with the diboson invariant mass of the boson pair $M_{V_1V_2}$ than the SM backgrounds. Figure 2 shows a parton-level comparison of the dijet invariant mass $M_{q_1'q_2'}$, jet pseudo-rapidity separation $\Delta\eta_{q_1'q_2'}$ and diboson invariant mass

[2]The s-channel diagram contributes also to VBS with opposite-sign WW or diphoton final states. However, these channels are not considered here.

JHEP06(2022)113

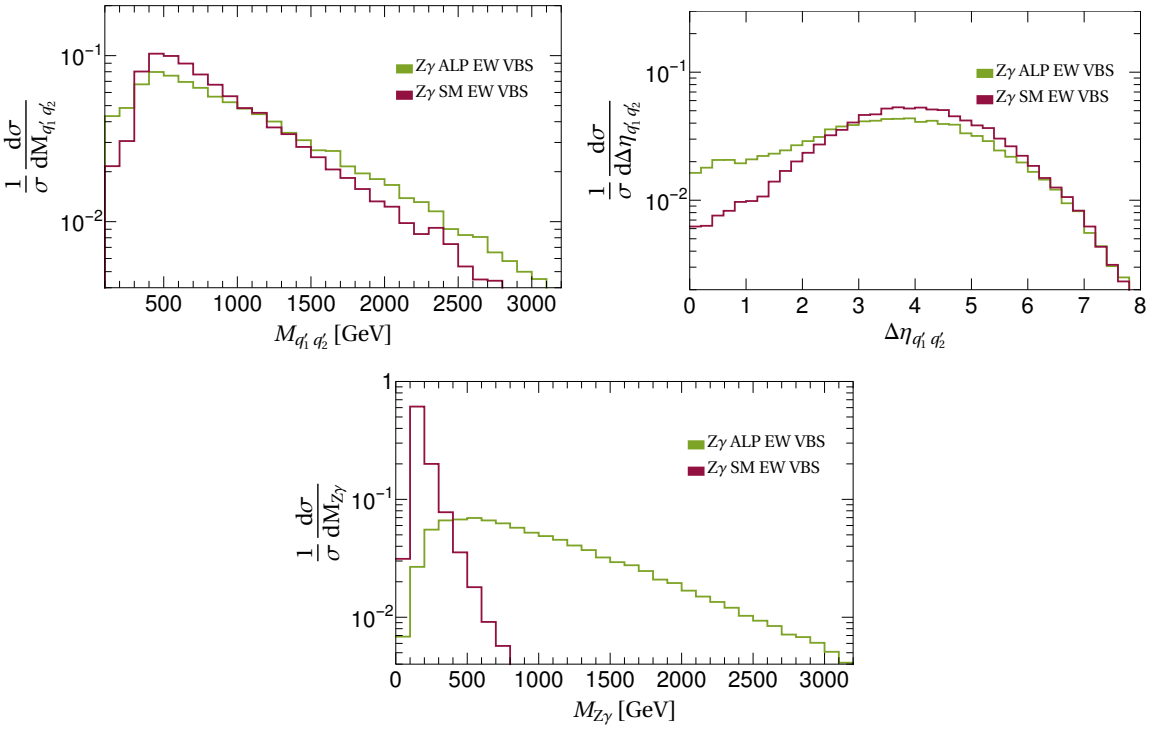

Figure 2. Normalized parton level distributions of the dijet invariant mass $M_{q_1' q_2'}$, jet pseudo-rapidity separation $\Delta\eta_{q_1' q_2'}$ and diboson invariant mass $M_{Z\gamma}$ for ALP EW VBS (green) and SM EW VBS (red) $Z\gamma$ production. The ALP curves include the pure signal and ALP-SM interference contributions, computed for $m_a = 1\,\text{MeV}$ and $c_{\widetilde{W}}/f_a = c_{\widetilde{B}}/f_a = 1\,\text{TeV}^{-1}$.

$M_{Z\gamma}$ distributions for ALP EW VBS and SM EW VBS $Z\gamma$ production. The ALP curves include the pure signal and ALP-SM interference contributions, computed for $m_a = 1\,\text{MeV}$ and $c_{\widetilde{W}}/f_a = c_{\widetilde{B}}/f_a = 1\,\text{TeV}^{-1}$. The dijet distributions are qualitatively similar, and dijet selection criteria designed to measure the SM EW VBS component should work efficiently for the ALP case as well. On the other hand, the very different tails of the diboson invariant mass distributions allow discrimination of the two processes for $M_{Z\gamma} \gtrsim 500\,\text{GeV}$. This general behavior holds for all ALP EW VBS final states, independently of the presence or absence of s-channel ALP Feynman diagrams.

3.1 Comments on the EFT power counting

Before discussing the details of the numerical analysis, a few comments on the validity of the EFT approach are in order. In particular, concerns might be raised about the fact that an ALP signal of $\mathcal{O}(f_a^{-4})$ is extracted from a Lagrangian defined at $\mathcal{O}(f_a^{-1})$. First of all, it should be noted that, because two insertions of ALP operators are always required in order to generate corrections to SM processes, the dimension-5 Lagrangian does provide complete VBS predictions up to $\mathcal{O}(f_a^{-2})$. However, it is indeed possible for $d \geq 6$ ALP operators to induce further contributions at $\mathcal{O}(f_a^{-3}, f_a^{-4})$ that are neglected in this work. Specifically, at tree-level, these missing terms can be exclusively corrections to $\sigma_{\text{interf.}}$ from ALP diagrams

JHEP06(2022)113

containing $d = 6$ or $d = 7$ operator insertions, while the expression for σ_{signal} is already complete to $\mathcal{O}(f_a^{-4})$. Note, in addition, that the parameterization in eq. (3.1) is complete to quartic order in the parameter space $(c_{\widetilde{B}}/f_a, c_{\widetilde{W}}/f_a)$, i.e. it accounts for *all* contributions up to $\mathcal{O}(f_a^{-4})$ generated by the $d = 5$ Lagrangian.[3] These considerations, together with the fact that the analysis presented in the next sections is numerically dominated by σ_{signal} (see e.g. table 6), suggest that the final results of this work would not change significantly if the missing $\mathcal{O}(f_a^{-4})$ terms were restored.[4]

For these reasons, we deem the Lagrangian in eq. (2.1) adequate for the scope of this work and we believe that the resulting constraints on $(c_{\widetilde{B}}/f_a, c_{\widetilde{W}}/f_a)$ are quite solid. We stress that these conclusions are based on considerations made *a posteriori*, having evaluated the sensitivity of LHC and HL-LHC VBS searches to $d = 5$ ALP couplings. They do not necessarily apply to processes different from VBS or in scenarios with very different sensitivity. A systematic and more quantitative assessment of the impact of higher-order ALP operators is left for future work. Note that this would require, among other things, the definition of a complete and non-redundant ALP operator basis beyond dimension-5, which has not been constructed to date.

4 ALP-mediated EW VBS simulation and analysis

In order to understand the potential of the LHC experiments, we perform a reinterpretation of the analyses recently published by the CMS Collaboration studying the production of ZZ [51], $Z\gamma$ [54], $W^{\pm}\gamma$ [52], $W^{\pm}Z$ [50] and same-sign $W^{\pm}W^{\pm}$ [50] bosons in association with two jets. All channels use leptonic (electron and muon) decays of the W and Z bosons in the final state.

The nonresonant ALP-mediated EW VBS diboson signal is simulated with the software MadGraph5_aMC@NLO 2.8.2 [59]. Employing the `ALP_linear` UFO model from [30, 60], we generate $q_1 q_2 \to V_1 V_2 q_1' q_2'$ events at leading order in the ALP and EW couplings and at zeroth order in the QCD coupling, using a 4-flavor-scheme. The parton distribution functions (PDFs) of the colliding protons are given by the NNPDF 3.0 PDF set [61] for all simulated samples. Kinematical cuts requiring

$$\begin{aligned} p_T(q'_{1,2}) > 20\,\text{GeV}\,, \quad \eta(q'_{1,2}) < 6\,, \qquad \Delta R(q'_1 q'_2) > 0.1\,, \quad M_{q'_1 q'_2} > 120\,\text{GeV}\,, \\ p_T(\gamma) > 10\,\text{GeV}\,, \qquad \eta(\gamma) < 2.5\,, \quad \Delta R(\gamma q'_{1,2}) > 0.4\,, \end{aligned} \tag{4.1}$$

are imposed at generation level for all VBS processes, except for the ZZ channel where the $M_{q'_1 q'_2}$ cut is removed. The angular separation is defined as $\Delta R = \sqrt{\Delta\eta^2 + \Delta\phi^2}$, with η the parton's pseudorapidity and ϕ its azimuthal angle. The ALP EW VBS signals are generated fixing $m_a = 1\,\text{MeV}$, $f_a = 1\,\text{TeV}$ and $\Gamma_a = 0$. The specific values of the ALP

[3] This is at variance e.g. with the SMEFT case, where the square of the $d = 6$ amplitude does not contain all $\mathcal{O}(c_6^2/\Lambda^4)$ contributions, because certain $d = 6$ operators can induce extra higher-order corrections, e.g. via redefinitions of SM fields or parameters, or via double insertions in a given diagram.

[4] The results could change significantly only if $d \geq 6$ ALP operators introduced very large kinematic enhancements to $\sigma_{\text{interf.}}$, sufficient to make it competitive with σ_{signal} within the region of sensitivity. Very preliminary considerations about the possible structure of such operators suggest that this is unlikely.

JHEP06(2022)113

mass and decay width do not have significant consequences in the nonresonant regime, see section 5.3. We generate separated samples for pure ALP-mediated production and the interference between the ALP and the SM EW VBS production. As discussed in section 3, the ALP EW VBS cross sections have a polynomial dependence on the parameters $c_{\widetilde{W}}$ and $c_{\widetilde{B}}$, whose coefficients need to be determined individually. This requires to evaluate the ALP-SM interference at a minimum of three linearly independent points in the $(c_{\widetilde{W}}, c_{\widetilde{B}})$ plane, and the pure ALP signal at a minimum of five points. This is achieved by exploiting the interaction orders syntax in MadGraph5_aMC@NLO, used both in independent event generations and with the MadGraph5 reweighting tool [62]. For cross-checking purposes, we consider a redundant set of points, namely

$$\begin{aligned} &p_0 = (1,1), \quad &&p_1 = (0,2), \quad &&p_2 = (1,0), \\ &p_3 = (1,-1), \quad &&p_4 = (1,-0.305), \quad &&p_5 = (1,-3.279)\,, \end{aligned} \tag{4.2}$$

where p_0 lies on the $c_{\widetilde{B}} = c_{\widetilde{W}}$ line, where $g_{a\gamma Z} = 0$; p_4 is on the photophobic $c_{\widetilde{B}} = -t_\theta^2 c_{\widetilde{W}}$ line, where $g_{a\gamma\gamma} = 0$; and p_5 is on the $c_{\widetilde{B}} = -c_{\widetilde{W}}/t_\theta^2$ line, where $g_{aZZ} = 0$. Here t_θ is the tangent of the Weinberg angle. We use five of these points to determine the polynomials and verify that the results extrapolated to the sixth point match those from direct simulation. This operation has been repeated on all possible subsets to verify the robustness of the predictions. The resulting polynomial expressions for the total cross sections, obtained after the full simulation and analysis procedure, are reported in appendix A. These can be employed to estimate the overall normalizations of the ALP signal for all distributions used in the final fits to the data. The production cross sections at $\sqrt{s} = 13\,\text{TeV}$ for benchmark points p_0 and p_4 are summarized in table 2. They have additionally a 11% systematic uncertainty related to the renormalization and factorization scales and a 4% systematic uncertainty related to the PDFs.

SM EW VBS diboson background events are generated with MadGraph5 at leading order in the EW couplings and zeroth order in the QCD coupling. This is an irreducible source of background for the analysis. Cross sections at $\sqrt{s} = 13\,\text{TeV}$ are presented in table 2.

For all the simulated samples in the analysis, parton showering, hadronization and decays are described by interfacing the event generators with PYTHIA 8 [63]. Massive EW bosons V_1 and V_2 are forced to decay leptonically (electrons and muons). No additional pileup pp interactions were added. All samples were processed through a simulation of the CMS detector and reconstruction of the experimental objects using DELPHES 3 [64], including FastJet [65] for the clustering of anti-k_T jets with a distance parameter of 0.4 (AK4 jets). The CMS DELPHES card was modified to improve the lepton isolation requirements and to reduce the lepton detection transverse momentum threshold to 5 GeV.

For the detector-level analysis, we apply the set of requirements designed to constrain anomalous quartic gauge couplings in the CMS publications. The most important cuts are those imposed on the dijet system, and on the photon transverse momentum if relevant, indicated in table 3. Differences between our generation and simulation procedure and the ones used by the CMS experiment are taken into account by comparing the predicted numbers of events after selection cuts for the SM EW VBS processes. In this context, the expected sources of discrepancy are calibration, efficiency or resolution effects in the

JHEP06(2022)113

Process	σ_{SM} [fb]	Point	$\sigma_{\text{interf.}}$ [fb]	σ_{signal} [fb]
$pp \to jjZZ$	98 ± 1	p_0	-13.5 ± 0.1	42.4 ± 0.2
		p_4	-9.3 ± 0.1	18.5 ± 0.1
$pp \to jjZ\gamma$	393 ± 1	p_0	0.3 ± 0.1	11.1 ± 0.1
		p_4	-9.1 ± 0.1	20.9 ± 0.1
$pp \to jjW^{\pm}\gamma$	994 ± 3	p_0	4.3 ± 0.1	28.7 ± 0.1
		p_4	1.7 ± 0.1	5.4 ± 0.1
$pp \to jjW^{\pm}Z$	386 ± 1	p_0	1.7 ± 0.1	18.4 ± 0.1
		p_4	0.1 ± 0.1	23.9 ± 0.1
$pp \to jjW^{\pm}W^{\pm}$	256 ± 1	p_0, p_4	-4.0 ± 0.1	16.0 ± 0.1

Table 2. EW VBS SM background and ALP signal partonic cross sections for $\sqrt{s} = 13\,\text{TeV}$, before decaying the vector bosons and applying only the selection cuts in eq. (4.1). The ALP signal cross sections are presented for two benchmark points p_0 and p_4 defined in eq. (4.2). For same-sign $W^{\pm}W^{\pm}$, both points give the same results. The reported errors are the statistical errors of the MadGraph5_aMC@NLO calculation.

Channel	Obs.	Lum. [fb^{-1}]	Selection Criteria	ρ
ZZ	M_{ZZ}	137	$M_{jj} > 100\,\text{GeV}$	0.8 ± 0.1
$Z\gamma$	$M_{Z\gamma}$	137	$M_{jj} > 500\,\text{GeV}$, $\Delta\eta_{jj} > 2.5$, $p_T^{\gamma} > 120\,\text{GeV}$	1.4 ± 0.2
$W^{\pm}\gamma$	$M_{W\gamma}$	35.9	$M_{jj} > 800\,\text{GeV}$, $\Delta\eta_{jj} > 2.5$, $p_T^{\gamma} > 100\,\text{GeV}$	3.1 ± 0.5
$W^{\pm}Z$	M_{WZ}^T	137	$M_{jj} > 500\,\text{GeV}$, $\Delta\eta_{jj} > 2.5$	1.5 ± 0.4
$W^{\pm}W^{\pm}$	M_{WW}^T	137	$M_{jj} > 500\,\text{GeV}$, $\Delta\eta_{jj} > 2.5$	1.3 ± 0.2

Table 3. Summary of the CMS VBS analyses: the diboson mass observable, the integrated luminosity, the most important selection criteria and the normalization scale factor ρ.

reconstruction of the experimental observables. We observe that all these affect primarily the normalization and therefore we define a scale factor ρ as the ratio of the number of expected events delivered by our generation and simulation procedure and the number of CMS expected events. We have verified that, after applying this rescaling, our simulation reproduces correctly the relevant kinematic distributions by CMS within the uncertainties. The same scale factors are then applied to the predictions for pure ALP-mediated EW VBS and ALP-SM interference simulated samples. For each channel, we assign an uncertainty to ρ, that stems from the uncertainty on the expected event yield for SM EW VBS production, reported in the CMS publications. A systematic uncertainty of 16% on the simulated ALP event yields is assigned, fully correlated across all channels. This is estimated as the average relative error on the scale factors ρ. A summary of the CMS VBS analyses is presented in table 3: the diboson mass observable, the integrated luminosity, the selection criteria and the normalization scale factor ρ.

JHEP06(2022)113

As anticipated in section 3, the discrimination between signal and background is based on the diboson mass distributions shown in appendix A. These include the fully reconstructed diboson invariant masses M_{ZZ} and $M_{Z\gamma}$; the diboson invariant mass $M_{W^{\pm}\gamma}$, where the longitudinal momentum of the neutrino is constrained by the condition $M_{\ell\nu} = m_W$ [52]; and the diboson transverse masses $M^T_{W^{\pm}W^{\pm}}$ and $M^T_{W^{\pm}Z}$, defined as

$$M^T_{V_1V_2} = \left[\left(\sum_i E_i\right)^2 - \left(\sum_i p_{z,i}\right)^2\right]^{1/2}, \tag{4.3}$$

where the index i runs over all the leptons in the final state, and assuming that the neutrinos longitudinal momenta are zero [50].

In order to provide a handle on possible issues concerning the validity of the ALP EFT expansion [66] and to estimate the impact of the highest-energy bins, we introduce an upper cut on $M_{V_1V_2}$, that is applied on the signal simulation only. We consider two benchmark selections: $M_{V_1V_2} < 2\,\text{TeV}$ and $M_{V_1V_2} < 4\,\text{TeV}$. These cuts are satisfied, respectively, by 85% and $> 99\%$ of the events in the ALP generated samples and mainly impact the signal predictions in the last bin of each distribution, as shown in figures 7–11.

The log-likelihood is constructed based on a Poisson distribution. For each VBS channel, it has the form:

$$\log L(c_{\widetilde{B}}, c_{\widetilde{W}}) = \sum_k \left[-\left(B_k + S_k(c_{\widetilde{B}}, c_{\widetilde{W}})\right) + D_k \log\left(B_k + S_k(c_{\widetilde{B}}, c_{\widetilde{W}})\right)\right] \tag{4.4}$$

where the index k runs over the bins of the relevant distribution. The number of events for the data (D_k) and for the SM background predictions (B_k) are taken from the CMS experimental publications. The expected number of signal events (S_k) accounts for both the pure ALP EW VBS signal and the ALP-SM interference contributions, that are parameterised as fourth- and second-degree polynomials in ($c_{\widetilde{W}}/f_a$, $c_{\widetilde{B}}/f_a$) respectively, as explained in section 3. The combined log-likelihood is simply constructed as the sum of $\log L$ for the individual channels.

Systematic uncertainties affecting the SM background distributions are considered fully correlated among bins of a distribution, but uncorrelated among different VBS channels. They are described by one nuisance parameter for each VBS channel, that multiplies both background and ALP signal yields, and is taken to be Gaussian-distributed. The systematic uncertainty on the signal prediction is implemented analogously and applied to S_k only. It is taken to be fully correlated across all channels and bins and we assign it a total size of 20%, obtained adding in quadrature the 16% uncertainty on the signal normalization, the 11% uncertainty on the renormalization and factorization scales choice and the 4% error related to the PDFs.

5 Results

5.1 Results from LHC Run 2 measurements

Table 4 shows the branching fractions and selection efficiencies for each VBS channel. The latter are relative to the simulated events in which the bosons are decayed to electrons and muons. The products of efficiencies and branching fractions range from 0.2% to 0.9%.

JHEP06(2022)113

Analysis	ZZ	$Z\gamma$	$W^{\pm}\gamma$	$W^{\pm}Z$	$W^{\pm}W^{\pm}$
Branching fraction	0.45%	6.7%	22%	1.5%	4.8%
Efficiency	35.7%	14.0%	1.6%	11.3%	17.0%

Table 4. Summary of branching fractions and selection efficiencies for each VBS channel. The efficiencies are relative to the simulated events in which the W and Z bosons decay to electrons or muons.

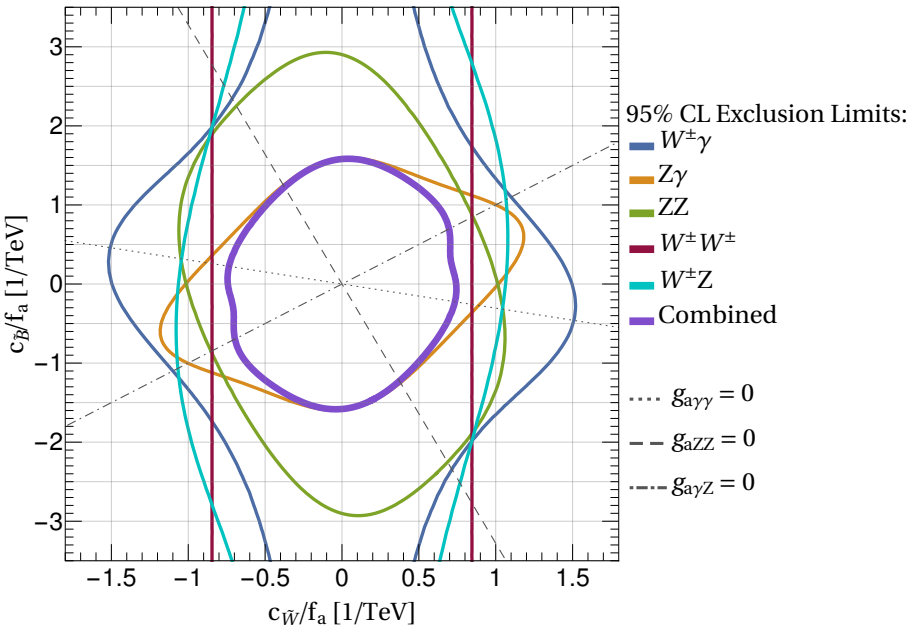

Figure 3. Observed 95% CL exclusion limits in the $(c_{\widetilde{W}}/f_a,\ c_{\widetilde{B}}/f_a)$ plane using the data of the Run 2 CMS publications and signal events with $M_{V_1V_2} < 4\,\text{TeV}$. The limits have been calculated individually for the five different experimental channels considered and for their combination. The thin dotted, dashed and dot-dashed lines indicate the directions of vanishing couplings to neutral gauge bosons.

Results are extracted from a maximum likelihood fit of signal and background to the diboson invariant mass (ZZ, $Z\gamma$ and $W^{\pm}\gamma$) or transverse mass ($W^{\pm}Z$ and $W^{\pm}W^{\pm}$) distributions, individually and simultaneously in all the experimental channels used in the analysis. The likelihood is defined as described in the previous section and the background-only hypothesis is tested against the combined background and signal hypothesis.

No significant excess was observed by CMS with respect to the SM expectations. ALP couplings $c_{\widetilde{W}}/f_a$ and $c_{\widetilde{B}}/f_a$ are considered excluded at 95% confidence level (CL) when the negative log likelihood (NLL) $(-\log L)$ of the combined signal and background hypothesis exceeds 3.84/2 units the NLL of the background-only hypothesis.

Figure 3 shows the observed 95% CL exclusion limits in the $(c_{\widetilde{W}}/f_a, c_{\widetilde{B}}/f_a)$ plane using the data of the Run 2 CMS publications and signal events with $M_{V_1V_2} < 4\,\text{TeV}$. The limits have been calculated individually for the five different experimental channels considered and for their combination. Table 5 reports the upper bounds obtained projecting the combined

JHEP06(2022)113

Coupling	Run 2 Observed (Expected)		$300\,\text{fb}^{-1}$		$3000\,\text{fb}^{-1}$	
$[\text{TeV}^{-1}]$	$M_{V_1V_2} < 4\,\text{TeV}$	$< 2\,\text{TeV}$	$< 4\,\text{TeV}$	$< 2\,\text{TeV}$	$< 4\,\text{TeV}$	$< 2\,\text{TeV}$
$\lvert c_{\widetilde{W}}/f_a \rvert$	0.75 (0.83)	0.86 (0.94)	0.71	0.80	0.55	0.62
$\lvert c_{\widetilde{B}}/f_a \rvert$	1.59 (1.35)	1.73 (1.47)	1.12	1.23	0.79	0.87
$\lvert g_{a\gamma\gamma} \rvert$	4.99 (4.24)	5.45 (4.63)	3.50	3.84	2.43	2.68
$\lvert g_{a\gamma Z} \rvert$	5.54 (4.74)	6.15 (5.25)	3.98	4.42	2.94	3.30
$\lvert g_{aZZ} \rvert$	2.84 (3.02)	3.19 (3.38)	2.53	2.81	1.94	2.16
$\lvert g_{aWW} \rvert$	2.98 (3.33)	3.43 (3.74)	2.84	3.18	2.21	2.49

Table 5. 95% CL upper limits on the absolute value of the Wilson coefficients $c_{\widetilde{W}}/f_a$ and $c_{\widetilde{B}}/f_a$ and projected onto the ALP couplings to physical bosons, eq. (2.2). The various columns report current bounds extracted from CMS Run 2 measurements and projected sensitivities for $\sqrt{s} = 14\,\text{TeV}$ and LHC higher luminosities, for signal events with $M_{V_1V_2}$ below 4 TeV or 2 TeV.

95% CL allowed region onto different directions in the $(c_{\widetilde{W}}/f_a, c_{\widetilde{B}}/f_a)$ plane, namely the two axes and the combinations corresponding to the ALP couplings to physical bosons defined in eq. (2.2), which are orthogonal to the dotted, dashed and dot-dashed lines in figure 3. Table 5 also presents the 95% CL limits obtained with the more conservative cut $M_{V_1V_2} < 2\,\text{TeV}$, which are about 10–15% weaker than the ones in figure 3. The modest impact of this additional cut indicates that the ALP VBS cross section does not grow indefinitely with energy (see also figure 2). Instead, only a small number of signal events populate the very high $M_{V_1V_2}$ region.

In most of the parameter space, the limits are dominated by the $Z\gamma$ measurement, that is the most stringent along the $c_{\widetilde{B}}$ direction. The only other measurement capable of bounding this parameter is ZZ, which however pays the price of the small $\text{Br}(Z \to \ell\ell)$ and the current loose selection cuts on the dijet system. The sensitivity of the $W^{\pm}\gamma$ channel is reduced by the smaller integrated luminosity of the published CMS analysis. A measurement of the $\gamma\gamma$ VBS final state at large diphoton invariant masses, that has not been performed by ATLAS or CMS to date, would bring additional sensitivity to $c_{\widetilde{B}}$, with a great potential for improving the current bounds [38].

5.2 Prospects for LHC Run 3 and HL-LHC

In this section we investigate the sensitivity of the nonresonant ALP VBS searches at the LHC Run 3 and HL-LHC. For simplicity, we apply the same selection criteria as the CMS Run 2 analyses, and rescale the integrated luminosities to $300\,\text{fb}^{-1}$ and $3000\,\text{fb}^{-1}$, respectively. An additional scaling factor κ is applied to account for an increase in the proton collision center-of-mass energy from 13 to 14 TeV. In our approximation, κ is taken to be constant over all distribution bins and identical for all VBS channels. Using MadGraph5_aMC@NLO and the cuts in eq. (4.1), we obtain κ-factors of 1.14, 1.26 and 1.20 for the SM background, the ALP EW VBS signal and their interference, respectively.

Figure 4 shows the projected 95% CL upper limits in the $(c_{\widetilde{W}}/f_a, c_{\widetilde{B}}/f_a)$ plane for $\sqrt{s} = 14\,\text{TeV}$, $M_{V_1V_2} < 4\,\text{TeV}$ and integrated luminosities $300\,\text{fb}^{-1}$ and $3000\,\text{fb}^{-1}$. For

JHEP06(2022)113

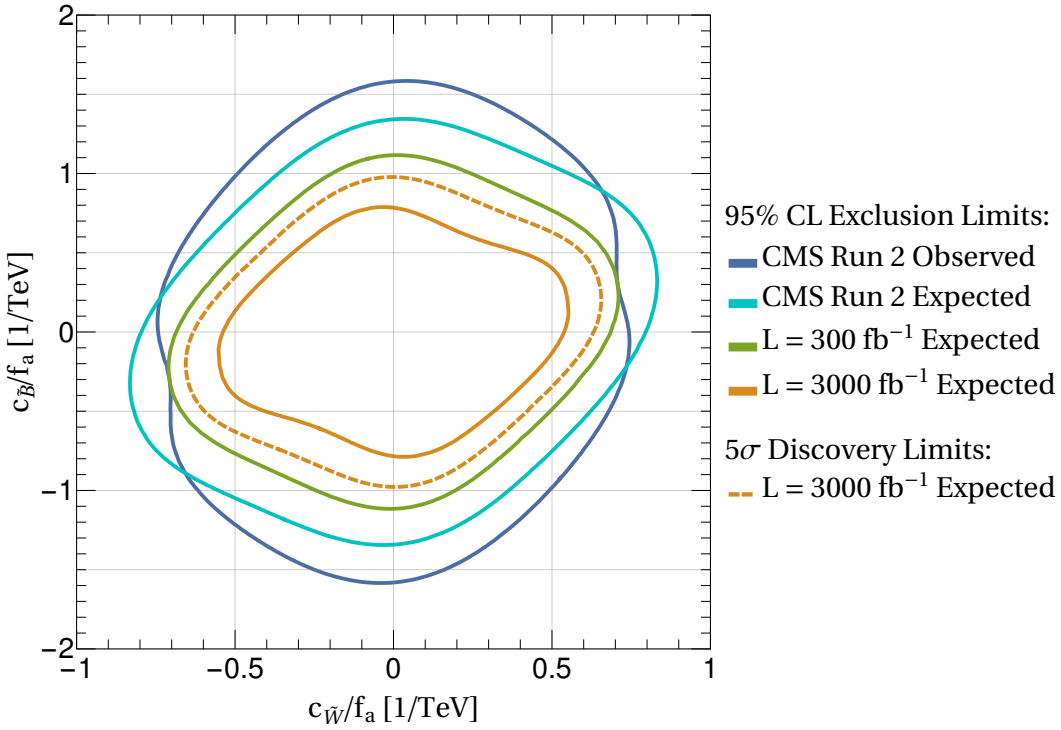

Figure 4. Projected 95% CL upper limits on the couplings $(c_{\widetilde{W}}/f_a, c_{\widetilde{B}}/f_a)$ for $\sqrt{s} = 14\,\text{TeV}$, $M_{V_1V_2} < 4\,\text{TeV}$ and integrated luminosities of 300 (green) and 3000 fb^{-1} (orange), obtained combining all VBS channels. The blue and light blue lines show, for comparison, the observed and expected limits with Run 2 luminosities. The dashed orange line marks the 5σ-discovery limit for the HL-LHC.

comparison, the observed and expected Run 2 limits have been included as well. The interplay between the individual channels is not shown in figure 4 as it remains qualitatively unchanged compared to figure 3. As expected, the largest individual improvement is found for the $W^{\pm}\gamma$ channel. However, the combined limits are still dominated by the $Z\gamma$ channel and with a significant contribution of $W^{\pm}W^{\pm}$ for the highest values of $c_{\widetilde{W}}/f_a$. We find that the bounds on $c_{\widetilde{B}}$ can improve by roughly a factor 2 at the HL-LHC compared to current constraints, while those on $c_{\widetilde{W}}$ by a factor ~ 1.4.

Figure 4 also shows, for reference, the curve corresponding to the expected discovery limit for $\sqrt{s} = 14\,\text{TeV}$, $M_{V_1V_2} < 4\,\text{TeV}$ and an integrated luminosity of $3000\,\text{fb}^{-1}$, defined as the set of $(c_{\widetilde{W}}/f_a, c_{\widetilde{B}}/f_a)$ values for which the SM point is excluded by 5 standard deviations, assuming that the measurement matches the predicted ALP EW VBS signal. The fact that it is fully contained inside the projected exclusion limits for current and Run 3 luminosities indicates that null results at previous LHC Runs will not exclude a priori the possibility of a discovery at the HL-LHC.

5.3 Dependence on the ALP mass and decay width

Our results were derived assuming that the ALP gives only off-shell contributions to all VBS processes considered. Specifically, in the simulations we fixed the ALP mass and decay width to $m_a = 1\,\text{MeV}, \Gamma_a = 0$, which satisfy $\sqrt{|p_a^2|} \gg m_a, \Gamma_a$, being p_a the momentum flowing

JHEP06(2022)113

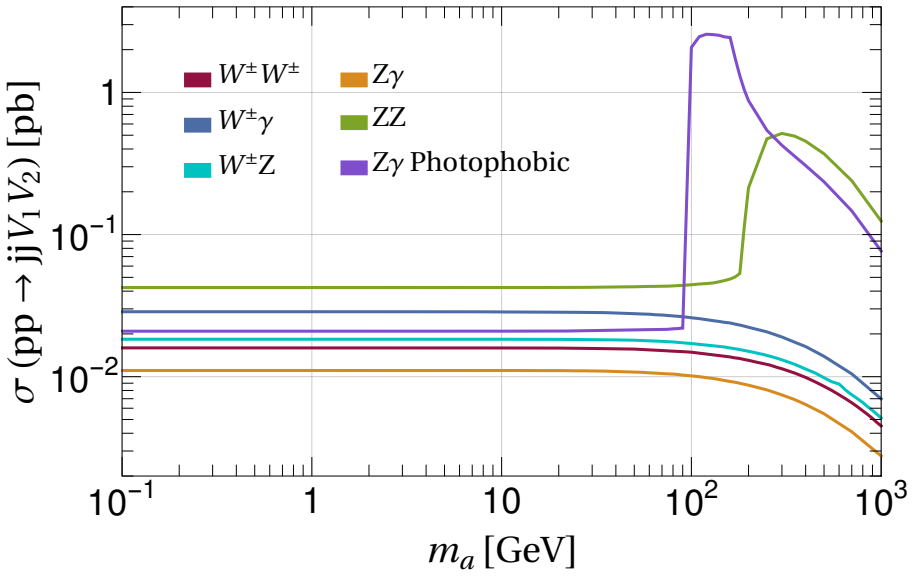

Figure 5. Total cross sections at $\sqrt{s} = 13\,\text{TeV}$ for the ALP contributions to the different VBS channels as a function of the ALP mass. All lines are evaluated at $c_{\widetilde{W}}/f_a = c_{\widetilde{B}}/f_a = 1\,\text{TeV}^{-1}$, that corresponds to the benchmark point p_0 in eq. (4.2). The exception is the "$Z\gamma$ photophobic" case, that is evaluated at p_4 instead. At each point in the plot, the ALP decay width was re-computed as a function of $m_a, c_{\widetilde{W}}$ and $c_{\widetilde{B}}$.

through the ALP propagator. As long as this kinematic condition is verified, the bounds are essentially independent of the specific m_a and Γ_a assumed. This is an important difference with respect to resonant searches, that only apply for limited mass and width windows.

Figure 5 provides a basic check of the validity of the off-shell approximation, showing the cross section for the ALP signal at $\sqrt{s} = 13\,\text{TeV}$ with the cuts in eq. (4.1), as a function of m_a for fixed values of $c_{\widetilde{W}}$, $c_{\widetilde{B}}$ and f_a. The width Γ_a was implicitly computed at every point as a function of m_a and of the ALP couplings, and it scales as $\Gamma_a \propto m_a^3 (c_i/f_a)^2$. The lines in figure 5 extend indefinitely to the left, confirming that the simulations apply to arbitrarily small m_a. In the direction of larger m_a the cross sections for $W^\pm Z, W^\pm\gamma, W^\pm W^\pm$ start falling once the t-channel propagator becomes kinematically dominated by the ALP mass. For the $Z\gamma$ and ZZ channels, the resonant behavior is visible for $(c_{\widetilde{W}}, c_{\widetilde{B}})$ benchmark points that allow the ALP exchange in s-channel. As $g_{a\gamma Z} = 0$ is enforced at p_0, we evaluate the $Z\gamma$ channel also at the "photophobic" point p_4 in order to test the resonant case.

Based on these indications, our results can be safely taken to hold up to $m_a \lesssim 100\,\text{GeV}$. At this mass, the ZZ and $W^\pm V$ cross sections have deviated by about 10% from their asymptotic values for $m_a \to 0$. At the same time, the $Z\gamma$ resonance is present but not visible in the CMS measurement, that requires $M_{Z\gamma} > 160\,\text{GeV}$ [54].

6 Comparison to existing bounds

Figure 6 shows the observed bounds obtained in this work as a function of the EW g_{aVV} couplings defined in eq. (2.2), and of m_a, compared to previously derived bounds. The

JHEP06(2022)113

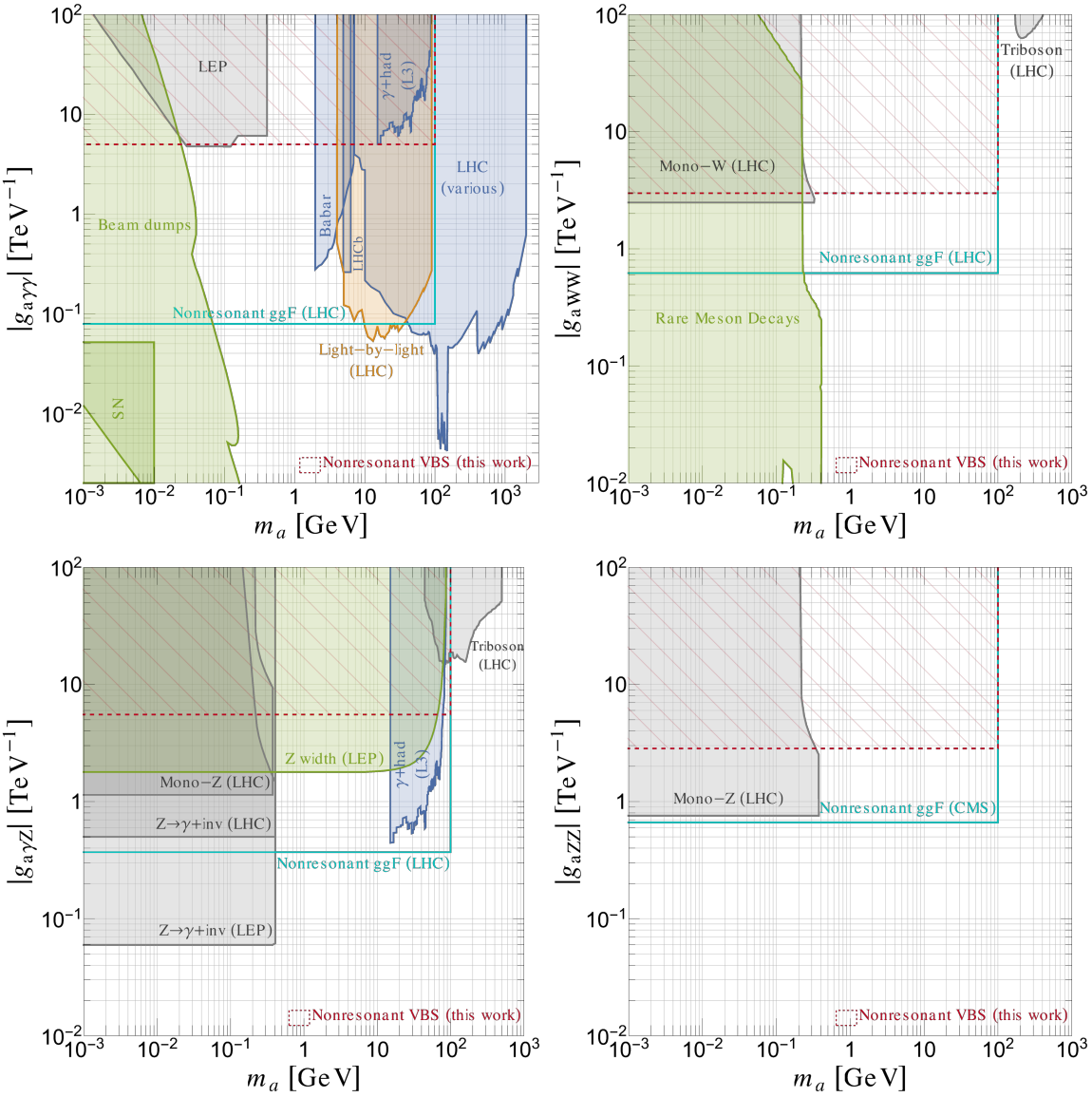

Figure 6. Summary of current constraints on ALP couplings to EW gauge bosons defined in eq. (2.2), as a function of the ALP mass m_a. Limits derived in this work are labeled "Nonresonant VBS" and shown in **red**. Previous constraints are shown with a color coding that indicates different underlying theory assumptions. **Orange** indicates a $\mathrm{Br}(a \to \gamma\gamma) = 1$ assumption, **dark blue** indicates an assumed gluon dominance $g_{agg} \gg g_{aV_1V_2}$, while bounds in **light blue** scale with $1/g_{agg}$ and are given for $g_{agg} = 1\,\mathrm{TeV}^{-1}$. **Grey** indicates more complex assumptions on the ALP EW couplings. Genuine bounds, that hold without further assumptions, are in **green**. See the main text for more details.

JHEP06(2022)113

numerical results of our study are also reported in table 5 for observed, expected and projected limits.

Most of the constraints shown in the figure are taken from the compilation in ref. [20] and updated to include more recent results. For ALP masses in the MeV-GeV window and within the range shown, the ALP coupling to photons is constrained by beam-dump experiments [67–70], by new physics searches in $e^+e^- \to 2\gamma, 3\gamma$ at LEP [29, 71] and by explosion energy arguments in supernovae [72, 73] (labeled "SN"). At higher ALP masses, all constraints on $g_{a\gamma\gamma}$ are due to searches at colliders, where the ALP decays resonantly either to hadrons or to photon pairs. In the first case, the relevant processes are $\Upsilon \to \gamma + \text{hadrons}$ at BaBar [74] and $e^+e^- \to \gamma + \text{hadrons}$ at L3 [75], that also constrains $g_{a\gamma Z}$. In the second case, the leading bounds stem from photon pair production at the LHC, both in proton-proton collisions [76, 77] (labeled "LHC" for those from ATLAS and CMS measurements and "LHCb" for those from LHCb searches [78]) and in light-by-light scattering $\gamma\gamma \to a \to \gamma\gamma$ measured in Pb-Pb collisions [79, 80] (labeled "Light-by-light (LHC)"). Most constraints on the couplings of the ALP to massive gauge bosons assume a stable ALP and cover the sub-GeV mass region. In this case, limits are inferred from mono-W and mono-Z [30] at the LHC and, for $g_{a\gamma Z}$, from the non-observation of exotic $Z \to \gamma + \text{invisible}$ decays at LEP [31] and at the LHC [81] (labeled "$Z \to \gamma + \text{inv.}$ (LHC)"). If the assumption of a stable ALP is relaxed, the latter constraint can be replaced by the more conservative bound due to the measurement of the total Z decay width at LEP, that extends up to $m_a \lesssim m_Z$ [30, 31]. In the region where the ALP can decay to hadrons, the same process leads to $Z \to \gamma + \text{hadrons}$ [75]. The ALP coupling to W bosons is the only one contributing to rare meson decays at 1-loop, which allow to set very stringent limits for light ALPs [18, 82]. For ALP masses above 100 GeV, the dominant bounds stem from resonant triboson searches [31]. Finally, nonresonant searches in diboson production via gluon fusion at the LHC (labeled "Nonresonant ggF") allow to constrain all four ALP interactions. Each nonresonant bound is extracted from a single process $gg \to a^* \to V_1V_2$: the constraint on $g_{a\gamma\gamma}$ was derived in ref. [34], those on $g_{aWW}, g_{a\gamma Z}$ in ref. [35], and the constraint on g_{aZZ} in ref. [36].

An important aspect to consider is that, in general, any given measurement can depend on several ALP couplings. In order to represent the corresponding bound in the 2D (m_a, g_{aVV}) plane, it is then necessary to define a projection rationale or introduce theoretical assumptions, which can vary significantly from constraint to constraint. These differences should be taken into account for a proper comparison. In figure 6, the bounds derived in this work (red dashed) are those corresponding to the 95% C.L. limits in table 5. As they are derived from the allowed region in the $(c_{\widetilde{W}}/f_a, c_{\widetilde{B}}/f_a)$ plane, they automatically take into account gauge invariance relations. Because of the arguments laid down in section 2, they also have limited sensitivity to the coupling to gluons. The remaining bounds are derived with alternative strategies, that we highlight with color coding in figure 6. Bounds that apply without extra assumptions, are reported in green. The bounds drawn in light blue, that include nonresonant $gg \to a^* \to V_1V_2$ processes, scale with $1/g_{agg}$ and for $c_{\widetilde{G}} \to 0$ are lifted completely. In the figure, they are normalized to $g_{agg} = 1\,\text{TeV}^{-1}$. Bounds drawn in dark blue assume gluon-dominance, i.e. $g_{agg} \gg g_{aV_1V_2}$, and in this limit they are largely

JHEP06(2022)113

independent of $c_{\widetilde{G}}$, see ref. [20]. Among these, bounds on $g_{a\gamma\gamma}$ labeled as "LHC" additionally assume negligible branching fractions to fermions and heavy EW bosons in the mass region where they are kinematically allowed. The limit from light-by-light scattering, shown in orange, assumes $\mathrm{Br}(a \to \gamma\gamma) = 1$, which corresponds to vanishing couplings to gluons and light fermions. Bounds that make more elaborate assumptions about the ALP parameter space or assumptions on the EW sector itself are shown in grey. Among these, triboson constraints on g_{aWW} and $g_{a\gamma Z}$ assume a photophobic ALP scenario [31]. All searches for a stable ALP (mono-W, mono-Z, $Z \to \gamma + \text{inv.}$) implicitly assume a small enough ALP decay width, which, in the relevant mass range, translates into assumptions on the coupling to photons, electrons and muons. The LEP constraints assume negligible branching fractions to leptons. Note also that this bound is truncated to $m_a \leq 3m_\pi \simeq 0.5\,\mathrm{GeV}$ because, beyond this threshold, hadronic ALP decay channels are kinematically open. This would introduce a further dependence on $c_{\widetilde{G}}$ whose modeling would require a dedicated analysis [20]. Constraints derived with assumptions that explicitly violate the gauge invariance relations, e.g. by explicitly requiring only one non-zero EW coupling, are omitted.

Overall, we find that the main value of nonresonant searches in VBS is that they probe the ALP interactions with EW bosons directly (at tree level) and independently of the coupling to gluons. In particular, nonresonant VBS constraints are stronger than those from nonresonant diboson production whenever g_{agg} is smaller than a certain threshold, that roughly ranges between $0.01\,\mathrm{TeV}^{-1}$ and $0.2\,\mathrm{TeV}^{-1}$ depending on the EW coupling of interest. For cases where the ALP-gluon coupling is very suppressed, such as Majorons,[5] VBS bounds are the most stringent in the 0.5–100 GeV mass region for g_{aWW}, g_{aZZ}, and in the 0.5–4 GeV region for $g_{a\gamma\gamma}$. In the case of $g_{a\gamma Z}$, the current best bounds for $m_a < m_Z$ come from the total Z width measurement at LEP.

7 Conclusions

We have investigated the possibility of constraining EW ALP interactions via the measurement of EW VBS processes at the LHC, where the ALP can induce nonresonant signals if it is too light to be produced resonantly. We have studied the production of ZZ, $Z\gamma$, $W^\pm\gamma$, $W^\pm Z$ and same-sign $W^\pm W^\pm$ pairs with large diboson invariant masses in association with two jets. New upper limits on ALP couplings to EW bosons have been derived from a reinterpretation of Run 2 public CMS VBS analyses. Among the channels considered, the most constraining ones are currently $Z\gamma$ and $W^\pm W^\pm$.

The limits have been calculated both in the plane of the gauge-invariant ALP EW couplings $(c_{\widetilde{W}}/f_a, c_{\widetilde{B}}/f_a)$ and projected onto the 4 mass-eigenstate couplings defined in eq. (2.2), to facilitate the comparison with other results. The constraints inferred on ALP couplings to ZZ, $W^\pm W^\pm$ and $Z\gamma$ pairs are very competitive with other LHC and LEP limits for ALP masses up to 100 GeV. They probe previously unexplored regions of the parameter space and have the advantage of being independent of the ALP coupling to

[5] A priori, the ALP-gluon interaction is not protected by any symmetry. Therefore, technically, it cannot be assumed to be exactly vanishing, even starting from a $c_{\widetilde{G}} = 0$ condition. In the Majoron case it is generated at 2-loops [83] and therefore remains very suppressed.

JHEP06(2022)113

gluons and of the ALP decay width. This is important in view of a global analysis of ALP couplings, where VBS can help disentangling EW from gluon interactions. All the constraints extracted in this work can be further improved in the future, for instance, by adopting a finer binning for the kinematic distributions, or by incorporating into the fit measurements by the ATLAS Collaboration or measurements of other VBS channels (e.g. opposite-sign $W^{\pm}W^{\pm}$ or semileptonic ZV).

Simple projections for integrated luminosities up to $3000\,\text{fb}^{-1}$ have been calculated, demonstrating the power of future dedicated analyses. Searches for nonresonant new physics signals in VBS production at the LHC Run 3 and HL-LHC performed by the ATLAS and CMS Collaborations will be able to probe the existence of ALPs for relevant values of their couplings to EW bosons.

Acknowledgments

We are grateful to G. Alonso and P. Quilez for providing code and information for the comparisons presented in section 6, to E. Vitagliano for guidance on the update of supernova constraints and to B. Gavela and V. Sanz for their continuous support. We also acknowledge the contributions of J.M. No to the initial phase of this work. J.B. and I.B. thank B. Heinemann, S. Heim, S. Bruggisser and P. Govoni for several illuminating discussions. The authors acknowledge the support of the CA16108 VBSCan COST Action. The work of J.B. was supported by the Spanish MICIU through the National Program FPU (grant number FPU18/03047). The work of J.M.R. was supported by the Spanish MICIU through the National Program FPI-Severo Ochoa (grant number PRE2019-089233). J.B. and J.M.R. acknowledge partial financial support by the Spanish MINECO through the Centro de excelencia Severo Ochoa Program under grant SEV-2016-0597, by the Spanish "Agencia Estatal de Investigacíon" (AEI) and the EU "Fondo Europeo de Desarrollo Regional" (FEDER) through the project PID2019-108892RB-I00/AEI/10.13039/501100011033. J.F.T. acknowledges support from the AEI and the EU FEDER through the project PID2020-116262RB-C43.

A Expected ALP EW VBS diboson mass distributions

Table 6 reports the expected ALP EW VBS pure signal and interference cross sections at $\sqrt{s} = 13\,\text{TeV}$ as a function of the Wilson coefficients $c_{\widetilde{W}}$ and $c_{\widetilde{B}}$ for $f_a = 1\,\text{TeV}$, after selection cuts and $M_{V_1V_2} < 4\,\text{TeV}$.

The diboson invariant mass or transverse mass distributions after selection cuts for the five VBS channels studied are shown in figures 7–11. The data points and the total SM background (orange line) are taken from the CMS publications. The dashed and solid green lines represent the total ALP EW VBS signal contributions for $c_{\widetilde{B}}/f_a = c_{\widetilde{W}}/f_a = 1\,\text{TeV}^{-1}$ with a cut of $M_{V_1V_2} < 2\,\text{TeV}$ and $4\,\text{TeV}$, respectively. As discussed in section 4, the total systematic uncertainty on the signal normalization is 20% (green band). The background systematics errors are taken bin-by-bin from the CMS publications (orange band).

JHEP06(2022)113

Process	ALP EW VBS Cross Section [fb]
$pp \to jjZZ$	$\sigma_{\text{interf.}} = \left(0.04\, c_{\widetilde{B}}^2 - 0.55\, c_{\widetilde{B}}\, c_{\widetilde{W}} - 1.80\, c_{\widetilde{W}}^2\right) \cdot 10^{-2}$ $\sigma_{\text{signal}} = \left(0.05\, c_{\widetilde{B}}^4 + 0.15\, c_{\widetilde{B}}^3\, c_{\widetilde{W}} + 1.55\, c_{\widetilde{B}}^2\, c_{\widetilde{W}}^2 + 1.66\, c_{\widetilde{B}}\, c_{\widetilde{W}}^3 + 3.39\, c_{\widetilde{W}}^4\right) \cdot 10^{-2}$
$pp \to jjZ\gamma$	$\sigma_{\text{interf.}} = \left(0.01\, c_{\widetilde{B}}^2 + 6.60\, c_{\widetilde{B}}\, c_{\widetilde{W}} - 6.56\, c_{\widetilde{W}}^2\right) \cdot 10^{-2}$ $\sigma_{\text{signal}} = \left(0.19\, c_{\widetilde{B}}^4 - 0.29\, c_{\widetilde{B}}^3\, c_{\widetilde{W}} + 2.04\, c_{\widetilde{B}}^2\, c_{\widetilde{W}}^2 - 2.07\, c_{\widetilde{B}}\, c_{\widetilde{W}}^3 + 1.23\, c_{\widetilde{W}}^4\right) \cdot 10^{-1}$
$pp \to jjW^{\pm}\gamma$	$\sigma_{\text{interf.}} = c_{\widetilde{W}} \left(-1.38\, c_{\widetilde{B}} + 0.29\, c_{\widetilde{W}}\right) \cdot 10^{-3}$ $\sigma_{\text{signal}} = c_{\widetilde{W}}^2 \left(5.20\, c_{\widetilde{B}}^2 + 2.12\, c_{\widetilde{B}}\, c_{\widetilde{W}} + 2.81\, c_{\widetilde{W}}^2\right) \cdot 10^{-2}$
$pp \to jjW^{\pm}Z$	$\sigma_{\text{interf.}} = c_{\widetilde{W}} \left(1.15\, c_{\widetilde{B}} - 0.55\, c_{\widetilde{W}}\right) \cdot 10^{-3}$ $\sigma_{\text{signal}} = c_{\widetilde{W}}^2 \left(0.90\, c_{\widetilde{B}}^2 - 1.00\, c_{\widetilde{B}}\, c_{\widetilde{W}} + 3.17\, c_{\widetilde{W}}^2\right) \cdot 10^{-2}$
$pp \to jjW^{\pm}W^{\pm}$	$\sigma_{\text{interf.}} = -0.0405\, c_{\widetilde{W}}^2$ $\sigma_{\text{signal}} = 0.135\, c_{\widetilde{W}}^4$

Table 6. Expected ALP EW VBS interference and pure signal cross sections at $\sqrt{s} = 13\,\text{TeV}$ as a function of the Wilson coefficients $c_{\widetilde{W}}$ and $c_{\widetilde{B}}$ for $f_a = 1\,\text{TeV}$ after selection cuts and requiring $M_{V_1V_2} < 4\,\text{TeV}$. These expressions can be used to estimate the overall normalizations of the ALP signal for all distributions used in the final fits to the data.

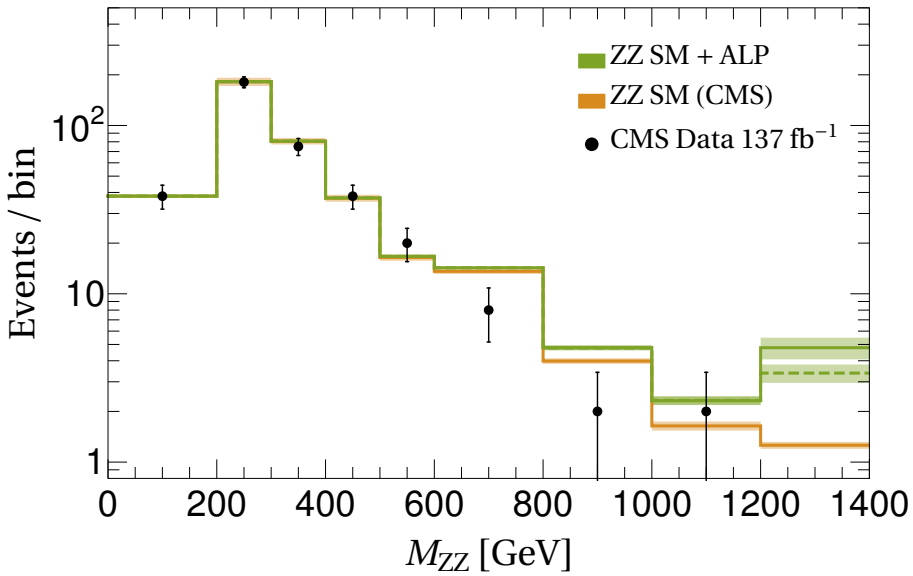

Figure 7. M_{ZZ} distribution for the $pp \to jjZZ \to jj\ell^+\ell^-\ell^+\ell^-$ channel. The data points and the total SM background (orange) are taken from the measurement in ref. [51]. The last bin contains the overflow events. The dashed and solid green lines show the total ALP EW VBS signal for $c_{\widetilde{B}}/f_a = c_{\widetilde{W}}/f_a = 1\,\text{TeV}^{-1}$ with a cut of $M_{ZZ} < 2\,\text{TeV}$ and $4\,\text{TeV}$, respectively.

JHEP06(2022)113

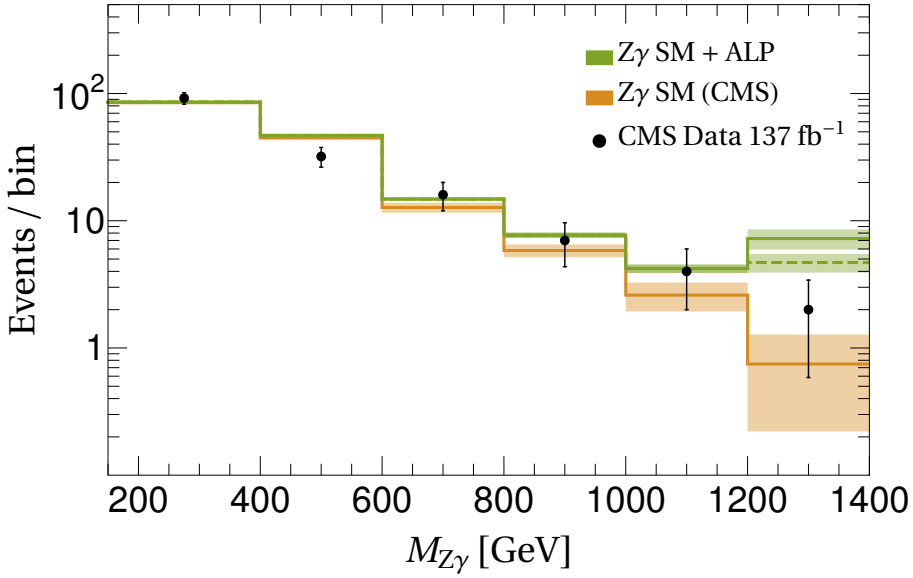

Figure 8. $M_{Z\gamma}$ distribution for the $pp \to jjZ\gamma \to jj\ell^+\ell^-\gamma$ channel. The data points and the total SM background (orange) are taken from the measurement in ref. [54]. The last bin contains the overflow events. The dashed and solid green lines show the total ALP EW VBS signal for $c_{\widetilde{B}}/f_a = c_{\widetilde{W}}/f_a = 1\,\text{TeV}^{-1}$ with a cut of $M_{Z\gamma} < 2\,\text{TeV}$ and 4 TeV, respectively.

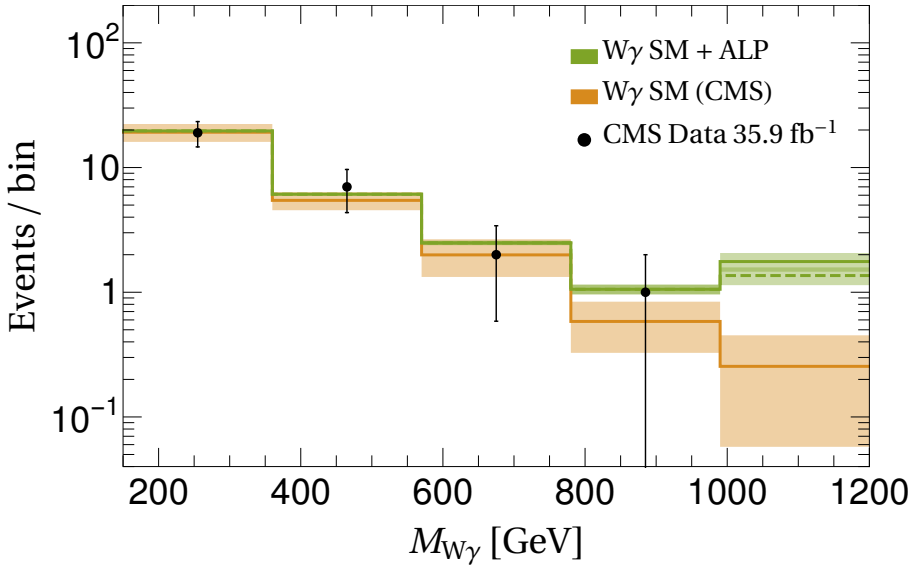

Figure 9. $M_{W\gamma}$ distribution for the $pp \to jjW^{\pm}\gamma \to jj\gamma\ell^{\pm}\nu$ channel.The data points and the total SM background (orange) are taken from the measurement in ref. [52]. The last bin contains the overflow events. The dashed and solid green lines show the total ALP EW VBS signal for $c_{\widetilde{B}}/f_a = c_{\widetilde{W}}/f_a = 1\,\text{TeV}^{-1}$ with a cut of $M_{W\gamma} < 2\,\text{TeV}$ and 4 TeV, respectively.

JHEP06(2022)113

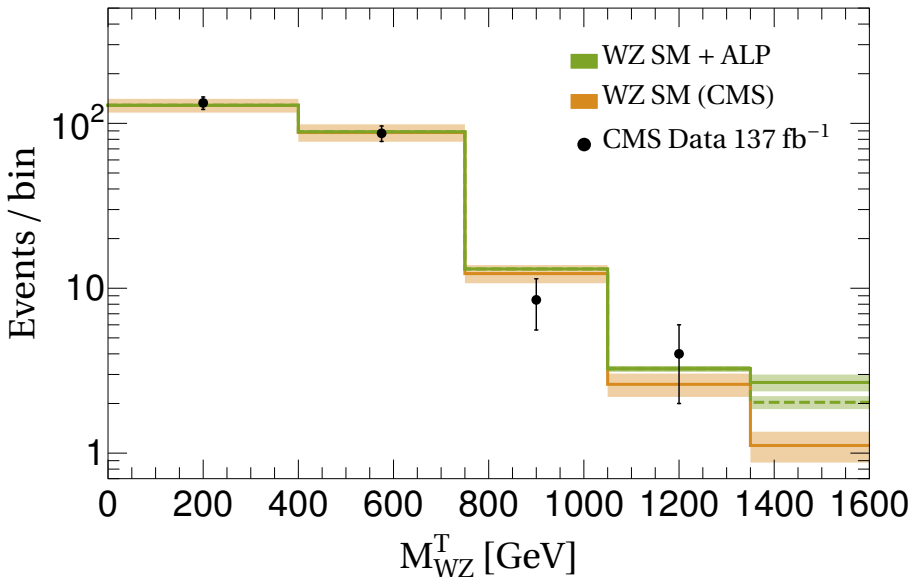

Figure 10. M^T_{WZ} distribution for the $pp \to jjW^{\pm}Z \to jj\ell^+\ell^-\ell'^{\pm}\nu$ channel.The data points and the total SM background (orange) are taken from the measurement in ref. [50]. The last bin contains the overflow events. The dashed and solid green lines show the total ALP EW VBS signal for $c_{\widetilde{B}}/f_a = c_{\widetilde{W}}/f_a = 1\,\text{TeV}^{-1}$ with a cut of $M_{WZ} < 2\,\text{TeV}$ and $4\,\text{TeV}$, respectively.

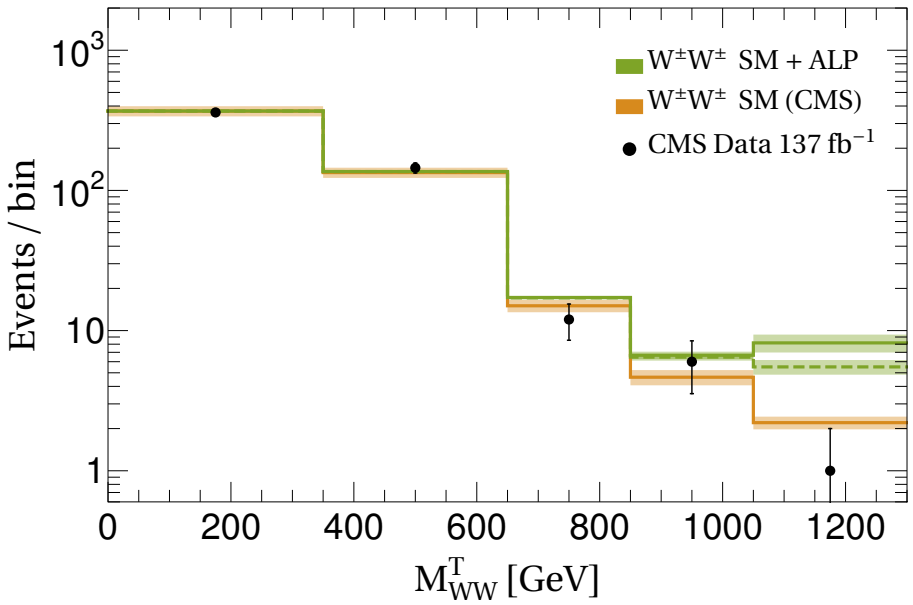

Figure 11. M^T_{WW} distribution for the $pp \to jjW^{\pm}W^{\pm} \to jj\ell^{\pm}\ell^{\pm}\nu\nu$ channel. The data points and the total SM background (orange) are taken from the measurement in ref. [50]. The last bin contains the overflow events. The dashed and solid green lines show the total ALP EW VBS signal for $c_{\widetilde{B}}/f_a = c_{\widetilde{W}}/f_a = 1\,\text{TeV}^{-1}$ with a cut of $M_{WW} < 2\,\text{TeV}$ and $4\,\text{TeV}$, respectively.

JHEP06(2022)113

References

[1] R.D. Peccei and H.R. Quinn, *CP Conservation in the Presence of Instantons*, *Phys. Rev. Lett.* **38** (1977) 1440 [INSPIRE].

[2] R.D. Peccei and H.R. Quinn, *Constraints Imposed by CP Conservation in the Presence of Instantons*, *Phys. Rev. D* **16** (1977) 1791 [INSPIRE].

[3] S. Weinberg, *A New Light Boson?*, *Phys. Rev. Lett.* **40** (1978) 223 [INSPIRE].

[4] F. Wilczek, *Problem of Strong P and T Invariance in the Presence of Instantons*, *Phys. Rev. Lett.* **40** (1978) 279 [INSPIRE].

[5] J.E. Kim, *Weak Interaction Singlet and Strong CP Invariance*, *Phys. Rev. Lett.* **43** (1979) 103 [INSPIRE].

[6] M.A. Shifman, A.I. Vainshtein and V.I. Zakharov, *Can Confinement Ensure Natural CP Invariance of Strong Interactions?*, *Nucl. Phys. B* **166** (1980) 493 [INSPIRE].

[7] M. Dine, W. Fischler and M. Srednicki, *A Simple Solution to the Strong CP Problem with a Harmless Axion*, *Phys. Lett. B* **104** (1981) 199 [INSPIRE].

[8] A.R. Zhitnitsky, *On Possible Suppression of the Axion Hadron Interactions* (in Russian), *Sov. J. Nucl. Phys.* **31** (1980) 260 [INSPIRE].

[9] M. Cicoli, *Axion-like Particles from String Compactifications*, in *9th Patras Workshop on Axions, WIMPs and WISPs*, pp. 235–242 (2013) [DOI] [arXiv:1309.6988] [INSPIRE].

[10] G.B. Gelmini and M. Roncadelli, *Left-Handed Neutrino Mass Scale and Spontaneously Broken Lepton Number*, *Phys. Lett. B* **99** (1981) 411 [INSPIRE].

[11] P. Langacker, R.D. Peccei and T. Yanagida, *Invisible Axions and Light Neutrinos: Are They Connected?*, *Mod. Phys. Lett. A* **1** (1986) 541 [INSPIRE].

[12] G. Ballesteros, J. Redondo, A. Ringwald and C. Tamarit, *Standard Model-axion-seesaw-Higgs portal inflation. Five problems of particle physics and cosmology solved in one stroke*, *JCAP* **08** (2017) 001 [arXiv:1610.01639] [INSPIRE].

[13] F. Wilczek, *Axions and Family Symmetry Breaking*, *Phys. Rev. Lett.* **49** (1982) 1549 [INSPIRE].

[14] Y. Ema, K. Hamaguchi, T. Moroi and K. Nakayama, *Flaxion: a minimal extension to solve puzzles in the standard model*, *JHEP* **01** (2017) 096 [arXiv:1612.05492] [INSPIRE].

[15] L. Calibbi, F. Goertz, D. Redigolo, R. Ziegler and J. Zupan, *Minimal axion model from flavor*, *Phys. Rev. D* **95** (2017) 095009 [arXiv:1612.08040] [INSPIRE].

[16] J. Beacham et al., *Physics Beyond Colliders at CERN: Beyond the Standard Model Working Group Report*, *J. Phys. G* **47** (2020) 010501 [arXiv:1901.09966] [INSPIRE].

[17] P. Agrawal et al., *Feebly-interacting particles: FIPs 2020 workshop report*, *Eur. Phys. J. C* **81** (2021) 1015 [arXiv:2102.12143] [INSPIRE].

[18] E. Izaguirre, T. Lin and B. Shuve, *Searching for Axionlike Particles in Flavor-Changing Neutral Current Processes*, *Phys. Rev. Lett.* **118** (2017) 111802 [arXiv:1611.09355] [INSPIRE].

JHEP06(2022)113

[19] M. Bauer, M. Neubert and A. Thamm, *Collider Probes of Axion-Like Particles*, *JHEP* **12** (2017) 044 [arXiv:1708.00443] [INSPIRE].

[20] G. Alonso-Álvarez, M.B. Gavela and P. Quilez, *Axion couplings to electroweak gauge bosons*, *Eur. Phys. J. C* **79** (2019) 223 [arXiv:1811.05466] [INSPIRE].

[21] M.B. Gavela, R. Houtz, P. Quilez, R. Del Rey and O. Sumensari, *Flavor constraints on electroweak ALP couplings*, *Eur. Phys. J. C* **79** (2019) 369 [arXiv:1901.02031] [INSPIRE].

[22] J. Ebadi, S. Khatibi and M. Mohammadi Najafabadi, *New probes for axionlike particles at hadron colliders*, *Phys. Rev. D* **100** (2019) 015016 [arXiv:1901.03061] [INSPIRE].

[23] F. Ertas and F. Kahlhoefer, *On the interplay between astrophysical and laboratory probes of MeV-scale axion-like particles*, *JHEP* **07** (2020) 050 [arXiv:2004.01193] [INSPIRE].

[24] S. Gori, G. Perez and K. Tobioka, *KOTO vs. NA62 Dark Scalar Searches*, *JHEP* **08** (2020) 110 [arXiv:2005.05170] [INSPIRE].

[25] K.J. Kelly, S. Kumar and Z. Liu, *Heavy axion opportunities at the DUNE near detector*, *Phys. Rev. D* **103** (2021) 095002 [arXiv:2011.05995] [INSPIRE].

[26] A.M. Galda, M. Neubert and S. Renner, *ALP — SMEFT interference*, *JHEP* **06** (2021) 135 [arXiv:2105.01078] [INSPIRE].

[27] J. Bonilla, I. Brivio, M.B. Gavela and V. Sanz, *One-loop corrections to ALP couplings*, *JHEP* **11** (2021) 168 [arXiv:2107.11392] [INSPIRE].

[28] M. Bauer, M. Neubert, S. Renner, M. Schnubel and A. Thamm, *Flavor probes of axion-like particles*, arXiv:2110.10698 [INSPIRE].

[29] K. Mimasu and V. Sanz, *ALPs at Colliders*, *JHEP* **06** (2015) 173 [arXiv:1409.4792] [INSPIRE].

[30] I. Brivio et al., *ALPs Effective Field Theory and Collider Signatures*, *Eur. Phys. J. C* **77** (2017) 572 [arXiv:1701.05379] [INSPIRE].

[31] N. Craig, A. Hook and S. Kasko, *The Photophobic ALP*, *JHEP* **09** (2018) 028 [arXiv:1805.06538] [INSPIRE].

[32] D. Wang, L. Wu, J.M. Yang and M. Zhang, *Photon-jet events as a probe of axionlike particles at the LHC*, *Phys. Rev. D* **104** (2021) 095016 [arXiv:2102.01532] [INSPIRE].

[33] J. Ren, D. Wang, L. Wu, J.M. Yang and M. Zhang, *Detecting an axion-like particle with machine learning at the LHC*, *JHEP* **11** (2021) 138 [arXiv:2106.07018] [INSPIRE].

[34] M.B. Gavela, J.M. No, V. Sanz and J.F. de Trocóniz, *Nonresonant Searches for Axionlike Particles at the LHC*, *Phys. Rev. Lett.* **124** (2020) 051802 [arXiv:1905.12953] [INSPIRE].

[35] S. Carra et al., *Constraining off-shell production of axionlike particles with $Z\gamma$ and WW differential cross-section measurements*, *Phys. Rev. D* **104** (2021) 092005 [arXiv:2106.10085] [INSPIRE].

[36] CMS collaboration, *Search for heavy resonances decaying to ZZ or ZW and axion-like particles mediating nonresonant ZZ or ZH production at $\sqrt{s} = 13$ TeV*, *JHEP* **04** (2022) 087 [arXiv:2111.13669] [INSPIRE].

[37] R. Covarelli, M. Pellen and M. Zaro, *Vector-Boson scattering at the LHC: Unraveling the electroweak sector*, *Int. J. Mod. Phys. A* **36** (2021) 2130009 [arXiv:2102.10991] [INSPIRE].

JHEP06(2022)113

[38] A. Flórez et al., *Probing axionlike particles with $\gamma\gamma$ final states from vector boson fusion processes at the LHC*, *Phys. Rev. D* **103** (2021) 095001 [arXiv:2101.11119] [INSPIRE].

[39] C.-X. Yue, H.-Y. Zhang and H. Wang, *Production of axion-like particles via vector boson fusion at future electron-positron colliders*, *Eur. Phys. J. C* **82** (2022) 88 [arXiv:2112.11604] [INSPIRE].

[40] Y. Liu and B. Yan, *Searching for the axion-like particle at the EIC*, arXiv:2112.02477 [INSPIRE].

[41] CMS collaboration, *Observation of electroweak production of same-sign W boson pairs in the two jet and two same-sign lepton final state in proton-proton collisions at $\sqrt{s} = 13$ TeV*, *Phys. Rev. Lett.* **120** (2018) 081801 [arXiv:1709.05822] [INSPIRE].

[42] ATLAS collaboration, *Observation of electroweak $W^{\pm}Z$ boson pair production in association with two jets in pp collisions at $\sqrt{s} = 13$ TeV with the ATLAS detector*, *Phys. Lett. B* **793** (2019) 469 [arXiv:1812.09740] [INSPIRE].

[43] CMS collaboration, *Measurement of electroweak WZ boson production and search for new physics in WZ + two jets events in pp collisions at $\sqrt{s} = 13$ TeV*, *Phys. Lett. B* **795** (2019) 281 [arXiv:1901.04060] [INSPIRE].

[44] CMS collaboration, *Search for anomalous electroweak production of vector boson pairs in association with two jets in proton-proton collisions at 13 TeV*, *Phys. Lett. B* **798** (2019) 134985 [arXiv:1905.07445] [INSPIRE].

[45] ATLAS collaboration, *Search for the electroweak diboson production in association with a high-mass dijet system in semileptonic final states in pp collisions at $\sqrt{s} = 13$ TeV with the ATLAS detector*, *Phys. Rev. D* **100** (2019) 032007 [arXiv:1905.07714] [INSPIRE].

[46] ATLAS collaboration, *Observation of electroweak production of a same-sign W boson pair in association with two jets in pp collisions at $\sqrt{s} = 13$ TeV with the ATLAS detector*, *Phys. Rev. Lett.* **123** (2019) 161801 [arXiv:1906.03203] [INSPIRE].

[47] ATLAS collaboration, *Evidence for electroweak production of two jets in association with a $Z\gamma$ pair in pp collisions at $\sqrt{s} = 13$ TeV with the ATLAS detector*, *Phys. Lett. B* **803** (2020) 135341 [arXiv:1910.09503] [INSPIRE].

[48] CMS collaboration, *Measurement of the cross section for electroweak production of a Z boson, a photon and two jets in proton-proton collisions at $\sqrt{s} = 13$ TeV and constraints on anomalous quartic couplings*, *JHEP* **06** (2020) 076 [arXiv:2002.09902] [INSPIRE].

[49] ATLAS collaboration, *Observation of electroweak production of two jets and a Z-boson pair with the ATLAS detector at the LHC*, arXiv:2004.10612 [INSPIRE].

[50] CMS collaboration, *Measurements of production cross sections of WZ and same-sign WW boson pairs in association with two jets in proton-proton collisions at $\sqrt{s} = 13$ TeV*, *Phys. Lett. B* **809** (2020) 135710 [arXiv:2005.01173] [INSPIRE].

[51] CMS collaboration, *Evidence for electroweak production of four charged leptons and two jets in proton-proton collisions at $\sqrt{s} = 13$ TeV*, *Phys. Lett. B* **812** (2021) 135992 [arXiv:2008.07013] [INSPIRE].

[52] CMS collaboration, *Observation of electroweak production of $W\gamma$ with two jets in proton-proton collisions at $\sqrt{s} = 13$ TeV*, *Phys. Lett. B* **811** (2020) 135988 [arXiv:2008.10521] [INSPIRE].

JHEP06(2022)113

[53] CMS collaboration, *Measurements of production cross sections of polarized same-sign W boson pairs in association with two jets in proton-proton collisions at* $\sqrt{s} = 13$ *TeV*, *Phys. Lett. B* **812** (2021) 136018 [arXiv:2009.09429] [INSPIRE].

[54] CMS collaboration, *Measurement of the electroweak production of* $Z\gamma$ *and two jets in proton-proton collisions at* $\sqrt{s} = 13$ *TeV and constraints on anomalous quartic gauge couplings*, *Phys. Rev. D* **104** (2021) 072001 [arXiv:2106.11082] [INSPIRE].

[55] CMS collaboration, *Evidence for WW/WZ vector boson scattering in the decay channel* $\ell\nu qq$ *produced in association with two jets in proton-proton collisions at* $\sqrt{s} = 13$ *TeV*, arXiv:2112.05259 [INSPIRE].

[56] CMS collaboration, *First observation of the electroweak production of a leptonically decaying* W^+W^- *pair in association with two jets in* $\sqrt{s} = 13$ *TeV pp collisions*, CMS-PAS-SMP-21-001 (2021).

[57] H. Georgi, D.B. Kaplan and L. Randall, *Manifesting the Invisible Axion at Low-energies*, *Phys. Lett. B* **169** (1986) 73 [INSPIRE].

[58] K. Choi, K. Kang and J.E. Kim, *Effects of* η' *in Low-energy Axion Physics*, *Phys. Lett. B* **181** (1986) 145 [INSPIRE].

[59] J. Alwall et al., *The automated computation of tree-level and next-to-leading order differential cross sections, and their matching to parton shower simulations*, *JHEP* **07** (2014) 079 [arXiv:1405.0301] [INSPIRE].

[60] http://feynrules.irmp.ucl.ac.be/wiki/ALPsEFT.

[61] NNPDF collaboration, *Parton distributions for the LHC Run II*, *JHEP* **04** (2015) 040 [arXiv:1410.8849] [INSPIRE].

[62] P. Artoisenet, V. Lemaitre, F. Maltoni and O. Mattelaer, *Automation of the matrix element reweighting method*, *JHEP* **12** (2010) 068 [arXiv:1007.3300] [INSPIRE].

[63] T. Sjöstrand et al., *An introduction to PYTHIA 8.2*, *Comput. Phys. Commun.* **191** (2015) 159 [arXiv:1410.3012] [INSPIRE].

[64] DELPHES 3 collaboration, *DELPHES 3, A modular framework for fast simulation of a generic collider experiment*, *JHEP* **02** (2014) 057 [arXiv:1307.6346] [INSPIRE].

[65] M. Cacciari, G.P. Salam and G. Soyez, *FastJet User Manual*, *Eur. Phys. J. C* **72** (2012) 1896 [arXiv:1111.6097] [INSPIRE].

[66] I. Brivio, O.J.P. Éboli and M.C. Gonzalez-Garcia, *Unitarity constraints on ALP interactions*, *Phys. Rev. D* **104** (2021) 035027 [arXiv:2106.05977] [INSPIRE].

[67] B. Döbrich, J. Jaeckel, F. Kahlhoefer, A. Ringwald and K. Schmidt-Hoberg, *ALPtraum: ALP production in proton beam dump experiments*, *JHEP* **02** (2016) 018 [arXiv:1512.03069] [INSPIRE].

[68] J.D. Bjorken et al., *Search for Neutral Metastable Penetrating Particles Produced in the SLAC Beam Dump*, *Phys. Rev. D* **38** (1988) 3375 [INSPIRE].

[69] E.M. Riordan et al., *A Search for Short Lived Axions in an Electron Beam Dump Experiment*, *Phys. Rev. Lett.* **59** (1987) 755 [INSPIRE].

[70] J. Blümlein and J. Brunner, *New Exclusion Limits on Dark Gauge Forces from Proton Bremsstrahlung in Beam-Dump Data*, *Phys. Lett. B* **731** (2014) 320 [arXiv:1311.3870] [INSPIRE].

JHEP06(2022)113

[71] J. Jaeckel and M. Spannowsky, *Probing MeV to 90 GeV axion-like particles with LEP and LHC*, *Phys. Lett. B* **753** (2016) 482 [arXiv:1509.00476] [INSPIRE].

[72] A. Caputo, G. Raffelt and E. Vitagliano, *Muonic boson limits: Supernova redux*, *Phys. Rev. D* **105** (2022) 035022 [arXiv:2109.03244] [INSPIRE].

[73] A. Caputo, H.-T. Janka, G. Raffelt and E. Vitagliano, *Low-Energy Supernovae Severely Constrain Radiative Particle Decays*, *Phys. Rev. Lett.* **128** (2022) 221103 [arXiv:2201.09890] [INSPIRE].

[74] BABAR collaboration, *Search for hadronic decays of a light Higgs boson in the radiative decay* $\Upsilon \to \gamma A^0$, *Phys. Rev. Lett.* **107** (2011) 221803 [arXiv:1108.3549] [INSPIRE].

[75] L3 collaboration, *Isolated hard photon emission in hadronic Z0 decays*, *Phys. Lett. B* **292** (1992) 472 [INSPIRE].

[76] J. Jaeckel, M. Jankowiak and M. Spannowsky, *LHC probes the hidden sector*, *Phys. Dark Univ.* **2** (2013) 111 [arXiv:1212.3620] [INSPIRE].

[77] A. Mariotti, D. Redigolo, F. Sala and K. Tobioka, *New LHC bound on low-mass diphoton resonances*, *Phys. Lett. B* **783** (2018) 13 [arXiv:1710.01743] [INSPIRE].

[78] X. Cid Vidal, A. Mariotti, D. Redigolo, F. Sala and K. Tobioka, *New Axion Searches at Flavor Factories*, *JHEP* **01** (2019) 113 [*Erratum ibid.* **06** (2020) 141] [arXiv:1810.09452] [INSPIRE].

[79] CMS collaboration, *Evidence for light-by-light scattering and searches for axion-like particles in ultraperipheral PbPb collisions at* $\sqrt{s_{\rm NN}} = 5.02$ *TeV*, *Phys. Lett. B* **797** (2019) 134826 [arXiv:1810.04602] [INSPIRE].

[80] ATLAS collaboration, *Measurement of light-by-light scattering and search for axion-like particles with* $2.2\,nb^{-1}$ *of Pb+Pb data with the ATLAS detector*, *JHEP* **03** (2021) 243 [*Erratum ibid.* **11** (2021) 050] [arXiv:2008.05355] [INSPIRE].

[81] ATLAS collaboration, *Search for dark matter in association with an energetic photon in pp collisions at* $\sqrt{s} = 13$ *TeV with the ATLAS detector*, *JHEP* **02** (2021) 226 [arXiv:2011.05259] [INSPIRE].

[82] BNL-E949 collaboration, *Study of the decay* $K^+ \to \pi^+ \nu\bar{\nu}$ *in the momentum region* $140 < P_\pi < 199$ *MeV/c*, *Phys. Rev. D* **79** (2009) 092004 [arXiv:0903.0030] [INSPIRE].

[83] J. Heeck and H.H. Patel, *Majoron at two loops*, *Phys. Rev. D* **100** (2019) 095015 [arXiv:1909.02029] [INSPIRE].

JHEP06(2022)113

Chapter 6

The cost of an ALP solution to the neutral B-anomalies

This chapter contains the publication in Ref. [3]. The purpose of this work is to analyze the neutral B-anomalies in terms of a tree-level exchange of an ALP with flavour off-diagonal couplings to quarks. The title of this chapter already suggests that the aim of the work was to precise the important theoretical stretching of the ALP arena required if those anomalies were confirmed. Such anomalies corresponded to a deviation with respect to the SM predictions measured in the lepton flavour universality (LFU) violating ratios R_K and R_{K^*}, which are defined as $R_{K^{(*)}} \equiv \frac{\mathcal{B}(B\to K^{(*)}\mu^+\mu^-)}{\mathcal{B}(B\to K^{(*)}e^+e^-)}$ for the rare decays of B-mesons into kaons and charged leptons. The SM prediction for these ratios is practically 1 due to LFU. The LHCb collaboration had presented several measurements of these quantities: R_{K^*} was measured in two bins of the di-lepton invariant mass squared, $q^2 \in [0.045, 1.1]$ and $[1.1, 6.0]\,\text{GeV}^2$, as well as R_K, measured only in the latter bin. According to the data published by the collaboration in Refs. [226,227], R_K showed the largest tension with respect to the SM prediction, at the level of 3.1σ; while in the low and central bins of R_{K^*} the tension appeared at the 2.3σ and 2.5σ level, exhibiting a preference for the decay channels into electrons rather than muons. The total combined deviation for the three measurement was at 4.3σ level.

The ALP Lagrangian is presented in Sec. 2. Off-diagonal ALP couplings to bottom and strange quarks were assumed, as well as diagonal couplings to electrons and muons. In addition, anomalous couplings to photons were also considered, as they play an important role for other flavour observables, such as anomalous magnetic moments of muons and electrons.

The phenomenological study is presented in Secs. 3, 4 and 5. Sec. 3 introduced a solution to the neutral B-anomalies in terms of a heavy ALP (heavier than the B-meson mass). First, we presented the resulting Lagrangian after integrating out the heavy ALP. In the fermion sector, scalar and pseudoscalar four-fermion operators are generated. However, no viable explanation of the neutral anomalies was found. In particular, numerical solutions to R_K compatible with other observables (except the muon anomalous magnetic moment) are found, but they are in strong conflict with the EFT validity conditions: in order to account for R_K, the very small ALP-quark couplings required by $B_s - \overline{B}_s$ oscillation data imposes in

turn ALP-lepton effective couplings unacceptably large from the theoretical point of view. On the other hand, in the case of R_{K^*}, all ALP mediated solutions were directly excluded by the data on the decay $B_s \to \ell^+\ell^-$, irrespective of EFT consistency considerations. Allowed regions of the ALP parameter space for this scenario are shown in Figs. 2, 3 and 5.

The situation of the very light ALP (lighter than twice the muon mass), introduced in Sec. 5, is similar to the heavy ALP scenario. Quantitative solutions to the neutral anomalies allowed within 2σ and in agreement with the previously mentioned flavour observables are found. Nevertheless, all solutions are excluded by the experimental bound on the electron anomalous magnetic moment and astrophysical bounds. This case is represented in Fig. 13 and 14.

The most acceptable solution was found in terms of a light ALP, lighter than the B mesons but with a mass value within any of the bin windows measured by the experiments. This scenario is presented in Sec. 4. Such ALP could be produced on-shell and enter the resonant regime. Thus, the $B \to K^{(*)}\ell^+\ell^-$ processes factorise into ALP on-shell production followed by its decay. The ALP coupling to muons must have been much smaller than that to electrons to explain the anomalies. Within the allowed parameter space for on-shell ALP exchange, a "golden" value of the ALP mass value was identified, which lies at the frontier between the two energy bins ($m_a = \sqrt{1.1}$ GeV), providing solutions which could a priori explain the three anomalies simultaneously. When the loop-level impact of the Lagrangian couplings are considered, it is demonstrated that solutions to the neutral B-anomalies are compatible with the experimental value of the electron anomalous magnetic moment. Once again the muon anomalous magnetic moment cannot be then accounted for, though. The allowed parameter space for these solutions is represented in Figs. $6 - 12$.

Nevertheless, since this work was published an update of these measurement by the LHCb collaboration was released in Ref. [228, 229]. The new experimental values for R_K and R_{K^*} differ from previous LHCb measurements, which they supersede. The new values move upwards from the previous results and closer to the SM predictions. Although these shifts can be attributed in part to statistical effects, the change is primarily due to systematic effects. For instance, in the case of R_K, the data sample is the same as in the previous publication, but subject to a revised analysis. The combined deviation of the current measurement is at 0.2σ level. In other words, the experiments find a remarkably good agreement with the SM predictions. Although this situation may seem to leave our work in Ref. [3] outdated, the truth is that our conclusions can still be used for ALP phenomenology. For instance, by implementing the most recent results in our analysis, we could instead identify the new excluded regions due to LFU and notably stringent upper limits on ALP off-diagonal couplings to quarks would be obtained.

Published for SISSA by Springer

Received: October 14, 2022
Revised: December 18, 2022
Accepted: February 4, 2023
Published: February 14, 2023

The cost of an ALP solution to the neutral B-anomalies

J. Bonilla, A. de Giorgi, B. Gavela, L. Merlo and M. Ramos

Departamento de Física Teórica and Instituto de Física Teórica UAM/CSIC, Universidad Autónoma de Madrid, Cantoblanco, 28049, Madrid, Spain

E-mail: jesus.bonilla@uam.es, arturo.degiorgi@uam.es, belen.gavela@uam.es, luca.merlo@uam.es, maria.pestanadaluz@uam.es

Abstract: The neutral anomalies in B decays are analysed in terms of the tree-level exchange of an axion-like-particle (ALP), within the effective field theory framework. The complete two-dimensional parameter space for ALP couplings to electrons and muons is explored. The solutions to R_K and to the two energy bins of R_{K^*} are confronted with the impact of ALP exchange on other observables (meson oscillations, leptonic and semileptonic decays of B mesons including searches for new resonances, astrophysical constraints), as well as with the theoretical domain of validity of the effective theory. Solutions based on ALPs heavier than B mesons, or lighter than twice the muon mass, are shown to be excluded. In contrast, the exchange of on-shell ALPs provides solutions to R_K and/or R_{K^*} within 2σ sensitivity which are technically compatible with those constraints. Furthermore, a "golden ALP mass" is identified at the frontier between the two energy bin windows of R_{K^*}, which could simultaneously explain these two R_{K^*} anomalies together with R_K; this calls for the convenience of different energy binning which would easily clear up this (unlikely) possibility. The impact of smearing on data analysis is also discussed. When loop effects are taken into account, the solutions found can be in addition compatible with the data on the $g-2$ of the electron but not simultaneously with those on the $g-2$ of the muon. Furthermore, loop effects may require fine-tunings of some coupling values.

Keywords: Axions and ALPs, Bottom Quarks, Lepton Flavour Violation (charged), Semi-Leptonic Decays

ArXiv ePrint: 2209.11247

https://doi.org/10.1007/JHEP02(2023)138

JHEP02(2023)138

Contents

1 Introduction

Despite the huge experimental and theoretical effort in direct searches at colliders and low-energy facilities, no new particle has been observed since the discovery of the Higgs boson [1–3] at the LHC [4, 5] a decade ago. Although this discovery constitutes a superb confirmation of the Standard Model of particle physics (SM), an explanation of the origin of neutrino masses, the nature of Dark Matter, the baryon asymmetry of the Universe and a quantum-level description of gravity are lacking.

Furthermore, in recent years anomalies associated with the B mesons have been observed as compared with SM expectations. Those include deviations in both neutral and

JHEP02(2023)138

charged current processes. Neutral current anomalous behaviour manifests in the angular distribution of $B^0 \to K^{0*}\mu^+\mu^-$ decay [6–9], and in the observed Lepton Flavour Universality (LFU)-violating quotient of the branching ratios for $B^\pm \to K^\pm\mu^+\mu^-$ vs. $B^\pm \to K^\pm e^+e^-$ and for $B^0 \to K^{0*}\mu^+\mu^-$ vs. $B^0 \to K^{0*}e^+e^-$ [10–13]. The LFU ratios are particularly clean observables theoretically and experimentally [14–16] and therefore represent an excellent window to new physics (NP). Their generic expression in terms of the dilepton invariant mass q^2 reads

$$R_X \equiv \frac{\displaystyle\int_{q^2_{\rm min}}^{q^2_{\rm max}} \frac{{\rm d}\Gamma\left(B \to X_s\,\mu^+\mu^-\right)}{{\rm d}q^2}{\rm d}q^2}{\displaystyle\int_{q^2_{\rm min}}^{q^2_{\rm max}} \frac{{\rm d}\Gamma\left(B \to X_s\,e^+e^-\right)}{{\rm d}q^2}{\rm d}q^2}\,, \tag{1.1}$$

where X_s stands for either a K or a K^* meson, and where — here and in what follows — the meson electric charges are implicit. Their most recent and precise determination results in

$$R_K = 0.846^{+0.042+0.013}_{-0.039-0.012} \qquad \text{for} \quad 1.1\ \text{GeV}^2 \leq q^2 \leq 6.0\ \text{GeV}^2 \qquad \text{central bin} \quad [13] \tag{1.2}$$

$$R_{K^*} = \begin{cases} 0.69^{+0.11}_{-0.07} \pm 0.05 & \text{for} \quad 1.1\ \text{GeV}^2 \leq q^2 \leq 6.0\ \text{GeV}^2 \quad \text{central bin} \\ 0.66^{+0.11}_{-0.07} \pm 0.03 & \text{for} \quad 0.045\ \text{GeV}^2 \leq q^2 \leq 1.1\ \text{GeV}^2 \quad \text{low bin} \end{cases} \quad [11] \tag{1.3}$$

where R_K refers to data from B^+ meson decays and R_{K^*} to data from B^0 decays, and where central/low bin refers to the higher/lower bin in q^2 for which experimental data are available. The SM prediction for R_K and R_{K^*} at the central bin region is 1.00 ± 0.01 [14, 15, 17], while for R_{K^*} at the low bin region is 0.92 ± 0.02 [18]. The measured deviations from these values represent the so-called neutral B-anomalies, with a significance of 3.1σ, 2.5σ and 2.3σ, respectively. Furthermore, anomalies in charged current processes have appeared in the form of LFU violation in the quotients of B semileptonic decay rates to τ leptons vs. those to electrons and muons.

The not very high significance of each individual channel/measurement calls for caution: a purely experimental resolution — statistical fluctuation or systematic effect — is not excluded. Nevertheless, the different deviations are intriguingly consistent with each other once treated in an effective field theory description, as first formulated in ref. [19] and recently updated in refs. [20–25]. Altogether, they could be interpreted as due to NP with a global statistical significance of 4.3σ [26]. Although no single flavour measurement exhibits a 5σ deviation from the SM, the emerging pattern could point to NP that violates lepton flavour universality, in particular in what concerns $R_{K^{(*)}}$. Other promising channels to test LFU are associated with $\Lambda_b^0 \to pK^-\ell^+\ell^-$, $B^+ \to K^+\pi^+\pi^-\ell^+\ell^-$ and $B^0 \to K^+\pi^-\ell^+\ell^-$ decays, which however are delicate observables as it is not known how the NP affects the hadronic structure of the final states involved (see ref. [27] for a possible strategy to overcome this problem).

The neutral LFU ratios are loop-level processes within the SM and the size of the observed deviations thus opens the possibility to explain those anomalies via tree-level exchanges of NP particles. The first attempts in this direction in the last decade mainly

JHEP02(2023)138

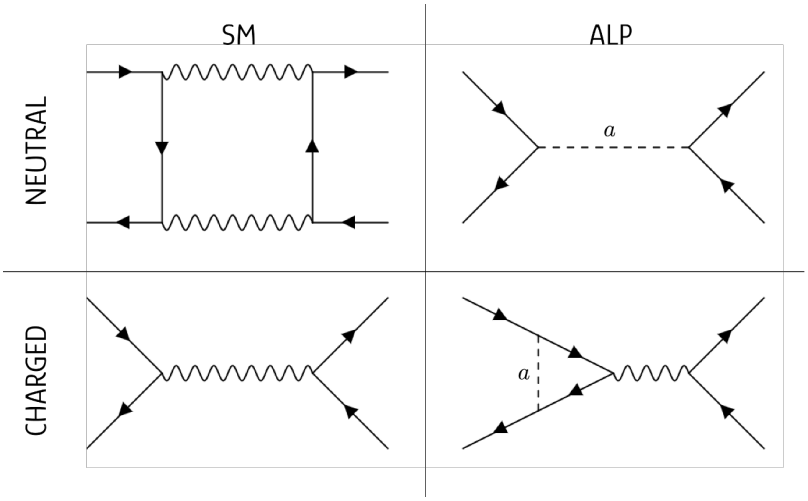

Figure 1. Sketchy illustrations of flavour-changing neutral and charged currents in the SM vs. those induced by flavour-non-diagonal ALP couplings. The wiggly lines denote SM electroweak gauge bosons, and all processes depicted are assumed to change flavour.

focused on Z' models [19, 28–31] or on lepto-quark scenarios [32–35]. In this paper, we will instead investigate the possibility that an axion-like-particle (ALP) reduces and eventually solves these neutral B-anomalies.

Axions have been originally introduced as the pseudo-Goldstone-bosons (pGBs) which result from the dynamical solution to the SM strong CP problem [36–39] through a global chiral U(1) symmetry — classically exact but anomalous at the quantum level. However, pGBs also appear in a plethora of theories that extend the SM even if not linked to a solution to the strong CP problem. These include among others the Majoron which stems from dynamical explanations of the lightness of active neutrino masses [40], pGBs from supersymmetric frameworks [41]; the Higgs boson itself which can have a pGB nature as in Composite-Higgs models [42]; and pGBs associated to extra-dimensional theories and string theories, which typically exhibit hidden U(1)'s [43]. Frequently these pGBs have anomalous couplings to gauge currents and are described by the generic name of ALPs.

In the SM, flavour-changing charged currents appear already as tree-level exchanges while neutral ones are one-loop suppressed processes. The exchange of ALPs exhibits generically the opposite pattern: it induces flavour-changing neutral currents already at tree-level while charged ones require one-loop transitions, see figure 1. We focus below on whether the tree-level exchange of ALPs can account for the neutral B-anomalies. Although this question has been previously formulated in ref. [44], we present for the first time the study of the complete parameter space, determining new solutions.

Both the case of a heavy ALP and of a light ALP are considered (heavy/light as compared to B meson masses). All the possible ranges for ALP masses will be carefully explored, and the compatibility of each of the neutral B-anomalies — R_K and R_{K^*} — with the SM prediction within the 1σ and 2σ levels will be determined, exposing the technical and theoretical cost of the solutions found. Moreover, we will explore whether there are

JHEP02(2023)138

specific values of the ALP mass for which all three neutral B-anomalies — i.e. R_K, R_{K^*} central bin and R_{K^*} low bin — could be simultaneously explained. The impact of the systematic errors in the analysis will be discussed, including the survival prospects for the solutions with the improvement of the experimental sensitivities. Moreover, we will check the consistency of ALP solutions to the neutral B anomalies with the constraints from other flavour observables, in particular with the data in the branching ratios for $B_s \to \ell^+\ell^-$ and $B \to K^{(*)}\ell^+\ell^-$ decays, and astrophysical constraints. In addition, the impact and compatibility of the ALP solutions with the data on the anomalous magnetic moment of the muon and of the electron will be discussed.

The charged B-anomalies in terms of ALP exchange will not be contemplated in this work. They would be one-loop processes — see figure 1: consistent solutions would require assuming flavour-blind ALP-fermion couplings, so that both the neutral and the charged B-anomalies would be induced only at loop-level. This is a very different setup, outside the scope of this work.

The structure of the paper can be inferred from the table of Contents.

2 The ALP Lagrangian

The construction of the ALP effective Lagrangian goes back to the late ′80s with the seminal works in refs. [45, 46]. It later underwent renewed interest [47–50] associated with an intense effort to investigate in detail its parameter space [44, 47, 51–64]. The ALP a is *defined here as a pseudoscalar field, singlet of the SM charges, and described by a Lagrangian invariant under the shift symmetry* $a \to a + constant$*, plus anomalous couplings which may break the shift invariance together with a small mass term*[1] $m_a \ll f_a$, where f_a is the NP ALP scale. We focus in this paper on the CP-even ALP Lagrangian at next-to-leading order (NLO) of the linear expansion, that is up to $\mathcal{O}(1/f_a)$ terms; this corresponds to operators with mass dimension up to five. The complete Lagrangian can be written as

$$\mathscr{L} = \mathscr{L}_{\rm SM} + \mathscr{L}_a \,, \tag{2.1}$$

where $\mathscr{L}_{\rm SM}$ denotes the SM Lagrangian,

$$\begin{aligned} \mathscr{L}_{\rm SM} = & -\frac{1}{4} X_{\mu\nu} X^{\mu\nu} + \sum_{\rm f} \bar{\rm f}\, i \not{D}\, {\rm f} + D_\mu \Phi^\dagger D^\mu \Phi - V\left(\Phi^\dagger \Phi\right) + \\ & - \left[\overline{Q'_L}\, Y_d\, \Phi\, d'_R + \overline{Q'_L}\, Y_u\, \widetilde{\Phi}\, u'_R + \overline{L'_L}\, Y_e\, \Phi\, e'_R + \text{h.c.} \right] , \end{aligned} \tag{2.2}$$

[1] There is a certain arbitrariness in the definition of an ALP. The customary underlying idea is inspired by the case of true axions: a global symmetry which is classically exact — and spontaneously realised — but explicitly broken only at the quantum level. This explicit breaking is precisely that given by the presence of gauge anomalous couplings (in fact, in true axion models that mass is a byproduct of the anomalous couplings of ALP to the strong gauge sector of the theory [38, 39, 65–84]). In all generality, their presence is expected to source a potential for the ALP, and thus a mass. The ALP mass is usually represented by a — more general — explicit mass term in the Lagrangian. Consistent with this underlying idea, all other shift-breaking operators are customarily expected to be even more suppressed than the mass term, and disregarded in phenomenological studies of ALP Lagrangians at leading order.

JHEP02(2023)138

$X_{\mu\nu}$ denotes the SM field strengths for the strong and electroweak (EW) gauge bosons, $\{X \equiv G, W, B\}$ respectively, and the sum over colour and weak gauge indices has been left implicit. The SM Higgs boson is denoted by Φ with $\widetilde{\Phi} \equiv i\sigma^2\Phi^*$, and $V\left(\Phi^\dagger\Phi\right)$ is the Higgs potential. The index f runs over the SM chiral fermion fields $\mathrm{f} \equiv \{Q'_L,\, u'_R,\, d'_R,\, L'_L,\, e'_R\}$, where the primes refer to the flavour basis. In turn, a complete set of independent and non-redundant ALP-SM couplings is encoded in

$$\mathscr{L}_a = \frac{1}{2}\partial_\mu a\, \partial^\mu a - \frac{m_a^2}{2}a^2 + \mathscr{L}_a^X + \mathscr{L}_{\partial a}^\psi\,, \tag{2.3}$$

where $\mathscr{L}_a^X$ encompasses the couplings of the ALP to anomalous currents,[2]

$$\mathscr{L}_a^X \;=\; -c_{\widetilde{W}}\frac{a}{f_a}W^i_{\mu\nu}\tilde{W}^{i\mu\nu} - c_{\widetilde{B}}\frac{a}{f_a}B_{\mu\nu}\tilde{B}^{\mu\nu} - c_{\widetilde{G}}\frac{a}{f_a}G^a_{\mu\nu}\tilde{G}^{a\mu\nu}\,, \tag{2.4}$$

while the ALP-fermion couplings contained in $\mathscr{L}_{\partial a}^\psi$ are derivative ones, i.e. invariant under constant shifts of the $a(x)$ field,

$$\mathscr{L}_{\partial a}^\psi = \frac{\partial_\mu a}{f_a}\left[\overline{Q}'_L\gamma^\mu \mathbf{c}'_Q Q'_L + \overline{u}'_R\gamma^\mu \mathbf{c}'_u u'_R + \overline{d}'_R\gamma^\mu \mathbf{c}'_d d'_R + \overline{L}'_L\gamma^\mu \mathbf{c}'_L L'_L + \overline{e}'_R\gamma^\mu \mathbf{c}'_e e'_R\right], \tag{2.5}$$

where $\mathbf{c}'_\mathrm{f}$ are hermitian 3×3 matrices in flavour space containing the Wilson coefficients of the corresponding operators: note that four of the couplings contained in these matrices are not independent, as they can be removed applying the conservation of baryon number and of the three independent lepton numbers (disregarding neutrino masses)[3] [44, 50]. Furthermore, a possible shift-invariant bosonic operator, $\mathcal{O}_{a\Phi} \equiv \partial_\mu a(\Phi^\dagger i\overleftrightarrow{D_\mu}\Phi)/f_a$, has *not* been included in eq. (2.3) as this would also be redundant given the choice made to consider all possible fermionic couplings (minus four) in $\mathscr{L}_{\partial a}^\psi$.[4] Finally, the condition of CP conservation implies that $\mathbf{c}'_\mathrm{f} = \mathbf{c}'^T_\mathrm{f}$ and thus all fermionic couplings are real.

The description above is explicitly invariant under the SM gauge group $\mathrm{SU}(3)\times\mathrm{SU}(2)\times\mathrm{U}(1)$ gauge group. At low energies after electroweak symmetry breaking, the total Lagrangian eq. (2.3) can be rewritten in the mass basis, in which $\mathscr{L}_a^X$ reads

$$\begin{aligned}\mathscr{L}_a^X = &-c_{a\gamma\gamma}\frac{a}{f_a}F_{\mu\nu}\tilde{F}^{\mu\nu} - c_{a\gamma Z}\frac{a}{f_a}F_{\mu\nu}\tilde{Z}^{\mu\nu} + \\ &- c_{aZZ}\frac{a}{f_a}Z_{\mu\nu}\tilde{Z}^{\mu\nu} - 2c_{\widetilde{W}}\frac{a}{f_a}W^+_{\mu\nu}\tilde{W}^{-\mu\nu} - c_{\widetilde{G}}\frac{a}{f_a}G^a_{\mu\nu}\tilde{G}^{a\mu\nu}\,.\end{aligned} \tag{2.6}$$

where $\{F^{\mu\nu}, Z^{\mu\nu}, W_{\mu\nu}, G_{\mu\nu}\}$ denote respectively the electromagnetic, Z-boson, W-boson and gluonic field strengths, and

$$c_{a\gamma\gamma} \equiv c_w^2 c_{\widetilde{B}} + s_w^2 c_{\widetilde{W}}\,, \qquad c_{a\gamma Z} \equiv 2c_s s_w\left(c_{\widetilde{W}} - c_{\widetilde{B}}\right), \qquad c_{aZZ} \equiv s_w^2 c_{\widetilde{B}} + c_w^2 c_{\widetilde{W}}\,, \tag{2.7}$$

[2] The coefficients of gauge anomalous terms are often defined with a suppression factor with respect to the notation used all throughout this paper, i.e. $c_i \to \alpha_i/(4\pi)c_i$, where α_i denotes the corresponding gauge field fine structure constant.

[3] The ALP-neutrino couplings will be argued to be irrelevant for the present tree-level analysis, and therefore neutrino masses and the PMNS mixing matrix are to be neglected throughout this work without loss of generality.

[4] Alternatively, one of the operators in $\mathscr{L}_{\partial a}^\psi$ could be substituted by $\mathcal{O}_{a\Phi}$ if wished, see for instance ref. [50].

JHEP02(2023)138

where the sine and cosine of the Weinberg angle are respectively denoted s_w and c_w. The chirality-conserving fermionic Lagrangian $\mathscr{L}^{\psi}_{\partial a}$ can also be written straightforwardly in the mass basis. Nevertheless, for practical purposes it is useful to use the equations of motion (EOM) supplemented with the anomaly contribution, to rewrite $\mathscr{L}^{\psi}_{\partial a}$ in terms of chirality-flip fermion couplings plus anomalous terms, i.e.

$$\begin{aligned}\mathscr{L}^{\psi}_{\partial a} = \mathscr{L}^{\psi}_{a} &- \Delta c_{a\gamma\gamma}\frac{a}{f_a}F_{\mu\nu}\tilde{F}^{\mu\nu} - \Delta c_{a\gamma Z}\frac{a}{f_a}F_{\mu\nu}\tilde{Z}^{\mu\nu} + \\ &- \Delta c_{aZZ}\frac{a}{f_a}Z_{\mu\nu}\tilde{Z}^{\mu\nu} - 2\Delta c_{a\widetilde{W}}\frac{a}{f_a}W^{+}_{\mu\nu}\tilde{W}^{-\mu\nu} - \Delta c_{a\widetilde{G}}\frac{a}{f_a}G^{a}_{\mu\nu}\tilde{G}^{a\mu\nu}\,,\end{aligned} \tag{2.8}$$

where $\mathscr{L}^{\psi}_{a}$ is a chirality-flip fermion Lagrangian that expressed in the mass basis reads

$$\mathscr{L}^{\psi}_{a} = -\frac{ia}{f_a}\sum_{\psi=u,d,e}\sum_{i,j}\left[(m_{\psi_i}-m_{\psi_j})\left(\mathbf{K}^{S}_{\psi}\right)_{ij}\overline{\psi}_i\,\psi_j + (m_{\psi_i}+m_{\psi_j})\left(\mathbf{K}^{P}_{\psi}\right)_{ij}\overline{\psi}_i\gamma_5\psi_j\right] + \ldots \tag{2.9}$$

where dots indicate ALP-fermion-Higgs interactions left implicit as they will not be used in this paper. In this equation, m_{ψ_i} denotes the mass of the four-component fermion field ψ_i, and the $\mathbf{K}_{\psi}$ coefficient matrices are defined as combinations of coefficients $\mathbf{c}_{\psi}$, possibly weighted down by the CKM mixing matrix. For instance, choosing a basis in which the down sector masses are diagonal, it follows that

$$\mathbf{K}^{S,P}_{u} \equiv \frac{\mathbf{c}_u \pm V_{\rm CKM}\mathbf{c}_Q V^{\dagger}_{\rm CKM}}{2}\,, \qquad \mathbf{K}^{S,P}_{d} \equiv \frac{\mathbf{c}_d \pm \mathbf{c}_Q}{2}\,, \qquad \mathbf{K}^{S,P}_{e} \equiv \frac{\mathbf{c}_e \pm \mathbf{c}_L}{2}\,, \tag{2.10}$$

with the sum (difference) of the operator coefficients $\mathbf{c}_{\psi}$ corresponding to the scalar (pseudoscalar) components of $\mathbf{K}_{\psi}$. The relation of the various $\mathbf{c}_{\psi}$ to the coefficient matrices in the flavour basis — see eq. (2.5) — is given by

$$\begin{aligned} &V^{\dagger}_u\mathbf{c}'_u V_u \equiv \mathbf{c}_u\,, \quad V^{\dagger}_d\mathbf{c}'_d V_d \equiv \mathbf{c}_d\,, \quad V^{\dagger}_e\mathbf{c}'_e V_e \equiv \mathbf{c}_e\,, \\ &U^{\dagger}_d\mathbf{c}'_Q U_d \equiv \mathbf{c}_Q\,, \quad U^{\dagger}_e\mathbf{c}'_L U_e \equiv \mathbf{c}_L\,, \end{aligned} \tag{2.11}$$

where U_{ψ} and V_{ψ} are the unitary rotations associated to the left- and right-handed fermions, respectively, which allow to diagonalise the fermion masses,

$$M_{\psi} \equiv \frac{v}{\sqrt{2}}U^{\dagger}_{\psi}\,Y_{\psi}\,V_{\psi}\,, \tag{2.12}$$

where $v = 246$ GeV is the EW vacuum expectation value (vev) and M_{ψ} denote real diagonal fermion mass matrices. In turn, the CKM matrix is given by[5]

$$V_{\rm CKM} = U^{\dagger}_u U_d\,. \tag{2.13}$$

The contributions to anomalous couplings which appear in eq. (2.8) (and are a consequence of the chiral rotation performed) are given by

$$\begin{aligned} &\Delta c_{a\gamma\gamma} \equiv c_w^2 K_B + s_w^2 K_W \quad \Delta c_{a\gamma Z} \equiv 2c_w s_w\,(K_W - K_B) \\ &\Delta c_{aZZ} \equiv s_w^2 K_B + c_w^2 K_W \quad \Delta c_{a\widetilde{W}} \equiv K_W \qquad\qquad \Delta c_{a\widetilde{G}} \equiv K_G\,, \end{aligned} \tag{2.14}$$

[5]Unlike for the SM, some combinations of the matrices V that rotate right-handed fields are now *a priori* physical.

JHEP02(2023)138

with the K_X coefficients given by the following combinations of fermionic couplings:

$$\begin{aligned} K_B &\equiv \frac{\alpha_{em}}{8\pi c_w^2}\mathrm{Tr}\left(\frac{1}{3}\mathbf{c}_Q - \frac{8}{3}\mathbf{c}_u - \frac{2}{3}\mathbf{c}_d + \mathbf{c}_L - 2\mathbf{c}_e\right) , \\ K_W &\equiv \frac{\alpha_{em}}{8\pi s_w^2}\mathrm{Tr}\Big(3\mathbf{c}_Q + \mathbf{c}_L\Big) , \\ K_G &\equiv \frac{\alpha_s}{8\pi}\mathrm{Tr}\Big(2\mathbf{c}_Q - \mathbf{c}_u - \mathbf{c}_d\Big) , \end{aligned} \tag{2.15}$$

where $\alpha_{em} = e^2/4\pi$ and $\alpha_s = g_s^2/4\pi$, e denotes the electric charge and g_s the strong gauge coupling. These Δc_i corrections can be reabsorbed in the arbitrary coefficients in eq. (2.6), $c_i \to c_i + \Delta c_i$ (e.g. $c_{a\gamma\gamma} \to c_{a\gamma\gamma} + \Delta c_{a\gamma\gamma}$ etc.) so that in all generality the complete ALP Lagrangian in eq. (2.3) can be rewritten as

$$\mathscr{L}_a = \frac{1}{2}\partial_\mu a\, \partial^\mu a - \frac{m_a^2}{2}a^2 + \mathscr{L}_a^X + \mathscr{L}_a^\psi , \tag{2.16}$$

with arbitrary operator coefficients. Nevertheless, this analysis illustrates that contributions from anomalous couplings are automatic and unavoidable when relating the initial chirality-conserving and explicitly shift-invariant ALP fermionic basis to chirality-flip fermion operators. In practice, for fermionic processes involving only tree-level ALP exchanges, it is completely equivalent to use either the chirality-conserving fermion Lagrangian $\mathscr{L}_{\partial a}^\psi$ in eq. (2.5) (or its mass-basis version) or the chirality-flip one $\mathscr{L}_a^\psi$ in eq. (2.9). On the contrary, consistency requires to take into account the complete combination of couplings in eq. (2.8) for some loop-level analyses of ALP exchanges involving fermions. For most of this work we focus only on tree-level exchange of ALPs, and $\mathscr{L}_a^\psi$ alone will thus suffice unless otherwise specified.

Eq. (2.9) shows then that only pseudoscalar couplings contribute at tree-level of the EFT to flavour-diagonal interactions, while both scalar and pseudoscalar contributions are present for the off-diagonal ones. Moreover, all tree-level ALP-fermion interactions are proportional to the masses of the fermions involved: the naive expectation is that couplings with light fermions are subdominant with respect to couplings with heavier fermions. In particular, the flavour-conserving ALP interactions pertinent to our analysis with electrons are much smaller than those with muons. It also follows from eq. (2.9) that ALP-mediated $B \to K$ transition amplitudes are proportional to (the 23 element of) the scalar coupling $\mathbf{K}_d^S$, while $B \to K^*$ ones are proportional to the pseudoscalar coupling $\mathbf{K}_d^P$.

It is pertinent to stress that the only NP couplings to be considered below — and as customary in the literature — are the ALP couplings to the quark bilinear $\bar{b}s$, and the lepton $\mu^+\mu^-$ and e^+e^- channels, i.e, in the notation of eq. (2.9):

$$\begin{aligned} \mathscr{L}_a^\psi \supset -\frac{ia}{f_a}\Big[&(m_s - m_b)\left(\mathbf{K}_d^S\right)_{sb}(\bar{s}\,b - \bar{b}\,s) + (m_s + m_b)\left(\mathbf{K}_d^P\right)_{sb}(\bar{s}\gamma_5 b + \bar{b}\gamma_5 s) + \\ &+ 2m_e\left(\mathbf{K}_e^P\right)_{ee}\bar{e}\gamma_5 e + 2m_\mu\left(\mathbf{K}_e^P\right)_{\mu\mu}\bar{\mu}\gamma_5\mu\Big] . \end{aligned} \tag{2.17}$$

Such a specific choice of parameters is part of the theoretical cost required to explain the neutral B anomalies through tree-level exchange of ALP couplings. Nevertheless, it may

JHEP02(2023)138

be natural to disregard ALP interactions with up-type quarks, in spite of fermionic ALP couplings being proportional to fermion masses, as their contribution to the neutral B anomalies is loop-suppressed. But the opposite could be argued for, for instance, ALP coupling to taus, etc. Overall, to suppress all fermionic ALP couplings in eq. (2.9) except those in eq. (2.17) is technically possible, as there are enough free parameters in the initial Lagrangian — eq. (2.3) — as to allow for it.

EFT validity. Finally, the question of the validity of the ALP EFT must be addressed. In order for the ALP Lagrangian to be approximately shift-invariant, the ALP mass m_a must be small compared with the EFT scale f_a, $m_a \ll f_a$. Furthermore, as the coupling dependence is of the form c_i/f_a, $c_i < 1$ must hold for all Lagrangian coefficients as indicated by naive dimensional analysis.

The absolute value of the ALP scale is also relevant. The consistency of formulating the effective field theory in terms of operators which are invariant under the EW symmetry, see eqs. (2.3)–(2.5), implies to consider in all cases f_a values larger than the EW scale, $f_a \gtrsim v$. We will adhere throughout this work to this condition, as an ALP scale below the EW scale is difficult to sustain in view of the non-observation of NP fields expected to accompany any renormalisable completion of the ALP scenario. Within this setup, we will explore two regimes: a "heavy ALP" and a "light ALP", where the denomination heavy/light refers to the ALP mass size compared to B meson masses.

The next sections are dedicated to the phenomenological analysis of the different possible ranges for the ALP mass: i) an ALP heavier than the B mesons, ii) an ALP with a mass within the energy bin windows considered for the neutral-B anomalies, and iii) a light ALP with mass 1 MeV $< m_a < 2m_\mu$ where m_μ denotes the muon mass. In the numerical computations, the exact values of the input parameters used can be read in table 3 of appendix A.

3 Heavy ALP

3.1 The low-energy Lagrangian

For an ALP heavier than the B mesons, the ALP can be safely integrated out to analyse its impact on B transitions. The result is an effective Lagrangian valid at energies lower than m_a, which in the mass basis can be decomposed as

$$\mathscr{L}_a^{\text{eff}} = \mathscr{L}_a^{\text{eff-4f}} + \mathscr{L}_a^{\text{mixed}} + \dots \tag{3.1}$$

where the dots encode pure gauge interactions — left implicit as they will have no impact on the results in this section, $\mathscr{L}_a^{\text{mixed}}$ encodes interactions involving two fermions and anomalous gauge currents, and $\mathscr{L}_a^{\text{eff-4f}}$ encodes the effective four-fermion couplings, which are specially significative for the analysis of B-anomalies and read

$$\mathscr{L}_a^{\text{eff-4f}} = -\frac{1}{2(f_a m_a)^2}\left[\sum_\psi \sum_{i,j}\left((m_{\psi_i} - m_{\psi_j})\left(\mathbf{K}_\psi^S\right)_{ij}\overline{\psi}_i\psi_j + (m_{\psi_i} + m_{\psi_j})\left(\mathbf{K}_\psi^P\right)_{ij}\overline{\psi}_i\gamma_5\psi_j\right)\right]^2. \tag{3.2}$$

JHEP02(2023)138

Among the effective operators in this last equation, only those composed of a s and a b quark fields together with flavour-diagonal leptonic currents are relevant to the tree-level phenomenological analysis of the neutral B-anomalies, i.e.

$$\mathscr{L}_a^{\text{eff-4f}} \supset -\frac{4m_\ell}{2(f_a m_a)^2}\Big[(m_s - m_b)\left(\mathbf{K}_d^S\right)_{sb}\,\bar{s}\,b + (m_s + m_b)\left(\mathbf{K}_d^P\right)_{sb}\,\bar{s}\,\gamma_5\,b\Big]\Big[\left(\mathbf{K}_e^P\right)_{\ell\ell}\,\bar{\ell}\,\gamma_5\,\ell\Big]\,. \tag{3.3}$$

It follows that only pseudoscalar leptonic interactions remain, while both scalar and pseudoscalar contributions will contribute to quark currents. It is useful to re-express this Lagrangian in a more compact way as

$$\mathscr{L}_a^{\text{eff-4f}} \supset -\frac{4G_F}{\sqrt{2}}\sum_{\ell=e,\mu,\tau} V_{tb}V_{ts}^*\left(C^\ell_{P_+}\,\mathcal{O}^\ell_{P_+} + C^\ell_{P_-}\,\mathcal{O}^\ell_{P_-}\right)\,, \tag{3.4}$$

where $G_F \equiv 1/(\sqrt{2}v^2)$ is the Fermi constant as extracted from muon decay, and the operators $\mathcal{O}^\ell_{P_\pm}$ are defined as

$$\mathcal{O}^\ell_{P_+} \equiv \frac{\alpha_{\text{em}}}{4\pi}\,(\bar{s}\,b)\left(\bar{\ell}\,\gamma_5\,\ell\right)\,, \qquad \mathcal{O}^\ell_{P_-} \equiv \frac{\alpha_{\text{em}}}{4\pi}\,(\bar{s}\,\gamma_5\,b)\left(\bar{\ell}\,\gamma_5\,\ell\right)\,, \tag{3.5}$$

where the $\pm$ subscripts remind the parity of the quark current component of the operators. The Wilson coefficients $C^\ell_{P_\pm}$ are then given by

$$C^\ell_{P_\pm} \equiv \frac{2\sqrt{2}\pi}{\alpha_{\text{em}}G_F V_{tb}V_{ts}^*}\frac{m_\ell}{(f_a m_a)^2}(m_s \mp m_b)\left(\mathbf{K}_d^{S,P}\right)_{sb}\left(\mathbf{K}_e^P\right)_{\ell\ell}\,. \tag{3.6}$$

It follows from the parity structure that $\mathcal{O}^\ell_{P_+}$ will contribute to $B \to K\ell^+\ell^-$ processes, while $\mathcal{O}^\ell_{P_-}$ can instead mediate both $B \to K^*\ell^+\ell^-$ and $B_s \to \ell^+\ell^-$ decays.

Yet another notation for four-fermion couplings is that customarily used in EFT analyses of B-anomalies, in which the combinations of couplings that can result from the tree-level integration of a heavy ALP read [32, 85, 86][6]

$$\mathscr{L}^{\text{eff}}_{\Delta B=1} \supset -\frac{4G_F}{\sqrt{2}}\sum_{\ell=e,\mu,\tau} V_{tb}V_{ts}^*\left(C^\ell_P\mathcal{O}^\ell_P + C^{\ell\prime}_P\mathcal{O}^{\ell\prime}_P\right)\,, \tag{3.7}$$

with

$$\mathcal{O}^{\ell(\prime)}_P \equiv \frac{\alpha_{\text{em}}}{4\pi}\left(\bar{s}P_{R(L)}b\right)\left(\bar{\ell}\gamma_5\ell\right)\,. \tag{3.8}$$

The relation between this formulation and the operators and Wilson coefficients in eq. (3.4) is simply

$$\mathcal{O}^\ell_{P_\pm} \equiv \mathcal{O}^\ell_P \pm \mathcal{O}^{\ell\prime}_P\,, \qquad C^\ell_{P_\pm} = \frac{C^\ell_P \pm C^{\ell\prime}_P}{2}\,. \tag{3.9}$$

[6] In other words, other dimension-six effective operators mediating LFU violation and encoded in $\mathscr{L}^{\text{eff}}_{\Delta B=1}$, such as for example $C_9^{(\prime)}$ and $C_{10}^{(\prime)}$, are disregarded here because they cannot be generated by the tree-level exchange of a heavy ALP.

JHEP02(2023)138

3.2 Phenomenology of a heavy ALP

As shown above, for a given lepton ℓ, the leading four-fermion effective operators induced by tree-level exchange of an ALP spans a two-parameter space $\{C^{\ell}_{P_+}, C^{\ell}_{P_-}\}$. Conversely, the parity analysis implies that typically these coefficients contribute to different observables, which can then be easily compared for electrons vs. muons (tau leptons are not considered here), e.g.

- $\mathcal{O}^{\ell}_{P_+}$: $\mathcal{O}^{e}_{P_+}$ and $\mathcal{O}^{\mu}_{P_+}$ will contribute to R_K.
- $\mathcal{O}^{\ell}_{P_-}$: $\mathcal{O}^{e}_{P_-}$ and $\mathcal{O}^{\mu}_{P_-}$ will contribute to R_{K^*}, as well as to $B_s \to \ell^+\ell^-$ decays.

Note that both $C^{\ell}_{P_+}$ and $C^{\ell}_{P_-}$ are proportional to the coupling combination $\mathbf{K}^P_e \sim (\mathbf{c}_e - \mathbf{c}_L)$ in eq. (2.10), while they differ on the dependence on quark couplings, that is $\mathbf{K}^S_d \sim (\mathbf{c}_d + \mathbf{c}_Q)$ and $\mathbf{K}^P_d \sim (\mathbf{c}_d - \mathbf{c}_Q)$, respectively. The proportionality to $\mathbf{K}^P_e$ will also appear in other observables to be discussed below, namely the anomalous magnetic moments of the muon and of the electron, while conversely $B_s - \overline{B}_s$ oscillations only depend on ALP-quark couplings.

The different observables of interest to our analysis are discussed next in more detail in terms of the contributions of the Wilson coefficients.

3.2.1 $B \to K\ell^+\ell^-$, R_K, ΔM_s and magnetic moments

The differential decay width for the $B \to K^{(*)}\ell^+\ell^-$ processes can be written as

$$\mathrm{d}\Gamma(B \to K^{(*)}\ell^+\ell^-) = \frac{1}{(2\pi)^3}\frac{1}{32M_B^3}\left|\overline{\mathcal{M}}\right|^2 \mathrm{d}q^2\mathrm{d}Q^2\,, \tag{3.10}$$

where $\overline{\mathcal{M}}$ is the matrix element of the process summed over the polarisations of the meson and leptons in the final state and M_B is the B meson mass, while the four-momenta are defined as $q^2 \equiv (p_{\ell^+} + p_{\ell^-})^2 \equiv (p-k)^2$ and $Q^2 \equiv (p_{\ell^+} + k)^2 = (p - p_{\ell^-})^2$, where p denotes the four-momentum of the initial state B-meson, k that of the $K^{(*)}$-meson, and $p_{\ell^\pm}$ those of the leptons $\ell^\pm$. For $m_a^2 \gg q^2$, the q^2-dependence can be neglected on the ALP propagator and a simple integration over q^2 remains.

$B \to K\ell^+\ell^-$. As a step previous to the analysis of R_K, we discuss next the semileptonic B decay widths into dilepton pairs, for which the experimental data available are shown In table 1. We compared the results obtained for the q^2 integration over the dilepton mass regions of interest for the anomaly — $1\ \mathrm{GeV}^2 < q^2 < 7\ \mathrm{GeV}^2$ — using two popular softwares, Flavio [87] and EOS [88], with the corresponding expression in ref. [17] — which is valid up to $\mathcal{O}(m_\ell^3)$ corrections,

$$\mathcal{B}(B \to K\ell^+\ell^-)^{7.0\ \mathrm{GeV}^2}_{1.0\ \mathrm{GeV}^2} = \left(\frac{\tau_{B^\pm}}{1.64\mathrm{ps}}\right)\left(1.91 + 0.08\,C^{\ell 2}_{P_+} - \frac{m_\ell}{\mathrm{GeV}}\frac{C^{\ell}_{P_+}}{1.46} - \frac{m_\ell^2}{\mathrm{GeV}^2}\frac{C^{\ell 2}_{P_+}}{5.18^2}\right), \tag{3.11}$$

where $\tau_{B^\pm}$ is the lifetime of the meson $B^\pm$ and the q^2 interval of integration $^{7.0\ \mathrm{GeV}^2}_{1.1\ \mathrm{GeV}^2}$ is indicated. We found a good agreement, as the numerical differences can be understood as a consequence of the more recent input data used in the softwares. The analytic expression

JHEP02(2023)138

Observable	q^2 [GeV^2]	Values	Heavy	On Bin	Light
$\mathrm{d}\mathcal{B}/\mathrm{d}q^2(B^+ \to K^+e^+e^-)$	(1.1, 6)	$(28.6^{+2.0}_{-1.7} \pm 1.4) \times 10^{-9}$ [12]	✓	✓	✓
$\mathcal{B}(B^+ \to K^+e^+e^-)$		$\left(14.01^{+0.98}_{-0.83} \pm 0.69\right) \times 10^{-8}$			
$\mathrm{d}\mathcal{B}/\mathrm{d}q^2(B^+ \to K^+\mu^+\mu^-)$	(1.1, 6)	$(24.2 \pm 0.7 \pm 1.2) \times 10^{-9}$ [89]	✓		✓
$\mathcal{B}(B^+ \to K^+\mu^+\mu^-)$		$(11.86 \pm 0.34 \pm 0.59) \times 10^{-8}$			
$\mathcal{B}(B^+ \to K^+a(\mu^+\mu^-))$	(0.06, 22.1)	$< 1 \times 10^{-9}$ [90]		✓	
$\mathcal{B}(B^0 \to K^{0*}e^+e^-)$	(1.1, 6)	$(1.8 \pm 0.6) \times 10^{-7}$ [91]	✓	✓	✓
	(0.1, 8)	$(3.7 \pm 1.0) \times 10^{-7}$ [91]		✓	
$\mathcal{B}(B^0 \to K^{0*}a(e^+e^-))$	(0.0004, 0.05)	$< 1.344 \times 10^{-7}$		✓	✓
	(0.05, 0.15)	$< 1.22 \times 10^{-8}$		✓	
	(0.25, 0.4)	$< 1.97 \times 10^{-8}$		✓	
	(0.4, 0.7)	$< 1.74 \times 10^{-8}$		✓	
	(0.7, 1)	$< 6.5 \times 10^{-9}$		✓	
$\mathcal{B}(B^0 \to K^{0*}\mu^+\mu^-)$	(1.1, 6)	$1.9^{+0.7}_{-0.6} \times 10^{-7}$ [91]	✓		✓
$\mathcal{B}(B^0 \to K^{0*}a(\mu^+\mu^-))$	(0.05, 18.9)	$< 3 \times 10^{-9}$ [92]		✓	

Table 1. The checkmarks correspond to the strongest bounds used in each mass regime analysed in this work. Notice that the second entries in the first two lines have been obtained from the corresponding first entry simply integrating over the bin window spread. For $\mathcal{B}(B^0 \to K^{0*}a(e^+e^-))$, no bound can be extracted for $q^2 \in [0.15, 0.25]\,\mathrm{GeV}^2$ as the data are incompatible with the SM prediction at more than 2σ.

above makes it easy to understand why the first term in this expression quadratic in the Wilson coefficients is the same for e and μ in the approximation considered, and it can even dominate over the linear term. Indeed, using Flavio and EOS (which agree with each other to very high accuracy), we find for the integration over the q^2 range of the central bin window

$$\begin{aligned}\mathcal{B}(B \to Ke^+e^-)^{6.0\ \mathrm{GeV}^2}_{1.1\ \mathrm{GeV}^2} &= 10^{-7} \times \left(1.5 - 3.4 \times 10^{-4}\, C^e_{P_+} + 7.1 \times 10^{-2}\, C^{e2}_{P_+}\right) , \\ \mathcal{B}(B \to K\mu^+\mu^-)^{6.0\ \mathrm{GeV}^2}_{1.1\ \mathrm{GeV}^2} &= 10^{-7} \times \left(1.5 - 7.0 \times 10^{-2}\, C^\mu_{P_+} + 7.1 \times 10^{-2}\, C^{\mu 2}_{P_+}\right) ,\end{aligned} \tag{3.12}$$

with a theoretical error of $\mathcal{O}(15)\%$ at 1σ. The corresponding 2σ bounds on the Wilson coefficients read:

$$C^e_{P_+} \in [-2.6, 2.6] \qquad \text{and} \qquad C^\mu_{P_+} \in [-1.3, 2.3]\,, \tag{3.13}$$

taking into account both experimental and theoretical errors. These constraints are depicted in grey in figure 2.

R_K. It follows from the previous expressions that the LFU ratio R_K can be written in terms of the two coefficients $C^\ell_{P_+}$:

$$R_K = 1 + \frac{0.21\, C^e_{P_+} - 4.67\, C^\mu_{P_+} + 4.73(\, C^{\mu 2}_{P_+} - C^{e2}_{P_+})}{100 - 0.21\, C^e_{P_+} + 4.73\, C^{e2}_{P_+}}\,. \tag{3.14}$$

JHEP02(2023)138

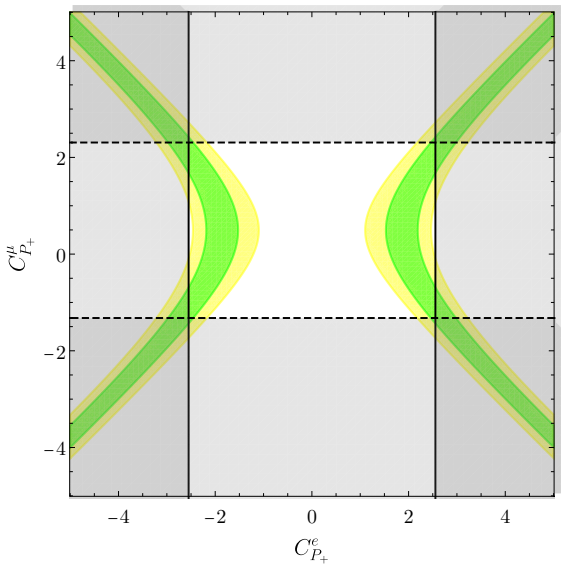

Figure 2. Parameter space for R_K, for an ALP heavier than B mesons. In yellow and green are respectively depicted the 1σ and 2σ solutions to the central bin of R_K. The grey regions around the frame of the figures are excluded at 2σ by data on semileptonic $B \to Ke^+e^-$ (solid black contours) and $B \to K\mu^+\mu^-$ (dashed black contours) decays.

The large theoretical errors reported for the semileptonic decays may be expected to cancel in this observable in general, and the largest source of uncertainty to determine the Wilson coefficients are the experimental errors. Given that experimentally $R_K < 1$, the second term in this equation should be negative.

Some naive conclusions can be obtained when leptonic NP contributions are assumed only for either the electron or the muon sector. For instance, let us consider the 2σ error range for R_K, $R_K \in [0.768, 0.935]$ [13]. In the absence of ALP-muon couplings, this would require the effective Wilson coefficients to lie in the range

$$C^e_{P_+} \in [1.2,\, 2.6] \vee [-2.6,\, -1.2] \qquad \text{for } C^{\mu}_{P_+} = 0\,. \tag{3.15}$$

On the contrary, if NP in the lepton sector would contribute only to muon couplings, i.e. $C^e_{P_+} = 0$, there is no value of $C^{\mu}_{P_+}$ that would solve the R_K anomaly at the 2σ level. This is easily understood noting that such a solution would require the $\mathcal{B}(B \to K\mu^+\mu^-)$ in eq. (3.12) to be suppressed with respect to the SM value, which in turns requires the term linear in $C^{\mu}_{P_+}$ to dominate over the quadratic one, i.e. $|C^{\mu}_{P_+}| < 1$. However, due to the suppression provided by the numerical prefactor of that linear term, the NP contribution would not be then large enough to generate a significant shift from the SM prediction.

In summary, it follows that R_K could be explained through ALP-electron couplings alone (in addition to the ALP-bs couplings), but not through ALP-muon couplings alone.

The two-dimensional enlargement of the parameter space as spanned by the variables $\{C^e_{P_+}, C^{\mu}_{P_+}\}$ is depicted in figure 2, which illustrates the 2σ region where both parameters could be simultaneously at play and account for R_K. Taking into account the bounds from

JHEP02(2023)138

semileptonic decays in eq. (3.13), the allowed area is given by

$$\begin{aligned} C^e_{P_+} &\in [1.2,\, 2.6] \vee [-2.6,\, -1.2] \\ C^\mu_{P_+} &\in [-1.3,\, 2.3]\,. \end{aligned} \tag{3.16}$$

Note that these two independent parameters can be traded by two specific combinations of the ALP-fermion couplings defined in the mass basis in the Lagrangian eq. (3.6),

$$\begin{aligned} C^e_{P_+} &\approx -1.3\times 10^4\ \text{GeV}^2 \left(\frac{10\ \text{GeV}}{m_a}\right)^2 \frac{(\mathbf{c}_d+\mathbf{c}_Q)_{sb}}{f_a}\frac{(\mathbf{c}_e-\mathbf{c}_L)_{ee}}{f_a}\,, \\ C^\mu_{P_+} &\approx -2.7\times 10^6\ \text{GeV}^2 \left(\frac{10\ \text{GeV}}{m_a}\right)^2 \frac{(\mathbf{c}_d+\mathbf{c}_Q)_{sb}}{f_a}\frac{(\mathbf{c}_e-\mathbf{c}_L)_{\mu\mu}}{f_a}\,. \end{aligned} \tag{3.17}$$

The limits obtained in eq. (3.16) translate then into the following constraints, for instance for $m_a = 10\,\text{GeV}$:

$$\begin{aligned} \frac{(\mathbf{c}_d+\mathbf{c}_Q)_{sb}\,(\mathbf{c}_e-\mathbf{c}_L)_{ee}}{f_a^2} &\in ([0.93,\, 2.02] \vee [-2.02,\, -0.93]) \times 10^{-4}\ \text{GeV}^{-2}\,, \\ \frac{(\mathbf{c}_d+\mathbf{c}_Q)_{sb}\,(\mathbf{c}_e-\mathbf{c}_L)_{\mu\mu}}{f_a^2} &\in [-0.87,\, 0.49] \times 10^{-6}\ \text{GeV}^{-2}\,. \end{aligned} \tag{3.18}$$

This result already implies that $(\mathbf{c}_e-\mathbf{c}_L)_{\mu\mu}$ needs to be about two orders of magnitude smaller than $(\mathbf{c}_e-\mathbf{c}_L)_{ee}$ to explain R_K via heavy ALP exchange. We consider next other relevant observables which are not describable in terms of $C^\ell_{P_\pm}$, but they are sensitive only to either the quark factor $(\mathbf{c}_d+\mathbf{c}_Q)_{sb}$ or the leptonic factors $(\mathbf{c}_e-\mathbf{c}_L)_{\ell\ell}$. Nevertheless, they will be shown to provide further restrictions on the ALP explanation of B-anomalies.

ΔM_s. The B_s meson mass difference ΔM_s measured in $B_s - \overline{B}_s$ oscillations can be defined as

$$\Delta M_s = \frac{1}{M_{B_s}} \left| \left\langle \overline{B}_s \left| \mathcal{H}^{\text{eff.}}_{\Delta B=2} \right| B_s \right\rangle \right|\,, \tag{3.19}$$

where M_{B_s} is the mass of the B_s meson and $\mathcal{H}^{\text{eff.}}_{\Delta B=2}$ is the effective Hamiltonian describing $\Delta B = 2$ transitions. The data imply that [93]

$$\Delta M_s = (17.7656 \pm 0.0057)\,\text{ps}^{-1}\,, \tag{3.20}$$

to be compared with the SM prediction that we take from ref. [94], $\Delta M_s^{\text{SM}} = (20.1^{+1.2}_{-1.6})\,\text{ps}^{-1}$. (Assuming the most recent results for the SM prediction [95] that are compatible with the SM within 1σ, the following conclusions do not change as the maximum NP couplings allowed by data at 2σ are in either case very alike. Nevertheless, the 1σ region in figure 3a would be in this case enlarged, constraining couplings $(\mathbf{c}_d+\mathbf{c}_Q)_{sb}/f_a \lesssim 6\times 10^{-5}\,\text{GeV}^{-1}$.)

The generic expression for the contribution of the tree-level exchange of a heavy ALP to ΔM_s has been recently presented in ref. [44], and we thus refrain from repeating that analysis here. It suffices to mention that the corresponding bound applies to the two ratios

$$\frac{(\mathbf{c}_d \pm \mathbf{c}_Q)_{sb}}{m_a\, f_a}\,. \tag{3.21}$$

JHEP02(2023)138

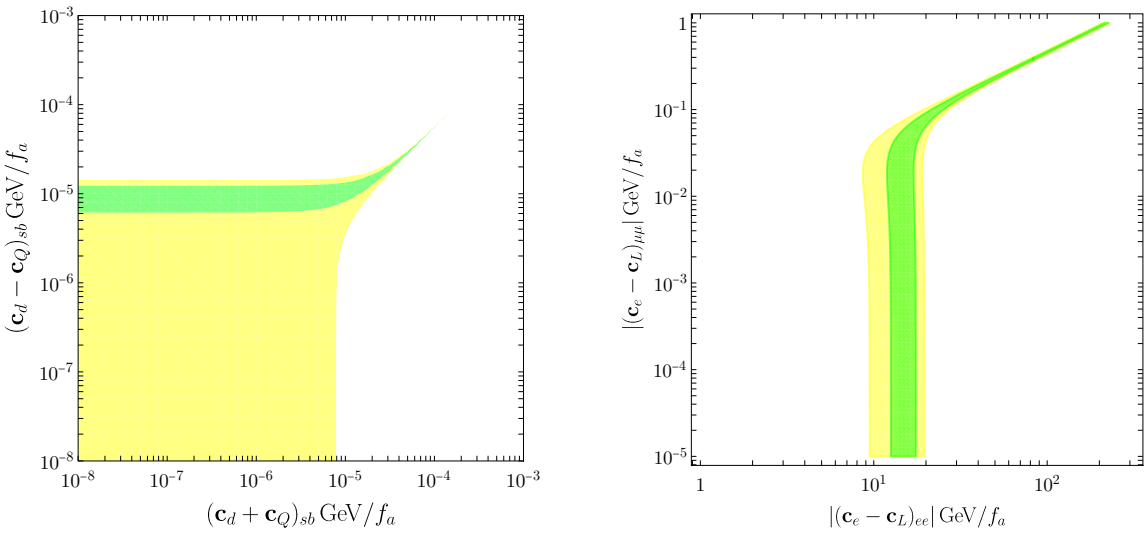

Figure 3. ALP heavier than B mesons. In figure 3a, $(\mathbf{c}_d \pm \mathbf{c}_Q)_{sb}/f_a$ parameter space allowed by B_s meson oscillation constraints, at 1σ (2σ) in green (yellow). This plot is symmetric with respect to any of the axes for negative values of the coordinates. In figure 3b, the parameter space for the combinations $(\mathbf{c}_e - \mathbf{c}_L)_{ee}/f_a$ and $(\mathbf{c}_e - \mathbf{c}_L)_{\mu\mu}/f_a$ that solve the R_K anomaly in figure 2 for the maximal allowed value $(\mathbf{c}_Q + \mathbf{c}_d)_{sb}/f_a = 10^{-5}$ GeV^{-1}. The ALP mass is fixed to $m_a = 10$ GeV in both plots.

The values allowed by data for these combinations are illustrated in figure 3a for the benchmark ALP mass value $m_a = 10\,\mathrm{GeV}$. They agree with those in ref. [44].[7] The figure illustrates that large values of $(\mathbf{c}_d \pm \mathbf{c}_Q)_{sb}/f_a$ up to $\sim 10^{-4}$ GeV^{-1} are allowed on a fine-tuned region of the parameter space (the spikes in the figure). Otherwise, in the 1σ region (in green) the solutions constrain $|(\mathbf{c}_d - \mathbf{c}_Q)_{sb}|/f_a$, while only an upper bound results for the orthogonal combination, $|(\mathbf{c}_d + \mathbf{c}_Q)_{sb}|/f_a$, which is the one relevant for R_K,

$$|(\mathbf{c}_d - \mathbf{c}_Q)_{sb}|/f_a \sim 10^{-5}\ \mathrm{GeV}^{-1}\,, \qquad |(\mathbf{c}_d + \mathbf{c}_Q)_{sb}|/f_a \lesssim 10^{-5}\ \mathrm{GeV}^{-1}\,. \tag{3.22}$$

At the 2σ level (in yellow) only an upper bound of $\mathcal{O}(10^{-5})$ GeV can be extracted for both combinations.

A naive estimation of the impact of ΔM_s on R_K can now be achieved by comparing these constraints on ALP-quark couplings with the products of ALP-quark and ALP-lepton couplings relevant for R_K, see eq. (3.17). For the illustrative case $(C^e_{P_+}, C^\mu_{P_+}) = (2, 0)$ in figure 2, $m_a = 10$ GeV and the value $|(\mathbf{c}_d + \mathbf{c}_Q)_{sb}|/f_a = 10^{-5}$ GeV^{-1} which saturates the bound in eq. (3.22), it would follow

$$\frac{|(\mathbf{c}_e - \mathbf{c}_L)_{ee}|}{f_a} \approx 16\ \mathrm{GeV}^{-1}\,. \tag{3.23}$$

This result leads right away to a clash with the validity of the EFT, though, as f_a is expected to be at least of the order of the electroweak scale, see eqs. (2.3) and (2.4), and

[7] Which expressed the result in terms of separate bounds for c_d and c_Q.

JHEP02(2023)138

$f_a > m_a > M_{B_s}$. This happens even for the smaller possible scale values, e.g.

$$f_a \approx 100 \text{ GeV} \Longrightarrow |(\mathbf{c}_e - \mathbf{c}_L)_{ee}| \approx 10^3 \,, \tag{3.24}$$

which are unacceptably large ALP-lepton couplings, well outside the perturbative regime of the EFT.[8]

Note that smaller ALP-quark couplings would not soften the issue as they would require even larger lepton-ALP couplings. The situation improves but is still problematic for $|(\mathbf{c}_Q + \mathbf{c}_d)_{sb}|/f_a$ values in the fine-tuned region, e.g. 10^{-4} GeV^{-1}, which would translate into $|(\mathbf{c}_e - \mathbf{c}_L)_{ee}| \approx 10^2$. To vary the ALP mass does not resolve the issue either, as the relevant combination of ALP-quark couplings scales with the ALP mass, see eq. (3.21): a larger m_a would lead to larger values of the combination of leptonic couplings involved, worsening the EFT validity prospects.

The exercise above assumed no NP contribution from the muon sector. Figure 3b considers the whole parameter space $|(\mathbf{c}_e - \mathbf{c}_L)_{ee}|$ vs. $\left|(\mathbf{c}_e - \mathbf{c}_L)_{\mu\mu}\right|$ that solves the R_K anomaly, again for $m_a = 10$ GeV and $|(\mathbf{c}_d + \mathbf{c}_Q)_{sb}|/f_a = 10^{-5}$ GeV^{-1}. The ΔM_s constraint in eq. (3.23) falls then within the green band of this plot. The figure shows that, necessarily,

$$\frac{|(\mathbf{c}_e - \mathbf{c}_L)_{ee}|}{f_a} \geq 10 \text{ GeV}^{-1} \tag{3.25}$$

and thus the conclusion described above holds even for a non-vanishing $C^{\mu}_{P_+}$: it is possible to explain the R_K anomaly consistently with data from semileptonic decays and B_s-meson oscillations, but the corresponding couplings are outside the range of validity of the ALP EFT.

Anomalous magnetic moment of the electron and the muon. The measurement of the electric dipole moment of the electron with Caesium atoms [97–99] and the measurement with Rubidium atoms [100] show deviations from the SM prediction in opposite directions. We will focus on the Caesium experimental determination, which is the one that shows the largest tension with the SM of about $\sim 2.4\sigma$,

$$\Delta a_e \equiv a_e^{\text{exp}} - a_e^{\text{SM}} = -(88 \pm 36) \times 10^{-14} \,, \tag{3.26}$$

and consider the 2σ interval as a bound on the range allowed. In turn, for the data on $g-2$ for the muon, a longstanding 4.2σ anomaly [101] indicates

$$\Delta a_\mu = (25.1 \pm 5.9) \times 10^{-10} \,, \tag{3.27}$$

with consistent results across different experiments [102, 103].[9]

[8] Such large values of the electron coupling can be attained e.g. selectively in electrophilic ALP models [96] where the electron coupling can be exponentially enhanced without increasing m_a or f_a.

[9] The BMW lattice QCD collaboration computed recently the leading hadronic vacuum polarisation contribution to the muon $g-2$ with sub percent precision [104], and using this result the tension would reduce to only 1.6σ. Recent results from other lattice groups and lattice methodologies [105, 106] are also converging towards a smaller tension with respect to the SM prediction, at least in the so-called "intermediate" range, while finding instead tensions in e^+e^- data. Waiting for further clarification, we will consider in this work the aforementioned value of Δa_μ in eq. (3.27).

JHEP02(2023)138

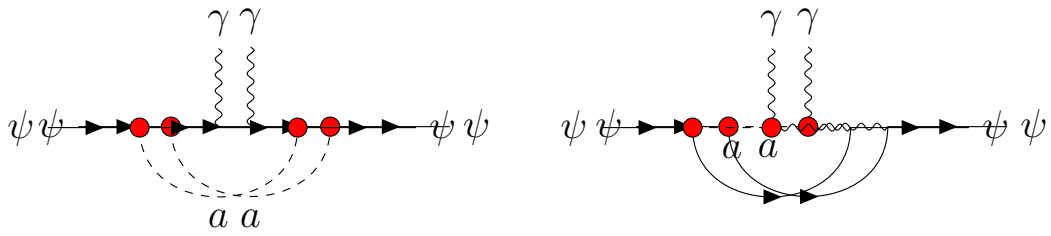

(a) Double ALP Fermion Coupling. **(b)** Single ALP Fermion Coupling.

Figure 4. One-loop ALP-mediated diagrams contributing to $(g-2)$ of the fermion ψ.

ALP exchange can contribute to both Δa_e [44] and Δa_μ. The effects appear at one-loop, as depicted in figure 4. In the chirality-flip basis eq. (2.9), the ALP-fermion couplings are mass dependent and their insertion in both internal vertices — figure 4a — is expected to be subdominant with respect to the amplitudes containing one insertion of ALP-anomalous gauge couplings — figure 4b, and in particular of the ALP-photon anomalous coupling. In the limit $m_a \gg m_\ell$ it results

$$\Delta a_\ell^{\rm ALP} \simeq A_\ell \, \frac{c_{a\gamma\gamma} + \Delta c_{a\gamma\gamma}}{f_a} \, \frac{(\mathbf{c}_e - \mathbf{c}_L)_{\ell\ell}}{f_a} \,, \tag{3.28}$$

where the constant in front of this expression reads

$$A_\ell \equiv \frac{m_\ell^2}{2\pi^2}\left(\log\frac{\Lambda^2}{m_a^2} - \frac{3}{2}\right) = \begin{cases} 1.02 \times 10^{-7}\ \text{GeV}^2 & \text{for the electron} \\ 4.36 \times 10^{-3}\ \text{GeV}^2 & \text{for the muon}\,, \end{cases} \tag{3.29}$$

with Λ assumed to be of $\mathcal{O}(1\ \text{TeV})$ and $\Lambda = 4\pi f_a$ by naive dimensional analysis. In the formula above, $c_{a\gamma\gamma}$ denotes the tree-level arbitrary anomalous gauge coupling in the initial Lagrangian, eq. (2.3). In contrast, $\Delta c_{a\gamma\gamma}$ is the anomalous contribution induced by the fermion rotation performed to pass to the chirality-flip basis, and it is given by a precise combination of fermion-ALP couplings, see eqs. (2.14)–(2.16), i.e.

$$\Delta c_{a\gamma\gamma} \simeq -\frac{\alpha_{em}}{4\pi}\left[(\mathbf{c}_e - \mathbf{c}_L)_{ee} + (\mathbf{c}_e - \mathbf{c}_L)_{\mu\mu}\right] , \tag{3.30}$$

which using eqs. (3.26) and (3.27) leads respectively to the following 2σ constraints:

$$\frac{1}{f_a}\left[(\mathbf{c}_e - \mathbf{c}_L)_{ee}\left((\mathbf{c}_e - \mathbf{c}_L)_{ee} + (\mathbf{c}_e - \mathbf{c}_L)_{\mu\mu} - \frac{4\pi}{\alpha_{em}}\, c_{a\gamma\gamma}\right)\right]^{1/2} \in [0.05,\, 0.16]\ \text{GeV}^{-1}\,, \tag{3.31}$$

and

$$\frac{1}{f_a}\left[(\mathbf{c}_e - \mathbf{c}_L)_{\mu\mu}\left(\frac{4\pi}{\alpha_{em}}\, c_{a\gamma\gamma} - (\mathbf{c}_e - \mathbf{c}_L)_{ee} - (\mathbf{c}_e - \mathbf{c}_L)_{\mu\mu}\right)\right]^{1/2} \in [0.023,\, 0.038]\ \text{GeV}^{-1}\,, \tag{3.32}$$

Were the bare anomalous coupling $c_{a\gamma\gamma}$ to vanish, an explanation of R_K in terms of heavy ALP exchange would be excluded, because the data on R_K and Δa_e cannot be simultaneously accommodated, given the bound in eq. (3.25) and the fact that $(\mathbf{c}_e - \mathbf{c}_L)_{\mu\mu} \ll (\mathbf{c}_e - \mathbf{c}_L)_{ee}$ — see discussion after eq. (3.18).

JHEP02(2023)138

Strictly speaking, though, the possibility to explain through heavy ALP exchange both R_K and Δa_ℓ cannot be completely excluded because $c_{a\gamma\gamma}$ is arbitrary. Its value can be fine-tuned to fit for instance R_K data and the Δa_e bound. Note that the coupling values then required would not allow to account in addition for the Δa_μ anomaly. Indeed, the expressions for $\Delta a_\mu^{\rm ALP}$ and $\Delta a_e^{\rm ALP}$ would then imply the constraint — at the 2σ level —

$$\frac{(\mathbf{c}_e - \mathbf{c}_L)_{\mu\mu}}{(\mathbf{c}_e - \mathbf{c}_L)_{ee}} \simeq \frac{\Delta a_\mu^{\rm ALP}}{\Delta a_e^{\rm ALP}} \frac{A_e}{A_\mu} \in -[0.02,\, 0.54]\,, \tag{3.33}$$

which is inconsistent with the hierarchy between $(\mathbf{c}_e - \mathbf{c}_L)_{ee}/f_a$ and $(\mathbf{c}_e - \mathbf{c}_L)_{\mu\mu}/f_a$ shown in figure 3b.

Building on the same freedom on the value of the initial $c_{a\gamma\gamma}$, one may still wonder whether it is technically possible a solution in which the amplitude of the second diagram in figure 4 cancels for either Δa_e or Δa_μ, forcing $c_{a\gamma\gamma} + \Delta c_{a\gamma\gamma} = 0$, so as to explain then the experimental value of that observable in terms of just the first diagram in that figure (which has been neglected up to now). This option leads to a dead end as well: i) for Δa_e, because its $(m_e)^4/(f_a m_a)^2$ suppression makes it totally negligible;[10] ii) for Δa_μ, because the $(m_\mu)^4/(f_a m_a)^2$ contribution is always negative, contrary to the experimental $\Delta a_\mu > 0$ value, and also the prediction for Δa_e would be incompatible with observation.

In summary, no simultaneous explanation in terms of tree-level heavy ALP exchange is possible for the three observables in the set $\{R_K, \Delta a_e, \Delta a_\mu\}$. Furthermore, although such an explanation is possible for the $\{R_K, \Delta a_e\}$ set, the data on R_K would always require a strong disregard of the EFT validity condition.

3.2.2 R_{K^*}, $B \to K^* \ell^+\ell^-$, and $B_s \to \ell^+\ell^-$

The analysis of R_{K^*} can be done in analogy with that for R_K and $B \to K\ell^+\ell^-$ above, although the data on $B_s \to \ell^+\ell^-$ will add an extra essential ingredient because the purely leptonic decays share with R_{K^*} the same dependence on the effective couplings $C_{P_-}^\ell$ only.

$B \to K^*\ell^+\ell^-$. Using the EOS software, we obtain

$$\begin{aligned}
\mathcal{B}(B \to K^*\mu^+\mu^-)_{1.1\ \text{GeV}^2}^{6.0\ \text{GeV}^2} &= 10^{-7} \times \left(1.9 - 7.4 \times 10^{-2}\, C_{P_-}^{\mu} + 7.5 \times 10^{-2}\, C_{P_-}^{\mu 2}\right)\,, \\
\mathcal{B}(B \to K^*e^+e^-)_{1.1\ \text{GeV}^2}^{6.0\ \text{GeV}^2} &= 10^{-7} \times \left(1.9 - 3.6 \times 10^{-4}\, C_{P_-}^{e} + 7.5 \times 10^{-2}\, C_{P_-}^{e 2}\right)\,,
\end{aligned} \tag{3.34}$$

and

$$\begin{aligned}
\mathcal{B}(B \to K^*\mu^+\mu^-)_{0.045\ \text{GeV}^2}^{1.1\ \text{GeV}^2} &= 10^{-7} \times \left(1.2 - 9.3 \times 10^{-3}\, C_{P_-}^{\mu} + 1.5 \times 10^{-3}\, C_{P_-}^{\mu 2}\right)\,, \\
\mathcal{B}(B \to K^*e^+e^-)_{0.045\ \text{GeV}^2}^{1.1\ \text{GeV}^2} &= 10^{-7} \times \left(1.3 - 4.8 \times 10^{-5}\, C_{P_-}^{e} + 1.6 \times 10^{-3}\, C_{P_-}^{e 2}\right)\,,
\end{aligned} \tag{3.35}$$

respectively for the central and low energy bin regions, see eq. (1.3). The theoretical errors are estimated to be at the 15% level at 1σ (similarly to those for the semileptonic $B \to K$ decays earlier on). The comparison of these equations with those for $B \to K$

[10] The same applies if the Δa_e value inferred from Rubidium was considered instead, in spite of its weaker strength.

JHEP02(2023)138

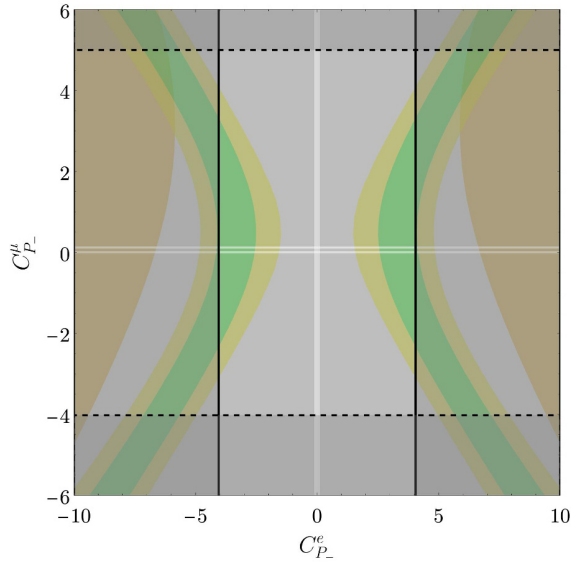

Figure 5. Parameter space for R_{K^*}, for an ALP heavier than B mesons. In yellow and green are respectively depicted the 1σ and 2σ solutions to the central bin, while in orange are indicated the 1σ solutions to the low bin. The grey regions around the frame of the figures are excluded at 2σ by data on semileptonic $B \to K^* e^+ e^-$ (solid black contours) and $B \to K^* \mu^+ \mu^-$ (dashed black contours) decays. The regions excluded by purely leptonic B_s decays reach the central area and are also depicted in grey (horizontally for the electron channel and vertically for the muon one) leaving available the narrow white strips.

semileptonic transitions in eqs. (3.12) shows a very similar structure, with in particular the terms quadratic on the Wilson coefficients being positive, and a very similar pattern for the prefactors of linear vs. quadratic terms. A comparison with the experimental data in table 1 results in the following 2σ bounds on the Wilson coefficients,

$$C^{e}_{P_-} \in [-4.0, 4.0] \qquad \text{and} \qquad C^{\mu}_{P_-} \in [-4.0, 5.0]\,, \tag{3.36}$$

which are illustrated in figure 5 as grey shaded regions delimitated by solid (electrons) and dashed (muons) black contours.

R_{K^*}. Analogous considerations to those for R_K will apply then to R_{K^*}, given the similarity between eqs. (3.12) and those above for the semileptonic R_{K^*} decays. In consequence, the experimental tension in R_{K^*} is expected to allow for an explanation in terms of ALP tree-level exchange only if the electron sector would receive NP contributions. We expatiate next on this point. From eqs. (3.34) and (3.35) it follows that

$$R_{K^*} = \begin{cases} 1 + \dfrac{0.02\, C^{e}_{P_-} - 3.89\, C^{\mu}_{P_-} + 3.95(\, C^{\mu 2}_{P_-} - C^{e2}_{P_-}\,)}{100 - 0.02\, C^{e}_{P_-} + 3.95\, C^{e2}_{P_-}} & \text{central bin} \\ 0.923 + \dfrac{0.03\, C^{e}_{P_-} - 7.15\, C^{\mu}_{P_-} + 1.15\, C^{\mu 2}_{P_-} - 1.13\, C^{e2}_{P_-}}{1000 - 0.04\, C^{e}_{P_-} + 1.23\, C^{e2}_{P_-}} & \text{low bin,} \end{cases} \tag{3.37}$$

with theoretical errors that are expected to be negligible with respect to the corresponding experimental ones.

JHEP02(2023)138

Let us first extract the values for $C_{P_-}^{e,\mu}$ that could solve the tension in R_{K^*} in case NP enters only in either the electron sector or the muon sector. For $C_{P_-}^{\mu} = 0$, the 2σ error bands for R_{K^*}, $R_{K^*} \in [0.519, 0.911]$ (central bin) and $R_{K^*} \in [0.504, 0.875]$ [11] (low bin) lead to

$$\text{For } C_{P_-}^{\mu} = 0\text{:} \quad \begin{cases} C_{P_-}^{e} \in [1.6,\, 4.8] \vee [-4.8,\, -1.6] & \text{central bin} \\ C_{P_-}^{e} \in [6.7,\, 26.1] \vee [-26.1,\, -6.7] & \text{low bin.} \end{cases} \tag{3.38}$$

These two sets of solutions do not overlap even partly and therefore there is no possible explanation in terms of a heavy ALP for the deviations in both energy bins. Alternatively, for $C_{P_-}^{e} = 0$, there is no $C_{P_-}^{\mu}$ value that can explain R_{K^*} with the sensitivity considered.

Let us finally consider the ALP explanations to R_{K^*} within the two-dimensional parameter space of couplings $\{C_{P_-}^{e}, C_{P_-}^{\mu}\}$. The solutions are depicted in figure 5 (in green, yellow and orange). This figure also shows, though, that when the data on $B \to K^* e^+ e^-$ $B \to K^* \mu^+ \mu^-$ are taken into account, the regions where the low bin anomaly can be explained are ruled out and those for the central bin one are reduced to

$$1.6 < |C_{P_-}^{e}| < 4\,, \qquad\qquad -3 < |C_{P_-}^{\mu}| < 4\,. \tag{3.39}$$

$B_s \to \ell^+\ell^-$. A second observable that directly depends on the operator $\mathcal{O}_{P_-}^{\ell}$ for a given charged lepton ℓ is the branching ratio $\mathcal{B}(B_s \to \ell^+\ell^-)$. The corresponding experimental measurements are in good agreement with the SM and therefore any NP effect should be at most marginal. By implementing the Flavio software, and after performing an interpolation procedure, we obtain the contribution of the SM plus those mediated by tree-level exchange of a heavy ALP:

$$\begin{aligned} \overline{\mathcal{B}}(B_s \to \mu^+\mu^-) &= 10^{-9} \times \left(3.67 - 1.15 \times 10^2\, C_{P_-}^{\mu} + 9.04 \times 10^2\, C_{P_-}^{\mu 2}\right), \\ \overline{\mathcal{B}}(B_s \to e^+e^-) &= 10^{-14} \times \left(8.58 - 5.57 \times 10^4 C_{P_-}^{e} + 9.05 \times 10^7\, C_{P_-}^{e2}\right), \end{aligned} \tag{3.40}$$

where the bar over the symbol for the branching ratio denotes untagged decays, that is, the time-integrated quantities which include the probability for the meson to oscillate before decaying (the tagged quantity is $\mathcal{O}(15\%)$ smaller than the results shown). If the EOS software is used instead of Flavio, the numerical output is 9% smaller than that in eq. (3.40); this difference is most probably due to some loop contributions considered in Flavio, as discussed in ref. [107]. The theoretical error on the SM prediction for these quantities is much smaller than that for semileptonic B decays and it is of $\mathcal{O}(4\%)$ at the 1σ level.

The size of the numerical factors appearing in front of the Wilson coefficients $C_{P_-}^{e,\mu}$ indicates that the latter should not exceed values of about $|C_{P_-}^{e,\mu}| \sim 0.1$. More precisely, the regions allowed in order to remain within the 2σ confidence level of the $B_s \to \ell^+\ell^-$ measurements, $\mathcal{B}\left(B_s \to \mu^+\mu^-\right) \in [2.2,\, 4.1] \times 10^{-9}$ [108] and $\mathcal{B}\left(B_s \to e^+e^-\right) < 11.2 \times 10^{-9}$ [109], are

$$\begin{aligned} C_{P_-}^{e} &\in [-0.11,\, 0.11]\,, \\ C_{P_-}^{\mu} &\in [-0.0033,\, 0.014] \vee [0.11,\, 0.13]\,. \end{aligned} \tag{3.41}$$

JHEP02(2023)138

These solutions are incompatible with the naive values in eq. (3.39). In summary, the data from purely leptonic B_s decays precludes an explanation of R_{K^*} in terms of a heavy ALP, even when the complete parameter space for ALP-electron and ALP-muon couplings is considered.[11] This is illustrated for R_{K^*} in figure 5: the bounds from purely leptonic B_s meson decays only allow very narrow (white) strips in the parameter space; the impact of $B_s \to e^+e^-$ in particular leaves no region to explain R_{K^*}, not even for the central energy bin window.

The comparison of our two-parameter space survey above can be contrasted with those in the one-parameter analysis in ref. [44]. While we find that an explanation for R_{K^*} in terms of a heavy ALP exchange is excluded, R_K could be accounted for technically, albeit at a heavy theoretical cost: to go out of the range of validity of the EFT. If the latter condition was nevertheless disregarded, it would be possible to accommodate at the same time the bound on Δa_e, but not the Δa_μ anomaly.

4 Light ALP

This section explores the option of an ALP lighter than the B mesons and whose mass is in the ballpark of the energy bin windows considered for the neutral B-anomalies. Therefore, the ALP field cannot be integrated out and resonant effects may become relevant. The analysis strongly depends on the precise value of m_a. We explore below two distinct scenarios:

- ALP mass well within the energy range of the bin under consideration.

- ALP mass outside the bin window but close to it.

4.1 ALP mass within the bin window

For the $B \to K^{(*)}\ell^+\ell^-$ processes, we rely on analytic computations of three body B decays which use the relativistic Breit-Wigner expression for the ALP propagator under the condition that the ALP decay width Γ_a is smaller than its mass, $\Gamma_a < m_a$. The matrix elements as computed in refs. [17, 111] will be used, together with the inputs in table 3 of appendix A for the SM Wilson coefficients. The form factors — which are the main source of theoretical uncertainties — are taken from refs. [112] and [111]. A detailed account of our computations can be found in appendix B, which includes a comparison between our results for the relevant decay widths with those obtained numerically via the Flavio software: we find a very accurate agreement in the energy bin regions relevant for the R_K and R_{K^*} anomalies.

Before presenting the numerical results, it is pertinent though to discuss analytically the validity of the narrow width approximation (NWA), which justifies that the ALP can be safely taken on-shell. In this approximation, the total branching ratio can be decomposed as

$$\mathcal{B}(B \to K^{(*)}\ell^+\ell^-) = \mathcal{B}(B \to K^{(*)}\ell^+\ell^-)^{\rm SM} + \mathcal{B}(B \to K^{(*)}a) \times \mathcal{B}(a \to \ell^+\ell^-)\,, \qquad (4.1)$$

[11] A combined analysis of the ATLAS, CMS and LHCb results on $\mathcal{B}\left(B_s \to \mu^+\mu^-\right)$ using data between 2011 and 2016, showed a small tension with the SM predictions at the 2σ level [110]. Was this combined result included, the conclusions above would not change. In any case, the more recent analysis by the LHCb collaboration which includes data till 2018 [108] shows a smaller deviation from the SM prediction.

JHEP02(2023)138

where the SM contributions can be found in table 4 while the expressions for $\mathcal{B}(B \to Ka)$ and $\mathcal{B}(B \to K^* a)$ are respectively given as a function of m_a by

$$\begin{aligned}\mathcal{B}(B \to Ka) &= \tau_B \frac{M_B \left[(\mathbf{c}_d + \mathbf{c}_Q)_{sb}\right]^2}{64\,\pi\, f_a^2} f_0^2[m_a^2]\, \lambda_{BKa}^{1/2} \left(1 - \frac{M_K^2}{M_B^2}\right)^2 , \\ \mathcal{B}(B \to K^* a) &= \tau_B \frac{\left[(\mathbf{c}_d - \mathbf{c}_Q)_{sb}\right]^2}{64\,\pi\, f_a^2\, M_B^3} A_0^2[m_a^2]\, \lambda_{BK^*a}^{3/2} ,\end{aligned} \tag{4.2}$$

where τ_B and M_B denote respectively the lifetime and mass of the B mesons (i.e. $B^{0,\pm}$) and $M_{K^{(*)}}$ is the neutral or charged kaon mass (see table 3). In turn, $f_0[m_a^2]$ and $A_0[m_a^2]$ are two form factors whose dependence on the ALP mass can be extracted from refs. [112] and [111], respectively,

$$\begin{aligned} f_0[m_a^2] &\approx 3.45 \times 10^{-1} + 2.84 \times 10^{-3}\, \frac{m_a^2}{\text{GeV}^2} + 6.97 \times 10^{-4}\, \frac{m_a^4}{\text{GeV}^4} , \\ A_0[m_a^2] &\approx\ 0.37 + 2.18 \times 10^{-2}\, \frac{m_a^2}{\text{GeV}^2} + 8.83 \times 10^{-4}\, \frac{m_a^4}{\text{GeV}^4} , \end{aligned} \tag{4.3}$$

where $\lambda_{BK^{(*)}a}$ are the Källén triangle functions $\lambda_{BK^{(*)}a} \equiv \lambda(M_B^2,\, M_{K^{(*)}}^2,\, m_a^2)$ such that

$$\lambda(a,\, b,\, c) \equiv a^2 + b^2 + c^2 - 2ab - 2bc - 2ca\,. \tag{4.4}$$

In turn, the purely leptonic decay width of an ALP reads,

$$\Gamma(a \to \ell^+ \ell^-) = \frac{m_a\, m_\ell^2}{8\,\pi\, f_a^2} \left[(\mathbf{c}_e - \mathbf{c}_L)_{\ell\ell}\right]^2 \left(1 - \frac{4m_\ell^2}{m_a^2}\right)^{1/2} . \tag{4.5}$$

Given the energy windows of the bins relevant for the R_K and R_{K^*} anomalies, an explanation in terms of the exchange of an on-shell ALP requires

$$m_a \geq 2m_\mu\,, \tag{4.6}$$

and in consequence, both leptonic decay channels are kinematically open. Nevertheless, in order to explain the neutral anomalies via an on-shell ALP, the electron-ALP coupling should dominate. Indeed, it follows from eq. (4.1) that

$$R_{K^{(*)}} \simeq 1 + \frac{\mathcal{B}(B \to K^{(*)} a)}{\mathcal{B}(B \to K^{(*)} e^+ e^-)^{\text{SM}}} \frac{\left(m_\mu^2 \left[(\mathbf{c}_e - \mathbf{c}_L)_{\mu\mu}\right]^2 - m_e^2 \left[(\mathbf{c}_e - \mathbf{c}_L)_{ee}\right]^2\right)}{\left(m_\mu^2 \left[(\mathbf{c}_e - \mathbf{c}_L)_{\mu\mu}\right]^2 + m_e^2 \left[(\mathbf{c}_e - \mathbf{c}_L)_{ee}\right]^2\right)} , \tag{4.7}$$

which requires for $R_{K^{(*)}} < 1$ that

$$\frac{|(\mathbf{c}_e - \mathbf{c}_L)_{ee}|}{|(\mathbf{c}_e - \mathbf{c}_L)_{\mu\mu}|} \geq \frac{m_\mu}{m_e} \sim 200\,. \tag{4.8}$$

It is therefore a good approximation to neglect the ALP-muon couplings in the solutions to the neutral B-anomalies.[12] This has a most important consequence: *the solutions to*

[12]The hierarchy suggests a UV structure with all lepton couplings vanishing, but the electron one. We have verified that this condition is RGE stable, with the induced ALP-muon coupling being two-loop suppressed with respect to the ALP-electron coupling.

JHEP02(2023)138

R_K and R_{K^*} in terms of resonant ALP exchange are basically independent of the precise values of the ALP coupling to leptons, because $\mathcal{B}(a \to e^+e^-) \sim 1$, see eq. (4.1). This is in stark contrast to the B anomaly solutions via a heavy ALP discussed earlier on, or a very light ALP (to be discussed in the next section), for which lepton couplings scale inversely proportional to quark couplings in the solutions to R_K and R_{K^*}, sourcing strong violations of the EFT validity conditions once other independent observables are considered.

On the validity of the NWA. As the use of the Breit-Wigner expression for the ALP propagator is meaningful only as far as the ALP decay rate is smaller than its mass, let us assume a conservative $\Gamma_a/m_a < 1/5$ condition. Given the constraint in eq. (4.8), it is reasonable as a working hypothesis to neglect the muon sector ALP couplings, $(\mathbf{c}_e - \mathbf{c}_L)_{\mu\mu} = 0$. It then follows from eq. (4.5) the constraint

$$\frac{|(\mathbf{c}_e - \mathbf{c}_L)_{ee}|}{f_a} \lesssim \sqrt{\frac{8\,\pi}{5\,m_e^2}} \simeq 4.4 \times 10^3 \text{ GeV}^{-1}\,. \tag{4.9}$$

This result is fairly independent of the ALP mass and is only slightly modified when considering non-vanishing ALP couplings to both electrons and muons. The corresponding numerical analysis is shown in figure 7b, in which the region excluded by the NWA validity is depicted in red. Its vertical border corresponds to eq. (4.9). The horizontal border stems instead from the analogous upper limit that can be set for the ALP-muon couplings by formally setting to zero those for electrons, $(\mathbf{c}_e - \mathbf{c}_L)_{ee} = 0$,

$$\frac{|(\mathbf{c}_e - \mathbf{c}_L)_{\mu\mu}|}{f_a} \lesssim \sqrt{\frac{8\,\pi}{5\,m_\mu^2}} \simeq 21 \text{ GeV}^{-1}\,. \tag{4.10}$$

Prompt ALP decay. The final leptons in the semileptonic B-decays are observed to come from the same point in which the $K^{(*)}$ meson is produced, and therefore the ALP needs to have a prompt decay. Considering the typical boost factors at LHCb, this leads to the requirement [113]

$$\Gamma_a \geq 0.02 \text{ eV}\,. \tag{4.11}$$

Accordingly to the previous discussion, assuming that the ALP decays only into electrons, we find a lower bound on the ALP-electron couplings given by:

$$\frac{|(\mathbf{c}_e - \mathbf{c}_L)_{ee}|}{f_a} \gtrsim \sqrt{\frac{0.16\,\pi \text{ eV}}{m_a\,m_e^2}} \simeq 4.4 \times 10^{-2} \left(\frac{1 \text{ GeV}}{m_a}\right) \text{ GeV}^{-1}\,. \tag{4.12}$$

This determines the vertical frontier of the region excluded by the condition of prompt decay, depicted in grey in figure 7b for the solutions to R_K, see further below. The horizontal frontier in that figure results similarly from the lower bound on muon couplings that follows by formally disregarding the electron contribution in the ALP total decay rate,

$$\frac{|(\mathbf{c}_e - \mathbf{c}_L)_{\mu\mu}|}{f_a} \gtrsim \sqrt{\frac{0.16\,\pi \text{ eV}}{m_a\,m_\mu^2}} \simeq 2.1 \times 10^{-4} \left(\frac{1 \text{ GeV}}{m_a}\right) \text{ GeV}^{-1}\,. \tag{4.13}$$

ΔM_s. We will refrain below from determining the impact of the meson oscillation data on R_K and R_{K^*} in the present case of an on-shell ALP, because the bounds to be obtained from semileptonic B decays are much stronger.

JHEP02(2023)138

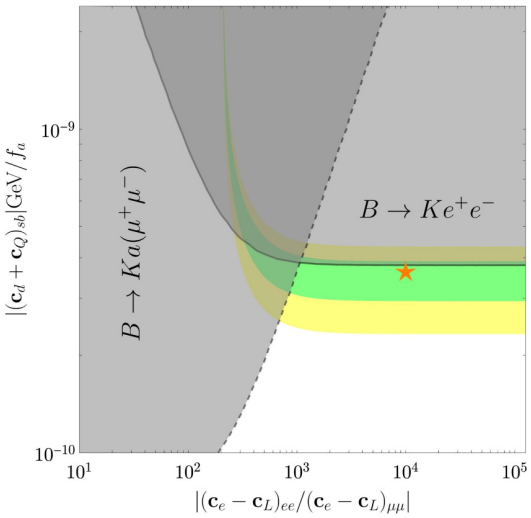

Figure 6. ALP mass within the central bin range. Constraints from semileptonic B-decays on the parameter space of ALP couplings to quarks and leptons. In grey the excluded regions, while in green (yellow) the solutions to R_K at 1σ (2σ). The orange star corresponds to the illustrative benchmark point $m_a = 1.2$ GeV with $(|(\mathbf{c}_e - \mathbf{c}_L)_{ee}|/f_a, |(\mathbf{c}_e - \mathbf{c}_L)_{\mu\mu}|/f_a) = (10^{-1}, 10^{-5})$ GeV^{-1}.

4.1.1 $B \to K\ell^+\ell^-$, R_K and magnetic moments

$B \to K\ell^+\ell^-$. For the range of ALP masses within the central bin range, the data on $B \to Ke^+e^-$ determined in the kinematic region of that bin, $1.1 < q^2 < 6.0$ GeV^2 see table 1, result in the 2σ bound

$$\frac{|(\mathbf{c}_d + \mathbf{c}_Q)_{sb}|}{f_a}\sqrt{\mathcal{B}(a \to e^+e^-)} \lesssim 3.8 \times 10^{-10}\ \text{GeV}^{-1}\,, \tag{4.14}$$

This result is fairly independent of the precise value of m_a as it enters only through a very mild dependence in the f_0 form factor. In the approximation $\mathcal{B}(a \to e^+e^-) \sim 1$, eq. (4.14) would directly imply $|(\mathbf{c}_d + \mathbf{c}_Q)_{sb}|/f_a \lesssim 3.8 \times 10^{-10}$, a bound that gets slightly relaxed though as a consequence of the branching ratio of $a \to e^+e^-$ being different from 1. This can be appreciated in figure 6: the excluded region for $|(\mathbf{c}_d + \mathbf{c}_Q)_{sb}|$ as a function of the ratio of lepton couplings $|(\mathbf{c}_e - \mathbf{c}_L)_{ee}/(\mathbf{c}_e - \mathbf{c}_L)_{\mu\mu}|$ is shown in grey.

The same combination of ALP-quark couplings can be independently bounded from analogous data on $B \to K\mu^+\mu^-$, which stem from dedicated searches at LHCb for exotic resonances as reported in table 1,

$$\frac{|(\mathbf{c}_d + \mathbf{c}_Q)_{sb}|}{f_a}\sqrt{\mathcal{B}(a \to \mu^+\mu^-)} \lesssim 7.4 \times 10^{-11}\ \text{GeV}^{-1}\,. \tag{4.15}$$

This does not translate into stronger bounds on $|(\mathbf{c}_d + \mathbf{c}_Q)_{sb}|$ than those stemming from eq. (4.14), once the values of $\mathcal{B}(a \to \mu^+\mu^-)$ are taken into account in the m_a range under discussion, except in the region where the ratio of leptonic couplings acquires the smallest values, see figure 6.

JHEP02(2023)138

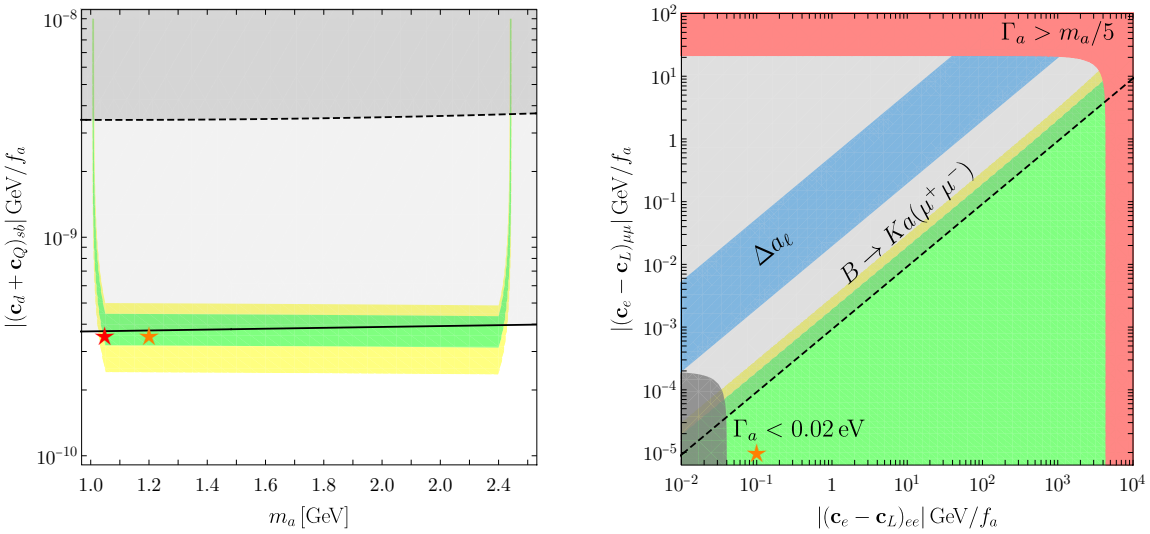

(a) Quark couplings vs. m_a for R_K.

(b) Lepton couplings for R_K.

Figure 7. ALP mass on-shell within the central bin range. In green (yellow) the 1σ (2σ) solutions to R_K. The stars correspond to the benchmark ALP-lepton couplings $(|(\mathbf{c}_e - \mathbf{c}_L)_{ee}|/f_a, |(\mathbf{c}_e - \mathbf{c}_L)_{\mu\mu}|/f_a) = (10^{-1}, 10^{-5})\ \mathrm{GeV}^{-1}$, for two different values of the ALP mass as discussed in the text. On the left: parameter space for ALP-quark couplings vs. m_a. In grey the experimental bounds from $B \to K\mu^+\mu^-$ (enclosed by the dashed line) and $B \to Ke^+e^-$ (enclosed by the solid line). On the right: parameter space $|(\mathbf{c}_e - \mathbf{c}_L)_{ee}|/f_a$ vs. $|(\mathbf{c}_e - \mathbf{c}_L)_{\mu\mu}|/f_a$, for $m_a = 1.2$ GeV and $|(\mathbf{c}_d + \mathbf{c}_Q)_{sb}|/f_a = 3.8 \times 10^{-10}$. The shaded red region corresponds to the exclusion condition $\Gamma_a < m_a/5$ in eqs. (4.9) and (4.10), while the dark grey one to the prompt decay condition in eqs. (4.12) and (4.13). The light grey region is excluded by the LHCb search for an exotic resonance decaying to muons. The blue band shows the parameter space compatible with Δa_μ once the photon coupling is fixed to comply with the Δa_e bound, both quantities taken at the 2σ level.

R_K. The parameter space in which the R_K anomaly can be explained through the on-shell exchange of an ALP within one (two) sigma is depicted in green (yellow) in the plots that follow. In all of them, the orange star corresponds to the illustrative benchmark point $m_a = 1.2$ GeV and $(|(\mathbf{c}_e - \mathbf{c}_L)_{ee}|/f_a, |(\mathbf{c}_e - \mathbf{c}_L)_{\mu\mu}|/f_a) = (10^{-1}, 10^{-5})\ \mathrm{GeV}^{-1}$. The parameter space is depicted as a function of:

- Quark couplings vs. lepton couplings in figure 6, for an ALP mass $m_a = 1.2$ GeV.
- Quark couplings vs. ALP mass in figure 7a. The limit on quark couplings obtained above, eq. (4.14), is depicted as a continuous line.
- Muon couplings vs. electron couplings in figure 7b, also for $m_a = 1.2$ GeV and for quark coupling values which saturate eq. (4.14). The upper-left half of the parameter space in this plot (in light grey) is excluded by the constraint in eq. (4.15); this constraint turns out to be stronger than that in eq. (4.8).

These figures indicate that indeed R_K could be explained by the on-shell exchange of an ALP and furthermore that the validity of the ALP EFT is maintained for those

JHEP02(2023)138

Observable	m_a^2 [GeV^2]	Values	$\lvert(\mathbf{c}_d - \mathbf{c}_Q)_{sb}\rvert\sqrt{\mathcal{B}_{a\to\ell^+\ell^-}}/f_a$[GeV^{-1}]
$\mathcal{B}(B^0 \to K^{0*}a(e^+e^-))$	$(0.0004, 0.05)$	$< 1.344 \times 10^{-7}$	$< 7.96 \times 10^{-10}$
	$(0.05, 0.15)$	$< 1.22 \times 10^{-8}$	$< 2.40 \times 10^{-10}$
	$(0.25, 0.4)$	$< 1.97 \times 10^{-8}$	$< 3.05 \times 10^{-10}$
	$(0.4, 0.7)$	$< 1.74 \times 10^{-8}$	$< 2.87 \times 10^{-10}$
	$(0.7, 1)$	$< 6.5 \times 10^{-9}$	$< 1.75 \times 10^{-10}$
$\mathcal{B}(B^0 \to K^{0*}a(\mu^+\mu^-))$	$(0.05, 18.9)$	$< 3 \times 10^{-9}$ [92]	$< 1.19 \times 10^{-10}$
$\mathcal{B}(B^0 \to K^{0*}e^+e^-)$	$(1.1, 6)$	$(1.8 \pm 0.6) \times 10^{-7}$ [91]	$< 6.46 \times 10^{-10}$
	$(0.1, 8)$	$(3.7 \pm 1.0) \times 10^{-7}$ [91]	$< 8.71 \times 10^{-10}$

Table 2. Constraints on the ALP-quark coupling from $B \to K^*\ell^+\ell^-$ and $B \to K^*a(a \to \ell^+\ell^-)$ decay processes used in the following figures of this section. The bounds in the last column are expressed at the 2σ level. For each bound, the value of m_a considered lies in the middle of the corresponding energy bin window. The values presented in the third column are those in table 1 and are copied here for convenience.

solutions which are located towards the lower left corner of figure 7b, an example being the benchmark point indicated by the orange star.

Anomalous magnetic moment of the electron and the muon. The analysis of anomalous magnetic moments for a heavy ALP applies as well to the resonant ALP considered in this section, because m_a is still larger than the electron and muon masses, and in consequence the expression in eq. (3.28) holds. It results that, taking now the value $m_a = 1.2\,\text{GeV}$, the bounds on the right hand side of eqs. (3.31) and eq. (3.32) are now multiplied by a factor ~ 0.8. Once again, it would be possible to remain within the EFT validity range and account simultaneously for the data in the set $\{R_K, \Delta a_e\}$ or for those of the two anomalies, $\{R_K, \Delta a_\mu\}$, while it would not be possible to account simultaneously for the data on the three observables $\{R_K, \Delta a_e, \Delta a_\mu\}$. Indeed, the blue region in figure 7b, for which the ALP-couplings are required within 2σ to both respect the Δa_e bound and to account for the a_μ anomaly falls outside the parameter space that would explain R_K.

4.1.2 $B \to K^*\ell^+\ell^-$, R_{K^*}, $B_s \to \ell^+\ell^-$ and magnetic moments

While $B \to K\ell^+\ell^-$ offered light on $|(\mathbf{c}_d + \mathbf{c}_Q)_{sb}|$, $B \to K^*\ell^+\ell^-$ tests the orthogonal combination $|(\mathbf{c}_d - \mathbf{c}_Q)_{sb}|$.

The experimental information on the decay $B \to K^*e^+e^-$ is more detailed than for its $B \to K$ counterpart, see table 2. The bounds on NP presented in the first row of this table and divided in several small-energy bins were not provided by the experimental collaborations, but are instead a recast from bounds on the differential distribution of the total number of events N, $dN/dq^2(B \to K^*e^+e^-)$, provided by the LHCb collaboration in their search of resonant new particles [114]; see appendix C for details.

Still regarding the electron channel, the constraints in the third block of table 2 result form the integration over two large windows in energy-bins [91], and they apply to the total

JHEP02(2023)138

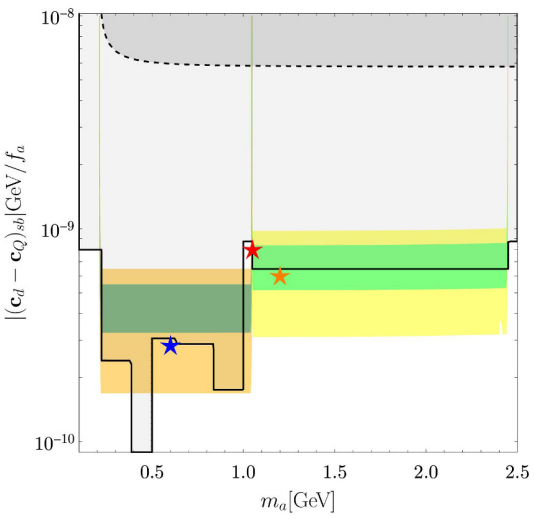

(a) Quark couplings vs. m_a for R_{K^*}.

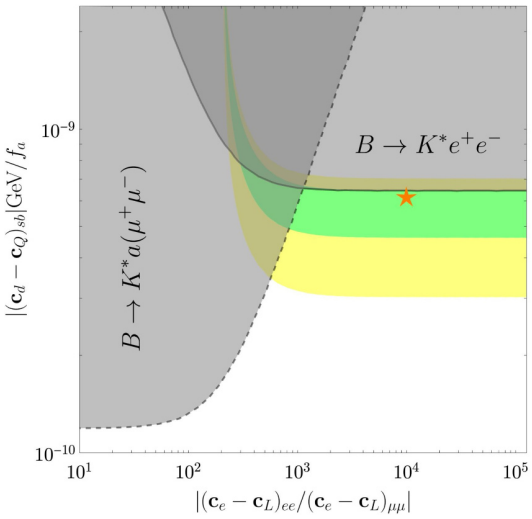

(b) Quark couplings vs. lepton coupling ratio for R_{K^*}.

Figure 8. Solutions to R_{K^*} with ALP masses within the bin window ranges. In green (yellow) the 1σ (2σ) solutions to the central bin. The coloured stars correspond to the benchmark ALP-lepton couplings $(|(\mathbf{c}_e - \mathbf{c}_L)_{ee}|/f_a, |(\mathbf{c}_e - \mathbf{c}_L)_{\mu\mu}|/f_a) = (10^{-1}, 10^{-5})$ GeV^{-1}, for different values of m_a. On the left: parameter space of ALP-quark couplings vs. m_a excluded by $B \to K^*\mu^+\mu^-$ data (enclosed by the dashed line) and by $B \to K^*e^+e^-$ data (enclosed by the solid line). For $m_a \in [0.39, 0.5]$ GeV data show a tension of more than 2σ with respect to the SM prediction and the additional contribution of the ALP could only worsen it (see figure 16). The dark green (dark yellow) shaded areas indicate ALP solutions to R_{K^*} low bin at 1σ (2σ). On the right: constraints from semileptonic B-decays on the parameter space of ALP couplings to quarks and leptons, for the reference value $m_a = 1.2$ GeV. In grey the regions excluded by $B \to K^{(*)}\mu^+\mu^-$ data (enclosed by the dashed line) and $B \to K^{(*)}e^+e^-$ data (enclosed by the solid line).

branching ratio which includes both the SM and the NP contributions. The limits involving the combination of ALP-quark couplings $|(\mathbf{c}_d - \mathbf{c}_Q)_{sb}|$ derived from the data and shown in the table have been extracted using the complete dependence on them. Finally, once again, the apparently stronger limits on those couplings in the last column which stem from muon channels turn out to be in fact weaker in a large fraction of the parameter space, once the true values of $\mathcal{B}_{a\to\ell^+\ell^-}$ are taken into account. This is illustrated in figure 8a for the specific value of the ALP-lepton couplings $(|(\mathbf{c}_e - \mathbf{c}_L)_{ee}|/f_a, |(\mathbf{c}_e - \mathbf{c}_L)_{\mu\mu}|/f_a) = (10^{-1}, 10^{-5})$ GeV^{-1}. Figure 8b focuses on the central energy bin and for the illustrative case $m_a = 1.2$ GeV: it shows that the constraint due to $B \to K^*e^+e^-$ depends only mildly on the ratio of ALP-lepton couplings. Once this ratio gets smaller enough, the dominant bound is provided by the $B \to K^*a(\mu^+\mu^-)$ decay instead. The plots in figure 8 are the siblings of those in figures 7a and 6, respectively, and the same colour code has been used.

The bounds obtained from $B \to K^*e^+e^-$ — see table 2 — can be used as conservative benchmarks for the ALP-quark couplings in our numerical analysis. Specifically, figure 9a and figure 9b illustrate the parameter space of ALP-couplings to leptons which can explain

JHEP02(2023)138

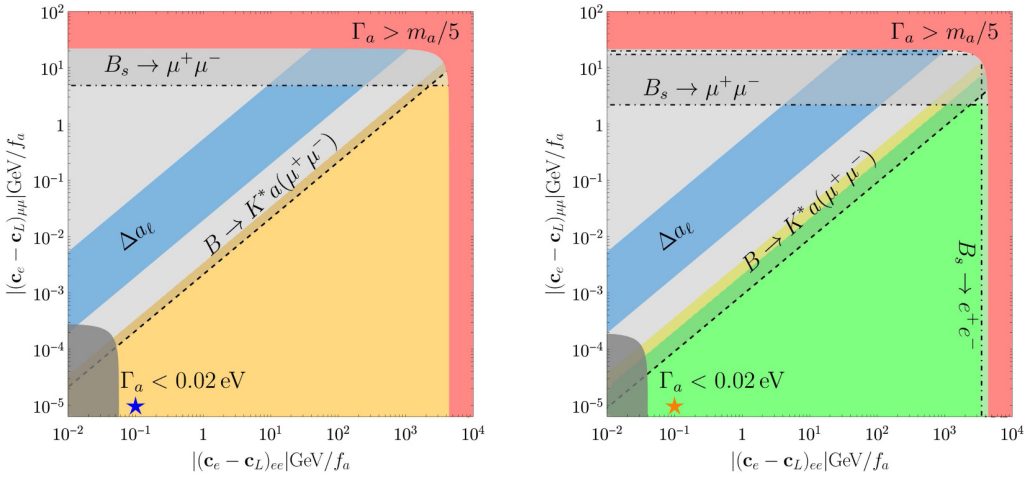

(a) Low bin R_{K^*}. **(b)** Central bin R_{K^*}.

Figure 9. ALP mass within the R_{K^*} bin windows. Parameter space $|(\mathbf{c}_e - \mathbf{c}_L)_{ee}|/f_a$ vs. $|(\mathbf{c}_e - \mathbf{c}_L)_{\mu\mu}|/f_a$ that solves the R_{K^*} anomaly, in the low energy-bin on the left and in the central energy-bin on the right. In green (yellow) the 1σ (2σ) sensitivity. The ALP mass is chosen to be $m_a = 0.6$ GeV ($m_a = 1.2$ GeV) on the left (right) plot together with, respectively, the values $|(\mathbf{c}_d - \mathbf{c}_Q)_{sb}|/f_a = 3.05 \times 10^{-10}\text{GeV}^{-1}$ and $|(\mathbf{c}_d - \mathbf{c}_Q)_{sb}|/f_a = 6.46 \times 10^{-10}\text{GeV}^{-1}$, chosen to comply with the $B \to K^* e^+ e^-$ bounds. The shaded red region corresponds to the exclusion condition $\Gamma_a < m_a/5$, while the dark grey one to the prompt decay condition. The light grey region delimited by an oblique dashed line is excluded by the LHCb search for an exotic resonance decaying to muons. The light grey regions delimited by horizontal and vertical dot-dashed lines are excluded by $B_s \to \mu^+\mu^-$ and $B_s \to e^+e^-$ data, respectively. The blue band shows the parameter space compatible with Δa_μ once the photon coupling is fixed to comply with bounds on Δa_e.

R_{K^*} via resonant ALP exchange, for the benchmark values

$$\frac{|(\mathbf{c}_d - \mathbf{c}_Q)_{sb}|}{f_a} = 3.05 \times 10^{-10}\text{GeV}^{-1} \quad , \quad \frac{|(\mathbf{c}_d - \mathbf{c}_Q)_{sb}|}{f_a} = 6.46 \times 10^{-10}\text{GeV}^{-1} \, , \tag{4.16}$$

respectively for the low bin ($m_a = 0.6$ GeV, blue star) and the central bin ($m_a = 1.2$ GeV, orange star). In both figures, the stars correspond to the (previously used) values of leptonic couplings $(|(\mathbf{c}_e - \mathbf{c}_L)_{ee}|/f_a, |(\mathbf{c}_e - \mathbf{c}_L)_{\mu\mu}|/f_a) = (10^{-1}, 10^{-5})$ GeV^{-1}.

These plots in figure 9 for R_{K^*} are very similar to that for R_K in figure 7b, and use the same colour code. Once again, the limits on ALP leptonic couplings from $B \to K^* a(\ell^+\ell^-)$ severely limit the allowed parameter space, in addition to those resulting from the validity conditions for the NWA and for prompt ALP decays in eqs. (4.9)–(4.13). On the other hand, the bounds from $B_s \to \ell^+\ell^-$ are at best of the same order of magnitude than the ones just mentioned. All in all, the lower-left area of the parameter space is the region where possible explanations to the R_{K^*} anomaly can be found within the validity range of the ALP EFT.

Finally, the compatibility of the data on leptonic anomalous magnetic moments and the solutions to the R_{K^*} anomaly through on-shell ALP exchange parallels the analysis for R_K in the previous subsection: when all data available are taken into account, it is

JHEP02(2023)138

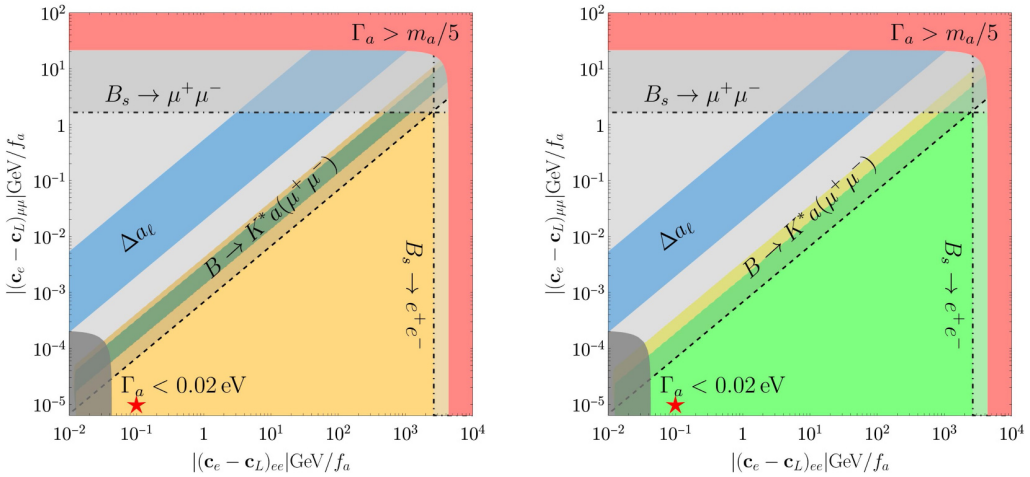

(a) Low bin R_{K^*}. Golden m_a. **(b)** Central bin R_{K^*}. Golden m_a.

Figure 10. Parameter space $|(\mathbf{c}_e - \mathbf{c}_L)_{ee}|/f_a$ vs. $|(\mathbf{c}_e - \mathbf{c}_L)_{\mu\mu}|/f_a$ interesting to explain the R_{K^*} anomaly, in the low energy-bin on the left and in the central energy-bin on the right, for the golden mass $m_a = \sqrt{1.1}$ GeV. In green (yellow) the 1σ (2σ) sensitivity. The ALP-quark coupling is fixed to $|(\mathbf{c}_d - \mathbf{c}_Q)_{sb}|/f_a = 8.71 \times 10^{-10}\text{GeV}^{-1}$. The colour code and lines follow the same description as in figure 9.

possible to account simultaneously for the data in the set $\{R_{K^*}, \Delta a_e\}$ within the theoretical region of validity of the ALP EFT. In contrast, the ensemble of the three observables $\{R_{K^*}, \Delta a_e, \Delta a_\mu\}$ cannot be simultaneously explained through such an ALP, see figure 9, and thus the Δa_μ anomaly would remain unexplained.

4.1.3 The golden mass

The analysis above explored whether R_K and the central-energy bin of R_{K^*} could be explained via ALP exchange, while the low-energy bin of the R_{K^*} anomaly was analysed separately. The respective benchmarks points were $m_a = 1.2$ GeV (orange star in figures 6, 7, 8 and 9b) and $m_a = 0.6$ GeV (blue star in figures 8a and 9a). It is a pertinent question, though, whether there exists some value of the ALP mass which could explain the data on all three neutral B anomalies, i.e. R_K and the two energy bins for R_{K^*}. We have identified a "golden mass" solution which could satisfy these three requirements within 2σ sensitivity (in yellow), located right at the edge of the two energy-bin windows, and which corresponds to

$$m_a = \sqrt{1.1}\ \text{GeV}\,. \tag{4.17}$$

This point is indicated by a red star in figures 7a, 8a and 10.

In particular, figure 10 depicts the same plots as those in figure 9 except that m_a is taken to be the golden mass value, indicated by the red star.[13] This figure shows that the exchange of an ALP with the mass given by eq. (4.17) could *a priori* account for the

[13]For this m_a value, the benchmark quark couplings that saturate the constraints from $B \to K^* e^+ e^-$ data are slightly different than those used previously: $|(\mathbf{c}_d - \mathbf{c}_Q)_{sb}|/f_a = 8.71 \times 10^{-10}\text{GeV}^{-1}$.

JHEP02(2023)138

anomalies in both energy bins of R_{K^*} within 2σ (in yellow). This result is strongly dependent on the value of the ALP-quark couplings, which ultimately regulates the impact of the on-shell contribution. Indeed, for smaller ALP-quark couplings, the resonant contributions disappear and no-overlap region is left between the low and central energy-bin anomalies.

The dependence on the ALP mass of the solutions to R_{K^*} is further scrutinised going back to figure 8a. It shows that:

- Within 1σ sensitivity (in green), all ALP solutions with masses within the low-energy bin of the R_{K^*} anomaly are excluded by other data. This conclusion agrees with that in ref. [113], where the parameter space of a generic resonance compatible only with this low bin anomaly was studied.

- The comparison with figure 7a shows that any ALP mass within the central bin range of R_{K^*} can accommodate a combined explanation of the two anomalies in the set $\{R_K, R_{K^*}\}$ within less than 2σ, for $\mathbf{c}_d \approx 3 \times 10^{-10}$ (which corresponds to $\mathcal{B}(B \to Ka) \sim 10^{-8}$). This possible explanation for the two neutral B anomalies via a resonance on the bin is a novel aspect of our work.

- Finally, the location of the red star in figure 7a and figure 8a illustrates that the on-shell exchange of a golden mass ALP could simultaneously account for the R_K anomaly *and* for the two anomalies in the two different R_{K^*} energy bins. The details of the mass dependence can be appreciated in the zoom-in view around the golden mass value depicted in figure 11.

Nevertheless, in spite of this last encouraging result, explanations of physics anomalies located at the frontier of energy bins are suspicious. The take-away message is that a different binning of the data is well-motivated and can quickly clarify the issue.

4.2 ALP mass close to the bin window: the smearing function

The aim of this section is twofold: the first is to consider the case in which the ALP mass is outside, but close to, a given energy-bin window; the second is to include in the previous analysis the finite experimental sensitivity. Indeed, if the value of the ALP mass lies outside the energy-bin window, the ALP is technically off-shell and its contribution to observables gets thus suppressed. On the other side, the experimental resolution in terms of bin distribution is not infinite and therefore it is possible that certain events with a q^2 close to the borders of a chosen window are simply not correctly taken into account.

To take into consideration these two sources of systematic errors, a Gaussian smearing function is traditionally adopted to modify the NWA expression. For the case of the semileptonic B-meson decays in eq. (4.1), it reads [113]

$$\mathcal{B}(B \to K^{(*)} a(\ell^+\ell^-)) = \mathcal{B}(B \to K^{(*)} a) \times \mathcal{B}(a \to \ell^+\ell^-) \times \mathcal{G}^{(r_\ell)}(q_{\text{min.}}, q_{\text{max.}})\,, \tag{4.18}$$

where $\mathcal{G}^{(r_\ell)}$ is a Gaussian smearing function defined as

$$\mathcal{G}^{(r_\ell)}(q_{\text{min.}}, q_{\text{max.}}) \equiv \frac{1}{\sqrt{2\pi} r_\ell} \int_{q_{\text{min.}}}^{q_{\text{max.}}} \mathrm{d}|q|\, e^{-\frac{(|q|-m_a)^2}{2r_\ell^2}}\,, \tag{4.19}$$

JHEP02(2023)138

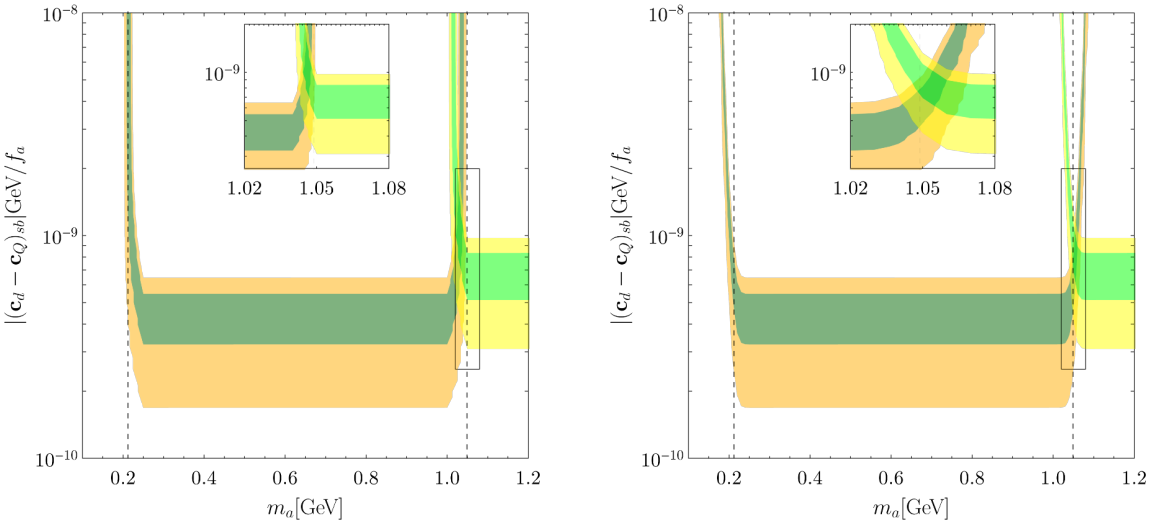

(a) Without smearing function.

(b) With smearing function.

Figure 11. Golden ALP mass. Impact of the smearing function in (a selected region of) the parameter space m_a vs. $|(\mathbf{c}_d - \mathbf{c}_Q)_{sb}|/f_a$ for the R_{K^*} anomaly. On the left (right) the case without (with) the effect of the smearing function. The benchmark point for the ALP-lepton couplings is $(|(\mathbf{c}_e - \mathbf{c}_L)_{ee}|/f_a, |(\mathbf{c}_e - \mathbf{c}_L)_{\mu\mu}|/f_a) = (10^{-1}, 10^{-5})$ GeV^{-1}. In green (yellow) the $1\sigma(2\sigma)$ allowed region for the low and central energy-bin window, with the darker colours corresponding to the low bin.

where $r_e = 10$ MeV [115] and $r_\mu = 2$ MeV [116] refer to the di-lepton mass resolution of the LHCb detector, and the boundaries of the integration range correspond to the extremes of the considered energy-bin window. The net effect of this function is to broaden the distributions found in the previous section near the borders of the energy-bin windows. We will explicitly show the impact of this smearing on the analysis of R_{K^*} in two mass ranges corresponding respectively to: the golden mass solution in between the two energy-bin windows, and the lowest energies within the low-energy bin region.

The golden mass solution. In figure 11 we zoom in the relevant part of the parameter space for R_{K^*} showed in figure 8a, for the same benchmark point of the ALP-lepton couplings. The impact of the smearing function around the golden mass region can be appreciated in figure 11b, as compared to figure 11a which does not include smearing effects. The overlap at the 2σ level of the ALP solutions common to the low and central energy-bin anomalies broadens now to an interval around the precise value $m_a = \sqrt{1.1}$ GeV, given by

$$m_a \in [1.04\,, 1.07]\ \text{GeV}\,. \tag{4.20}$$

The kinematic solution to the low-bin anomaly. Let us focus now instead on the lower boundary of the low-energy bin of R_{K^*}. This is of particular interest because this boundary is higher than the di-muon threshold: an ALP with mass $m_a < 2m_\mu$ cannot decay into muons but only into electrons, which *a priori* opens the possibility of a kinematic

JHEP02(2023)138

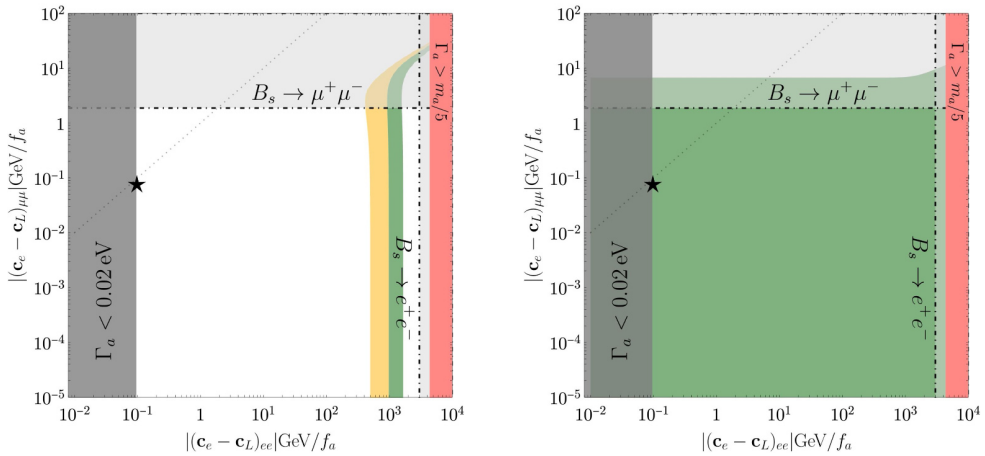

(a) Without smearing function. **(b)** With smearing function.

Figure 12. ALP mass just under the low bin window. Impact of the smearing function in the parameter space $|(\mathbf{c}_e - \mathbf{c}_L)_{ee}|/f_a$ vs. $|(\mathbf{c}_e - \mathbf{c}_L)_{\mu\mu}|/f_a$ of solutions to the low bin R_{K^*} anomaly; $1\sigma(2\sigma)$ allowed regions depicted in green (yellow), for $m_a = 210$ MeV and $|(\mathbf{c}_d - \mathbf{c}_Q)_{sb}|/f_a = 7.96 \times 10^{-10}$ GeV^{-1}. The figure on the left (right), does not (does) include the smearing function. The dotted line represents the flavour universal setup for the lepton couplings and the black star the smallest allowed value. The dark grey regions are excluded by the prompt decay condition, while the light grey ones are excluded by $B_s \to \ell^+\ell^-$ data.

explanation of the low energy-bin R_{K^*} anomaly [113]. While this is not possible without the effect of the smearing function, as shown in the previous section, now it appears to be a viable possibility, see figure 11b.

The kinematic solution is further illustrated in figure 12 for the particular case of an ALP mass slightly below the di-muon threshold, $m_a = 210$ MeV. The allowed parameter space for lepton couplings is depicted (the ALP-quark coupling has been fixed to a reference value that allows us to avoid conflict with the semileptonic B-decay constraints). The comparison of the left and right plots of this figure shows that the effect of the smearing is to substantially enlarge the relevant 2σ region that explains the anomaly. Furthermore, an oblique dotted line in these plots indicates the location of the flavour universal solutions: the particular case analysed in ref. [44] is represented by a black star and shown to be excluded without smearing effects and viable once smearing effects are included. The expectation is that the future experimental improvements in these observables will increase the sensitivity and thus the effect of the smearing will get progressively reduced; in the absence of a discovery, the realistic analysis should ultimately converge towards figure 12a as final result.

4.3 Impact of sizeable couplings

We have previously discussed that a large ALP-electron coupling induces a non-negligible ALP-photon coupling in the context of $(g-2)$ data. A similar effect occurs for flavour-violating couplings of the ALP to quarks, which are generated by the ALP-electron coupling

JHEP02(2023)138

at the two-loop level.[14] Indeed, given the large $|(\mathbf{c}_e - \mathbf{c}_L)_{ee}|$ values required to explain the neutral B-anomalies and the very high precision on some data, these effects might become, in some cases, relevant for the present study. It is beyond the scope of the present work to include such effects in the analysis. However, following the discussion in ref. [44], we remark that the loop induced ALP-bs coupling could become larger than the value in eq. (4.14). The experimental bound on $\mathcal{B}(B \to K e^+ e^-)$ in fact applies to the effective coupling

$$\frac{(\mathbf{c}_d + \mathbf{c}_Q)_{sb}}{f_a} \sim \frac{(\mathbf{c}_d + \mathbf{c}_Q)^{\text{tree}}_{sb}}{f_a} + \frac{\alpha^2_{em}}{s^4_w (4\pi)^2} \frac{(\mathbf{c}_L)_{ee}}{f_a} \log \frac{\Lambda}{m_B} \,, \tag{4.21}$$

as it can be estimated from the renormalization group equations of the ALP EFT. Hence, as we discussed in the context of magnetic moments, a cancellation between tree and loop level contributions can become necessary in order to satisfy this experimental constraint. Note that this type of fine-tuning can be avoided in certain UV models, such as those producing only right-handed lepton couplings to the ALP, where this loop contribution can be naturally suppressed.

5 Very light ALP

We address next whether the neutral B anomalies could be mediated by ALPs even lighter than those discussed in the previous section, that is lighter than twice the muon mass. In consequence, the ALP cannot decay into two muons but it can decay into two electrons.

Astrophysical constraints on non-negligible ALP-electron couplings [44] exclude ALPs lighter than 1 MeV, though, and in consequence, the range of masses to be explored in this section is

$$1 \text{ MeV} < m_a \lesssim 2\, m_\mu \,. \tag{5.1}$$

For this range of masses, additional bounds from Beam Dump experiments and from supernova data analysis constrain the possible values for the ALP-electron coupling to be outside of a small interval [44], approximately $|(c_e - c_L)_{ee}|/f_a \notin [10^{-4}, 10^{-1}]$ GeV^{-1} and $[10^{-6}, 10^{-4}]$ GeV^{-1}, respectively.

Furthermore, for $m_a < 2m_\mu$, astrophysical upper limits on the ratio between the effective ALP-photon couplings and the scale f_a would be very strong, of the order of 10^{-11} GeV^{-1},[15] but they can be evaded using the freedom on the value of the tree-level $c_{a\gamma\gamma}$ coefficient in eq. (2.6).

A peculiar feature of this mass regime is the similarity of the final expressions for R_K and R_{K^*} with those in the heavy ALP scenario discussed in section 3. Indeed, for $m_a^2 \ll q^2$, the m_a dependence in the ALP propagator can be neglected, which leaves only its q^2 dependence. Once the integration over q^2 is performed with Flavio and EOS, the final expressions for the SM plus ALP contributions to $B \to K^{(*)} \ell^+ \ell^-$ read, for the central

[14] We thank the referee for recalling the relevance of the two-loop effects in these couplings.

[15] Even stronger bounds could follow from cosmological constraints, which however depend on the specific assumption of the cosmological model considered.

JHEP02(2023)138

bin of $B \to K$ semileptonic decays,

$$\begin{aligned}\mathcal{B}(B \to K\mu^+\mu^-)^{6.0\ \text{GeV}^2}_{1.1\ \text{GeV}^2} &= 10^{-7} \times \left(1.5 - 2.4 \times 10^{-2}\, \widetilde{C}^{\mu}_{P_+} + 6.6 \times 10^{-3}\, \widetilde{C}^{\mu 2}_{P_+}\right) , \\ \mathcal{B}(B \to Ke^+e^-)^{6.0\ \text{GeV}^2}_{1.1\ \text{GeV}^2} &= 10^{-7} \times \left(1.5 - 1.2 \times 10^{-4}\, \widetilde{C}^{e}_{P_+} + 6.7 \times 10^{-3}\, \widetilde{C}^{e 2}_{P_+}\right) ,\end{aligned} \tag{5.2}$$

while for the central bin of $B \to K^*$ semileptonic transitions, it results

$$\begin{aligned}\mathcal{B}(B \to K^*\mu^+\mu^-)^{6.0\ \text{GeV}^2}_{1.1\ \text{GeV}^2} &= 10^{-7} \times \left(1.9 - 2.3 \times 10^{-2}\, \widetilde{C}^{\mu}_{P_-} + 6.2 \times 10^{-2}\, \widetilde{C}^{\mu 2}_{P_-}\right) , \\ \mathcal{B}(B \to K^*e^+e^-)^{6.0\ \text{GeV}^2}_{1.1\ \text{GeV}^2} &= 10^{-7} \times \left(1.9 - 1.1 \times 10^{-4}\, \widetilde{C}^{e}_{P_-} + 6.3 \times 10^{-3}\, \widetilde{C}^{e 2}_{P_-}\right) ,\end{aligned} \tag{5.3}$$

and for its low-energy bin they read

$$\begin{aligned}\mathcal{B}(B \to K^*\mu^+\mu^-)^{1.1\ \text{GeV}^2}_{0.045\ \text{GeV}^2} &= 10^{-7} \times \left(1.2 - 2.4 \times 10^{-2}\, \widetilde{C}^{\mu}_{P_-} + 6.3 \times 10^{-3}\, \widetilde{C}^{\mu 2}_{P_-}\right) , \\ \mathcal{B}(B \to K^*e^+e^-)^{1.1\ \text{GeV}^2}_{0.045\ \text{GeV}^2} &= 10^{-7} \times \left(1.3 - 1.4 \times 10^{-4}\, \widetilde{C}^{e}_{P_-} + 7.7 \times 10^{-3}\, \widetilde{C}^{e 2}_{P_-}\right) .\end{aligned} \tag{5.4}$$

For all these quantities, the theoretical error is estimated to be $\mathcal{O}(15)\%$. The comparison of these expressions with their corresponding siblings for the heavy ALP case in eqs. (3.12), (3.34) and (3.35) shows that the numerical coefficients in front of the NP Wilson coefficients have a similar order of magnitude, and similar considerations can be applied to the analysis of both cases. Using the available data on non-resonant searches presented in table 1, the 2σ bounds on the corresponding Wilson coefficients read:

$$\begin{aligned}\widetilde{C}^{e}_{P_+} &\in [-8.3, 8.3] , \qquad \widetilde{C}^{\mu}_{P_+} \in [-4.2, 7.8] , \\ \widetilde{C}^{e}_{P_-} &\in [-14.0, 14.0] , \quad \widetilde{C}^{\mu}_{P_-} \in [-4.8, 5.1] .\end{aligned} \tag{5.5}$$

Before proceeding to compare with other observables, it is useful to rewrite these $\widetilde{C}^{\ell}_{P_\pm}$ coefficients in terms of ALP-fermion couplings. They can be expressed in terms of the $C^{\ell}_{P_\pm}$ coefficients defined in eq. (3.6) as

$$\widetilde{C}^{\ell}_{P_\pm} \equiv -m_a^2 \frac{C^{\ell}_{P_\pm}}{\text{GeV}^2} = -\frac{2\sqrt{2}\pi}{\alpha_{\text{em}} G_F V_{tb} V_{ts}^*} \frac{m_\ell}{(f_a\ \text{GeV})^2} (m_s \mp m_b) \left(\mathbf{K}_d^{S,P}\right)_{sb} \left(\mathbf{K}_e^{P}\right)_{\ell\ell} . \tag{5.6}$$

which can be simplified to

$$\begin{aligned}\widetilde{C}^{e}_{P_\pm} &\approx \pm 1.3 \times 10^{6}\ \text{GeV}^2\, \frac{(\mathbf{c}_d \pm \mathbf{c}_Q)_{sb}}{f_a} \frac{(\mathbf{c}_e - \mathbf{c}_L)_{ee}}{f_a} , \\ \widetilde{C}^{\mu}_{P_\pm} &\approx \pm 2.7 \times 10^{8}\ \text{GeV}^2\, \frac{(\mathbf{c}_d \pm \mathbf{c}_Q)_{sb}}{f_a} \frac{(\mathbf{c}_e - \mathbf{c}_L)_{\mu\mu}}{f_a} .\end{aligned} \tag{5.7}$$

Note that these relations are independent of the specific value of the ALP mass, in contrast with the case of a heavy ALP, see eq. (3.17).

5.1 R_K, ΔM_s and magnetic moments

R_K. In the illustrative case $\widetilde{C}^{\mu}_{P_+} = 0$, the regions in parameter space which now allow to explain R_K within the 2σ region are $\widetilde{C}^{e}_{P_+} \in [-8.2, -3.9] \vee [4.0, 8.2]$. When the complete

JHEP02(2023)138

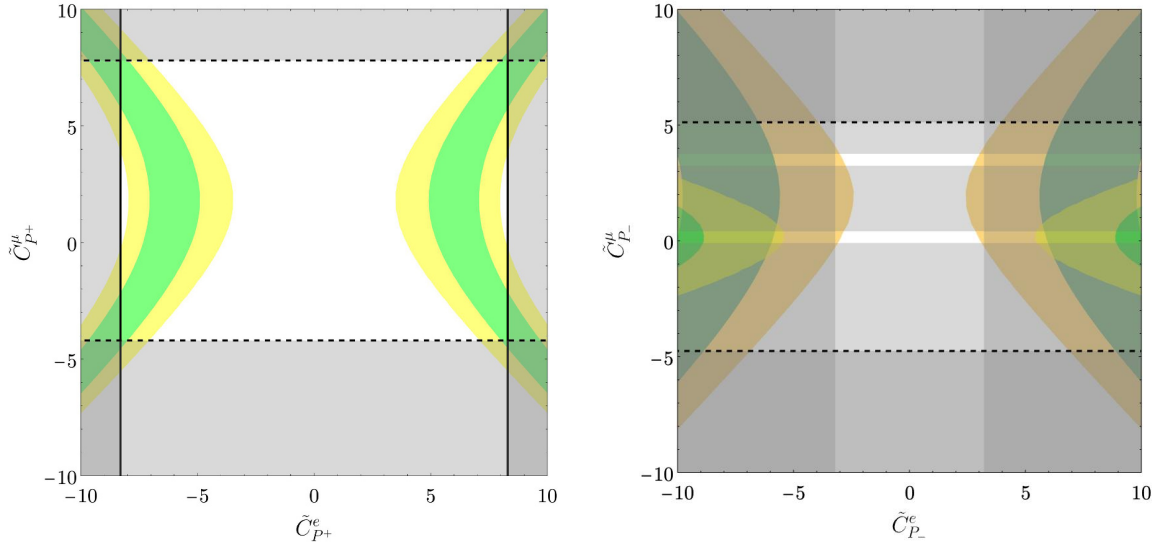

(a) R_K. **(b)** R_{K^*}.

Figure 13. Parameter space for R_K (left) and R_{K^*}(right) for an ALP lighter than $2m_\mu$. In light yellow and light green are respectively depicted the 1σ and 2σ solutions to the central bin of R_{K^*}, while darker shades of those colours on the right plot denote the corresponding solutions for the low bin of R_{K^*}. The grey regions around the frame of the figures are excluded at 2σ by data on semileptonic $B \to K^{(*)}\mu^+\mu^-$ (dashed black contours) decays, and on the left plot also by $B \to Ke^+e^-$ data (solid black contours). On the right plot, regions excluded by purely leptonic B_s decays reach the central area and are also depicted in grey.

bi-dimensional parameter space $\{C^e_{P_+}, C^\mu_{P_+}\}$ is considered, the allowed regions in parameter space can be seen in figure 13a, leading to the 2σ allowed range:

$$\begin{aligned} \widetilde{C}^e_{P_+} &\in [-8.3,\, -3.5] \vee [3.5,\, 8.3]\,, \\ \widetilde{C}^\mu_{P_+} &\in [-4.2,\, 7.8]\,, \end{aligned} \tag{5.8}$$

where the bounds which stem from the data on semileptonic $B \to K$ decays have already been taken into account. Comparing these results with the expressions in eq. (5.7), a naive estimation for the ratio between electron-ALP and muon-ALP couplings is obtained:

$$\left|\frac{(\mathbf{c}_e - \mathbf{c}_L)_{\mu\mu}}{(\mathbf{c}_e - \mathbf{c}_L)_{ee}}\right| \approx 4.8 \times 10^{-3} \left|\frac{\widetilde{C}^\mu_{P_+}}{\widetilde{C}^e_{P_+}}\right| \lesssim 10^{-2}\,. \tag{5.9}$$

ΔM_s. The data on meson oscillations provide bounds on quark-ALP couplings similar to those previously obtained for the heavy ALP,[16]

$$\frac{(\mathbf{c}_d \pm \mathbf{c}_Q)_{sb}}{f_a} \lesssim 10^{-5}\ \text{GeV}^{-1}\,, \tag{5.10}$$

[16]Stronger bounds will be obtained further below from semileptonic resonant searches for $(\mathbf{c}_d - \mathbf{c}_Q)_{sb}$ in a particular range of m_a, see eq. (5.22).

JHEP02(2023)138

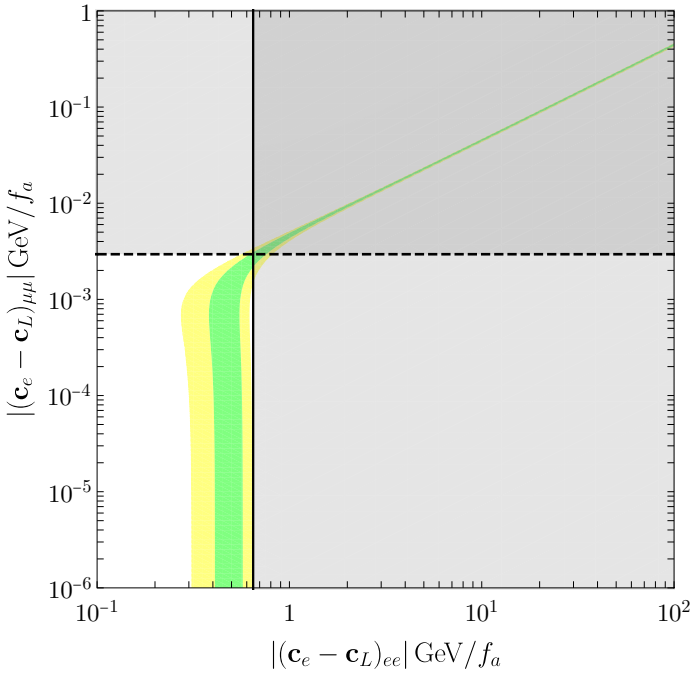

Figure 14. Very light ALP ($m_a \leq 2m_\mu$). Parameter space $(\mathbf{c}_e - \mathbf{c}_L)_{ee}/f_a$ vs. $(\mathbf{c}_e - \mathbf{c}_L)_{\mu\mu}/f_a$ that solves the R_K anomaly assuming $(\mathbf{c}_Q + \mathbf{c}_d)_{sb}/f_a = 10^{-5}$ GeV^{-1}. The green (yellow) regions correspond to the allowed parameter space at 1σ (2σ). In grey are represented the experimental bounds from $B \to K\mu^+\mu^-$ (enclosed by the dashed line) and $B \to Ke^+e^-$ (enclosed by the solid line).

which, taking into account eq. (5.7) and the range of solutions for R_K in eq. (5.8), implies

$$\frac{|\,(\mathbf{c}_e - \mathbf{c}_L)_{ee}\,|}{f_a} \gtrsim 0.3\ \text{GeV}^{-1}\,, \qquad \frac{|\,(\mathbf{c}_e - \mathbf{c}_L)_{\mu\mu}\,|}{f_a} \gtrsim 1.6 \times 10^{-3}\ \text{GeV}^{-1}\,, \tag{5.11}$$

in order to solve R_K. At least for the electron case, these large values for ALP-lepton coupling are borderline with respect to the validity of the EFT.

Anomalous magnetic moment of the electron and the muon. Similarly to the case of larger m_a values explored in previous sections, for the very light ALP the contribution from the diagram in figure 4a would be largely insufficient by itself to either saturate the Δa_e bound or to account for the Δa_μ anomaly. The dominant contribution would then stem from the insertion of gauge anomalous ALP-couplings in figure 4b, and in particular from the photon-photon one.

Given the ALP mass range under consideration, 1 MeV $< m_a < 2m_\mu$, the expression in eq. (3.28) and the ensuing bound from Δa_e still applies to this very light ALP case because $m_a > m_e$. In contrast, a new analysis is in order for the ALP contribution to Δa_μ, which results in

$$\Delta a_\mu^{\text{ALP}} \simeq \widetilde{A}_\mu \, \frac{c_{a\gamma\gamma} + \widetilde{\Delta} c_{a\gamma\gamma}}{f_a} \, \frac{(\mathbf{c}_e - \mathbf{c}_L)_{\ell\ell}}{f_a}\,, \tag{5.12}$$

JHEP02(2023)138

where

$$\widetilde{A}_\mu \equiv \frac{m_\mu^2}{2\pi^2}\left(\log\frac{\Lambda^2}{m_\mu^2}-1\right) = 1.0\times 10^{-2}\ \text{GeV}^2\,, \tag{5.13}$$

for $\Lambda = 4\pi f_a \approx 1$ TeV. In the $m_a \ll m_\mu$ limit the $\Delta c_{a\gamma\gamma}$ coefficient — induced by the anomalous chiral rotations needed to reach the mass basis — is modified, as the anomalous contribution proportional to $(\mathbf{c}_e - \mathbf{c}_L)_{\mu\mu}$ cancels exactly with the one-loop corrections from the pseudoscalar ALP-muon coupling to the $aF\tilde{F}$ coupling [50]. Thus, a different coefficient, $\widetilde{\Delta} c_{a\gamma\gamma}$, is defined, which only contains the anomalous contribution proportional to the ALP-electron coupling constant $(\mathbf{c}_e - \mathbf{c}_L)_{ee}$, i.e.

$$\widetilde{\Delta} c_{a\gamma\gamma} \equiv -\frac{\alpha_{em}}{4\pi}\,(\mathbf{c}_e - \mathbf{c}_L)_{ee}\ , \tag{5.14}$$

and replaces $\Delta c_{a\gamma\gamma}$ in the $m_a \ll m_\mu$ limit. This means that the strong astrophysical bounds apply to the combination

$$c_{a\gamma\gamma} + \widetilde{\Delta} c_{a\gamma\gamma} \simeq c_{a\gamma\gamma} - \frac{\alpha_{em}}{4\pi}\,(\mathbf{c}_e - \mathbf{c}_L)_{ee} < 10^{-11}\ \text{GeV}^{-1}\,. \tag{5.15}$$

It follows that an explanation at the 2σ level of the data on $g-2$ of the electron and the muon in terms of the exchange of a very light ALP leads respectively to the requirements

$$\frac{1}{f_a}\left[(\mathbf{c}_e - \mathbf{c}_L)_{ee}\left((\mathbf{c}_e - \mathbf{c}_L)_{ee} - \frac{4\pi}{\alpha_{em}}\,c_{a\gamma\gamma}\right)\right]^{1/2} \in [0.03,\, 0.10]\ \text{GeV}^{-1}\,, \tag{5.16}$$

and

$$\frac{1}{f_a}\left[(\mathbf{c}_e - \mathbf{c}_L)_{\mu\mu}\left(\frac{4\pi}{\alpha_{em}}c_{a\gamma\gamma} - (\mathbf{c}_e - \mathbf{c}_L)_{ee}\right)\right]^{1/2} \in [0.02,\, 0.03]\ \text{GeV}^{-1}\,, \tag{5.17}$$

where $m_a = 10$ MeV has been used as illustration.

Given the constraint in eq. (5.15), the very large values of $(\mathbf{c}_e - \mathbf{c}_L)_{ee}$ required to satisfy Δa_e in eq. (5.16) are incompatible with the possible explanations of R_K in terms of the exchange of a very light ALP; see figure 14. Thus, experimental data exclude by themselves such a solution to R_K. Note that even if this had not been the case, the very large values of $(\mathbf{c}_e - \mathbf{c}_L)_{ee}$ required would have lied outside the regime of validity of the EFT by several orders of magnitude.

5.2 R_{K^*}, $B \to K^* a(e^+e^-)$, $B_s \to \ell^+\ell^-$ and magnetic moments

R_{K^*}. An explanation of the R_{K^*} anomalies in terms of the exchange of a very light ALP leads to

$$\text{for } \widetilde{C}^\mu_{P_-} = 0\text{:} \qquad \begin{cases} \widetilde{C}^e_{P_-} \in [-14.0,\,-5.4] \vee [5.4,\,15.3] & \text{central bin} \\ \widetilde{C}^e_{P_-} \in [-14.0,\,-3.0] \vee [3.0,\,15.3] & \text{low bin} \end{cases} \tag{5.18}$$

while figure 13b illustrates the enlarged range for $\widetilde{C}^\mu_{P_-} \neq 0$, which translates into a parameter space of solutions $\{\widetilde{C}^e_{P_-}, \widetilde{C}^\mu_{P_-}\}$ with

$$\widetilde{C}^\mu_{P_-} \in [-4.8,\,5.1] \qquad \text{central and low bin} \tag{5.19}$$

JHEP02(2023)138

and

$$\begin{cases} \widetilde{C}^e_{P_-} \in [-14.0,\, -5.4] \vee [5.4,\, 14.0] & \text{central bin} \\ \widetilde{C}^e_{P_-} \in [-14.0,\, -2.4] \vee [2.4,\, 14.0] & \text{low bin} \end{cases} \tag{5.20}$$

As before, these bounds already take into account the non-resonant semileptonic $B \to K^*$ constraints. It follows from eq. (5.7) that

$$\left| \frac{(\mathbf{c}_e - \mathbf{c}_L)_{\mu\mu}}{(\mathbf{c}_e - \mathbf{c}_L)_{ee}} \right| \approx 4.8 \times 10^{-3} \left| \frac{\widetilde{C}^\mu_{P_-}}{\widetilde{C}^e_{P_-}} \right| \lesssim \begin{cases} 5 \times 10^{-3} & \text{central bin} \\ 10^{-2} & \text{low bin} \end{cases} \tag{5.21}$$

which shows the necessity of a moderate hierarchy between the electronic and muonic couplings of the ALP.

$B \to K^* a(e^+e^-)$. For a light ALP with mass value within the q^2 bin $(0.0004, 0.05)$ GeV^2, that is with $m_a > 10$ MeV, data from resonant $B \to K^* a(e^+e^-)$ searches are available. As the ALP is on-shell, it is possible to use the NWA as in the previous section. Because $\mathcal{B}(a \to e^+e^-) = 1$, it is then possible to infer directly from those data a very strong bound on ALP-quark couplings, given by

$$\frac{(\mathbf{c}_d - \mathbf{c}_Q)_{sb}}{f_a} \lesssim 8 \times 10^{-10}\,\text{GeV}^{-1}\,, \tag{5.22}$$

which in order to account now for the R_{K^*} anomaly leads to the following constraints on ALP-lepton couplings, in that range of m_a,

$$\frac{|\,(\mathbf{c}_e - \mathbf{c}_L)_{\mu\mu}\,|}{f_a} \in [-23.8,\, 22.4] \qquad \text{central and low bin}\,, \tag{5.23}$$

together with

$$\begin{cases} \dfrac{|\,(\mathbf{c}_e - \mathbf{c}_L)_{ee}\,|}{f_a} \in [-13.5,\, -5.2] \times 10^3 \vee [5.2,\, 13.5] \times 10^3 & \text{central bin} \\ \dfrac{|\,(\mathbf{c}_e - \mathbf{c}_L)_{ee}\,|}{f_a} \in [-13.5,\, -2.3] \times 10^3 \vee [2.3,\, 13.5] \times 10^3 & \text{low bin} \end{cases} \tag{5.24}$$

again strongly at odds with the range of validity of the EFT.

$B_s \to \ell^+\ell^-$. The contributions of the SM plus ALP exchange to the branching ratios for the purely leptonic decays of the B_s meson are given by

$$\begin{aligned} \overline{\mathcal{B}}(B_s \to \mu^+\mu^-) &= 10^{-9} \times \left(3.67 - 3.99\,\tilde{C}^\mu_{P_-} + 1.09\,\tilde{C}^{\mu 2}_{P_-}\right)\,, \\ \overline{\mathcal{B}}(B_s \to e^+e^-) &= 10^{-14} \times \left(8.58 - 1.93 \times 10^3 \tilde{C}^e_{P_-} + 1.09 \times 10^5\,\tilde{C}^{e2}_{P_-}\right), \end{aligned} \tag{5.25}$$

with a theoretical error of 4% at the 1σ level. It follows that the 2σ allowed regions in parameter space are

$$\begin{cases} \widetilde{C}^e_{P_-} & \in [-3.2,\, 3.2]\,, \\ \widetilde{C}^\mu_{P_-} & \in [-0.095,\, 0.41] \vee [3.2,\, 3.8]\,. \end{cases} \tag{5.26}$$

JHEP02(2023)138

This is an interesting point for this very light ALP case, as illustrated in figure 13b. It shows that — in contrast with the scenario for a heavy ALP — there is 2σ *compatibility between the solutions to the* R_{K^*} *anomaly — low bin — and the data on* $B_s \to \mu^+\mu^-$ *and* $B_s \to e^+e^-$: the four small yellow square regions with white background in figure 13b survive, corresponding to

$$\left(\widetilde{C}^e_{P_-}, \widetilde{C}^\mu_{P_-}\right) \simeq \Big\{(-3,\,0),\,(-3,\,3.4),\,(3,\,0),\,(3,\,3.4)\Big\}\,. \tag{5.27}$$

The prize in this case is again theoretical, as these solutions imply ALP-lepton couplings outside the range of validity of the EFT. Indeed, applying the bounds from dedicated resonant searches in eq. (5.22), the four points listed above translate into the following unacceptably large values for ALP-lepton couplings:

$$\left(\frac{(\mathbf{c}_e - \mathbf{c}_L)_{ee}}{f_a},\,\frac{(\mathbf{c}_e - \mathbf{c}_L)_{\mu\mu}}{f_a}\right) \simeq \Big\{(\pm 3\times 10^3,\,0),\,(\pm 3\times 10^3,\,17)\Big\}\ \text{GeV}^{-1}\,. \tag{5.28}$$

Anomalous magnetic moment of the electron and the muon. The analysis of ALP exchange on leptonic magnetic moments, compared with the solutions to R_{K^*}, parallels that for the solutions to R_K above. In particular, the data on the set of observables $\{R_{K^*}, \Delta a_e\}$ require tree-level photon couplings that are too large to comply with the existent astrophysical constraints [55] (and are also incompatible with the EFT validity conditions).

6 Conclusions

We have analysed the technical *and* the theoretical cost required to explain the neutral anomalies in B-meson decays via the tree-level exchange of an ALP. Within the ALP effective field theory and assuming ALP-bs couplings, the complete two-dimensional parameter space for flavour-diagonal ALP couplings to electrons and muons is explored (considering, in addition, ALP-photon couplings when certain loop-level effects require it). The range of ALP masses contemplated sweeps from heavy ALPs, i.e. heavier than the B mesons, to very light ALPs down to 1 MeV — which is the lower value allowed by astrophysical constraints on the ALP-electron coupling.

The predictions for R_K and the two bins of R_{K^*} are confronted with the impact of ALP exchange on other observables, namely meson oscillations (ΔM_s), $B_s \to \ell^+\ell^-$ decays, $B \to K^{(*)}\ell^+\ell^-$ decays — including searches for new resonances — and astrophysical constraints. The data on these observables severely limit the available parameter space. Furthermore, we have analysed the impact of the solutions found on the $g-2$ of the electron and of the muon.

The solutions allowed are then compared with the theoretical conditions for the validity of the ALP EFT, requiring to remain within the perturbative domain of the effective theory on the assumption that the ALP scale is at least of the order of the electroweak scale, and the ALP mass under it.

For a heavy ALP, no viable explanation of the neutral anomalies in terms of tree-level ALP exchange survives. Solutions to R_K compatible with other observables — except the

JHEP02(2023)138

Δa_μ anomaly — are found. Nevertheless, they are in strong conflict with the EFT validity conditions: in order to account for R_K, the very small ALP-quark couplings required by ΔM_s data require in turn ALP-lepton effective couplings unacceptably large from the theoretical point of view. In the case of R_{K^*}, all ALP mediated solutions are directly excluded by the data on $B_s \to \ell^+\ell^-$ irrespective of EFT consistency considerations.

A similar fate applies to the other extreme of the ALP mass range: ALPs with mass smaller than the energies of the low-energy bin of R_{K^*} are also excluded. In fact, we do find solutions to the R_K or the R_{K^*} anomalies allowed within 2σ by the other observables mentioned; for instance the explanation of R_{K^*} and the $B_s \to \ell^+\ell^-$ data are in this case compatible within 2σ. From the theoretical point of view, the validity constraints of the EFT are (in)compatible by themselves with the values required by the R_K (R_{K^*}). Nevertheless, all solutions via these very light ALPs are excluded by the experimental bound on Δa_e, since in this case, astrophysical bounds set strong constraints on the effective photon coupling.

In contrast to the above, an ALP lighter than the B mesons but with a mass value within any of the bin windows provides an altogether different perspective. The ALP exchanged can then be on-shell and enter a resonant regime: $B \to K^{(*)}\ell^+\ell^-$ processes factorise into ALP on-shell production followed by decay. In this situation, the ALP coupling to muons must be much smaller than that to electrons to explain the neutral B-anomalies and thus $\mathcal{B}(a \to e^+e^-) \sim \mathcal{O}(1)$. The latter implies in turn that R_K and/or R_{K^*} become rather independent of the precise values of ALP leptonic couplings, and the solutions, therefore, escape from the theoretical problems with the EFT validity encountered for either heavy or extremely light ALPs. In this mass regime, we have also taken into account the validity requirements for the narrow-width approximation and for prompt ALP decays. The latter defines a minimum electron coupling for the solutions to $R_{K^{(*)}}$ and hence the parameter space compatible with the EFT validity constraints is reduced even in this on-shell regime.

Within the allowed parameter space for on-shell ALP exchange, we have furthermore identified a golden ALP mass value which lies at the frontier between the two energy bins for R_{K^*}, $m_a = \sqrt{1.1}$ GeV, and which becomes a broader mass range when smearing effects — associated to the finite experimental precision — are estimated. These golden mass values provide solutions which could *a priori* explain the three anomalies, i.e. R_K together with the two bins of R_{K^*}, always remaining compatible with the observables mentioned above and with the EFT validity constraints. While solutions in-between bins are always suspect, they are technically allowed and prompt the convenience to perform a slightly different experimental binning, which could easily clean up this avenue.

When the loop-level impact of the Lagrangian couplings are considered for an on-shell ALP, it is also possible to account simultaneously for the data in the sets $\{R_{K^{(*)}}, \Delta a_e\}$, while once again the Δa_μ anomaly cannot be then accounted for. Nonetheless, given the large electron couplings required by the analysis, their loop-level impact becomes relevant for some set of data. Correspondingly, some level of fine-tuning is called for to comply with the experimental bounds on Δa_e, as well as those obtained via $B \to K^{(*)}a(e^+e^-)$ searches. This adds to the already established theoretical cost of the ALP solution to the neutral B-anomalies. A complete loop-analysis is beyond the scope of this paper. Along the same

JHEP02(2023)138

line, we have not addressed the so-called charged flavour B-anomalies, as they cannot be explained by tree-level ALP exchanges.

We have exposed the high cost and conditions required to explain the neutral B-anomalies via tree-level ALP exchange. This is furthermore within the assumption — customary in the literature — that the only new physics couplings present in Nature are non-diagonal bs-ALP couplings and diagonal electron and muon ALP couplings as defined in the mass basis, instead of the most natural flavour basis. Nevertheless, the potential groundbreaking implications of the flavour B-anomalies, would they turn to be definitely confirmed by experiment, prompt to let no stone unturned. The broad ALP arena is a generic and compelling option to explore.

Acknowledgments

The authors acknowledge Cristopher Bobeth, Gudrun Hiller and José Miguel No for useful discussions. The authors acknowledge as well partial financial support by the Spanish Research Agency (Agencia Estatal de Investigación) through the grant IFT Centro de Excelencia Severo Ochoa No CEX2020-001007-S and by the grant PID2019-108892RB-I00 funded by MCIN/AEI/ 10.13039/501100011033, by the European Union's Horizon 2020 research and innovation programme under the Marie Skłodowska-Curie grant agreement No 860881-HIDDeN. The work of J.B. was supported by the Spanish MICIU through the National Program FPU (grant number FPU18/03047). The work of A.d.G. and M.R. was supported by the European Union's Horizon 2020 Marie Skłodowska-Curie grant agreement No 860881-HIDDeN.

A The input data and SM predictions

The parameters used for the computations, as well as the SM predictions used to derive the constraints along this work, are shown in table 3 and table 4, respectively.

B Details of $B \to K^{(*)}\ell\ell$ computations

The differential semileptonic decay rates considered in this work depend strongly on the values of the form factors, which have been calculated using different models and methods in the literature. The central values of the $B \to K$ form factors presented in ref. [112] have been used in this work, under the standard BCL parameterisation [118]. In the $B \to K^*$ case the central values reported in ref. [111] have been used instead.

We have cross-checked our analytical expressions, used in all figures presented in section 4 and to cross-check the results in other sections, by comparing the differential distributions $\mathrm{d}\mathcal{B}(B \to K^{(*)}\ell^+\ell^-)/\mathrm{d}q^2$ assuming only the SM with the output from Flavio; see figure 15. The accuracy between the two results is evident. The corresponding error bands, obtained with the same software, are also shown. Such theoretical uncertainties, together with the experimental ones, have been included to estimate the bounds on the new physics couplings. On the other hand, we neglect the theory errors associated to the

JHEP02(2023)138

Parameter	Value	Unit of Measure
$\alpha_{\text{em}}(m_b)$	0.007518797	—
G_F	$1.1663787(6) \times 10^{-5}$	GeV^{-2}
m_e	0.000510999	GeV
m_μ	0.105658	GeV
$\bar{m}_s(2\text{ GeV})$	$0.093^{+0.011}_{-0.005}$	GeV
$\bar{m}_b(m_b)$	$4.18^{+0.03}_{-0.02}$	GeV
M_{B_s}	5.36688 ± 0.00014	GeV
M_{B^0}	5.27965 ± 0.00012	GeV
$M_{B^\pm}$	5.27934 ± 0.00012	GeV
$M_{K^\pm}$	0.493677 ± 0.000016	GeV
$M_{K^{0*}}$	0.89555 ± 0.0008	GeV
τ_{B_s}	$(1.516 \pm 0.004) \times 10^{-12}$	s
τ_{B^0}	$(1.519 \pm 0.004) \times 10^{-12}$	s
$\tau_{B^\pm}$	$(1.638 \pm 0.004) \times 10^{-12}$	s
$\lvert V_{ts}\rvert$	$0.04065^{+0.00040}_{-0.00055}$	—
$\lvert V_{tb}\rvert$	$0.999142^{+0.000018}_{-0.000023}$	—
C_7	-0.33726473	—
C_9	4.27342842	—
C_{10}	-4.16611761	—

Table 3. Parameters used for the computations. The quark masses are estimates of the $\overline{\text{MS}}$ scheme at the given renormalisation scale [117]. The values of the WET Wilson coefficients are those used in EOS [88].

new physics branching ratios, as they are expected to have a negligible impact compared to the SM ones. In fact, the former are typically $\mathcal{O}(15\%)$ of the latter.

Using the new form factors presented by the FLAG collaboration [119], the results from our analytical expressions remain compatible with the Flavio output, although the central values in figure 15 show variations of $\mathcal{O}(7\%)$.

C Bounds from binned $B \to K^* e^+ e^-$ data

Bounds from the differential distribution of the observed number of events in the $B \to K^* e^+ e^-$ decay, $\mathrm{d}N/\mathrm{d}q^2(B \to K^* e^+ e^-)$, measured at LHCb [114] constrain the product $\mathcal{B}(B \to K^* a) \times \mathcal{B}(B \to e^+ e^-)$ for ALP masses within the 6 measured bins of q^2. In order to obtain such constraints, we have estimated the efficiency effects by comparing the number of events resulting from the Monte Carlo simulation of the SM, reported in the experimental paper, with the predictions from Flavio [87]; see table 4. In this way, we can

JHEP02(2023)138

SM Prediction	q^2 [GeV]^2	Value
$\mathcal{B}(B \to K\ell^+\ell^-)$	[1.1, 6.0]	$(1.71 \pm 0.29) \times 10^{-7}$
$\mathcal{B}(B \to K^*\ell^+\ell^-)$	[0.0004, 0.05]	e^+e^-: $(1.65 \pm 0.31) \times 10^{-7}$ $\mu^+\mu^-$: $(1.28 \pm 0.24) \times 10^{-9}$
$\mathcal{B}(B \to K^*\ell^+\ell^-)$	[0.05, 0.15]	e^+e^-: $(3.94 \pm 0.69) \times 10^{-8}$ $\mu^+\mu^-$: $(3.28 \pm 0.60) \times 10^{-8}$
$\mathcal{B}(B \to K^*\ell^+\ell^-)$	[0.15, 0.25]	e^+e^-: $(1.96 \pm 0.34) \times 10^{-8}$ $\mu^+\mu^-$: $(1.92 \pm 0.33) \times 10^{-8}$
$\mathcal{B}(B \to K^*\ell^+\ell^-)$	[0.25, 0.4]	e^+e^-: $(1.94 \pm 0.31) \times 10^{-8}$ $\mu^+\mu^-$: $(1.92 \pm 0.30) \times 10^{-8}$
$\mathcal{B}(B \to K^*\ell^+\ell^-)$	[0.4, 0.7]	e^+e^-: $(2.62 \pm 0.38) \times 10^{-8}$ $\mu^+\mu^-$: $(2.61 \pm 0.37) \times 10^{-8}$
$\mathcal{B}(B \to K^*\ell^+\ell^-)$	[0.7, 1]	e^+e^-: $(1.98 \pm 0.26) \times 10^{-8}$ $\mu^+\mu^-$: $(1.97 \pm 0.29) \times 10^{-8}$
$\mathcal{B}(B \to K^*\ell^+\ell^-)$	[1.1, 6.0]	$(2.53 \pm 0.36) \times 10^{-7}$
$\mathcal{B}(B \to K^*\ell^+\ell^-)$	[0.1, 8.0]	e^+e^-: $(4.87 \pm 0.65) \times 10^{-7}$ $\mu^+\mu^-$: $(4.82 \pm 0.68) \times 10^{-7}$
$\overline{\mathcal{B}}(B_s \to \mu^+\mu^-)$	—	$(3.67 \pm 0.15) \times 10^{-9}$
$\overline{\mathcal{B}}(B_s \to e^+e^-)$	—	$(8.58 \pm 0.35) \times 10^{-14}$

Table 4. SM predictions relevant for the analyses discussed in this work, computed directly from flavio [87].

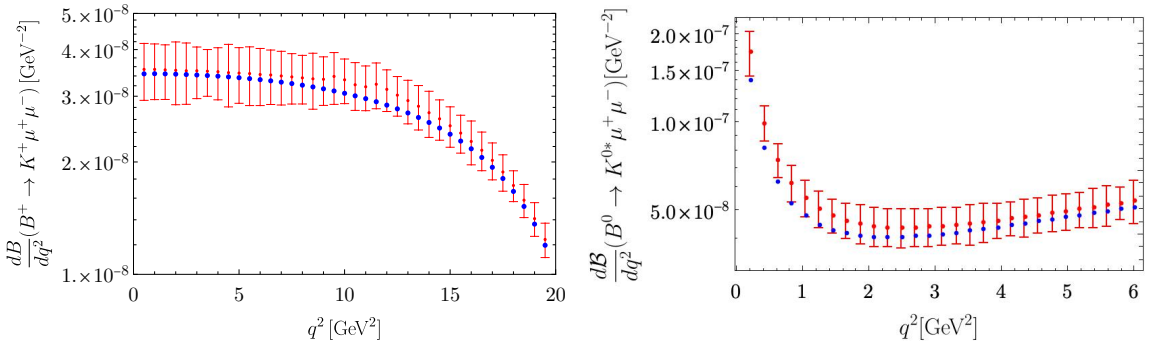

Figure 15. The SM prediction for the differential distributions obtained using Flavio (red dots) vs. our analytical formulas (blue dots). Error bars include the theoretical uncertainties in the SM prediction.

JHEP02(2023)138

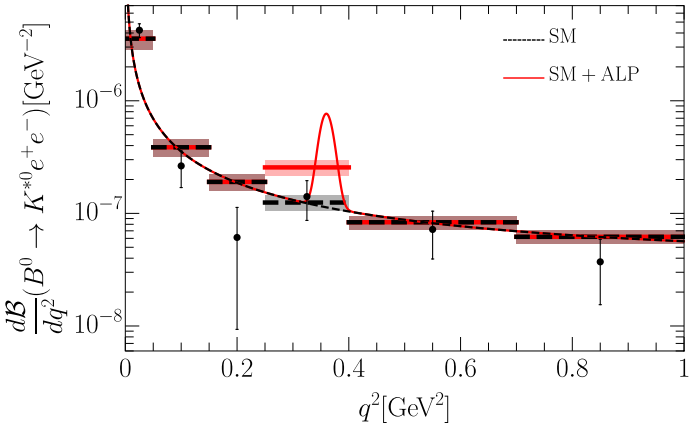

Figure 16. The experimental limits on the differential branching ratio $\mathrm{d}\mathcal{B}/\mathrm{d}q^2(B \to K^* e^+ e^-)$ obtained from ref. [114], together with the SM (in black) and the NP (in red) predictions. Both the continuous and binned distributions, divided in the 6 measured bins of q^2, are presented. For the NP, we have assumed an ALP with $m_a = 0.6\,\mathrm{GeV}$ and decaying $\approx 100\%$ into electrons. The quark coupling is set to $|(\mathbf{c}_d - \mathbf{c}_Q)_{sb}|/f_a = 3.05 \times 10^{-10}\,\mathrm{GeV}^{-1}$.

relate the two relevant quantities N and $\mathcal{B}$ by

$$N(B \to K^* e^+ e^-) = \mathcal{B}(B \to K^* e^+ e^-)\, \sigma^B\, \mathcal{L}\, \epsilon\,, \tag{C.1}$$

where σ^B is the production cross-section of a B meson at LHCb, $\mathcal{L}$ is the integrated luminosity and ϵ is the detector efficiency for a given energy bin. Hence, knowing the SM predictions for the branching fraction and the expected number of events, the quotient $N^{\mathrm{data}}/\mathcal{B}^{\mathrm{data}}$ can be obtained from $N^{\mathrm{SM}}/\mathcal{B}^{\mathrm{SM}}$.

The resulting bounds, taking into account both experimental and the SM theoretical errors,[17] are reported in table 2 with exception of one interval, $q^2 \in [0.15, 0.25]\,\mathrm{GeV}^2$, where a tension of more than 2σ with respect to the SM prediction is observed in data, that would be worsened by the presence of NP. No beyond SM contributions are therefore considered in this bin; see figure 8a.

These bounds are represented in figure 16 along with the SM predictions. In addition, the contribution from a resonant ALP with a mass of 0.6 GeV is also shown. For the fermionic couplings, we have adopted the benchmark defined by $(|(\mathbf{c}_e - \mathbf{c_L})_{ee}|/f_a,\, |(\mathbf{c}_e - \mathbf{c_L})_{\mu\mu}|/f_a) = (10^{-1}, 10^{-5})\,\mathrm{GeV}^{-1}$ and $|(\mathbf{c}_d - \mathbf{c_Q})_{bs}|/f_a| = 3.05 \times 10^{-10}\,\mathrm{GeV}^{-1}$ corresponding to the blue star in figures 8a and 9a. It becomes clear the potential of these measurements to probe the ALP parameter space relevant to the B anomalies and, in particular, the advantages of using a smaller binning in order to resolve the ALP resonant peak.

[17] Correlations across bins are ignored in this procedure. The former are taken into account in ref. [113] where a similar procedure was adopted using only the first two bins of q^2 determined in the experimental analysis; the resulting bounds are very similar to those we have obtained.

JHEP02(2023)138

References

[1] F. Englert and R. Brout, *Broken symmetry and the mass of gauge vector mesons*, *Phys. Rev. Lett.* **13** (1964) 321 [INSPIRE].

[2] P.W. Higgs, *Broken symmetries, massless particles and gauge fields*, *Phys. Lett.* **12** (1964) 132 [INSPIRE].

[3] P.W. Higgs, *Broken symmetries and the masses of gauge bosons*, *Phys. Rev. Lett.* **13** (1964) 508 [INSPIRE].

[4] ATLAS collaboration, *Observation of a new particle in the search for the standard model Higgs boson with the ATLAS detector at the LHC*, *Phys. Lett. B* **716** (2012) 1 [arXiv:1207.7214] [INSPIRE].

[5] CMS collaboration, *Observation of a new boson at a mass of 125 GeV with the CMS experiment at the LHC*, *Phys. Lett. B* **716** (2012) 30 [arXiv:1207.7235] [INSPIRE].

[6] LHCb collaboration, *Measurement of form-factor-independent observables in the decay* $B^0 \to K^{*0}\mu^+\mu^-$, *Phys. Rev. Lett.* **111** (2013) 191801 [arXiv:1308.1707] [INSPIRE].

[7] LHCb collaboration, *Angular analysis of the* $B^0 \to K^{*0}\mu^+\mu^-$ *decay using* $3\,fb^{-1}$ *of integrated luminosity*, *JHEP* **02** (2016) 104 [arXiv:1512.04442] [INSPIRE].

[8] LHCb collaboration, *Measurement of CP-averaged observables in the* $B^0 \to K^{*0}\mu^+\mu^-$ *decay*, *Phys. Rev. Lett.* **125** (2020) 011802 [arXiv:2003.04831] [INSPIRE].

[9] LHCb collaboration, *Angular analysis of the* $B^+ \to K^{*+}\mu^+\mu^-$ *decay*, *Phys. Rev. Lett.* **126** (2021) 161802 [arXiv:2012.13241] [INSPIRE].

[10] LHCb collaboration, *Test of lepton universality using* $B^+ \to K^+\ell^+\ell^-$ *decays*, *Phys. Rev. Lett.* **113** (2014) 151601 [arXiv:1406.6482] [INSPIRE].

[11] LHCb collaboration, *Test of lepton universality with* $B^0 \to K^{*0}\ell^+\ell^-$ *decays*, *JHEP* **08** (2017) 055 [arXiv:1705.05802] [INSPIRE].

[12] LHCb collaboration, *Search for lepton-universality violation in* $B^+ \to K^+\ell^+\ell^-$ *decays*, *Phys. Rev. Lett.* **122** (2019) 191801 [arXiv:1903.09252] [INSPIRE].

[13] LHCb collaboration, *Test of lepton universality in beauty-quark decays*, *Nature Phys.* **18** (2022) 277 [arXiv:2103.11769] [INSPIRE].

[14] G. Hiller and F. Kruger, *More model-independent analysis of* $b \to s$ *processes*, *Phys. Rev. D* **69** (2004) 074020 [hep-ph/0310219] [INSPIRE].

[15] M. Bordone, G. Isidori and A. Pattori, *On the standard model predictions for* R_K *and* R_{K^*}, *Eur. Phys. J. C* **76** (2016) 440 [arXiv:1605.07633] [INSPIRE].

[16] G. Isidori, S. Nabeebaccus and R. Zwicky, *QED corrections in* $\overline{B} \to \overline{K}\ell^+\ell^-$ *at the double-differential level*, *JHEP* **12** (2020) 104 [arXiv:2009.00929] [INSPIRE].

[17] C. Bobeth, G. Hiller and G. Piranishvili, *Angular distributions of* $\bar{B} \to \bar{K}\ell^+\ell^-$ *decays*, *JHEP* **12** (2007) 040 [arXiv:0709.4174] [INSPIRE].

[18] B. Capdevila, A. Crivellin, S. Descotes-Genon, J. Matias and J. Virto, *Patterns of new physics in* $b \to s\ell^+\ell^-$ *transitions in the light of recent data*, *JHEP* **01** (2018) 093 [arXiv:1704.05340] [INSPIRE].

[19] S. Descotes-Genon, J. Matias and J. Virto, *Understanding the* $B \to K^*\mu^+\mu^-$ *anomaly*, *Phys. Rev. D* **88** (2013) 074002 [arXiv:1307.5683] [INSPIRE].

JHEP02(2023)138

[20] M. Ciuchini, M. Fedele, E. Franco, A. Paul, L. Silvestrini and M. Valli, *Lessons from the $B^{0,+} \to K^{*0,+}\mu^+\mu^-$ angular analyses*, *Phys. Rev. D* **103** (2021) 015030 [arXiv:2011.01212] [INSPIRE].

[21] M. Algueró, B. Capdevila, S. Descotes-Genon, J. Matias and M. Novoa-Brunet, *$b \to s\ell^+\ell^-$ global fits after R_{K_S} and $R_{K^{*+}}$*, *Eur. Phys. J. C* **82** (2022) 326 [arXiv:2104.08921] [INSPIRE].

[22] W. Altmannshofer and P. Stangl, *New physics in rare B decays after Moriond* 2021, *Eur. Phys. J. C* **81** (2021) 952 [arXiv:2103.13370] [INSPIRE].

[23] L.-S. Geng, B. Grinstein, S. Jäger, S.-Y. Li, J. Martin Camalich and R.-X. Shi, *Implications of new evidence for lepton-universality violation in $b \to s\ell^+\ell^-$ decays*, *Phys. Rev. D* **104** (2021) 035029 [arXiv:2103.12738] [INSPIRE].

[24] T. Hurth, F. Mahmoudi, D.M. Santos and S. Neshatpour, *More indications for lepton nonuniversality in $b \to s\ell^+\ell^-$*, *Phys. Lett. B* **824** (2022) 136838 [arXiv:2104.10058] [INSPIRE].

[25] C. Cornella, D.A. Faroughy, J. Fuentes-Martin, G. Isidori and M. Neubert, *Reading the footprints of the B-meson flavor anomalies*, *JHEP* **08** (2021) 050 [arXiv:2103.16558] [INSPIRE].

[26] G. Isidori, D. Lancierini, P. Owen and N. Serra, *On the significance of new physics in $b \to s\ell^+\ell^-$ decays*, *Phys. Lett. B* **822** (2021) 136644 [arXiv:2104.05631] [INSPIRE].

[27] G. Isidori, D. Lancierini, A. Mathad, P. Owen, N. Serra and R. Silva Coutinho, *A general effective field theory description of $b \to s\ell^+\ell^-$ lepton universality ratios*, *Phys. Lett. B* **830** (2022) 137151 [arXiv:2110.09882] [INSPIRE].

[28] W. Altmannshofer and D.M. Straub, *New physics in $B \to K^*\mu\mu$?*, *Eur. Phys. J. C* **73** (2013) 2646 [arXiv:1308.1501] [INSPIRE].

[29] A.J. Buras and J. Girrbach, *Left-handed Z' and Z FCNC quark couplings facing new $b \to s\mu^+\mu^-$ data*, *JHEP* **12** (2013) 009 [arXiv:1309.2466] [INSPIRE].

[30] A. Crivellin, G. D'Ambrosio and J. Heeck, *Explaining the LHC flavour anomalies*, in 50th *Rencontres de Moriond on EW interactions and unified theories*, (2015), p. 101 [arXiv:1505.02026] [INSPIRE].

[31] A. Celis, J. Fuentes-Martin, M. Jung and H. Serodio, *Family nonuniversal Z' models with protected flavor-changing interactions*, *Phys. Rev. D* **92** (2015) 015007 [arXiv:1505.03079] [INSPIRE].

[32] R. Alonso, B. Grinstein and J. Martin Camalich, *Lepton universality violation and lepton flavor conservation in B-meson decays*, *JHEP* **10** (2015) 184 [arXiv:1505.05164] [INSPIRE].

[33] L. Calibbi, A. Crivellin and T. Ota, *Effective field theory approach to $b \to s\ell\ell^{(')}$, $B \to K^{(*)}\nu\overline{\nu}$ and $B \to D^{(*)}\tau\nu$ with third generation couplings*, *Phys. Rev. Lett.* **115** (2015) 181801 [arXiv:1506.02661] [INSPIRE].

[34] R. Barbieri, G. Isidori, A. Pattori and F. Senia, *Anomalies in B-decays and U(2) flavour symmetry*, *Eur. Phys. J. C* **76** (2016) 67 [arXiv:1512.01560] [INSPIRE].

[35] D. Buttazzo, A. Greljo, G. Isidori and D. Marzocca, *B-physics anomalies: a guide to combined explanations*, *JHEP* **11** (2017) 044 [arXiv:1706.07808] [INSPIRE].

JHEP02(2023)138

[36] R.D. Peccei and H.R. Quinn, *CP conservation in the presence of instantons*, *Phys. Rev. Lett.* **38** (1977) 1440 [INSPIRE].

[37] R.D. Peccei and H.R. Quinn, *Constraints imposed by CP conservation in the presence of instantons*, *Phys. Rev. D* **16** (1977) 1791 [INSPIRE].

[38] S. Weinberg, *A new light boson?*, *Phys. Rev. Lett.* **40** (1978) 223 [INSPIRE].

[39] F. Wilczek, *Problem of strong P and T invariance in the presence of instantons*, *Phys. Rev. Lett.* **40** (1978) 279 [INSPIRE].

[40] G.B. Gelmini and M. Roncadelli, *Left-handed neutrino mass scale and spontaneously broken lepton number*, *Phys. Lett. B* **99** (1981) 411 [INSPIRE].

[41] B. Bellazzini, A. Mariotti, D. Redigolo, F. Sala and J. Serra, *R-axion at colliders*, *Phys. Rev. Lett.* **119** (2017) 141804 [arXiv:1702.02152] [INSPIRE].

[42] H. Georgi and D.B. Kaplan, *Composite Higgs and custodial* SU(2), *Phys. Lett. B* **145** (1984) 216 [INSPIRE].

[43] M. Cicoli, *Axion-like particles from string compactifications*, in 9th *Patras workshop on axions, WIMPs and WISPs*, DESY-PROC 235-242 (2013), p. 235 [arXiv:1309.6988] [INSPIRE].

[44] M. Bauer, M. Neubert, S. Renner, M. Schnubel and A. Thamm, *Flavor probes of axion-like particles*, *JHEP* **09** (2022) 056 [arXiv:2110.10698] [INSPIRE].

[45] H. Georgi, D.B. Kaplan and L. Randall, *Manifesting the invisible axion at low-energies*, *Phys. Lett. B* **169** (1986) 73 [INSPIRE].

[46] K. Choi, K. Kang and J.E. Kim, *Effects of η' in low-energy axion physics*, *Phys. Lett. B* **181** (1986) 145 [INSPIRE].

[47] I. Brivio et al., *ALPs effective field theory and collider signatures*, *Eur. Phys. J. C* **77** (2017) 572 [arXiv:1701.05379] [INSPIRE].

[48] M. Chala, G. Guedes, M. Ramos and J. Santiago, *Running in the ALPs*, *Eur. Phys. J. C* **81** (2021) 181 [arXiv:2012.09017] [INSPIRE].

[49] M. Bauer, M. Neubert, S. Renner, M. Schnubel and A. Thamm, *The low-energy effective theory of axions and ALPs*, *JHEP* **04** (2021) 063 [arXiv:2012.12272] [INSPIRE].

[50] J. Bonilla, I. Brivio, M.B. Gavela and V. Sanz, *One-loop corrections to ALP couplings*, *JHEP* **11** (2021) 168 [arXiv:2107.11392] [INSPIRE].

[51] M. Freytsis, Z. Ligeti and J. Thaler, *Constraining the axion portal with $B \to K\ell^+\ell^-$*, *Phys. Rev. D* **81** (2010) 034001 [arXiv:0911.5355] [INSPIRE].

[52] K. Mimasu and V. Sanz, *ALPs at colliders*, *JHEP* **06** (2015) 173 [arXiv:1409.4792] [INSPIRE].

[53] J. Jaeckel and M. Spannowsky, *Probing MeV to* 90 *GeV axion-like particles with LEP and LHC*, *Phys. Lett. B* **753** (2016) 482 [arXiv:1509.00476] [INSPIRE].

[54] E. Izaguirre, T. Lin and B. Shuve, *Searching for axionlike particles in flavor-changing neutral current processes*, *Phys. Rev. Lett.* **118** (2017) 111802 [arXiv:1611.09355] [INSPIRE].

[55] M. Bauer, M. Neubert and A. Thamm, *Collider probes of axion-like particles*, *JHEP* **12** (2017) 044 [arXiv:1708.00443] [INSPIRE].

JHEP02(2023)138

[56] N. Craig, A. Hook and S. Kasko, *The photophobic ALP*, *JHEP* **09** (2018) 028 [arXiv:1805.06538] [INSPIRE].

[57] C. Frugiuele, E. Fuchs, G. Perez and M. Schlaffer, *Relaxion and light (pseudo)scalars at the HL-LHC and lepton colliders*, *JHEP* **10** (2018) 151 [arXiv:1807.10842] [INSPIRE].

[58] M. Bauer, M. Heiles, M. Neubert and A. Thamm, *Axion-like particles at future colliders*, *Eur. Phys. J. C* **79** (2019) 74 [arXiv:1808.10323] [INSPIRE].

[59] J. Ebadi, S. Khatibi and M. Mohammadi Najafabadi, *New probes for axionlike particles at hadron colliders*, *Phys. Rev. D* **100** (2019) 015016 [arXiv:1901.03061] [INSPIRE].

[60] L. Merlo, F. Pobbe, S. Rigolin and O. Sumensari, *Revisiting the production of ALPs at B-factories*, *JHEP* **06** (2019) 091 [arXiv:1905.03259] [INSPIRE].

[61] M.B. Gavela, J.M. No, V. Sanz and J.F. de Trocóniz, *Nonresonant searches for axionlike particles at the LHC*, *Phys. Rev. Lett.* **124** (2020) 051802 [arXiv:1905.12953] [INSPIRE].

[62] M. Bauer, M. Neubert, S. Renner, M. Schnubel and A. Thamm, *Axionlike particles, lepton-flavor violation, and a new explanation of a_μ and a_e*, *Phys. Rev. Lett.* **124** (2020) 211803 [arXiv:1908.00008] [INSPIRE].

[63] M. Bauer, M. Neubert, S. Renner, M. Schnubel and A. Thamm, *Consistent treatment of axions in the weak chiral lagrangian*, *Phys. Rev. Lett.* **127** (2021) 081803 [arXiv:2102.13112] [INSPIRE].

[64] J. Bonilla, I. Brivio, J. Machado-Rodríguez and J.F. de Trocóniz, *Nonresonant searches for axion-like particles in vector boson scattering processes at the LHC*, *JHEP* **06** (2022) 113 [arXiv:2202.03450] [INSPIRE].

[65] V.A. Rubakov, *Grand unification and heavy axion*, *JETP Lett.* **65** (1997) 621 [hep-ph/9703409] [INSPIRE].

[66] Z. Berezhiani, L. Gianfagna and M. Giannotti, *Strong CP problem and mirror world: the Weinberg-Wilczek axion revisited*, *Phys. Lett. B* **500** (2001) 286 [hep-ph/0009290] [INSPIRE].

[67] L. Gianfagna, M. Giannotti and F. Nesti, *Mirror world, supersymmetric axion and gamma ray bursts*, *JHEP* **10** (2004) 044 [hep-ph/0409185] [INSPIRE].

[68] S.D.H. Hsu and F. Sannino, *New solutions to the strong CP problem*, *Phys. Lett. B* **605** (2005) 369 [hep-ph/0408319] [INSPIRE].

[69] A. Hook, *Anomalous solutions to the strong CP problem*, *Phys. Rev. Lett.* **114** (2015) 141801 [arXiv:1411.3325] [INSPIRE].

[70] H. Fukuda, K. Harigaya, M. Ibe and T.T. Yanagida, *Model of visible QCD axion*, *Phys. Rev. D* **92** (2015) 015021 [arXiv:1504.06084] [INSPIRE].

[71] C.-W. Chiang, H. Fukuda, M. Ibe and T.T. Yanagida, *750 GeV diphoton resonance in a visible heavy QCD axion model*, *Phys. Rev. D* **93** (2016) 095016 [arXiv:1602.07909] [INSPIRE].

[72] S. Dimopoulos, A. Hook, J. Huang and G. Marques-Tavares, *A collider observable QCD axion*, *JHEP* **11** (2016) 052 [arXiv:1606.03097] [INSPIRE].

[73] T. Gherghetta, N. Nagata and M. Shifman, *A visible QCD axion from an enlarged color group*, *Phys. Rev. D* **93** (2016) 115010 [arXiv:1604.01127] [INSPIRE].

[74] A. Kobakhidze, *Heavy axion in asymptotically safe QCD*, arXiv:1607.06552 [INSPIRE].

JHEP02(2023)138

[75] P. Agrawal and K. Howe, *Factoring the strong CP problem*, *JHEP* **12** (2018) 029 [arXiv:1710.04213] [INSPIRE].

[76] P. Agrawal and K. Howe, *A flavorful factoring of the strong CP problem*, *JHEP* **12** (2018) 035 [arXiv:1712.05803] [INSPIRE].

[77] M.K. Gaillard, M.B. Gavela, R. Houtz, P. Quilez and R. Del Rey, *Color unified dynamical axion*, *Eur. Phys. J. C* **78** (2018) 972 [arXiv:1805.06465] [INSPIRE].

[78] M.A. Buen-Abad and J. Fan, *Dynamical axion misalignment with small instantons*, *JHEP* **12** (2019) 161 [arXiv:1911.05737] [INSPIRE].

[79] A. Hook, S. Kumar, Z. Liu and R. Sundrum, *High quality QCD axion and the LHC*, *Phys. Rev. Lett.* **124** (2020) 221801 [arXiv:1911.12364] [INSPIRE].

[80] C. Csáki, M. Ruhdorfer and Y. Shirman, *UV sensitivity of the axion mass from instantons in partially broken gauge groups*, *JHEP* **04** (2020) 031 [arXiv:1912.02197] [INSPIRE].

[81] T. Gherghetta and M.D. Nguyen, *A composite Higgs with a heavy composite axion*, *JHEP* **12** (2020) 094 [arXiv:2007.10875] [INSPIRE].

[82] A. Hook, *Solving the hierarchy problem discretely*, *Phys. Rev. Lett.* **120** (2018) 261802 [arXiv:1802.10093] [INSPIRE].

[83] L. Di Luzio, B. Gavela, P. Quilez and A. Ringwald, *An even lighter QCD axion*, *JHEP* **05** (2021) 184 [arXiv:2102.00012] [INSPIRE].

[84] L. Di Luzio, B. Gavela, P. Quilez and A. Ringwald, *Dark matter from an even lighter QCD axion: trapped misalignment*, *JCAP* **10** (2021) 001 [arXiv:2102.01082] [INSPIRE].

[85] G. Buchalla, A.J. Buras and M.E. Lautenbacher, *Weak decays beyond leading logarithms*, *Rev. Mod. Phys.* **68** (1996) 1125 [hep-ph/9512380] [INSPIRE].

[86] K.G. Chetyrkin, M. Misiak and M. Munz, *Weak radiative B meson decay beyond leading logarithms*, *Phys. Lett. B* **400** (1997) 206 [*Erratum ibid.* **425** (1998) 414] [hep-ph/9612313] [INSPIRE].

[87] D.M. Straub, *flavio: a python package for flavour and precision phenomenology in the standard model and beyond*, arXiv:1810.08132 [INSPIRE].

[88] EOS Authors collaboration, *EOS: a software for flavor physics phenomenology*, *Eur. Phys. J. C* **82** (2022) 569 [arXiv:2111.15428] [INSPIRE].

[89] LHCb collaboration, *Differential branching fractions and isospin asymmetries of $B \to K^{(*)}\mu^+\mu^-$ decays*, *JHEP* **06** (2014) 133 [arXiv:1403.8044] [INSPIRE].

[90] LHCb collaboration, *Search for long-lived scalar particles in $B^+ \to K^+\chi(\mu^+\mu^-)$ decays*, *Phys. Rev. D* **95** (2017) 071101 [arXiv:1612.07818] [INSPIRE].

[91] Belle collaboration, *Test of lepton-flavor universality in $B \to K^*\ell^+\ell^-$ decays at Belle*, *Phys. Rev. Lett.* **126** (2021) 161801 [arXiv:1904.02440] [INSPIRE].

[92] LHCb collaboration, *Search for hidden-sector bosons in $B^0 \to K^{*0}\mu^+\mu^-$ decays*, *Phys. Rev. Lett.* **115** (2015) 161802 [arXiv:1508.04094] [INSPIRE].

[93] LHCb collaboration, *Precise determination of the B_s^0-$\overline{B}_s^0$ oscillation frequency*, *Nature Phys.* **18** (2022) 1 [arXiv:2104.04421] [INSPIRE].

JHEP02(2023)138

[94] Fermilab Lattice and MILC collaborations, *$B^0_{(s)}$-mixing matrix elements from lattice QCD for the standard model and beyond*, *Phys. Rev. D* **93** (2016) 113016 [arXiv:1602.03560] [INSPIRE].

[95] L. Di Luzio, M. Kirk, A. Lenz and T. Rauh, *ΔM_s theory precision confronts flavour anomalies*, *JHEP* **12** (2019) 009 [arXiv:1909.11087] [INSPIRE].

[96] L. Darmé, L. Di Luzio, M. Giannotti and E. Nardi, *Selective enhancement of the QCD axion couplings*, *Phys. Rev. D* **103** (2021) 015034 [arXiv:2010.15846] [INSPIRE].

[97] R.H. Parker, C. Yu, W. Zhong, B. Estey and H. Müller, *Measurement of the fine-structure constant as a test of the standard model*, *Science* **360** (2018) 191 [arXiv:1812.04130] [INSPIRE].

[98] D. Hanneke, S. Fogwell and G. Gabrielse, *New measurement of the electron magnetic moment and the fine structure constant*, *Phys. Rev. Lett.* **100** (2008) 120801 [arXiv:0801.1134] [INSPIRE].

[99] D. Hanneke, S.F. Hoogerheide and G. Gabrielse, *Cavity control of a single-electron quantum cyclotron: measuring the electron magnetic moment*, *Phys. Rev. A* **83** (2011) 052122 [arXiv:1009.4831] [INSPIRE].

[100] L. Morel, Z. Yao, P. Cladé and S. Guellati-Khélifa, *Determination of the fine-structure constant with an accuracy of* 81 *parts per trillion*, *Nature* **588** (2020) 61 [INSPIRE].

[101] T. Aoyama et al., *The anomalous magnetic moment of the muon in the standard model*, *Phys. Rept.* **887** (2020) 1 [arXiv:2006.04822] [INSPIRE].

[102] Muon g-2 collaboration, *Final report of the muon E821 anomalous magnetic moment measurement at BNL*, *Phys. Rev. D* **73** (2006) 072003 [hep-ex/0602035] [INSPIRE].

[103] Muon g-2 collaboration, *Measurement of the positive muon anomalous magnetic moment to* 0.46 *ppm*, *Phys. Rev. Lett.* **126** (2021) 141801 [arXiv:2104.03281] [INSPIRE].

[104] S. Borsanyi et al., *Leading hadronic contribution to the muon magnetic moment from lattice QCD*, *Nature* **593** (2021) 51 [arXiv:2002.12347] [INSPIRE].

[105] M. Cè et al., *Window observable for the hadronic vacuum polarization contribution to the muon $g-2$ from lattice QCD*, *Phys. Rev. D* **106** (2022) 114502 [arXiv:2206.06582] [INSPIRE].

[106] C. Alexandrou et al., *Lattice calculation of the short and intermediate time-distance hadronic vacuum polarization contributions to the muon magnetic moment using twisted-mass fermions*, arXiv:2206.15084 [INSPIRE].

[107] M. Beneke, C. Bobeth and R. Szafron, *Power-enhanced leading-logarithmic QED corrections to $B_q \to \mu^+\mu^-$*, *JHEP* **10** (2019) 232 [*Erratum ibid.* **11** (2022) 099] [arXiv:1908.07011] [INSPIRE].

[108] LHCb collaboration, *Analysis of neutral B-meson decays into two muons*, *Phys. Rev. Lett.* **128** (2022) 041801 [arXiv:2108.09284] [INSPIRE].

[109] LHCb collaboration, *Search for the rare decays $B^0_s \to e^+e^-$ and $B^0 \to e^+e^-$*, *Phys. Rev. Lett.* **124** (2020) 211802 [arXiv:2003.03999] [INSPIRE].

[110] ATLAS collaboration, *Combination of the ATLAS, CMS and LHCb results on the $B^0_{(s)} \to \mu^+\mu^-$ decays*, Tech. Rep. ATLAS-CONF-2020-049, CERN, Geneva, Switzerland (2020) [INSPIRE].

JHEP02(2023)138

[111] A. Bharucha, D.M. Straub and R. Zwicky, *$B \to V\ell^+\ell^-$ in the standard model from light-cone sum rules*, *JHEP* **08** (2016) 098 [arXiv:1503.05534] [INSPIRE].

[112] J.A. Bailey et al., *$B \to K\ell^+\ell^-$ decay form factors from three-flavor lattice QCD*, *Phys. Rev. D* **93** (2016) 025026 [arXiv:1509.06235] [INSPIRE].

[113] W. Altmannshofer et al., *Light resonances and the low-q^2 bin of R_{K^*}*, *JHEP* **03** (2018) 188 [arXiv:1711.07494] [INSPIRE].

[114] LHCb collaboration, *Angular analysis of the $B^0 \to K^{*0}e^+e^-$ decay in the low-q^2 region*, *JHEP* **04** (2015) 064 [arXiv:1501.03038] [INSPIRE].

[115] P. Ilten, J. Thaler, M. Williams and W. Xue, *Dark photons from charm mesons at LHCb*, *Phys. Rev. D* **92** (2015) 115017 [arXiv:1509.06765] [INSPIRE].

[116] LHCb collaboration, *LHCb detector performance*, *Int. J. Mod. Phys. A* **30** (2015) 1530022 [arXiv:1412.6352] [INSPIRE].

[117] Particle Data Group collaboration, *Review of particle physics*, *PTEP* **2022** (2022) 083C01 [INSPIRE].

[118] C. Bourrely, I. Caprini and L. Lellouch, *Model-independent description of $B \to pi\ell\nu$ decays and a determination of $|V_{ub}|$*, *Phys. Rev. D* **79** (2009) 013008 [*Erratum ibid.* **82** (2010) 099902] [arXiv:0807.2722] [INSPIRE].

[119] Flavour Lattice Averaging Group (FLAG) collaboration, *FLAG review* 2021, *Eur. Phys. J. C* **82** (2022) 869 [arXiv:2111.09849] [INSPIRE].

[120] BaBar collaboration, *Search for an axionlike particle in B meson decays*, *Phys. Rev. Lett.* **128** (2022) 131802 [arXiv:2111.01800] [INSPIRE].

JHEP02(2023)138

Part III

Conclusions

Conclusions

Axion and ALP interactions can be depicted by the same ALP effective Lagrangian. This fact, accompanied by the ubiquity of ALPs in many BSM models, have fomented a flourishing period on the theoretical studies and the landscape of experimental searches for axions and ALPs, covering orders of magnitude in energy scale and using very different techniques. These searches have reached a level of precision and are so diverse that experimental sensitivity requires to compute the one-loop impact of effective ALP couplings. These have been presented in this thesis in Ch. 4, which contains the work from Ref. [5]. First, an extensive classification of the different ALP operators was presented. Non-redundant degrees of freedom within the ALP EFT were identified and relations between different operators have been demonstrated. We introduced the complete set of one-loop corrections to the most general non-redundant ALP Lagrangian. The corrections were computed in a covariant R_ξ gauge for off-shell ALPs and on-shell SM legs. Additionally, several kinematic limits for the ALP momentum and SM particle masses were presented, which may be useful for particular experimental setups.

In order to demonstrate the power of one-loop corrections, some phenomenological consequences of the computations were discussed. In particular, we studied the implication of the loop-impact of the ALP-top interaction in other ALP couplings which are well tested experimentally. On one hand, we considered the resonant decay of a heavy ALP into a pair of top quarks. In such process, ALPs were assumed to be produced by gluon-gluon fusion via a top quark loop. Even though the process is loop-suppressed it still counts with a significant cross section which may be measured at LHC experiments. For instance, ATLAS experiment data for ditop events was used to set new bounds on the ALP-top interaction in the region of $m_a \subset [1.5, 4.5]$ TeV. On the other hand, we also explored the impact of such interaction on low-energy ALP searches. For instance, it induces a significant one-loop contribution to the ALP-electron that is enhanced by the top mass. Therefore, limits on the ALP-electron interaction can be recasted into new upper bounds for the ALP-top interaction in the mass region $m_a \lesssim 1$ MeV, which was previously unconstrained. These results were presented in Figs. 10 and 11 from the same chapter.

Another interesting point is the one-loop modification of the electroweak tree-level gauge invariance relations. Since all four phenomenological couplings to EW gauge bosons $\{g_{a\gamma\gamma}, g_{a\gamma Z}, g_{aZZ}, g_{aWW}\}$ are induced by only two independent EW couplings above EWSB $\{c_{\widetilde{B}}, c_{\widetilde{W}}\}$, they cannot be linearly independent. In other words, at tree-level, those couplings are related by fixed expressions which can be used, for instance, to correlate experimental

bounds within the ALP EW sector (see Ref. [101]). It was demonstrated that such relations were actually modified once the one-loop corrected Lagrangian was taken into account. This apparent breaking of EW gauge symmetry was however understood and explained in terms of higher dimensional ALP effective operators involving the Higgs doublet, which are generated at one-loop order from the $d = 5$ Lagrangian.

An extensive study of the EW ALP parameters was accomplished in the second work included in this thesis, in Ref. [2] and in Ch. 5, which lies closer to the frontier between theory and experiment. In this chapter we studied the impact of ALPs in high-energy processes at the LHC. A novel search for ALPs was proposed and explored, which focuses on EW diboson production in VBS processes. ALPs, given their derivative nature, could contribute to such processes with significant cross sections which could be measured at the LHC or in future collider experiments.

In particular, and in contrast with most previous works in the literature, we focused on processes mediated by nonresonant ALPs (where the ALP is assumed to be too light to be produced on-shell). These assumptions have the advantage that cross sections become independent on the ALP mass and decay width, which allows to explore huge regions of the parameter space at a time. Additionally, again due to the derivative nature of ALP couplings, ALP-mediated VBS process tends to produce a higher rate of events for larger values of the diboson invariant mass, compared with the SM counterpart. Therefore, instead of looking for a resonant peak in the invariant mass distribution of events, nonresonant searches aim to see a distortion in the "tails" of the event distributions.

We employed Run 2 public data by the CMS experiment on the EW production of diboson events in VBS processes. The final states considered included the production of ZZ, $Z\gamma$, $W^{\pm}\gamma$, $W^{\pm}Z$ and same-sign $W^{\pm}W^{\pm}$ pairs with large diboson invariant mass in association with two forward jets in VBS processes [217–220]. Additionally, heavy EW bosons were required to decay into leptons. No significant discrepancy with respect to the SM prediction have been measured within such analyses. Thus, new upper limits on the ALP parameters were derived.

The VBS channels considered could get contributions from the phenomenological ALP couplings to the EW gauge bosons: $\{g_{a\gamma\gamma}, g_{a\gamma Z}, g_{aZZ}, g_{aWW}\}$. In the analysis, tree-level ALP-fermion interactions were demonstrated to be negligible, since their contribution to the amplitude is proportional to fermion masses. Furthermore, ALP-gluon interactions are disregarded, but it was proven that if those are included in addition, this only leads to an enhancement of the ALP signal cross section, which would imply slightly better limits on the ALP parameters. This is also a strength with respect to previous analysis which relied on ALP-gluon couplings as the dominant ALP production channel. Moreover, the functional dependence of the pure ALP processes and the ALP-SM interference was discussed in a full gauge invariant way in terms on the EW couplings $\{c_{\widetilde{B}}, c_{\widetilde{W}}\}$, which implies that the limits derived were completely general and do not rely on further assumptions on the ALP EFT.

The experimental upper bounds on ALP EW couplings which follow were shown in Figs. 3, 4 and 6 of Ch. 4. Fig. 3 represented the limits obtained in the $\{c_{\widetilde{B}}/f_a, c_{\widetilde{W}}/f_a\}$ plane for the individual VBS channels, and the combined limit. These bounds were proven to be valid for ALP masses up to $m_a \lesssim 100$ GeV. Additionally, projection limits for the combined channel for Run 3 LHC (with an estimated luminosity of $\mathcal{L} = 300$ fb^{-1}) and HL-LHC

($\mathcal{L} = 3000$ fb^{-1}) were estimated and represented in Fig. 4. Finally, a comparison with other existing bounds was included in Fig. 6 for the four phenomenological ALP EW couplings. Our results were shown to be competitive with other ALP searches and, in particular, they comprise the best limit on g_{aZZ} and g_{aWW} in the ALP mass region from 1 to 100 GeV, which was previously unconstrained.

Regarding future improvements of this work, stronger results could be found for example by the implementation of a refined binning in the region of large invariant masses for the event distribution. They could also be improved by defining a signal region more focused on the ALP signal prediction for the diboson production processes. Finally, this work could also be extended by incorporating into the fit measurements by the ATLAS Collaboration or measurements of other VBS channels, e.g. opposite-sign $W^{\pm}W^{\pm}$ production or semileptonic decays of heavy bosons (WV and ZV production, with $V \to jj$).

Finally, another phenomenological quest of interest is whether ALP physics can explain standing experimental anomalies. That was the case of the third work included in this thesis in Ch. 6 from Ref. [3]. In this chapter, the neutral B-anomalies within the lepton flavour universality (LFU) ratios R_K and R_{K^*} were confronted with an explanation in terms of ALP interactions. It should be noticed that more recently the statistical significance of the anomalies have diminished in new measurements by the LHCb collaboration. Although this situation may seem to leave Ref. [3] outdated, this work could still be used for ALP phenomenology studies. For instance, the best regions of the ALP parameter space for explaining the anomalies could be identified now as new excluded regions and notably stringent upper limits on ALP off-diagonal couplings to quarks would be established.

Within the ALP EFT and assuming ALP-bs couplings, the complete two-dimensional parameter space for flavour-diagonal ALP couplings to electrons and muons was explored. Additionally, ALP-photon couplings were also taken into account when certain loop-level effects required it, since they contribute significantly to other flavour observables, e.g. charged lepton anomalous magnetic moments. Several mass ranges were considered for ALPs, which include: i) m_a heavier than the B-meson mass, ii) light masses bellow twice the muon mass and iii) intermediate masses between those two values. Among these three ranges, only the latter could give a resonant contribution to the decay process of B-mesons.

The predictions for R_K and R_{K^*} were also confronted with the impact of ALPs on other observables. These include $B_s - \overline{B}_s$ meson oscillations, $B_s \to \ell^+\ell^-$ decays, $B \to K^{(*)}\ell^+\ell^-$ decays and astrophysical observables. The data on these observables severely limited the available parameter space. Furthermore, the impact of the solutions found on the charged lepton anomalous magnetic moments was also explored. Then, the available parameter space that could explain the anomalies was compared with the theoretical conditions for EFT validity, requiring to remain within the perturbative domain.

For an ALP heavier than the B-meson, no viable explanation to the anomalies was found. Solutions to R_{K^*} were completely excluded from data on $B_s \to \ell^+\ell^-$. On the other hand, numerical solutions to R_K were found. However, in order to satisfy constraints from meson oscillations, ALP-lepton couplings were required to be excessively large, exceeding EFT validity conditions. Analogously, ALPs lighter than twice the muon mass face similar outcomes. Quantitative solutions to R_{K^*} were found but again incompatible with validity conditions. On the other hand, solutions to R_K were however excluded by data on the electron anomalous magnetic moment and astrophysical constraints.

In contrast to the above, an ALP with an intermediate mass, lighter than the B-meson but with a mass value within any of the bin windows, was found to provide a viable solution to the anomalies. Such ALP could be exchanged on-shell and enter a resonant regime: $B \to K^{(*)}\ell^+\ell^-$ processes factorise into ALP on-shell production followed by decay. In this situation, the ALP coupling to muons must be much smaller than that to electrons, and thus a had to decay mostly into electrons. The latter implies in turn that R_K and/or R_{K^*} are rather independent of the precise values of ALP leptonic couplings, and the solutions, therefore, avoid the theoretical problems with the EFT validity encountered for either heavy or extremely light ALPs. Within the allowed parameter space, a "golden" ALP mass value at the frontier between the two energy bins for R_{K^*} was identified: $m_a = \sqrt{1.1}$ GeV. Such golden mass offered a simultaneous solution to all the anomalies within the experimental limits from the other flavour observables taken into consideration and within the EFT validity region. When smearing effects associated to the experimental resolution were considered, the golden mass becomes a broader mass range. Notwithstanding, it is noteworthy that while solutions in-between bins are always suspect, they are technically allowed and prompt the convenience to perform a slightly different experimental binning, which could easily clean up this avenue.

In resume, in this thesis I have explored axion and ALP phenomenology within the EFT framework. The tree and loop-level structure of ALP couplings was studied, together with their phenomenological implications in collider experiments, or as a solution to experimental anomalies. The landscape of axions and ALPs is undergoing a flourishing period with huge efforts from both the experimental and theoretical point of view. This thesis has both sizeably reduced the ALP parameter space open to exploration, and developed ALP-EFT at loop level, with direct impact on these searches. The results also suggest new possibilities and potential avenues for continuing this discovery quest.

Conclusiones

Las interacciones de axiones y PTAs pueden ser representadas por el mismo Lagrangiano efectivo de las PTAs. Este hecho, junto con la ubicuidad de las PTAs en diferentes modelos más allá del ME, ha fomentado un período próspero tanto en los estudios teóricos y como en el panorama de las búsquedas experimentales de axiones y PTAs, que abarca órdenes de magnitud en las escalas de energía y utiliza técnicas muy diferentes. Estas búsquedas han alcanzado un nivel de precisión y son tan diversas que la sensibilidad experimental requiere de calcular el impacto a un loop en los acoplos efectivos de las PTAs. En esta tesis se presentan estos cálculos en el Cap. 4, que contiene el trabajo incluido en la Ref. [5]. En primer lugar, se presentó una extensa clasificación de los diferentes operadores de las PTAs. Se identificaron los grados de libertad no redundantes presentes en la teoría de campos efectiva (TCE) de las PTAs y se derivaron las relaciones entre los diferentes operadores. Introdujimos el conjunto completo de correcciones a un loop para el Lagrangiano no redundante de las PTAs más general posible. Las correcciones se calcularon en un gauge covariante R_ξ para PTAs fuera de su capa de masas y para las partículas del ME en su capa de masas. Además, se presentaron varios límites cinemáticos para el momento de la PTA y las masas de las partículas del ME, que pueden ser útiles para diversos experimentos.

Con el fin de demostrar el poder de las correcciones a un loop, se discutieron algunas consecuencias fenomenológicas de los cálculos. En particular, se estudió la implicación del impacto a un loop de la interacción PTA-top en otros acoplamientos de las PTAs que han sido testados experimentalmente. Por un lado, consideramos la desintegración resonante de una PTA pesada en un par de quarks top. En dicho proceso, se supuso que las PTAs son producidas por fusión de gluones a través de un loop de quarks top. Aunque el proceso está suprimido por un loop, todavía cuenta con una sección eficaz significativa que puede medirse en experimentos del LHC. Por ejemplo, se utilizaron los datos del experimento ATLAS para eventos con dos tops con el fin de establecer nuevos límites en la interacción PTA-top en la región de $m_a \subset [1{,}5, 4{,}5]$ TeV. Por otro lado, también se exploró el impacto de dicha interacción en las búsquedas de PTAs a bajas energías. Por ejemplo, esta induce una contribución significativa a un loop al acoplo PTA-electrón, que es proporcional la masa del quark top. Por lo tanto, los límites en la interacción PTA-electrón se pueden reformular en términos de nuevas cotas superiores para la interacción PTA-top en la región de masa $m_a \lesssim 1$ MeV, que anteriormente no estaba constreñida. Estos resultados se presentaron en las Figs. 10 y 11 del mismo capítulo.

Otro punto interesante es la modificación a un loop de las relaciones a nivel árbol de

la invariancia gauge electrodébil. Dado que todos los cuatro acoplamientos fenomenológicos a bosones gauge ED $\{g_{a\gamma\gamma}, g_{a\gamma Z}, g_{aZZ}, g_{aWW}\}$ son inducidos por solo dos acoplamientos ED independientes por encima de la ruptura espontánea de simetría ED $\{c_{\widetilde{B}}, c_{\widetilde{W}}\}$, estos no pueden ser linealmente independientes. En otras palabras, a nivel de árbol, esos acoplamientos están relacionados por expresiones fijas que se pueden utilizar, por ejemplo, para correlacionar límites experimentales dentro del sector ED de las PTAs (ver Ref. [101]). Se demostró que dichas relaciones se modifican una vez se tiene en cuenta el Lagrangiano corregido a un loop. Sin embargo, esta aparente ruptura de la simetría gauge ED se entendió y explicó en términos de operadores efectivos de las PTAs de dimensión superior que involucran al doblete de Higgs, que se generan a nivel loop a partir del Lagrangiano $d = 5$.

Una extensa investigación de los parámetros ED de las PTAs se llevó a cabo en el segundo trabajo incluido en esta tesis, en la Ref. [2] y en el Cap. 5, que se encuentra más cerca de la frontera entre la teoría y el experimento. En este capítulo, estudiamos el impacto de las PTAs en procesos de alta energía en el LHC. Se propuso y se exploró una nueva búsqueda de PTAs, que se enfoca en la producción de dibosones ED en procesos de dispersión de bosones vectoriales (DBV). Las PTAs, debido a su naturaleza derivativa, podrían contribuir a tales procesos con secciones eficaces significativas, que podrían medirse en el LHC o en futuros experimentos de colisionadores.

En particular, y en contraste con la mayoría de los trabajos previos de la literatura, nos centramos en procesos mediados por PTAs no resonantes (donde se asume que la PTA es demasiado ligera para ser producida en su capa de masas). Estas suposiciones tienen la ventaja de que las secciones eficaces se vuelven independientes de la masa y de la anchura de desintegración de la PTA, lo que permite explorar grandes regiones del espacio de parámetros simultameamente. Además, nuevamente debido a la naturaleza derivativa de los acoplamientos de las PTAs, el proceso de DBV mediado por PTAs tiende a producir una tasa más alta de eventos para valores más grandes de la masa invariante de los dibosones, en comparación con el caso del ME. Por lo tanto, en lugar de buscar un pico resonante en la distribución de masas invariantes de los eventos, las búsquedas no resonantes buscan ver una distorsión en las "colas" de las distribuciones de eventos.

Utilizamos datos públicos del Run 2 del experimento CMS sobre la producción ED de eventos de dibosones en procesos de DBV. Los estados finales considerados incluyeron la producción de pares ZZ, $Z\gamma$, $W^{\pm}\gamma$, $W^{\pm}Z$ y $W^{\pm}W^{\pm}$ con alta masa invariante en asociación con dos jets no transvesales en procesos de DBV [217–220]. Además, se requirió que los bosones ED pesados se desintegren en leptones. No se ha medido ninguna discrepancia significativa con respecto a la predicción del ME en dichos análisis. Por lo tanto, se derivaron nuevos límites superiores para los parámetros de las PTAs.

Los canales DBV considerados podrían recibir contribuciones de los acoplamientos fenomenológicos de las PTAs a los bosones gauge ED: $\{g_{a\gamma\gamma}, g_{a\gamma Z}, g_{aZZ}, g_{aWW}\}$. En el análisis, se demostró que las interacciones PTA-fermión a nivel de árbol eran despreciables, ya que su contribución a la amplitud es proporcional a la masa de los fermiones. Además, no se consideraron las interacciones PTA-gluón, pero se demostró que si estas también se incluyen, esto solo conduce a una mejora de la sección eficaz de la señal de mediada por PTAs, lo que implicaría límites ligeramente mejores en los parámetros de las PTA. Esto también es una fortaleza en comparación con los análisis previos que se basaban en los acoplamientos PTA-gluón como el canal dominante de producción de la PTA. Además, se discutió la dependencia funcional de los procesos puros de PTA y la interferencia PTA-ME en un marco completa-

mente invariante gauge en términos de los acoplamientos ED $\{c_{\widetilde{B}}, c_{\widetilde{W}}\}$, lo que implica que los límites derivados eran completamente generales y no se basaban en suposiciones adicionales sobre la TCE de las PTAs.

Los límites superiores experimentales para los acoplamientos ED de las PTA que se derivaron se mostraron en las Figs 3, 4 y 6 del Cap. 5. La Fig. 3 representó los límites obtenidos en el plano $\{c_{\widetilde{B}}/f_a, c_{\widetilde{W}}/f_a\}$ para los canales DBC individuales y el límite combinado. Se demostró que estos límites eran válidos para masas de PTA de hasta $m_a \lesssim 100$ GeV. Además, se estimaron los límites proyectados para el canal combinado para el Run 3 del LHC (con una luminosidad estimada de $\mathcal{L} = 300$ fb^{-1}) y HL-LHC ($\mathcal{L} = 3000$ fb^{-1}) y se representaron en la Fig. 4. Finalmente, se incluyó una comparación con otros límites existentes en la Fig. 6 para los cuatro acoplamientos ED de la PTA. Se probó que nuestros resultados eran competitivos con otras búsquedas de PTAs y, en particular, constituyen el mejor límite en g_{aZZ} y g_{aWW} en la región de masa de las PTAs de 1 a 100 GeV, anteriormente no constreñida.

En cuanto a las mejoras de este trabajo en el futuro, se podrían encontrar resultados más sólidos, por ejemplo, mediante la implementación de una separación experimental de intervalos de masa más refinada en la región de grandes masas invariantes para la distribución de eventos. También podrían mejorarse definiendo una región de la señal más centrada en la predicción de la señal de PTA para los procesos de producción de dibosones. Finalmente, este trabajo también podría ampliarse incorporando en el análisis medidas de la Colaboración ATLAS o medidas de otros canales de DBC, como la producción de $W^{\pm}W^{\pm}$ de signo opuesto o desintegraciones semileptónicas de los bosones pesados (producción de un par WV y ZV, con $V \to jj$).

Finalmente, otro objetivo fenomenológico de interés es si la física de las PTAs puede explicar anomalías experimentales. Este fue el caso del tercer trabajo incluido en esta tesis en el Cap. 6 que incluye la Ref. [3]. En este capítulo, se tratan de explicar las anomalías neutras de los mesones B observadas en los ratios R_K y R_{K^*} de la Universalidad del Sabor Leptónico (USL) en términos de las interacciones de las PTAs. Cabe señalar que más recientemente, la significancia estadística de estas anomalías ha disminuido en las nuevas mediciones de la Colaboración LHCb. Aunque esta situación pueda parecer que la Ref. [3] quedaría obsoleta, este trabajo aún podría usarse para estudios de la fenomenología de las PTAs. Por ejemplo, las regiones del espacio de parámetros de las PTAs que mejor explicaban las anomalías podrían identificarse ahora como nuevas regiones excluidas y se establecerían límites superiores notablemente más estrictos en los acoplos no diagonales de las PTAs a los quarks.

Dentro de la TCE de las PTAs y asumiendo acoplos PTA-bs, se exploró el espacio de parámetros bidimensional compuesto por los acoplamientos diagonales de sabor de las PTAs a electrones y muones. Además, también se tuvieron en cuenta los acoplamientos PTA-fotón cuando ciertos efectos a nivel loop lo requerían, ya que contribuyen significativamente a otros observables de sabor, como los momentos magnéticos anómalos de los leptones cargados. Se consideraron varios rangos de masas para las PTAs, que incluyen: i) m_a más pesadas que la masa del mesón B, ii) masas ligeras por debajo del doble de la masa del muón y iii) masas intermedias entre esos dos valores. Entre estos tres rangos, solo las PTA con masas intermedias podrían dar una contribución resonante al proceso de desintegración de los mesones B.

Las predicciones para R_K y R_{K^*} también se compararon con el impacto de las PTAs en otros observables. Estos incluyen oscilaciones de los mesones $B_s - \overline{B}_s$, desintegraciones

$B_s \to \ell^+\ell^-$, desintegraciones $B \to K^{(*)}\ell^+\ell^-$ y observables astrofísicos. El valor de estos observables limitó severamente el espacio de parámetros disponible. Además, se exploró el impacto de las soluciones encontradas en los momentos magnéticos anómalos de los leptones cargados. Posteriormente, se comparó el espacio de parámetros disponible que podría explicar las anomalías con las condiciones teóricas sobre la validez de la TCE, imponiendo que las soluciones encontradas permanezcan dentro del régimen perturbativo.

Para una PTA más pesada que el mesón B, no se encontró una explicación viable para las anomalías. Las soluciones para R_{K^*} fueron completamente excluidas por los datos en $B_s \to \ell^+\ell^-$. Por otro lado, se encontraron soluciones numéricas para R_K. Sin embargo, para satisfacer las restricciones de las oscilaciones de mesones, se requería que los acoplamientos PTA-leptón fueran excesivamente grandes, superando las condiciones de validez de la TCE. De manera análoga, las PTAs más ligeras que el doble de la masa del muón se enfrentan a una situación similar. Se encontraron soluciones cuantitativas para R_{K^*}, pero nuevamente estas eran incompatibles con las condiciones de validez. Por otro lado, las soluciones para R_K fueron excluidas por los datos sobre el momento magnético anómalo del electrón y las observaciones astrofísicas.

En contraste con lo anterior, se encontró que una PTA con una masa intermedia, más ligera que el mesón B pero con un valor de masa dentro de alguno de los intervalos de energía, proporcionó una solución viable para las anomalías. Esta PTA podría ser producida en su capa de masas y entrar en el régimen resonante: los procesos $B \to K^{(*)}\ell^+\ell^-$ se factorizan en la producción de la PTA en su capa de masas seguida de su desintegración. En esta situación, el acoplamiento de la PTA a los muones debe ser mucho menor que el de los electrones, y por lo tanto, a debe desintegrarse principalmente en electrones. Lo anterior implica, a su vez, que R_K y/o R_{K^*} son entonces independientes de los valores concretos de los acoplamientos leptónicos de la PTA, y las soluciones, por lo tanto, consiguen eludir los problemas teóricos sobre la validez de la TCE a los que se enfrentan las PTAs pesadas o extremadamente ligeras. Dentro del espacio de parámetros permitido, se identificó un valor de masa "dorada" de la PTA en la frontera entre los dos intervalos de energía para R_{K^*}: $m_a = \sqrt{1{,}1}$ GeV. Dicha masa dorada ofreció una solución simultánea a todas las anomalías dentro de los límites experimentales de todos los observables de sabor considerados y dentro de la región de validez de la TCE. Cuando se consideraron los efectos de difusión asociados a la resolución experimental, la masa dorada se convirtió en un rango de masa más amplio. Sin embargo, es importante destacar que, si bien las soluciones entre intervalos de energía siempre son sospechosas, técnicamente están permitidas y sugirieren la conveniencia de realizar una separación experimental de intervalos de energía ligeramente diferente, lo que podría eliminar fácilmente esta posibilidad.

En resumen, en esta tesis he explorado la fenomenología de los axiones y las PTAs dentro del marco de la teoría efectiva. Se ha estudiado la estructura a nivel árbol y loop de los acoplamientos de las PTAs, junto con sus implicaciones fenomenológicas en experimentos de colisionadores o como solución a anomalías experimentales. El panorama de los axiones y las PTAs está experimentando un período próspero con enormes esfuerzos tanto desde el punto de vista experimental como teórico. Esta tesis ha reducido considerablemente el espacio de parámetros de las PTAs permitido para su exploración y ha desarrollado la teoría efectiva de las PTA a nivel loop, con un impacto directo en estas búsquedas. Los resultados también sugieren nuevas posibilidades y posibles enfoques para continuar esta labor de descubrimiento.

References

[1] J. Bonilla, I. Brivio, M. B. Gavela and V. Sanz, *One-loop corrections to ALP couplings*, *JHEP* **11** (2021) 168, [2107.11392].

[2] J. Bonilla, I. Brivio, J. Machado-Rodríguez and J. F. de Trocóniz, *Nonresonant searches for axion-like particles in vector boson scattering processes at the LHC*, *JHEP* **06** (2022) 113, [2202.03450].

[3] J. Bonilla, A. de Giorgi, B. Gavela, L. Merlo and M. Ramos, *The cost of an ALP solution to the neutral B-anomalies*, *JHEP* **02** (2023) 138, [2209.11247].

[4] J. Bonilla, A. de Giorgi and M. Ramos, *Neutral B-anomalies from an on-shell scalar exchange*, 2211.05135.

[5] J. Bonilla, I. Brivio, M. B. Gavela and V. Sanz, *One-loop corrections to ALP effective couplings*, *PoS* **EPS-HEP2021** (2022) 497, [2111.14750].

[6] J. Bonilla, I. Brivio, J. Machado and J. F. de Trocóniz, *Nonresonant Searches for Axion-Like Particles at the LHC: Implications for Vector Boson Scattering*, *PoS* **EPS-HEP2021** (2022) 692.

[7] J. Bonilla, *ALP one-loop corrections and nonresonant searches*, in *56th Rencontres de Moriond on Electroweak Interactions and Unified Theories*, 5, 2022. 2205.09156.

[8] C.-N. Yang and R. L. Mills, *Conservation of Isotopic Spin and Isotopic Gauge Invariance*, *Phys. Rev.* **96** (1954) 191–195.

[9] S. L. Glashow, *Partial Symmetries of Weak Interactions*, *Nucl. Phys.* **22** (1961) 579–588.

[10] S. Weinberg, *A Model of Leptons*, *Phys. Rev. Lett.* **19** (1967) 1264–1266.

[11] A. Salam, *Weak and Electromagnetic Interactions*, *Conf. Proc. C* **680519** (1968) 367–377.

[12] F. Englert and R. Brout, *Broken Symmetry and the Mass of Gauge Vector Mesons*, *Phys. Rev. Lett.* **13** (1964) 321–323.

[13] P. W. Higgs, *Broken Symmetries and the Masses of Gauge Bosons*, *Phys. Rev. Lett.* **13** (1964) 508–509.

[14] A. Einstein, *On the electrodynamics of moving bodies*, *Annalen Phys.* **17** (1905) 891–921.

[15] Y. Nambu and G. Jona-Lasinio, *Dynamical Model of Elementary Particles Based on an Analogy with Superconductivity. 1.*, *Phys. Rev.* **122** (1961) 345–358.

[16] J. Goldstone, *Field Theories with Superconductor Solutions*, *Nuovo Cim.* **19** (1961) 154–164.

[17] ATLAS collaboration, G. Aad et al., *Observation of a new particle in the search for the Standard Model Higgs boson with the ATLAS detector at the LHC*, *Phys. Lett. B* **716** (2012) 1–29, [1207.7214].

[18] CMS collaboration, S. Chatrchyan et al., *Observation of a New Boson at a Mass of 125 GeV with the CMS Experiment at the LHC*, *Phys. Lett. B* **716** (2012) 30–61, [1207.7235].

[19] Particle Data Group collaboration, R. L. Workman et al., *Review of Particle Physics*, *PTEP* **2022** (2022) 083C01.

[20] N. Cabibbo, *Unitary Symmetry and Leptonic Decays*, *Phys. Rev. Lett.* **10** (1963) 531–533.

[21] M. Kobayashi and T. Maskawa, *CP Violation in the Renormalizable Theory of Weak Interaction*, *Prog. Theor. Phys.* **49** (1973) 652–657.

[22] S. Weinberg, *Baryon and Lepton Nonconserving Processes*, *Phys. Rev. Lett.* **43** (1979) 1566–1570.

[23] T. Yanagida, *Horizontal Symmetry and Masses of Neutrinos*, *Prog. Theor. Phys.* **64** (1980) 1103.

[24] B. Pontecorvo, *Mesonium and anti-mesonium*, *Sov. Phys. JETP* **6** (1957) 429.

[25] Z. Maki, M. Nakagawa and S. Sakata, *Remarks on the unified model of elementary particles*, *Prog. Theor. Phys.* **28** (1962) 870–880.

[26] I. Esteban, M. C. Gonzalez-Garcia, M. Maltoni, T. Schwetz and A. Zhou, *The fate of hints: updated global analysis of three-flavor neutrino oscillations*, *JHEP* **09** (2020) 178, [2007.14792].

[27] O. W. Greenberg, *CPT violation implies violation of Lorentz invariance*, *Phys. Rev. Lett.* **89** (2002) 231602, [hep-ph/0201258].

[28] A. A. Belavin, A. M. Polyakov, A. S. Schwartz and Y. S. Tyupkin, *Pseudoparticle Solutions of the Yang-Mills Equations*, *Phys. Lett. B* **59** (1975) 85–87.

[29] G. 't Hooft, *Computation of the Quantum Effects Due to a Four-Dimensional Pseudoparticle*, *Phys. Rev. D* **14** (1976) 3432–3450.

[30] C. G. Callan, Jr., R. F. Dashen and D. J. Gross, *Toward a Theory of the Strong Interactions*, *Phys. Rev. D* **17** (1978) 2717.

[31] S. Weinberg, *The U(1) Problem*, *Phys. Rev. D* **11** (1975) 3583–3593.

[32] G. 't Hooft, *Symmetry Breaking Through Bell-Jackiw Anomalies*, *Phys. Rev. Lett.* **37** (1976) 8–11.

[33] G. 't Hooft, *How Instantons Solve the U(1) Problem*, *Phys. Rept.* **142** (1986) 357–387.

[34] S. L. Adler, *Axial vector vertex in spinor electrodynamics*, *Phys. Rev.* **177** (1969) 2426–2438.

[35] J. S. Bell and R. Jackiw, *A PCAC puzzle: $\pi^0 \to \gamma\gamma$ in the σ model*, *Nuovo Cim. A* **60** (1969) 47–61.

[36] K. Fujikawa, *Path Integral Measure for Gauge Invariant Fermion Theories*, *Phys. Rev. Lett.* **42** (1979) 1195–1198.

[37] D. Lee, U.-G. Meißner, K. A. Olive, M. Shifman and T. Vonk, *θ -dependence of light nuclei and nucleosynthesis*, *Phys. Rev. Res.* **2** (2020) 033392, [2006.12321].

[38] E. P. Shabalin, *Electric Dipole Moment of Quark in a Gauge Theory with Left-Handed Currents*, *Sov. J. Nucl. Phys.* **28** (1978) 75.

[39] M. B. Gavela, A. Le Yaouanc, L. Oliver, O. Pene, J. C. Raynal and T. N. Pham, *CP Violation Induced by Penguin Diagrams and the Neutron Electric Dipole Moment*, *Phys. Lett. B* **109** (1982) 215–220.

[40] M. B. Gavela, A. Le Yaouanc, L. Oliver, O. Pene, J. C. Raynal and T. N. Pham, *Contribution of the Triangle Graphs to the Neutron Electric Dipole Moment*, *Z. Phys. C* **23** (1984) 251.

[41] A. Czarnecki and B. Krause, *Neutron electric dipole moment in the standard model: Valence quark contributions*, *Phys. Rev. Lett.* **78** (1997) 4339–4342, [hep-ph/9704355].

[42] S. Dar, *The Neutron EDM in the SM: A Review*, hep-ph/0008248.

[43] V. Baluni, *CP Violating Effects in QCD*, *Phys. Rev. D* **19** (1979) 2227–2230.

[44] R. J. Crewther, P. Di Vecchia, G. Veneziano and E. Witten, *Chiral Estimate of the Electric Dipole Moment of the Neutron in Quantum Chromodynamics*, *Phys. Lett. B* **88** (1979) 123.

[45] K. Kanaya and M. Kobayashi, *Strong CP Violation in the Chiral σ Model*, *Prog. Theor. Phys.* **66** (1981) 2173.

[46] H. J. Schnitzer, *The Soft Pion Skyrmion Lagrangian and Strong CP Violation*, *Phys. Lett. B* **139** (1984) 217–222.

[47] P. Cea and G. Nardulli, *A realistic calculation of the electric dipole moment of the neutron induced by strong cp violation*, *Physics Letters B* **144** (1984) 115–118.

[48] M. M. Musakhanov and Z. Z. Israilov, *THE ELECTRIC DIPOLE MOMENT OF THE NEUTRON IN THE CHIRAL BAG MODEL*, *Phys. Lett. B* **137** (1984) 419–421.

[49] M. A. Morgan and G. A. Miller, *The Neutron Electric Dipole Moment in the Cloudy*

Bag Model, *Phys. Lett. B* **179** (1986) 379–384.

[50] Particle Data Group collaboration, R. L. Workman and Others, *Review of Particle Physics*, *PTEP* **2022** (2022) 083C01.

[51] R. K. Ellis et al., *Physics Briefing Book: Input for the European Strategy for Particle Physics Update 2020*, 1910.11775.

[52] J. Alexander et al., *The storage ring proton EDM experiment*, 2205.00830.

[53] J. Gasser and H. Leutwyler, *Quark Masses*, *Phys. Rept.* **87** (1982) 77–169.

[54] D. R. Nelson, G. T. Fleming and G. W. Kilcup, *Is strong CP due to a massless up quark?*, *Phys. Rev. Lett.* **90** (2003) 021601, [hep-lat/0112029].

[55] S. Aoki et al., *Review of lattice results concerning low-energy particle physics*, *Eur. Phys. J. C* **77** (2017) 112, [1607.00299].

[56] J. Frison, R. Kitano and N. Yamada, *$N_f = 1 + 2$ mass dependence of the topological susceptibility*, *PoS* **LATTICE2016** (2016) 323, [1611.07150].

[57] J. Frison, R. Kitano and N. Yamada, *Topological susceptibility with a single light quark flavour*, *EPJ Web Conf.* **175** (2018) 14017, [1710.06643].

[58] Flavour Lattice Averaging Group (FLAG) collaboration, Y. Aoki et al., *FLAG Review 2021*, *Eur. Phys. J. C* **82** (2022) 869, [2111.09849].

[59] A. E. Nelson, *Naturally Weak CP Violation*, *Phys. Lett. B* **136** (1984) 387–391.

[60] S. M. Barr, *A Natural Class of Nonpeccei-quinn Models*, *Phys. Rev. D* **30** (1984) 1805.

[61] S. M. Barr, *Solving the Strong CP Problem Without the Peccei-Quinn Symmetry*, *Phys. Rev. Lett.* **53** (1984) 329.

[62] M. Dine and P. Draper, *Challenges for the Nelson-Barr Mechanism*, *JHEP* **08** (2015) 132, [1506.05433].

[63] G. 't Hooft, *Naturalness, chiral symmetry, and spontaneous chiral symmetry breaking*, *NATO Sci. Ser. B* **59** (1980) 135–157.

[64] J. R. Ellis and M. K. Gaillard, *Strong and Weak CP Violation*, *Nucl. Phys. B* **150** (1979) 141–162.

[65] R. D. Peccei and H. R. Quinn, *CP Conservation in the Presence of Instantons*, *Phys. Rev. Lett.* **38** (1977) 1440–1443.

[66] R. D. Peccei and H. R. Quinn, *Constraints Imposed by CP Conservation in the Presence of Instantons*, *Phys. Rev. D* **16** (1977) 1791–1797.

[67] S. Weinberg, *A New Light Boson?*, *Phys. Rev. Lett.* **40** (1978) 223–226.

[68] F. Wilczek, *Problem of Strong P and T Invariance in the Presence of Instantons*, *Phys. Rev. Lett.* **40** (1978) 279–282.

[69] J. E. Kim, *Weak Interaction Singlet and Strong CP Invariance*, *Phys. Rev. Lett.* **43** (1979) 103.

[70] M. A. Shifman, A. I. Vainshtein and V. I. Zakharov, *Can Confinement Ensure Natural CP Invariance of Strong Interactions?*, *Nucl. Phys. B* **166** (1980) 493–506.

[71] M. Dine, W. Fischler and M. Srednicki, *A Simple Solution to the Strong CP Problem with a Harmless Axion*, *Phys. Lett. B* **104** (1981) 199–202.

[72] A. R. Zhitnitsky, *On Possible Suppression of the Axion Hadron Interactions. (In Russian)*, *Sov. J. Nucl. Phys.* **31** (1980) 260.

[73] K. Choi and J. E. Kim, *DYNAMICAL AXION*, *Phys. Rev. D* **32** (1985) 1828.

[74] V. A. Rubakov, *Grand unification and heavy axion*, *JETP Lett.* **65** (1997) 621–624, [hep-ph/9703409].

[75] Z. Berezhiani, L. Gianfagna and M. Giannotti, *Strong CP problem and mirror world: The Weinberg-Wilczek axion revisited*, *Phys. Lett. B* **500** (2001) 286–296, [hep-ph/0009290].

[76] L. Gianfagna, M. Giannotti and F. Nesti, *Mirror world, supersymmetric axion and gamma ray bursts*, *JHEP* **10** (2004) 044, [hep-ph/0409185].

[77] S. D. H. Hsu and F. Sannino, *New solutions to the strong CP problem*, *Phys. Lett. B* **605** (2005) 369–375, [hep-ph/0408319].

[78] A. Hook, *Anomalous solutions to the strong CP problem*, *Phys. Rev. Lett.* **114** (2015) 141801, [1411.3325].

[79] H. Fukuda, K. Harigaya, M. Ibe and T. T. Yanagida, *Model of visible QCD axion*, *Phys. Rev. D* **92** (2015) 015021, [1504.06084].

[80] C.-W. Chiang, H. Fukuda, M. Ibe and T. T. Yanagida, *750 GeV diphoton resonance in a visible heavy QCD axion model*, *Phys. Rev. D* **93** (2016) 095016, [1602.07909].

[81] S. Dimopoulos, A. Hook, J. Huang and G. Marques-Tavares, *A collider observable QCD axion*, *JHEP* **11** (2016) 052, [1606.03097].

[82] T. Gherghetta, N. Nagata and M. Shifman, *A Visible QCD Axion from an Enlarged Color Group*, *Phys. Rev. D* **93** (2016) 115010, [1604.01127].

[83] A. Kobakhidze, *Heavy axion in asymptotically safe QCD*, 1607.06552.

[84] P. Agrawal and K. Howe, *Factoring the Strong CP Problem*, *JHEP* **12** (2018) 029, [1710.04213].

[85] P. Agrawal and K. Howe, *A Flavorful Factoring of the Strong CP Problem*, *JHEP* **12** (2018) 035, [1712.05803].

[86] M. K. Gaillard, M. B. Gavela, R. Houtz, P. Quilez and R. Del Rey, *Color unified dynamical axion*, *Eur. Phys. J. C* **78** (2018) 972, [1805.06465].

[87] M. A. Buen-Abad and J. Fan, *Dynamical axion misalignment with small instantons*,

JHEP **12** (2019) 161, [1911.05737].

[88] A. Hook, S. Kumar, Z. Liu and R. Sundrum, *High Quality QCD Axion and the LHC*, *Phys. Rev. Lett.* **124** (2020) 221801, [1911.12364].

[89] C. Csáki, M. Ruhdorfer and Y. Shirman, *UV Sensitivity of the Axion Mass from Instantons in Partially Broken Gauge Groups*, *JHEP* **04** (2020) 031, [1912.02197].

[90] T. Gherghetta and M. D. Nguyen, *A Composite Higgs with a Heavy Composite Axion*, *JHEP* **12** (2020) 094, [2007.10875].

[91] A. Hook, *Solving the Hierarchy Problem Discretely*, *Phys. Rev. Lett.* **120** (2018) 261802, [1802.10093].

[92] L. Di Luzio, B. Gavela, P. Quilez and A. Ringwald, *An even lighter QCD axion*, *JHEP* **05** (2021) 184, [2102.00012].

[93] L. Di Luzio, B. Gavela, P. Quilez and A. Ringwald, *Dark matter from an even lighter QCD axion: trapped misalignment*, 2102.01082.

[94] B. Gavela, P. Quílez and M. Ramos, *Multiple QCD axion*, 2305.15465.

[95] K. Choi, K. Kang and J. E. Kim, *Effects of η' in Low-energy Axion Physics*, *Phys. Lett. B* **181** (1986) 145–149.

[96] H. Georgi, D. B. Kaplan and L. Randall, *Manifesting the Invisible Axion at Low-energies*, *Phys. Lett. B* **169** (1986) 73–78.

[97] P. Di Vecchia, G. Rossi, G. Veneziano and S. Yankielowicz, *Spontaneous CP breaking in QCD and the axion potential: an effective Lagrangian approach*, *JHEP* **12** (2017) 104, [1709.00731].

[98] D. S. M. Alves and N. Weiner, *A viable QCD axion in the MeV mass range*, *JHEP* **07** (2018) 092, [1710.03764].

[99] D. B. Kaplan, *Opening the Axion Window*, *Nucl. Phys. B* **260** (1985) 215–226.

[100] G. Grilli di Cortona, E. Hardy, J. Pardo Vega and G. Villadoro, *The QCD axion, precisely*, *JHEP* **01** (2016) 034, [1511.02867].

[101] G. Alonso-Álvarez, M. Gavela and P. Quilez, *Axion couplings to electroweak gauge bosons*, *Eur. Phys. J. C* **79** (2019) 223, [1811.05466].

[102] L. Di Luzio, F. Mescia and E. Nardi, *Redefining the Axion Window*, *Phys. Rev. Lett.* **118** (2017) 031801, [1610.07593].

[103] L. Chuzhoy and E. W. Kolb, *Reopening the window on charged dark matter*, *JCAP* **07** (2009) 014, [0809.0436].

[104] M. L. Perl, E. R. Lee and D. Loomba, *Searches for fractionally charged particles*, *Ann. Rev. Nucl. Part. Sci.* **59** (2009) 47–65.

[105] J. Preskill, M. B. Wise and F. Wilczek, *Cosmology of the Invisible Axion*, *Phys. Lett. B* **120** (1983) 127–132.

[106] L. F. Abbott and P. Sikivie, *A Cosmological Bound on the Invisible Axion*, *Phys. Lett. B* **120** (1983) 133–136.

[107] M. Dine and W. Fischler, *The Not So Harmless Axion*, *Phys. Lett. B* **120** (1983) 137–141.

[108] D. J. E. Marsh, *Axion Cosmology*, *Phys. Rept.* **643** (2016) 1–79, [1510.07633].

[109] G. B. Gelmini and M. Roncadelli, *Left-Handed Neutrino Mass Scale and Spontaneously Broken Lepton Number*, *Phys. Lett. B* **99** (1981) 411–415.

[110] P. Langacker, R. D. Peccei and T. Yanagida, *Invisible Axions and Light Neutrinos: Are They Connected?*, *Mod. Phys. Lett. A* **1** (1986) 541.

[111] G. Ballesteros, J. Redondo, A. Ringwald and C. Tamarit, *Standard Model—axion—seesaw—Higgs portal inflation. Five problems of particle physics and cosmology solved in one stroke*, *JCAP* **08** (2017) 001, [1610.01639].

[112] M. Cicoli, *Axion-like Particles from String Compactifications*, in *9th Patras Workshop on Axions, WIMPs and WISPs*, 9, 2013. 1309.6988. DOI.

[113] H. Georgi and D. B. Kaplan, *Composite Higgs and Custodial SU(2)*, *Phys. Lett. B* **145** (1984) 216–220.

[114] F. Wilczek, *Axions and Family Symmetry Breaking*, *Phys. Rev. Lett.* **49** (1982) 1549–1552.

[115] L. Calibbi, F. Goertz, D. Redigolo, R. Ziegler and J. Zupan, *Minimal axion model from flavor*, *Phys. Rev. D* **95** (2017) 095009, [1612.08040].

[116] Y. Ema, K. Hamaguchi, T. Moroi and K. Nakayama, *Flaxion: a minimal extension to solve puzzles in the standard model*, *JHEP* **01** (2017) 096, [1612.05492].

[117] I. Brivio, M. B. Gavela, L. Merlo, K. Mimasu, J. M. No, R. del Rey et al., *ALPs Effective Field Theory and Collider Signatures*, *Eur. Phys. J. C* **77** (2017) 572, [1701.05379].

[118] M. Chala, G. Guedes, M. Ramos and J. Santiago, *Running in the ALPs*, 2012.09017.

[119] M. Bauer, M. Neubert, S. Renner, M. Schnubel and A. Thamm, *The Low-Energy Effective Theory of Axions and ALPs*, *JHEP* **04** (2021) 063, [2012.12272].

[120] M. Freytsis, Z. Ligeti and J. Thaler, *Constraining the Axion Portal with $B \to K l^+ l^-$*, *Phys. Rev. D* **81** (2010) 034001, [0911.5355].

[121] K. Mimasu and V. Sanz, *ALPs at Colliders*, *JHEP* **06** (2015) 173, [1409.4792].

[122] J. Jaeckel and M. Spannowsky, *Probing MeV to 90 GeV axion-like particles with LEP and LHC*, *Phys. Lett. B* **753** (2016) 482–487, [1509.00476].

[123] E. Izaguirre, T. Lin and B. Shuve, *Searching for Axionlike Particles in Flavor-Changing Neutral Current Processes*, *Phys. Rev. Lett.* **118** (2017) 111802, [1611.09355].

[124] M. Bauer, M. Neubert and A. Thamm, *Collider Probes of Axion-Like Particles*, *JHEP* **12** (2017) 044, [1708.00443].

[125] N. Craig, A. Hook and S. Kasko, *The Photophobic ALP*, *JHEP* **09** (2018) 028, [1805.06538].

[126] C. Frugiuele, E. Fuchs, G. Perez and M. Schlaffer, *Relaxion and light (pseudo)scalars at the HL-LHC and lepton colliders*, *JHEP* **10** (2018) 151, [1807.10842].

[127] M. Bauer, M. Heiles, M. Neubert and A. Thamm, *Axion-Like Particles at Future Colliders*, *Eur. Phys. J. C* **79** (2019) 74, [1808.10323].

[128] J. Ebadi, S. Khatibi and M. Mohammadi Najafabadi, *New probes for axionlike particles at hadron colliders*, *Phys. Rev. D* **100** (2019) 015016, [1901.03061].

[129] L. Merlo, F. Pobbe, S. Rigolin and O. Sumensari, *Revisiting the production of ALPs at B-factories*, *JHEP* **06** (2019) 091, [1905.03259].

[130] M. Gavela, J. No, V. Sanz and J. de Trocóniz, *Nonresonant Searches for Axionlike Particles at the LHC*, *Phys. Rev. Lett.* **124** (2020) 051802, [1905.12953].

[131] M. Bauer, M. Neubert, S. Renner, M. Schnubel and A. Thamm, *Axionlike Particles, Lepton-Flavor Violation, and a New Explanation of a_μ and a_e*, *Phys. Rev. Lett.* **124** (2020) 211803, [1908.00008].

[132] M. Bauer, M. Neubert, S. Renner, M. Schnubel and A. Thamm, *Consistent Treatment of Axions in the Weak Chiral Lagrangian*, *Phys. Rev. Lett.* **127** (2021) 081803, [2102.13112].

[133] M. Bauer, M. Neubert, S. Renner, M. Schnubel and A. Thamm, *Flavor Probes of Axion-Like Particles*, 2110.10698.

[134] A. Salvio, A. Strumia and W. Xue, *Thermal axion production*, *JCAP* **01** (2014) 011, [1310.6982].

[135] M. B. Gavela, J. Gonzalez-Fraile, M. C. Gonzalez-Garcia, L. Merlo, S. Rigolin and J. Yepes, *CP violation with a dynamical Higgs*, *JHEP* **10** (2014) 044, [1406.6367].

[136] J. Martin Camalich, M. Pospelov, P. N. H. Vuong, R. Ziegler and J. Zupan, *Quark Flavor Phenomenology of the QCD Axion*, *Phys. Rev. D* **102** (2020) 015023, [2002.04623].

[137] J. S. R. Chisholm, *Change of variables in quantum field theories*, *Nucl. Phys.* **26** (1961) 469–479.

[138] S. Kamefuchi, L. O'Raifeartaigh and A. Salam, *Change of variables and equivalence theorems in quantum field theories*, *Nucl. Phys.* **28** (1961) 529–549.

[139] J. C. Criado and M. Pérez-Victoria, *Field redefinitions in effective theories at higher orders*, *JHEP* **03** (2019) 038, [1811.09413].

[140] C. O'Hare, "cajohare/AxionLimits:AxionLimits (version v1.0)." July, 2020, "https://doi.org/10.5281/zenodo.3932430".

[141] D. A. Dicus, E. W. Kolb, V. L. Teplitz and R. V. Wagoner, *Astrophysical Bounds on the Masses of Axions and Higgs Particles*, *Phys. Rev. D* **18** (1978) 1829.

[142] G. Raffelt and L. Stodolsky, *Mixing of the Photon with Low Mass Particles*, *Phys. Rev. D* **37** (1988) 1237.

[143] CAST collaboration, S. Andriamonje et al., *An Improved limit on the axion-photon coupling from the CAST experiment*, *JCAP* **04** (2007) 010, [hep-ex/0702006].

[144] CAST collaboration, V. Anastassopoulos et al., *New CAST Limit on the Axion-Photon Interaction*, *Nature Phys.* **13** (2017) 584–590, [1705.02290].

[145] ADMX collaboration, S. J. Asztalos et al., *A SQUID-based microwave cavity search for dark-matter axions*, *Phys. Rev. Lett.* **104** (2010) 041301, [0910.5914].

[146] ADMX collaboration, N. Du et al., *A Search for Invisible Axion Dark Matter with the Axion Dark Matter Experiment*, *Phys. Rev. Lett.* **120** (2018) 151301, [1804.05750].

[147] ADMX collaboration, T. Braine et al., *Extended Search for the Invisible Axion with the Axion Dark Matter Experiment*, *Phys. Rev. Lett.* **124** (2020) 101303, [1910.08638].

[148] ADMX collaboration, C. Bartram et al., *Search for Invisible Axion Dark Matter in the 3.3–4.2 μeV Mass Range*, *Phys. Rev. Lett.* **127** (2021) 261803, [2110.06096].

[149] N. Crisosto, P. Sikivie, N. S. Sullivan, D. B. Tanner, J. Yang and G. Rybka, *ADMX SLIC: Results from a Superconducting LC Circuit Investigating Cold Axions*, *Phys. Rev. Lett.* **124** (2020) 241101, [1911.05772].

[150] S. Lee, S. Ahn, J. Choi, B. R. Ko and Y. K. Semertzidis, *Axion Dark Matter Search around 6.7 μeV*, *Phys. Rev. Lett.* **124** (2020) 101802, [2001.05102].

[151] J. Jeong, S. Youn, S. Bae, J. Kim, T. Seong, J. E. Kim et al., *Search for Invisible Axion Dark Matter with a Multiple-Cell Haloscope*, *Phys. Rev. Lett.* **125** (2020) 221302, [2008.10141].

[152] CAPP collaboration, O. Kwon et al., *First Results from an Axion Haloscope at CAPP around 10.7 μeV*, *Phys. Rev. Lett.* **126** (2021) 191802, [2012.10764].

[153] Y. Lee, B. Yang, H. Yoon, M. Ahn, H. Park, B. Min et al., *Searching for Invisible Axion Dark Matter with an 18 T Magnet Haloscope*, *Phys. Rev. Lett.* **128** (2022) 241805, [2206.08845].

[154] J. Kim et al., *Near-Quantum-Noise Axion Dark Matter Search at CAPP around 9.5 μeV*, *Phys. Rev. Lett.* **130** (2023) 091602, [2207.13597].

[155] A. K. Yi et al., *Axion Dark Matter Search around 4.55 μeV with Dine-Fischler-Srednicki-Zhitnitskii Sensitivity*, *Phys. Rev. Lett.* **130** (2023) 071002, [2210.10961].

[156] S. De Panfilis, A. C. Melissinos, B. E. Moskowitz, J. T. Rogers, Y. K. Semertzidis, W. Wuensch et al., *Limits on the Abundance and Coupling of Cosmic Axions at*

4.5-Microev < m(a) < 5.0-Microev, *Phys. Rev. Lett.* **59** (1987) 839.

[157] HAYSTAC collaboration, L. Zhong et al., *Results from phase 1 of the HAYSTAC microwave cavity axion experiment*, *Phys. Rev. D* **97** (2018) 092001, [1803.03690].

[158] HAYSTAC collaboration, K. M. Backes et al., *A quantum-enhanced search for dark matter axions*, *Nature* **590** (2021) 238–242, [2008.01853].

[159] HAYSTAC collaboration, M. J. Jewell et al., *New results from HAYSTAC's phase II operation with a squeezed state receiver*, *Phys. Rev. D* **107** (2023) 072007, [2301.09721].

[160] D. Alesini et al., *Galactic axions search with a superconducting resonant cavity*, *Phys. Rev. D* **99** (2019) 101101, [1903.06547].

[161] D. Alesini et al., *Search for invisible axion dark matter of mass $m_a = 43$ μeV with the QUAX–$a\gamma$ experiment*, *Phys. Rev. D* **103** (2021) 102004, [2012.09498].

[162] D. Alesini et al., *Search for Galactic axions with a high-Q dielectric cavity*, *Phys. Rev. D* **106** (2022) 052007, [2208.12670].

[163] B. T. McAllister, G. Flower, J. Kruger, E. N. Ivanov, M. Goryachev, J. Bourhill et al., *The ORGAN Experiment: An axion haloscope above 15 GHz*, *Phys. Dark Univ.* **18** (2017) 67–72, [1706.00209].

[164] A. P. Quiskamp, B. T. McAllister, P. Altin, E. N. Ivanov, M. Goryachev and M. E. Tobar, *Direct search for dark matter axions excluding ALP cogenesis in the 63- to 67-μeV range with the ORGAN experiment*, *Sci. Adv.* **8** (2022) abq3765, [2203.12152].

[165] D. Noordhuis, A. Prabhu, S. J. Witte, A. Y. Chen, F. Cruz and C. Weniger, *Novel Constraints on Axions Produced in Pulsar Polar Cap Cascades*, 2209.09917.

[166] A. Ayala, I. Domínguez, M. Giannotti, A. Mirizzi and O. Straniero, *Revisiting the bound on axion-photon coupling from Globular Clusters*, *Phys. Rev. Lett.* **113** (2014) 191302, [1406.6053].

[167] M. J. Dolan, F. J. Hiskens and R. R. Volkas, *Advancing globular cluster constraints on the axion-photon coupling*, *JCAP* **10** (2022) 096, [2207.03102].

[168] A. Caputo, H.-T. Janka, G. Raffelt and E. Vitagliano, *Low-Energy Supernovae Severely Constrain Radiative Particle Decays*, 2201.09890.

[169] D. Wadekar and Z. Wang, *Strong constraints on decay and annihilation of dark matter from heating of gas-rich dwarf galaxies*, *Phys. Rev. D* **106** (2022) 075007, [2111.08025].

[170] E. Müller, F. Calore, P. Carenza, C. Eckner and M. C. D. Marsh, *Investigating the gamma-ray burst from decaying MeV-scale axion-like particles produced in supernova explosions*, 2304.01060.

[171] M. Regis, M. Taoso, D. Vaz, J. Brinchmann, S. L. Zoutendijk, N. F. Bouché et al., *Searching for light in the darkness: Bounds on ALP dark matter with the optical*

MUSE-faint survey, *Phys. Lett. B* **814** (2021) 136075, [2009.01310].

[172] D. Grin, G. Covone, J.-P. Kneib, M. Kamionkowski, A. Blain and E. Jullo, *A Telescope Search for Decaying Relic Axions*, *Phys. Rev. D* **75** (2007) 105018, [astro-ph/0611502].

[173] K. Nakayama and W. Yin, *Anisotropic cosmic optical background bound for decaying dark matter in light of the LORRI anomaly*, *Phys. Rev. D* **106** (2022) 103505, [2205.01079].

[174] P. Carenza, G. Lucente and E. Vitagliano, *Probing the blue axion with cosmic optical background anisotropies*, *Phys. Rev. D* **107** (2023) 083032, [2301.06560].

[175] J. W. Foster, M. Kongsore, C. Dessert, Y. Park, N. L. Rodd, K. Cranmer et al., *Deep Search for Decaying Dark Matter with XMM-Newton Blank-Sky Observations*, *Phys. Rev. Lett.* **127** (2021) 051101, [2102.02207].

[176] K. Perez, K. C. Y. Ng, J. F. Beacom, C. Hersh, S. Horiuchi and R. Krivonos, *Almost closing the νMSM sterile neutrino dark matter window with NuSTAR*, *Phys. Rev. D* **95** (2017) 123002, [1609.00667].

[177] K. C. Y. Ng, B. M. Roach, K. Perez, J. F. Beacom, S. Horiuchi, R. Krivonos et al., *New Constraints on Sterile Neutrino Dark Matter from NuSTAR M31 Observations*, *Phys. Rev. D* **99** (2019) 083005, [1901.01262].

[178] B. M. Roach, S. Rossland, K. C. Y. Ng, K. Perez, J. F. Beacom, B. W. Grefenstette et al., *Long-exposure NuSTAR constraints on decaying dark matter in the Galactic halo*, *Phys. Rev. D* **107** (2023) 023009, [2207.04572].

[179] F. Calore, A. Dekker, P. D. Serpico and T. Siegert, *Constraints on light decaying dark matter candidates from 16 yr of INTEGRAL/SPI observations*, *Mon. Not. Roy. Astron. Soc.* **520** (2023) 4167–4172, [2209.06299].

[180] F. Capozzi, R. Z. Ferreira, L. Lopez-Honorez and O. Mena, *CMB and Lyman-α constraints on dark matter decays to photons*, 2303.07426.

[181] H. Liu, W. Qin, G. W. Ridgway and T. R. Slatyer, *Exotic energy injection in the early universe II: CMB spectral distortions and constraints on light dark matter*, 2303.07370.

[182] D. Cadamuro, *Cosmological limits on axions and axion-like particles*. PhD thesis, Munich U., 2012. 1210.3196.

[183] P. F. Depta, M. Hufnagel and K. Schmidt-Hoberg, *Robust cosmological constraints on axion-like particles*, *JCAP* **05** (2020) 009, [2002.08370].

[184] K. Langhoff, N. J. Outmezguine and N. L. Rodd, *Irreducible Axion Background*, *Phys. Rev. Lett.* **129** (2022) 241101, [2209.06216].

[185] CHARM collaboration, F. Bergsma et al., *Search for Axion Like Particle Production in 400-GeV Proton - Copper Interactions*, *Phys. Lett. B* **157** (1985) 458–462.

[186] E. M. Riordan et al., *A Search for Short Lived Axions in an Electron Beam Dump*

Experiment, *Phys. Rev. Lett.* **59** (1987) 755.

[187] M. J. Dolan, T. Ferber, C. Hearty, F. Kahlhoefer and K. Schmidt-Hoberg, *Revised constraints and Belle II sensitivity for visible and invisible axion-like particles*, *JHEP* **12** (2017) 094, [1709.00009].

[188] J. Blumlein et al., *Limits on neutral light scalar and pseudoscalar particles in a proton beam dump experiment*, *Z. Phys. C* **51** (1991) 341–350.

[189] NA64 collaboration, D. Banerjee et al., *Search for Axionlike and Scalar Particles with the NA64 Experiment*, *Phys. Rev. Lett.* **125** (2020) 081801, [2005.02710].

[190] CMS collaboration, A. M. Sirunyan et al., *Evidence for light-by-light scattering and searches for axion-like particles in ultraperipheral PbPb collisions at* $\sqrt{s_{\mathrm{NN}}} = 5.02$ *TeV*, *Phys. Lett. B* **797** (2019) 134826, [1810.04602].

[191] ATLAS collaboration, G. Aad et al., *Measurement of light-by-light scattering and search for axion-like particles with 2.2* nb^{-1} *of Pb+Pb data with the ATLAS detector*, *JHEP* **03** (2021) 243, [2008.05355].

[192] S. Knapen, T. Lin, H. K. Lou and T. Melia, *Searching for Axionlike Particles with Ultraperipheral Heavy-Ion Collisions*, *Phys. Rev. Lett.* **118** (2017) 171801, [1607.06083].

[193] Belle-II collaboration, F. Abudinén et al., *Search for Axion-Like Particles produced in* e^+e^- *collisions at Belle II*, *Phys. Rev. Lett.* **125** (2020) 161806, [2007.13071].

[194] BESIII collaboration, M. Ablikim et al., *Search for an axion-like particle in radiative* J/ψ *decays*, *Phys. Lett. B* **838** (2023) 137698, [2211.12699].

[195] D. Aloni, C. Fanelli, Y. Soreq and M. Williams, *Photoproduction of Axionlike Particles*, *Phys. Rev. Lett.* **123** (2019) 071801, [1903.03586].

[196] NA62 collaboration, E. Cortina Gil et al., *Measurement of the very rare* $K^+ \to \pi^+ \nu\overline{\nu}$ *decay*, *JHEP* **06** (2021) 093, [2103.15389].

[197] G. Haghighat, D. Haji Raissi and M. Mohammadi Najafabadi, *New collider searches for axionlike particles coupling to gluons*, *Phys. Rev. D* **102** (2020) 115010, [2006.05302].

[198] ATLAS collaboration, G. Aad et al., *Search for new phenomena in events with an energetic jet and missing transverse momentum in pp collisions at* $\sqrt{s}$ *=13 TeV with the ATLAS detector*, *Phys. Rev. D* **103** (2021) 112006, [2102.10874].

[199] F. A. Ghebretinsaea, Z. S. Wang and K. Wang, *Probing axion-like particles coupling to gluons at the LHC*, *JHEP* **07** (2022) 070, [2203.01734].

[200] R. Z. Ferreira, M. C. D. Marsh and E. Müller, *Strong supernovae bounds on ALPs from quantum loops*, *JCAP* **11** (2022) 057, [2205.07896].

[201] GERDA collaboration, M. Agostini et al., *First Search for Bosonic Superweakly Interacting Massive Particles with Masses up to 1 MeV/*c^2 *with GERDA*, *Phys. Rev. Lett.* **125** (2020) 011801, [2005.14184].

[202] XENON collaboration, E. Aprile et al., *Light Dark Matter Search with Ionization Signals in XENON1T*, *Phys. Rev. Lett.* **123** (2019) 251801, [1907.11485].

[203] XENON collaboration, E. Aprile et al., *Excess electronic recoil events in XENON1T*, *Phys. Rev. D* **102** (2020) 072004, [2006.09721].

[204] XENON collaboration, E. Aprile et al., *Emission of single and few electrons in XENON1T and limits on light dark matter*, *Phys. Rev. D* **106** (2022) 022001, [2112.12116].

[205] XENON collaboration, E. Aprile et al., *Search for New Physics in Electronic Recoil Data from XENONnT*, *Phys. Rev. Lett.* **129** (2022) 161805, [2207.11330].

[206] F. Capozzi and G. Raffelt, *Axion and neutrino bounds improved with new calibrations of the tip of the red-giant branch using geometric distance determinations*, *Phys. Rev. D* **102** (2020) 083007, [2007.03694].

[207] P. F. Depta, M. Hufnagel and K. Schmidt-Hoberg, *Updated BBN constraints on electromagnetic decays of MeV-scale particles*, *JCAP* **04** (2021) 011, [2011.06519].

[208] L. Waites, A. Thompson, A. Bungau, J. M. Conrad, B. Dutta, W.-C. Huang et al., *Axionlike particle production at beam dump experiments with distinct nuclear excitation lines*, *Phys. Rev. D* **107** (2023) 095010, [2207.13659].

[209] S. N. Gninenko, D. V. Kirpichnikov, M. M. Kirsanov and N. V. Krasnikov, *The exact tree-level calculation of the dark photon production in high-energy electron scattering at the CERN SPS*, *Phys. Lett. B* **782** (2018) 406–411, [1712.05706].

[210] NA64 collaboration, Y. M. Andreev et al., *Search for pseudoscalar bosons decaying into e^+e^- pairs in the NA64 experiment at the CERN SPS*, *Phys. Rev. D* **104** (2021) L111102, [2104.13342].

[211] Y. M. Andreev et al., *Improved exclusion limit for light dark matter from e+e- annihilation in NA64*, *Phys. Rev. D* **104** (2021) L091701, [2108.04195].

[212] J. D. Bjorken, S. Ecklund, W. R. Nelson, A. Abashian, C. Church, B. Lu et al., *Search for Neutral Metastable Penetrating Particles Produced in the SLAC Beam Dump*, *Phys. Rev. D* **38** (1988) 3375.

[213] A. Bross, M. Crisler, S. H. Pordes, J. Volk, S. Errede and J. Wrbanek, *A Search for Shortlived Particles Produced in an Electron Beam Dump*, *Phys. Rev. Lett.* **67** (1991) 2942–2945.

[214] M. Davier and H. Nguyen Ngoc, *An Unambiguous Search for a Light Higgs Boson*, *Phys. Lett. B* **229** (1989) 150–155.

[215] CMS collaboration, A. M. Sirunyan et al., *Search for the production of $W^{\pm}W^{\pm}W^{\mp}$ events at $\sqrt{s} = 13$ TeV*, *Phys. Rev. D* **100** (2019) 012004, [1905.04246].

[216] M. Buschmann, C. Dessert, J. W. Foster, A. J. Long and B. R. Safdi, *Upper Limit on the QCD Axion Mass from Isolated Neutron Star Cooling*, *Phys. Rev. Lett.* **128** (2022) 091102, [2111.09892].

[217] CMS collaboration, A. M. Sirunyan et al., *Evidence for electroweak production of four charged leptons and two jets in proton-proton collisions at $\sqrt{s}$ = 13 TeV*, *Phys. Lett. B* **812** (2021) 135992, [2008.07013].

[218] CMS collaboration, A. Tumasyan et al., *Measurement of the electroweak production of $Z\gamma$ and two jets in proton-proton collisions at $\sqrt{s}$ = 13 TeV and constraints on anomalous quartic gauge couplings*, *Phys. Rev. D* **104** (2021) 072001, [2106.11082].

[219] CMS collaboration, A. M. Sirunyan et al., *Observation of electroweak production of $W\gamma$ with two jets in proton-proton collisions at $\sqrt{s}$ = 13 TeV*, *Phys. Lett. B* **811** (2020) 135988, [2008.10521].

[220] CMS collaboration, A. M. Sirunyan et al., *Measurements of production cross sections of WZ and same-sign WW boson pairs in association with two jets in proton-proton collisions at $\sqrt{s}$ = 13 TeV*, *Phys. Lett. B* **809** (2020) 135710, [2005.01173].

[221] J. Alwall, R. Frederix, S. Frixione, V. Hirschi, F. Maltoni, O. Mattelaer et al., *The automated computation of tree-level and next-to-leading order differential cross sections, and their matching to parton shower simulations*, *JHEP* **07** (2014) 079, [1405.0301].

[222] feynrules.irmp.ucl.ac.be/wiki/ALPsEFT.

[223] T. Sjöstrand, S. Ask, J. R. Christiansen, R. Corke, N. Desai, P. Ilten et al., *An introduction to pythia 8.2*, *Computer Physics Communications* **191** (2015) 159–177.

[224] J. Favereau, C. Delaere, P. Demin, A. Giammanco, V. Lemaitre, A. Mertens et al., *Delphes 3, a modular framework for fast simulation of a generic collider experiment*, *Journal of High Energy Physics* **2014** (07, 2013) .

[225] M. Cacciari, G. P. Salam and G. Soyez, *FastJet User Manual*, *Eur. Phys. J. C* **72** (2012) 1896, [1111.6097].

[226] LHCb collaboration, R. Aaij et al., *Test of lepton universality with $B^0 \to K^{*0}\ell^+\ell^-$ decays*, *JHEP* **08** (2017) 055, [1705.05802].

[227] LHCb collaboration, R. Aaij et al., *Test of lepton universality in beauty-quark decays*, 2103.11769.

[228] LHCb collaboration, *Test of lepton universality in $b \to s\ell^+\ell^-$ decays*, 2212.09152.

[229] LHCb collaboration, *Measurement of lepton universality parameters in $B^+ \to K^+\ell^+\ell^-$ and $B^0 \to K^{*0}\ell^+\ell^-$ decays*, 2212.09153.